

**Data Modeling and Analysis for the  
TFTR Differential Phase Reflectometer  
With Applications to ICRH**

A Thesis  
Presented to  
The Academic Faculty  
by  
**Iván Collazo-López**

In Partial Fulfillment  
for the Degree of  
**DOCTOR OF PHILOSOPHY  
IN NUCLEAR ENGINEERING**

Georgia Institute of Technology  
March 1996

**Data Modeling and Analysis for the  
TFTR Differential Phase Reflectometer  
With Applications to ICRH**

APPROVED:

\_\_\_\_\_, 12-11-95  
W. M. Stacey, Jr., Chairman Date

\_\_\_\_\_  
C. E. Thomas, Co-chairman  
D. A.

\_\_\_\_\_  
J. Mandrekas

\_\_\_\_\_  
E. W. Thomas

\_\_\_\_\_  
A. Larson

\_\_\_\_\_  
J. B. Wilgen  
D. A.

\_\_\_\_\_  
N. Bretz

*Dedicated to my parents  
Francisco Collazo-González and María Del Carmen López-Pujolz,  
and my beloved wife  
Stephanie Ann May.*

## Acknowledgments

I will like to give special thanks to my advisors, Drs. J.B. Wilgen, T.S. Bigelow and N. Bretz for their help, support, and encouragement through these years of slavery at Georgia Tech. Since most of this work was done at the Princeton Plasma Physics Laboratory, I am in debt to all the wonderful people with whom I worked there and to the people at the Oak Ridge National Laboratory, that helped me and supported me through this entire and misearble adventure.

To all of them, my deepest and most sincere THANKS.



# Table of Contents

<b>Acknowledgments</b>	<b>iv</b>
<b>Table of Contents</b>	<b>v</b>
<b>List of Tables</b>	<b>xvi</b>
<b>List of Figures</b>	<b>xviii</b>
<b>Summary</b>	<b>xxxiii</b>
<b>CHAPTER</b>	
<b>I. Introduction</b>	<b>1</b>
1.1 Fusion . . . . .	2
1.2 Reflectometry . . . . .	3
1.3 Fusion Experiments . . . . .	8
1.4 Tokamak Fusion Test Reactor . . . . .	10
<b>II. Reflectometry</b>	<b>16</b>
2.1 Introduction . . . . .	16
2.2 History of Reflectometry . . . . .	16
2.2.1 The beginnings . . . . .	16
2.2.2 First experiments in Russia . . . . .	17
2.2.3 First experiment in USA . . . . .	17
2.3 Propagation of Electromagnetic Waves in Plasmas . . . . .	18
2.3.1 Maxwell equations . . . . .	18
2.3.2 The dielectric tensor . . . . .	20

2.3.3	Properties of the O- and X-modes . . . . .	27
	The Ordinary mode . . . . .	27
	The eXtraordinary mode . . . . .	28
2.3.4	Advantages and disadvantages of each mode . . . . .	29
	O-mode . . . . .	29
	X-mode . . . . .	31
2.3.5	Solution to the wave equation in a plasma . . . . .	32
	Geometrical optics solution . . . . .	34
	Series solution . . . . .	36
	Solution at the reflection layer . . . . .	37
	One dimensional full wave analysis. . . . .	38
2.4	Reflectometry Techniques . . . . .	45
2.4.1	Fixed frequency . . . . .	45
2.4.2	Narrow band swept frequency . . . . .	46
2.4.3	Broadband swept frequency . . . . .	46
2.4.4	AM technique . . . . .	48
2.4.5	Dual frequency phase difference technique . . . . .	51
2.4.6	Pulse radar technique . . . . .	51
2.4.7	Other techniques . . . . .	52
	Measurement of magnetic fluctuations . . . . .	52
	Small scale edge fluctuations . . . . .	52
2.5	Measuring Density Fluctuations . . . . .	53
2.5.1	Using the O-mode . . . . .	55
2.5.2	Using the X-mode . . . . .	56
2.6	Measuring the Density Profile . . . . .	56
2.6.1	Profile reconstruction using the O-mode . . . . .	56
2.6.2	Profile reconstruction using the X-mode . . . . .	60

	Full phase technique . . . . .	60
	Phase difference technique . . . . .	61
2.7	Complications and Error Sources . . . . .	63
2.7.1	Electron Cyclotron Resonance absorption . . . . .	63
2.7.2	Tunneling . . . . .	66
2.7.3	Magnetic shear . . . . .	71
2.7.4	Motion/fluctuation of the cutoff layer . . . . .	73
2.7.5	Fluctuation correlation length . . . . .	74
2.7.6	Relativistic effects . . . . .	75
2.7.7	Uncertainty in $\omega_X$ . . . . .	79
2.8	Summary . . . . .	81
<b>III.</b>	<b>Ion Cyclotron Resonance Heating</b>	<b>83</b>
3.1	Introduction . . . . .	83
3.2	Theory . . . . .	85
3.2.1	Radio frequency heating schemes . . . . .	85
3.2.2	Multiple species dielectric tensor . . . . .	86
3.3	ICRH and Plasma Edge Interaction . . . . .	88
3.3.1	Pre-history . . . . .	90
3.3.2	The impurity problem . . . . .	91
3.3.3	Antenna phasing . . . . .	93
3.3.4	The sheath rectification effect . . . . .	94
3.3.5	Self sputtering and avalanche . . . . .	95
3.3.6	Increased diffusion at the edge . . . . .	95
3.3.7	Quiver induced losses . . . . .	96
3.3.8	Ponderomotive effects . . . . .	96
3.4	Antennas in Fusion Experiments . . . . .	97
3.5	TFTR Antenna . . . . .	99

3.6	Summary . . . . .	107
<b>IV.</b>	<b>TFTR Reflectometer System Design</b>	<b>108</b>
4.1	Introduction . . . . .	108
4.2	Development . . . . .	109
4.3	Description of the Reflectometer . . . . .	121
4.4	Major Components of the Reflectometer System . . . . .	122
4.4.1	Frequency signal sources . . . . .	124
4.4.2	Fixed frequency sources . . . . .	126
4.4.3	Directional couplers . . . . .	130
4.4.4	Active frequency multipliers and amplifiers . . . . .	132
	Frequency doublers . . . . .	133
	Frequency triplers . . . . .	133
	Amplifiers . . . . .	135
4.4.5	Quadrature phase detector . . . . .	137
	The I & Q Network as a detector . . . . .	139
	The phase Comparator . . . . .	140
	Merrimac IQM-A series . . . . .	141
4.4.6	Detectors and mixers . . . . .	141
	Small signal analysis of diodes . . . . .	143
	Diodes as detectors . . . . .	146
	Single-ended mixers . . . . .	148
4.4.7	Filters . . . . .	153
4.4.8	Equalizer . . . . .	154
4.4.9	Waveguides/antenna system . . . . .	155
4.4.10	Power budget . . . . .	157
4.5	Summary . . . . .	157

<b>V.</b>	<b>Operation, Verification and Calibration</b>	<b>160</b>
5.1	Introduction . . . . .	160
5.2	Description of the Normal Operation . . . . .	160
5.2.1	Some parameters . . . . .	160
5.2.2	Normal operation . . . . .	162
	Waveguide setup . . . . .	162
	Getting on the <i>shot cycle</i> . . . . .	162
	Setting the reflectometer's digitizers . . . . .	162
	Normal setting of frequency sources . . . . .	164
	Take bypass loop data . . . . .	167
	Recognizing good data . . . . .	167
5.3	Verification and Testing the Operation of the System . . . . .	168
5.3.1	Bypass loop verification and testing . . . . .	168
5.3.2	Effects of the plasma on the reflectometer data . . . . .	169
	Magnetic fields . . . . .	169
	Electron Cyclotron Emission of the plasma . . . . .	169
5.3.3	Maximizing the return signal . . . . .	172
5.4	Absolute Bypass Loop Calibration . . . . .	172
5.4.1	Setting of the bypass loop switches . . . . .	173
5.4.2	Uses of the bypass loop data . . . . .	174
5.5	Absolute Waveguide Run Calibration . . . . .	179
5.5.1	Reflectometer initial settings . . . . .	179
5.5.2	Absolute waveguide run calibration using metal reflector . . . . .	180
5.5.3	Translation of reference plane . . . . .	181
5.5.4	Initial calibration of the reflectometer . . . . .	183
5.6	Summary . . . . .	184

<b>VI.</b>	<b>Simulation Software</b>	<b>186</b>
6.1	Introduction . . . . .	186
6.2	Theory for Profile Reconstruction . . . . .	187
6.2.1	Profile reconstruction based on Doyle's method . . . . .	191
6.2.2	The parabolic method . . . . .	196
	Parabolic fit . . . . .	196
	Parabolic fit with non-equal step size . . . . .	197
	Simplifying the non-equal step size . . . . .	199
	Parabolic fit with the derivative condition . . . . .	200
6.2.3	Error on the parabolic method . . . . .	201
	Error in the parabolic fits . . . . .	202
	Error in the increment on the cutoff position . . . . .	204
	Error in the density using the parabolic method . . . . .	207
6.2.4	Limits of the parabolic method . . . . .	212
	Limit of equal step size . . . . .	212
	Limit of small step size . . . . .	215
6.2.5	An accurate (density expansion) method . . . . .	216
6.3	Program . . . . .	221
6.3.1	Density and phase models . . . . .	221
6.3.2	Frequency vs cutoff position mapping . . . . .	227
6.3.3	Integrals calculation . . . . .	228
6.3.4	Cubic integrals error . . . . .	231
6.4	Modeling Results . . . . .	232
6.4.1	Phase difference dynamic range . . . . .	234
6.4.2	Effect of the density shape . . . . .	234
	Central density slope . . . . .	236
	Effect of the density edge shape . . . . .	237

	Effect of the central density . . . . .	239
6.4.3	Effect of the edge position . . . . .	239
6.4.4	Effect of fluctuations . . . . .	242
6.4.5	Modeling the smoothing . . . . .	249
6.4.6	Frequency range . . . . .	251
6.4.7	Analytical limits on the phase difference . . . . .	253
6.4.8	Effect of the frequency separation . . . . .	256
6.5	Sensitivity and Error Analysis . . . . .	262
6.5.1	Systematic errors in absolute phase calibration . . . . .	262
6.5.2	Effect of the magnetic field error . . . . .	263
6.5.3	Conclusion on sensitivity/error analysis . . . . .	263
6.6	Benchmarking: Comparison With Hanson's Code . . . . .	268
6.6.1	Differences on the reconstruction technique . . . . .	268
6.6.2	Differences in integration techniques . . . . .	270
6.6.3	Effect of the choice of the cutoff . . . . .	271
6.6.4	Density model before the first cutoff . . . . .	271
6.6.5	Magnetic field model . . . . .	272
6.7	Benchmarking: Comparison Using the $B_0 = 0$ Case . . . . .	272
6.8	Summary . . . . .	278
<b>VII.</b>	<b>Data Analysis Software</b>	<b>281</b>
7.1	Introduction . . . . .	281
7.2	Data Reduction and Phase Extraction . . . . .	284
7.2.1	Data description . . . . .	284
7.2.2	Processing the data . . . . .	285
7.3	Density Profile Reconstruction Program . . . . .	291
7.3.1	Description of the density reconstruction program . . . . .	291
7.3.2	Benchmarking the program . . . . .	296

7.4	Errors . . . . .	298
7.4.1	Random errors (error bars) . . . . .	298
	Random error formula . . . . .	300
	Radial position error formula . . . . .	301
	Phase error formula . . . . .	301
	Calculated phase random error . . . . .	303
7.4.2	Systematic errors . . . . .	309
	Systematic error sources . . . . .	311
	Position of the reference plane error . . . . .	313
	First cutoff position systematic error . . . . .	314
	Magnetic field error formula . . . . .	315
	Practical approach to systematic error . . . . .	316
7.5	Summary . . . . .	319
<b>VIII.</b>	<b>Experimental Data and Interpretation</b>	<b>320</b>
8.1	Introduction . . . . .	320
8.2	Results of Phase I . . . . .	320
8.2.1	Different field strength operation . . . . .	321
	Operation at 3.3 Tesla . . . . .	321
	Operation at 3.7 Tesla . . . . .	322
	Operation at 4.5 Tesla . . . . .	322
	Operation at 4.8 Tesla . . . . .	326
8.2.2	Plasma radial scan . . . . .	328
8.2.3	Central density scan . . . . .	333
8.2.4	Effect of the ICRH . . . . .	333
8.2.5	Conclusions of phase I . . . . .	339
8.3	Results of Phase II . . . . .	340
8.3.1	Initial data . . . . .	340



8.3.2	Effect of the ICRH on the plasma edge . . . . .	341
8.3.3	Conclusions of phase II . . . . .	347
8.4	Summary . . . . .	347
<b>IX.</b>	<b>Summary</b>	<b>349</b>
9.1	Discussion . . . . .	349
9.2	Important Results and Accomplishment . . . . .	352
9.3	Suggestions for Future Work . . . . .	354
<b>A.</b>	<b>Gaussian Beam Optics</b>	<b>356</b>
A.1	Introduction . . . . .	356
A.2	Pre-History of Lasers . . . . .	358
A.3	Paraxial Ray Analysis . . . . .	358
A.3.1	Ray transfer matrix . . . . .	359
A.3.2	Periodic sequences . . . . .	362
A.4	Wave Analysis of Laser Beams . . . . .	363
A.4.1	Solution to the beam's wave equation . . . . .	364
A.4.2	Propagation law for the fundamental mode . . . . .	365
<b>APPENDIX</b>		
<b>B.</b>	<b>Simulation Program</b>	<b>369</b>
B.1	Introduction . . . . .	369
B.2	Description . . . . .	369
B.2.1	Code description . . . . .	369
B.2.2	Code graphic subroutines . . . . .	370
B.2.3	Data file . . . . .	372
B.2.4	Subroutine/Functions description . . . . .	375
	Function MU2 . . . . .	378

Function SN . . . . .	378
Function SNREC . . . . .	379
Function MU2REC . . . . .	379
Function RZERO . . . . .	379
Function REZERO . . . . .	380
Function DENSITY . . . . .	380
Function BFIELD . . . . .	380
B.3 Computer Code . . . . .	381
<b>C. Data Analysis Program</b>	<b>459</b>
C.1 Introduction . . . . .	459
C.2 Reflectometer Data Files . . . . .	459
C.3 Description . . . . .	461
C.3.1 Generation of the phase data files . . . . .	461
C.3.2 Subroutine/Function description . . . . .	462
Graphic package . . . . .	462
Subroutine YO_INFO . . . . .	462
Subroutine YO_DATA . . . . .	463
Subroutine CONVERT . . . . .	463
Subroutine GET_INDEX . . . . .	463
Subroutine COMPRES . . . . .	463
Subroutine SMOOTH . . . . .	464
Subroutine DAT_AVE . . . . .	465
Subroutine YO_PHASE . . . . .	465
Subroutine IQ_AVE . . . . .	465
Subroutine PH_SIGMA . . . . .	465
Subroutine MATCH_TO_AVE . . . . .	466
C.4 Computer Code . . . . .	466

<b>D.</b>	<b>Density Reconstruction Program</b>	<b>534</b>
D.1	Introduction . . . . .	534
D.2	Description . . . . .	534
D.3	Computer Code . . . . .	535
<b>E.</b>	<b>Call Numbers for the Bibliography</b>	<b>563</b>
	<b>BIBLIOGRAPHY</b>	<b>565</b>
	<b>Vita</b>	

## List of Tables

1.1	Key plasma parameters: achieved and required. . . . .	6
1.2	Some fusion experiments and their corresponding locations. . . .	9
1.3	Some stellarators and their corresponding parameters. (FRG is Federal Republic of Germany) . . . . .	12
1.4	Some of ATF major parameters. . . . .	12
1.5	Some major parameters of TFTR. . . . .	14
1.6	Some of TFTR diagnostics. . . . .	15
3.1	Radio frequency (rf) experiments list. . . . .	103
3.2	TFTR antenna design parameters. . . . .	104
4.1	Some of the digitizer major parameters. . . . .	116
4.2	Some of the reflectometer system major components. . . . .	122
4.3	Some of the DROs main specifications. . . . .	130
4.4	Some of the doubler main specifications. . . . .	134
4.5	Some of the tripler main specifications. . . . .	135
4.6	Some of the amplifier main specifications. . . . .	135
4.7	Some of the constant phase limiting amplitude amplifier main specifications. . . . .	136
4.8	Common specifications of an I & Q phase detector. . . . .	143

4.9	Frequencies and related amplitudes of the Square-Law output of a detected AM signal. . . . .	147
4.10	Main parameters of the filters. . . . .	154
4.11	Main parameters of the equalizer. . . . .	155
5.1	Table of the pull down menu options for the YOMENU program. . . . .	165
5.2	Table showing the drift/change in frequency of the DROs. . . . .	165
5.3	Table showing the drift/change in frequency of the DROs. . . . .	179
5.4	Table showing the drift/change in frequency of the source. . . . .	180
5.5	Table showing the waveguide losses for the fluctuation reflectometer waveguide system. . . . .	181
7.1	A short description of the data analysis and reconstruction programs. . . . .	282
A.1	Ray transfer matrices of six elementary structures. ©1966 IEEE . . . . .	361
B.1	List of the different types of plots that the simulation program can do and its importance. . . . .	371
B.2	List of the plotting code for the AG2 plotting subroutines. . . . .	377
B.3	List of the function names of the modeling code and a short description of their purpose. . . . .	377

## List of Figures

1.1	Fusion reactivity as a function of ion temperature. . . . .	4
1.2	Artist's conception of a fusion reaction. . . . .	5
1.3	Schematics of the closed toroidal confinement concepts and a tokamak schematic. . . . .	11
1.4	An artist's sketch of ATF's vacuum chamber and magnetic field coil system. . . . .	13
2.1	CMA diagram (Swanson) with all boundaries and the wave normal surfaces. . . . .	30
2.2	Plot of the different frequencies for a plasma with a density profile of the type $n_e(r) \propto \left(1 - \left(\frac{r}{a}\right)^\alpha\right)^\beta$ and with a magnetic field (in Teslas) of the form $B(R) \propto \frac{1}{R}$ , where $r$ is the minor radius, $a$ is the plasma edge minor radius and $R$ is the major radius. DENS0 is the center density. . . . .	33
2.3	Generic diagram for an AM reflectometer system. . . . .	49
2.4	Schematics for PBX-M AM reflectometer system. . . . .	50
2.5	Basic schematic of a reflectometer. . . . .	54
2.6	Typical cutoff and resonance frequencies on JT-1. . . . .	65
2.7	Reflection and transmission coefficients for a typical TFTR plasma (upper plot). The assumed density profile is included (lower plot) and it is of the form $n_e \propto \left(1 - \left(\frac{r}{a}\right)^\alpha\right)^\beta$ where all the parameters have been defined before. . . . .	69

2.8	Density profile for a typical TFTR plasma and corresponding radial spacing for the probing side bands. . . . .	76
2.9	Relativistic effect on the index of refraction and the location of the cutoff using the weakly relativistic model. $\mu_r$ is the refractive index and $T_e \approx 10$ KeV for plots <i>a</i> to <i>e</i> . . . . .	78
2.10	Comparison of the actual and reconstructed density profile using the weakly relativistic model. . . . .	80
3.1	Typical parabolic density profiles of the form: $\left(1 - \left(\frac{r}{a}\right)^2\right)^\alpha$ and antenna loading vs the profile shape exponent, $\alpha$ , and the scrapeoff decay length, $\lambda$ . (Batchelor, et al., Fusion Tech., Vol. 21 (1992) p. 1214) . . . . .	89
3.2	Loop antenna and circuit representation of both, the short and long loop versions. . . . .	98
3.3	Long loop antenna used in Alcator-C. . . . .	99
3.4	Typical cavity antenna and its equivalent circuit. . . . .	100
3.5	Resonant Double Loop antenna and its equivalent circuit. The symmetric version has $\alpha = 0.5$ . . . . .	101
3.6	The U-slot antenna, as proposed by McDonnell Douglas Astronautics Company and its equivalent circuit. . . . .	102
3.7	TFTR antenna layout. . . . .	105
3.8	TFTR antenna cavity box. Most of the Faraday screen elements have been removed to show the current strap housing and the straps relative size. . . . .	106

4.1	TFTR plasmas showing the density profile (Thomson Scattering at $t = 4.1$ seconds) and magnetic field (time history) range for shot 67024. . . . .	112
4.2	TFTR plasmas showing the density profile (Thomson Scattering at $t = 3.5$ seconds) and magnetic field (history) range for shot 67877. . . . .	113
4.3	TFTR fluctuation reflectometer waveguide to vessel interface. . . . .	116
4.4	Side view layout of the reflectometer for the second phase of the project. Dimension are in inches. . . . .	117
4.5	Front view of the ICRH antenna rf box showing the launcher position (center) with respect to the ICRH antenna. The launcher is tilted at the same angle as the Faraday Shield screen elements. . . . .	118
4.6	Radiation pattern of the launcher in two orthogonal planes, parallel ( $\phi = 0$ ) and perpendicular ( $\phi = 90$ ) to the widest dimension of the waveguide. The $x$ -axis is the pattern angle, $\theta$ , and the $y$ -axis is the beam relative amplitude in decibels (dB). . . . .	119
4.7	Calculated TFTR's reflectometer launcher Gaussian pattern (unfolded). . . . .	120
4.8	Reflectometer system design schematic. The receiver mixer is a 3 <sup>rd</sup> harmonic mixer, which allow us to spare of a tripler in the design and construction. . . . .	123
4.9	Plots of the dispersion relations ( $\omega = \omega(\beta)$ ) for a forward wave (a) and a backward wave (b), where $\omega$ is the frequency and $\beta$ is the wave-number. . . . .	126
4.10	Backward wave amplifier schematic. . . . .	127
4.11	The $TE_{01}$ mode used in cylindrical dielectric resonators, with the electric, E, and the magnetic, H, fields lines. . . . .	129



4.12 Basic operation of a two hole directional coupler. . . . .	132
4.13 Basic microstrip or stripline power divider. . . . .	133
4.14 Frequency doubler package outline. . . . .	134
4.15 Frequency tripler package outline. . . . .	136
4.16 Basic schematic of an I & Q Network. . . . .	138
4.17 Geometry of a 3 dB 90° hybrid coupler. $Z_0$ is the impedance of the connection and $\lambda$ is the wavelength of the wave. . . . .	138
4.18 The Phase Comparator. . . . .	141
4.19 Package outline of the quadrature phase detector. . . . .	142
4.20 Basic operations of rectification, detection, and mixing of a signal. (a) Diode acting as a rectifier. (b) Diode acting as a modulated signal detector. (c) Mixer. . . . .	144
4.21 $V-I$ characteristic curve of a diode. . . . .	145
4.22 Output spectrum of a detected Amplitude Modulated (AM) signal. . . . .	148
4.23 Square-law region for a typical diode detector. . . . .	149
4.24 Frequency conversion of a mixer in a receiver and transmitter ap- plication. (a) Down-conversion in a heterodyne receive. (b) Up- conversion in a transmitter. . . . .	151
4.25 Single-ended mixer circuit. . . . .	152
4.26 Calculated TFTR's Gaussian beam geometry and intersection in- side the vacuum chamber. . . . .	156
4.27 Reflectometer system power budget diagram. . . . .	158

5.1	Plot of the family of lines of the cutoff frequencies as a function of density and radial position. Three density curves with their corresponding cutoff frequency and cutoff position are shown. ( $B_0 = 4.5$ Teslas) . . . . .	163
5.2	Sweeper voltage signal to the Backward Wave Oscillator. The sweeping time and the reset time of the Backward Wave Oscillator can be calculated from this plot. . . . .	166
5.3	Bypass calibration loop data with no magnetic field. (A) Plot of the amplitude of the signal. (B) Plot of the phase difference data. (Attenuation setting was 30 dB.) . . . . .	170
5.4	Bypass calibration loop data for a plasma with a magnetic field of 3.2 Tesla. (A) Plot of the amplitude of the signal. (B) Plot of the phase difference data. (Attenuation setting was 30 dB.) . . . . .	171
5.5	Waveguide switches and calibration loop setup for the reflectometer system. Components and/or symbols are not to scale. . . . .	175
5.6	Reflectometer phase data for the bypass test loop (attenuator set to 30 db). The upper plot is the signal amplitude and the lower plot is the calculated phase difference data. . . . .	176
5.7	Reflectometer phase data of the bypass loop for two different days with no change on the calibration phase data (attenuator set to 30 dB). The upper plot is the calculated phase difference data for the two plasma shot numbers in the figure and the lower plot is the difference between the two data sets. . . . .	177

5.8	Reflectometer phase data of the bypass loop for two different days with a 0.05 of a fringe change on the data (attenuator set to 30 dB). The upper plot is the phase difference data and the lower curve is the difference between the data sets. . . . .	178
5.9	Phase difference data for one of the first bypass loop calibration data shots taken with the reflectometer system. Comparison with other calibration data sets show a good similarity between the data sets. (Attenuation setting was 40 dB.) . . . . .	185
6.1	Curves of the index of refraction for the upper and lower probing frequencies. . . . .	188
6.2	Graphical representation of the trapezoidal rule used by Doyle (solid straight diagonal line) to calculate the increment on the radial position and the parabolic method (dash line). The refractive index (dot-dash line) is plotted as a function of the position for the upper frequencies. The error of the technique is the difference in the zero crossing of the curves. . . . .	192
6.3	Examples of the index of refraction as a function of the minor radius for an assumed density profile. The upper plot is the assumed density profile ( $n_e = 3.5 \times 10^{19} \left(1 - \left(\frac{r}{a}\right)^\alpha\right)^\beta$ ) ( $\alpha = 6$ and $\beta = 2$ ). The lower plot is the calculated index of refraction for the frequencies of 117, 110, 100, and 93 GHz (from most left to most right curve respectively). . . . .	193
6.4	Plot of the maximum fractional error as a function of the frequency separation of the probing beams. This is typical for all the parabolic methods presented here. . . . .	211

6.5	Plot of the density profiles and the percent error (dot-dash curve) between the reconstructed and assumed profiles when using the parabolic method with the derivative condition. . . . .	213
6.6	Reconstructed density profile using a real index of refraction fit near the cutoff to calculate the increments between cutoffs and the density profile. Both the real assumed density and the reconstructed density profile are shown. The percent error due to this method is shown on the right hand side axis for the increment in cutoff and for the calculated density on the left hand side axis. Step size is of the order of $10^{-6}$ m. . . . .	218
6.7	Plot of the error as a function of the step size for the new density expansion method. For this plot, the code was run five times with five different increments on the step size. Then the error of the first 9 points of the profile from every run where used as data. . . . .	222
6.8	Flow chart of the modeling program. . . . .	225
6.9	Typical plotting output for the simulation or modeling code. (A) Plot of the phase difference data calculated from the assumed density profile. Negative frequencies in plot (A) are used to force the plotting routine to write numbers from right to left, thus providing a mapping between the frequency and radial axis. Real frequencies are actually positive. (B) Plot of the assumed density profile (in dash line) and the corresponding reconstructed density profile (solid line) calculated using the phase difference data from plot (A). . . . .	226
6.10	Cutoff frequency of the propagating wave vs its cutoff radial position (major radius). . . . .	229

6.11	(A) Plot of the phase difference dynamic range for a plasma density of the $\alpha$ - $\beta$ form with $\alpha = 6$ and $\beta = 2$ . (B) Plot of the assumed density profile used to calculate the phase data and the reconstructed density using the phase difference data. . . . .	235
6.12	Effect of the slope at the center of the density profile on the phase difference data and the reconstructed density profile. (A) The phase difference data calculated from the assumed density profile. (B) The assumed density profile and the reconstructed density profile. . .	238
6.13	Effect of the shape of the density edge on the phase difference data and the reconstructed density profile. (A) Calculated phase difference for different plasma edge slopes. (B) Assumed density profile used to calculate the phase difference data over-plotted with the corresponding reconstructed density profile. . . . .	240
6.14	Effect of the different central density values on the phase difference and the reconstructed profile. Notice how the phase data at the higher part of the frequency band (corresponding to the center area of the profile) increases as the scanned part of the profile becomes flatter. (A) Calculated phase difference for different central maximum densities. (B) Assumed density profiles and corresponding reconstructed density profiles. . . . .	241
6.15	Plots showing the effect of the change in the plasma edge position on the phase data and the reconstructed density profile. (A) Calculated phase difference data for different density displacements. (B) Assumed density profile (hyperbolic tangent) and reconstructed density profile from the phase difference data. . . . .	243

6.16 (A) The calculated phase difference data for a density profile with a periodic density perturbation with a wavelength of $\lambda = 1$ cm. (B) The assumed density profile used to calculate the phase difference data and the resulting reconstructed density profile calculated from the phase data. . . . .	245
6.17 (A) Calculated phase difference data for a density profile with a periodic density perturbation with a wavelength of $\lambda = 5$ cm. (B) Assumed density profile and reconstructed density profile. . . . .	246
6.18 (A) Calculated phase difference data for a density profile with a periodic density perturbation with a wavelength of $\lambda = 10$ cm. (B) Assumed density profile and reconstructed density profile. . .	247
6.19 (A) Plot of the calculated phase difference data for an assumed density profile including density fluctuations ( $\approx 25\%$ rms) with a typical spatial wave-number spectrum. (B) Plot of the assumed and reconstructed density profile for the above phase difference data. .	250
6.20 (A) Plot of the phase difference data after the smoothing or averaging. (B) Plot of the assumed and reconstructed density profile for the phase difference data after the smoothing. . . . .	252
6.21 The upper plot is a contour plot of the cutoff layers for an assumed typical TFTR plasma density profile. The profile assumed is of the $\alpha$ - $\beta$ type defined previously and with $B_0 = 4.5$ Tesla. The lower plot shows the assumed density profile at the horizontal midplane.	254
6.22 Plots showing the limiting value of the phase difference data to be $\approx 6$ as the density profile goes to 0. (A) Phase difference data calculated from the assumed density profile. (B) Assumed density profile and reconstructed density profile. . . . .	257

6.23	Plot of the radial separation of the cutoffs and the phase difference data for a typical TFTR plasma density profile. Frequency separation is $\Delta\omega = 0.25$ GHz. (A) Plot of the phase difference data dynamic range. (B) Plot of the cutoffs separation as a function of the radial position. . . . .	260
6.24	Radial separation of the cutoffs and the phase difference data for a typical TFTR plasma density profile. Frequency separation is $\Delta\omega = 0.125$ GHz. (A) Plot of the phase difference data. (B) Plot of the cutoff separation as a function of the radial position. . . . .	261
6.25	Effect of the constant offset function $(-0.25, 0, +0.25)$ on the reconstructed density profile. The important feature here is that as the phase offset decreases the profile becomes steeper and as the phase offset increases the profile becomes flatter. (A) Plot of the phase difference data and the associated phase offset added to the phase data. (B) Plot of the assumed density profile and the reconstructed density profile using the phase data above. . . . .	264
6.26	Effect of the slope of the offset function (with intersection at 120 GHz) on the reconstructed density profile. (A) Plot of the family of curves for the phase difference and the associated offset functions. (B) Plot of the assumed density profile and the reconstructed density profile for the corresponding phase difference data in plot (A). . . . .	265
6.27	Effect of the slope of the offset function (with intersection at 90 GHz) on the reconstructed density profile. (A) Plot of the family of curves for the phase difference data and their corresponding offset functions. (B) Plot of the assumed density profile and the reconstructed density profile for the associated phase difference data. . . . .	266

6.28	Effect of the uncertainty of the magnetic field on the reconstructed density profile. (A) Plot of the phase difference curves calculated with an error on the magnetic field of -1%, 0%, and 1% (corresponding to curves 1, 2, and 3 respectively). (B) Plot of the assumed density profile and the reconstructed density profile for the phase difference data calculated with the error on the magnetic field. . .	267
6.29	Plot of the difference between the calculated density profile from author's program and the one provided by Hanson. The two curves seem to blend together. The difference between the density points is shown by the x-axis. . . . .	269
6.30	Plot of the density profiles for the author's technique and Hanson's technique. The error is shown in the lower curve by the x-axis. The exponential model is used by both codes in this plot. . . . .	273
6.31	Plot of the density profiles for the author's technique and Hanson's technique using an exponential profile for the edge. A shift of the position of the first cutoff in the author's profile provides a much better fit at the steep part of the profile as compared with the previous plot. . . . .	274
6.32	Plots of (A) the phase difference data and (B) the assumed and reconstructed density profiles for the case of $B_0 = 0$ . . . . .	276
6.33	Plot of the Abel inversion density profile using the phase data from the previous figure, the reconstructed profile using the author's technique, and the assumed profile for comparison and verification. The match between curves makes it difficult to distinguish between them. The percent error is the difference between the reconstructed and Abel inverted profiles. . . . .	277



7.1	Flow chart of the analysis and phase extraction program. . . . .	283
7.2	Raw data for the $I$ ( $= \sin \Delta\phi$ , $\times$ points) and $Q$ ( $= \cos \Delta\phi$ , $\circ$ points) signals and the corresponding calculated raw phase data for the signal. No smoothing is in effect for this data set. . . . .	288
7.3	The same raw data as before, but using smoothing (10 points) and averaging (10 sweeps) on the signal data. . . . .	289
7.4	Reconstructed density profile (labeled "REFL." in the legend of the plot) for a good choice on the position of the first cutoff and the initial offset phase. Match to the Thomson Scattering (TS) data is acceptable. . . . .	292
7.5	Reconstructed density profile for a different choice of the position of the first cutoff. . . . .	293
7.6	Reconstructed density profile for a different choice of the initial offset phase. . . . .	294
7.7	Flow chart for the density reconstruction program. . . . .	295
7.8	Plot of the density profile from the modeling code and the density profile of the reconstructing code. The difference between the curves is shown along the right hand side $y$ -axis of the plot. Agreement between the curves is acceptable. . . . .	299
7.9	Plot of the average phase (solid line) for a set of data points (scattered points), and the standard deviation. . . . .	304
7.10	Plot of the average phase and the standard deviation where a 16 sweep average was done to the data. . . . .	306
7.11	Plot of the reconstructed density profile with the corresponding error bars. The error bars in most cases are of the order of the thickness of the lines and are some what hard to see in the plots. . . .	310

7.12	Plots of (A) the phase difference data with a $\pm 0.21$ fringes of systematic error, and (B) the corresponding reconstructed density profiles with a shift in the position of the first cutoff corresponding to an error of $\pm 5$ cm. This is 5 times the expected systematic error. . .	318
8.1	Plots of (A) the phase difference data and (B) the corresponding reconstructed density profiles for a plasma with sawtooth oscillations. The MIRI data points used the $\times$ symbol as noted in the legend of the figure. . . . .	323
8.2	(A) Phase data and (B) corresponding reconstructed density profile for a low density plasma and small minor radius at a toroidal field current of 55 Kamps ( $B_0 = 3.7$ Tesla). . . . .	324
8.3	Plots of the toroidal field current (upper plot) and the minor radius (lower plot) for plasma shot 67875. . . . .	325
8.4	(A) Phase data for a typical 67 Kamps ( $B_0 = 4.5$ Tesla) shot, with (B) the corresponding reconstructed density profile. . . . .	327
8.5	Contour plot of the reflection layers for a high magnetic field modeled plasma and the center plane line density. Magnetic field is $B_0 \approx 4.8$ Tesla and the profile model is the typical $n_e \propto \left(1 - \left(\frac{r}{a}\right)^\alpha\right)^\beta$ profile, where $\alpha = 6$ and $\beta = 2$ . . . . .	329
8.6	Signal level for a high magnetic field plasma ( $B_0 \approx 4.8$ Tesla). Notice how the signal level increases rapidly just before 100 GHz. . .	330
8.7	(A) Phase difference data and (B) corresponding reconstructed density profile for a plasma with a toroidal field current of $I_{tj} = 72$ Kamps ( $B_0 = 4.8$ Tesla) shown before. . . . .	331

8.8	(A) Phase difference data and (B) corresponding reconstructed density profile for $R_{edge} = 3.30, 3.40, 3.50$ , and $3.55$ m (corresponding to curves 1, 2, 3, and 4 respectively). . . . .	332
8.9	(A) Phase data and (B) corresponding reconstructed density profiles for a plasma with central density of $\approx 2.0, 4.0, 4.5$ , and $6.0 \times 10^{19} \text{ part/m}^3$ . NBI power is $P_{NBI} \approx 0, 12, 22$ , and $27$ MegaWatts (corresponding to curves 1, 2, 3, and 4 respectively). . . . .	334
8.10	Plot of the phase difference during an ICRH modulation. The curves have been separated by adding a constant offset of $0.2$ fringes in order to distinguish them. . . . .	336
8.11	Plot of the reconstructed density profile using the phase data in the previous figure. Curves have been separated by adding a constant offset of $0.2 \times 10^{19} \frac{\text{particles}}{\text{m}^3}$ in order to show the different curves and show any changes in the profiles. As the legend shows, the solid line is the difference between the two curves. . . . .	337
8.12	Plot of the ICRH power deposition on the plasma for the time interval of the reflectometer. . . . .	338
8.13	Plots of the plasma major and minor radius for the time interval of the jog. . . . .	342
8.14	(A) Phase data and (B) reconstructed density profile for the time interval of the plasma jog. Data times are before ( $3.498$ sec, curve 2), during ( $3.548$ sec, curve 1), and after ( $3.598$ sec, curve 3). It can be seen that the before (curve 2) and after (curve 3) data are not too different. . . . .	343

8.15	Plot of (A) the phase difference data and (B) the corresponding reconstructed density profile for a plasma with a magnetic field of $B_0 = 4.5$ Tesla and a central density of $n_{e0} = 5.0 \times 10^{19} \frac{\text{part}}{\text{m}^3}$ during and after the ICRH. . . . .	345
8.16	Same plot as Figure 8.15, but the lower end of the frequency band and the corresponding far edge of the reconstructed density profile have been enlarge to show the effect of the ICRH on both the phase difference data and the density profile. . . . .	346
A.1	Calculated TFTR's beam geometry and intersection inside the vacuum chamber. . . . .	357
A.2	Optical system diagram and parameters. An arbitrary ray and its corresponding parameters are also shown. ©1966 IEEE . . . . .	360
A.3	Diagram of an infinite sequence of systems (lenses) each characterized by an equal ray transfer matrix. ©1966 IEEE . . . . .	363
B.1	"NAMELIST" data file used to initialize the parameters for the modeling program. . . . .	376

## Summary

This thesis presents a description of reflectometry with particular attention to eXtraordinary mode (X-mode) reflectometry using the novel technique of dual frequency differential phase, and the results obtained using this novel technique of dual frequency phase difference reflectometry. For this purpose a dual frequency phase difference reflectometer was designed and constructed at the Oak Ridge National Laboratory (ORNL), and later tested at the Toroidal Fusion Test Reactor (TFTR) at the Princeton Plasma Physics Laboratory (PPPL). The advantage of using an X-mode wave is that it can probe the edge of the plasma with significantly higher resolution and using a much smaller frequency range than with the Ordinary mode (O-mode). Other technical advantages include better focusing properties (or smaller launchers), its shorter skin depth, and its accessibility to a larger region of the plasma for a given frequency range. The general problem with previous full phase reflectometry techniques has to do with keeping track of the phase (on the order of 1000 fringes) as the frequency is swept over the band. The dual frequency phase difference technique has the advantage that since it keeps track of the phase difference of two frequencies with a constant frequency separation, then the fringe counting was on the order of only 3 to 6 fringes. This fringe count, combined with the high resolution of the X-mode wave and the small plasma access requirements of reflectometry, make X-mode reflectometry a very attractive diagnostic for today's experiments and future fusion devices.

The reason for building this new reflectometer was to be able to make measurements of the induced changes on the edge density profile in front of the ICRF antenna during the ICRF high power heating experiments. The edge of

the plasma is where the density fluctuations are the largest, thus, measurement of these changes on the plasma edge with other conventional reflectometers is rather hard or impossible, because of the multiple value nature of the reflectometer's phase data and the fringe skips due to the fluctuations.

At the beginning of this project, the ORNL group (including but not only: Drs. John Wilgen, Tim Bigelow, Greg Hanson, etc ...) was given the task to design, construct, test, install, collect and analyze the data for an edge density profile reflectometer on TFTR for the purpose of measuring and help to understand the edge density changes induced by the ICRH power deposition on the plasma. My role as the Graduate Research Assistant (GRA) of the team was to assist in all parts and stages of the project as much as possible. During the beginnings of the project, I had the opportunity to contribute on the initial concept development, component, and schematic design. As the concept and idea became well defined the opportunity to develop a computer model of the reflectometer data was given to me. This modeling code provided many interesting results before the reflectometer was built (as explained in the corresponding chapters of the thesis), of which the most important was the reduction of the phase fluctuation due to density fluctuations and the reduction of the phase dynamic range to the order of  $\approx 6$  fringes. This modeling code provided a test bench for the reconstruction technique as well. Testing of the reflectometer and its components was done at the microwave laboratory under the supervision of Drs. John Wilgen, Tim Bigelow and Greg Hanson. After the successful construction and testing of the reflectometer, it was moved and installed on TFTR at the Princeton Plasma Physics Laboratory. Calibration data was taken during the test phase of the reflectometer. Once the reflectometer was installed and data collected, I was given the opportunity to write computer codes to read, process, analyze, extract the phase data and reconstruct the corresponding density profile.

# CHAPTER I

## INTRODUCTION

With the recent war in the Persian Gulf the need to reduce our dependance on foreign oil has become strikingly evident. In an attempt to reduce and/or eliminate this dependance the need for new long term energy sources has become obvious. With its almost inexhaustible resources, nuclear fusion has the potential to satisfy our constantly increasing need for inexpensive and clean energy. To reach the goal of nuclear fusion a full understanding of the plasma and transport phenomena must come first. For this purpose the understanding of the main plasma parameters (such as density, temperature, transport coefficients, etc.) is essential.

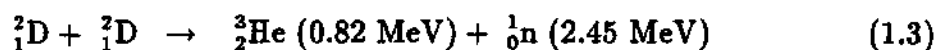
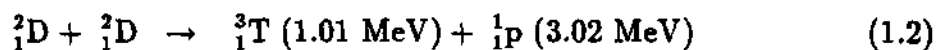
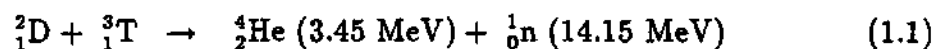
In this thesis the principles of reflectometry as a diagnostic tool will be discussed. A novel technique using two wave frequencies with a constant  $\delta\omega$  will be discussed, and its potential use for probing the plasma and extracting density profiles under different configurations and plasma conditions will be examined.

This chapter will present an introduction to fusion, reflectometry and a description of the major parameters of the Tokamak Fusion Test Reactor (TFTR) at the Princeton Plasma Physics Laboratory in Princeton, New Jersey.

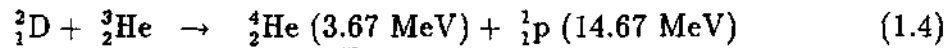
## 1.1 Fusion

As far as is known, fusion is the primary source of energy in the universe. Nuclear fusion is the process in which two light nuclei (the parents) join together to form a new nucleus (daughter or products) of bigger mass than the individual parent nuclei, but with nuclear mass slightly smaller (for exothermic reactions) than the combined mass of the parents. The mass difference is transformed into kinetic energy<sup>1</sup> (since mass is energy, as proved by Einstein with his famous formula  $E = mc^2$ ) and distributed among the daughters of the fusion reaction. Fusion reactions in which energy is released (exothermic reactions) can occur between elements that are below iron (Fe) in the periodic table. Fusion of elements heavier than Fe is generally endothermic. This is because Fe has the lowest energy per nucleon in the periodic Table.<sup>2</sup> This explains why fission of heavy elements such as  $^{235}\text{U}$  is exothermic.

Hydrogen is the most abundant element in the universe. This and other characteristics (such as reactivity, energy released per reaction, etc.) make it an excellent fuel source for a fusion reactor. To accomplish fusion, the positively charged nuclei must overcome the Coulomb repulsive electrostatic force and get close enough so that the attractive nuclear forces can take action and fuse the nuclei permanently together. From the hydrogen family the two best candidates for fusion fuel are *Deuterium* ( $^2_1\text{D}$ ) and *Tritium* ( $^3_1\text{T}$ ), mainly because of their high fusion reactivity at low temperature when compared with other elements, as can be seen from Figure 1.1.<sup>1</sup> The fusion reactions of most interest using hydrogen isotopes are:<sup>3</sup>







and the approach for equation 1.1 is shown in Figure 1.2.

A secondary advantage of the Deuterium-Tritium reaction (or D-T reaction) is that about 20% of the energy goes to the Helium (He) ion which can be confined in the plasma and helps to heat the plasma. The remaining 80% of the energy goes to the neutron, which has no net charge, so it leaves the plasma and deposits its energy in the vacuum vessel and/or neutron blanket. The energy deposited in the blanket can be used to make steam and drive a standard steam power plant. To sustain the D-T reaction, the plasma and energy necessary for the reaction must be contained in the vacuum vessel for a reasonable length of time. Some key plasma parameters for the achieved and required values are shown in Table 1.1.<sup>3</sup> To this day, anomalous transport, short energy confinement times, and some engineering difficulties have prevented us from developing fusion to its full potential. The goal of the fusion program is to overcome all these problems and develop a commercially attractive fusion reactor.

## 1.2 Reflectometry

Reflectometry is a technique developed during the 1960s and works on the same principle as the *RADAR* (RADio Detection And Ranging). That is, it measures the distance (position) between a transmitter (source) and a target (plasma) using the delay time (phase difference) between the incident and reflected wave.<sup>5-8</sup>

Reflectometry is a technique that relies on the total reflection of an electromagnetic microwave signal to obtain information about the density profile and the density fluctuations of the plasma. This reflection occurs when the local index

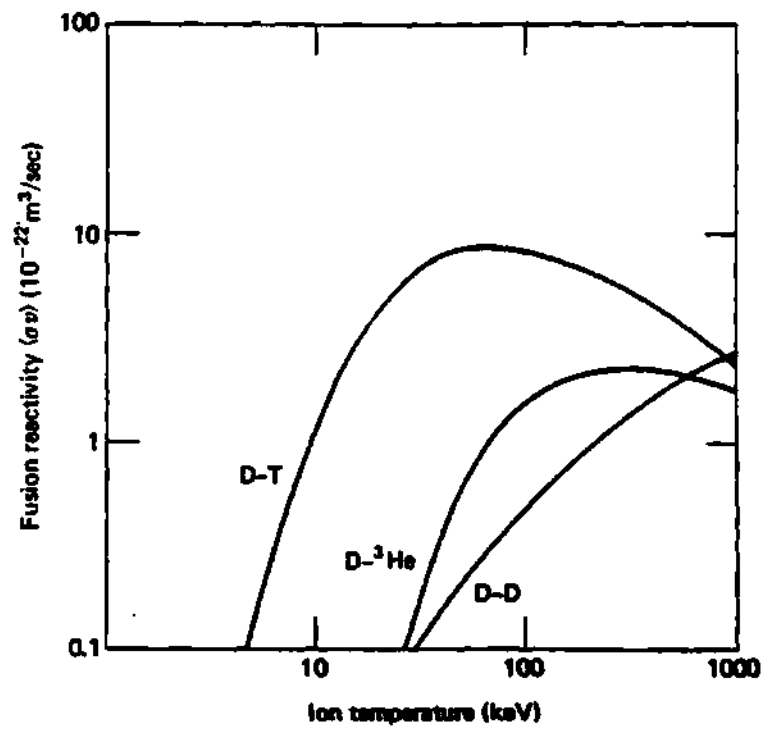


Figure 1.1: Fusion reactivity as a function of ion temperature.

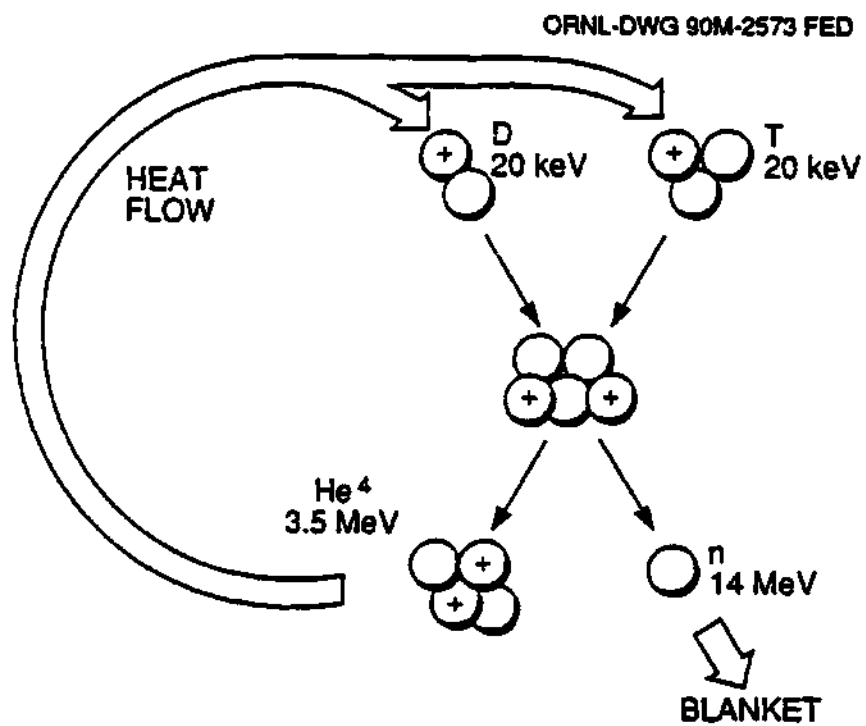


Figure 1.2: Artist's conception of a fusion reaction.

Table 1.1: Key plasma parameters: achieved and required.

Parameter	1971	1981	1991	Steady State
Central ion temp. $T_{i0}$ (KeV)	0.5	7.0	35	30
Central electron temp. $T_{e0}$ (KeV)	1.5	3.5	15	30
Energy confinement time $\tau_E$ (sec)	0.007	0.02	1.4	3.0
Triple product $n_{i0}T_{i0}\tau_E$ (KeV $\frac{\text{sec}}{\text{m}^3}$ )	$1.5 \times 10^{17}$	$5.5 \times 10^{18}$	$9.0 \times 10^{20}$	$7.0 \times 10^{21}$
Plasma pressure $\beta = \frac{2\mu_0 p}{B^2}$	0.1%	3%	11%	5%
Current-drive parameter $\eta_{CD} = \frac{n_{e0}RI_p}{P_{CD}} \left( \frac{A}{\text{m}^2 W} \right)$	—	$8 \times 10^{18}$	$3.4 \times 10^{19}$ + bootstrap	$3 \times 10^{19}$ + bootstrap
Fusion reactivity: D-D reactions/sec D-T reactions/sec	— —	$3 \times 10^{14}$ —	$1 \times 10^{17}$ $\approx 6 \times 10^{17}$	— $10^{21}$

of refraction of the wave goes to 0,  $n \rightarrow 0$ , which is equivalent to the wavelength going to infinity,  $\lambda \rightarrow \infty$ , or the phase velocity going to infinity,  $v_{\text{phase}} \rightarrow \infty$ . This defines the cutoff of a wave. Depending on the orientation of the wave's electric field with respect to the plasma's magnetic field, the wave will be classified as the Ordinary wave ( $E \parallel B$ ), with a cutoff given by:

$$\omega_O = \left( \frac{n_e q_e^2}{\epsilon_0 m_e} \right)^{\frac{1}{2}} \quad (1.5)$$

or as an eXtraordinary wave ( $E \perp B$ ) with a cutoff given by:

$$\omega_X = \pm \frac{\omega_{ec}}{2} + \left( \omega_{pe}^2 + \left( \frac{\omega_{ec}}{2} \right)^2 \right)^{\frac{1}{2}} \quad (1.6)$$

where  $\omega_{ec}$  is the electron cyclotron frequency of the plasma and  $\omega_{pe}$  is the plasma electron frequency. Either one of these two modes of propagation can be used to probe the plasma and obtain the density data.

Reflectometry has many advantages over other density profile diagnostics, such as Thomson Scattering, Multichannel Infra Red Interferometer, Langmuir probes and Heavy Ion Beam Probe. It requires little viewing access to the plasma, it is non-disturbing to the plasma (i.e., it requires no structures in the plasma as compared to Langmuir probes), can probe the edge as well as the center of the plasma, its components are relative cheap and available, it provides a remote measurement as opposed to an intrusive measurement (like Langmuir probes), it can provide continuous time density profiles (as opposed to a one shot profile like Thomson Scattering) and it can provide density fluctuation information as well as density profile information depending on the technique being used. These characteristics make it ideal for measuring the changes of the edge density profile in front of the ICRH antenna due to the power deposition on the plasma. In general Langmuir probes can not survive the high temperatures and densities of the plasma in front of the ICRH antenna. Viewing access for diagnostics like Thomson Scattering and MIRI is generally insufficient in front of the ICRH antenna. As it will be discussed, the edge density profile in front of the ICRH antenna can be modified by ponderomotive forces, impurity production, sheath rectification effects, self sputtering, quiver induced losses, etc. This has the effect of changing the loading and therefore the coupling of the ICRH power to the plasma.

A reflectometer is the first choice to do a direct measurement of the changes on the plasma edge density profile in front of the ICRH antenna due to these phenomena. The information obtained from the reflectometer can be used to better understand the plasma edge and to maximize the coupling and power deposition to the plasma, which is of great importance to the success of ICRH as a primary source of auxiliary heating and to the achievement of temperatures at the fusion reactor regime.

A more detailed history of the development of reflectometry is offered in

section 2.2 beginning on page 16. This work presented a library search in the field of reflectometry, with emphasis on the techniques to measure density profiles.

### 1.3 Fusion Experiments

Presently magnetic fusion research takes place mainly in relatively large machines of three main types: *Tokamaks*, *Stellarators* and *Torsatrons*. There are other less popular configurations<sup>9</sup> like the Symmotron, the modular stellarator, heliac (a type of helical axis stellarator), the spheromak, etc.,<sup>14-16</sup> but they will not be discussed here. Table 1.2 shows a list of fusion experiments and their corresponding locations.<sup>3</sup> The most common and popular of these three machines is the tokamak, where the name comes from the soviet words for toroidal magnetic chamber.

These machines rely on a helical magnetic field to confine the hot plasma to achieve fusion. What differentiates them is the way in which they achieve this helical magnetic field. The tokamak uses a set of toroidal field coils to produce the toroidal component of the helical magnetic field and a transformer set of coils to induce a current in the plasma that produces the poloidal component of the helical magnetic field.<sup>1</sup> A simplified schematic is presented in Figure 1.3,<sup>1</sup> top picture, together with a more detailed diagram of a fusion experiment showing the helical magnetic field line through the cutout section, which is a product of the vectorial addition of the Poloidal and Toroidal magnetic fields. The stellarator and torsatron are characterized by a set of external helical coils that produce the magnetic field with no internal plasma current.<sup>9</sup> The stellarator has helical coils with alternating antiparallel currents that produce a net poloidal magnetic field and no net toroidal field. Because of the zero net toroidal field, a separate set of toroidal field coils is used to provide the toroidal component of the helical

**Table 1.2: Some fusion experiments and their corresponding locations.**

Device	Status	Location
Alc-C-M	On	Alcator-C Modified, Plasma Fusion Center, MIT
PLT	Off	Princeton Large Tokamak, Princeton Plasma Phy. Lab.
ATC	Off	Adiabatic Toroidal Compressor, PPPL
PBX-M	On	Princeton Divertor Experiment, PPPL
TFTR	On	Tokamak Fusion Test Reactor, PPPL
BPX		Burning Plasma Exp., PPPL (proposed)
DIID-D	On	Doublet III-D, General Atomics, San Diego, Ca.
ORMAK	Off	Oak Ridge Tokamak, Oak Ridge Nat. Lab.
ISX-B	Off	Impurity Studies Experiment B, ORNL
ATF	Off	Advanced Toroidal Facility, ORNL
ITER		Inter. Thermonuclear Exp. Reactor (proposed)
ASDEX-U	On	Axially Symmetric Divertor Experiment, Max Planck Institute for Plasma Physics, Garching, Germany
Textor	On	Jülich, Federal Republic of Germany
JET	On	Joint European Torus, Abingdon, England
JFT-2M	On	Japan Atomic Energy Research Ins., Takai, Japan
JT-60U	On	Japan Atomic Energy Research Ins., Naka, Japan
T-3	On	Kurchatov Institute, Moscow
T-10	On	Kurchatov Institute, Moscow
Toresupra	On	Centre d'Etudes de Cadarache, France

magnetic field. A list of some major stellarators<sup>9-11</sup> is shown in Table 1.3 with their corresponding main parameters. On the torsatron (a subclass of the stellarator) the currents run parallel to each other, creating poloidal and toroidal magnetic fields; thus, no extra toroidal field coils are needed, but vertical field coils are used to provide stabilization and positioning of the plasma. An example of a torsatron is the Advanced Toroidal Facility (ATF) at the Oak Ridge National Laboratory, shown in Figure 1.4.<sup>9</sup> Some of its main parameters are listed in Table 1.4.

## 1.4 Tokamak Fusion Test Reactor

The Tokamak Fusion Test Reactor (TFTR) experiment, originally conceived in 1974, became operational in December 1982. The original basic objectives of TFTR are the following:<sup>12</sup>

1. to achieve temperatures (10 KeV) and densities ( $10^{14} \frac{\text{part}}{\text{cm}^3}$ ) pertinent to a fusion reactor in plasmas with currents of 2.5 MAmps
2. to achieve approximate energy break-even between the power input to and neutron power output from the plasma ( $Q \approx 1$ ) at reactor-like fusion power densities ( $\approx 1 \frac{\text{Watts}}{\text{cm}^3}$ ).

The TFTR program goals are to understand plasma transport in reactor relevant regimes, to achieve conditions in deuterium plasmas that project to energy breakeven in D-T plasmas, to carry out physics research and development for TPX (Tokamak Physics eXperiment) and ITER (International Thermonuclear Experimental Reactor), and to achieve breakeven conditions in D-T plasmas. Some

---

\*If things go well, start date maybe some time after 2000.



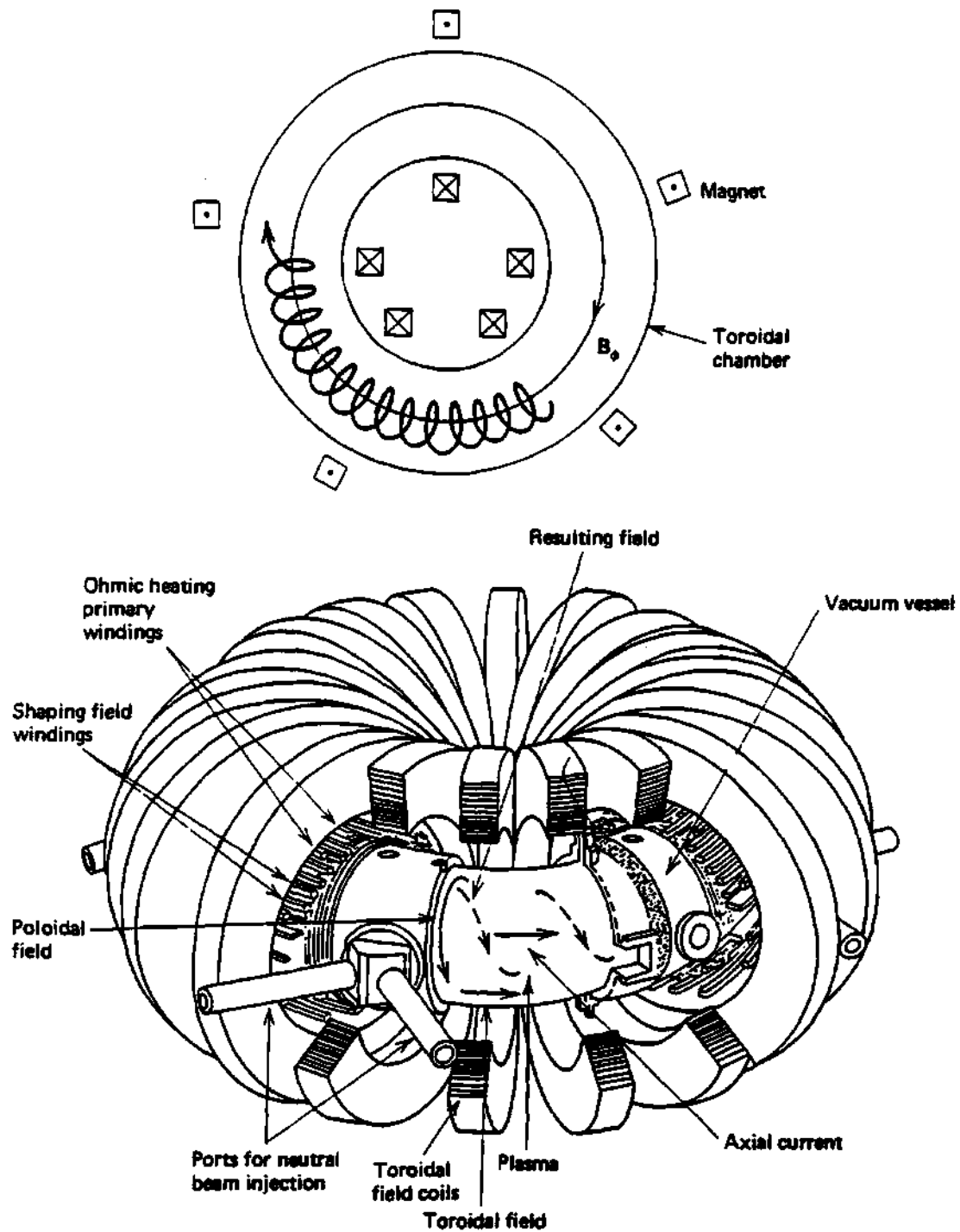


**Figure 1.3: Schematics of the closed toroidal confinement concepts and a tokamak schematic.**

**Table 1.3: Some stellarators and their corresponding parameters. (FRG is Federal Republic of Germany)**

Device	Location	Start Date	$l$	$m$	$R$ (m)	$a$ (m)	$B$ (T)	Main Feature
ATF	USA	1987	2	12	2.1	0.27	1.9	Flexibility
CAT	USA	1990	1,2	5	0.53	0.11	0.1	Torsatron
IMS	USA	1989	3	7	0.4	0.04	0.3	Modular Stel.
L-2	Russia	1976	2	14	1.0	0.11	1.5	Stellarator
URAGAN-2	Ukraine	1993	2,4	4	1.7	0.2	2.4	Torsatron
URAGAN-3	Ukraine	1982	3	9	1.0	0.13	1.2	Divertor
Wend. 7-A	FRG	1976	NA	5	2.0	0.1	3.5	Shearless
Wend. 7-AS	FRG	1987	NA	5	2.0	0.2	2.5	Modular coils
Wend. 7-X	FRG	200?*	NA	5	5.5	0.5	2.5	Advance Stel.
Heliotron-E	Japan	1981	2	19	2.2	0.2	1.9	High $\bar{\iota}$ , shear
CHS	Japan	1988	2	8	1.0	0.2	2.0	Heliotron
LHD	Japan	1997	2	10	3.9	0.65	3.0	Heliotron
TJ IU	Spain	1994	1	6	0.6	0.1	0.5	Torsatron
TJ-II	Spain	1996	1	4	1.5	0.25	1.0	Helical axis
H-1	Australia	1993	1	3	1.0	0.2	1.0	Flexible Heliac

**Table 1.4: Some of ATF major parameters.**

Dimensions	Major radius, $R_0$	2.1 m
	Minor radius, $a$	0.27 m
	Plasma volume, $V_p$	3.0 m <sup>3</sup>
	Vacuum vessel volume	10.5 m <sup>3</sup>
Magnetic configuration	Maximum field on axis, $B_0$	1.9 Teslas
	Field flattop time at 1.9 T	5 sec
	Field flattop time at 0.95 T	20 sec
	Poloidal multipolarity, $l$	2
	Number of field periods, $m$	12
	Standard central transform, $\bar{\iota}(0)$	0.3
	Standard edge transform, $\bar{\iota}(a)$	1.0
Plasma Heating	ECH, 53 GHz, steady state	0.4 MW
	NBI, 30 kv, 0.3 sec	2 MW
	ICH, 29 MHz, 0.1 sec	1.0 MW

## ADVANCED TOROIDAL FACILITY

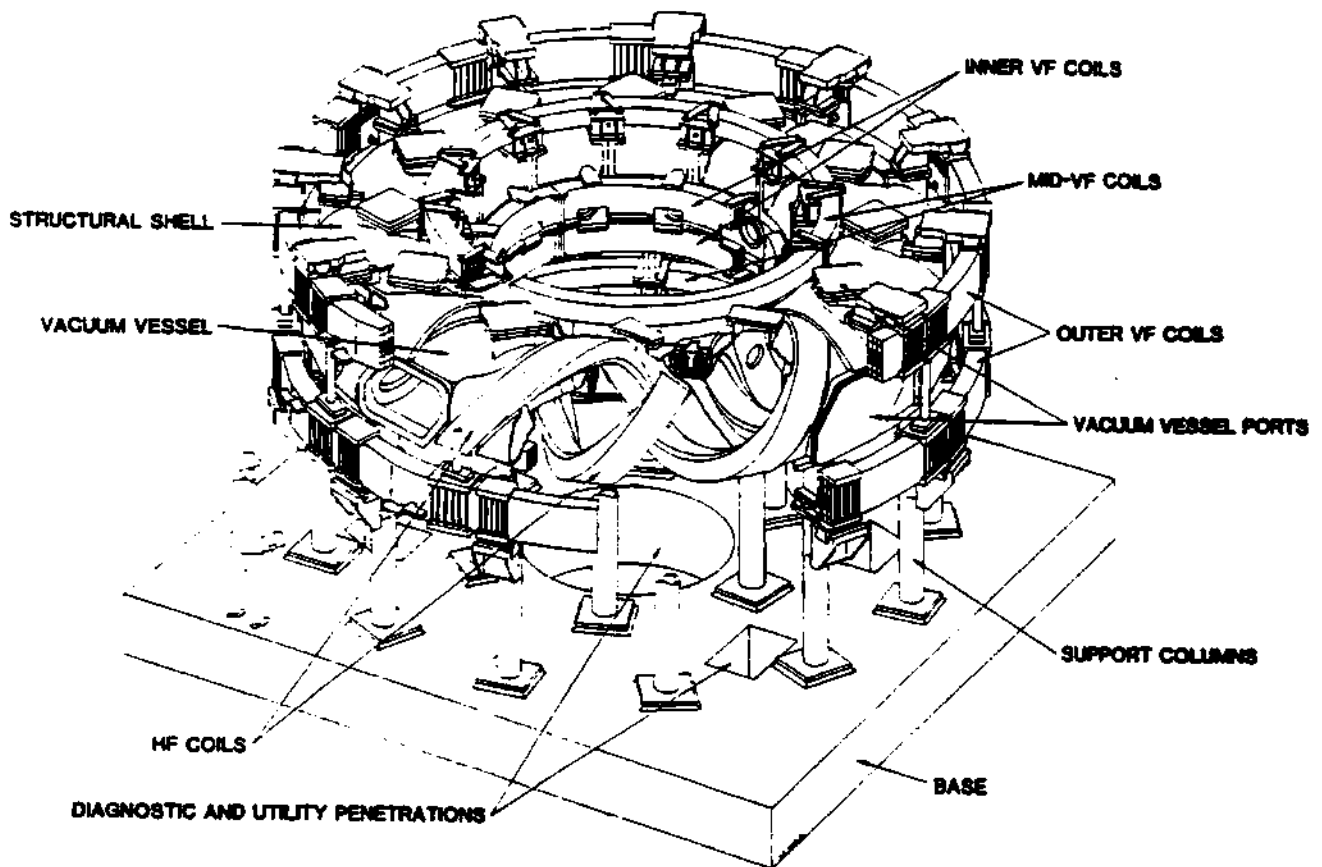


Figure 1.4: An artist's sketch of ATF's vacuum chamber and magnetic field coil system.

**Table 1.5: Some major parameters of TFTR.**

Major radius, $R_0$	2.63 m
Minor radius, $a$	0.97 m
Plasma volume, $V_p$	46 m <sup>3</sup>
Toroidal magnetic field, $B_0$	6.0 T
Plasma current (maximum), $I_p$	3 MA
Plasma density, $n_e$	$5 \times 10^{19} \frac{\text{part}}{\text{m}^3}$
Neutral beam power, $P_{NBI}$	35 MW
ICRH power, $P_{ICRH}$	12 MW

machine parameters are shown in Table 1.5,<sup>4,13</sup> and some diagnostics are presented in Table 1.6<sup>12,13</sup> (a very good article is the one by Orlinskij).

Table 1.6: Some of TFTR diagnostics.

Diagnostic	Measurement	# Data Channels	Data Points
1 mm Interferometer	$\int n_e dl$	2	32 K
Torus Pressure Gauges	Torus pressure	2	8 K
Residual Gas Analysis	Gas impurity concentration	2	—
Rogowski Loops	$I_p$	4	32 K
Position Coils	Plasma position	37	108 K
Mirnov Coils	Magnetic oscillations	43	195 K
Voltage Loops/Saddle Coils	Vol. around torus, position	44	88 K
Diamagnetic Loop	Plasma pressure	4	4 K
Hard X-ray Monitors	Effects of runaway electrons	5	40 K
Plasma TV	Plasma pictures, position	1	—
Fast Scan. Het. Radiometer	$T_e(r, t)$	2	32 K
X-ray Pulse-height Analyzer	$T_e, n_{Fe}, Z_{eff}$	9	102 K
Horizontal Charge Exchange	$T_i(t)$	198	198 K
$^{235}\text{U}$ , $\text{BF}_3$ , $^3\text{He}$ Neutron Proportional Counters	Neutrons $T_i(t)$	12	44 K
Bolometers	Radiated (and C-EX) power	34	34 K
UV Survey Spectrometer	Impurity Spectrum ( $t$ )	2	64 K
Interference Filter Array	$Z_{eff}(t)$ , $H_\alpha$ light ( $t$ ), $n_e(r, t)$	64	16 K

## CHAPTER II

### REFLECTOMETRY

#### 2.1 Introduction

This chapter presents a short history of the beginnings of reflectometry, and describes its basic principles, the propagation of electromagnetic waves in fusion plasmas, and the different reflectometry techniques.

#### 2.2 History of Reflectometry

##### 2.2.1 The beginnings

Since the 1960's research programs in fusion, ionospheric physics, and astrophysics have led to developments in the study of plasma physics. Reflectometry has its origins in the field of ionospheric physics,<sup>5,6,8</sup> in which the altitude (position) of an atmospheric density layer is calculated from the delay time of an electromagnetic wave after it is reflected off a plasma layer (the cutoff layer) for which the electron plasma frequency ( $\omega_{pe}^2 = \frac{q_e^2 n_e}{\epsilon_0 m_e}$ ) is equal to the wave frequency  $\omega$ . Reflectometry works under the same principle as the famous *RADAR* principle (Radio Detection And Ranging), except that the reflectometer is reflecting from a plasma and not from a solid object. For the particular case of laboratory plasmas, the time delays are so small (of the order of nanoseconds) that the phase difference between the incident and the reflected waves is measured, rather than the time delay.

### 2.2.2 First experiments in Russia

The first use of reflectometry on fusion plasmas was performed in what at that time was known as the Union of Soviet Socialist Republics (USSR) and now consists of many different and independent nations<sup>17,18</sup> (now frequently referred to as the “Former Soviet Union” or the Soviet DisUnion). In this experiment Anisimov used three sources of microwaves to probe the plasma at three different densities. It was a very simple method compared to today’s technology, but it made a proof of principle of the potentials of the technique. Many others, such as Colchin,<sup>19,20</sup> Simonet,<sup>21</sup> Anoshkin,<sup>18</sup> Calderon,<sup>25</sup> Sánchez,<sup>28–32</sup> etc. followed up on the idea and developed it to its present more sophisticated state.

### 2.2.3 First experiment in USA

The first reflectometry (underground) experiment in the United States was done by Colchin<sup>19,20</sup> in ORMAK (Oak Ridge tokaMAK) and as he explains in his report “...it cost almost nothing. The equipment was entirely borrowed; setup, and most of the runs were made after hours. Hence the ‘underground’ in the title.” They used a frequency swept microwave source in an attempt to make time resolved density profiles. The success of this effort indicated that the microwave sweeper held out the promise of detailed time-resolved density measurements on a shot-to-shot basis.

Since that time, reflectometry at fixed frequencies, narrowband swept frequencies, and broad band swept frequencies has been used in many fusion experiments over the world. For example, reflectometry at fixed frequencies has been used on the ATC tokamak<sup>37</sup> (Adiabatic Toroidal Compresor), on the TORSO stellarator,<sup>42</sup> on JET<sup>141</sup> (Joint European Torus), on TFTR<sup>102–104,116,107–110</sup> and on TFR<sup>77</sup> to measure density fluctuations. Reflectometry over a narrow range was used on TFR to follow the lateral movement of the discharge and to determine

when a particular density was reached in the plasma<sup>78</sup> and on PLT to control auxiliary high-power plasma heating systems.<sup>80</sup> Broadband reflectometry was used on DIII-D to measure density profiles of the plasma<sup>95-97</sup> and density fluctuations.<sup>95</sup>

## 2.3 Propagation of Electromagnetic Waves in Plasmas

This section will present a brief derivation of the equations that describe the propagation of electromagnetic waves in plasmas with an emphasis on fusion plasmas.

### 2.3.1 Maxwell equations

No work about electromagnetism can be complete without a presentation of Maxwell's equations. This section will present some important equations and some definitions that are the basis of electromagnetism and most of the present work.

Maxwell's equations describe the propagation of electromagnetic waves in a medium (or plasma). These are (in MKS units):<sup>49</sup>

$$\vec{\nabla} \cdot (\vec{\epsilon} \cdot \vec{E}) = \rho \quad (\text{Gauss' electric field law}) \quad (2.1)$$

$$\vec{\nabla} \cdot \vec{B} = 0 \quad (\text{Gauss' magnetic field law}) \quad (2.2)$$

$$\vec{\nabla} \times \vec{E} = -\frac{\partial \vec{B}}{\partial t} \quad (\text{Faraday's induction law}) \quad (2.3)$$

$$\vec{\nabla} \times \vec{B} = \mu_0 \left( \vec{J} + \frac{\partial (\vec{\epsilon} \cdot \vec{E})}{\partial t} \right) \quad (\text{generalized Ampère's law}) \quad (2.4)$$

where:

1.  $\vec{E}$  = Electric vector field in Volts/meter.



2.  $\vec{D}$  = Electric displacement vector field =  $\vec{\epsilon} \cdot \vec{E}$  in Coulombs/meter<sup>2</sup>, where  $\vec{\epsilon}$  is the permittivity (dielectric tensor) of the medium.
3.  $\vec{B}$  = Magnetic induction vector field =  $\mu \vec{H}$  in Teslas, where  $\mu$  is the permeability of the medium.
4.  $\vec{H}$  = Magnetic field in Ampère-turn/meter.
5.  $\rho$  = Electrical charge density in Coulombs/meter<sup>3</sup>.
6.  $\vec{J}$  = Electrical current density vector field in Ampère/meter<sup>2</sup>.
7.  $c = 299,792,456.2 \pm 1.1$  meters/second.<sup>50</sup>
8.  $\epsilon_0 = 8.854187817 \times 10^{-12} \frac{F}{m}$  is the permittivity of vacuum.
9.  $\mu_0 = 4\pi \times 10^{-7} \frac{N}{Amp^2}$  is the permeability of vacuum.
10.  $m_e = 9.1093897 \times 10^{-31}$  kg is the electron rest mass.
11.  $q_e = 1.60217733 \times 10^{-19}$  C is the electron charge.

Among the consequences of Maxwell equations, there is the continuity equation:

$$\vec{\nabla} \cdot \vec{J} + \frac{\partial \rho}{\partial t} = 0 \quad (2.5)$$

which is derived by taking the divergence ( $\vec{\nabla} \cdot$ ) of equation 2.4 above.

A useful quantity in plasma studies is the electric conductivity tensor,  $\vec{\sigma}$ , defined by:

$$\vec{J} \equiv \vec{\sigma} \cdot \vec{E} \quad (2.6)$$

which relates the current density,  $\vec{J}$ , to the applied external electric field in an anisotropic medium.

The polarization vector field,  $\vec{P}$ , is another quantity of importance, defined together with the susceptibility tensor,  $\bar{\bar{\chi}}$ , as:

$$\vec{P} \equiv \epsilon_0 \bar{\bar{\chi}} \cdot \vec{E} \quad (2.7)$$

and it represents the reaction of the medium (plasma) to the external applied electric field. Among the conveniences of defining the polarization vector and electric susceptibility is that it provides us with a divergence-free electric displacement field in the medium, that is:

$$\vec{\nabla} \cdot \vec{D} = 0 \quad (2.8)$$

where:

$$\vec{D} \equiv \epsilon_0 \vec{E} + \vec{P} \quad (2.9)$$

where by using eq. 2.7 one obtains:

$$\vec{D} = \epsilon_0 \vec{E} + \epsilon_0 \bar{\bar{\chi}} \cdot \vec{E} \quad (2.10)$$

and since:

$$\vec{D} = \bar{\bar{\epsilon}} \cdot \vec{E} \quad (2.11)$$

then:

$$\bar{\bar{\epsilon}} = \epsilon_0 (\bar{\bar{1}} + \bar{\bar{\chi}}) \quad (2.12)$$

All of this leads to the polarization charge density:

$$\rho = -\vec{\nabla} \cdot \vec{P} \quad (2.13)$$

### 2.3.2 The dielectric tensor

The propagation of an electromagnetic wave in a plasma can be described and/or modeled by the dielectric tensor, which represents a measurement of the response of a dielectric medium to an externally applied electromagnetic field. For such a model it will be assumed that:<sup>5,8,48,51-55,137</sup>

1. The fields and the velocities are Fourier transformable.
2. The velocity of the species are all the same. This means that the particles have no thermal motion.

This description addresses what is known as the cold plasma model; and even though the model is very simple, these idealizations capture, to a large extent, the main characteristics of a plasma response to an external electromagnetic wave. The term “cold” is used to indicate that the electrons and ions have no thermal velocities, except the one that it is induced by the electromagnetic fields of the wave and the natural gyration motion of the electrons. More details on the dielectric tensor can be found in the references, such as D. G. Swanson,<sup>48</sup> T. H. Stix,<sup>53-55</sup> W. P. Allis,<sup>52</sup> H. Meuth,<sup>137</sup> K. G. Budden,<sup>5</sup> M. Bornatici,<sup>51</sup> V. I. Ginzburg<sup>8</sup> and others.

Next consider a particle of mass  $m_s$  and charge  $q_s$  that moves with velocity  $\vec{v}_s$  under the influence of the Lorentz force in an electric field  $\vec{E}$  and magnetic field  $\vec{B}$ ;<sup>5,48,51-55,137,8</sup>

$$\frac{d\vec{v}_s}{dt} = \frac{q_s}{m_s} (\vec{E} + \vec{v}_s \times \vec{B}) \quad (2.14)$$

along with two of Maxwell's equations:

$$\vec{\nabla} \times \vec{E} = -\frac{\partial \vec{B}}{\partial t} \quad (2.15)$$

$$\vec{\nabla} \times \vec{B} = \mu_0 \left( \vec{J} + \epsilon_0 \frac{\partial \vec{E}}{\partial t} \right) \quad (2.16)$$

where the term  $\epsilon_0 \frac{\partial \vec{E}}{\partial t}$  is known as the displacement current of the externally applied electric field. The equation for the current density is given by:

$$\vec{J} = \sum_s n_s q_s \vec{v}_s \quad (2.17)$$

which includes all the species of the plasma, and it assumes that the plasma is locally uniform and homogenous. For the study of the oscillatory properties of the

plasma, it can be assumed that the  $\vec{E}$ ,  $\vec{B}$  and  $\vec{v}_s$  fields can be Fourier transformed and that they have the form:

$$\vec{E}(\vec{r}, t) = \vec{E} e^{i(\vec{k} \cdot \vec{r} - \omega t)} \quad (2.18)$$

$$\vec{B}(\vec{r}, t) = \vec{B}_0 + \vec{B} e^{i(\vec{k} \cdot \vec{r} - \omega t)} \quad (2.19)$$

$$\vec{v}_s(\vec{r}, t) = \vec{v}_s e^{i(\vec{k} \cdot \vec{r} - \omega t)} \quad (2.20)$$

where  $\vec{B}_0$  is the static part of the magnetic field and it is assumed, without loss of generality, that it is in the  $z$ -direction of the coordinate system, and that  $|\vec{B}| \ll |\vec{B}_0|$ .

Substituting equations 2.18, 2.19, and 2.20 into the equation of motion, eq. 2.14, and keeping the terms of first order yields:

$$-i\omega m_s \vec{v}_s = q_s (\vec{E} + \vec{v}_s \times \vec{B}_0) \quad (2.21)$$

This is a system of three equations in the three unknown components of the velocity,  $\vec{v}_s$ . When it is solved, this  $3 \times 3$  system of equations for the components of  $\vec{v}_s$  yields:

$$v_{sx} = \frac{iq_s}{m_s(\omega^2 - \omega_{sc}^2)} (\omega E_x + i\epsilon_s \omega_{sc} E_y) \quad (2.22)$$

$$v_{sy} = \frac{iq_s}{m_s(\omega^2 - \omega_{sc}^2)} (-i\epsilon_s \omega_{sc} E_x + \omega E_y) \quad (2.23)$$

$$v_{sz} = \frac{iq_s}{m_s \omega} E_z \quad (2.24)$$

where:

$$\epsilon_s = \frac{q_s}{|q_s|} \quad (2.25)$$

represent the sign of the charge and:

$$\omega_{sc} = \frac{|q_s| B_0}{m_s} \quad (2.26)$$

is the species cyclotron frequency of the plasma.

This solution can be seen as a matrix multiplied by a vector, that is:

$$\begin{pmatrix} v_{sx} \\ v_{sy} \\ v_{sz} \end{pmatrix} = \begin{pmatrix} \frac{iq_s \omega}{m_s(\omega^2 - \omega_{sc}^2)} & \frac{-\epsilon_s q_s \omega_{sc}}{m_s(\omega^2 - \omega_{sc}^2)} & 0 \\ \frac{\epsilon_s q_s \omega_{sc}}{m_s(\omega^2 - \omega_{sc}^2)} & \frac{iq_s \omega}{m_s(\omega^2 - \omega_{sc}^2)} & 0 \\ 0 & 0 & \frac{iq_s}{m_s \omega} \end{pmatrix} \cdot \begin{pmatrix} E_x \\ E_y \\ E_z \end{pmatrix} \quad (2.27)$$

Now this matrix can be diagonalized by the rotation of the coordinate system or what is equivalent, by choosing a coordinate system such that the matrix becomes diagonal. This coordinate system is given by the transformations:

$$v_{\pm} = v_x \pm i v_y \quad (2.28)$$

$$E_{\pm} = E_x \pm i E_y \quad (2.29)$$

which are obtained by the usual method of row multiplication and addition such that the matrix becomes diagonal. Substituting the values for the  $v_{sx}$  and  $v_{sy}$  from equations 2.22 and 2.23 into equation 2.28, the components of the velocity in the diagonalized coordinate system become:

$$v_{\pm} = \frac{iq_s}{m_s(\omega \mp \epsilon_s \omega_{sc})} E_{\pm} \quad (2.30)$$

In a similar fashion, the current density can be expressed in vector form as:

$$\begin{pmatrix} J_x \\ J_y \\ J_z \end{pmatrix} = \begin{pmatrix} \sum_s \frac{n_s q_s^2}{m_s} \left( \frac{i\omega E_x - \epsilon_s \omega_{sc} E_y}{\omega^2 - \omega_{cs}^2} \right) \\ \sum_s \frac{n_s q_s^2}{m_s} \left( \frac{\epsilon_s \omega_{cs} E_x + i\omega E_y}{\omega^2 - \omega_{cs}^2} \right) \\ \sum_s \frac{n_s q_s^2}{m_s} \frac{E_z}{\omega} \end{pmatrix} \quad (2.31)$$

or in the diagonalized coordinate system as:

$$J_{\pm} = i\epsilon_0 \sum_s \frac{\omega_{ps}^2}{\omega \mp \epsilon_s \omega_{sc}} E_{\pm} \quad (2.32)$$

$$J_z = i\epsilon_0 \sum_s \frac{\omega_{ps}^2}{\omega} E_z \quad (2.33)$$

where:

$$\omega_{ps}^2 \equiv \frac{n_s q_s^2}{m_s \epsilon_0} \quad (2.34)$$

is the species plasma frequency in the coordinate system of diagonalization.

Next consider Maxwell's equation 2.16, in particular the current terms on the right hand side of the equation. This equation can be used to define a new useful quantity, the dielectric tensor,  $\bar{\bar{K}}$ , as:

$$\vec{J} - i\omega\epsilon_0\vec{E} = -i\omega\epsilon_0\bar{\bar{K}} \cdot \vec{E} \quad (2.35)$$

where the dielectric tensor  $\bar{\bar{K}}$  is given by:

$$\bar{\bar{K}} \equiv \begin{pmatrix} S & -iD & 0 \\ iD & S & 0 \\ 0 & 0 & P \end{pmatrix} \quad (2.36)$$

where:

$$S \equiv \frac{1}{2}(R + L) \equiv 1 - \sum_s \frac{\omega_{ps}^2}{\omega^2 - \omega_{sc}^2} \quad (2.37)$$

$$D \equiv \frac{1}{2}(R - L) \equiv \sum_s \frac{\epsilon_s \omega_{ps}^2 \omega_{sc}}{\omega(\omega^2 - \omega_{sc}^2)} \quad (2.38)$$

$$P \equiv 1 - \sum_s \frac{\omega_{ps}^2}{\omega^2} \quad (2.39)$$

$$R \equiv S + D \equiv 1 - \sum_s \frac{\omega_{ps}^2}{\omega(\omega + \epsilon_s \omega_{sc})} \quad (2.40)$$

$$L \equiv S - D \equiv 1 - \sum_s \frac{\omega_{ps}^2}{\omega(\omega - \epsilon_s \omega_{sc})} \quad (2.41)$$

The notation used here is the familiar notation first used by Stix<sup>53</sup> and are mnemonics for the words: Sum, Difference, Plasma, Right and Left.

The advantages of these definitions and formulae are that they make an excellent launch path for the derivation of the dispersion relation for a wave in a plasma, which follows next.

Starting with Maxwell's equations 2.3 and 2.4, by taking the *curl* (i.e.,  $\nabla \times$ ) of equation 2.3 and 2.4, it can be shown that:<sup>48,53</sup>

$$\vec{\nabla} \times (\vec{\nabla} \times \vec{E}) = \vec{\nabla} \times \left( -\frac{\partial \vec{B}}{\partial t} \right) \quad (2.42)$$

$$\vec{\nabla} \times \vec{B} = \mu_0 \left( \vec{J} + \frac{\partial \vec{\epsilon} \vec{E}}{\partial t} \right) \quad (2.43)$$

which under the assumption that the fields are Fourier transformable, becomes:

$$\vec{k} \times (\vec{k} \times \vec{E}) = \vec{k} \times \omega \vec{B} \quad (2.44)$$

$$\vec{k} \times \vec{B} = -\omega \epsilon_0 \mu_0 \vec{K} \cdot \vec{E} \quad (2.45)$$

Substituting equation 2.44 into equation 2.45 and defining the index of refraction vector as:

$$\vec{n} \equiv \frac{\vec{k}c}{\omega} \quad (2.46)$$

whose magnitude,  $n = |\vec{n}|$ , represents the ratio of the velocity of light in the medium to the phase velocity of the wave, yields:

$$\vec{n} \times (\vec{n} \times \vec{E}) + \vec{K} \cdot \vec{E} = 0 \quad (2.47)$$

where the identity:

$$c^2 = \frac{1}{\epsilon_0 \mu_0} \quad (2.48)$$

has been used.

Now, without loss of generality, assume the direction of propagation,  $\vec{k}$ , of the wave to be in the  $x$ - $z$  plane, and since  $\vec{B}$  has been already chosen in the  $z$ -direction, equation 2.47 becomes:

$$\begin{pmatrix} S - n^2 \cos^2 \theta & -iD & n^2 \cos \theta \sin \theta \\ iD & S - n^2 & 0 \\ n^2 \cos \theta \sin \theta & 0 & P - n^2 \sin^2 \theta \end{pmatrix} \begin{pmatrix} E_x \\ E_y \\ E_z \end{pmatrix} = 0 \quad (2.49)$$

where  $\theta$  is the angle between the propagation vector  $\vec{k}$  and the  $z$ -axis. This is the famous dispersion relationship of the "cold" plasma, and it describes the propagation modes of waves in the plasma.<sup>48,53</sup>

In order to have a nontrivial solution the determinant of the matrix must be zero. This condition gives the final form of the dispersion relation as:

$$An^4 - Bn^2 + C = 0 \quad (2.50)$$

where:

$$A \equiv S \sin^2 \theta + P \cos^2 \theta \quad (2.51)$$

$$B \equiv (S + D)(S - D) \sin^2 \theta + PS(1 + \cos^2 \theta) \quad (2.52)$$

$$C \equiv P(S + D)(S - D) = PLR \quad (2.53)$$

The solutions can be written in terms of the angle as follows. Start by substituting equations 2.51, 2.52, and 2.53 into equation 2.50 to obtain:

$$0 = (S \sin^2 \theta + P \cos^2 \theta) n^4 - [LR \sin^2 \theta + PS(1 + \cos^2 \theta)] n^2 + PLR \quad (2.54)$$

where the identity  $LR = (S - D)(S + D)$  has been used. Next, use equation 2.54 twice. The first time express all the sines in terms of cosine using the formula  $\sin^2 \theta = 1 - \cos^2 \theta$  and the second time express all the cosine in terms of the sines in order to obtain two equations, one in terms of cosine only and another one in terms of sines only. After moving the corresponding terms around in both equations:

$$Sn^4 - (LR + PS)n^2 + PLR = \cos^2 \theta [(P - S)n^4 + (LR - PS)n^2] \quad (2.55)$$

$$Pn^4 - 2PSn^2 + PLR = \sin^2 \theta [(P - S)n^4 + (LR - PS)n^2] \quad (2.56)$$

Taking the ratio of equations 2.55 and 2.56 above, yields:

$$\frac{\sin^2 \theta}{\cos^2 \theta} = \frac{Pn^4 - 2PSn^2 + PLR}{Sn^4 - (LR + PS)n^2 + PLR} \quad (2.57)$$

The numerator and denominator can be factored into the form:

$$\tan^2 \theta = -\frac{P(n^2 - R)(n^2 - L)}{(Sn^2 - RL)(n^2 - P)} \quad (2.58)$$

where the general condition for resonance (where  $n^2 \rightarrow \infty$  or  $\lambda \rightarrow 0$ ) is given by:

$$\tan^2 \theta = -\frac{P}{S} \quad (2.59)$$



and the general condition for cutoff (where  $n^2 = 0$  or  $\lambda \rightarrow \infty$ ) is given by:

$$C = P(S + D)(S - D) = 0 \quad (2.60)$$

There are two special cases for the propagation of a wave in a plasma. These are propagation parallel and perpendicular to the magnetic field. This work deals only with propagation perpendicular to the magnetic field. For such waves there exist two modes of propagation:

1.  $n^2 = P$ , known as the Ordinary mode or O-mode.
2.  $n^2 = \frac{RL}{S}$ , known as the eXtraordinary mode or X-mode.

### 2.3.3 Properties of the O- and X-modes

This section presents some of the properties of the solution to a wave propagating perpendicular to the magnetic field of the plasma, the so called Ordinary and eXtraordinary waves. From here on, only the first order terms will be considered on the formulas and derivations.

**The Ordinary mode** The Ordinary wave follows the dispersion relation given by:

$$n_O^2 = P = 1 - \sum_s \frac{\omega_{ps}^2}{\omega^2} \quad (2.61)$$

or when only the electrons are considered, in the simpler form:

$$n_O^2 = P = 1 - \frac{\omega_{pe}^2}{\omega^2} \quad (2.62)$$

which shows the dependence of the wave on the local density, since  $\omega_{pe}^2(r) = \frac{n_e(r)q_e^2}{m_e\epsilon_0}$ . The dispersion relation, equation 2.62, does not show any dependence on the magnetic field. This is because the electric field,  $\vec{E}$ , of the Ordinary wave is parallel to the magnetic field,  $\vec{B}$ , so that the particles (electrons) do not experience any

effect from the magnetic field. There is no resonance (except for  $\omega = 0$ , which does not count because it is basically D.C.) and the cutoff condition,  $n^2 = 0$ , occurs only at  $\omega = \omega_{pe}(r_c)$ , the electron plasma frequency. There can be no propagation (as discussed in section 2.7.2) for  $\omega < \omega_{pe}$ , since this makes  $n^2 < 0$ , and  $n^2 \rightarrow 1$  as  $\omega \rightarrow \infty$ , making the O-mode dispersion relation among the simplest and easiest to work with.

The propagation of the O-mode is characterized by a direction of propagation,  $\vec{k}$ , perpendicular to the magnetic field,  $\vec{B}_0$ , and an electric field,  $\vec{E}$ , parallel to the externally applied magnetic field,  $\vec{B}_0$ .

**The eXtraordinary mode** For the eXtraordinary wave the story becomes a little more complicated, with a dispersion relation given by:

$$n_X^2 = \frac{(S + D)(S - D)}{S} \quad (2.63)$$

which can be expressed in terms of the electron frequencies as:

$$n_X^2 = 1 - \frac{\omega_{pe}^2}{\omega^2} \frac{\omega^2 - \omega_{pe}^2}{\omega^2 - \omega_{pe}^2 - \omega_{ec}^2} \quad (2.64)$$

The resonances,  $n_X^2 \rightarrow \infty$ , for the X-mode are given by the equations:

$$\omega_{UH}^2 = \omega_{pe}^2 + \omega_{ec}^2 \quad (2.65)$$

$$\omega_{LH}^2 = \omega_{ec}\omega_{ic} \left( \frac{\omega_{pe}^2 + \omega_{ec}\omega_{ic}}{\omega_{pe}^2 + \omega_{ec}^2} \right) \quad (2.66)$$

where the subscripts refer to the Upper-Hybrid and Lower-Hybrid respectively, and some terms of the order  $\frac{m_e}{m_i}$  have been neglected. The cutoff,  $n^2 \rightarrow 0$ , occurs at:

$$\omega_X = \pm \frac{\omega_{ec}}{2} + \left[ \omega_{pe}^2 + \left( \frac{\omega_{ec}}{2} \right)^2 \right]^{\frac{1}{2}} \quad (2.67)$$

where two negative roots have been discarded. The two cutoffs are referred to as the upper (+) and the lower (−) cutoffs,<sup>68</sup> or as the right (+) and left (−) cutoffs,<sup>53,85</sup> or as the fast (+) and slow (−) waves<sup>48</sup> (because of their phase velocities),

respectively. Because of the number of different solutions and the many variables involved in plasma wave propagation problems, the solutions become extremely complicated. A popular way to sketch these solutions is the famous Clemmow-Mullaly-Allis diagram or *CMA* diagram.<sup>48</sup> In this type of diagram the cutoffs and resonances are plotted as curves as a function of the normalized density,  $\frac{\omega_p^2}{\omega^2}$ , and the normalized magnetic field,  $\frac{\omega_{ce}}{\omega}$ , for a one species plasma. An example is shown in Figure 2.1.<sup>48</sup> The  $x$  and  $y$  axes are not linear. This is done to be able to include all of the boundaries in a clear fashion. A complete description of the CMA can be found in the references, such as Budden,<sup>5</sup> Ginzburg,<sup>8</sup> Swanson,<sup>48</sup> and others.<sup>51-55,137</sup>

For the propagation of the X-mode the propagation vector,  $\vec{k}$ , is again perpendicular to the magnetic field,  $\vec{B}_0$ , but the electric field,  $\vec{E}$ , is perpendicular to the magnetic field,  $\vec{B}_0$ .

#### 2.3.4 Advantages and disadvantages of each mode

**O-mode** The O-mode has the advantage of having an extremely simple dispersion equation. Because of this, the formulae associated with the calculation of the density profile can be done analytically using an *Abel* inversion technique, as described in section 2.6.1. The problem with the Abel inversion is that it has an integral over frequency space from 0 to  $\omega_{reflection}$ , something technically hard to do because there is no microwave generator that can go from 0 Hz to about 100 GHz in a reasonable amount of time. The way that physicists have gone around this problem is by assuming a density profile at the edge and starting the frequency sweep at a more reasonable frequency.<sup>80,43</sup> While this introduces some error in the technique, generally good agreement has been found between this and other diagnostic techniques. Because of the simplicity of the dispersion equation, it is the oldest technique in laboratory reflectometry and the one that people have the most experience with.

## 2.2. THE CMA DIAGRAM

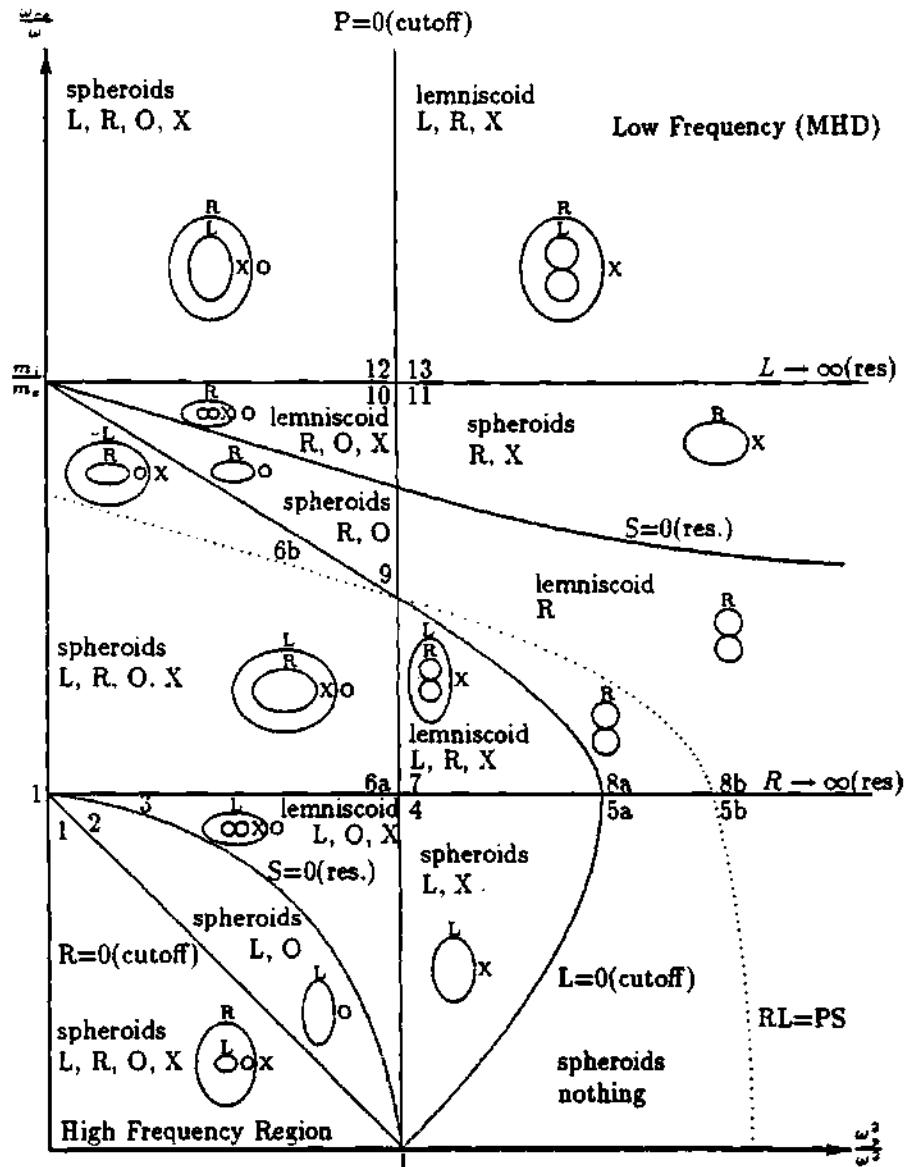


Figure 2.1: CMA diagram (Swanson) with all boundaries and the wave normal surfaces.

A minor disadvantage of the O-mode is that it cannot probe the back of the density profile on toroidal devices (where  $B(R) = \frac{B_0 R_0}{R}$ ), past the point of maximum density because of the single dependence of the dispersion relation on the density profile. Nor can it be used to probe the outer edge of the plasma, because the long wavelengths of the frequencies necessary to probe the plasma edge will reduce and degrade the spatial resolution of the beam.

**X-mode** Because the X-mode has a more complicated dispersion equation (compared with the one for the O-mode), an analytical inversion is not possible or known. However it has the advantage of being able to probe the edge of the plasma<sup>31</sup> starting with the electron cyclotron frequency (equation 2.26) at that point,<sup>131</sup> whereas the O-mode has to use very low frequencies at such low densities. At the edge of the plasma, where  $n_e \rightarrow 0$ , the cutoff and the electron resonance layers become closer; thus, some of the waves may pass through the evanescent part of the plasma and be absorbed at the electron resonance layer. Regardless of this, the X-mode wave makes it easier to probe the edge of the plasma (as compared to the O-mode). This advantage has been used in ASDEX (R. Schubert<sup>131</sup>) to study the density profile at the edge of the plasma in front of the RF-heating antenna.

Another advantage of the X-mode is that because of the dual dependance of the dispersion relation on the density and the magnetic field, the X-mode wave can propagate past the point of maximum density and probe the back of the density profile (this is for toroidal devices, because  $B(R) \propto \frac{1}{R}$  and as long as the density is sufficiently low). Some knowledge of the magnetic field profile is needed, but this is not a major obstacle because the usual assumption that  $B(R) \propto \frac{1}{R}$  can be used. The scanning capabilities of the X-mode are restricted by the position of the second harmonic resonance layer and not by the peakedness of the density

profile as compared with the O-mode wave. This does not present a problem, since as can be seen in Figure 2.2, for a typical  $n_e \propto [1 - (\frac{r}{a})^\alpha]^\beta$  density profile, the first frequency for the second harmonic resonance corresponds to the probing frequency for the innermost part of the density profile. This region is usually of less interest, because the radial profile is normally assumed to be symmetric in the minor radius. The density profile has been superimposed to show its effect on the cutoff frequencies (X-mode upper and lower cutoff) and on the Upper and Lower Hybrid resonance frequencies. Figure 2.2 shows some of the different resonances and cutoffs for an X-mode wave; from the position of these resonances, it is clear that a wave in the frequency range of the reflectometer (90 to 120 GHz) launched from the low field side of the plasma will always reach the cutoff before it reaches the Upper Hybrid and/or Electron Cyclotron resonances. The toroidal field coil current,  $I_{tf}$ , the corresponding magnetic field,  $B_0$ , the central density,  $n_e(0)$ , and coefficients for the assumed density profile ( $\alpha$  and  $\beta$ ) are shown in the figure. The density profile is plotted to show the general shape of a typical plasma and to show the effect of the density profile on the plasma frequencies.

### 2.3.5 Solution to the wave equation in a plasma

The wave equation has the general form:

$$\vec{\nabla}^2 \vec{E}(\vec{r}, t) + \frac{1}{c^2} \frac{\partial^2 \vec{E}(\vec{r}, t)}{\partial t^2} = 0 \quad (2.68)$$

where the general electric vector field has a dependance on both the position,  $\vec{r}$ , and the time,  $t$ . Solution of this equation at any point and time is rather difficult. So, as usual, different approximations for different conditions and regions of the plasma have been found. The importance of finding such solutions for reflectometry is that the *phase* of the reflecting wave can be obtained from such solutions, and from the phase, the density profile can be reconstructed. Some of these approximations and solutions follow.

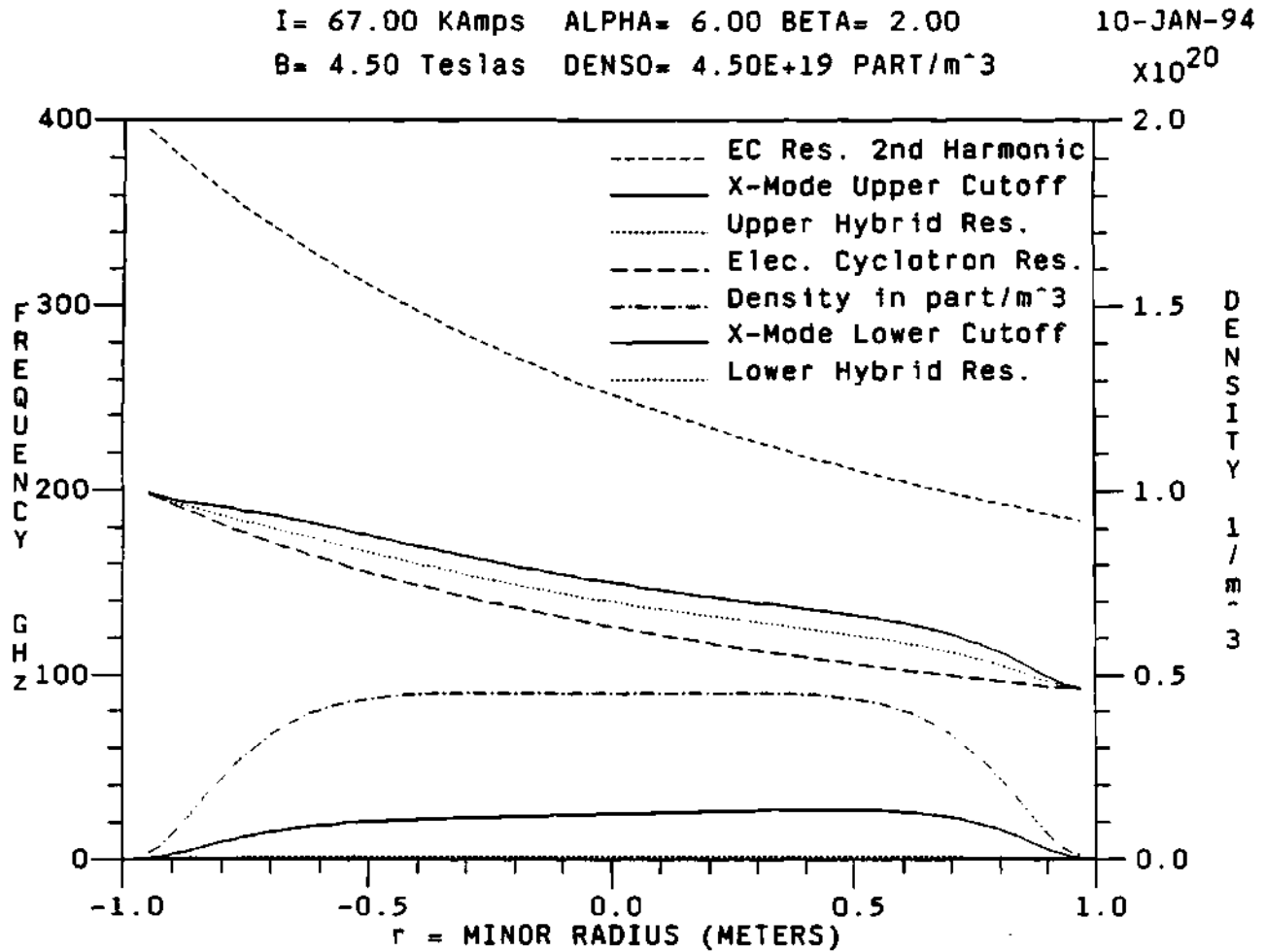


**Figure 2.2:** Plot of the different frequencies for a plasma with a density profile of the type  $n_e(r) \propto \left(1 - \left(\frac{r}{a}\right)^\alpha\right)^\beta$  and with a magnetic field (in Teslas) of the form  $B(R) \propto \frac{1}{R}$ , where  $r$  is the minor radius,  $a$  is the plasma edge minor radius and  $R$  is the major radius. DENS0 is the center density.

**Geometrical optics solution** The geometric optical approximation can be used to calculate the phase for a wave propagating in a fusion plasma given that some assumptions about the plasma medium are made. These assumptions are:<sup>5-8,309</sup>

1. The effects of the toroidal curvature will be ignored. This is a valid assumption, since the wave is launched along the minor radius and the beam width is much smaller than the major radius of the device. Any waves not propagating in the direction of the major radius will be reflected away from the collecting antenna and are very unlikely to be detected.
2. The electron density,  $n_e$ , has only a radial dependence. As long as the data is collected in about 200  $\mu$ -seconds the average density will be time independent.
3. The magnetic field,  $\vec{B}$ , has only a radial dependence too. Here again, the effects of the toroidal curvature are ignored and a time independent magnetic field is assumed for the time scales of the collection of the data.
4. The fields are Fourier transformable in time.
5. Absorption is neglected.

On the basis of the above assumptions, equation 2.68 becomes:

$$\frac{d^2 \vec{E}(\vec{r})}{dr^2} + \frac{\omega^2}{c^2} \epsilon_r(\vec{r}, \omega) \vec{E}(\vec{r}) = 0 \quad (2.69)$$

where  $\epsilon_r(\vec{r}, \omega) = n^2$  is the relative permittivity and  $n$  is the index of refraction.

For a 100% homogeneous plasma, i.e., for  $\epsilon_r = n^2 = \text{constant}$ , the solution becomes:

$$E(r) = E_0 e^{\pm i \frac{\omega}{c} n r} \quad (2.70)$$



where  $E_0$  is simply a constant and the phase is given by:

$$\phi = \frac{\omega n r}{c} \quad (2.71)$$

To add more reality to the problem, consider  $\epsilon_r(r)$  as a slowly changing function of  $r$ ; in such a case, a reasonable approximation is to substitute the term  $n r$  in equation 2.71 by the average refraction coefficient over the ray path. Then the phase will become:

$$\phi = \frac{\omega}{c} \int_{r_1}^{r_2} n(r, \omega) dr \quad (2.72)$$

where  $r_1, r_2$  are the end points of the path along the minor radius of the plasma.

This by itself is the solution of the geometrical optics approximation, or the WKB or WKBJ approximation, first introduced by Jeffreys<sup>88</sup> and developed for quantum mechanics and the Schrödinger equation by Wentzel,<sup>89</sup> Kramers,<sup>90</sup> and Brillouin.<sup>91</sup> It holds only when  $\epsilon_r(r)$  changes slowly over the length of an electromagnetic wave, that is, when:

$$\lambda(r) \frac{d\epsilon_r(r)}{dr} \ll \epsilon_r(r) \quad (2.73)$$

for which  $\lambda(r)$  is the wavelength at position  $r$ . This condition is equivalent to:

$$\frac{\lambda}{L_{n_e}} \ll 1 \quad (2.74)$$

for the O-mode and to:

$$\frac{\lambda}{L_{n_e}}, \frac{\lambda}{L_B} \ll 1 \quad (2.75)$$

for the X-mode, where  $L_{n_e}$  is the electron density gradient scale length:

$$L_{n_e} = n_e \left( \frac{dn_e}{dr} \right)^{-1} \quad (2.76)$$

and  $L_B$  is the magnetic field gradient scale length:

$$L_B = B \left( \frac{dB}{dr} \right)^{-1} \quad (2.77)$$

**Series solution** Others have obtained solutions by assuming other forms for the solution. Ginzburg<sup>8</sup> seeks a solution by assuming a solution in the form of a series, as:

$$E(r) = \sum_{j=0}^{\infty} \left(\frac{c}{\omega}\right)^j E_j(r) e^{\pm i \frac{\omega}{c} \psi(r)} \quad (2.78)$$

where  $\psi(r)$  and  $E_j(r)$  are unknown functions. Substituting equation 2.78 into equation 2.69, collecting terms of equal powers in  $\frac{c}{\omega}$  and setting the terms of each of the powers of  $\frac{c}{\omega}$  to 0, yields:

$$\psi(r) = \pm \int_{r_1}^r n(r', \omega) dr' \quad (2.79)$$

$$E_0(r) = A_0 (n(r, \omega))^{-\frac{1}{2}} \quad (2.80)$$

$$E_1(r) = (n(r, \omega))^{-\frac{1}{2}} \int_{r_1}^r \frac{1}{2i} \left( \frac{d^2 E_0(x)}{dx^2} \right) \Big|_{x=r'} (n(r', \omega))^{-\frac{1}{2}} dr' \quad (2.81)$$

$$\vdots \quad (2.82)$$

Assuming that only the first term of the series is significant, the solution is:

$$E(r) = A_0 (n(r, \omega))^{-\frac{1}{2}} e^{\pm i \frac{\omega}{c} \int_{r_1}^r n(r', \omega) dr'} \quad (2.83)$$

which is very similar to the solution for constant  $n(r, \omega)$  and even more interesting is that the phase solution is exactly the same.

If  $n(r, \omega)$  is monotonic, a sufficient condition for the validity of equation 2.83 is that:

$$\frac{\omega}{c} \frac{n^2}{\left| \frac{dn}{dr} \right|} = \frac{2\pi L_n}{\lambda} \gg 1 \quad (2.84)$$

where  $L_n \equiv n^2 \left( \frac{dn}{dr} \right)^{-1}$  is the gradient scale length of the refractive index,  $n$ . Physically, the above equation means that the local wavelength of the probing wave must be much smaller than the local gradient scale length of the refractive index.

**Solution at the reflection layer** An exact solution for the wave equation in the neighborhood of the reflecting layer has been calculated for an electromagnetic wave moving in the ionosphere.<sup>5,8</sup> The assumptions to reach this solution are:

1. The plasma electron density is monotonically increasing with decreasing minor radius.
2. The plasma is collisionless.
3. The density,  $n_e(r)$ , is approximately linear around the neighborhood of the reflection layer. In his derivation, Budden<sup>5</sup> shows that a sufficient condition for  $n_e(r)$  to be considered quasi-linear is that:

$$\frac{d^2 n_e(r)}{dr^2} |r - r_c| \ll \frac{dn_e}{dr} \quad (2.85)$$

where  $r_c$  is the position where the wave is reflected or the cutoff position.

In this region of quasi-linearity the relative permittivity of the plasma can be expressed as:

$$\epsilon_r = a_0 (r - r_c) \quad (2.86)$$

where  $a_0$  is a constant. Under this condition the wave equation becomes:

$$\frac{d^2 \vec{E}(\vec{r})}{dr^2} + \frac{\omega^2}{c^2} a_0 (r - r_c) \vec{E}(\vec{r}) = 0 \quad (2.87)$$

This happens to be one of Stokes' differential equations with solutions in terms of the famous *Airy* integrals.<sup>144</sup> In his derivation, Budden<sup>5</sup> shows that the solution at the reflection layer matches the solution of the geometrical optics approximation with a difference of a term of  $\frac{\pi}{2}$  due to the reflection of the wave. The final solution for the phase is:

$$\phi = 2 \frac{\omega}{c} \int_{r_1}^{r_2} n(r, \omega) dr - \frac{\pi}{2} \quad (2.88)$$

in which the factor of 2 comes from assuming a symmetrical path of the incident and reflected wave to and from the reflecting layer.

**One dimensional full wave analysis.** A one dimensional full wave solution to the wave equation of a reflectometer beam has been done and studied by Hutchinson.<sup>34</sup> The analysis is based on the first Born approximation (which is not a full wave solution, but another type of solution), dating back at least to Pitteway (1959).<sup>36</sup> Even though it is a one dimensional approach, Hutchinson's solution includes some features (such as, wave attenuation due to beam divergence and/or absorption by the medium) that correspond to multidimensional analysis of the wave. This is done by considering the case where the wave number,  $k$ , and the solution to the wave equation are complex. This analysis differs from the more usual WKB approximation<sup>5,8</sup> in offering a solution consistent with the full wave problem but requiring that the perturbations to the density profile be small. In comparison, the WKB approximation ignores the finite wavelength but can be applied to zero-order problems, and hence to large perturbations, at least in principle.

The assumptions for this model are:

1. Consider a plasma slab in which all gradients are perpendicular to the magnetic field.
2. Without loss of generality, assume that the magnetic field,  $\vec{B}$ , is in the  $\hat{z}$ -direction and the wave propagates in a direction parallel to the gradients, which it is taken in the  $\hat{x}$ -direction.
3. Next, assume that the plasma can be described by a local response in the form of a dielectric tensor,  $\vec{\epsilon}$ , that is a function only of the frequency,  $\omega$ , and the position,  $x$ , such that the wave equation is:

$$\vec{\nabla} \times (\vec{\nabla} \times \vec{E}) - \frac{\omega^2}{c^2} \vec{\epsilon} \cdot \vec{E} = 0 \quad (2.89)$$

4. Finally, assume that the cross terms  $\epsilon_{xz}$  and  $\epsilon_{yz}$  are zero.

Under these assumptions, equation 2.89 can be separated into the two decoupled scalar wave equations:

$$\left[ \frac{d^2}{dx^2} + \frac{\omega^2}{c^2} \right] E_z = 0 \quad (2.90)$$

for the O-mode, and:

$$\left[ \frac{d^2}{dx^2} + \frac{\omega^2}{c^2} \left( \epsilon_{yy} - \frac{\epsilon_{yx}\epsilon_{xy}}{\epsilon_{xx}} \right) \right] E_y = 0 \quad (2.91)$$

for the X-mode, where the values for the components of the dielectric tensor are given by:

$$\epsilon_{xx} = 1 - \frac{\omega_{pe}^2}{\omega^2 - \omega_{ec}^2} \quad (2.92)$$

$$\epsilon_{yy} = \epsilon_{xx} \quad (2.93)$$

$$\epsilon_{xy} = i \frac{\omega_{pe}^2 \omega_{ec}}{\omega (\omega^2 - \omega_{ec}^2)} \quad (2.94)$$

$$\epsilon_{yx} = -\epsilon_{xy} \quad (2.95)$$

$$\epsilon_{zz} = \frac{\omega_{pe}^2}{\omega^2} \quad (2.96)$$

Both of equations 2.90 and 2.91 are of the Helmholtz type, that is, of the form:

$$\frac{d^2 \psi}{dx^2} + k^2(x) \psi = 0 \quad (2.97)$$

where the parameter  $k(x)$  is an arbitrary function of  $x$ . In the particular case of the O-mode,  $k$  is given by:

$$k^2(x) = \frac{\omega^2 - \omega_{pe}^2(x)}{c^2} \quad (2.98)$$

$$= k_v^2 \left( 1 - \frac{n_e(x)}{n_e(x_c)} \right) \quad (2.99)$$

where  $k_v = \frac{\omega}{c}$  and  $n_e(x_c)$  is the critical density, or the density at the cutoff, given by:

$$n_e(x_c) = \frac{\omega^2 \epsilon_0 m_e}{q^2} \quad (2.100)$$

and  $n_e(x)$  is the local density. While for the X-mode,  $k$  is given by:

$$k^2(x) = k_v^2 \left[ 1 - \frac{\omega_{pe}^2(x) (\omega^2 - \omega_{pe}^2(x))}{\omega^2 (\omega^2 - \omega_{ec}^2(x) - \omega_{pe}^2(x))} \right] \quad (2.101)$$

Equation 2.97 is a second order linear differential equation with two linearly independent solutions, call them  $\psi_1$  and  $\psi_2$ . The one that represents the physical solution has to go to zero as  $x \rightarrow \infty$ . Without loss of generality, it can be assume that  $\psi_1$  is such a solution. A perturbation on the amplitude of the density (like the fluctuations due to MHD and other instabilities) will induce a similar perturbation on the wave number,  $k$ , because as it can be seen from equations 2.98 and 2.101 above:

$$k = k(w_{pe}) \quad (2.102)$$

$$= k(w_{pe}(n_e)) \quad (2.103)$$

for both the O-mode and the X-mode. So, by adding a small perturbation to the  $k$  due to the perturbation on the density, the new solution to equation 2.97 can be found by using perturbation theory, as follows. The new perturbation equation can be found by using the substitutions:

$$k^2 \rightarrow k_0^2 + \tilde{k}^2 \quad (2.104)$$

and

$$\psi \rightarrow \psi_0 + \tilde{\psi} \quad (2.105)$$

where the symbol  $\tilde{\phantom{x}}$  stands for the perturbed part of the new solution. Then equation 2.97 becomes:

$$\frac{d^2 \tilde{\psi}}{dx^2} + k_0^2 \tilde{\psi} = -\tilde{k}^2 \psi_0 \quad (2.106)$$

which still is in the form of Helmholtz equations and its solution can be found using the ubiquitous Green functions. Green's theory says that given an equation of the form:

$$\frac{d^2 \psi}{dx^2} + k^2 \psi = f(x) \quad (2.107)$$

with boundary conditions:

$$\psi(x \rightarrow \infty) = 0 \quad (2.108)$$

$$U(\psi(x_0)) = 0 \quad (2.109)$$

where  $U(\psi)$  is a linear combination operator of  $\psi$  and  $\frac{d\psi}{dx}$ , evaluated at some reference point,  $x_0$ , inside of the vacuum region, then the solution to the boundary value problem is given by:

$$\psi(x) = \int_{x_0}^{\infty} G(x, y) f(y) dy \quad (2.110)$$

where  $G(x, y)$  is the solution to the equation:

$$\frac{d^2 G(x, y)}{dx^2} + k^2 G(x, y) = \delta(x - y) \quad (2.111)$$

and  $G(x, y)$  is given by:

$$G(x, y) = \psi_1(y) \left( \psi_2(x) - \frac{U(\psi_2(x_0))}{U(\psi_1(x_0))} \psi_2(x) \right) \frac{1}{W(y)}, \text{ for } x < y \quad (2.112)$$

$$= \psi_1(x) \left( \psi_2(y) - \frac{U(\psi_2(x_0))}{U(\psi_1(x_0))} \psi_2(y) \right) \frac{1}{W(y)}, \text{ for } y < x \quad (2.113)$$

where  $W(x)$  is the Wronskian, given by:

$$W(x) = \psi_1(x) \psi_2'(x) - \psi_2(x) \psi_1'(x) \quad (2.114)$$

where the primes symbol, ', denotes differentiation with respect to the argument of the function. The Green's function solution for the perturbation problem will be good provided that  $\tilde{\psi} \ll \psi_0$  for all  $x$ . Setting the zeroth solution to be:

$$\psi_0 = \psi_1 \quad (2.115)$$

and setting:

$$f(x) = -\tilde{k}^2 \psi_1 \quad (2.116)$$

on equation 2.107, together with the boundary condition that equation 2.110 is evaluated at a point on the vacuum region, then the solution for the perturbed part of the solution for the wave equation is of the form:

$$\bar{\psi}(x) = - \left( \psi_2(x) - \frac{U(\psi_2)}{U(\psi_1)} \psi_1(x) \right) \int_{x_0}^{\infty} \bar{k}^2(\xi) \frac{(\psi_1(\xi))^2}{W(\xi)} d\xi \quad (2.117)$$

Thus, the first order perturbation solution to the wave equation using Green's functions is a linear combination of the two independent solutions to the unperturbed problem, with coefficients given by equation 2.117.

In his work, Hutchinson<sup>34</sup> proposes that the key principal effects of transverse wave spreading can reasonably be modelled by the addition of an imaginary part to  $k^2$ . This imaginary part is regarded as a parameter that can be adjusted to model approximately the effect of a specific antenna configuration.

Continuing with the derivation, it is assumed that in the vacuum region, where  $k_v$  is constant, the unperturbed solution,  $\psi_1$ , can be decomposed into forward and backward propagating waves; that is:

$$\psi_1 = A_1 e^{ik_v(x-x_0)} + B_1 e^{-ik_v(x-x_0)} \quad (2.118)$$

where the time dependent factor  $e^{-i\omega t}$  is understood and  $A_1$  and  $B_1$  are the complex amplitudes of the forward and backward waves. Then at the reference point position,  $x_0$ , the amplitudes of the wave are:

$$A_1 = \frac{1}{2} \left( \psi_1 - \frac{i\psi_1'}{k_v} \right) \quad (2.119)$$

$$B_1 = \frac{1}{2} \left( \psi_1 + \frac{i\psi_1'}{k_v} \right) \quad (2.120)$$

The second solution,  $\psi_2$ , can be expressed in a similar form, that is, with amplitudes  $A_2$  and  $B_2$  which are free to choose as needed, as long as the result is linearly independent of the solution  $\psi_1$ . Thus, the amplitudes for the second solution,  $\psi_2$ ,



can be:

$$A_2 = -iA_1 \quad (2.121)$$

$$B_2 = iB_1 \quad (2.122)$$

For such solutions the Wronskian at the point  $x = x_0$  is:

$$W(x_0) = (A_1 + B_1)ik_v(A_2 - B_2) - (A_2 + B_2)ik_v(A_1 - B_1) \quad (2.123)$$

$$= 4k_v A_1 B_1 \quad (2.124)$$

$$= k_v \left( \psi_1^2 + \frac{\psi_1'^2}{k_v^2} \right) \quad (2.125)$$

From general Wronskian theory<sup>36</sup> it is known that for an equation of the form of equation 2.97, which has no first order term, the Wronskian, equation 2.114, is a constant independent of  $x$ . Thus, for the present case, the value of  $W(x)$  given by equation 2.123 at the point  $x_0$  is the same for all  $x$  in the plasma.

Under the assumption that the physical situation to be described is one in which the launched (forward) wave amplitude is determined by the apparatus used and is fixed, then the boundary condition to be applied to the forward amplitude of the perturbation should be zero. This will require the condition:

$$U(\psi) = \frac{1}{2} \left( \psi - \frac{i}{k_v} \psi' \right) \Big|_{x_0} \quad (2.126)$$

From this choice of amplitude and boundary conditions it can be obtained:

$$\frac{U(\psi_2)}{U(\psi_1)} = \frac{A_2}{A_1} \quad (2.127)$$

and consequently the perturbation gives forward and backward amplitudes of:

$$\tilde{A} = 0 \quad (2.128)$$

and:

$$\tilde{B} = - \left( B_2 - B_1 \frac{A_2}{A_1} \right) \int k^2 \frac{\psi_1^2}{W} dx \quad (2.129)$$

$$= -2iB_1 \int k^2 \frac{\psi_1^2}{W} dx \quad (2.130)$$

which is the general form of the perturbation solution and its importance is that from it the phase difference of the reflected wave can be obtained. The phase can be calculated from equation 2.129 for the total reflected wave,  $B_1 + \tilde{B}$ , whose phase angle relative to  $B_1$  is:

$$\tilde{\phi} = -2\Re \left( \int \tilde{k}^2 \frac{\psi_1^2}{W} dx \right) \quad (2.131)$$

where the perturbation  $\tilde{\phi}$  is small and  $\Re(f)$  is the real part operator of  $f$ . Thus the perturbation on the phase of a wave can be calculated from the perturbation on the  $k(n_e)$  of the wave. This approach to calculate the phase of the wave can be used when the perturbations to the density profile (and the  $k$ ) are small, but the effect of these perturbations on the phase are not negligible.

This section presented a derivation to calculate the phase changes due to the effects of density fluctuations on the traveling wave as it propagates through the plasma. The solution can be used to study fluctuations in the phase of the wave due to such effects as line density ripple interference and Bragg effect from density fluctuations. This solution provides a relatively simple one-dimensional full wave analysis that includes some effects (like beam dispersion and absorption by the plasma) which are characteristic of multidimensional analysis, without the usual complications that accompany multidimensional analysis derivations.

## 2.4 Reflectometry Techniques

Reflectometry techniques have the advantages of requiring little access to the plasma, being non disturbing to the plasma, can probe the edge as well as the center of the plasma and providing density fluctuation information and/or density profile information, depending on the mode of operation and the technique being used. Each of these techniques has its advantages and disadvantages. A description of these follows.

### 2.4.1 Fixed frequency

Fixed frequency reflectometry has been used to provide information on the inception of a cutoff layer (that is, when a particular density or the peak density is reached some where in the plasma)<sup>17,18,38,79</sup>; for movements and/or fluctuations of the cutoff layer<sup>23,30,133</sup> (fluctuations in the density); for drift waves and transport studies,<sup>27,30,81,82,100,103,106-108,122</sup> and for correlation fluctuations studies in which the signals from two or more independent sources are correlated<sup>105,85-87</sup> to obtain information on radial coherence.<sup>93,123-125</sup> In principle, these fixed frequency techniques are simple, compared with broad band swept frequency techniques, since there is only one frequency to observe and availability of components and matching is easy and reliable. The first experiments using fixed frequency reflectometry were done by Anisimov<sup>17</sup> and Anoshkin<sup>18</sup> in the Alpha device in the 1960s.

After Anoshkin's experiments, fixed frequency reflectometry for density fluctuations became extremely popular. Other diagnostics can provide density fluctuation information, but they are confined to the edge and disturb the plasma around them (like Langmuir probes), or are more complicated in design, are expensive, and require more access to the plasma, such as the Heavy Ion Beam Probe (HIBP), or may have poor spatial resolution (e.g., Far Infrared scattering because

of the large scattering volume).

Two or more probing beam frequencies in the same antenna system can be used to do fluctuation correlation studies, in which the fluctuations at the radial reflection points of the corresponding probing beams can be cross correlated to obtain information such as the correlation length, normalized coherence, cross power spectral intensity (CPSI), cross phase of the fluctuation, and the radial width of a coherent fluctuation.<sup>85,86</sup>

#### **2.4.2 Narrow band swept frequency**

Narrow band or FM reflectometers have been used to measure the approximate position and movement of the cutoff layer,<sup>78,23</sup> to determine the inception of the cutoff density (as in PLT<sup>80</sup>), to control auxiliary high power plasma heating systems and to infer density profiles if multiple sources are used.<sup>94,95,45,46</sup> They are very much like narrow band FM radar as described by Doane<sup>80</sup> and Lehecka.<sup>94,95</sup> The idea of using multiple sources to calculate the density profile of a plasma was first mentioned by A. I. Anisimov<sup>17</sup> in 1961, and it is used in tokamaks like RTP.<sup>24</sup>

#### **2.4.3 Broadband swept frequency**

Broadband reflectometry was first proposed by Cano and Cavallo<sup>145</sup> in 1980. They proposed the determination of the density profile of a tokamak plasma by sweeping the probing frequency beam over the whole bandwidth of the waveguide and calculating the density profile out of the recorded phase of the reflected wave. After that, the method was tested by F. Simonet<sup>21,22</sup> on the TFR tokamak using the O-mode of propagation and by others in different experiments, like Petula-B,<sup>43,44</sup> DIII-D,<sup>94-99</sup> TF-1,<sup>68</sup> JET,<sup>70</sup> Wendelstein VII-AS,<sup>31,126</sup> RFX,<sup>127</sup> ASDEX,<sup>128-132</sup> TORE-SUPRA<sup>134</sup> and others.

The method was able to provide very detailed profiles, but it was apparent that determining the complete density profile for a large tokamak plasma would require a large number of reflectometers working at adjacent frequency bands. This appeared to be an inherent problem with the O-mode propagation because to scan a plasma from an edge density of 0 to a density of  $n_0$  the frequency band has to be from 0 Hz to  $\omega_0$ . On a fusion plasma with  $\omega_0 = 50$  GHz, it puts an impossible demand on the swept wave oscillator and the waveguide, since there is no oscillator with a frequency band from 0 to 50 GHz and no waveguide that works over that entire frequency band. Sweeping from some  $\omega_{min} \rightarrow \omega_0$  has been done, but the error introduced by the missing information can be significant. This is an advantage of the X-mode over the O-mode, since to probe the plasma from the edge at density 0 to some point inside the plasma at density  $n_0$  the X-mode wave frequency goes from the electron cyclotron frequency (some 50 GHz for a typical plasma) to the frequency of the cutoff. This makes it possible in principle to reduce the number of waveguides penetrating the vacuum vessel to one or two. The problem with the X-mode is that its index of refraction depends on the total magnetic field as well as the density profile, so a reasonable knowledge or model of the magnetic field in the region of propagation must be available.

The profile inversion is among the important differences between the O-mode and the X-mode. For the O-mode the density profile can be obtained by an Abel inversion of the data. This is possible because of the relatively simple form of the index of refraction and the single dependence on the density. For the X-mode, the index of refraction is a complicated function of the density and the local magnetic field. So an analytical solution as in the case of the Abel inversion for the O-mode is not known, and a numerical solution is necessary. Numerical algorithms have been developed by H. Bottollier et al.<sup>43</sup> and by E. J. Doyle.<sup>96,99</sup> Bottollier's method has some numerical instability problems during the profile inversion. Doyle's method

is similar to Bottollier's but it does not suffer from the numerical instability problems encountered by Bottollier.

#### 2.4.4 AM technique

On the Amplitude Modulated (AM) reflectometer the amplitude of the probing signal (in the range of GHz) is modulated (with a sinusoidal envelope) at a frequency on the order of MHz before launching it to the plasma. The advantage of this method is that phase tracking of the wave can be done at the modulation frequency of the sinusoidal envelope, reducing the phase shift. The group delay time,  $\tau$ , of the reflected signal can be easily evaluated from the phase delay,  $\Delta\phi$ , as:

$$\tau = \frac{\partial\phi}{\partial\omega} = \frac{\Delta\phi}{\Omega} \quad (2.132)$$

where  $\Omega$  is the modulation frequency of the probing wave. A generic block diagram of a typical AM (sinusoidal modulation) reflectometer<sup>28,32</sup> system is shown in Figure 2.3. This technique has been used in machines like PBX-M<sup>33</sup> to measure the edge density profile. The schematics for the AM reflectometer used in PBX-M is shown in Figure 2.4. Note the simplicity of the diagram as compared to the dual frequency phase difference reflectometer in Figure 4.8.

Some of the problems with an AM reflectometer are fast density fluctuations, pulse/envelope deformation, and parasitic reflections. The fast density fluctuations affect the signal by phase and amplitude oscillations. This effect can be significantly reduced provided that the modulation frequency is larger than the frequencies of the amplitude oscillations of the reflected signal. Pulse deformation is due to the response of the square law detector to higher order derivatives of the phase delay versus frequency and spectra deformation by dispersive effects of the waveguides and plasma. This presents a problems for pulse reflectometry (section 2.4.6), because of the broad spectrum of the square pulse. Since the AM

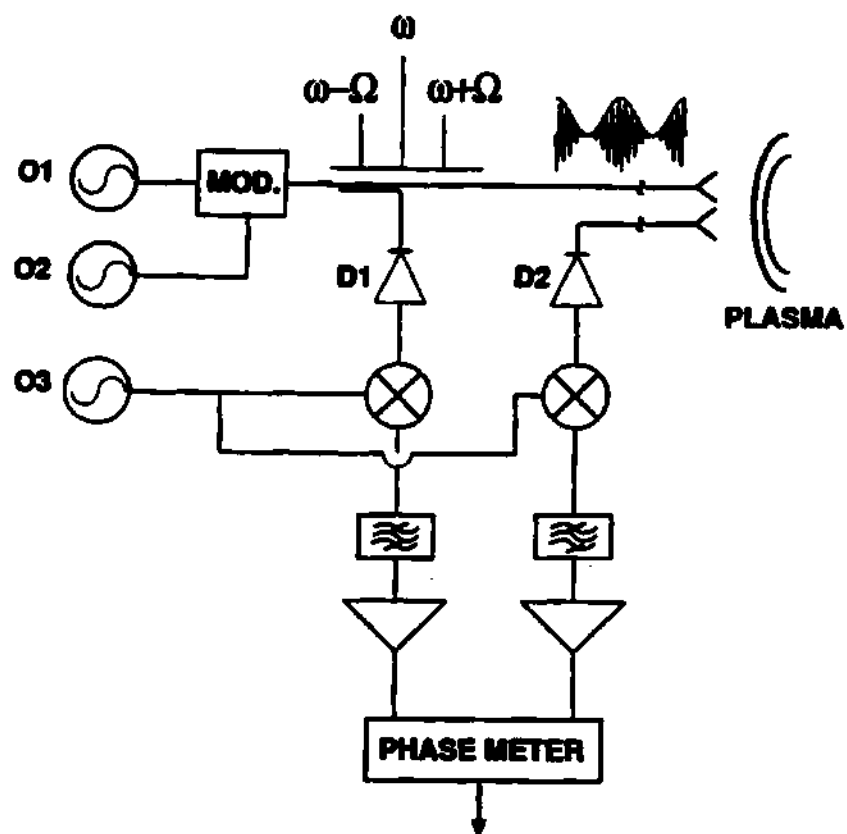
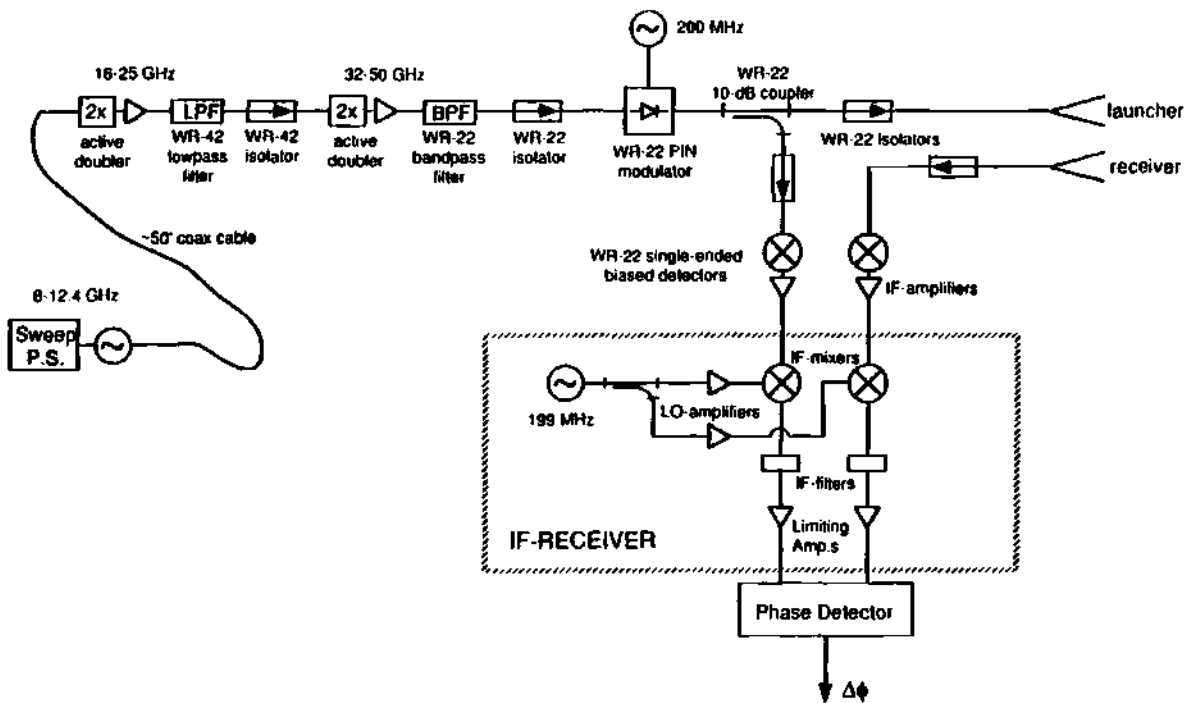


Figure 2.3: Generic diagram for an AM reflectometer system.

11 September, 1992

**PBX AM Reflectometer Schematic:**  
**DRAFT**



**Figure 2.4: Schematics for PBX-M AM reflectometer system.**



(sinusoidal modulation) signal is made up of only three frequency components, the deformation due to dispersion of the waveguide and plasma is minimal, and it can be totally suppressed by removing the carrier frequency or one of the side bands.<sup>28,32</sup>

#### 2.4.5 Dual frequency phase difference technique

The dual frequency phase difference technique uses the difference in phase between two probing frequencies that are separated by a constant  $\delta\omega$  and a technique similar to the one used by Doyle<sup>96,99</sup> to reconstruct the density profile by adding the pieces of phase differences as the density profile is reconstructed. Since this technique uses the phase difference between the side bands, the fringe count is smaller than it is with the full phase detection technique. With the continuous full phase detection scheme a count of over 1000 fringes is observed, and keeping track is extremely difficult. With the dual frequency phase difference, the fringe count is on the order of 5 fringes, an easy task for the hardware.<sup>28,39,40</sup> More details are presented in section 2.6.2.

#### 2.4.6 Pulse radar technique

A radar pulse of microwaves can be used to determine the density profile by either calculating the time of flight of the pulse (as is done in ionospheric studies<sup>5,6,8</sup>) or by using the change in shape of the reflected pulse. The time of flight has been used on ionospheric plasmas for a long time. The use of this technique for laboratory plasmas was first proposed by Golant<sup>138</sup> and later implemented on T-10 by Vershkov.<sup>139</sup>

Hughenoltz<sup>83,84</sup> and others<sup>41,138,140,143</sup> have proposed using an ultrafast microwave radar pulse to determine the plasma density. They proposed sending into the plasma a square radar pulse of waves composed of a broad band of frequencies.

The reflection of the different frequencies at different density layers will change the shape of the returning radar pulse. The deformation on the pulse signal is due to the response of the square law detector to higher order derivatives of the phase delay versus frequency, and spectra deformation by dispersive effects of the waveguides and plasma. This presents some problems for pulse reflectometry, because of the broad spectrum of the square pulse. Nevertheless, from the new shape of the reflected pulse, the information on the density can be decoded. Computer simulations of this concept indicate that a pulse rise/fall time on the order of 200 picoseconds will be required to see any measurable change. For time delay measurements, a rise/fall time of about 1 nanosecond is necessary to get a reflected pulse of the same shape as the incident pulse.

#### **2.4.7 Other techniques**

**Measurement of magnetic fluctuations** Recent research by Bretz and Vahala,<sup>118,119</sup> and others<sup>70-72,74,75</sup> has suggested that the fluctuations in the magnetic field can be determined by the study of the  $O \rightarrow X$  mode conversion. The interested reader is referred to the original articles in the references.

**Small scale edge fluctuations** It has been proposed by García<sup>121</sup> that the spatial location of small scale fluctuations at the edge of a fusion plasma can be determined by analyzing the enhanced scattering of a reflectometry signal on the reflection layer at the edge of the plasma, where the nonhomogeneous fluctuations of the plasma are strong. For his theory, García considers a slab model and an O-mode of propagation for the wave.

## 2.5 Measuring Density Fluctuations

Reflectometry works on the principle of the total reflection of an electromagnetic wave by a cutoff layer in a plasma. Such reflection occurs at the point where the index of refraction becomes equal to zero, i.e.,  $n^2 = 0$ .

The basic principle of the reflectometer is shown in Figure 2.5. From this basic schematic it can be seen that the signal from the source is divided into two signals: the reference signal and the probing signal. The probing signal is launched into the plasma, and as the wave propagates through the plasma, the index of refraction decreases until it becomes zero, at which point the wave is reflected back, collected by a second antenna, and fed into the phase detector to be compared in phase with the reference signal.

Analytically, the process can be seen as follows. First, ignore the effect of the plasma in front of the reflection layer on the incident wave. Under this assumption the signal path length,  $L_s$ , is equal to a certain number of wavelengths, call it  $a$ , then:

$$L_s = a\lambda \quad (2.133)$$

$$= \frac{\phi_s}{2\pi} \lambda \quad (2.134)$$

A similar argument is true for the signal in the reference path, that is:

$$L_r = b\lambda \quad (2.135)$$

$$= \frac{\phi_r}{2\pi} \lambda \quad (2.136)$$

where  $\phi_s$  and  $\phi_r$  are the probing signal phase and the reference signal phase, respectively. Solving for the phases and using  $c = \lambda f$  gives:

$$\phi_s = L_s \frac{\omega}{c} \quad (2.137)$$

$$\phi_r = L_r \frac{\omega}{c} \quad (2.138)$$

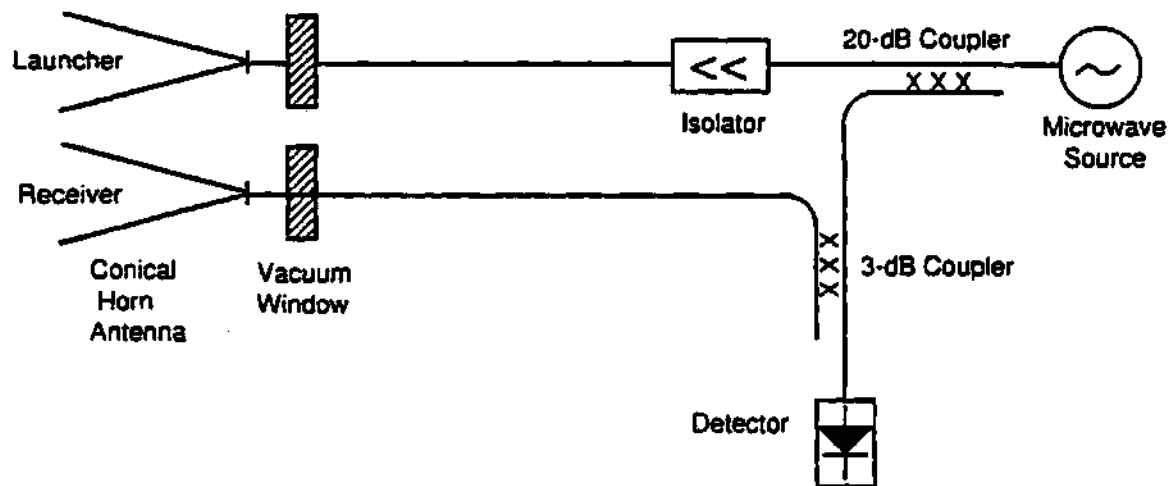


Figure 2.5: Basic schematic of a reflectometer.

Then the phase difference at the detector becomes:

$$\phi = \phi_s - \phi_r = (L_s - L_r) \frac{\omega}{c} \quad (2.139)$$

where  $\phi$  is the phase difference between the probing signal and the reference signal.

For a reflectometer, a change in the phase difference,  $\delta\phi$ , can be produced by a change in frequency,  $\omega$ , or by a change and/or motion of the reflection layer, thus producing a change in the signal path length,  $L_s$ . The reference path remains electrically constant. Then using the definition of the derivative, the change in the phase difference,  $\delta\phi$ , is given by:

$$\delta\phi = \delta(L_s - L_r) \frac{\omega}{c} + (L_s - L_r) \frac{\delta\omega}{c} \quad (2.140)$$

From this equation it can be seen that in the case that the frequency,  $\omega$ , is held constant ( $\delta\omega = 0$ ), the changes in the phase difference can only come from changes in the probing signal path,  $L_s$ , and this is a direct measurement of the motion of the reflection layer. For the other mode, in which it is assumed that there are no changes in the probing signal path ( $\delta(L_s - L_r) = 0$ ), the changes in the phase difference can only come from the change in frequency,  $\delta\omega$ .

Thus in the fixed frequency ( $\delta\omega = 0$ ) mode of operation, the changes in phase difference can be used to measure changes (fluctuations) in the density layer. While in the swept frequency mode (assuming  $\delta(L_s - L_r) = 0$ ) the value of  $L_s - L_r$  can be calculated, and the position of the density layer and hence the density profile can also be calculated.

### 2.5.1 Using the O-mode

Because of the single dependence on the density, the availability of frequency sources in the range of the O-mode, and the simple form of the index of refraction, equation 2.62, the O-mode was the first to gain popularity in the

fusion community. Among the first to work with the O-mode were Anisimov,<sup>17</sup> Anoshkin,<sup>18</sup> and Colchin.<sup>19,20</sup> Some modern fusion experiments using O-mode reflectometers are TFR,<sup>21,77,78</sup> JET,<sup>70,71,141</sup> TFTR,<sup>108</sup> PLT,<sup>80</sup> ASDEX,<sup>129,130</sup> DIII-D,<sup>94-98,135,147</sup> RTP,<sup>24</sup> JT-60,<sup>136</sup> TEXT,<sup>135</sup> and ATF.<sup>85,86</sup>

### 2.5.2 Using the X-mode

Because of the dependence on both the density and the magnetic field, and the complicated form of the index of refraction, equation 2.63, X-mode reflectometry was explored later than O-mode. Some users of X-mode reflectometers are TFTR,<sup>108,109</sup> Wendelstein VII-AS,<sup>26,31</sup> ATF,<sup>85,86</sup> DIII-D,<sup>98-99</sup> ASDEX,<sup>129-132</sup> Uragan-3M,<sup>128</sup> and Petula-B.<sup>43</sup>

## 2.6 Measuring the Density Profile

### 2.6.1 Profile reconstruction using the O-mode

The reconstruction of the density profile using the O-mode is achieved with an Abel inversion technique.<sup>5,8,47,85</sup> The derivation starts with equation 2.88:

$$\phi(\omega) = \frac{2\omega}{c} \int_{r_c(\omega)}^{r_0} n(r, \omega) dr - \frac{\pi}{2} \quad (2.141)$$

which represents the phase change of a probing wave of frequency  $\omega$  after reflection on the cutoff layer. Proceed by differentiating with respect to the probing frequency,  $\omega$ , to obtain:

$$\frac{d\phi(\omega)}{d\omega} = \frac{d}{d\omega} \left( \frac{2\omega}{c} \int_{r_c(\omega)}^{r_0} n(r, \omega) dr - \frac{\pi}{2} \right) \quad (2.142)$$

$$= \frac{2}{c} \left[ \int_{r_c(\omega)}^{r_0} \frac{d}{d\omega} (\omega n(r, \omega)) dr - \omega n(r_c(\omega), \omega) \frac{dr_c(\omega)}{d\omega} \right] \quad (2.143)$$

using the cutoff condition at  $r_c(\omega)$  for  $\omega$ , gives  $n^2(r_c(\omega), \omega) = 0$ , so that the second term above vanishes as long as  $\frac{dr_c(\omega)}{d\omega}$  is bounded. Now equation 2.143 transforms

into:

$$\frac{d\phi(\omega)}{d\omega} = \frac{2}{c} \int_{r_c(\omega)}^{r_0} \frac{d}{d\omega} (\omega n(r, \omega)) dr \quad (2.144)$$

It has been shown by Budden<sup>5</sup> that a packet of waves of frequency  $\omega$  travels with velocity  $V_z$  parallel to the density gradient, where  $V_z$  is given by:

$$\frac{c}{V_z} = \frac{d}{d\omega} (\omega n(r, \omega)) \quad (2.145)$$

where  $V_z$  is the component of the group velocity,  $V_g$ , parallel to the density gradient of the plasma. Then the group refractive index is defined as:

$$n'(r, \omega) = \frac{c}{V_g} \quad (2.146)$$

$$= \frac{d}{d\omega} (\omega n(r, \omega)) \quad (2.147)$$

which allows equation 2.144 to be written as:

$$\frac{d\phi(\omega)}{d\omega} = \frac{2}{c} \int_{r_c(\omega)}^{r_0} n'(r, \omega) dr \quad (2.148)$$

and

$$\tau = \frac{d\phi(\omega)}{d\omega} \quad (2.149)$$

where  $\tau$  is defined as the delay time.<sup>142</sup>

For the particular case of the O-mode, the refractive index is given by equation 2.62 as:

$$n_O(r, \omega) = \left( 1 - \frac{\omega_{pe}^2(r)}{\omega^2} \right)^{\frac{1}{2}} \quad (2.150)$$

where the plasma frequency,  $\omega_{pe}$ , is related to the local electron density by equation 2.34:

$$\omega_{pe}^2(r) \equiv \frac{n_e(r) q_e^2}{m_e \epsilon_0} \quad (2.151)$$

and the probing frequency,  $\omega$ , is given by a similar equation:

$$\omega^2 \equiv \frac{n_e(r_c) q_e^2}{m_e \epsilon_0} \quad (2.152)$$

where  $n_e(r_c)$  is the density at the reflection layer for the probing frequency  $\omega$  (or the cutoff density or the critical density).

From equation 2.150 the group refractive index can be derived, that is:

$$n'(r, \omega) = \left(1 - \frac{\omega_{pe}^2(r)}{\omega^2}\right)^{-\frac{1}{2}} \quad (2.153)$$

Substituting into equation 2.148 yields:

$$\frac{d\phi(\omega)}{d\omega} = \frac{2}{c} \int_{r_c(\omega)}^{r_0} \left(1 - \frac{\omega_{pe}^2(r)}{\omega^2}\right)^{-\frac{1}{2}} dr \quad (2.154)$$

or

$$\frac{d\phi(\omega)}{d\omega} = \frac{2}{c} \int_{r_c(\omega)}^{r_0} \left(\frac{\omega^2}{\omega^2 - \omega_{pe}^2(r)}\right)^{\frac{1}{2}} dr \quad (2.155)$$

Assuming that the function:

$$\omega_{pe} = \omega_{pe}(r) \quad (2.156)$$

is 1 to 1 and onto in the radial and frequency range of the plasma under study, a change of variable on the integration, from  $r \rightarrow \omega_{pe}$ , can be performed, since from equation 2.156 there is an inverse function such that:

$$r = r(\omega_{pe}) \quad (2.157)$$

which is 1 to 1 and onto. Thus equation 2.155 becomes:

$$\frac{1}{\omega} \frac{d\phi(\omega)}{d\omega} = \frac{2}{c} \int_{\omega}^0 \frac{1}{(\omega^2 - \omega_{pe}^2)^{\frac{1}{2}}} \frac{dr}{d\omega_{pe}} d\omega_{pe} \quad (2.158)$$

This transforms it into an Abel-like form:

$$\frac{1}{2\omega} \frac{d\phi(\omega)}{d\omega} = \frac{1}{c} \int_{\omega}^0 \frac{1}{(\omega^2 - \omega_{pe}^2)^{\frac{1}{2}}} \frac{dr}{2\omega_{pe} d\omega_{pe}} 2\omega_{pe} d\omega_{pe} \quad (2.159)$$

$$\frac{d\phi(\omega)}{d(\omega^2)} = \frac{1}{c} \int_{\omega}^0 \frac{1}{(\omega^2 - \omega_{pe}^2)^{\frac{1}{2}}} \frac{dr}{d(\omega_{pe}^2)} d(\omega_{pe}^2) \quad (2.160)$$



Substituting  $\omega_{pe}^2 \rightarrow t$ ,  $\omega^2 \rightarrow x$ , gives:

$$\frac{d\phi(x)}{dx} = \frac{-1}{c} \int_0^x \frac{1}{(x-t)^{\frac{1}{2}}} \frac{dr(t)}{dt} dt \quad (2.161)$$

By making the substitutions:

$$f(x) = \frac{d\phi(x)}{dx} \quad (2.162)$$

and

$$\varphi(t) = \frac{-1}{c} \frac{dr(t)}{dt} \quad (2.163)$$

one obtains the Abel equation given in Arfken:<sup>47</sup>

$$f(x) = \int_0^x \frac{\varphi(t)}{(x-t)^{\frac{1}{2}}} dt \quad (2.164)$$

with solution:

$$\varphi(x) = \frac{1}{\pi} \frac{d}{dx} \int_0^x \frac{f(t)}{(x-t)^{\frac{1}{2}}} dt \quad (2.165)$$

Substituting equations 2.162 and 2.163 into equation 2.165 gives:

$$\frac{-1}{c} \frac{dr(x)}{dx} = \frac{1}{\pi} \frac{d}{dx} \int_0^x \frac{1}{(x-t)^{\frac{1}{2}}} \left( \frac{d\phi(t)}{dt} \right) dt \quad (2.166)$$

Integrating with respect to  $x$ , gives:

$$r(x) - r_0 = \frac{-c}{\pi} \int_0^x \frac{1}{(x-t)^{\frac{1}{2}}} \left( \frac{d\phi(t)}{dt} \right) dt \quad (2.167)$$

Substituting  $\omega_{pe}^2 = t$  and  $\omega^2 = x$ , then yields:

$$r(\omega) = r_0 - \frac{c}{\pi} \int_0^{\omega^2} \frac{1}{(\omega^2 - \omega_{pe}^2)^{\frac{1}{2}}} \left( \frac{d\phi(\omega_{pe})}{d\omega_{pe}} \right) d\omega_{pe} \quad (2.168)$$

which is the final form of the reconstruction formula.

Note that in order to reconstruct the radius it is necessary to know the derivative of the phase delay with respect to the frequency,  $\left( \frac{d\phi(\omega_{pe})}{d\omega_{pe}} \right)$ , rather than the phase delay itself. This is accomplished easily using the identity:

$$\frac{d\phi(\omega)}{d\omega} = \frac{d\phi}{dt} \frac{dt}{d\omega} \quad (2.169)$$

$$= \frac{d\phi}{dt} \left( \frac{d\omega}{dt} \right)^{-1} \quad (2.170)$$

or by other numerical means. Another point to notice is that the integral starts at 0 Hz. A sweep from 0 Hz to some 50 GHz is an impossible task for any known hardware at this time. A way to avoid this problem is to assume a density profile that corresponds to the frequencies from 0 Hz to some more reasonable  $\omega_{low}$  such that the corresponding region of the integral can be calculated numerically and the frequency band is narrow enough for the hardware limitations.

### 2.6.2 Profile reconstruction using the X-mode

**Full phase technique** The refractive index for the X-mode depends on both the density profile and the magnetic field, as shown in equation 2.63:

$$n_X^2 = 1 - \frac{\omega_{pe}^2}{\omega^2} \frac{\omega^2 - \omega_{pe}^2}{\omega^2 - \omega_{pe}^2 - \omega_{ec}^2} \quad (2.171)$$

$$\omega_{pe}^2(r) = \frac{n_e(r)q_e^2}{m_e \epsilon_0} \quad (2.172)$$

$$\omega_{ec}(r) = \frac{q_e B(r)}{m_e} \quad (2.173)$$

where  $\omega_{pe}(r)$  carries the dependence on the density and  $\omega_{ec}(r)$  carries the dependence on the magnetic field. Therefore an analytical inversion such as the one for the O-mode is not known, and numerical methods are necessary to extract the solution.

A particularly nice method has been developed by Doyle<sup>96,99</sup> and will be explained here. Doyle starts by assuming a knowledge of the density profile up to the  $j^{th}$  frequency of the probing array. Then the phase delay for the probing wave of frequency  $\omega_j$  is given by equation 2.88:

$$\phi(\omega_j) = \frac{2\omega_j}{c} \int_{r_c(\omega_j)}^{r_0} n(r, \omega_j) dr \quad (2.174)$$

where the order of the limits has been changed to ensure a positive phase and a term of  $\frac{\pi}{2}$  has been dropped.

For the next frequency,  $\omega_{j+1}$ , Doyle represents the measured phase by the equation:

$$\phi(\omega_{j+1}) = \frac{2\omega_{j+1}}{c} \left\{ \int_{r_c(\omega_j)}^{r_0} n(r, \omega_{j+1}) dr + \frac{1}{2} [n(r_c(\omega_j), \omega_{j+1}) + n(r_c(\omega_{j+1}), \omega_{j+1})] \Delta r(\omega_{j+1}) \right\} \quad (2.175)$$

where  $\Delta r(\omega_{j+1})$  is the increment in radial distance between the reflection point of  $\omega_j$  and the reflection point of  $\omega_{j+1}$ . This equation is like a Simpson's rule representation of the integral of equation 2.174 for the frequency  $\omega_{j+1}$ . Now, by definition of the cutoff condition:

$$n(r_c(\omega_{j+1}), \omega_{j+1}) = 0 \quad (2.176)$$

and from equation 2.175 the increment on  $r$  of the reflection point can be solved as:

$$\Delta r(\omega_{j+1}) = 2 \frac{\phi(\omega_{j+1}) \frac{c}{2\omega_{j+1}} - \int_{r_c(\omega_j)}^{r_0} n(r, \omega_{j+1}) dr}{n(r_c(\omega_j), \omega_{j+1})} \quad (2.177)$$

From this, the new point of reflection for frequency  $\omega_{j+1}$  can be calculated, that is:

$$r_c(\omega_{j+1}) = r_c(\omega_j) + \Delta r(\omega_{j+1}) \quad (2.178)$$

and the density of the cutoff at this point can be calculated from the cutoff condition on the refractive index, i.e., a density can be found such that:

$$n(r_c(\omega_{j+1}), n_{e,j+1}, \omega_{j+1}) = 0 \quad (2.179)$$

to obtain the density at the cutoff point,  $r_c(\omega_{j+1})$ . Now this new cutoff point,  $r_c(\omega_{j+1})$ , and density,  $n_e(\omega_{j+1})$ , can be incorporated into the density profile and the process repeated to the next frequency in an inductive way.

**Phase difference technique** In the dual frequency phase difference technique the phase difference data can be seen as the parts of a puzzle, which

when put together in the right order will give the desired picture. To elaborate on this, start by assuming knowledge of the position  $R_1$  at which the first frequency of the frequency array,  $\omega_1$ , is reflected. This  $R_1$  can be the position of the outer most flux surface or the scrapeoff layer of the limiter. From this assumption the value of the density at  $R_1$  can be calculated, this is  $n_{e1} = n_e(R_1)$ , by using the cutoff condition, i.e.,  $n(R_1, n_{e1}, \omega_1) = 0$ . Now that there is an  $R_1$ ,  $n_{e1}$ , and  $\omega_1$ , one can assume a linear model<sup>96,99</sup> for the density from the edge of the plasma (where the density  $n_e \approx 0$ ) to the first point of reflection ( $R_1, n_{e1}$ ), such that Doyle's method can be used and the full phase data can be reconstructed by using the equation:

$$\phi_{j+1} = \phi_j + \Delta\phi_j \quad (2.180)$$

where  $\Delta\phi_j$  is the phase difference data.

## 2.7 Complications and Error Sources

The validity of the equations for the dielectric tensor, equation 2.36, dispersion relation, equation 2.49, etc; is governed by the validity of the WKB approximation and the geometrical optics approximation. Many conditions in the plasma such as electron cyclotron resonance (ECR) absorption, tunneling, magnetic shear, Doppler effect, movement of the reflection layer with time, etc; can produce breakdown of the initial assumptions and complicate the data beyond recognition. These conditions and their effect on the phase of the reflecting wave will be discussed next.<sup>21,43,70,80,85,86,96-99,141,146</sup>

### 2.7.1 Electron Cyclotron Resonance absorption

Electron Cyclotron Resonance (ECR) absorption of an electromagnetic wave in the plasma occurs when the frequency of the probing wave matches the natural frequency (or the harmonics) of gyration of the electrons at a particular magnetic field strength in the plasma. For the case of toroidal fusion plasmas, the probing wave is launched from the low field side of the plasma in the direction of increasing field and density. For this case there are four possible resonances of concern, two for the O-mode and two for the X-mode. As an example, characteristic cutoff and resonance frequencies for a JT-1 plasma along the minor radius in the equatorial plane and assuming a parabolic density profile with  $n_e(0) = 1.0 \times 10^{19} \text{part}/\text{m}^3$  and  $B_T(0) = 1 \text{ Tesla}$  are shown<sup>69</sup> in Figure 2.6. The curves are as follows:

- A. Upper (fast wave,  $\omega_{X+}$ ) and Lower (slow wave,  $\omega_{X-}$ ) X-mode cutoff frequencies, given by equation 2.67:

$$\omega_{X+} = \frac{\omega_{ec}}{2} + \left( \omega_{pe}^2 + \left( \frac{\omega_{ec}}{2} \right)^2 \right)^{\frac{1}{2}} \quad (2.181)$$

$$\omega_{X-} = -\frac{\omega_{ec}}{2} + \left( \omega_{pe}^2 + \left( \frac{\omega_{ec}}{2} \right)^2 \right)^{\frac{1}{2}} \quad (2.182)$$

B. Plasma frequency, given by equation 2.34:

$$\omega_{pe}^2 = \frac{n_e q_e^2}{m_e \epsilon_0} \quad (2.183)$$

C. First and second harmonics of the electron cyclotron frequency, given by equation 2.26:

$$\omega_{ec} = \frac{q_e B_0}{m_e} \quad (2.184)$$

D. The Upper Hybrid frequency, given by equation 2.65:

$$\omega_{UH}^2 = \omega_{pe}^2 + \omega_{ec}^2 \quad (2.185)$$

For the O-mode there is the electron cyclotron resonance and its harmonics, given by equation 2.26. While for the X-mode there is the Upper and Lower Hybrid resonance frequencies, given by equations 2.65 and 2.66. For the particular case of the X-mode:

$$\omega_{LH} < \omega_{UH} < \omega_X \quad (2.186)$$

where  $\omega_X$  is the cutoff frequency of the X-mode and the right inequality  $\omega_{UH} < \omega_X$  can be shown as follows:

$$\begin{aligned} \left( \omega_{pe}^2 + \omega_{ec}^2 \right)^{\frac{1}{2}} &< \frac{\omega_{ec}}{2} + \left( \omega_{pe}^2 + \left( \frac{\omega_{ec}}{2} \right)^2 \right)^{\frac{1}{2}} \\ \omega_{ec}^2 &< \frac{\omega_{ec}^2}{2} + \omega_{ec} \left( \omega_{pe}^2 + \left( \frac{\omega_{ec}}{2} \right)^2 \right)^{\frac{1}{2}} \\ \frac{\omega_{ec}}{2} &< \left( \omega_{pe}^2 + \left( \frac{\omega_{ec}}{2} \right)^2 \right)^{\frac{1}{2}} \\ 0 &< \omega_{pe}^2 \end{aligned}$$

This shows that for the X-mode the probing wave will always reach the cutoff layer before it can find the absorption layer, except at the very edge of the plasma, where

- A. Lower (slow wave) and upper (fast wave) cutoff frequency, given by equation 2.67.
- B. Plasma frequency, given by equation 2.34.
- C. First and second harmonics of the electron cyclotron frequency, given by equation 2.26.
- D. The Upper Hybrid frequency, given by equation 2.65.

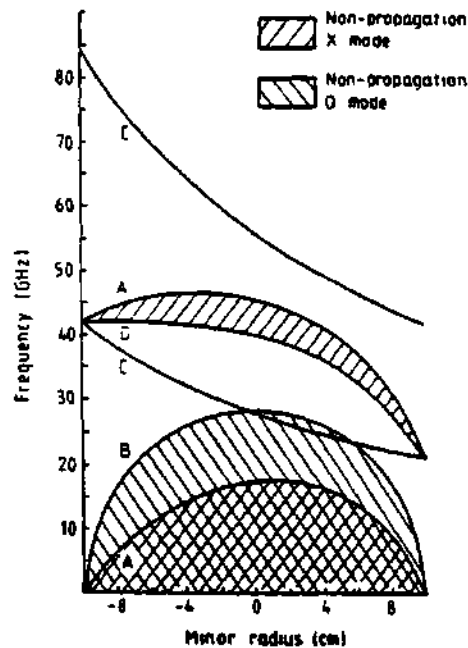


**Figure 2.6: Typical cutoff and resonance frequencies on JT-1.**

the resonance and the cutoff are so close together that some of the power may be absorbed because of tunneling<sup>5,44</sup> and other coupling effects. Another problem at the edge of the plasma is the validity of the geometrical optics approximation condition, equation 2.84:

$$\frac{\omega}{c} \frac{n^2}{\left| \frac{dn}{dr} \right|} = \frac{2\pi L_n}{\lambda} \gg 1 \quad (2.187)$$

where  $L_n \equiv n^2 \left| \frac{dn}{dr} \right|^{-1}$  is the gradient scale length of the refraction index,  $n$ . This condition states that in order for the geometric optics approximation to be valid, the gradient scale length of the index of refraction must be larger than the wavelength of the probing wave.

From the above formulae it can be seen that the lower cutoff (slow wave) and upper hybrid will not interfere with the probing wave, but that the second harmonic of the electron cyclotron resonance may impair the ability to probe the far minor radius of the plasma because of absorption of the probing wave by the the second harmonic of the electron cyclotron resonance at the plasma edge. As an example, using Figure 2.6, for a probing frequency of 45 GHz it can be seen that the wave will be absorbed at the edge of the plasma by the second harmonic of the electron cyclotron resonance and little power will be able to reach the upper cutoff (fast wave) of the X-mode at the inner part of the plasma. Absorption at higher harmonics may be reached, but its coupling to the plasma is usually considered in general weak.<sup>86,51</sup>

### 2.7.2 Tunneling

Early in this chapter, page 37, the solution of the wave equation at the reflecting layer was discussed. In order to obtain a solution it was assumed that the density was *increasing linearly* at the point of reflection. This condition is embodied in equation 2.85 and it is valid throughout most of the plasma except at



the point where the density peaks or flattens out. In this region of flat density the density gradient goes to 0, while the width of the reflection layer and the curvature of the profile becomes large, and the condition for quasi-linearity, equation 2.85, is not valid.

Under the condition of tunneling, a fraction of the wave power will be reflected and another fraction will pass through the point of reflection. The fraction of wave that tunnels may be reflected by the vacuum wall or at some other part of the plasma, producing mixing of the real signal and a *phantom* signal in the detector, thus complicating the extraction of the density profile.

K. G. Budden<sup>5</sup> (1955) also analyzed the interesting occurrence of back-to-back linear and singular turning points.<sup>53,44</sup> This physical situation occurs in our case when the X-wave propagates to the reflection point and tunnels through the evanescent region to reach the Upper Hybrid resonance layer, as it may occur at the very edge of a fusion plasma. Budden considered the wave equation in the form:

$$\frac{d^2 E}{dx^2} + \left( \frac{\gamma}{x} + \frac{\gamma^2}{\eta^2} \right) E = 0 \quad (2.188)$$

and used the substitutions:

$$\xi = \frac{\pm 2i\gamma x}{\eta} \quad (2.189)$$

to reduce the equation to the standard form given by E. T. Whittaker and G. N. Watson<sup>56</sup> (1927) for the confluent hypergeometric function. This gives left and right running waves. The right moving wave passes the zero first and then comes to the singularity and suffers reflection, transmission, and absorption. The coefficients of reflection ( $R$ ) and of transmission ( $T$ ) are:

$$|R| = 1 - \exp(-\pi\eta) \quad (2.190)$$

$$|T| = \exp\left(-\frac{1}{2}\pi\eta\right) \quad (2.191)$$

where  $\eta$  is given by:<sup>53</sup>

$$\eta = |k_{\infty} \Delta x| \quad (2.192)$$

and it represents the number of free space wavelengths (i.e., the wavelength as  $|x| \rightarrow \infty$ ) between the point of  $n = 0$  and the singularity.<sup>53</sup> When the number of wavelengths is small, appreciable tunneling occurs through the evanescent region. When the spacing is large, no tunneling occurs, and the reflection or absorption of the wave is determined entirely by the first turning point encountered by the wave. For the conditions expected in TFTR the reflection and transmission coefficients are plotted in Figure 2.7 for a typical  $n_e \propto \left(1 - \left(\frac{r}{a}\right)^{\alpha}\right)^{\beta}$  density profile plasma and a toroidal field current of  $I_{tf} = 67$  Kamps which gives a magnetic field of  $B_0 = 4.5$  Teslas.

For conditions of very low density (as in the edge of the plasma) and where  $\omega_{ec} \gg \omega_{pe}$ , an expression for the radial spacing in between the Upper Hybrid and the reflection layers is possible. First express  $\omega_{UH}$  and  $\omega_X$  using the binomial expansion theorem and keeping the first order terms, that is, for  $\omega_{UH}$ :

$$\omega_{UH} = \left(\omega_{ec}^2 + \omega_{pe}^2\right)^{\frac{1}{2}} \quad (2.193)$$

$$= \omega_{ec} + \frac{1}{2} \frac{\omega_{pe}^2}{\omega_{ec}} \quad (2.194)$$

and similarly for  $\omega_X$ :

$$\omega_X = \frac{\omega_{ec}}{2} + \left(\omega_{pe}^2 + \left(\frac{\omega_{ec}}{2}\right)^2\right)^{\frac{1}{2}} \quad (2.195)$$

$$= \omega_{ec} + \frac{\omega_{pe}^2}{\omega_{ec}} \quad (2.196)$$

where only the first order terms have been kept.

Next, for any given probing frequency,  $\omega$ , there is the condition:

$$\omega_{UH}(R) = \omega_X(R + \Delta R) \quad (2.197)$$

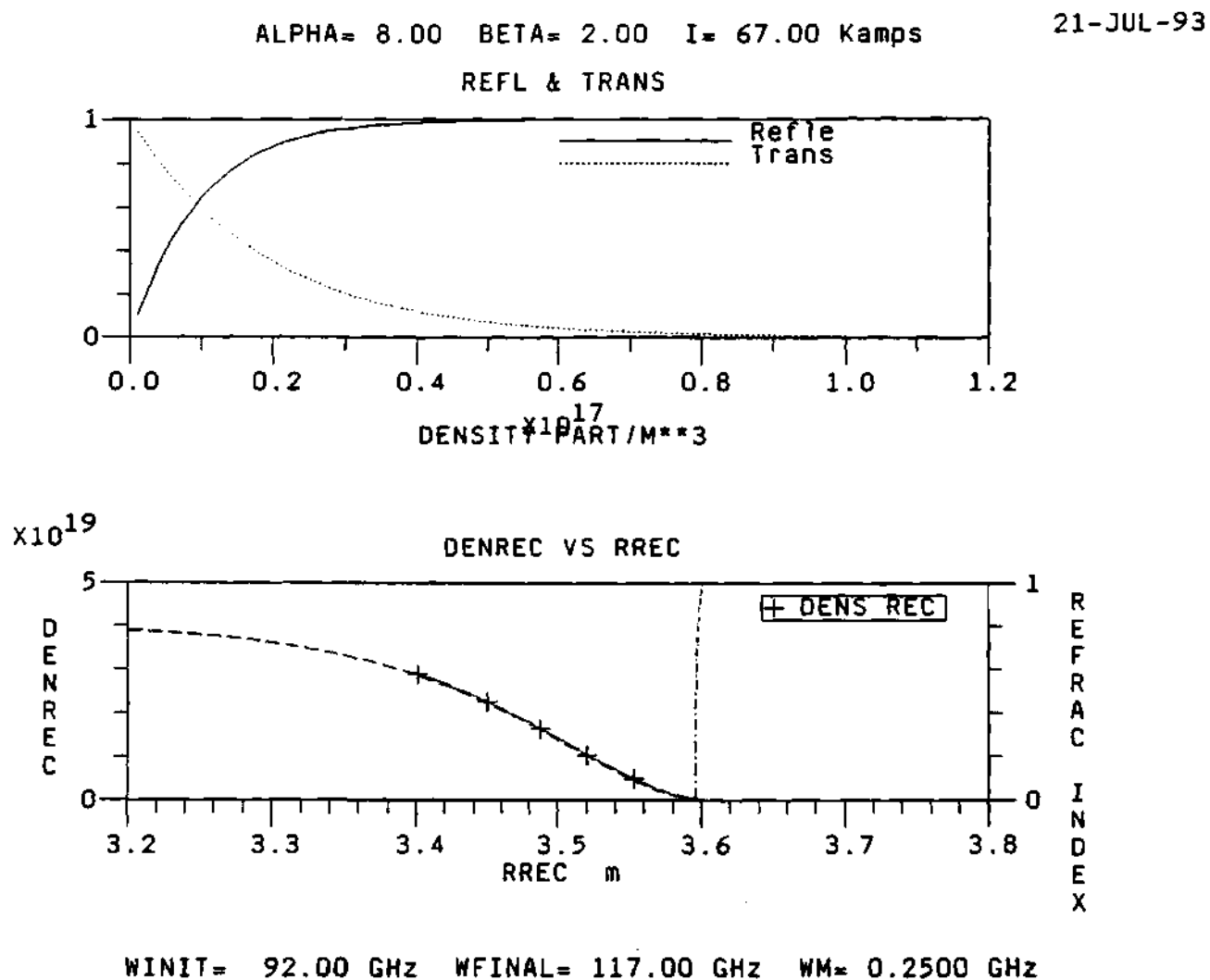


**Figure 2.7:** Reflection and transmission coefficients for a typical TFTR plasma (upper plot). The assumed density profile is included (lower plot) and it is of the form  $n_e \propto \left(1 - \left(\frac{z}{a}\right)^\alpha\right)^\beta$  where all the parameters have been defined before.

which represents the matching condition of the probing wave at both the reflecting layer and the resonance layer. Now, by substituting equations 2.196 and 2.194 into equation 2.197 above and using the definitions for the  $\omega_{pe}$  and  $\omega_{ec}$  (equations 2.34 and 2.26), one finds:

$$\frac{q_e B_0 R_0}{m_e R} + \frac{1}{2} \frac{q_e n_e(R)}{\epsilon_0 B_0 R_0} R = \frac{q_e B_0 R_0}{m_e (R + \Delta R)} + \frac{q_e n_e(R + \Delta R)}{\epsilon_0 B_0 R_0} (R + \Delta R) \quad (2.198)$$

Using the binomial expansion on the term  $(R + \Delta R)^{-1}$  yields:

$$\frac{q_e B_0 R_0}{m_e R} + \frac{1}{2} \frac{q_e n_e(R)}{\epsilon_0 B_0 R_0} R = \frac{q_e B_0 R_0}{m_e R} - \frac{q_e B_0 R_0 \Delta R}{m_e R^2} + \frac{q_e n_e(R + \Delta R)}{\epsilon_0 B_0 R_0} (R + \Delta R) \quad (2.199)$$

which can be simplified to:

$$\frac{B_0 R_0 \Delta R}{m_e R^2} = \frac{(n_e(R + \Delta R) - \frac{1}{2} n_e(R))}{\epsilon_0 B_0 R_0} R + \frac{n_e(R + \Delta R)}{\epsilon_0 B_0 R_0} \Delta R \quad (2.200)$$

for a final result of:

$$\Delta R = \frac{\frac{(n_e(R + \Delta R) - \frac{1}{2} n_e(R))}{\epsilon_0 B_0 R_0} R}{\frac{B_0 R_0}{m_e R^2} - \frac{n_e(R + \Delta R)}{\epsilon_0 B_0 R_0}} \quad (2.201)$$

which holds at the edge of the plasma, where the density is small enough such that  $\omega_{ec} \gg \omega_{pe}$ . For a TFTR plasma, with an edge density of  $n_e(a) \approx 0.1 \times 10^{19} \frac{\text{part}}{\text{m}^3}$  the separation is  $\Delta R \approx 1.5$  cm. The importance of this result is that it provides an analytical formula for the radial spacing between the upper cutoff (fast wave) of the X-mode and the Upper Hybrid resonance frequency layer on the plasma edge. This explains why the amplitude of the receiving signal tends to be rather small at the beginning of the edge of the plasma and increases for frequencies cutoff farther in the plasma.

It is possible to simplify equation 2.201 a little more to the expense of credibility of the result. This is, by taking the limit as the density goes to 0 a

simpler equation can be obtained. In the limit as the density goes to 0,  $n_e \rightarrow 0$ , the following substitutions can be done on equation 2.201:

$$\lim_{n_e \rightarrow 0} \left( n_e(R + \Delta R) - \frac{1}{2} n_e(R) \right) = \frac{1}{2} n_e(R) \quad (2.202)$$

$$\lim_{n_e \rightarrow 0} \left( \frac{B_0 R_0}{m_e R^2} - \frac{n_e(R + \Delta R)}{\epsilon_0 B_0 R_0} \right) = \frac{B_0 R_0}{m_e R^2} \quad (2.203)$$

where the approximation  $n_e(R + \Delta R) \approx n_e(R)$  has been used. Then the radial spacing,  $\Delta R$ , becomes:

$$\Delta R \approx \frac{\frac{1}{2} n_e(R) R}{\frac{\epsilon_0 B_0 R_0}{B_0 R_0} \frac{m_e R^2}{m_e R^2}} \quad (2.204)$$

or as:

$$\Delta R \approx \frac{n_e(R) m_e R^3}{2 \epsilon_0 B_0^2 R_0^2} \quad (2.205)$$

which can be simplified to:

$$\frac{\Delta R}{R} \approx \frac{1}{2} \frac{\omega_{pe}^2}{\omega_{ec}^2} \quad (2.206)$$

### 2.7.3 Magnetic shear

For the geometrical optics approximation in section 2.3.5, it was assumed that there is no coupling in between the X- and O-mode of propagation, i.e., that both modes propagate through the plasma independently of each other. This is not always true for fusion plasmas.<sup>70,74-76,85,118,127,146</sup> The change of the magnetic field angle with respect to the toroidal axis, and therefore the magnetic shear, can produce a coupling of one mode to another.<sup>74</sup> As an example, assume that an O-mode wave is launched (and therefore with  $\vec{E} \parallel \vec{B}$ ) into the plasma. As the wave propagates, the magnetic field will rotate, producing a component of the  $\vec{E}$  field that is parallel to  $\vec{B}$  (for an O-mode wave) and an  $\vec{E}$  component that is perpendicular to  $\vec{B}$  (for an X-mode wave). Therefore, some of the power has been converted from one mode to the other. The resulting mixing of modes makes the

interpretation of the data much more difficult, since the two modes have different refractive indexes and therefore different propagation velocities.<sup>146</sup> In addition, because of the different refraction indexes of the X-mode and O-mode waves, their reflection points and corresponding phase will be different.

The fact that the electron cyclotron emission is generated in two modes of propagation was first noted by Engelmann and Curatolo.<sup>73</sup> They suggested that this phenomena could be used to measure the orientation of the magnetic field at the source of the radiation. Clearly, if the electron cyclotron radiation emerged from the plasma with the same orientation as the electric field at the point of the source, then an experimental determination of its orientation will fix the orientation of the magnetic field at the position of the source. Unfortunately, it has been shown that as the radiation propagates from its source through the plasma and across the sheared magnetic field, there is a tendency of the electric vector field to rotate with the magnetic field.<sup>74-76</sup> Thus, in general, the electric field will not emerge with the same orientation that it had at the position of the source, but at some angle given by the direction of the magnetic field in some low plasma density region near the plasma edge.

In his paper, Boyd<sup>76</sup> gives a set of equations to determine the boundary where the anisotropy overwhelms the shear effects of the magnetic field. The formula is:

$$S = \frac{2c}{\omega} \frac{d\theta}{dr} \approx 2 \frac{\lambda_0}{a} \frac{\psi}{\pi} \quad (2.207)$$

where  $S$  is the shear,  $\lambda_0$  is the free space wavelength,  $a$  is the radius of the plasma and  $\psi$  is the maximum value of the angle between the magnetic field and the toroidal axis,  $\theta$ . Boyd calculates that for a circular cross section tokamak, some typical values are:  $\psi \approx \frac{\pi}{30}$ ,  $\lambda \approx 2 \times 10^{-3}$  m,  $a \approx 0.5$  m, and therefore the value for the shear is  $S \approx 3 \times 10^{-4}$ . This value for the shear will give a very low critical density, and therefore the direction of polarization of the emission will be rotated

due to the magnetic shear.

#### 2.7.4 Motion/fluctuation of the cutoff layer

In section 2.5 the change in phase difference, equation 2.140, was derived for a probing wave in a simplified propagation model. When the frequency sweep method is used, it is assumed that the density layers do not move; that is:

$$\delta(L_s - L_r) = 0 \quad (2.208)$$

Under such conditions the density profile is easily obtainable. The effect of the motion of the reflection layer is best illustrated by the use of an example.<sup>83</sup> Assume the following parameters:

- probing frequency,  $f = 30$  GHz
- frequency sweep,  $\delta f = 0.1$  GHz
- path difference,  $L_s - L_r = 6$  m
- change in path difference,  $\delta(L_s - L_r) = 0.5$  mm.

With this set of parameters, equation 2.140 gives a phase difference of  $\delta\phi = 0.1\pi + 4\pi$ . The term  $0.1\pi$  corresponds to the error associated with the motion of the reflecting layer. The magnitude of this error can lead to serious problems, especially when the frequency is swept slowly over a broad band of frequencies.<sup>69,21</sup> The way to reduce this error is to increase the sweeping rate and reduce the frequency band.

Doyle<sup>99</sup> and others<sup>129,131</sup> report that in measuring the phase delay,  $\phi_p(f)$ , the biggest experimental problem is the one of intrinsic plasma density fluctuations. These density fluctuations add a random Doppler shift to the probing frequency of the measured fringes that can severely distort and/or entirely mask

the desired profile information. The effect of this Doppler shift can be minimized by minimizing the sweep time of the probing beam.<sup>99</sup> Doyle's argument is based on the idea that using a random walk argument, the *rms* deviation from what the count would be in the absence of fluctuations is proportional to  $\sqrt{t}$ , where  $t$  is the sweep time. Therefore, the influence of both forms of phase distortion (fluctuations and Doppler shift) can be minimized by reducing the sweep time, while the desired profile induced phase shift,  $\phi$ , is independent of the sweep time,  $t$ .

### 2.7.5 Fluctuation correlation length

The radial spacing between the reflection points of the Upper and Lower side bands depends on the density gradient in between the two points and the density fluctuations around them. If the reflection points are at places in the plasma where the density fluctuations are uncorrelated, then the radial spacing in between them might fluctuate significantly because of the density fluctuations. This depends on the gradient and size of the fluctuations, and the frequency and time resolution of the reflectometer. On the other hand, if the reflection points are at places in the plasma where the density fluctuations are correlated, then the radial spacing in between them may fluctuate only mildly. Thus, to reduce the fluctuation errors in the measurements the local correlation length of the density fluctuations must be bigger than the local radial spacing in between the reflections points of the side bands.

For TFTR, typical correlation lengths are between 2-4 cm.<sup>110-116</sup> For a typical TFTR density profile, (i.e.,  $n_e \propto \left(1 - \left(\frac{r}{a}\right)^\alpha\right)^\beta$ , with  $\alpha = 8$ ,  $\beta = 2$ , and a toroidal field current of  $I_{tf} = 67$  Kamps which gives a magnetic field of  $B_0 \approx 4.5$  Teslas), shown in Figure 2.8, the model program<sup>117</sup> shows that the expected side band radial spacing is between 0.25 to 0.5 cm, corresponding to the edge and the peak of the density profile. These are well within acceptable boundaries for



the correlation length.<sup>110,112-116</sup>

### 2.7.6 Relativistic effects

Even though the temperature of today's fusion plasmas (10 KeV) is small compared to the rest mass energy of the electron (511 KeV), it has been found<sup>57-62,101</sup> that significant relativistic shifts of the position of the cutoff and modifications of the index of refraction can occur at such low temperatures. This is believed to be caused partially by the high sensitivity of the index of refraction in the vicinity of the cutoff to the plasma response<sup>57-61</sup> due to simple relativistic mass shift.<sup>63</sup> It can be shown, too, that the relativistic modifications of the Hermitian part of the dielectric tensor are larger ( $\times 2$  or  $3$ ) than would be expected from a comparison of the electron temperature with the electron rest mass energy. For the X-mode this can produce a considerable shift of the cutoff (5-10 cm at  $\frac{r}{a} \approx \frac{1}{2}$ ) and an underestimation of the density profile if the cold plasma model is used.<sup>62,63,101</sup> For the X-mode the Upper (right) cutoff effect is considerably larger than for the Lower (left) cutoff.<sup>63</sup>

The Cold and Hot dielectric models are well known and can be found in references such as: Budden,<sup>5</sup> Ginzburg,<sup>8</sup> Swanson,<sup>48</sup> Bornatici,<sup>51</sup> Stix,<sup>53-55</sup> and others.<sup>52,137</sup> The fully relativistic dielectric tensor has been derived by Trubnikov<sup>64</sup> and by Bornatici<sup>51</sup> and the weakly relativistic dielectric tensor by Shkarofsky<sup>65</sup> from Trubnikov's result. The relativistic effect on the index of refraction and the density of the cutoff can be seen in Figure 2.9 for the weakly relativistic model as compared to the cold and hot dielectric models.<sup>58-61</sup> From plots "a", "b", "c", and "d" it can be seen that the refraction index of the wave for the cold and hot models does not change very much ( $T_e \approx 10$  KeV). On the other hand, for the weakly relativistic case, there is a significant difference as compared to the cold and hot models, especially for the X-mode of propagation as compared to the O-mode of

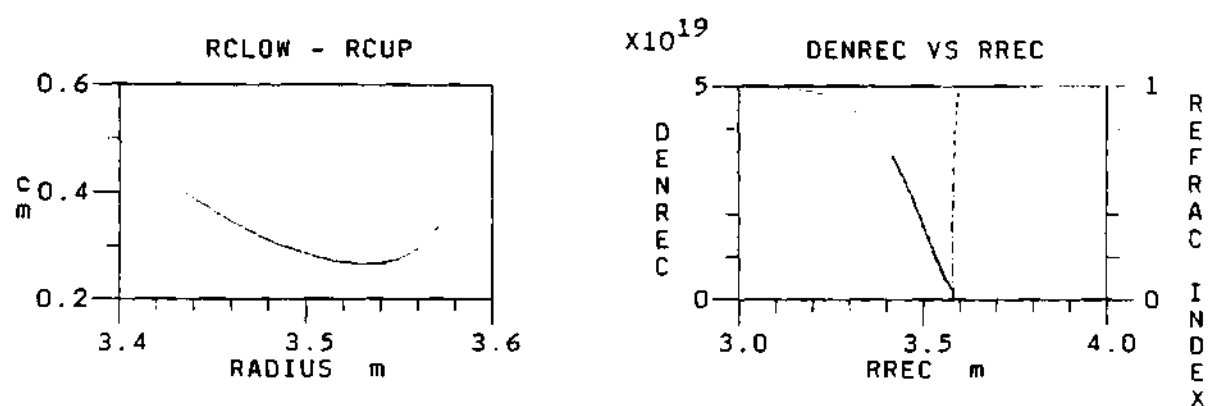


**Figure 2.8: Density profile for a typical TFTR plasma and corresponding radial spacing for the probing side bands.**

propagation. That is, from plots "a" and "b" it can be seen that the change in the density of the O-mode cutoff is much less than that for the X-mode. The frequency for plot "b" is twice that for plot "a", and the change in the density of the cutoff is small, while the frequency change in between plots "c" and "d" is only 10 GHz, and the change of the density is much larger as compared to the O-mode. Plot "f" shows the effect of the temperature on the cutoff density for the X-mode of propagation. A significant change in the cutoff density can be observed as the temperature increases. Even at the common plasma temperature value of  $T_e \approx 10$  KeV, a non-negligible increase of the cutoff density is observed.

The cutoff is deeper into the plasma for the weakly relativistic model, thus causing an underestimation of the reconstructed density profiles, as can be seen from Figure 2.10.<sup>58-61</sup> In these plots the curves for the assumed (actual) density profiles are compared with the reconstructed density profiles using the weakly relativistic refractive index for different plasma temperatures for both the O-mode and the X-mode. A significant underestimation on the density profile can be observed, especially for the X-mode, when plots "a" and "c" are compared with the actual assumed density profile. It can also be seen that the X-mode underestimates the reconstructed density profile more than the O-mode. The plots in Figure 2.10 are as follows:

- A. Plot "a)" shows the actual (assumed) density profile together with the reconstructed density profiles for different plasma temperatures using the O-mode wave.
- B. Plot "b)" shows the actual (assumed) density profile together with the reconstructed density profiles for different plasma temperatures for an X-mode wave.
- C. Plot "c)" is similar to the previous plot but the center density of the plasma

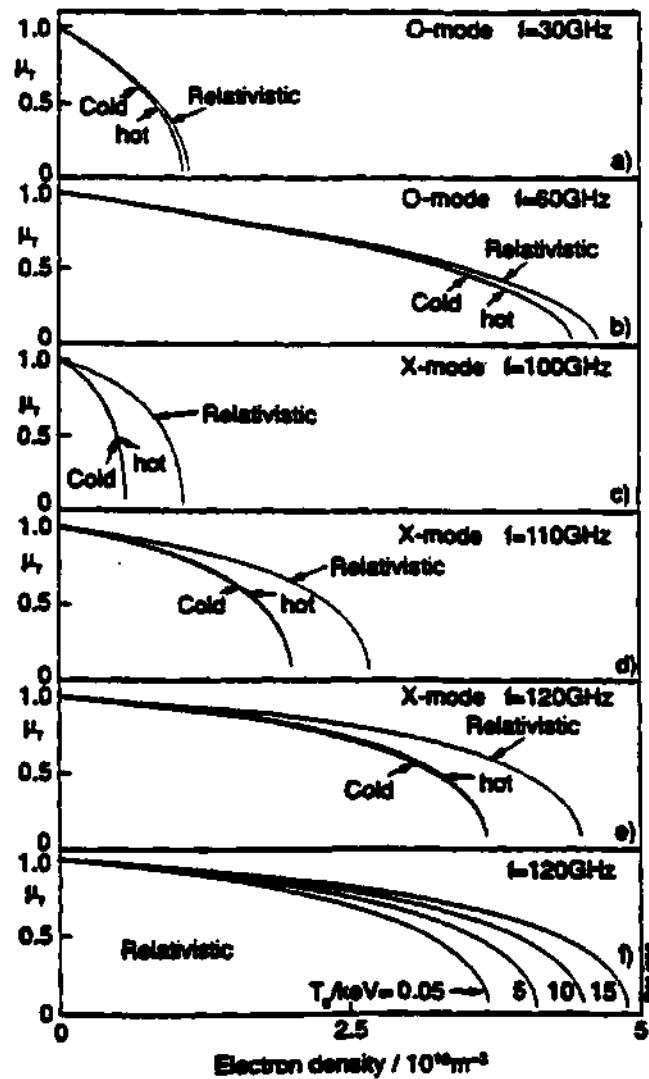


Figure 2.9: Relativistic effect on the index of refraction and the location of the cutoff using the weakly relativistic model.  $\mu_r$  is the refractive index and  $T_e \approx 10 \text{ KeV}$  for plots a to e.

and the magnetic field have been changed to  $n_e(R_0) \approx 3.0 \times 10^{19} \frac{\text{part}}{\text{m}^3}$  and  $B_0 \approx 3.4$  Teslas. An even bigger disagreement between the O-mode and the X-mode can be seen in these plots.

### 2.7.7 Uncertainty in $\omega_X$

The uncertainty in the measurement of the cutoff frequency can be calculated using the propagation of error formula given by Bevington<sup>66</sup> as:

$$\sigma_{\omega_X}^2 = \sigma_{\omega_{ec}}^2 \left( \frac{\partial \omega_X}{\partial \omega_{ec}} \right)^2 + \sigma_{\omega_{pe}}^2 \left( \frac{\partial \omega_X}{\partial \omega_{pe}} \right)^2 \quad (2.209)$$

where  $\sigma_{\omega_X}$  is the uncertainty on the cutoff frequency,  $\sigma_{\omega_{ec}}$  is the uncertainty on the electron cyclotron frequency, and  $\sigma_{\omega_{pe}}$  is the uncertainty on the plasma electron frequency.

Using equation 2.67 for the upper cutoff (fast wave):

$$\omega_X = \frac{\omega_{ec}}{2} + \left( \omega_{pe}^2 + \left( \frac{\omega_{ec}}{2} \right)^2 \right)^{\frac{1}{2}} \quad (2.210)$$

it follows that:

$$\frac{\partial \omega_X}{\partial \omega_{ec}} = \frac{1}{2} + \frac{1}{4} \frac{\omega_{ec}}{\left( \omega_{pe}^2 + \left( \frac{\omega_{ec}}{2} \right)^2 \right)^{\frac{1}{2}}} \quad (2.211)$$

and:

$$\frac{\partial \omega_X}{\partial \omega_{pe}} = \frac{\omega_{pe}}{\left( \omega_{pe}^2 + \left( \frac{\omega_{ec}}{2} \right)^2 \right)^{\frac{1}{2}}} \quad (2.212)$$

for the final result:

$$\sigma_{\omega_X}^2 = \sigma_{\omega_{ec}}^2 \frac{1}{4} \left( 1 + \frac{\omega_{ec}}{2 \left( \omega_{pe}^2 + \left( \frac{\omega_{ec}}{2} \right)^2 \right)^{\frac{1}{2}}} \right)^2 + \sigma_{\omega_{pe}}^2 \left( \frac{\omega_{pe}}{\left( \omega_{pe}^2 + \left( \frac{\omega_{ec}}{2} \right)^2 \right)^{\frac{1}{2}}} \right)^2 \quad (2.213)$$

where  $\sigma_{\omega_{ec}}$  and  $\sigma_{\omega_{pe}}$  are the corresponding uncertainties in the electron cyclotron and plasma electron frequencies, respectively.

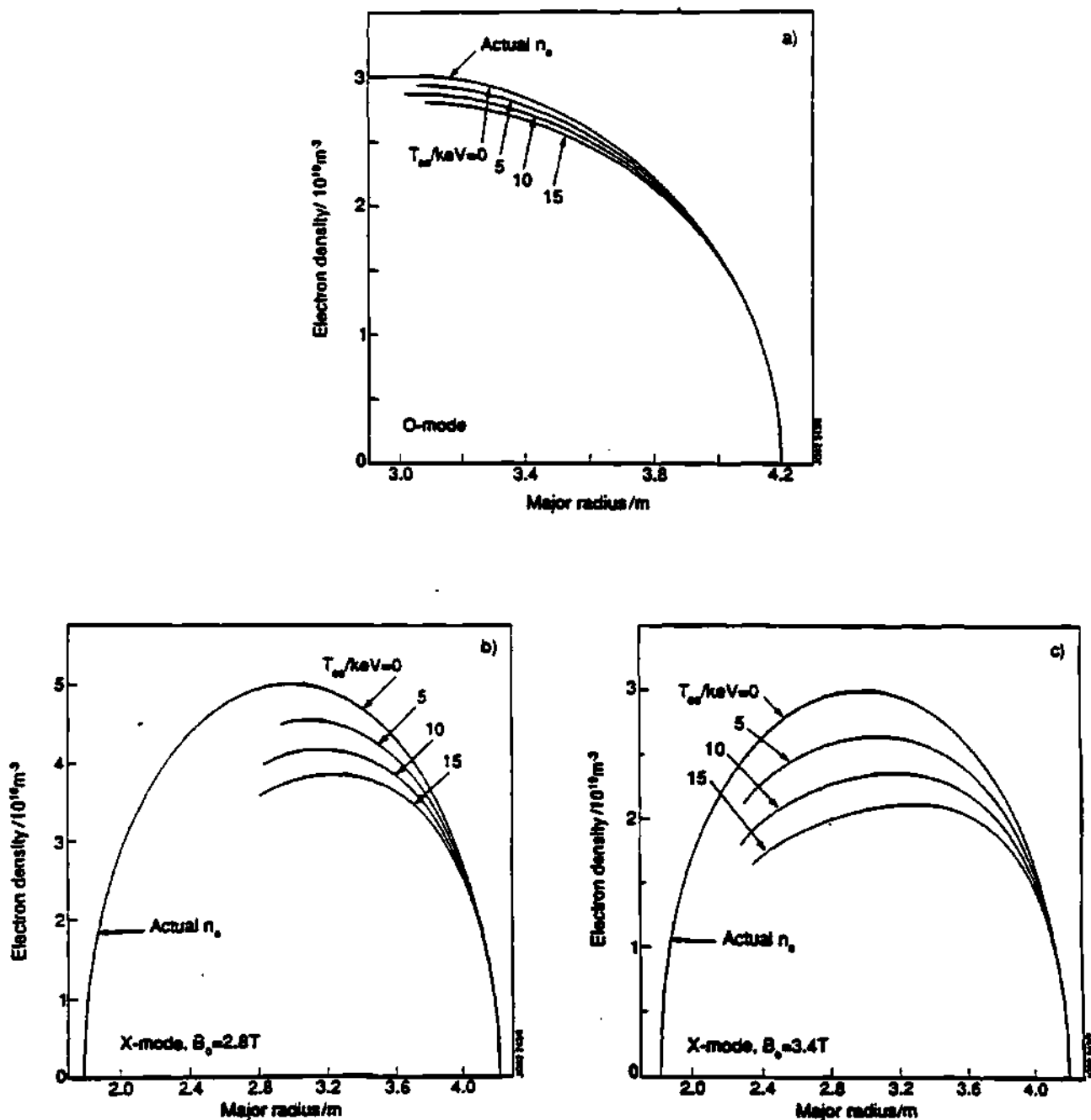


Figure 2.10: Comparison of the actual and reconstructed density profile using the weakly relativistic model.

Next, this uncertainty can be expressed in terms of the uncertainties of the density,  $\sigma_{n_e}$ , and the magnetic field,  $\sigma_B$ , by using the equation:

$$\omega_{pe}^2 = \frac{q_e^2}{m_e \epsilon_0} n_e \quad (2.214)$$

Using propagation of error gives:

$$2\omega_{pe}\sigma_{\omega_{pe}} = \frac{q_e^2}{m_e \epsilon_0} \sigma_{n_e} \quad (2.215)$$

Dividing both sides by equation 2.214 yields:

$$\frac{\sigma_{\omega_{pe}}}{\omega_{pe}} = \frac{1}{2} \frac{\sigma_{n_e}}{n_e} \quad (2.216)$$

And for  $\omega_{ec}$ :

$$\omega_{ec} = \frac{q_e B}{m_e} \quad (2.217)$$

$$\sigma_{\omega_{ec}} = \frac{q_e}{m_e} \sigma_B \quad (2.218)$$

$$\frac{\sigma_{\omega_{ec}}}{\omega_{ec}} = \frac{\sigma_B}{B} \quad (2.219)$$

for a final result of:

$$\sigma_{\omega_x}^2 = \frac{1}{4} \left( \frac{\sigma_B}{B} \right)^2 \left( \omega_{ec} + \frac{\omega_{ec}^2}{(4\omega_{pe}^2 + \omega_{ec}^2)^{\frac{1}{2}}} \right)^2 + \left( \frac{\sigma_{n_e}}{n_e} \right)^2 \left( \frac{\omega_{pe}^2}{(4\omega_{pe}^2 + \omega_{ec}^2)^{\frac{1}{2}}} \right)^2 \quad (2.220)$$

which express the uncertainty of the frequency of the upper cutoff (fast wave) in terms of the uncertainties of the magnetic field and the density. This equation can be used to calculate the uncertainty on the reconstructed density profile if all the other parameters are known or are measurable from other diagnostics.

## 2.8 Summary

This chapter presents a brief history of the beginnings of reflectometry, a derivation of the cold plasma dielectric tensor, a description of the different

reflectometry techniques, and a discussion of the complications and error sources that one can expect to find on this type of diagnostic.

This review of electromagnetic theory in plasma is essential to understanding plasmas and reflectometry. This gives the researcher the knowledge needed to understand the different phenomena that occur in a plasma and how any electromagnetic wave, including that of a reflectometer, propagates through the plasma. This chapter and the theory covered within it provide a set of formulae that can be used to calculate parameters such as the frequency band for the cutoffs, the relative position of the cutoffs, and the electron cyclotron resonances; the formulae necessary to calculate the theoretical phase to model the wave propagation and test the technique; and complications that can be associated with the measurement.



## CHAPTER III

### ION CYCLOTRON RESONANCE HEATING

#### 3.1 Introduction

In order to achieve fusion, the particles must have enough kinetic energy to overcome the Coulomb repulsive force during a collision. Such energy is provided in the form of heat, and the temperatures must be on the order of 10 to 20 KeV.<sup>1,169</sup> This is the range at which the cross section of the D-T reaction is the greatest.<sup>1,169</sup> Among present day heat sources for plasmas there are:

1. Ohmic heating (OH)
2. Neutral Beam Injection (NBI)
3. Electron Cyclotron Resonance Heating (ECRH)
4. Adiabatic compression
5. Ion Cyclotron Resonance Heating (ICRH)
6. Fusion Alpha Heating
7. Lower Hybrid Heating (usually associated with current drive)

For ohmic heating the current that flows in the plasma transfers its energy to the particles through collisions and frictional effects, providing an intrinsic

heating mechanism. Unfortunately, it can be shown that the ohmic power transfer saturates as the temperature increases (at around 3-4 KeV);<sup>1,169</sup> thus, fusion probably can not depend entirely on ohmic heating to achieve fusion temperatures.

Neutral Beam Injection (NBI) has successfully provided additional heating and refueling capabilities, but it has been found that it degrades confinement of energy in toroidal devices. Neutral Beam Injection has a coupling in between heating and refueling of the plasma. For experimental purposes it makes it more complicated to study the independent effect of heating and refueling on the plasma. Electron Cyclotron Resonance Heating (ECRH) is starting to prove itself as a heating method and has a high dollars/Watt.<sup>160</sup> Adiabatic compression does not work well in small volumes (requires large volumes), for heating electrons, and it does not have the positioning capabilities of RF schemes and NBI.<sup>169</sup>

Ion Cyclotron Resonance Heating (ICRH) methods have been used successfully to heat ions in fusion plasmas for the past 25 years, particularly in tokamaks<sup>148-151</sup> and other<sup>9,152-155</sup> fusion devices, over a wide range of confinement regimes, including H-mode.<sup>156</sup> In addition to provide a main source of auxiliary heating, several other functions are served by ICRH (RF) such as plasma ionization, plasma temperature profile control, MagnetoHydroDynamic (MHD) stabilization and current drive. One major advantage of ICRH (or radio frequency heating, or rf) is that the position of the energy absorption layer is highly controllable as compared with other heating mechanisms such as Ohmic heating and Adiabatic compression.<sup>169</sup> Thus, the position of the absorption layer can be controlled so as to change the current density and temperature profiles.<sup>1,169</sup> These changes in the density and temperature profiles can be coordinated to suppress plasma instabilities (like sawteeth<sup>171,172</sup>), enhance confinement, and control plasma transport.<sup>169</sup> Another major advantage of ICRH (rf) is in the area of current drive, since when a wave is sent into a tokamak at an angle to the major radius, it is capable of being

absorbed in such a way as to set up a directional drift of electrons around the torus.<sup>169</sup> This together with the control of the position of the absorption layer can be used to change the current profile. This is of extreme importance, since many important MagnetoHydroDynamic (MHD) instabilities in tokamaks are current driven.<sup>169,157-159</sup> Thus, the ICRH (rf) power deposition profile might be controlled so that MHD instabilities can be avoided or suppressed.

At the moment NBI and ICRH (rf) are the methods most widely used to heat large tokamaks. For example, JET has 22 MW of ICRH power while TFTR has 12.5 MW<sup>161</sup> of power available in the rf range.<sup>160,263</sup> Due to its flexibility and relative low cost, ICRH is becoming a leading supplemental heat source for toroidal experiments.

## 3.2 Theory

### 3.2.1 Radio frequency heating schemes

The schemes that have been used for rf heating in tokamaks fall into four main frequency ranges; within which waves excited at the edge of the plasma may propagate into the central region of the plasma where they can be absorbed. The frequencies involved depend on many plasma parameters. The values given here are simply indicators of what is typical in present day fusion experiments. The lowest in frequency is the Alfvén wave, involving waves at a frequency of a few megahertz. This is well below the ion cyclotron frequency of a typical tokamak, so the waves involved are the shear and the compressional Alfvén waves. Next comes the ion cyclotron range of frequencies at a few tens of megahertz. This is presently the method most widely used to heat large tokamaks. Increasing the frequency to a few gigahertz leads to the Lower Hybrid range, which has been particularly successful for current drive experiments. Finally, electron cyclotron

heating (also called UH resonance or electron cyclotron harmonic) occurs at frequencies of around 30 GHz and upward. Development of this method has, to some extent, been held back by the difficulties of manufacturing high power sources at the necessary high frequencies.

### 3.2.2 Multiple species dielectric tensor

The theory of wave propagation and absorption in the ion cyclotron range of frequencies is the same one discussed in section 2.3 for the propagation of the reflectometer beam in the plasma. In this section this theory will be reviewed, which can explain more complicated heating mechanisms like ion-ion heating and minority species heating. The effects of multiple species (electrons and different kinds of ions) is included in the current density as:

$$\vec{J} = \sum_s n_s q_s \vec{v}_s \quad (3.1)$$

and the equation of motion of each species as:

$$\frac{d\vec{v}_s}{dt} = \frac{q_s}{m_s} (\vec{E} + \vec{v}_s \times \vec{B}) \quad (3.2)$$

where the subscript "s" is used to designate the species (electrons and/or ions) and the other variables are the density,  $n_s$ ; particle charge,  $q_s$ ; velocity,  $\vec{v}_s$  and mass,  $m_s$  of the particular species. Following the procedure in section 2.3.2 and using the equations for the current density, equation 3.1, and the equation of motion, equation 3.2, the velocity components for the particles of species "s" are given by:

$$v_{sx} = \frac{q_s (i\omega E_x - \epsilon_s \omega_{cs} E_y)}{m_s (\omega^2 - \omega_{cs}^2)} \quad (3.3)$$

$$v_{sy} = \frac{q_s (\epsilon_s \omega_{cs} E_x + i\omega E_y)}{m_s (\omega^2 - \omega_{cs}^2)} \quad (3.4)$$

$$v_{sz} = \frac{iq_s}{m_s \omega} E_z \quad (3.5)$$

or in matrix form as:

$$\begin{pmatrix} v_{sx} \\ v_{sy} \\ v_{sz} \end{pmatrix} = \begin{pmatrix} \frac{iq_s \omega}{m_s(\omega^2 - \omega_{cs}^2)} & -\frac{\epsilon_s q_s \omega_{cs}}{m_s(\omega^2 - \omega_{cs}^2)} & 0 \\ \frac{\epsilon_s q_s \omega_{cs}}{m_s(\omega^2 - \omega_{cs}^2)} & \frac{iq_s \omega}{m_s(\omega^2 - \omega_{cs}^2)} & 0 \\ 0 & 0 & \frac{iq_s}{m_s \omega} \end{pmatrix} \cdot \begin{pmatrix} E_x \\ E_y \\ E_z \end{pmatrix} \quad (3.6)$$

where  $\omega$  is the frequency of the electromagnetic wave,  $\omega_{cs}$  is the corresponding cyclotron resonance frequency of species "s", and  $\epsilon = \frac{q_s}{|q_s|}$ .

Next, substituting the equation for the species velocities, equation 3.6, into the current density, equation 3.1, it can be obtained:

$$\begin{pmatrix} J_x \\ J_y \\ J_z \end{pmatrix} = \begin{pmatrix} \sum_s \frac{n_s q_s^2}{m_s} \left( \frac{i\omega E_x - \epsilon_s \omega_{cs} E_y}{\omega^2 - \omega_{cs}^2} \right) \\ \sum_s \frac{n_s q_s^2}{m_s} \left( \frac{\epsilon_s \omega_{cs} E_x + i\omega E_y}{\omega^2 - \omega_{cs}^2} \right) \\ \sum_s \frac{n_s q_s^2}{m_s} \frac{E_z}{\omega} \end{pmatrix} \quad (3.7)$$

which can be substituted on the right hand side of the generalized Ampère's law as:

$$\vec{J} - i\omega\epsilon_0\vec{E} = -i\omega\epsilon_0\vec{K} \quad (3.8)$$

where the dielectric tensor is defined by:

$$\vec{K} \equiv \begin{pmatrix} S & -iD & 0 \\ iD & S & 0 \\ 0 & 0 & P \end{pmatrix} \quad (3.9)$$

where:

$$S \equiv \frac{1}{2}(R + L) \equiv 1 - \sum_s \frac{\omega_{ps}^2}{\omega^2 - \omega_{cs}^2} \quad (3.10)$$

$$D \equiv \frac{1}{2}(R - L) \equiv \sum_s \frac{\epsilon_s \omega_{ps}^2 \omega_{cs}}{\omega(\omega^2 - \omega_{cs}^2)} \quad (3.11)$$

$$P \equiv 1 - \sum_s \frac{\omega_{ps}^2}{\omega^2} \quad (3.12)$$

$$R \equiv S + D \equiv 1 - \sum_s \frac{\omega_{ps}^2}{\omega(\omega + \epsilon_s \omega_{cs})} \quad (3.13)$$

$$L \equiv S - D \equiv 1 - \sum_s \frac{\omega_{ps}^2}{\omega(\omega - \epsilon_s \omega_{cs})} \quad (3.14)$$

$$\omega_{ps}^2 \equiv \frac{n_s q_s^2}{m_s \epsilon_0} \quad (3.15)$$

$$\omega_{cs} \equiv \frac{q_s B}{m_s} \quad (3.16)$$

These equations are very similar to the ones derived in the previous chapters, but they include the effect of multiple ion species, which describe other more subtle effects like ion-ion and minority heating in fusion plasma.

### 3.3 ICRH and Plasma Edge Interaction

The plasma edge has always been of utmost importance to ICRH experiments, since it is the interface in between the antenna/launching structure and the bulk of the plasma interior. This interaction is becoming more important because of its role in understanding the plasma confinement and the control of the plasma composition. This interaction is bidirectional and sometimes even circular, in the sense that the ICRH influences the plasma edge directly or indirectly, through power deposition, ponderomotive effects, waves, sheath effects, induced electric field, and fluctuations. The plasma edge influences the ICRH by its effects on the antenna coupling and loading, see Figure 3.1,<sup>193</sup> impurity production, sputtering, etc. Most of the different phenomena and effects appeared to be specific to each machine and depend significantly on the different wall and limiter configurations, as well as the different plasma and heating conditions of the experiments, e.g., TFR,<sup>174,211</sup> PLT,<sup>175,176,214,233</sup> TORE SUPRA,<sup>177</sup> MACROTOR,<sup>229</sup> JIPPT-IIU,<sup>179</sup> JFT-2M,<sup>215,180</sup> URAGAN-3,<sup>181,182</sup> Alcator C,<sup>183,184</sup> ASDEX,<sup>185,230,235</sup> TEXTOR,<sup>186-189</sup> JET,<sup>241,190,191</sup> JT-60,<sup>192</sup> etc.

This section will describe the most important ICRH and plasma edge interactions; cause and effects (which are easily confused) will be presented.

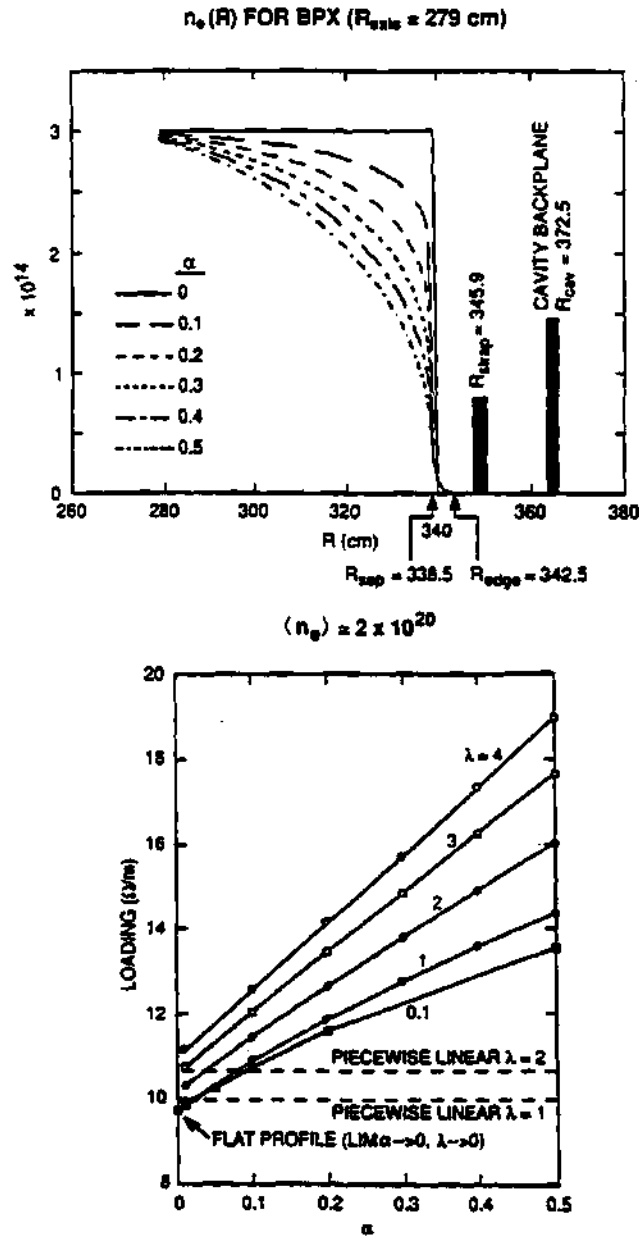


Figure 3.1: Typical parabolic density profiles of the form:  $\left(1 - \left(\frac{r}{a}\right)^2\right)^\alpha$  and antenna loading vs the profile shape exponent,  $\alpha$ , and the scrapeoff decay length,  $\lambda$ . (Batchelor, et al., Fusion Tech., Vol. 21 (1992) p. 1214)

### 3.3.1 Pre-history

For the ion cyclotron resonance frequency domain, the cold plasma dispersion relation has two branches that can be used to heat up the plasma. These are the slow wave (or also called the shear wave, or the torsional Alfvén wave, or the left hand wave), which propagates below the frequency of the ion cyclotron gyration frequency and can only penetrate to the central core of the medium density machines of the early times<sup>194</sup> and the fast wave (or compressional wave, or hydromagnetic wave, or right hand wave), which propagates above a minimum density.<sup>195</sup> The slow wave was initially used in early machines because it has a simple damping mechanism, since its electric field is circularly polarized in the ion gyration direction. During the early high power experiments in the C-stellarator,<sup>196</sup> researchers observed a massive influx of impurities following the start of the ICRH power, accompanied by an anomalous loading of the coil, and they originally ascribed this phenomenon to the coupling to a mode called the “Mode X”. The origin of the impurities was localized in the vicinity of the induction coil. This impurity influx was due to the sheath rectification effect. This occurred because the electric field component,  $E_z$ , parallel to the magnetic field,  $B_z$ , between the turns of the induction coil would penetrate the tenuous outer plasma layer. This caused the electrons to be accelerated in the  $B_z$  direction, producing a spatial charge buildup, which in turn accelerated the ions into the wall. This effect has been observed 20 years earlier in linear plasmas discharges,<sup>197</sup> and its mechanism has been explained by Butler.<sup>198</sup> Short ICRH pulses had been used in the early machines to try to reduce the influx of impurities. Later, the implementation of a Faraday shield screen shorted out these  $E_z$  fields and reduced the impurity influx by an order of magnitude.

With the increasing success of the tokamak with higher densities and longer pulse times, the poor coupling of the slow wave at the higher densities became a



concern, and the use of short rf pulses could not be used to avoid the impurity production problem. This was when the studies of the fast wave for ICRF heating became important. Experiments using the fast wave for ICRH were performed in tokamaks like TM-1 VCh in Moscow<sup>198-202</sup> and in the ST-tokamak at Princeton.<sup>203-205</sup> Even though the fast wave is circularly polarized in the direction of gyration of the electrons and the damping mechanism is not as simple as for the slow wave, three damping methods were found to absorb the wave in the plasma. These methods are:

1. Using the second harmonic of the wave, since even in single species plasmas the wave has a component in the ion gyration direction.
2. The wave can be damped by the minority species of a two species plasma.
3. By launching the wave from the high field side of the plasma, the wave can reach the ion-ion hybrid resonance, at which it can be mode converted and damped.

### 3.3.2 The impurity problem

As solutions to the problems of launching and propagation of the wave were found, the problem of the effectiveness of heating became a concern. The negative effects of ICRH, and in particular the problem of increased impurity influx in the plasma, could no longer be ignored by shortening the ICRH pulse length. In order to pinpoint the possible causes of impurity influx, the specific machine dependent effects had to be avoided. For example, in TFR it took first the avoidance of ripple trapped ions to realize that the direct rf interaction with the edge was the cause of the additional impurity problems.<sup>206</sup> The influx of particles was strongly reduced by operating in the mode conversion regime rather than the minority

heating regime. After a lot of debate, the cause for this specifically edge related increased impurity production was attributed to two possible causes:

1. ICRH and plasma edge interaction can increase impurity production.
2. ICRH could be changing the transport of impurities from the edge to the center of the plasma.

In both cases it was important to identify where and how the change was taking place.

As higher ICRH power became possible, an increased influx of metallic impurities to the plasma center was observed. With the increase in plasma pulse length, the increase in impurities produced a decrease in central electron temperature of the plasma. The attention turned to changing the materials of the antenna to avoid and/or reduce the production of impurities.<sup>207-211</sup> Experiments with different materials for the antenna and Faraday shields reduced significantly the production of impurities, but could not reduce the high amounts of Nickel (Ni) in the center of the plasma, thus pointing to the vacuum wall as a non-negligible source of impurities.<sup>211,212</sup> Measurements of the density and temperature at the scrapeoff layer showed an increase in the density and temperature for both the ions and the electrons. These were seen as the main reasons for the increased interaction with the wall.<sup>211,212</sup> After a lot of work, the mechanism was thought to be related to direct interaction between the rf and the plasma edge.<sup>211,212</sup>

Careful planning and selection of the ICRH antenna material has been shown to reduce significantly the production of impurities in the plasma. An example of this is the PLT tokamak at Princeton, in which the use of Carbon limiters and strong Titanium gettering to reduce Oxygen content in the plasma helped to reduce impurity production. This allowed for the study of other sources of impurities, such as the enhanced influx of particles from the surface of the

plasma due to the rf interaction.<sup>213</sup> Detailed analysis of the changes in density at the edge were performed using a low-energy neutral spectrometer. A large increase of the low-energy neutral hydrogen efflux during ICRF heating was observed.<sup>213</sup> The edge density increased by an order of magnitude in some cases. Thus, it was concluded that the application of ICRH increases the radial transport, thereby increasing the edge density and the plasma interaction with the vacuum wall.<sup>213</sup> Further experiments with the position of the resonance layer and the minority concentration pointed out a correlation between the density increase and the wave absorption.<sup>214</sup> That is, the increase in plasma edge density was a minimum when the wave absorption was a maximum.

Other effects seem to be responsible for the impurity production in other machines. In JFT-2M, sputtering induced by ions accelerated by the electric field near the antenna was proposed as an explanation for the impurity production.<sup>215-217</sup> The effect of this mechanism could be controlled in two possible ways: the phasing of the antennas and the choice of the material in the antenna neighborhood. The operation of the antennas out of phase (i.e., the electric field of the radiating elements of the antennas are  $\pi$  radians out of phase) reduced the levels of metallic impurities significantly,<sup>218,219</sup> while the installation of carbon blocks on the wall in the vicinity of the antennas greatly reduced the difference between the in phase and out of phase operation,<sup>220</sup> supporting the theoretical prediction that the electric field near the antenna played a dominant role in inducing the metallic impurity release. Reduction of metallic impurities has been observed in TFTR when the ICRH antennas are operating in an out-of-phase mode.<sup>249</sup>

### 3.3.3 Antenna phasing

The influence of antenna phasing is one of the most important phenomena studied in ICRH plasmas. In almost all experiments with two or more radiating

elements (antennas), there is a distinct advantage to driving the antennas in an out of phase configuration (dipole configuration) as opposed to driving the antennas in an in phase configuration (monopole configuration). Heating efficiencies are 20–30% lower, and both low- and high-Z impurities are 30–50% higher when the antennas are used in the in phase (monopole) configuration.<sup>250</sup> Local arcing of the antennas has been observed only during the operation of the in phase (monopole) configuration.

### 3.3.4 The sheath rectification effect

The sheath rectification effect was first seen 20 years ago in linear plasma discharges.<sup>222,223</sup> This effect works by creating a potential in the direction of the field lines in front of the antenna. Where these field lines intercept the Faraday screen, the rf potential will be rectified, and the ions around these field lines will be accelerated into the screen, creating impurity ions off the Faraday screen that will migrate to the plasma. Calculations have shown that under these conditions, the electric field would be enhanced in the immediate vicinity of the Faraday screen, resulting in an increased induced potential.<sup>221</sup> Numerical simulations indicated that field lines in the antenna neighborhood can acquire an rf potential, even if not by direct induction, so that the sheath rectification effect could be retained as the fundamental driving mechanism for the impurity generation.<sup>222,223</sup>

Perkins<sup>224,225</sup> and Myra<sup>226</sup> have proposed a mechanism in which parallel electric fields associated with the antenna can give rise to a significant increase of the energy of the ions impacting the Faraday shield. As a result of the parallel electric fields, the sputtering yield is much higher than the one expected for ions that fall through the normal Bohm sheath. The source of the parallel electric fields may come from the rf sheath (image charges) that are produced from the misalignment between the Faraday shield elements and the magnetic field lines.<sup>224,225</sup>

Caughman<sup>227,228</sup> and others<sup>229,230</sup> have found evidence of increased electron temperature, plasma potential and ion energy near the Faraday shield. In his experiment, the time varying floating potential followed the magnetic field pattern of the antenna, indicating that the electromagnetic field is responsible for the potential formation. The increase in the ion energy can be at least partially explained by an increase in the sheath potential, which in turn is caused by an increase in the electron temperature. These high energy ions that are produced in front of the ICRH antenna contribute to the sputtering and the production of impurities into the plasma.<sup>231</sup>

### **3.3.5 Self sputtering and avalanche**

The different reactions of the different materials to the antenna induced impurity and the sheath rectification effect was resolved by a theoretical model proposed for JET.<sup>235</sup> The sputtered impurities produced by the sheath rectification effect could be re-ionized and accelerated back into the wall, producing more impurities; hence, the name self-sputtering. This process could become unstable and self-amplifying, producing an avalanche effect in the generation of sputtering ions.

### **3.3.6 Increased diffusion at the edge**

Radial electric fields were observed in early fusion experiments. It has been suggested that these radial electric fields could create flows in the plasma.<sup>233-237</sup> This will create convective flow cells that will change the edge transport. Convective cells flow was analyzed by D'Ippolito<sup>238</sup> and it was found that radial electric fields could lead to the required rf enhanced diffusion at the edge. Direct evidence of convective cell was found by measurements of the electric field in the edge and by edge fluctuation measurements.<sup>239,240</sup> Edge electric fields are observed in H-mode

transition layers in DIII-D.<sup>115</sup>

Associated with these effects are changes in the edge scrapeoff layer. This typically includes an increase in the electron temperature, increase in the edge density and an increase of the scrapeoff lengths.<sup>241,242</sup> This is significant, since the last of these suggests that an rf-induced edge transport mechanism is in effect. Work by Greene,<sup>243</sup> Taylor,<sup>233</sup> and Van Nieuwenhove<sup>244</sup> demonstrated the formation of D.C. edge potentials considerably larger than the ones expected from the normal Bohm sheaths.

### 3.3.7 Quiver induced losses

Because of the high electromagnetic fields at the interface between the plasma and the antenna, the *quiver* motion of particles (the velocity component associated with the effect of the rf fields as the particles pass by the antenna) passing near the antenna can drift into the Faraday shield and wall, thus producing direct losses of particle and inducing sputtering into the plasma. It was found<sup>245</sup> that the quiver motion of ions can lead to particle energies considerably in excess of thermal energies, and that the rf can induce ion transport into the Faraday shield. The Faraday shield small scale non-uniformity produces a significant perpendicular ponderomotive force on the ions, leading to a diffusion coefficient of about two times Bohm.

### 3.3.8 Ponderomotive effects

Lehrman<sup>245</sup> has done an analysis of the trajectories for the electrons and ions due to the antenna near fields. It was found that the electrons were mainly unperturbed, while the ions experience a strong perpendicular ponderomotive drift force due to the large evanescent fields in the vicinity of the Faraday shield. The flow in the vicinity of the Faraday shield is alternatively radially inward and out-

ward as a consequence of the local electric fields in the shield gaps. Because ions reaching the Faraday shields are lost, there is an outward flux of particles.

### 3.4 Antennas in Fusion Experiments

There are many kinds of antennas currently in use in fusion plasmas.<sup>246</sup> They have different characteristics with respect to coupling to the plasma, resistance to the plasma environment, power delivered, voltage limits, frequency domain, etc. M. Kwon<sup>259</sup> made some measurements of the coupling of these parameters to the Faraday shields on different ICRH antennas. The most common antennas in use today are:<sup>246-257</sup>

1. The simple (short) loop is characterized by a total length that is short compared to the free space wavelength of the wave. It can be represented by an inductor and a resistor in series, as shown in Figure 3.2. It is not matched at the feed point.
2. A natural extension of the short loop is the long loop antenna shown in Figure 3.2 and used on Alcator-C,<sup>246,247,260,261</sup> Figure 3.3. Because the dimensions are large compared to the wavelength, the circuit representation must be a distributed circuit. Like its relative the short loop antenna, it requires matching.
3. The cavity antenna shown in Figure 3.4 follows. This kind of antenna is used in the DIII-D experiment.<sup>170,246</sup> It uses a tuning capacitor and corresponding feed point to provide a match at the feed point for a certain load.
4. The Resonant Double Loop (RDL) and the Asymmetric Resonant Double Loop (ARDL), shown in Figure 3.5, which are both matched at the feed

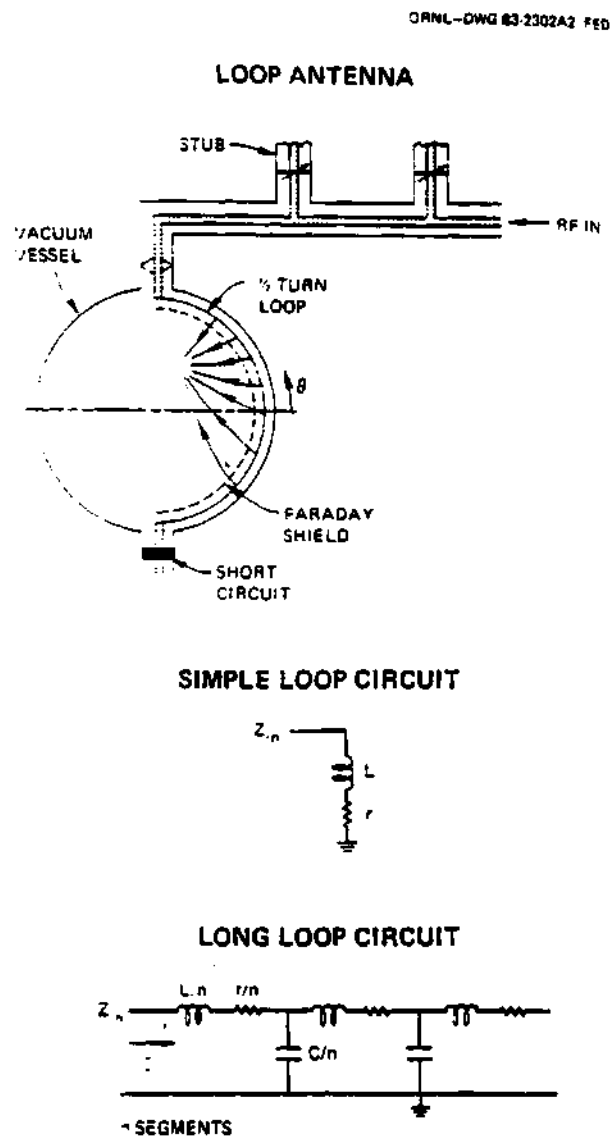


**Figure 3.2: Loop antenna and circuit representation of both, the short and long loop versions.**



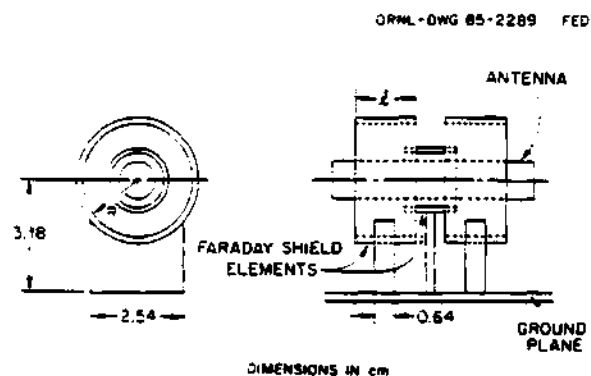


**Figure 3.3: Long loop antenna used in Alcator-C.**

point over both frequency and load ranges by means of two tuning capacitors. RDL antennas have been used successfully in TFTR,<sup>247</sup> TORE-SUPRA<sup>247,257,259</sup> and elsewhere.<sup>173</sup> Their particular details can be found in the references.<sup>246,247</sup>

5. Finally, the U-slot antenna, shown in Figure 3.6,<sup>262</sup> which is tunable over load and frequency ranges by two tuning capacitors.

A list of experiments and corresponding operational parameters is shown in Table 3.1.<sup>162-168</sup>

### 3.5 TFTR Antenna

TFTR's ICRF antenna has been the subject of much work. Some of the references are: J. R. Wilson,<sup>248</sup> D. J. Hoffman,<sup>246,247</sup> D. T. Taylor,<sup>257</sup> J. F. King,<sup>256</sup> J. E. Stevens,<sup>249,250</sup> G. L. Chen,<sup>251</sup> F. W. Baity,<sup>252</sup> W. L. Gardner<sup>253</sup> and others.<sup>254,255</sup>

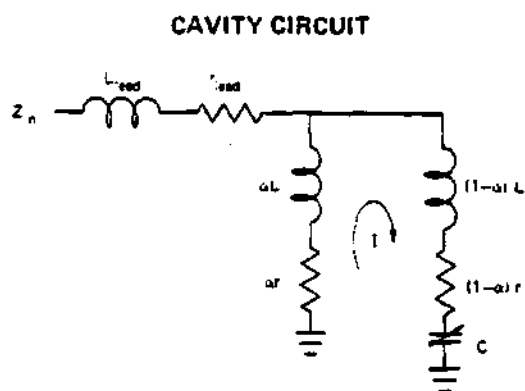
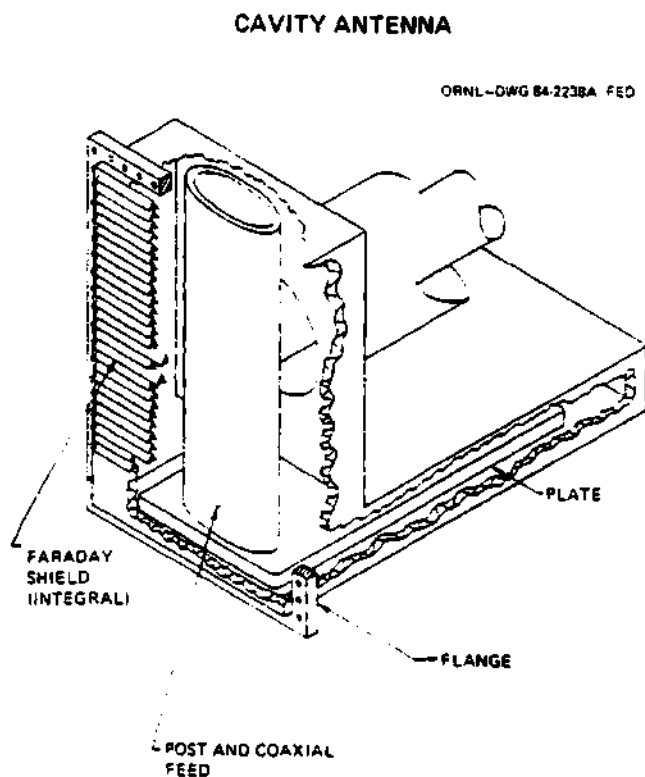
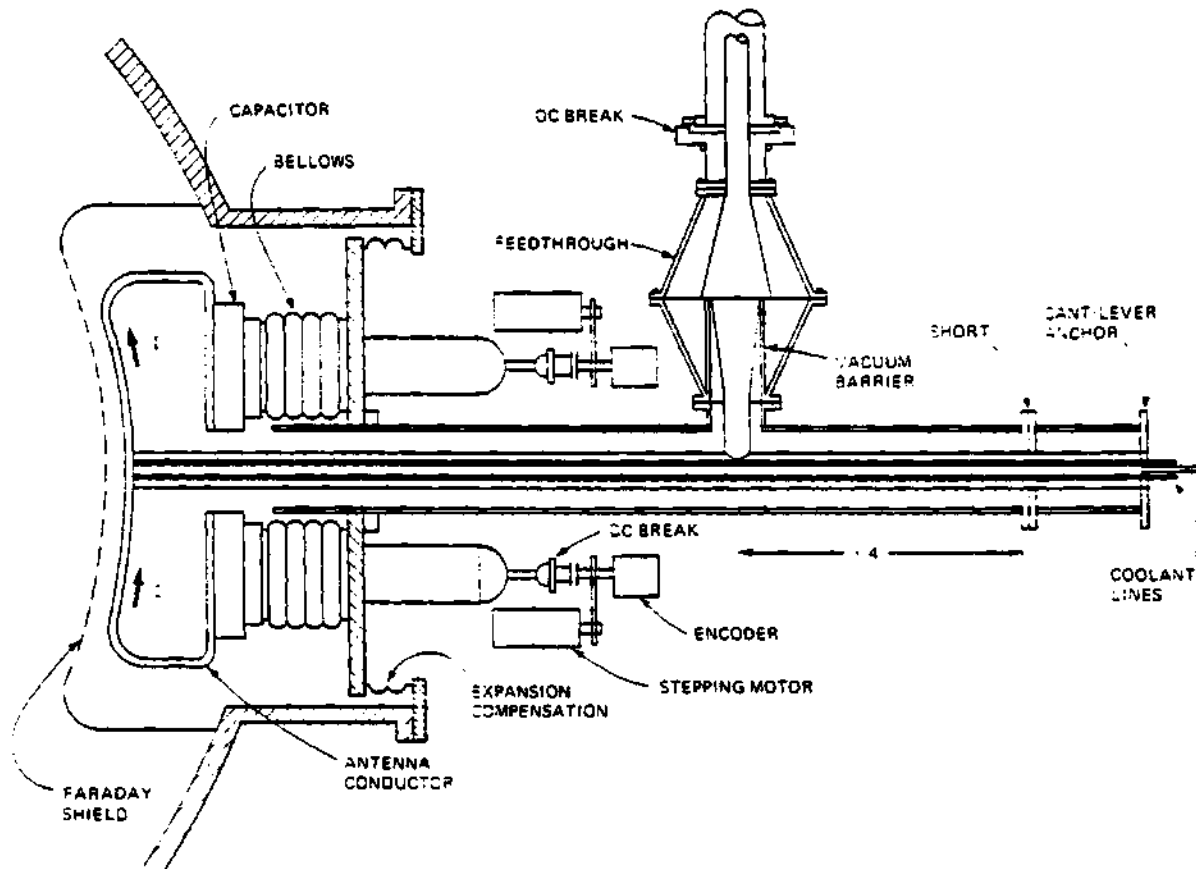


**Figure 3.4: Typical cavity antenna and its equivalent circuit.**

### RESONANT DOUBLE LOOP (SIMPLE OR ASYMMETRIC)

CRNL-DWG 85-2276A FE0



### RDL AND ARDL CIRCUIT

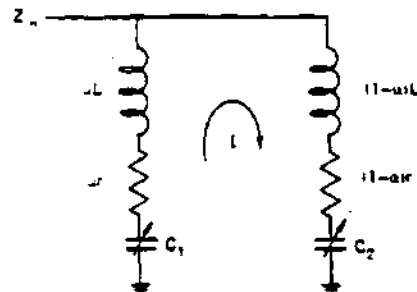


**Figure 3.5: Resonant Double Loop antenna and its equivalent circuit. The symmetric version has  $\alpha = 0.5$ .**

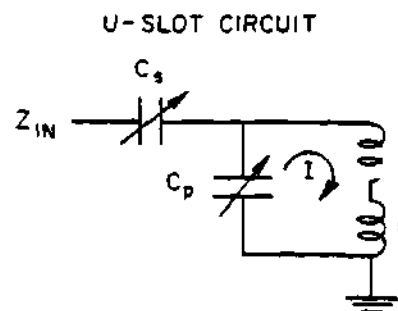
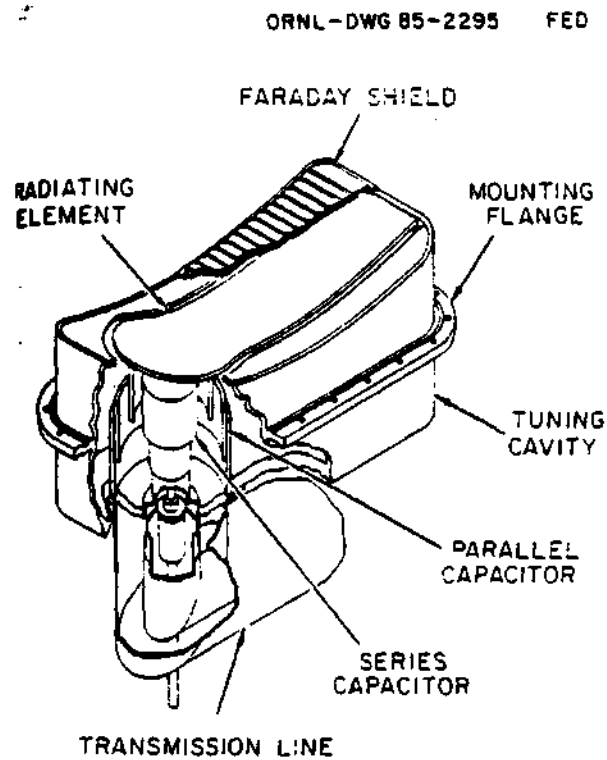


**Figure 3.6: The U-slot antenna, as proposed by McDonnell Douglas Astronautics Company and its equivalent circuit.**

Table 3.1: Radio frequency (rf) experiments list.

Exp.	R m	a m	$\bar{n}_e$ $10^{19} m^{-3}$	f MHz	$P_{rf}$ MW	$t_{rf}$ sec	Heating scheme
TFTR	2.6	0.96	$\leq 5.0$	43,64	12.5	3	D(H) ICRH
JET	3	1.2	$\leq 4$	25-55 48	20	$\leq 8$	D(H), D( $^3He$ ) ICRH + NI
Tore Supra	2.35	0.78	$\leq 5.0$	35-80	4.2	2.0	ICRH
DIII-D	1.67	0.67	$\leq 14$	30-60	2	5	D(H) ICRH
JT-60U	3.3	1.0	$\leq 4$	110-130	$\leq 2.5$	$\leq 2$	$2\omega_{CH}$ in H
TEXTOR	1.75	0.46	$\leq 6$	25-29	2.2	$\leq 2$	MC(D(H))
ASDEX	1.67	0.40	$\leq 9$	30-115 33.5/67	2.2	$\leq 2$	D(H), $2\omega_{CH}$ H and H/D, ICRH + NI
JFT-2M	1.31	0.42	$\leq 5$	15./17.	2	0.3	MC(D(H)) ICRH + NI
JIPPT -IIU	0.91	0.23	$\leq 7$	40	2.2	$\leq 0.1$	MC(D(H)) IBW
ALC-C	0.64	0.13	$\leq 20$	180	0.5	0.07	D(H), $2\omega_{CH}$ IBW
HEL-E	2	0.2	$\leq 2.5$	26.7	1.5	$\leq 0.2$	MC(D(H)) IBW

**Table 3.2: TFTR antenna design parameters.**

Description	TFTR
Power into the port	4 MW
Power per current strap	2 MW
Port dimension	60 × 90 cm × cm
Total frequency range	40 – 80 MHz
Frequency range, first band	40 – 60 MHz
rf pulse length	2 sec
Capacitor designer	ORNL
Capacitor voltage peak	50 kV
Capacitor current (rms)	800 Amp
Capacitor electric field	43 kV/cm
Antenna electric field	23 kV/cm
Faraday shields losses	100 W/cm <sup>2</sup>
Antenna power density	1160 W/cm <sup>2</sup>
Antenna motion range	11 cm

Table 3.2 lists the antenna's main design parameters.<sup>246</sup> Figure 3.7 and Figure 4.5 shows layouts of an antenna used on TFTR. While Figure 3.8 shows the cavity box of the antenna in more detail. The antenna consisted of a pair of resonant loops, separated by a solid dividing septum, in a single movable housing designed to fit through a horizontal midplane port of approximately 60 cm by 70–90 cm. Each loop was designed to launch up to 2 MW of power, for a total of 4 MW per port in two bands from 40–80 MHz. A pair of capacitors was used to tune the antenna and match its impedance to 50  $\Omega$ . The tuning capacitors were designed at ORNL to minimize electric field at the expense of tuning range. A single Faraday shield protects the antennas. It consist of two tiers of actively cooled Inconel tubes, the front tier was covered with semicircular graphite sleeves to minimize the introduction of high-Z impurities into the plasma from the Faraday shield. The TFTR antenna was designed for 2 seconds pulses.

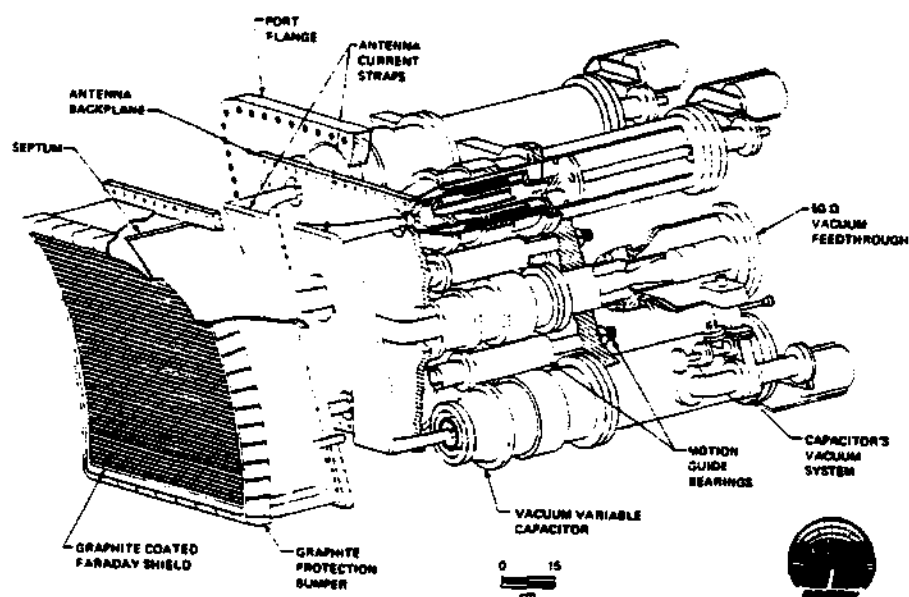
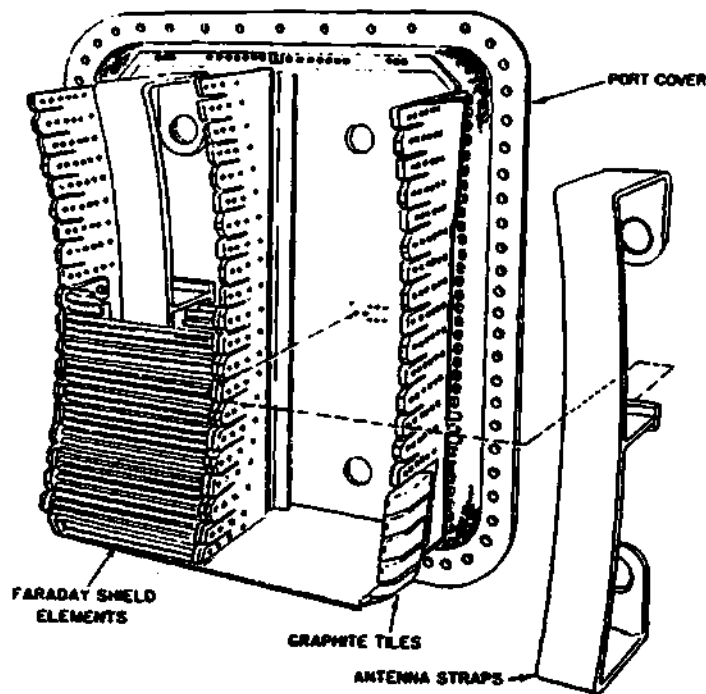


Figure 3.7: TFTR antenna layout.



**Figure 3.8: TFTR antenna cavity box. Most of the Faraday screen elements have been removed to show the current strap housing and the straps relative size.**



### 3.6 Summary

In this chapter the basis for rf wave heating has been reviewed, together with the effects of the rf power on the plasma edge. Some of the rf effects include: impurity generation, sheath rectification, self sputtering and avalanche, quiver motion, ponderomotive effects and antenna phasing. A presentation of the typical heating antennas used in fusion experiments was given, along with a description of TFTR's ICRF antenna. The importance of the effect of the edge density profile on the ICRH antenna coupling and loading was presented in section 3.3 and in Figure 3.1, emphasizing the importance of the measurement of the plasma edge density in front of the ICRH antenna for calculations and comparisons between the theoretical and calculated loading and coupling of the plasma.

## CHAPTER IV

# TFTR REFLECTOMETER SYSTEM DESIGN

### 4.1 Introduction

The purpose of the new reflectometer for the Toroidal Fusion Test Reactor (TFTR) was to study the edge density profile in front of the Ion Cyclotron Resonance Heating (ICRH) antenna, from within the high power environment of the antenna; thus making a direct measurement of the changes of the radio frequency (rf) power on the plasma edge. Changes in the edge density profile can change the coupling and loading of the antenna which can change the rf power deposition on the plasma.

The reflectometer system designed and installed on the TFTR was discussed in detail in the references<sup>39,40,280-282</sup> and it will be completely described in the following sections. The system had one source at the range of 8 to 12.4 GHz that provided the swept part of the probing wave. Up-conversion and frequency multiplication are used to increased the frequency of the probing wave to the frequency range of the plasma reflection layers, that is, to  $\approx 90$  to 120 GHz of frequency range, corresponding to the first 20 to 30 cm of the plasma edge (depending on the magnetic field and the edge density gradient).

At the beginning of this project, the ORNL group (including Drs. John Wilgen, Tim Bigelow, Greg Hanson, C. E. Thomas, and others) was given the task to design, construct, test, install, collect, and analyze the data for an edge density profile reflectometer on TFTR. The purpose of the study was to measure

and increase the understanding of the edge density changes induced by the ICRH power deposition on the plasma. The author's role as the Graduate Research Assistant (GRA) of the team was to assist as much as possible in all parts and stages of the project. The author contributed to the initial concept development and component and schematic design of the project. The unique contributions of the author were in the computer simulation of the system and the development of the data analysis and reconstruction technique. As the concept and idea became well defined, the author developed a computer model of the reflectometer data. This modeling code provided a test bench for the reconstruction technique. Testing of the reflectometer and its components was done at the microwave laboratory under the supervision of Drs. John Wilgen, Tim Bigelow and Greg Hanson. After the successful construction and testing of the reflectometer and technique, the reflectometer was moved and installed on TFTR at the Princeton Plasma Physics Laboratory (PPPL). Calibration data were taken during the test phase of the reflectometer. With the reflectometer installed and collecting data, the author was given the opportunity to develop computer codes and new data analysis techniques to read, process, analyze, and extract the phase data, and to reconstruct the corresponding density profile.

## 4.2 Development

Because of the TFTR requirements and working conditions, the new reflectometer could not be a copy of any pre-existent reflectometer system. These conditions include:

1. *Inaccessibility*: Because of the Deuterium-Tritium operation (D-T phase) of TFTR, access to the tokamak was difficult and infrequent. Placing the reflectometer electronics outside the TFTR enclosure with the corresponding

waveguide of 100 feet or more posed other design problems (such as dispersion of the waveguide and power loss).

2. *Long distances:* The long waveguide length made phase detection quite difficult for conventional reflectometers. Therefore, the phase difference technique was developed to minimize the fringe skipping associated with density fluctuations and to reduce the fringe count.
3. *Frequency range:* Edge probing using conventional O-mode operation reflectometers required a very wide range of frequency. This was limited by the waveguide band limits, and involved relatively long wavelengths at the edge, which degraded the spatial resolution. Therefore, the X-mode of propagation was chosen for the probing wave. The X-mode reflectometer can start the frequency sweep at the local electron cyclotron resonance frequency on the edge, which is  $\approx 90$  GHz.
4. *New inversion technique:* X-mode phase difference data inversion techniques are more complicated but provided all the necessary information once they were understood and developed.
5. *Very high frequency electronic components:* Because of the high magnetic field operating environment of TFTR, high frequency waves (on the order of 100 GHz) were needed to probe the plasma.
6. Density fluctuations at the edge can reach levels as high as  $\frac{\delta n_e}{n_e} \approx 100\%$ .<sup>63,107</sup>  
 "This causes rapid large changes in the local refractive index, creating a difficult environment for probing with EM waves."<sup>178</sup>

TFTR can produce a wide range of plasma scenarios for the study of plasma transport, ICRH heating and other important parameters relevant to D-T operation. The plasma edge densities can range from  $\approx 1.0 \times 10^{16}$  to  $2.0 \times$

$10^{19} \frac{\text{part}}{\text{m}^3}$ , over the first 20 to 30 cm of the plasma edge depending on the magnetic configuration and the peak density of the plasma. The central magnetic field strength can range from 3.2 Tesla (toroidal field current of  $I_{tf} \approx 48$  Kamps) to 4.9 Tesla ( $I_{tf} \approx 72$  Kamps). Some examples of TFTR plasma shots are shown in Figure 4.1 for a low density and magnetic field plasma, and in Figure 4.2 for a high density and magnetic field. This parameter range gives a frequency range of 90 to 120 GHz, which is able to probe the first 20 to 30 cm of the plasma edge (and even the plasma center if a low density and low magnetic field configuration is used). The selection of the X-mode of propagation reduced the required frequency range as explained previously. After studying different reflectometer designs and prospects, the final version of the reflectometer and its electronic components was determined as shown in Figure 4.8<sup>39,40,280-282</sup> of section 4.3.

A two phase development program was sought at the time to prove the feasibility of the project:

1. *Proof of principle phase:* This allowed for a timely and low cost checkout of the dual frequency phase difference concept. By using the pre-existing waveguide (which uses low loss corrugated circular waveguide) and interface system (shown in Figure 4.3<sup>294</sup>) of TFTR's fluctuation reflectometer, a "test" of the reflectometer and technique was able to be done without going through the expense of building a waveguide run (Figure 4.4) to the ICRH antenna. These data provided a baseline of information about how the edge effects, if any, were modified away from the ICRH antennas. This had some inconveniences, such as:

- The launcher for the TFTR fluctuation reflectometer was designed for probing highly localized fluctuations. Focused Gaussian beams were

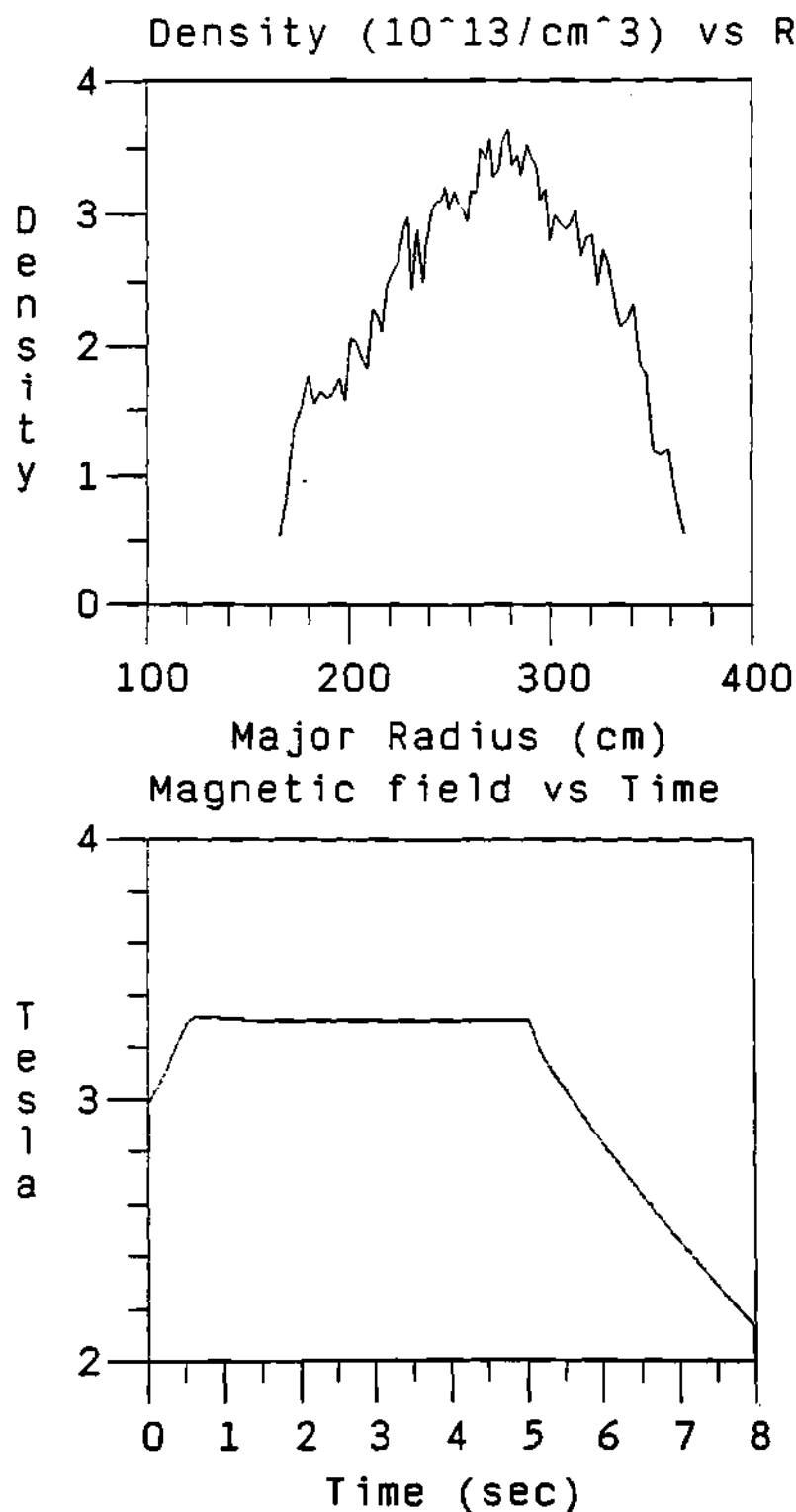


**Figure 4.1:** TFTR plasmas showing the density profile (Thomson Scattering at  $t = 4.1$  seconds) and magnetic field (time history) range for shot 67024.

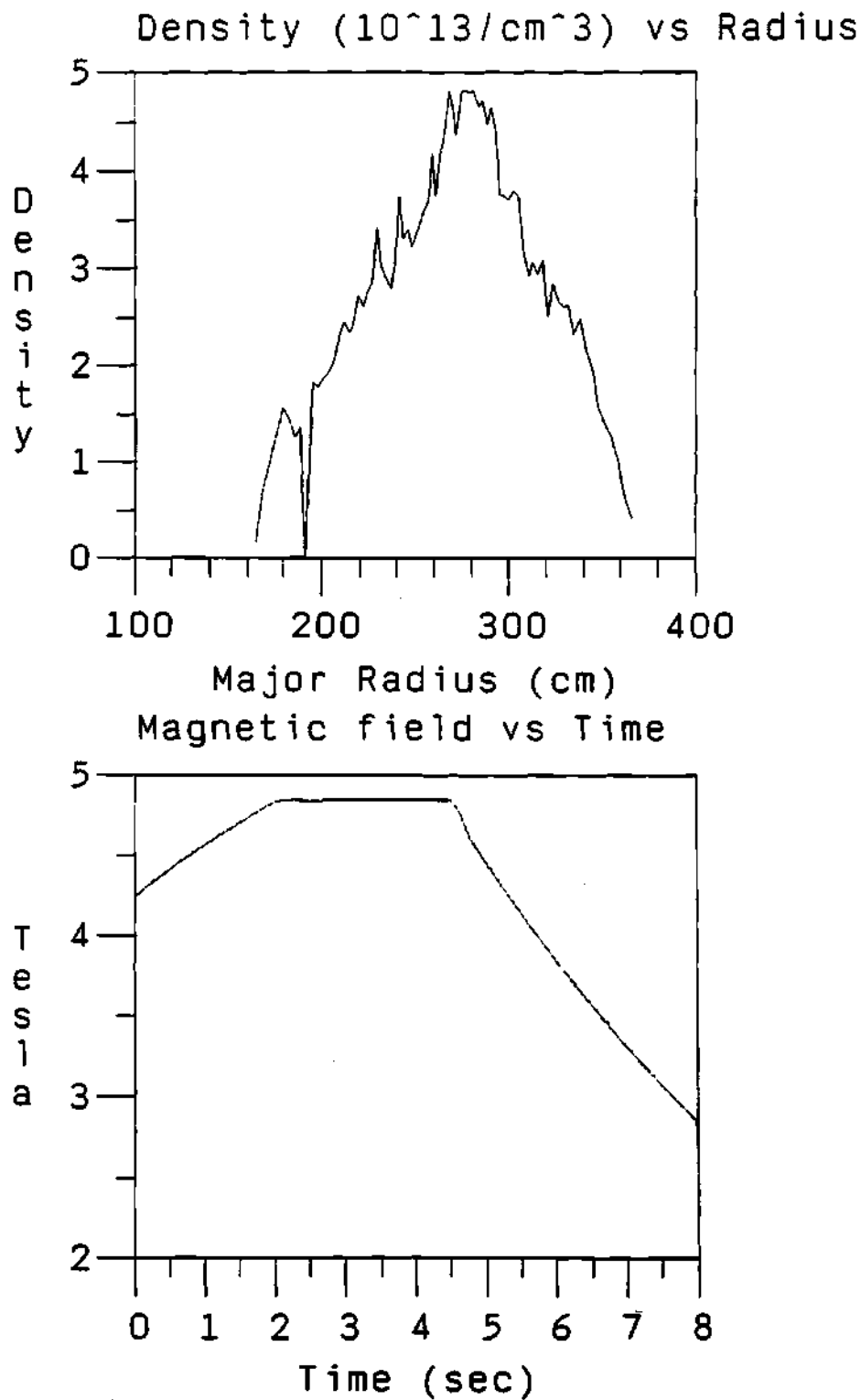


**Figure 4.2:** TFTR plasmas showing the density profile (Thomson Scattering at  $t = 3.5$  seconds) and magnetic field (history) range for shot 67877.

generated that intersect at the plasma midplane (see Figure 4.26), not at the edge.

- Remotely controlled mirrors were available to aim the beams, but it was difficult to make the beams cross at the edge (i.e, the system was not optimized for plasma edge coupling) as can be seen in Figure 4.7.
- The beam cross section may have been too small to cover the entire part of interest of the profile. This was particularly true at the edge of the plasma, where the intersection area of the two beams was small.
- Low reflected signal levels were frequently encountered. This is probably because of the poor beam crossing and coupling at the edge.
- The launcher system was not close to the ICRH antennas, and the local effects of the ICRH power may not have been seen directly.

2. *Full system configuration:* In this phase the reflectometer was moved to a location in the basement under TFTR's vacuum vessel where it could reach the ICRH antenna mounted launcher (using a 450 in long waveguide transmission line), shown in Figure 4.4<sup>283,284</sup> and Figure 4.5,<sup>283,284</sup> which had been optimized for the operation of the reflectometer and ICRH coupling studies. The radiation pattern of the reflectometer beam was not the highly focused Gaussian beam from the TFTR fluctuation reflectometer, but was a divergent beam pattern which had the advantage that the launcher is much closer to the edge of the plasma. This radiation pattern for the antenna is presented in Figure 4.6, where two perpendicular profiles of the pattern have been plotted. The coordinate system that was used for the plot is a spherical coordinate system  $(r, \theta, \phi)$ ; where the  $z$ -axis is in the direction of the propagation of the wave, the  $z$ -axis is along the long side of the waveguide, and the  $y$ -axis is along the short side of the waveguide. Thus,



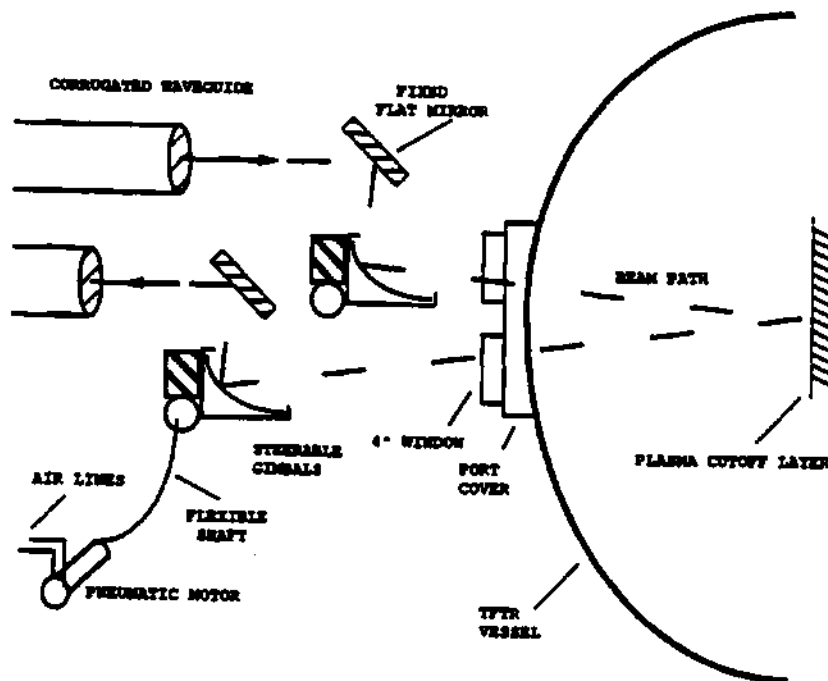
the curve with the dotted line is the pattern for an  $x$ -axis cross section, while the continuous line is the pattern for a  $y$ -axis cross section of the main pattern. This corresponds to a cross section profile for  $\phi = 0$  (along the  $x$ -axis) and for  $\phi = 90$  degrees (along the  $y$ -axis), respectively. In contrast to the TFTR fluctuation reflectometer system, this system was able to receive a good signal from the edge of the plasma but not from the center of the plasma. Another major change on the reflectometer was that the frequency spacing of the two probing waves was reduced from the original 0.25 GHz to 0.125 GHz. This was done to reduce the phase dynamic range and the phase fluctuations associated with density fluctuations.

The reflectometer had two main output ports. These were the I and Q signals of the quadrature phase detection system (or I & Q Network), given by:

$$I = A_s \sin(\psi) \quad (4.1)$$

$$Q = A_s \cos(\psi) \quad (4.2)$$

where  $A_s$  was the amplitude of the signal, and  $\psi$  was the phase of the wave. The quadrature detection system was a super heterodyne system, which gave good signal-to-noise ratio and large dynamic range. A LeCroy 6810 CAMAC digitizer module was used to digitize these signals with a ramp voltage proportional to the frequency of the swept frequency source. Some of the digitizer settings and parameters are presented in Table 4.1. The data was moved automatically by the Princeton Plasma Physics Laboratory (PPPL) computer system from the LeCroy 6810 memory to the designated storage media, where it could be accessed for analysis and reconstruction of the density profile. The phase difference was calculated by fringe counting the I and Q signals from the raw data. The data analysis programs allowed for the special creation and processing of calibration data files, which could be used later to calibrate the general raw data files.

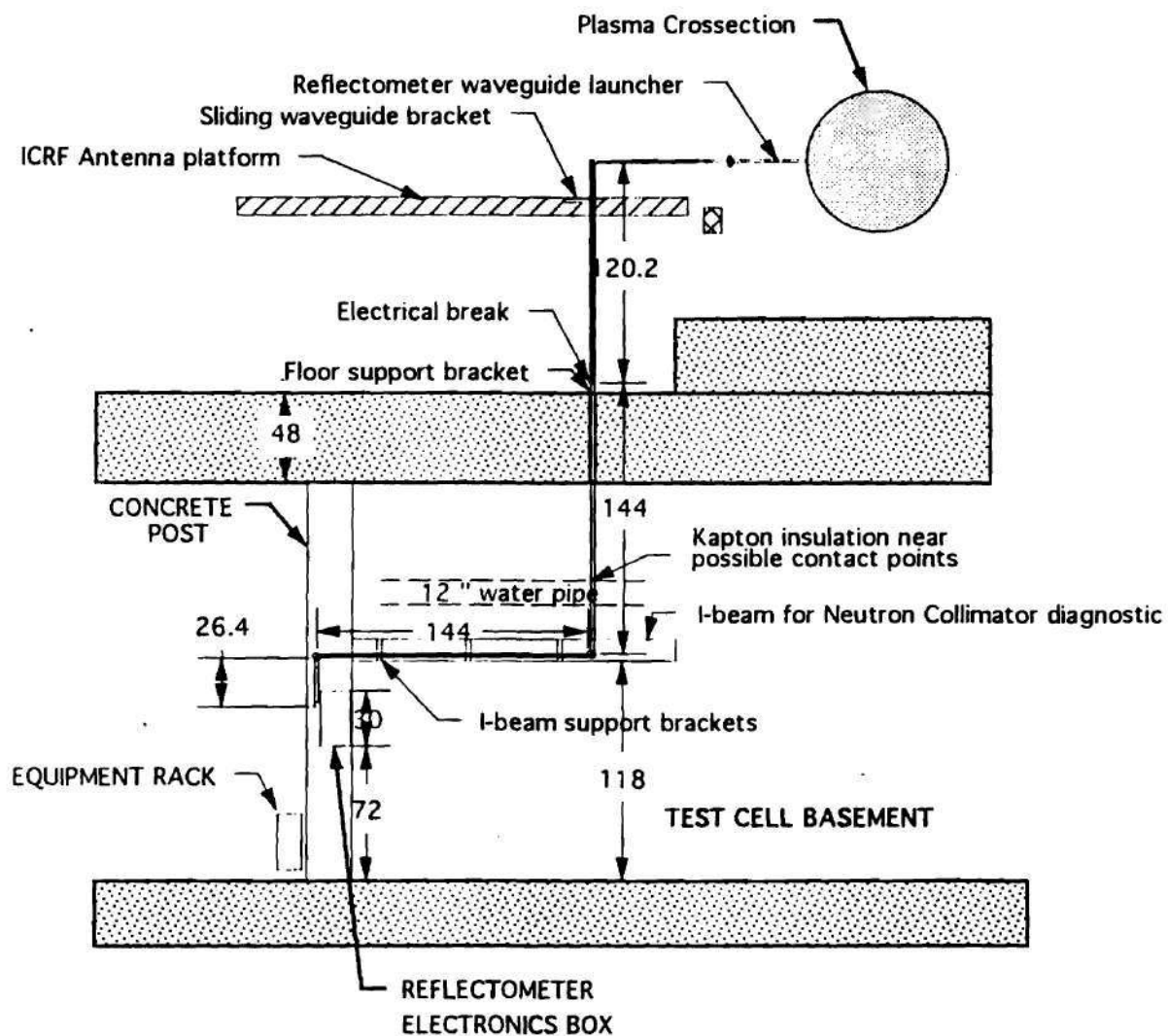


WAVEGUIDE TO VESSEL INTERFACE

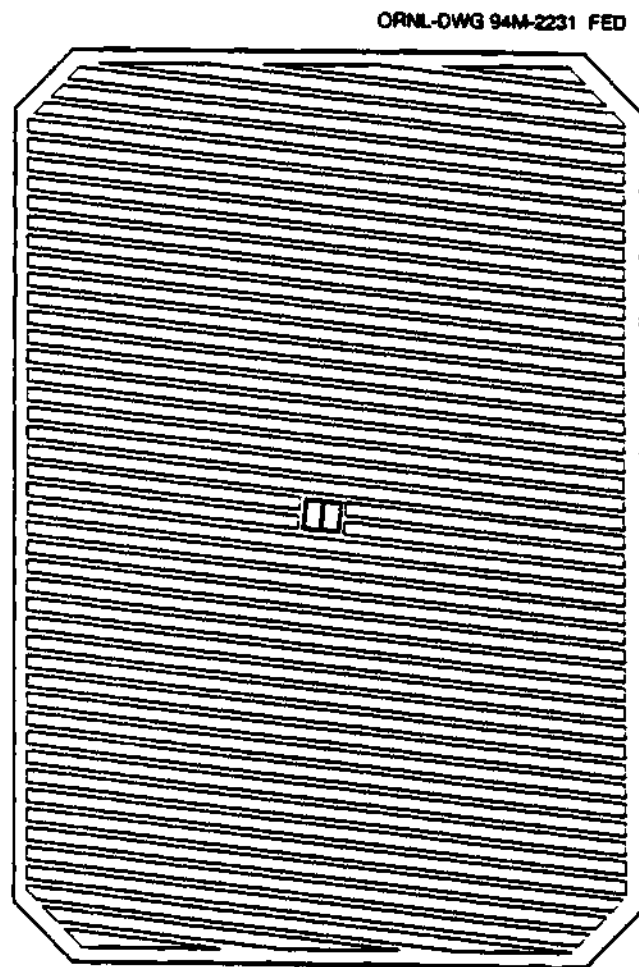
Figure 4.3: TFTR fluctuation reflectometer waveguide to vessel interface.

Table 4.1: Some of the digitizer major parameters.

Description	LeCroy 6810
Number of channels	4
Memory size per channel	128 K
Typical digitizing rate	1 MHz
Data window	128 msec
Number of bits	12
Voltage range	$\pm 12.8$ Volts
Signal range	$\pm 6.5$ Volts



**Figure 4.4: Side view layout of the reflectometer for the second phase of the project. Dimension are in inches.**



**Figure 4.5: Front view of the ICRH antenna rf box showing the launcher position (center) with respect to the ICRH antenna. The launcher is tilted at the same angle as the Faraday Shield screen elements.**

### NEAR FIELD PATTERN

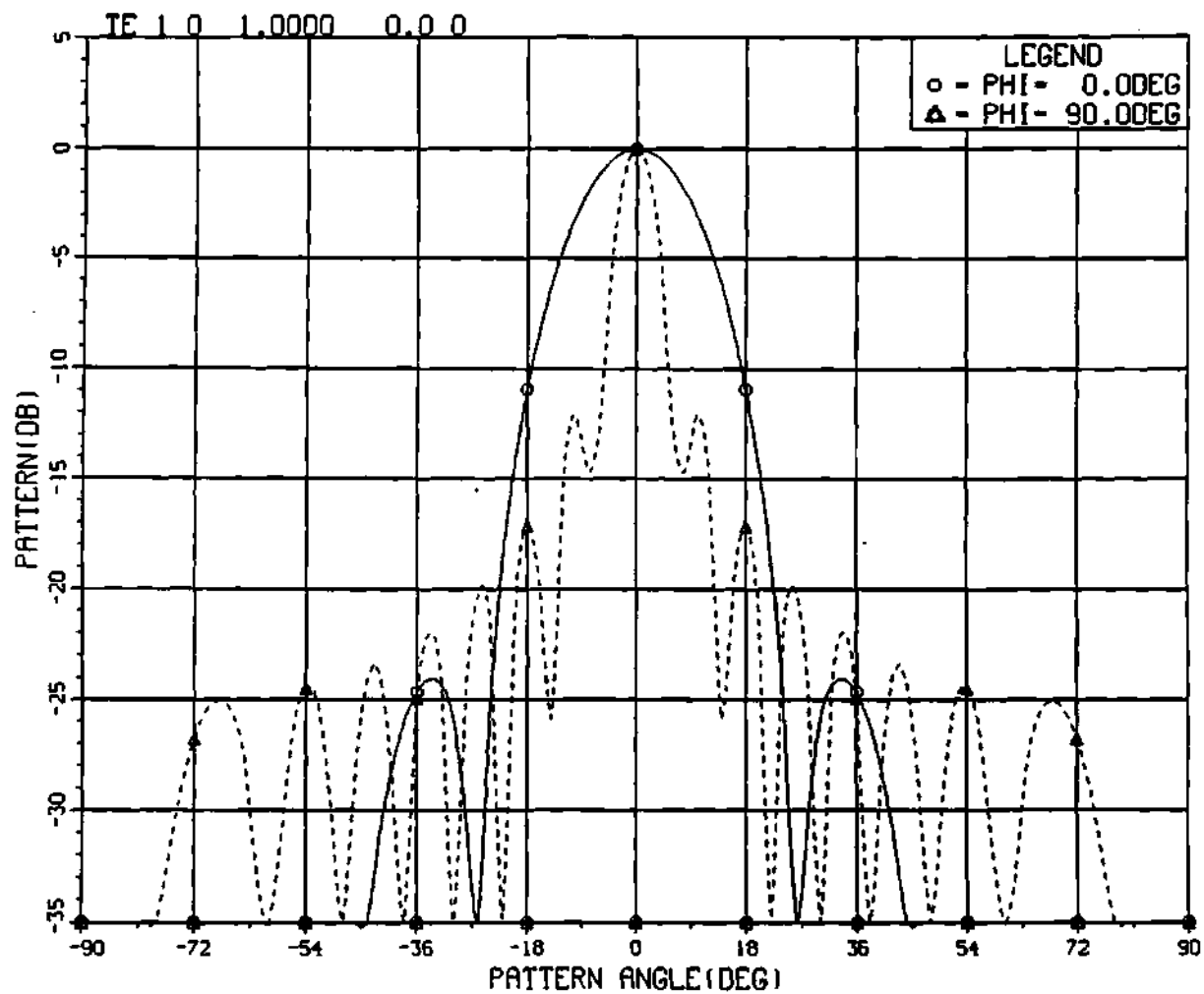


**Figure 4.6: Radiation pattern of the launcher in two orthogonal planes, parallel ( $\phi = 0$ ) and perpendicular ( $\phi = 90$ ) to the widest dimension of the waveguide. The  $x$ -axis is the pattern angle,  $\theta$ , and the  $y$ -axis is the beam relative amplitude in decibels (dB).**

## CALCULATED TFTR REFLECTOMETER LAUNCHER PATTERN (UNFOLDED)

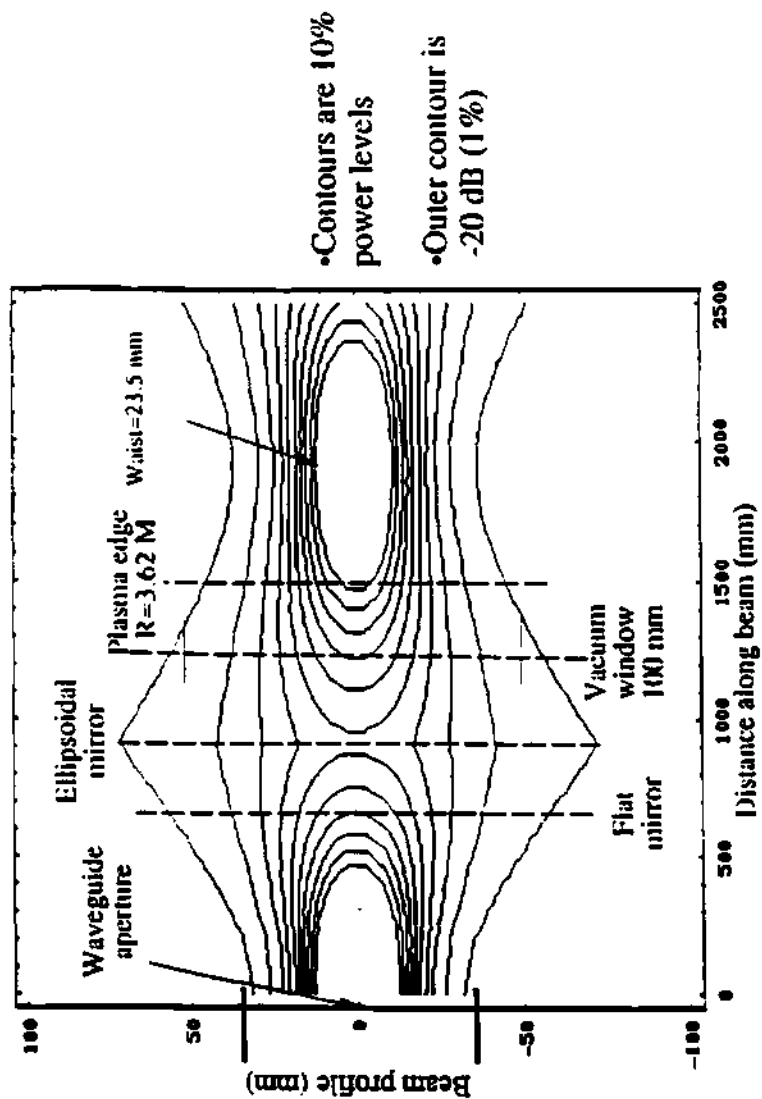


Figure 4.7: Calculated TFTR's reflectometer launcher Gaussian pattern (unfolded).

### 4.3 Description of the Reflectometer

The reflectometer had one Backward Wave Oscillator (BWO) source in the frequency range of 8 to 12.4 GHz, which provided the capability for sweeping the frequency of the probing beam. This is shown in Figure 4.8 with the label "8-12.4 GHz". The BWO's signal is divided in three ways, as shown in Figure 4.8. The top two signal paths on the diagram are almost identical circuits. The difference is the frequency of the Dielectric Resonant Oscillator (DRO) Local Oscillator used by the up-converters, labeled f1 and f2 in the figure. These frequencies are set to have a difference equal to  $\Delta\omega = 0.25$  for the phase I and to  $\Delta\omega = 0.125$  for the phase II of the project, respectively. After the signal goes through the up-converters, it goes through the Band Pass Filters (label BPF1) to reduce the amplitude of inter-modulation products from the mixers, and then through the active frequency doubler (labeled 2 $\times$ ) and tripler (labeled 3 $\times$ ) to increase the frequency of the probing beam to the range of 90 to 120 GHz. Finally, the two signals are added together (plasma probing signal) in a directional coupler (or power combiner) where a small part of the probing signal is sampled and combined in a singled ended mixer to produce a reference signal (at the beat frequency) for the phase detector. The third signal (Local Oscillator or LO) that comes out of the BWO oscillator source, goes through a similar circuit path as the other two signals, except that the frequency (f3) of the up converter DRO is different and the active tripler is substituted by a 3<sup>rd</sup> harmonic mixer (with Intermediate Frequency (IF) preamplifier) where the plasma probing signal and the carrier signal are mixed together. This has the effect of down converting the two probing signals from the plasma to an Intermediate Frequency (IF) range where they can be easily amplified. Constant phase limiting amplifiers are used to remove amplitude modulations caused by density fluctuations in the plasma and to provide proper

**Table 4.2: Some of the reflectometer system major components.**

Component	Model	Freq. GHz	Section
Freq. sweeper	Micronow BWO	8-12.5	4.4.1
LO Freq. sources	Resotech DRO-7300-EMA	7.3, 7.35, 7.4	4.4.2
Power combiner	Aerowave	90-120	4.4.3
Pre-amp. MiTeq	AFS3-00111200-20-13P-4	0.1-2.0	4.4.4
Limiting amps.	Veritech VMLA102-170	1.0-2.0	4.4.4
Active doublers	Milliwave S91-1822B	13.3-20.0	4.4.4
Triplers	Millitech FTT-10-3-S	30-40	4.4.4
Phase detector	Merrimac IQM-A series	0.125, 0.25, 0.5	4.4.5
Millitech mixers	MSH-10	90-120	4.4.6
Up-conv. mixer	Miteq Inc. MDZ0088	8.0-12.5	4.4.6
DADEN Filters	BA125-16-555	0.125, 0.25, 0.5	4.4.7
Equalizer	SMT, SM31183	8-12.5	4.4.8

signal levels to the mixer inputs. The two probing signals are combined in the IF balanced mixer to produce an IF signal at the difference frequency containing the phase difference data which is fed into a quadrature phase detector system. The  $I (= A_r \sin(\psi))$  and  $Q (= A_r \cos(\psi))$  signals from the quadrature phase detection system are digitized together with the ramp voltage of the sweeper source and later transferred from the CAMAC module's memory to the computer disk system.

#### **4.4 Major Components of the Reflectometer System**

A list of the reflectometer's major components is shown in Table 4.2. While a description of the specific components is available in the corresponding books on microwave engineering, a short description of some of the most important components is provided in the following sections.





#### 4.4.1 Frequency signal sources

The main frequency generator of the reflectometer was a *Backward Wave Oscillator* (BWO). This produced a wave in the frequency range of 8 to 12.5 GHz with a sweeping time of 10 msec with the built-in sweeper. An external sweeper driver was used to reduce the sweeping time to 1 msec to reduce the effect of density fluctuations on the phase data and the corresponding fringe skips associated with the induced fluctuations on the phase.

The BWO is characterized as having a traveling wave rf circuit for which the energy of the traveling wave moves in the opposite direction of the phase velocity of the wave.<sup>297-299</sup> This is shown in Figure 4.9,<sup>297-299</sup> where the frequency,  $\omega$ , as a function of the wave number,  $\beta$ , is plotted for a forward wave and backward wave. This function,  $\omega(\beta)$ , is called the dispersion relation. The phase velocity of a wave is defined by:

$$V_p = \frac{\omega}{\beta} \quad (4.3)$$

where  $\omega$  is the frequency and  $\beta$  is the wave number. While the group velocity is defined by:

$$V_g = \frac{d\omega}{d\beta} \quad (4.4)$$

which can be interpreted as the local value of the slope at a given point in the  $\omega(\beta)$  curve. The phase information of the wave travels in the direction of the phase velocity, while the energy information of the wave travels in the direction of the group velocity. The curve in Figure 4.9a give a positive value for the phase velocity,  $V_p$ , and a positive value for the group velocity,  $V_g$ ; thus the phase information and the energy information of the wave travel in the same direction. On the other hand, for the plot in Figure 4.9b, the phase velocity has a positive value while the group velocity has a negative value because the slope of the curve at point "A" is negative; thus the phase information of the wave moves in the positive direction while the energy information of the wave is moving in the negative direction.

Figure 4.10<sup>297-299</sup> shows a simplified schematic of a Backward Wave Amplifier (BWA) that could be transformed to a BWO by using a properly adjusted feedback network between the input and output terminals, as is the case in any amplifier device. An electron beam is formed from the accelerated cathode emission by means of the potential  $V_a$ . The beam moves parallel to a uniform magnetic field  $B_0$  that extends the length of the tube; the beam is then collected by the collector electrode. The collector potential,  $V_c$ , determines the beam velocity and the anode screen potential  $V_a$  determines the beam current,  $I_b$ . While the input signal travels toward the cathode, the electrons are bunched somewhere near the collector electrode.<sup>297-299</sup> The bunching of the electrons in the beam can be explained as follows. The electron beam has an uniform velocity  $u_0$  when it enters the slow wave structure, which guides electromagnetic waves with phase velocity smaller than the speed of light,  $v_{ph} \ll c$ . When the velocity of the beam electrons and the wave phase velocity are approximately equal, the electrons in the beam "see" essentially a static electric field with sinusoidal spatial distribution. At the input of the tube the beam has a uniform electron density distribution, but as the electrons travel along the slow wave structure with the wave, the electrons tend to bunch.<sup>301</sup> Even when the electrons in the beam are moving initially slightly faster than the wave, the electrons tend to be trapped and slowed down to the phase velocity of the wave. The decrease in the electrons' kinetic energy is accompanied by an increase of the wave amplitude. The bunched electrons interact with the helix slow wave in such a way as to cause the net energy to be transferred from the bunched electrons to the helix fields. This permits wave amplification to occur. The input wave is moving in the negative direction (to the cathode at left of the figure). Since the energy of the wave moves in the same direction as the wave, then the energy and therefore the group velocity are in the negative direction. On the other hand, the electron beam is moving in the positive direction (to the right). Since this is backward wave circuit, the phase velocity of the wave (carrying the

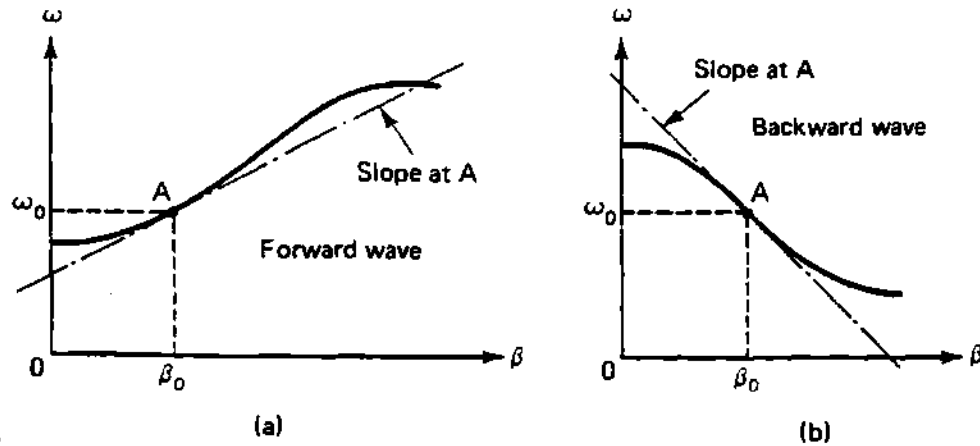


**Figure 4.9:** Plots of the dispersion relations ( $\omega = \omega(\beta)$ ) for a forward wave (a) and a backward wave (b), where  $\omega$  is the frequency and  $\beta$  is the wave-number.

phase information) is moving in the positive direction, while the group velocity (carrying the energy information) is moving in the negative direction. Thus, the energy of the electron beam (which is moving positive direction or in the direction of the phase velocity) is coupled to the input wave, causing amplification of the input wave. More information can be found in the references.<sup>297-299,301,302</sup>

#### 4.4.2 Fixed frequency sources

Dielectric Resonator Oscillators (DRO) represent a good compromise of cost, size, and performance compared to alternative signal sources, such as high-quality factor (Q) cavity oscillators, microstrip oscillators, or multiplied crystal oscillators.<sup>297,298</sup> Dielectric resonators, since they can be easily integrated in microwave integrated circuits (MICs), can be used directly as the frequency determining element for stable microwave sources. The primary characteristics of the

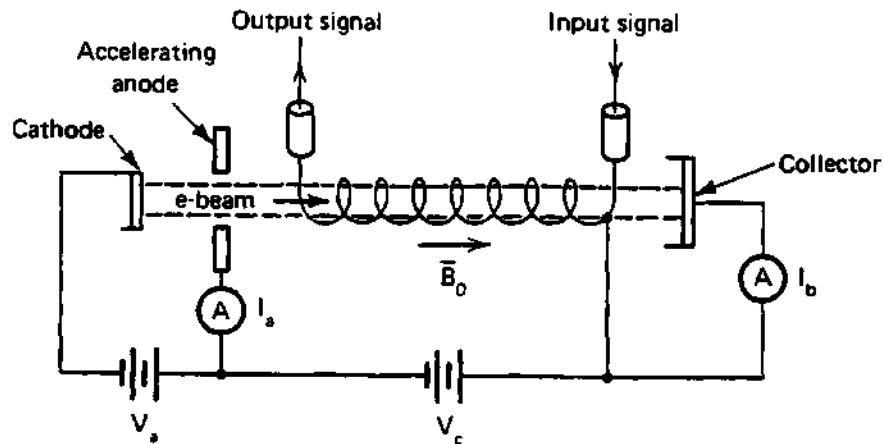


Figure 4.10: Backward wave amplifier schematic.

ceramic material to be used for dielectric resonators are:<sup>297,298</sup>

- $Q$ , which is approximately equal to the inverse of the loss tangent (where the loss tangent is defined as the ratio of the real to the imaginary parts of the total displacement current<sup>297</sup>).
- The temperature coefficient of the resonant frequency ( $\tau_f$ ), which includes the combined effects of the temperature coefficient of the dielectric constant and the thermal expansion of the dielectric resonator and the shielding package.
- The dielectric constant ( $\epsilon_r$ ).

The values of  $Q$ ,  $\tau_f$ , and  $\epsilon_r$  required for various applications differ, and in general, satisfactory oscillator operation under most conditions can be achieved by choosing an appropriate material composition. Until several years ago, the lack of suitable materials severely limited dielectric resonator applications. Materials

such as rutile-phase  $TiO_2$  which has an unloaded  $Q$  of about 10,000 at 4 GHz and  $\epsilon_r$  of 100, were most often used. However,  $TiO_2$  has a resonant frequency value of 400 PPM/ $^{\circ}C$ , which makes it impractical for most applications.<sup>297,298</sup>

At present, several ceramic compositions have been developed offering excellent dielectric properties. Complex peroxide compounds have proven to possess acceptable properties for dielectric resonators. These compounds have dielectric constants between 20 and 40, high  $Q$ s (some greater than 10,000 at 10 GHz), and a temperature coefficient that can be varied through modification of the ceramic composition. It is impossible to say that any of the commercially available dielectric compositions are better than any other because other factors, such as the ease of ceramic processing and the ability of a manufacturer to hold tolerances on the dielectric properties, must also be considered. Performance limitations, if any, of the lower dielectric constant materials remain to be determined, since most component work reported (thus far) has used dielectric resonators with  $\epsilon_r$  in the range of 30 to 90. The lower dielectric constant material is likely to be more sensitive to shielding, because of the increase of fields outside the resonator.<sup>297,298</sup>

A dielectric resonator made of low-loss, high permittivity ceramic material resonates at various modes at frequencies determined by its dimensions and its surroundings. Although the geometrical form of a dielectric resonator is extremely simple, an exact solution of the Maxwell equations is considerably more difficult than for the hollow metallic cavity. Therefore, the exact resonant frequency of a particular resonant mode, such as the most commonly used  $TE_{01}$  mode, shown in Figure 4.11,<sup>297,298</sup> can only be computed by rigorous numerical procedures.<sup>297,298</sup>

The DROs employ a high- $Q$ , temperature-stable dielectric resonator in a passive resonator circuit. The dielectric resonator is weakly coupled to maximize the loaded  $Q$  of the circuit, minimizing changes in frequency with temperature variations, pulling, and pushing. The DROs are designed with a series feedback

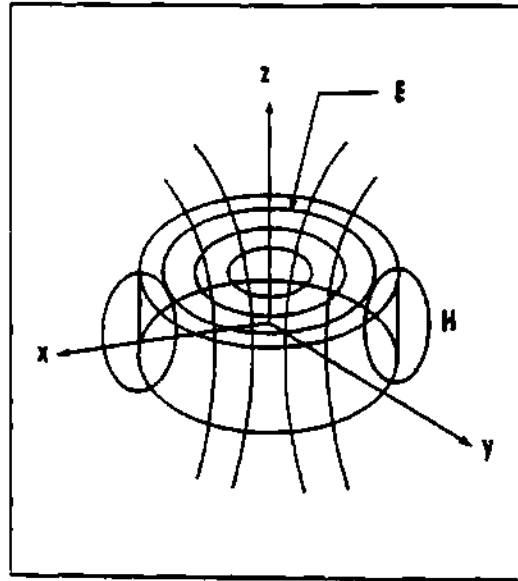


Figure 4.11: The  $TE_{01}$  mode used in cylindrical dielectric resonators, with the electric,  $E$ , and the magnetic,  $H$ , fields lines.

circuit topology in which the oscillator transistor (a Gallium Arsenic Field Effect Transistor, or GaAs FET) is linked to an output isolator or buffer amplifier by using an impedance matching network. Voltage regulation is included to reduce the frequency variations that occur from changes in load and supply voltage. General specifications include at least +13 dBm output power from 5 to 12 GHz and at least +10 dBm output power from 12 to 18 GHz. Maximum second harmonic levels are -25 dBc at all frequencies.<sup>297,298</sup>

The reflectometer uses some fixed frequency sources for the up-converting process of the probing beam. Resotech's fundamental frequency free-running Dielectric Resonator Oscillators (DROs), which operated at frequencies from 3 to 13 GHz were used. Regardless of the operating frequency, two versions were available, a basic model and a high frequency stability model. The basic model consisted of a single transistor DRO, while the high frequency stability version consisted of a basic model followed by a 10 dB attenuator pad and a buffer am-

Table 4.3: Some of the DROs main specifications.

Parameter	7300-EMA	7350-EMA	7400-EMA
Center Frequency, MHz	7300	7350	7400
Mechanical tuning range, MHz	7143-7500	7190-7550	7197-7600
Electrical tuning range, MHz	16	19	20
Tuning voltage, VDC	0-30	0-30	0-30
Power output, mW	30	35	37
Pulling (3:1 load VSWR), KHz	$\pm 90$	$\pm 150$	$\pm 250$
2 <sup>nd</sup> harmonic, below carrier, dBm	-24	-28	-28
Spurious, below carrier, dBm	< -80	< -80	< -80

plifier. This high frequency stability model topology provided excellent isolation from output load Voltage Standing Wave Ratio (VSWR) variation, thereby creating outstanding frequency stability (less than 2ppm/°C over the temperature range). Electrically tuned DROs can be obtained with features like electrical tuning ranges of up to 2% with excellent phase noise performance. The standard electrical tuning range option is 0.2 to 0.3%, with a tuning linearity of better than 2:1, and a mechanical tuning range of 3 to 4% minimum and tuning resolution of 0.001%. All GaAs FET DROs (4 to 13 GHz) incorporate a voltage regulator (with reverse polarity and over-voltage protection) which makes the DRO performance insensitive to power supply voltage level (+7 to +18 VDC). Table 4.3 shows the main parameters for the reflectometer's DROs. The model numbers (DRO-7300-EMA, DRO-7350-EMA, DRO-7400-EMA) give the center frequency of the DRO. The last three letter are the options of the model, which are: "E" for Electrical tuning, "M" for Mechanical tuning, and "A" for buffer Amplifier.<sup>303</sup>

#### 4.4.3 Directional couplers

Directional couplers are four-port devices in which the power incident into port 1 will couple to port 2 (the through port) and to port 3 (the coupled port)



but not to port 4 (the isolated port).<sup>297,298</sup> The coupler is symmetric with respect to port 2, that is, power incident into port 2 will couple to port 1 and port 4 but not to port 3. Thus, port 1 and port 4 are decoupled, and port 2 and port 3 are decoupled. They are used to take samples of the signal on the input port without disturbing or decreasing the signal going to the output port. The fraction of power from port 1 to port 3 is called the coupling factor,  $C$ , as defined by:

$$C = 10 \log \frac{P_1}{P_3}. \quad (4.5)$$

The leakage of power from port 1 to port 4 is called the isolation,  $I$ , given by:

$$I = 10 \log \frac{P_1}{P_4}. \quad (4.6)$$

The power fraction between port 3 and port 4 is called the directivity,  $D$ , given by:

$$D = I - C = 10 \log \frac{P_3}{P_4}. \quad (4.7)$$

The ideal coupler is characterized solely by the coupling factor, since the isolation and directivity are both infinite. (In reality, directivities of 30 to 40 dB are typical in the millimeter frequency range.)

Many types of couplers are available, including: Directional couplers, aperture couplers, Bethe hole, coupled line, branch line, Lange coupler, Moreno cross guide, multi-hole waveguide, Riblet short slot, ring hybrid, Schwinger reversed phase, and others.<sup>297</sup> Couplers can come in waveguide form, microstrip form, or cable form, depending on the frequency range and the type of coupler needed. Waveguide couplers are generally made by two waveguides connected together by one of their side walls. In this connecting wall there are one or more holes (coupling holes) through which a part or fraction of the electromagnetic wave passes from one waveguide to the other, thus dividing the wave and its power in some way determined by the geometry of the coupling holes. A simple diagram of a

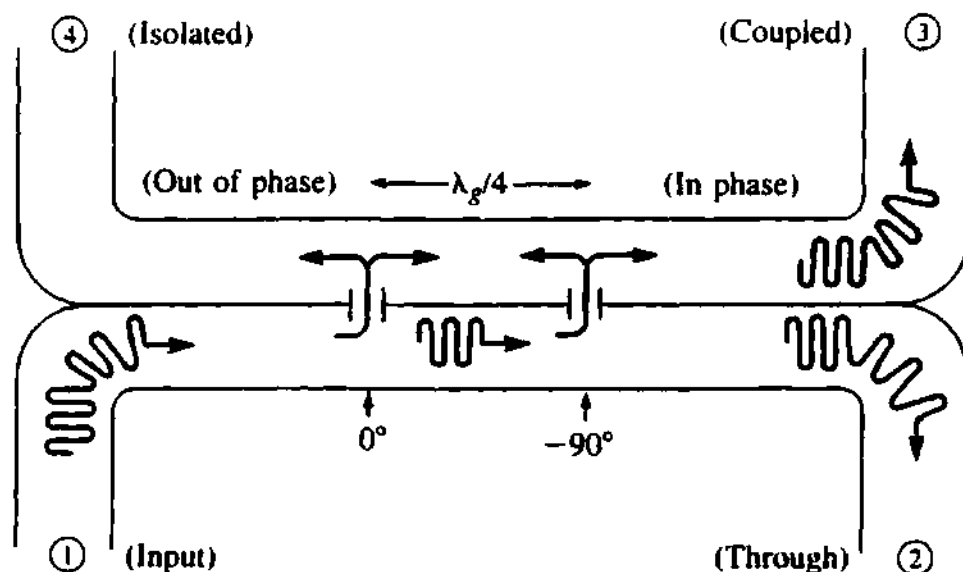
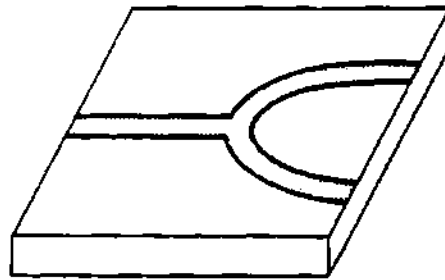


Figure 4.12: Basic operation of a two hole directional coupler.

two-hole directional coupler is shown in Figure 4.12<sup>297</sup> to visualize the coupling of the wave from one waveguide to the other.  $\lambda_g$  is the wavelength of the wave in the waveguide. This is basically how the coupler before the launcher in Figure 4.8 works. The power dividers at the output of the 8 to 12.4 GHz source and in front of the 3<sup>th</sup> harmonic mixer are of the microstrip or stripline type of coupler, shown in Figure 4.13.

#### 4.4.4 Active frequency multipliers and amplifiers

A frequency multiplier (doubler or tripler) is a device that increases the frequency of a signal by an integer multiple of the signal's frequency. The reflectometer uses frequency doublers and triplers to increase the frequency of the probing beam to the range necessary to probe the plasma. A description of the devices follows.



**Figure 4.13: Basic microstrip or stripline power divider.**

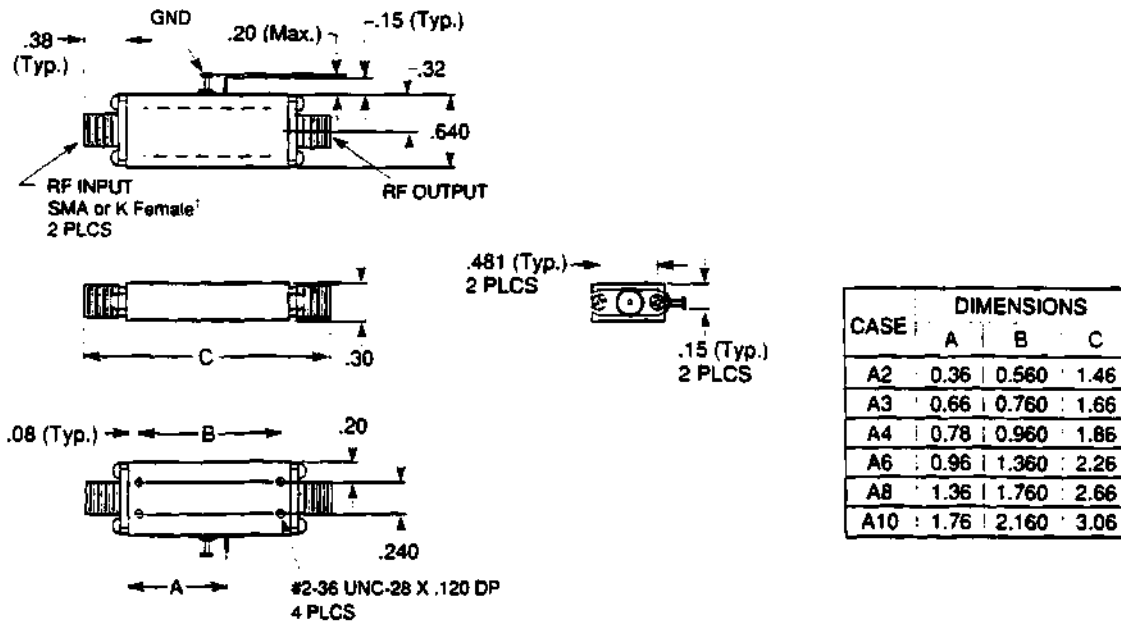
**Frequency doublers** The frequency doublers used in the reflectometer were made by Sierra Microwave Technology (SMT). The model used was the FA-20405, which combined the functions of frequency multiplication and amplification into a single miniature package while maintaining a high level of signal purity. A list of the specifications for the doubler is shown in Table 4.4 and a package outline is shown in Figure 4.14.<sup>304</sup>

**Frequency triplers** The frequency triplers have the same function as the doublers, that is, to increase the frequency of the probing wave by an integer multiple of the signal's frequency. The tripler used by the reflectometer is the Millitech FTT-10-3-S (custom made). A list of its specifications is shown in Table 4.5<sup>305</sup> and an outline of the package is shown in Figure 4.15.<sup>306</sup> Series FTT triplers are fixed-tuned varactor triplers offering coverage of 20% fractional bandwidths. These units are very flat over specified frequency ranges and offer higher

Table 4.4: Some of the doubler main specifications.

Parameter	Value
Input frequency	13.3-20.0 GHz
Output frequency	26.5-40.0 GHz
Output power	+15 dBm
Harmonic output	20 dBc
DC input	12 V @ 450 mAmp
Case type	A6

### A Series Case, SMA, 3mm, 2.4mm



NOTE:  
1. Also available in 2.4mm connector.

Figure 4.14: Frequency doubler package outline.

**Table 4.5: Some of the tripler main specifications.**

Model	Freq.	EIA	Power
FTT-10-3	GHz	Waveguide	mW
Input	30-36.7	WR-28	30
Output	90-115	WR-10	1.3

**Table 4.6: Some of the amplifier main specifications.**

Parameter	VMLA 102-170
Frequency	0.1-2.0 GHz
Min. gain	36 dB
Max gain Flatness	$\pm 1$ dB
Max VSWR input	2:1
Max VSWR output	2:1
Output power @ 1 dBm	+13 dBm
Voltage	+15 Volts
Measured Current	123 mAmps

output power than MUT series, but over a more narrow band.<sup>305</sup>

**Amplifiers** One of the amplifiers used in the reflectometer was the Miteq model AFS3-00100200-20-13P-4. Table 4.6 shows some of its main parameters. Other types of amplifiers were also used, including the Veritech Microwave Inc. "Constant Phase" limiting amplifier models VMLA 102-170 and VMA 812-127. Table 4.7 shows some of the main parameters of these models.

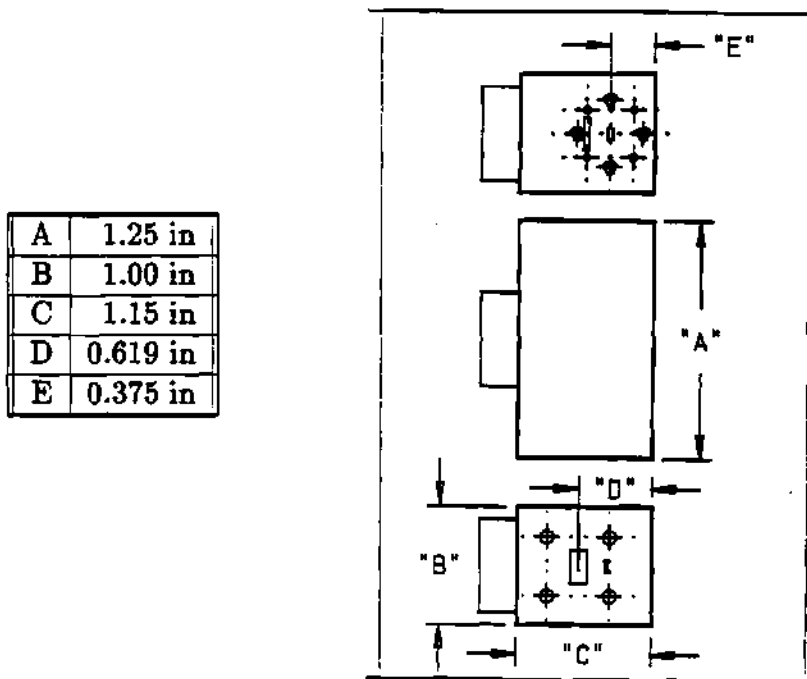


Figure 4.15: Frequency tripler package outline.

Table 4.7: Some of the constant phase limiting amplitude amplifier main specifications.

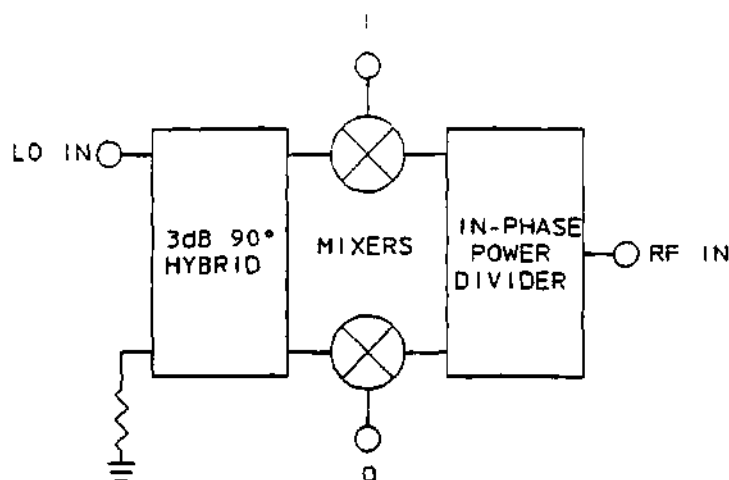
Parameter	VMLA 102-170	VMA 812-127
Freq range	1.0-2.0 GHz	8.0-12.4 GHz
Sat. Power	+14/+16 dBm	+12/+14 dBm
Noise Figure	6.5 dB	5.0 dB
Gain	68 min, 75 typ. dB	26 min, 27 typ. dB
Gain ripple	$\pm 1.0$ dB max	$\pm 0.4$ typ. / $\pm 0.7$ max dB
Output power	+14 dBm min.	+14 dBm
Output power var.	$\pm 1.0$ dB	$\pm 1.0$ dB
Dynamic range	-43/+10 dBm	-43/+10 dBm
Noise output	-3 dBm typ.	-3 dBm typ.
DC @+15 Volts	360 mAmps	360 mAmps

#### 4.4.5 Quadrature phase detector

The *quadrature phase detector* or I & Q Network, as it is commonly known, is perhaps one of the most widely used networks in communications, control systems, and signal processing systems. When fed by rf and Local Oscillator (LO) signals, it produces two equal amplitude signals that are in phase quadrature, i.e., the signals are at  $90^\circ$  off-phase.<sup>306,307</sup> The basic components of an I & Q Network are shown in Figure 4.16 (i.e., 3 dB  $90^\circ$  hybrid coupler, in-phase power divider, and two mixers). The 3 dB  $90^\circ$  hybrid coupler (or Quadrature hybrid) is a 3 dB directional coupler with a  $90^\circ$  phase difference in the outputs of the through and coupled arms.<sup>297</sup> This type of hybrid is often made in microstrip or stripline form as shown in Figure 4.17.<sup>297</sup> The I & Q Network is called a variety of different names depending on its application, including:

1. I & Q Phase Detectors
2. Phase Comparators
3. QPSK Modulators/Demodulators
4. Quadrature Generators/Phase Detectors
5. Quadraphase Modulators/Demodulators
6. Quadrature Intermediate Frequency (IF) Mixers
7. Vector Modulators

With additional passive components, the I & Q Networks form the basis of such circuits as Single Sideband Modulators, Image Reject Mixers, Phase Correlators and, Phase Lock Loop systems.



**The Basic I & Q Network**

**Figure 4.16: Basic schematic of an I & Q Network.**

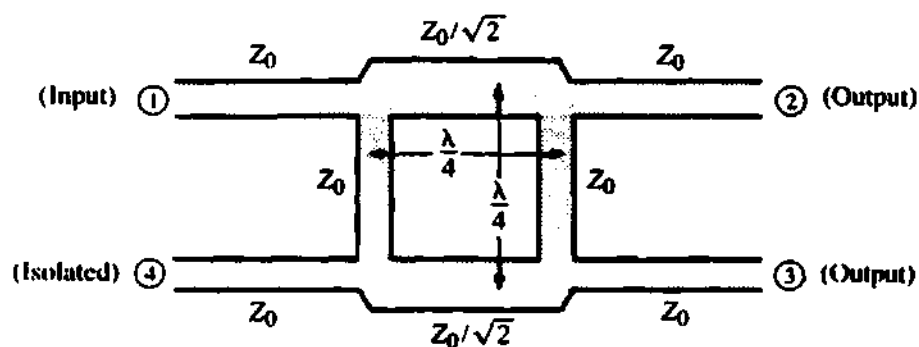


**Figure 4.17: Geometry of a 3 dB 90° hybrid coupler.  $Z_0$  is the impedance of the connection and  $\lambda$  is the wavelength of the wave.**



**The I & Q Network as a detector** One of the disadvantages of a simple phase detector is that its output is dependent on both the phase and the amplitude of the rf signal.<sup>306</sup> This is immediately overcome by the use of an I & Q Phase Detector (or I & Q Network), since the detected output is used to form the inverse tangent ( $\tan^{-1}$ ) by the ratio of the I and Q outputs.<sup>308</sup> This can be seen mathematically as:

$$\phi = \tan^{-1} \left( \frac{I}{Q} \right) \quad (4.8)$$

where:

$$I = A_s \sin(\phi_s) \quad (4.9)$$

$$Q = A_s \cos(\phi_s) \quad (4.10)$$

where  $A_s$  is the amplitude of the signal and  $\phi_s$  is the phase of the signal. The phase can be expressed as:

$$\phi = \tan^{-1} \left( \frac{A_s \sin(\phi_s)}{A_s \cos(\phi_s)} \right) \quad (4.11)$$

$$= \tan^{-1} \left( \frac{\sin(\phi_s)}{\cos(\phi_s)} \right) \quad (4.12)$$

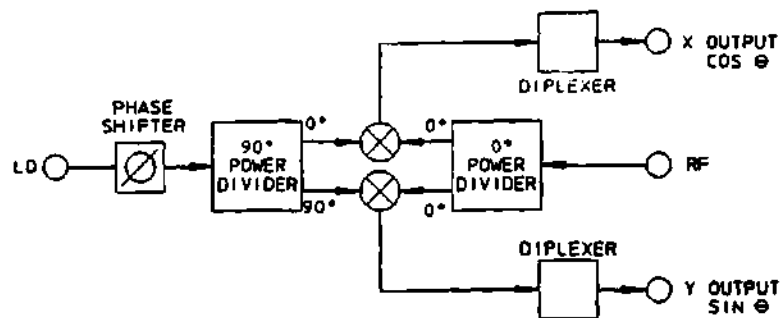
where the amplitude of the signal,  $A_s$ , cancels out of the fraction inside the  $\tan^{-1}$  function. This makes it essentially independent of any amplitude variations. In digital transmission systems the number of permitted states is limited to 2 (Biphase), 4 (Quadrature), 8 (Eight Phase), or more phase angles. Each time the number of states is increased, the demands on the I & Q detector are increased.

Of the four components in the I & Q Network, all but the 90° Quadrature Hybrid are wideband by design; therefore, the bandwidth of the hybrid coupler will limit the frequency range. For this reason the LO signal (which is often fixed frequency) is fed into this port, and the rf into the 0° power divider, and it is the LO

frequency range that determines the bandwidth requirements. The video bandwidth of an I & Q Network is inherently unlimited, unless diplexers are included to cut off unwanted harmonics and spurious signals. In practice, the bandwidth is at least 0 to 500 MHz, allowing the processing of wideband data signals. The quadrature and isolation of the 90° quadrature hybrid at the LO frequency is also important for ensuring accuracy. Equally, the mixers should be well matched to both inputs, with minimum variation over frequency and temperature, to avoid internal reflections and their associated errors.

Of particular note are the In-Circuit Adjustable models which provide the user the ability to trim either or both the phase and amplitude balance, for near perfect quadrature operation, limited only by the variations over temperature.

**The phase Comparator** The Phase Comparator provides two output voltages that together permit unambiguous phase comparisons to be made over the whole 0° to 360° range of phase angles. One output is proportional to the *sine* of the phase difference between the reference (LO) and the unknown (rf) input signals, while the other output is proportional to the *cosine*. The integrated components, shown in Figure 4.18, are essentially an I & Q Network, with a phase shifter in the LO path to set a reference phase and force the zero amplitude crossing of the *sine* and *cosine* outputs to occur at an rf-LO phase difference of 0° or 90°, respectively. Two diplexers are added in the I & Q output paths to band limit the video information and attenuate the error producing second harmonic ( $2f_0$ ) level. A Phase Comparator is most suited to *Test and Measurement* applications rather than dynamic information detection, where a basic I & Q demodulator circuit excels.



**The Phase Comparator**

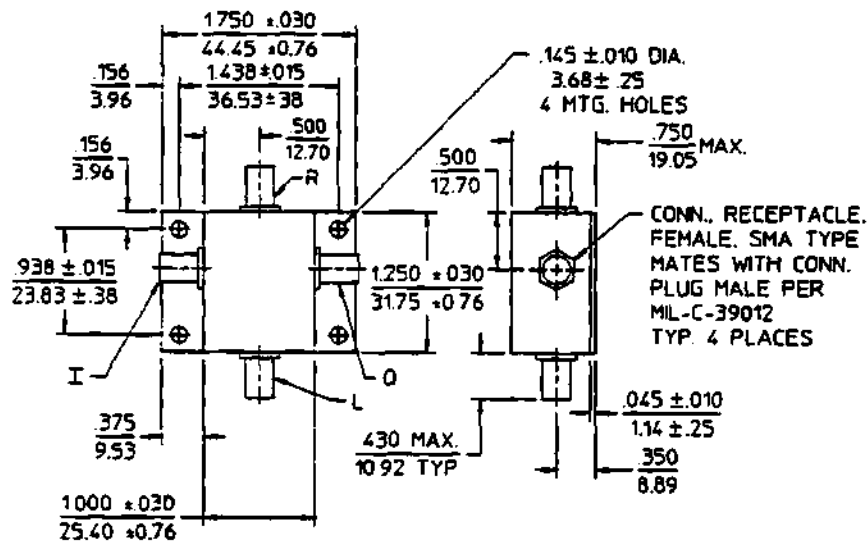
**Figure 4.18: The Phase Comparator.**

**Merrimac IQM-A series** The quadrature phase detector used in the reflectometer was a Merrimac IQM-A series connectorized I & Q demodulator. The basic components diagram is shown in Figure 4.16, and the package outline is shown in Figure 4.19. Corresponding data are shown in Table 4.8. Merrimac I & Q Demodulators are integrated networks that, when fed by an rf and LO signal, produce two equal amplitude signals that are in phase quadrature. This IQM-A series of connectorized I & Q Phase Detectors uses lumped circuit technologies for small size and high performance. I & Q Phase Detectors are popular for applications in image reflection and single sideband modulator circuits, whereby complete systems are formed with the addition of an external IF 90° Hybrid coupler.

#### 4.4.6 Detectors and mixers

The reflectometer uses detectors and mixers directly or indirectly to process the signals and produce the desired probing beam characteristics.<sup>297-299</sup> This

### Package Outline



NOTES: 1. Tolerance on 3 place decimals  $\pm$  .020(.51) except as noted.  
2. Dimensions in inches over millimeters.

Figure 4.19: Package outline of the quadrature phase detector.

Table 4.8: Common specifications of an I &amp; Q phase detector.

rf and LO Input Characteristics	Impedance	50 $\Omega$ nom.
	VSWR	1.5:1 max.
	rf Power Level	0 dBm nom.
	LO Power Level	+10 dBm nom.
I & Q Output Characteristics	Conversion loss (rf to I or Q)	10 dB typ., 12 dB max.
	Phase Balance (I to Q) IQM-20A series	90° $\pm$ 1° typ., $\pm$ 2° (fixed LO)
	Phase Balance (I to Q) IQM-20A series	90° $\pm$ 3° typ., $\pm$ 5° (LO with 10% Bandwidth)
	Amplitude balance (I to Q) IQM-20A series	0.1 dB typ., 0.2 db max.
Amplitude balance (I to Q)	Video Bandwidth	DC to 50 MHz nom.
	Output Impedance	50 $\Omega$
	Weight, nom.	2 oz (57 g)
	Operating temperature	-55° to +85°C

is shown in Figure 4.8 as the single-ended mixer, the up-converter mixers, the 3<sup>rd</sup> harmonic mixer, etc. Detectors and mixers use a nonlinear device to achieve frequency conversion of an input signal. Microwave diodes (PIN and/or Schottky) are most commonly used as the nonlinear element, but transistors can also be used. Figure 4.20<sup>297-299</sup> illustrates the three basic frequency conversion functions of rectification, detection, and mixing. The following sections will first discuss the nonlinear voltage-current characteristics of a diode, and then use a small-signal analysis to describe the operation of various circuits that perform these functions.

**Small signal analysis of diodes** A diode is basically a nonlinear resistor, with a DC  $V$ - $I$  characteristic function that can be expressed as:<sup>297-299</sup>

$$I(V) = I_s (e^{\alpha V} - 1) \quad (4.13)$$

where:

$$\alpha = \frac{q}{nkT} \quad (4.14)$$

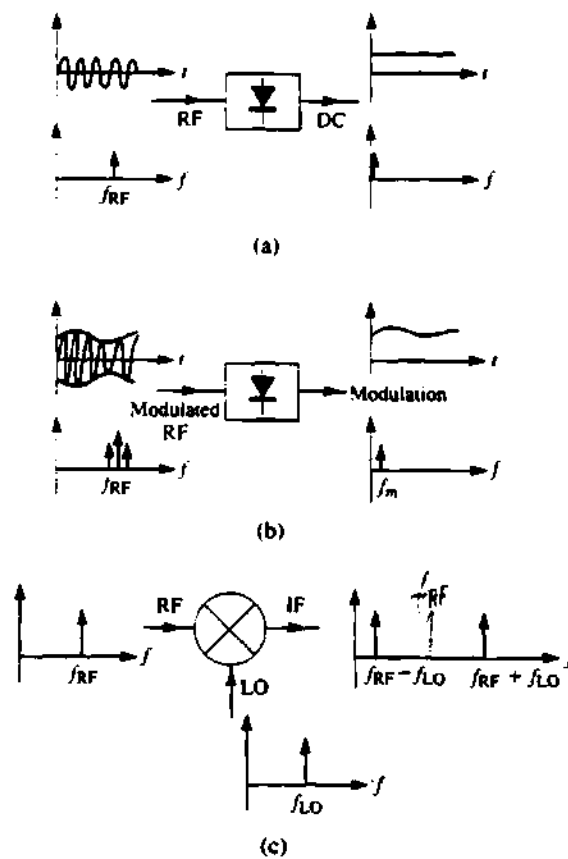


**Figure 4.20: Basic operations of rectification, detection, and mixing of a signal. (a) Diode acting as a rectifier. (b) Diode acting as a modulated signal detector. (c) Mixer.**

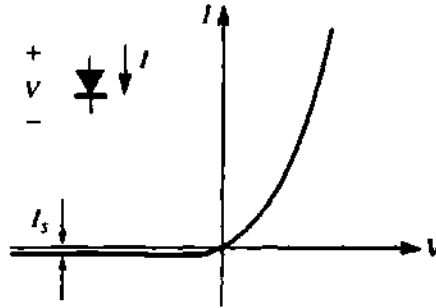


**Figure 4.21:  $V$ - $I$  characteristic curve of a diode.**

and  $q$  is the charge of the electron,  $k$  is Boltzmann's constant,  $T$  is the temperature,  $n$  is the ideality factor, and  $I_s$  is the saturation current.<sup>288,289</sup> Typically,  $I_s$  is between  $10^{-6}$  and  $10^{-15}$  Amps, and  $\alpha$  is approximately  $\frac{1}{25mV}$  for  $T = 290^\circ$  K. The ideality factor,  $n$ , depends on the structure of the diode itself and can vary from 1.2 for Schottky barrier diodes to about 2.0 for point-contact silicon diodes. Figure 4.21<sup>297-298</sup> shows typical diode  $V$ - $I$  characteristics.

Now let the diode voltage be given by:

$$V = V_0 + v \quad (4.15)$$

where  $V_0$  is the Direct Current (DC) bias voltage and  $v$  is a small AC signal voltage. Then the current, equation 4.13, can be expanded in a Taylor series about the DC bias voltage value,  $V_0$ , as follows:

$$I(V) = I_0 + v \left( \frac{dI}{dV} \right) \Big|_{V_0} + \left( \frac{v^2}{2} \frac{d^2I}{dV^2} \right) \Big|_{V_0} + \dots \quad (4.16)$$

where  $I_0 = I(V_0)$  is the DC bias current. The first derivative on the Taylor expansion can be evaluated as:

$$\left. \frac{dI}{dV} \right|_{V_0} = \alpha I_s e^{\alpha V_0} \quad (4.17)$$

$$= \alpha (I_0 + I_s) \quad (4.18)$$

$$= G_d \quad (4.19)$$

$$= \frac{1}{R_j} \quad (4.20)$$

which defines  $R_j$ , the junction resistance of the diode, and  $G_d = \frac{1}{R_j}$ , the dynamic conductance of the diode. The second derivative is given by:<sup>297-299</sup>

$$\left. \frac{d^2 I}{dV^2} \right|_{V_0} = \left. \frac{d^2 G_d}{dV^2} \right|_{V_0} \quad (4.21)$$

$$= \alpha^2 I_s e^{\alpha V_0} \quad (4.22)$$

$$= \alpha^2 (I_0 + I_s) \quad (4.23)$$

$$= \alpha G_d \quad (4.24)$$

$$= G'_d \quad (4.25)$$

The Taylor expansion, equation 4.16, can be rewritten as the sum of the DC bias current,  $I_0$ , and an AC current,  $i$ , as:

$$I(V) = I_0 + i \quad (4.26)$$

$$= I_0 + v G_d + \frac{v^2}{2} G'_d + \dots \quad (4.27)$$

The three-term approximation for the diode current in equation 4.27 is called the *small-signal approximation*, and is adequate for most purposes. The small-signal approximation is based on the DC voltage-current relationship of equation 4.13, and shows that the equivalent circuit of a diode will involve a nonlinear resistance.

**Diodes as detectors** In a detector application the nonlinearity of a diode is used to demodulate an amplitude modulated rf carrier signal. For this case, the diode voltage can be expressed as:

$$v(t) = v_0 [1 + m \cos(\omega_m t)] \cos(\omega_0 t) \quad (4.28)$$



**Table 4.9: Frequencies and related amplitudes of the Square-Law output of a detected AM signal.**

Frequency	Relative amplitude
0	$1 + \frac{m^2}{2}$
$\omega_m$	$2m$
$2\omega_m$	$\frac{m^2}{2}$
$2\omega_0$	$1 + \frac{m^2}{2}$
$2\omega_0 \pm \omega_m$	$m$
$2(\omega_0 \pm \omega_m)$	$\frac{m^2}{4}$

where  $\omega_m$  is the modulation frequency,  $\omega_0$  is the rf carrier frequency ( $\omega_0 \gg \omega_m$ ), and  $m$  is the modulation index ( $0 \leq m \leq 1$ ). Substituting equation 4.28 into equation 4.27, the diode AC current is given as:

$$\begin{aligned}
 i(t) &= v_0 G_d [1 + m \cos(\omega_m t)] \cos(\omega_0 t) + \frac{v_0^2}{2} G'_d [1 + m \cos(\omega_m t)]^2 \cos^2(\omega_0 t) \\
 &= v_0 G_d \left[ \cos(\omega_0 t) + \frac{m}{2} \sin(\omega_0 + \omega_m)t + \frac{m}{2} \sin(\omega_0 - \omega_m)t \right] \\
 &\quad + \frac{v_0^2}{4} G'_d \left[ 1 + \frac{m^2}{2} + 2m \cos(\omega_m t) + \frac{m^2}{2} \cos(2\omega_m t) + \cos(\omega_0 t) \right. \\
 &\quad \left. + m \sin(2\omega_0 + \omega_m)t + m \sin(2\omega_0 - \omega_m)t + \frac{m^2}{2} \cos(2\omega_0 t) \right. \\
 &\quad \left. + \frac{m^2}{4} \sin 2(\omega_0 + \omega_m)t + \frac{m^2}{4} \sin 2(\omega_0 - \omega_m)t \right] \quad (4.29)
 \end{aligned}$$

The frequency spectrum of this output is shown in Figure 4.22.<sup>297-299</sup> The output current terms, which are linear in the diode voltage (terms multiplying  $v_0 G_d$ ), have frequencies of  $\omega_0$  and  $\omega_0 \pm \omega_m$ ; while the terms that are proportional to the square of the diode voltage (terms multiplying  $\frac{v_0^2 G'_d}{2}$ ) include the frequencies and relative amplitudes listed in Table 4.9.

The desired demodulated output of frequency  $\omega_m$  is easily separated from the undesired components with a low-pass filter. The amplitude of the current is  $\frac{m v_0^2 G'_d}{2}$ , which is proportional to the power of the input signal. This *square-law*

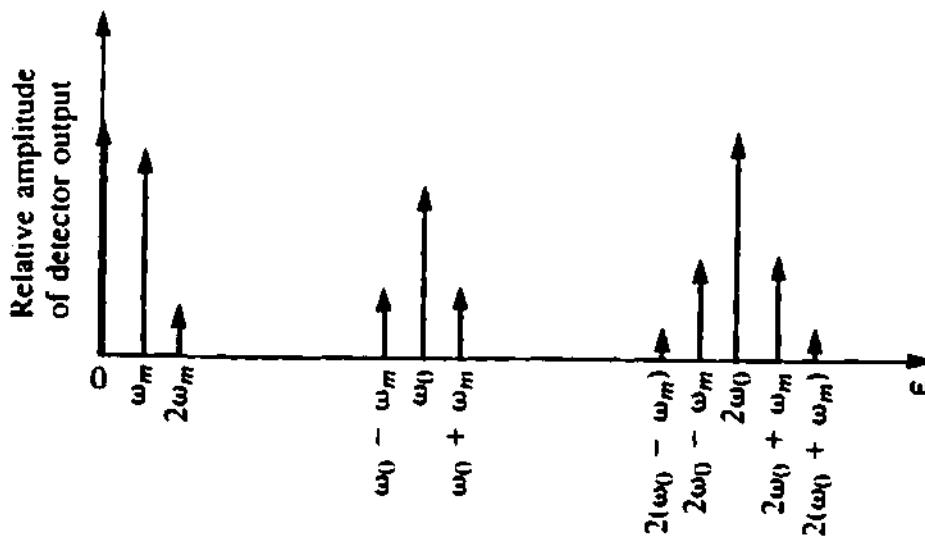
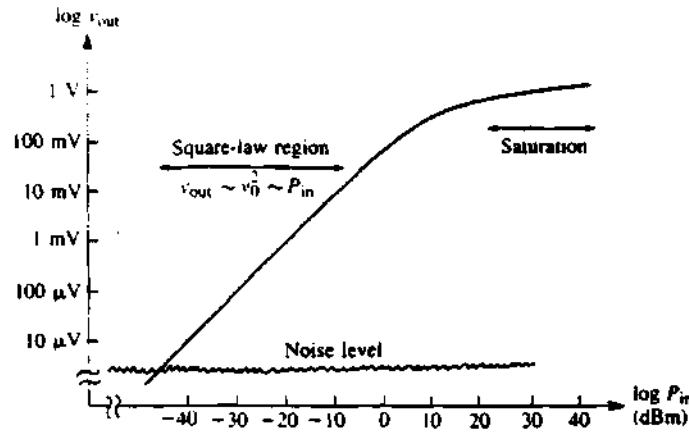


Figure 4.22: Output spectrum of a detected Amplitude Modulated (AM) signal.

behavior is the usual operating condition for detector diodes, but can be obtained only over a restricted range of input powers. If the input power is too large, small-signal conditions will not apply, and the output will become saturated and approach a linear, and then a constant  $i$  versus  $P$  characteristic. At very low signal levels the input signal will be lost in the noise floor of the device. Figure 4.23<sup>297-299</sup> shows the typical  $v_{out}$  versus  $P_{in}$  characteristic, where the output voltage can be considered as the voltage drop across a resistor in series with the diode. Square-law operation is particularly important for applications where power levels are inferred from detector voltage, as in Standing Wave Ratio (SWR) indicators and signal level indicators. Detectors may be DC biased to an operating point that provides the best sensitivity.

**Single-ended mixers** Mixing may be broadly defined as the conversion of a signal from one frequency to another by combining it with a local oscillator voltage in a nonlinear device. The nonlinear device is essential to the mixing



**Figure 4.23: Square-law region for a typical diode detector.**

process. By the principle of superposition, the addition of two frequencies in a linear device never results in additional (beat) frequencies and only the two original frequencies will exist in the Fourier spectrum of the resulting disturbance. If, however, the device is nonlinear, it will generate the sum and difference frequencies of the applied signals. These newly created frequencies will, in turn, beat with each other and with the originally applied signals to create still more frequencies, and so on *ad infinitum*.

A mixer uses the nonlinearity of a diode to generate an output spectrum consisting of the sum and difference frequencies of two input signals. In a receiver application, a low-level rf signal and a Local Oscillator (LO) signal are mixed together to produce an intermediate frequency (IF), such that:

$$f_{IF} = f_{rf} - f_{LO} \quad (4.30)$$

and a much higher frequency,  $f_{rf} + f_{LO}$ , which is generally filtered out, shown in Figure 4.24a.<sup>297-299</sup> The IF signal usually has a frequency between 10 and 100 MHz and can be amplified with a low-noise amplifier. This is called a super heterodyne

receiver, and is useful because it has much better sensitivity and noise characteristics (using an IF amplifier minimizes  $\frac{1}{f}$  noise) than the direct detection scheme discussed in the previous section. A super heterodyne system also has the advantage of being able to tune over a band by simply changing the LO frequency, without the need for a high-gain, wideband rf amplifier.

As shown in Figure 4.24b,<sup>297-299</sup> a mixer can also be used in a transmitter to offset the frequency of an rf signal by an amount equal to  $f_{IF}$ . This is a convenient technique, because it allows the use of identical local oscillators in the transmitter and receiver; a single oscillator may serve this purpose in a radar or transceiver system.

There are several types of mixer circuits, but the simplest is the single-ended mixers. Single-ended mixer are often used as part of more sophisticated mixers, such as the image rejection mixer and I & Q Networks. A typical single-ended mixer circuit is shown in Figure 4.25,<sup>297-299</sup> where an rf signal given by:

$$v_{rf} = v_r \cos(\omega_r t) \quad (4.31)$$

is combined with an LO signal, given by:

$$v_{LO} = v_0 \cos(\omega_0 t) \quad (4.32)$$

and fed into a diode. The combiner may be a simple T-junction combiner or a directional coupler. An rf matching circuit may precede the diode, and the diode may be biased through chokes that allow DC to pass while blocking rf. From equation 4.27, the diode current will consist of a constant DC bias term, and rf and LO signals of frequencies  $\omega_r$  and  $\omega_0$ , due to the term which is linear in  $v$ . The  $v^2$  term will give rise to the following output current:

$$i = \frac{G'_d}{2} [v_r \cos(\omega_r t) + v_0 \cos(\omega_0 t)]^2 \quad (4.33)$$

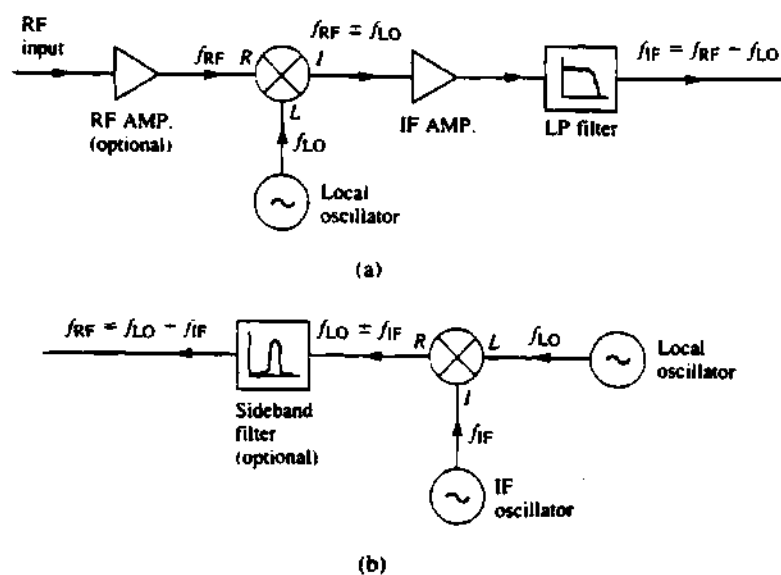


**Figure 4.24: Frequency conversion of a mixer in a receiver and transmitter application. (a) Down-conversion in a heterodyne receiver. (b) Up-conversion in a transmitter.**

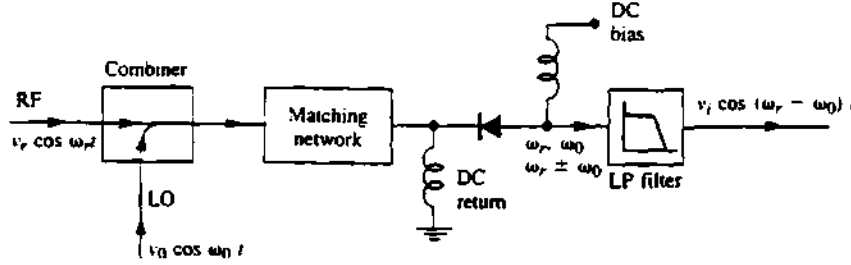


Figure 4.25: Single-ended mixer circuit.

$$= \frac{G'_d}{2} \left[ v_r^2 \cos^2(\omega_r t) + 2v_r v_0 \cos(\omega_r t) \cos(\omega_0 t) + v_0^2 \cos^2(\omega_0 t) \right] \quad (4.34)$$

$$= \frac{G'_d}{4} \left[ v_r^2 + v_0^2 + v_r^2 \cos(2\omega_r t) + v_0^2 \cos(2\omega_0 t) \right. \\ \left. + 2v_r v_0 \sin(\omega_r - \omega_0) t + 2v_r v_0 \sin(\omega_r + \omega_0) t \right] \quad (4.35)$$

The DC terms can be ignored, and the  $2\omega_r$  and  $2\omega_0$  terms will be filtered out. The most important terms are those of frequency  $\omega_r \pm \omega_0$ .

There is another approach to show or model mathematically the operation of a mixer. This is by applying fourier analysis to the conversion transconductance of the mixer.<sup>300</sup> The conversion transconductance of a mixer is determined by considering the modulation of the LO frequency by the signal inside the mixer. The general type of analysis that will be given here may be applied to any type of mixer. If the signal voltages are assumed small and the LO voltage large, the transconductance from the signal electrode to the output of the mixer will be a function of the LO voltage alone. This transconductance may, therefore, be considered as varying periodically at the LO frequency and can be written as a Fourier series:

$$g_m = a_0 + a_1 \cos(\omega_0 t) + a_2 \cos(2\omega_0 t) + \dots \quad (4.36)$$

where  $\omega_0$  is the frequency of the Local Oscillator and  $a_n$  are the terms of the Fourier expansion. If a small signal given by:

$$v_s = e_s \sin(\omega_s t) \quad (4.37)$$

is applied to the signal electrode, the resulting alternating plate current will be given by the expression:

$$i_p = g_m v_s \quad (4.38)$$

$$= g_m e_s \sin(\omega_s t) \quad (4.39)$$

$$= a_0 e_s \sin(\omega_s t) + e_s \sum_{n=1}^{\infty} a_n \sin(\omega_s t) \cos(n\omega_0 t) \quad (4.40)$$

$$= a_0 e_s \sin(\omega_s t) + \frac{1}{2} e_s \sum_{n=1}^{\infty} a_n \sin(\omega_s + n\omega_0) t \quad (4.41)$$

$$+ \frac{1}{2} e_s \sum_{n=1}^{\infty} a_n \sin(\omega_s - n\omega_0) t \quad (4.42)$$

where only the first-order terms in  $e_s$  have been retained. As  $n$  may be any integer, the intermediate frequency may be chosen equal to the signal frequency minus any multiple of the LO frequency. This is true even if the LO signal is a pure sine wave, since the harmonics are introduced by the time variation of the signal transconductance. This formula agrees with the previous result in this section.

#### 4.4.7 Filters

Filters were used to remove unwanted signals from the system. These can be seen in Figure 4.8 labeled as BPF (Band Pass Filter). Table 4.10 shows some of the main parameters of the reflectometer system filters. These are made by DADEN and models BA125-16-555, BA250-30-555, and BA500-65-555, where the first number corresponds to the central frequency of the filter. A microwave filter is a two-port network or device used to control the frequency response at a certain point in a microwave system by providing transmission at frequencies within the

Table 4.10: Main parameters of the filters.

Center frequency, $\omega_c$ , MHz		125	250	500
Passband insertion loss, dB	@ $\omega_c$	2.0	2.0	1.2
Impedance Ohms	input	50	50	50
	output	50	50	50
VSWR less than 1.5:1 MHz	from	118.75	237.5	475
	to	131.25	262.5	525
2.0 dB relative bandwidth MHz	from	118.75	237.5	475
	to	131.25	262.5	525
3 dB relative bandwidth MHz	from	117	235	467.5
	to	133	265	532.5
Stopband insertion loss dBm	@ $\frac{4}{5}\omega_c$	40	40	40
	@ $\frac{6}{5}\omega_c$	40	40	40

frequency passband of the filter, and attenuation in the frequency stopband of the filter. Typical frequency responses include low-pass, high-pass, bandpass, and band-reject characteristics. Applications can be found in virtually any type of microwave communication, radar, or test and measurement system. The filters used in the reflectometer are of the Chebyshev and tubular type.

The subject of microwave filters is quite extensive, because of the importance of these components in practical systems and the wide variety of possible implementations. More information can be found in the references.<sup>290-293</sup>

#### 4.4.8 Equalizer

Equalizers are devices that fill such needs as leveling attenuation characteristics of long transmission line runs and correcting excessive system gain vs frequency slope. The equalizer used for the reflectometer is the Sierra Microwave Technology model SM31183. Some of the main characteristic parameters of this model are shown in Table 4.11. It basically works like a cavity resonator filter over the band and is labeled in Figure 4.8 as “equalizer”.



**Table 4.11: Main parameters of the equalizer.**

Parameter	Value
Attenuation @ 8.0 GHz	6.2 dB
Attenuation @ 10.25 GHz	2.95 dB
Insertion loss @ 12.5 GHz	0.51 dB
VSWR J1 1.7:1 Max	1.54:1
VSWR J2 1.7:1 Max	1.35:1

#### 4.4.9 Waveguides/antenna system

For the first phase of the experiment, the reflectometer used/shared the TFTR's fluctuation reflectometer waveguide system. This is shown in Figure 4.3<sup>294</sup> and Figure 4.26. Shared access to the waveguide system is done using two waveguide switches that can be set to allow the fluctuation reflectometer system or the phase difference reflectometer system (but not both) to have access/use of the waveguide. The waveguide system vacuum interface is done by using a sophisticated set of planar mirrors and parabolic mirrors that focus and direct the microwave beam into a particular area inside the vacuum vessel. This system was designed and constructed to study highly localized plasma fluctuations at the center of the plasma of TFTR, not to study the edge of the plasma as was done for the ORNL reflectometer. Thus, focusing and intersecting the Gaussian beams at the edge of the plasma was hard to do and in most cases it was very inefficient for use in getting a strong reflected signal amplitude back from the plasma. This is seen in Figure 4.26, where the Gaussian beam patterns are shown with their intersection volume and the mirrors of the TFTR's fluctuation reflectometer waveguide system. On the other hand, the system was able to give good signal amplitude for the center part of the plasma when the reflection layers were away from the edge in some plasma configurations.

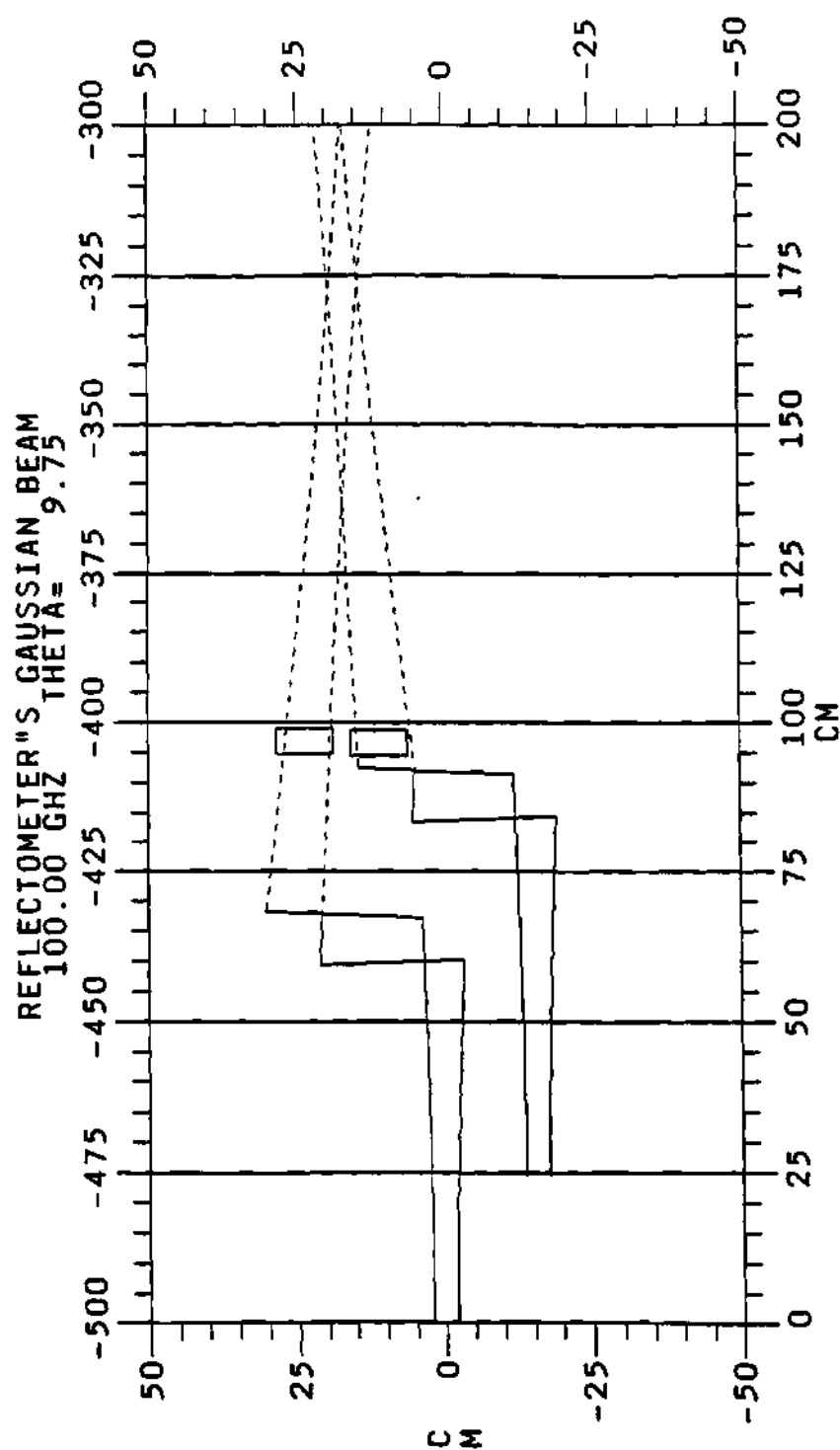


Figure 4.26: Calculated TFTR's Gaussian beam geometry and intersection inside the vacuum chamber.

#### 4.4.10 Power budget

A power budget was done for the reflectometer system and it is shown in Figure 4.27. The diagram shows the power ratio of each major component in units of dBm (decibels with respect to 1 milliWatt of input power) or dB (decibels). From the diagram the power of the Backward Wave Oscillator (BWO),  $P_{BWO}$ , can be calculated as:

$$13 = 10 \log \left( \frac{P_{BWO}}{1 \text{ mWatt}} \right) \quad (4.43)$$

$$1.3 = \log \left( \frac{P_{BWO}}{1 \text{ mWatt}} \right) \quad (4.44)$$

$$\frac{P_{BWO}}{1 \text{ mWatt}} = 10^{1.3} \quad (4.45)$$

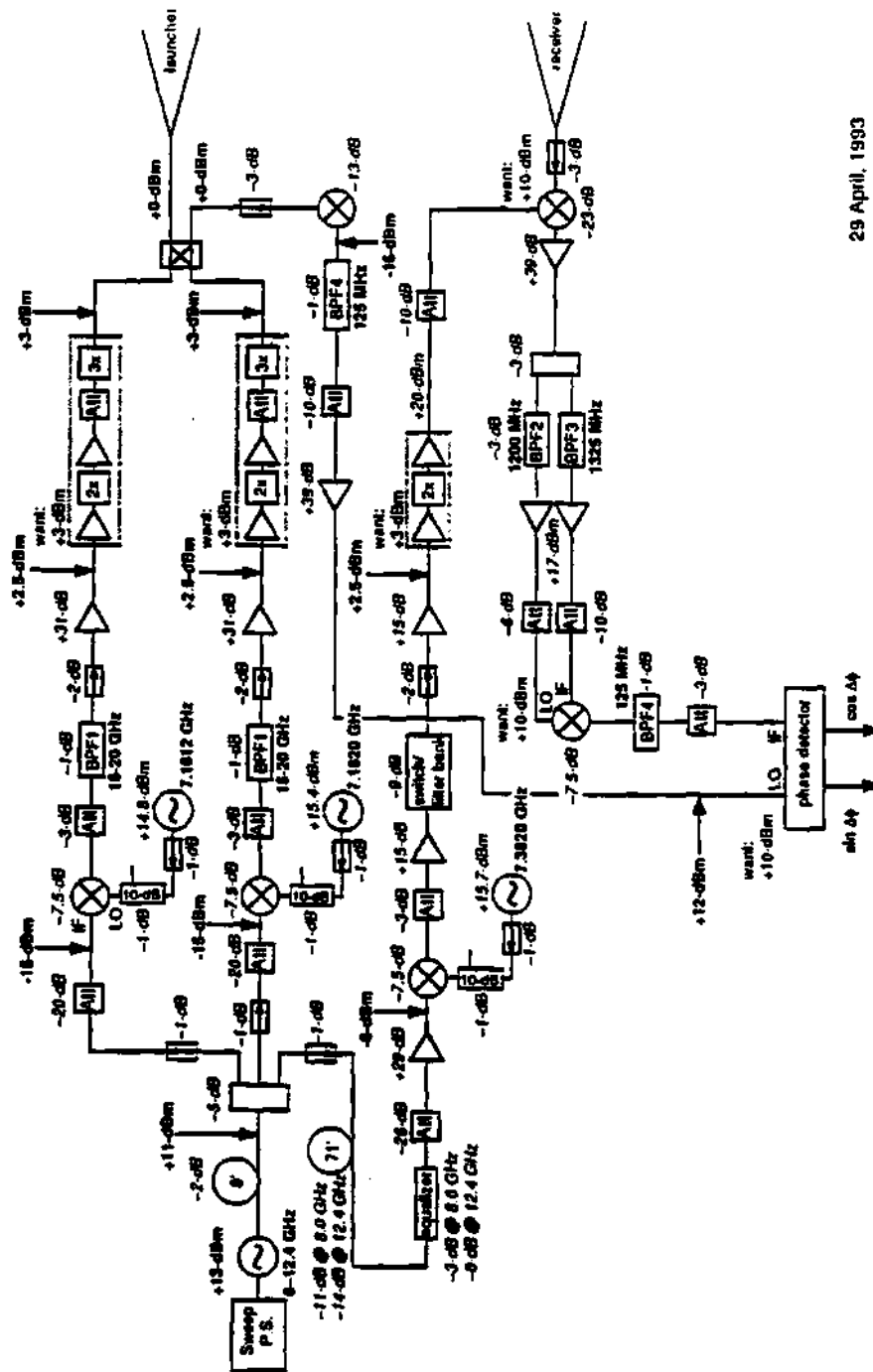
$$P_{BWO} = 10^{1.3} \cdot 1 \text{ mWatt} \quad (4.46)$$

$$P_{BWO} = 20 \text{ mWatt} \quad (4.47)$$

and from the value at the launcher the power sent to the plasma is about 1 mWatt. The full waveguide run had a loss of  $\approx 10$  dB according to McCarthy<sup>294</sup> and as discussed in section 5.5.2. The plasma can have a loss of  $\approx 40$  dB<sup>309</sup> depending on the plasma conditions and the position of the first cutoff layer. This gives to a total loss of  $\approx 50$  dB for a plasma and both ways through the waveguides. Finally, the power received by the reflectometer receiver will be  $\approx 10^{-5}$  mWatt.

## 4.5 Summary

This chapter presents the development, requirements, and description for the Dual Frequency Phase Difference reflectometer for TFTR. The development of the reflectometer was divided into a two phase program. The first was a cheap and fast way to test the capabilities of the reflectometer by using the pre-existent waveguide system of the TFTR fluctuation reflectometer. This was used on a



29 April, 1993

Figure 4.27: Reflectometer system power budget diagram.

shared basis with the fluctuation reflectometer group (Dr. Ernesto Mazzucato and Dr. Rafi Nazikian). From this waveguide system it was possible to collect data on the plasma at a position away from the ICRH antenna; thus, no direct measurements of the density changes at the ICRH antenna environment could be made. However, any global changes in the edge density profile and center of the plasma (for different values of the magnetic field,  $B_0$ ) could be measured using the highly focused Gaussian beams of the TFTR fluctuation reflectometer system. This provided a base line data base for the performance of the reflectometer. After a successful proof of principle test on the TFTR fluctuation reflectometer system, the Dual Frequency Phase Difference reflectometer was ready for the second phase of the project. A description of the reflectometer components and how these components generate the dual frequency probing signal used for the measurement was presented.

# CHAPTER V

## OPERATION, VERIFICATION AND CALIBRATION

### 5.1 Introduction

This chapter presents the procedures used to operate the reflectometer and verify its proper operation. A step by step list of procedures is presented to describe the proper use, setting, operation, and verification of the reflectometer. Both operation and verification are related and a great effort was made to try to explain them separately. Description of the procedures to collect and calculate the calibration data for the bypass loop and for the full waveguide run of the reflectometer are presented. The calculation for the translation of the reference plane from the position of the right angle metal reflector to a position two wavelengths away from it is presented. The conclusions for these calibrations are given in the chapter summary.

### 5.2 Description of the Normal Operation

#### 5.2.1 Some parameters

In order to better understand the reflectometer a short description of some of its main parameters is important. The frequency range for the reflectometer is  $\approx 92$  to  $117$  GHz. The sweeping time of the Backward Wave Oscillator (BWO) is  $\approx 1$  msec. The voltage range of the signal depends on the plasma scenario, and can range from 3 Volts for a low signal to 6 Volts or higher for a good signal. The

number of data points taken depends on the digitization rate of the digitizers and the sweep rate of the BWO. The basic formula is:

$$N_{points} = t_{sweep} \cdot f_{digitizer} \quad (5.1)$$

where  $N_{points}$  is the number of points per sweep,  $t_{sweep}$  is the time to make a frequency sweep, and  $f_{digitizer}$  is the digitization frequency (or the digitizing rate) of the digitizers. For a typical sweeping time of  $t_{sweep} = 1 \frac{msec}{sweep}$  and a digitizing rate of  $f_{digitizer} = 500$  or  $1000$  KHz the number of points was about 500 or 1000 points per sweep. This number is a compromise between having a good number of points to describe the plasma and being able to collect data for a reasonable interval of time, because the amount of memory available in the digitizer is limited. That is, higher digitizing rates will give more data points per sweep, but because the limited amount of memory the time interval to take data will have to be smaller.

The radial scanning range of the reflectometer is determined by the radial position of the reflection layers of the plasma. A contour plot of the cutoff frequencies as function of the minor radius and the density is shown in Figure 5.1 together with some density profiles. The points of cutoff frequencies and cutoff positions for each profile are marked as A, B, and C for the reflectometer's maximum frequency of 117 GHz. The importance of this plot is that the maximum cutoff density and cutoff position is determined by the line of constant cutoff frequency for the frequency of 117 GHz. The maximum scanning density and maximum scanning radial position can be found for any given density profile by finding the intersection of the density profile with the curve of constant cutoff frequency in Figure 5.1 (where the density profiles A, B and C are only examples). For the example of Figure 5.1 the cutoff position and cutoff density for a low density plasma like the one of curve A in Figure 5.1 are  $(r_c, n_e) = (0.6, 2.2)$ , while the cutoff position and cutoff density for a high density plasma like the one of curve C will be  $(r_c, n_e) = (0.72, 2.75)$ , where the units are given in the figure. Therefore, the

cutoff position and cutoff density for any density profile can be found by plotting the density profile in Figure 5.1 and finding the intersection between the density profile curve and the curve of constant cutoff frequency of interest.

### 5.2.2 Normal operation

Waveguide setup As discussed previously, the phase difference reflectometer was using the fluctuation reflectometer waveguide run on a shared basis. Therefore, before using the waveguide it was necessary to request permission for the use of the waveguide. To set the phase difference reflectometer to use the waveguide all that was necessary was to set the waveguide switches to the position where the switches would send the phase difference reflectometer's signal to the waveguide instead of the bypass calibration loop.

Getting on the shot cycle As with all TFTR diagnostics there was a series of steps to be done in order to have the reflectometer running and ready to take data. One of the first things to do was to request to the TFTR operator to put the reflectometer diagnostic on the "shot cycle" for some particular experiment of interest (in general it was for the entire day). This authorized and/or ordered the computers to collect the data of the reflectometer from the digitizer's memory and put it in the disk area of the PPPL computer system.

Setting the reflectometer's digitizers Setting the digitizers is an operation that must be done before the plasma shot. The parameters of the digitizers include: the start time for the data window, number of active channels, digitizing rate, voltage range of the channels, etc. To do the setting of the digitizers there is a program named "YOMENU" that runs on the "Gould" computer system which is used to control the digitizers of the reflectometer. The program uses a menu



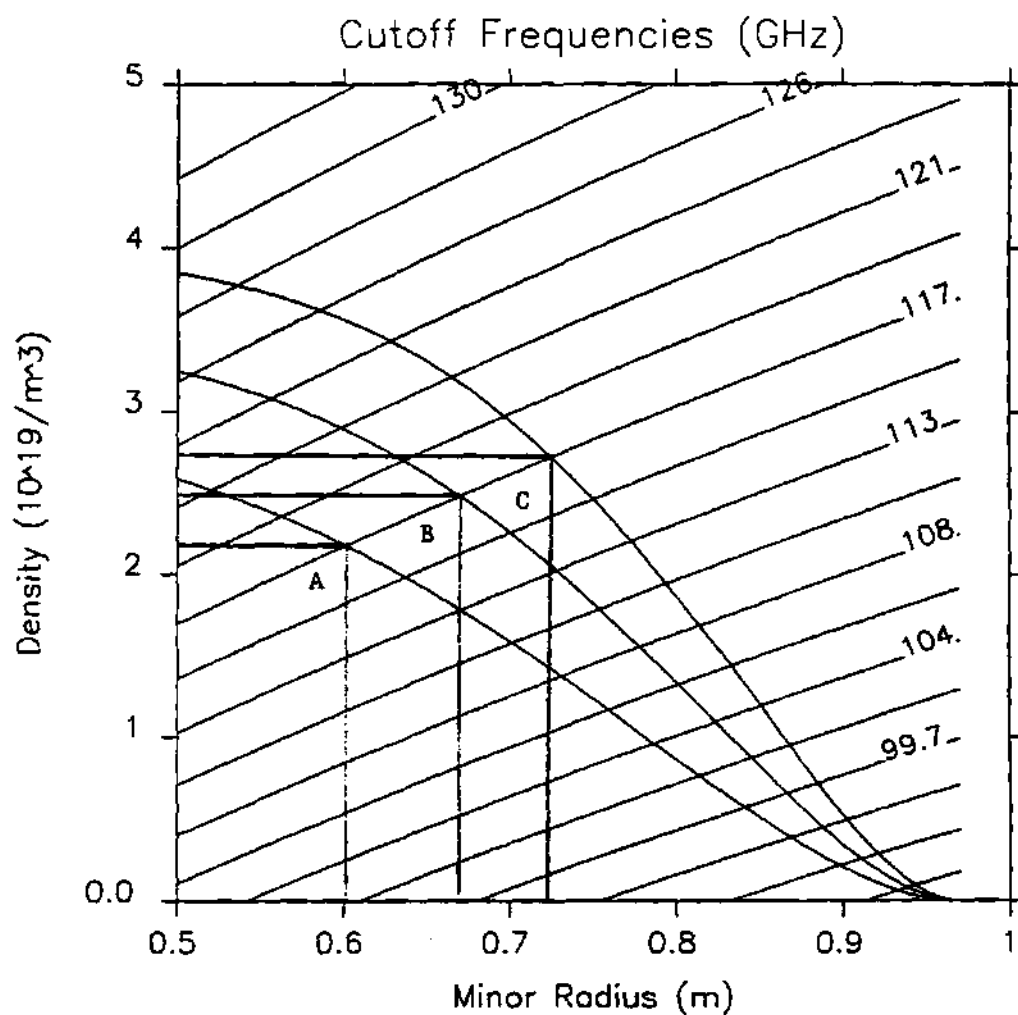


**Figure 5.1:** Plot of the family of lines of the cutoff frequencies as a function of density and radial position. Three density curves with their corresponding cutoff frequency and cutoff position are shown. ( $B_0 = 4.5$  Teslas)

driven interface for operation and setting of the digitizers.

The new settings of the digitizers are recorded on the parameters file (PFT *ShotNumber* file) for the particular plasma shot and the settings will remain the same for all the following shots.

**Normal setting of frequency sources** The sweeper ramp signal for the Backward Wave Oscillator (BWO) is shown in Figure 5.2 for a normal setting. From this figure the total time per sweep is about 3.0 msec, of which 1.0 msec are for the ramp voltage of the sweeping signal to the BWO and the other 2.0 msec are the reset time for the BWO. Therefore, the only data that is useful is the data collected during the 1.0 msec of the sweep ramp.

The Backward Wave Oscillator source is set with the help of a cavity wave meter connected to an oscilloscope with a detector diode. The sweeper signal is set in one channel of the oscilloscope and the output of the detector diode is on the other channel of the oscilloscope. The way in which this setup works is that the cavity wave meter is tuned until it reaches the resonance frequency of the source at the lower or upper end of the sweep. The point of resonance of the cavity wave meter will be shown on the oscilloscope as a low signal point in the signal of the diode detector. The frequency at the lower or upper end of the frequency sweep can be read from the cavity wave meter.

The fixed frequency sources are set manually with the help of a microwave frequency counter. The Dielectric Resonator Oscillators (DROs) can be set by using a mechanical tuning button or can be electrically tuned to the desired frequency of operation, as described in section 4.4.2. The settings for the DROs are shown in Table 5.2.

**Table 5.1: Table of the pull down menu options for the YOMENU program.**

<b>Help Menu</b>			
(N)	next field	(G)	Go to field No.
(P)	previous field	(A)	accept settings
(F)	first field	(X)	go to main menu
(L)	last field		
<b>Segment Size</b>			
(0)	1k	(4)	16k
(1)	2k	(5)	32k
(2)	4k	(6)	64k
(3)	8k	(7)	128k
<b>Sampling Rate</b>			
(9)	10 kHz	(13)	200 kHz
(10)	20 kHz	(14)	500 kHz
(11)	50 kHz	(15)	1 MHz
(12)	100 kHz	(16)	2 MHz/2 channels
<b>Sensitivity</b>			
(3)	4.096		
(4)	10.24		
(5)	25.60		

**Table 5.2: Table showing the drift/change in frequency of the DROs.**

	Frequency (GHz)
DR01	7.1410
DR02	7.1818
DR03	7.2818

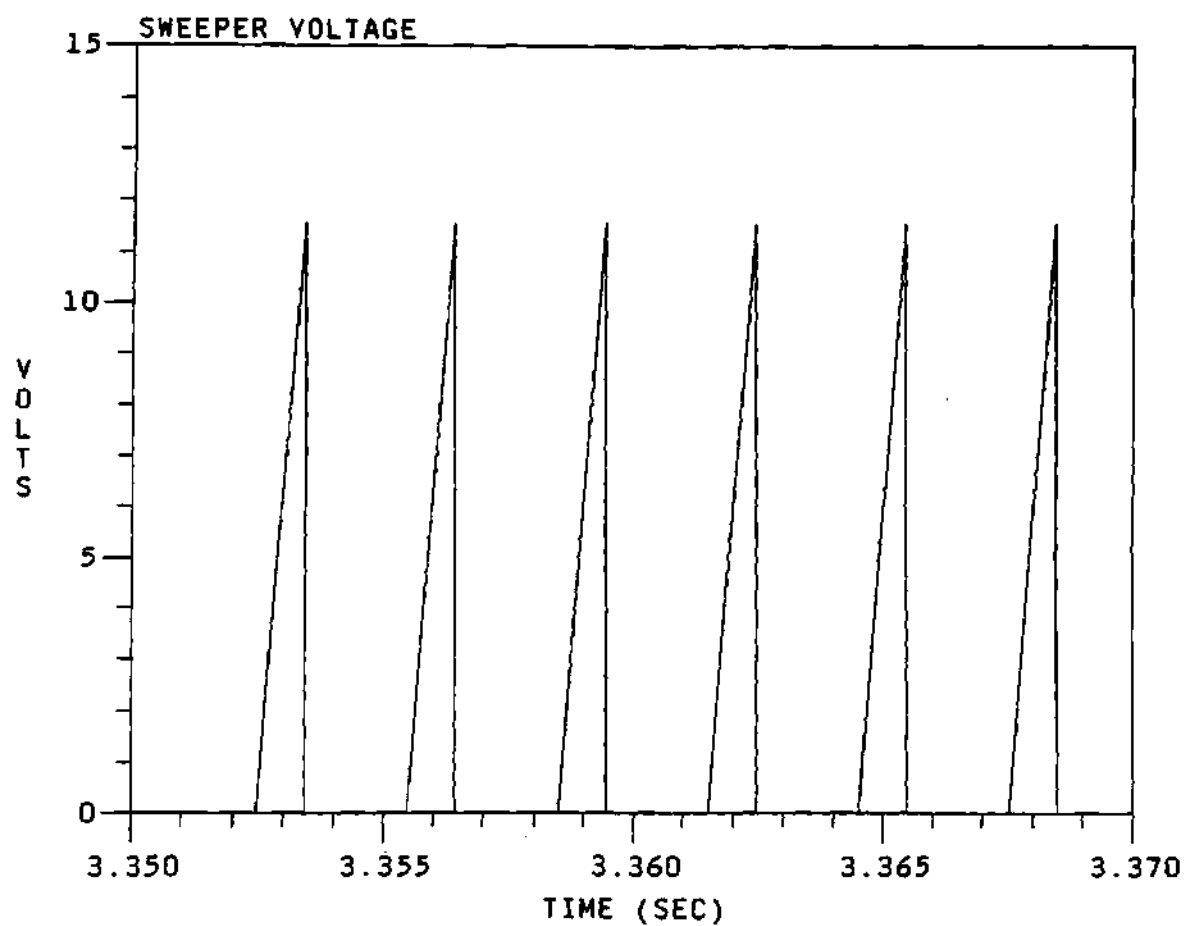


**Figure 5.2: Sweeper voltage signal to the Backward Wave Oscillator. The sweeping time and the reset time of the Backward Wave Oscillator can be calculated from this plot.**

**Take bypass loop data** Before the first plasma shot data set was taken, it was useful to take a bypass loop calibration shot data set, as described in section 5.4. This data had the phase information of the reflectometer electronics components. The bypass loop data was not only useful to calibrate the plasma shots data, but it was used as a signature or finger print that the phase of the components and the reflectometer had not changed due to malfunction or other reasons. Examples of the bypass loop calibration data are shown in section 5.4.

After the bypass loop calibration was taken and the diagnostic was ready to take data, then the shutters of the waveguide system could be opened to release the reflectometer signal to go in and out of the vacuum vessel.

**Recognizing good data** Once the reflectometer was taking data there were two criteria to determine if it was good data or not. The first criterion was to look at the signal amplitude from the plasma. If the signal amplitude was too small, then the return signal from the plasma would not have enough power to drive the receiver mixer, and the signal would be lost in the receiver noise. A good signal amplitude for a plasma shot is around 6 Volts, while a poor signal level would be anything below 3 Volts. The second criterion was to look at the phase fluctuations of the raw phase calculated from the  $I = A_r \sin(\phi)$  and the  $Q = A_r \cos(\phi)$  signals of the reflectometer. If the level of fluctuations of the calculated phase was so large that the tracking of the phase was erratic, then the data was not usable. In order for the phase to be easy to track, the phase fluctuations have to have an amplitude much less than  $\frac{1}{2\sqrt{3}}$  fringes rms.

### **5.3 Verification and Testing the Operation of the System**

#### **5.3.1 Bypass loop verification and testing**

Unlike most commercial electronic equipment (like a laser printers and/or oscilloscopes) the reflectometer does not have a test button nor a simple and direct way to test it for proper operation. Thus the only options available are to check the electronic components one by one, or having the reflectometer take a sample data set from the bypass calibration loop. The first option is some what complicated in the sense that a good knowledge of the reflectometer electronics and/or components, plus the necessary hardware (oscilloscope, etc. . . ) and a considerable period of time will be needed. The second option is easier to perform since all that is required is to set the waveguides switches to the calibration bypass loop and the proper software to see the data collected from the bypass loop. This is the very same procedure used to take the calibration data, and it provides plots of the signal amplitude and the phase delay of the bypass loop as a function of the swept frequency. The calibration data obtained in this way can be compared with the calibration data from previous days or the data obtained during the testing of the reflectometer at Oak Ridge to make sure that the phase due to the different components had not changed. This calibration data is stored in the computer as a regular data file. It not only provides the convenience of plotting the phase delay of the bypass loop as a function of the sweeping frequency, but it keeps this data in the computer's storage system, thus providing for the comparison of different data sets from different days whenever necessary. In this way the phase changes due to things such as the malfunction of one of the reflectometer's components can be monitored. An example of this is shown in Figure 5.8 where the phase of the calibration data was changed from one day to another due to some change in the electronics components of the reflectometer (possibly tightening of a connector

or a change in one of the microwave components). This added an extra phase of 0.05 fringes to the data, but the system was still in general working conditions.

### 5.3.2 Effects of the plasma on the reflectometer data

**Magnetic fields** The magnetic field environment of fusion experiments and in particular the one of TFTR can affect the performance of some electrical equipment that is sensitive to strong magnetic fields such as the one encountered in the TFTR proximity. Nevertheless, this was not the case with the phase difference reflectometer. As noted in the reflectometer's log book: "No problems noticed with TFTR field, scope deflected slightly, but frequency or power not changed in DRO3." This can be shown better using the data from the bypass loop. That is, comparing the data sets for the bypass loop during a real plasma shot (with magnetic field) and the bypass loop data for a shot without a plasma (without magnetic field). These are shown in Figure 5.3 for a bypass loop data set without magnetic field and in Figure 5.4 for a plasma with magnetic field. As can be seen from these two figures, there is no significant change on the amplitude of the signal or the phase difference data for these two bypass loop calibration data sets, that is, there is no significant change like a shift of frequency (negative or positive) for the frequency band of the sweep, or the vertical values for the plots. The two graphs are basically identical, therefore it is safe to say that there is no significant effect of the magnetic field on the reflectometer. For the Dielectric Resonator Oscillators (DROs) there was not significant change on the frequencies during the plasma shots. Therefore, it is safe to conclude that the reflectometer diagnostic is not sensitive to the magnetic fields of the TFTR experiment.

**Electron Cyclotron Emission of the plasma** Another issue was the effect of the Electron Cyclotron Emissions (ECE) on the receiver and density

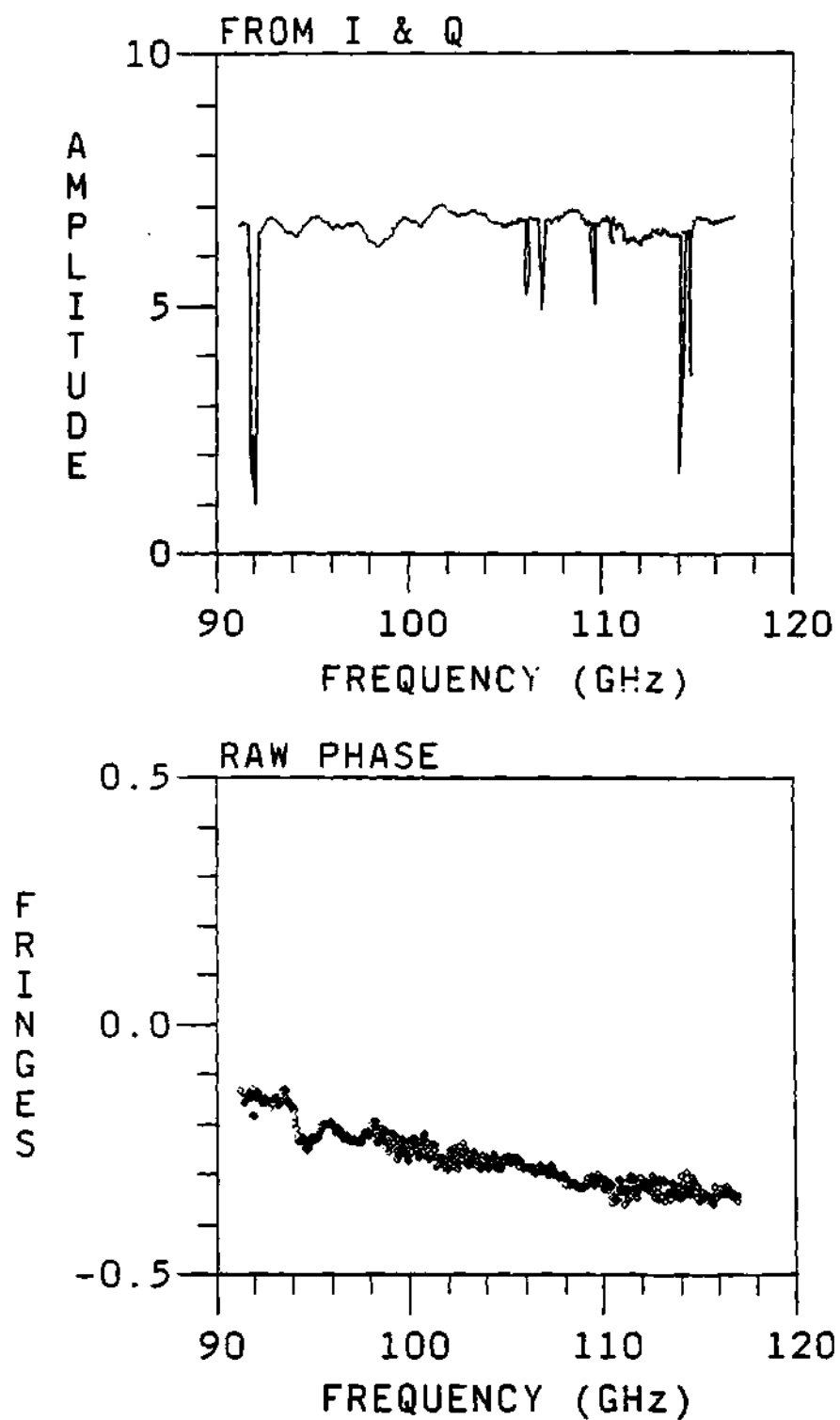


**Figure 5.3: Bypass calibration loop data with no magnetic field. (A) Plot of the amplitude of the signal. (B) Plot of the phase difference data. (Attenuation setting was 30 dB.)**



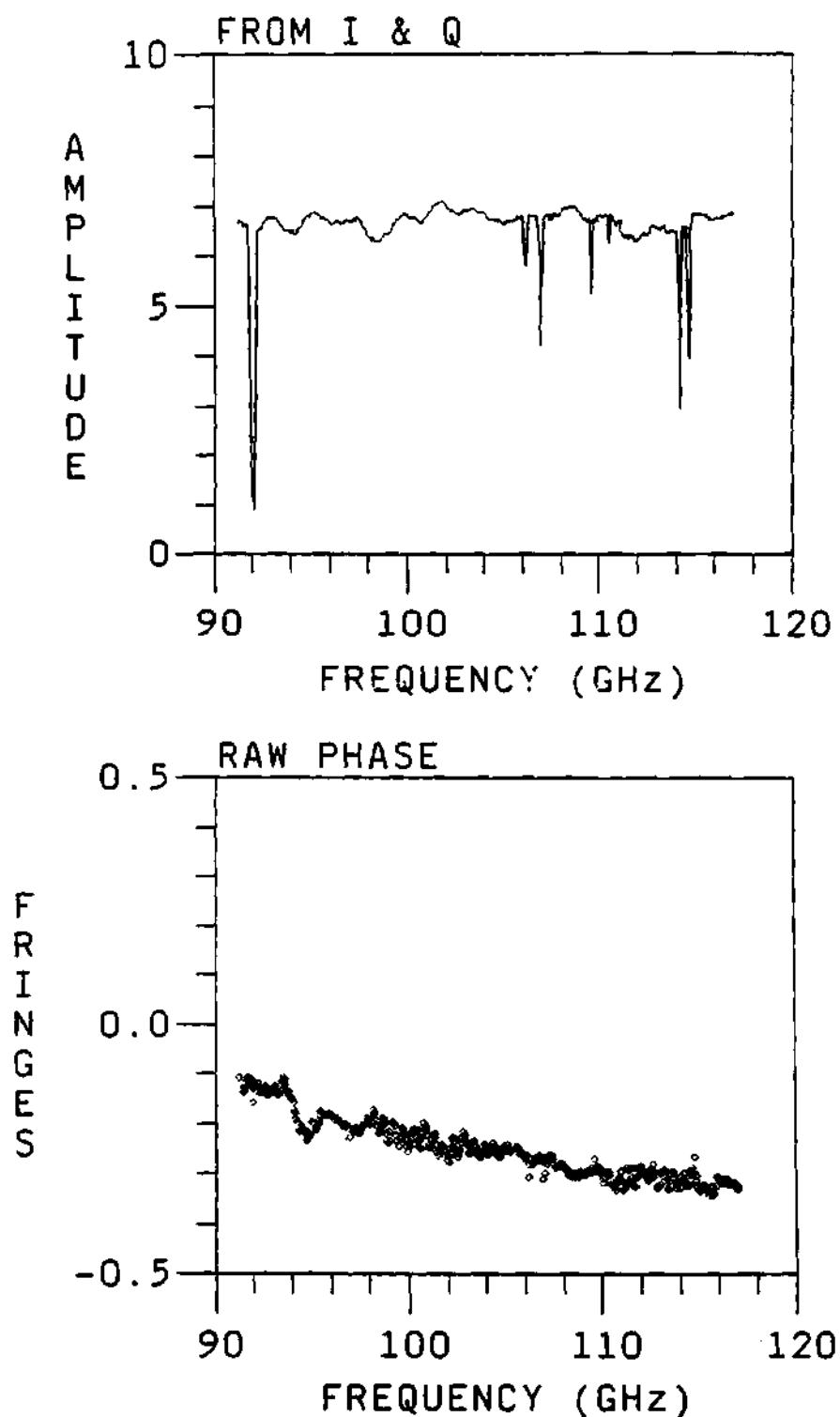


**Figure 5.4:** Bypass calibration loop data for a plasma with a magnetic field of 3.2 Tesla. (A) Plot of the amplitude of the signal. (B) Plot of the phase difference data. (Attenuation setting was 30 dB.)

fluctuations on the calculated phase data. It was observed that the signal level of the amplitude fluctuations was in some cases larger in magnitude than the noise of the receiver, while the noise of the receiver and the ECE of the plasma were comparable in signal amplitude. Therefore, the effect of the receiver noise and the ECE of the plasma was not significant to the plasma signal for most of the cases and that the plasma signal dominates the signal amplitude at the receiver.

### **5.3.3 Maximizing the return signal**

The waveguide and mirror system of the TFTR fluctuation reflectometer was designed to study highly localized fluctuations in the center of the plasma, not the edge. Because of this incompatibility with the original design of the focusing mirrors, the probing of the plasma edge was complicated by the clipping of the Gaussian beams by the vacuum windows. It was hard to get the beams to intersect with a big enough cross section to have an acceptable signal strength from the plasma edge. This was additionally complicated by the risk that driving the mirrors beyond their scanning range could lock them into a position where they were useless to the fluctuation reflectometry team. The mirror positions for maximum signal coupling were obtained by simply scanning the mirrors for different angles and plasma shots.

## **5.4 Absolute Bypass Loop Calibration**

Because of imperfections on the reflectometer's components, resistive losses and dispersion of the probing wave while propagating in the waveguide system, the probing beam measures a phase difference not directly associated with the propagation of the probing beam in the plasma. Since the waveguide system and the reflectometer's components change little during plasma shots, the associated

phase due to these effects can be measured and subtracted from the plasma data to correct for these errors.

Calibration of the reflectometer's data is done by subtracting the phase data due to the propagation of the wave from the reflectometer to a test mirror and back to the reflectometer. This phase data is due to two main contributions: the phase due to the reflectometer electronics and the phase due to the waveguide run to the vacuum vessel.

#### **5.4.1 Setting of the bypass loop switches**

The calibration data from the bypass loop is obtained simply by setting the waveguide switches of the waveguide system so that the probing wave goes through the calibration loop and not to the plasma. This setup is shown in Figure 5.5, where the two "baseball" switches and the attenuators (depicted by an adjustable resistor symbol) are shown in their relative position with respect to the fluctuation reflectometer and the phase difference reflectometer. As soon as the digitizers are triggered by the TFTR plasma shot, data is collected with the phase information of the bypass calibration loop and the reflectometer electronics. There exist Fortran computer programs to read and analyze the data. These programs will be discussed in sections 7.2 and 7.3.

The bypass calibration loop is a piece of waveguide connecting two attenuators to the waveguide switches such that the probing wave makes a short loop back to the reflectometer. These two attenuators can be adjusted to simulate the losses due to the actual waveguide transmission line and plasma, thus making a continuous test data file of the performance of the reflectometer circuits. This data contains the phase due to the test loop plus the phase due to the non-linearities of the reflectometer system. Since the bypass loop data contains the phase data due to the reflectometer's electronics, it can change from one day to another due to

changes in the components of the reflectometer. This can be monitored to detect for problems with the reflectometer electronic's components. An example of this type of calibration data is shown in Figure 5.6 for the bypass test loop. Notice how the phase changes in a quasi-linear way with some fluctuations added to it. The negative spikes at both ends of the amplitude plot are due to inter-modulation frequencies of the electronic components.

#### **5.4.2 Uses of the bypass loop data**

The bypass phase calibration shows changes in the phase and components of the reflectometer electronics, thus revealing when a change in the phase due to the internal components occurs. This can be seen more clearly from Figure 5.7 which shows the phase data comparison for two calibration shots on different days. The upper plot of Figure 5.7 shows the calibration phase data for two different days overlayed on each other. The close match makes it difficult to distinguish between the curves. The lower plot in Figure 5.7 shows the point by point difference in between the data sets of the upper plot. The bypass loop phase remains the same on the average, this is shown by the curve in lower plot of Figure 5.7, which has a zero average value. Figure 5.8 shows the phase data for the calibration of two different days which shows a constant increment on the calibration phase data of about 0.05 of a fringe. This constant change in the phase pointed out a possible problem with one of the components of the reflectometer.

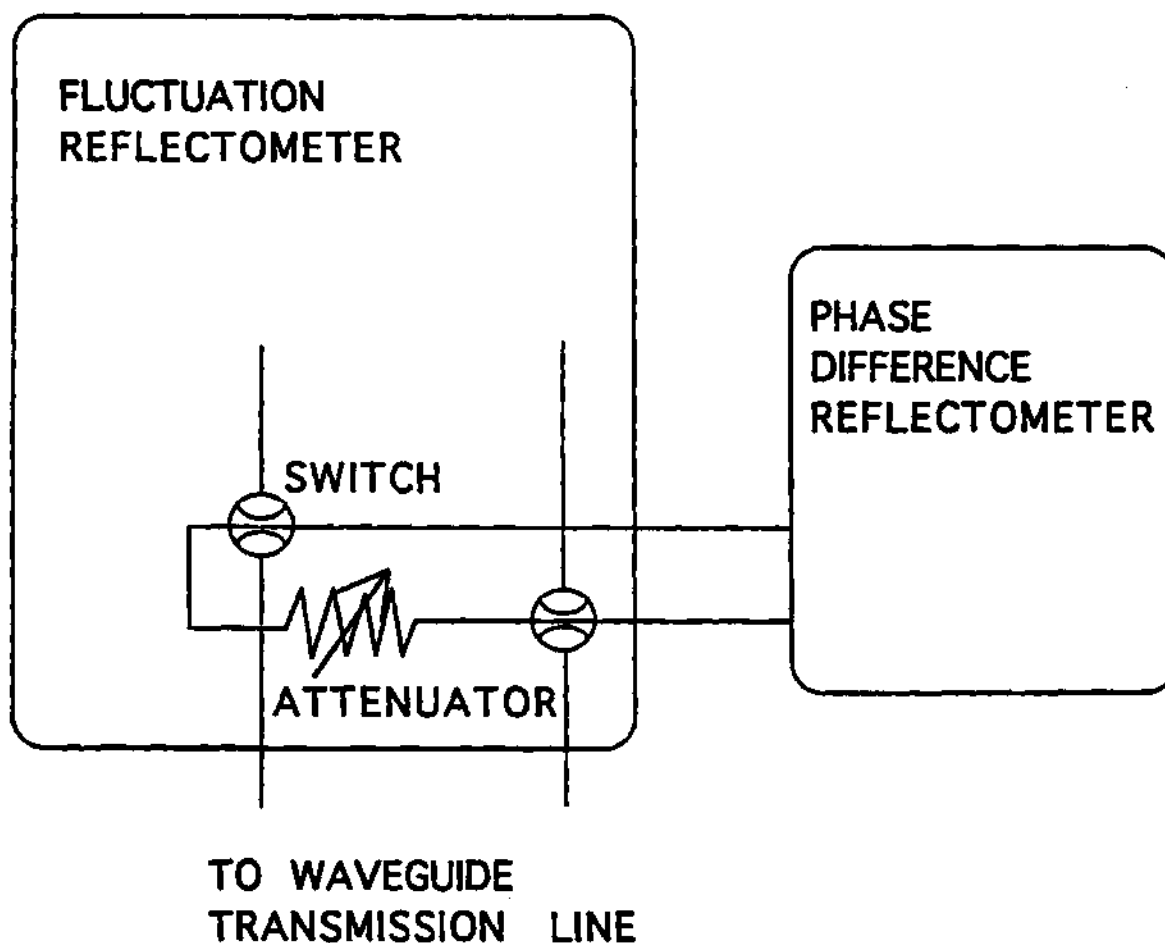


**Figure 5.5:** Waveguide switches and calibration loop setup for the reflectometer system. Components and/or symbols are not to scale.

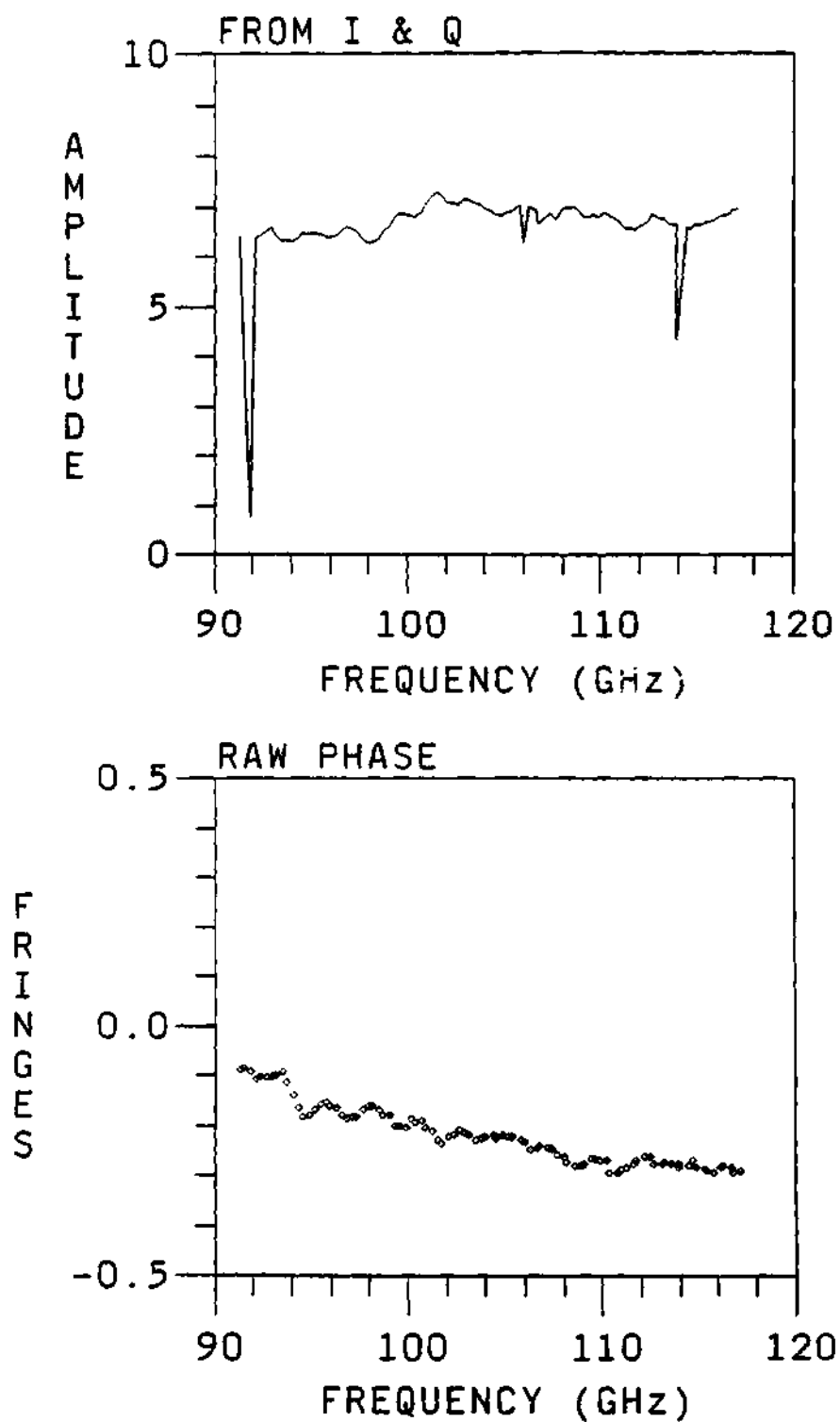


**Figure 5.6: Reflectometer phase data for the bypass test loop (attenuator set to 30 db). The upper plot is the signal amplitude and the lower plot is the calculated phase difference data.**

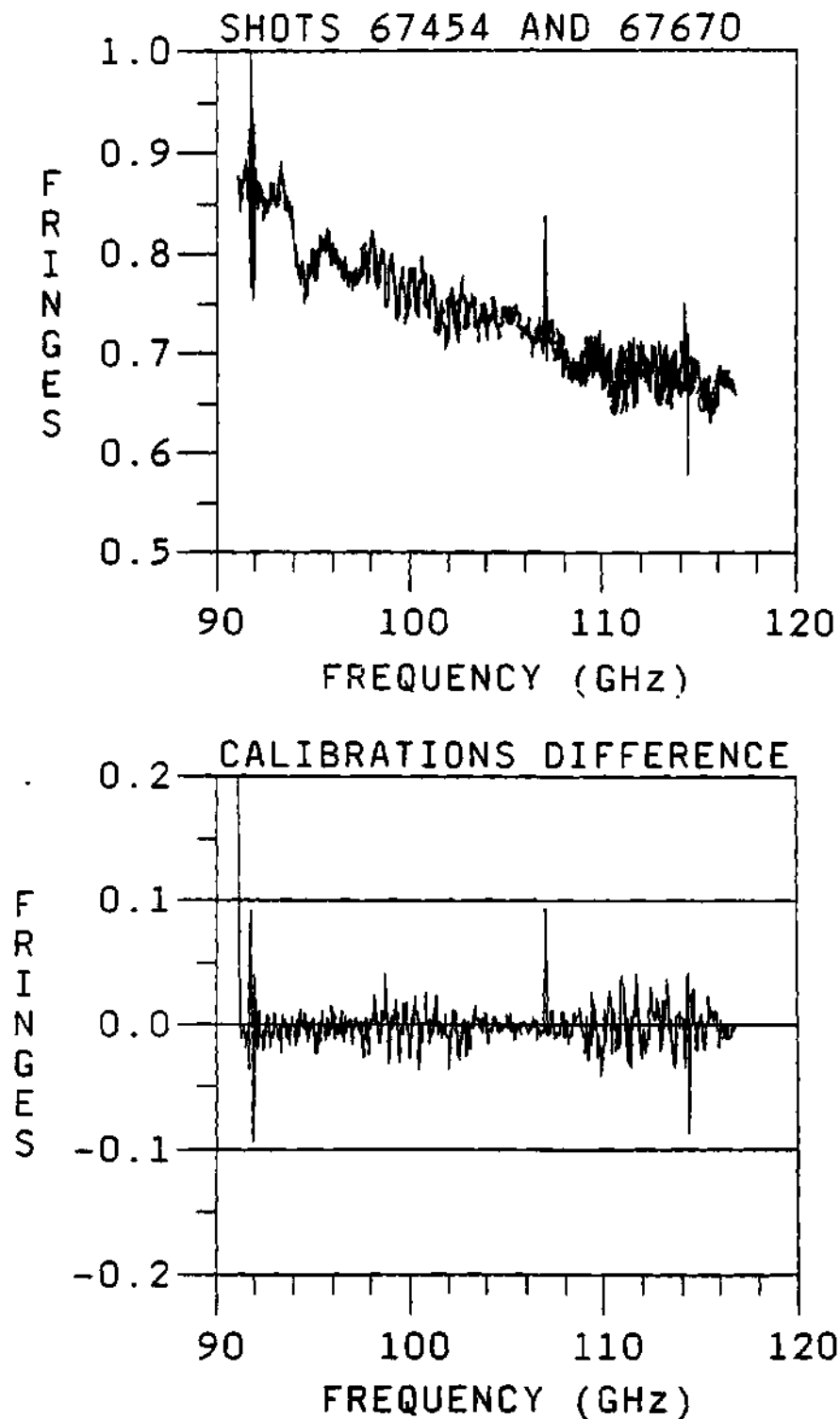
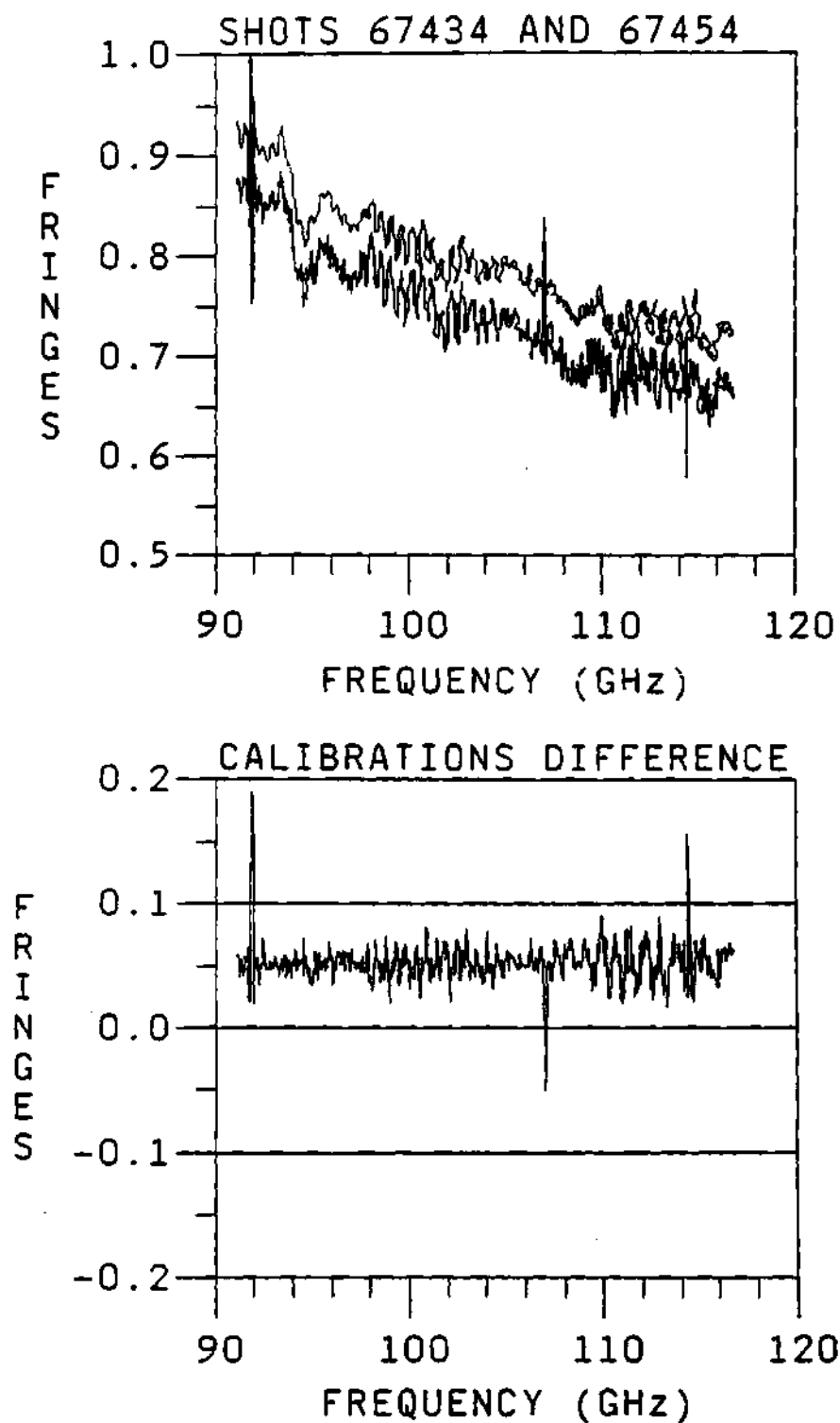


Figure 5.7: Reflectometer phase data of the bypass loop for two different days with no change on the calibration phase data (attenuator set to 30 dB). The upper plot is the calculated phase difference data for the two plasma shot numbers in the figure and the lower plot is the difference between the two data sets.



**Figure 5.8: Reflectometer phase data of the bypass loop for two different days with a 0.05 of a fringe change on the data (attenuator set to 30 dB). The upper plot is the phase difference data and the lower curve is the difference between the data sets.**



**Table 5.3:** Table showing the drift/change in frequency of the DROs.

DRO#	From (GHz)	To (GHz)	Power (dBm)
1	7.1410	7.1400	-2.6
2	7.1818	7.1817	-1.5
3	7.2818	7.2817	-0.7

## 5.5 Absolute Waveguide Run Calibration

### 5.5.1 Reflectometer initial settings

The first "run data" of the reflectometer was measured on 8-26-1992. This was a TFTR shot with the reflectometer signal running through a test loop. Initial settings of the DRO's were 7.140, 7.182, and 7.2818 GHz for DROs 1, 2, and 3, respectively. A test of the sweeper source showed that a 10 msec sweep was possible. For the initial operation and testing a YIG (Yttrium Iron Garnet) frequency source was used (instead of the BWO). The YIG source was set to have a starting frequency of 8.00 GHz and an ending frequency of 12.40 GHz. Sweeper power level was set to  $\approx 2.0$  mW to get saturated signal at full band. Later tests (10-8-1992) of the stability of the DRO sources revealed that a very small adjustment was needed. These are shown in Table 5.3, which shows that the stability of the DROs is good. Testing of the initial and final frequencies of the source on 11-19-1992 using a cavity wave meter showed that these frequencies were very close to the original values, as shown in Table 5.4. The stability of the source has been very acceptable.

**Table 5.4:** Table showing the drift/change in frequency of the source.

Source (11-19-92)	Starting (GHz)	Final (GHz)
Measured	7.98	12.38
Ideal setting	8.00	12.40

### 5.5.2 Absolute waveguide run calibration using metal reflector

The calibration data of the full waveguide system contains the phase information due to the propagation of the probing beam from the reflectometer through the waveguide and back to the reflectometer. This is the phase data used to subtract the phase contribution of the waveguide from the plasma shot phase data, thus moving the reference plane of the phase data to a position within the waveguide launcher and the vacuum vessel.

The calibration of the full waveguide system is done by taking data with a reflector at the end of the full waveguide run. This was accomplished by clamping a 90° angle corner at the end of the TFTR reflectometer waveguide system, so as to reflect the incoming probing signal without it going inside the vacuum chamber. This data has the phase information due to the path of the waveguide and the reflectometer electronics. The data is collected on the digitizer's memory and transferred to the computer by means of a manual trigger or asynchronous trigger signal to the digitizers. This generates a data file for analysis and extraction of the phase information. This calibration data file is used to subtract the phase of the waveguide run from the phase data of the plasma shots.

Using a network analyzer it was verified that the power loss due to propagation through the corrugated waveguide transmission line was an average of  $\approx 10$  dB. This compares favorably with that reported by M. McCarthy,<sup>284</sup> given

**Table 5.5:** Table showing the waveguide losses for the fluctuation reflectometer waveguide system.

Component	Quantity	Loss	Total
Tapers	2	1.3 dB/taper	2.6 dB
Mode conversion	2	3 dB/taper	6 dB
Corrugated waveguide	2	1 dB/line	2 dB
System total loss			10.6 dB

in Table 5.5.

### 5.5.3 Translation of reference plane

The calibration with the metal reflector provided the phase information of the full waveguide run to the reference plane of the metal reflector. The reference plane of the metal reflector is outside of the vacuum vessel, so the reference plane has to be translated to the plasma edge inside the vacuum vessel. This is done using the periodicity of the inverse tangent function. That is, for free space propagation (as in air) the phase of the probing beam will increase one fringe every wavelength,  $\lambda = 60$  cm, of displacement. Therefore, the phase at an integer multiple of the wavelength is the same as the one calculated at the reference plane, as calculated by the inverse tangent function. Thus, moving the reference plane a distance of  $2\lambda$  from the reference plane of the calibration will not change the value of the calibration data. For the translation calculations it is assumed that the wave is propagating in free space since the wave is propagating essentially in air. The procedure to perform this translation is described next.

During the calibration using a right angle metal reflector to couple the microwave signal of the waveguides, the beam travels vertically a distance of about 5.8 in (14.73 cm) between the two surfaces of the metal right angle reflector. The

center of the beam path for that vertical jog is a distance of 25 in (63.5 cm) from the surface of the TFTR port flange. The inner wall of the flange is at a major radius position of 155 in (393.7 cm). The thickness of the flange is approximately 1.5 in (3.81 cm). Therefore, the position of the jog with respect to the major radius is:

$$R_{jog} = 155.0 + 1.5 + 25.0 = 181.5 \text{ in} \quad (5.2)$$

$$= 461. \text{ cm} \quad (5.3)$$

The path lengths from the same points on the surface of the reflector to a reference plane ( $R_{ref}$ ) at a major radius position of 365 cm ( $R_{ref} = 143.7$  in) are approximately given by the change in major radius plus a vertical jog of 10.4 to 10.8 in, which turns out to be:

$$\Delta R = R_{jog} - R_{ref} \quad (5.4)$$

$$= (181.5 - 143.7) + 10.6 \quad (5.5)$$

$$= 48.4 \text{ in} \quad (5.6)$$

$$= 122.9 \text{ cm} \quad (5.7)$$

The above should be a pretty good first order estimate, to be compared with the results of a more detailed calculation that follows.

For the lower beam path, the beam travels:

- Horizontally 19.3 in from  $R=181.5$  to 162.25 (first mirrors)
- Vertically 10.4 in to focusing mirror
- Distance of 18.77 in sloping upwards at an angle of  $8.81^\circ$  to the intersection point on midplane at  $R=143.7$  in
- Lower total = 48.47 in (123.1 cm)

For the upper beam path, the beam travels:

- Horizontally 9.75 in from R=181.5 to 171.75 (first mirror)
- vertically 10.8 in to focusing mirror
- Distance of 28.24 in sloping downwards at an angle of  $6.73^\circ$  with respect to the horizontal to the intersection point at R=143.7 in
- Upper total = 48.79 in (123.9 cm)

Therefore the increase in path length to a reference plane at TFTR major radius,  $R = 365$  cm, as compared to the path length with the reflector in place is:

$$(48.47 + 48.79) - 5.8 = 91.46 \text{ in} \quad (5.8)$$

$$123.1 + 123.9 - 14.7 = 232.3 \text{ cm} \quad (5.9)$$

Note that in terms of the beat wavelength of the transmitter frequencies this is  $\frac{232.3}{130} = 1.936$  wavelengths, or  $23^\circ$  short of two wavelengths. The original drawing for the calculation can be found in page 241 of *The Log Book*.<sup>303</sup>

#### 5.5.4 Initial calibration of the reflectometer

The first calibration of the full waveguide run of the reflectometer was done on 9-29-1992. For this calibration a piece of a metal plate, bent at a right angle was positioned in front of the launchers, at the end of the waveguide run to act as a reflector and reflect the reflectometer's signal back to the receiving waveguide run. This gives a measurement of the phase difference changes due to the dispersion properties of the waveguide run from the reflectometer black box to the end of the waveguide run and launcher. The original first data was displayed on an oscilloscope, of which a black and white picture was taken for *The*

*Log Book.*<sup>303</sup> For subsequent calibration data sets, the data was taken during the TFTR plasma shots, thus that data was automatically stored as a PFT and RDT data file in the TFTR data file system. A plot of the phase difference data for one of these first calibration data shots is shown in Figure 5.9.

## 5.6 Summary

This chapter presented a description of the procedures used to do the bypass loop calibration and the full waveguide transmission line calibration for the reflectometer. The bypass calibration data has been useful to calibrate the phase difference data and to verify the proper operation of the reflectometer. The full waveguide calibration data provides the phase data due to the dispersive properties of the full waveguide run and a measurement of the power losses due the resistive losses of the waveguide. These calibrations were used to remove the phase changes due to the propagation of the probing beam through the waveguide transmission line and the reflectometer electronics. The bypass loop calibration data proved to be useful to provide information on the phase changes due to the reflectometer electronics and on the performance of the reflectometer components, since changes in the phase of the bypass loop calibration could be associated with changes on the performance of the individual components of the reflectometer. The bypass loop calibration phase data was used to show that the effects of the magnetic fields of TFTR are negligible to the reflectometer components (in particular to the frequency sources).

Procedures to perform the operation and verification of the reflectometer were presented.

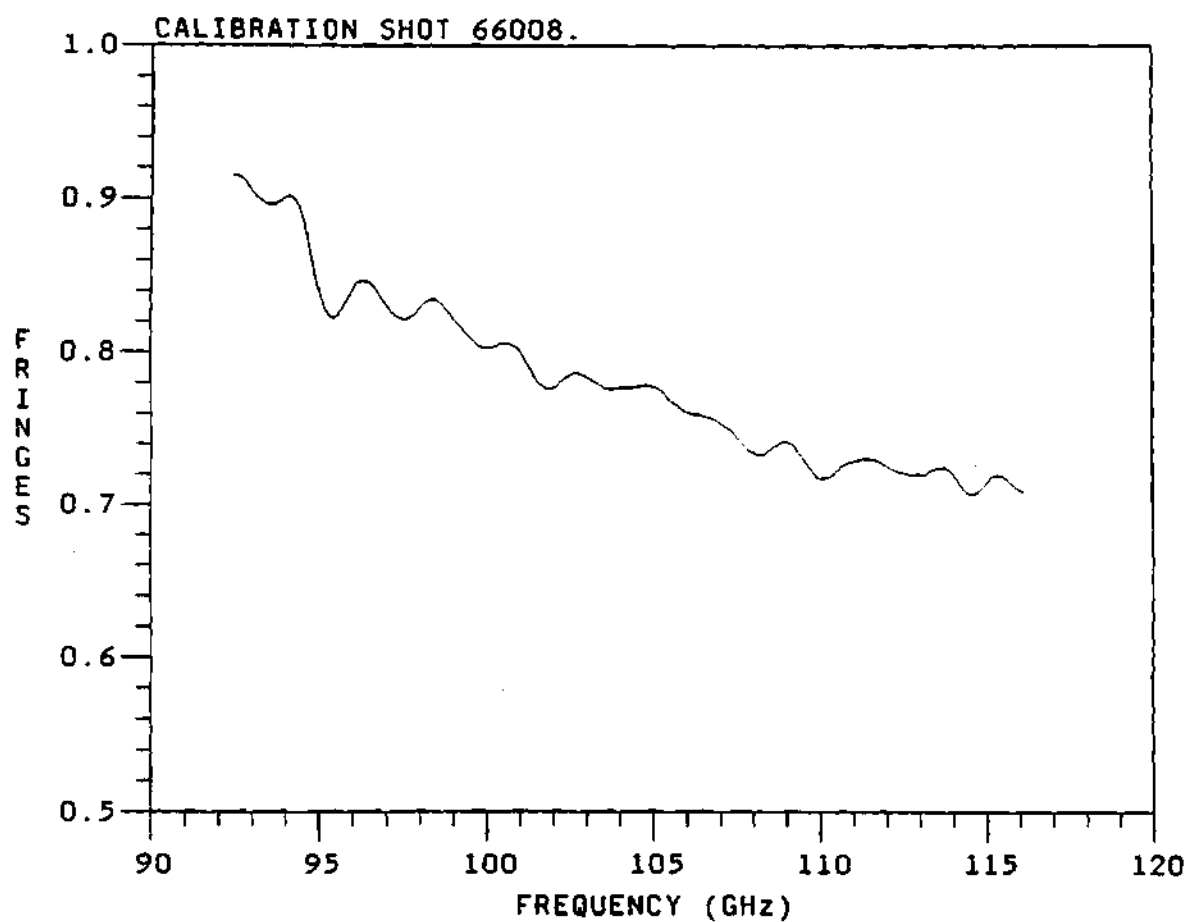


**Figure 5.9:** Phase difference data for one of the first bypass loop calibration data shots taken with the reflectometer system. Comparison with other calibration data sets show a good similarity between the data sets. (Attenuation setting was 40 dB.)

## CHAPTER VI

### SIMULATION SOFTWARE

#### 6.1 Introduction

Computer modeling can provide great insight into the development and construction of a diagnostic. Things like data dynamic range, response to different plasma parameters and/or configurations, and diagnostic limitations can be simulated with a good, accurate and carefully written computer model. This may not be feasible for all diagnostics, but it has been possible for the dual frequency phase difference reflectometer. Thus, this chapter will discuss the simulation and modeling program that was written (by the author) to test the density profile reconstruction technique, get some insight on the dynamic phase data range and other variables, study the effect of fluctuations on the phase data and the reconstruction technique, and examine other parameters. Simulation of the experiment was the first and most cost effective way to test the feasibility of the conceptual idea for the dual frequency phase difference reflectometer. Computer modeling may not provide proof of principle for a diagnostic, but in general, an accurate model can provide useful and important information with respect to the diagnostics and its operational limits. Therefore, the computer simulation was extremely important for designing the reflectometer, and has been very useful in gaining insight into the reflectometer data.



## 6.2 Theory for Profile Reconstruction

The idea for the reconstruction of the profile is relatively simple. The phase of the wave is the area under its index of refraction curve. Two of these index of refraction curves are plotted in Figure 6.1 (dot-dash line curves) from the reference plane ( $r_{ref} = 3.60$ ) to their respective position of cutoffs. These curves represent the index of refraction for the lower (right curve) and upper (left curve) frequency waves. The phase difference as measured by the diagnostic is the difference of the areas of the two index of refraction curves, or the area between the index of refraction curves. The density profile is assumed to be known up to the position of the lower cutoff. Therefore, the index of refraction curve for the upper frequency wave can be calculated up to that position, and the difference between index of refraction curves up to that point can be calculated, that is, the part of the phase difference in the known part of the profile can be calculated. What is left to do is to find a way to calculate the area under the curve of the upper index of refraction curve and between the lower cutoff position and the upper cutoff position. Then the phase difference will be defined as the area between the lower and upper index of refraction up to the lower cutoff plus the area under the index of refraction of the upper frequency wave between the lower and upper cutoffs. The calculation of this area is done by fitting some reasonable function to the index of refraction in this unknown part of the density profile. This function can be inverted to solve for the distance between upper and lower cutoffs of the wave.

The words in the previous paragraph can be expressed in formulas as follows. The phase difference from the diagnostic is defined as:

$$\delta\phi = \int_{r_u}^{r_{ref}} n(r, \omega_u) dr - \int_{r_l}^{r_{ref}} n(r, \omega_l) dr \quad (6.1)$$

where  $n(r, \omega_u)$  is the index of refraction for the upper frequency,  $n(r, \omega_l)$  is the index of refraction for the lower frequency,  $r_u$  is the upper cutoff position,  $r_l$  is the

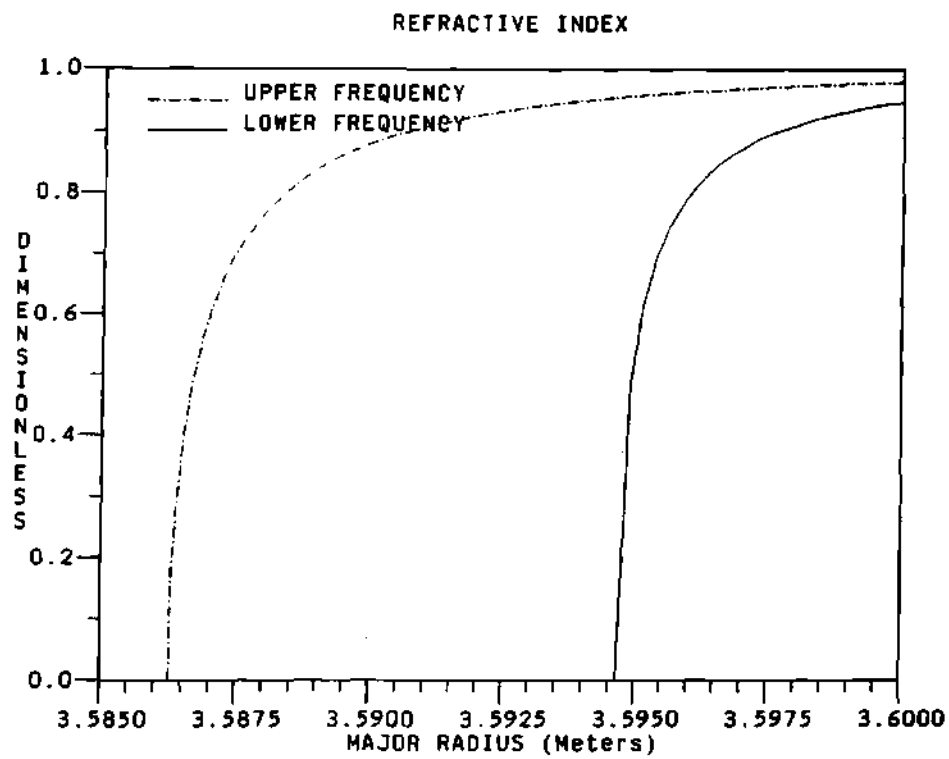


Figure 6.1: Curves of the index of refraction for the upper and lower probing frequencies.

lower cutoff position,  $r_{ref}$  is the reference plane position,  $\omega_u$  is the upper cutoff frequency, and  $\omega_l$  is the lower cutoff frequency. The density is assumed known to the position  $r_l$ . Then, the integral for the upper frequency can be written as:

$$\delta\phi = \int_{r_u}^{r_l} n(r, \omega_u) dr + \int_{r_l}^{r_{ref}} n(r, \omega_u) dr - \int_{r_l}^{r_{ref}} n(r, \omega_l) dr \quad (6.2)$$

where all what was done was to break the integral of the upper index of refraction into two pieces, at the lower cutoff position. If all the known, calculable, and/or measurable quantities are move to the left hand side, then the equation can be simplified to:

$$\delta\phi - \left( \int_{r_l}^{r_{ref}} n(r, \omega_u) dr - \int_{r_l}^{r_{ref}} n(r, \omega_l) dr \right) = \int_{r_u}^{r_l} n(r, \omega_u) dr \quad (6.3)$$

$$\Delta\phi = \int_{r_u}^{r_l} n(r, \omega_u) dr \quad (6.4)$$

where  $\Delta\phi$  is the phase due to the index of refraction past the last known point of density ( $r_l$ ) into the unknown part of the density profile. The curve of the upper frequency index of refraction past the last point of know density is the unknown or missing part of the index of refraction. This part of the index of refraction for the upper frequency wave can be approximated or fitted with a function (polynomial) to solve for the distance between the limits of the integral on the right hand side of the equation. This can be expressed in the equations as:

$$\Delta\phi = \int_{r_u}^{r_l} f(r) dr \quad (6.5)$$

$$\Delta\phi = F(\Delta r) \quad (6.6)$$

where  $f(r)$  is the fitting function (or polynomial) used to approximate the index of refraction in the unknown part of the density profile (past  $r_l$ ),  $F(\Delta r)$  is the integral of the index of refraction fit past the last point of know density ( $r_l$ ) and  $\Delta r = r_l - r_u$  is the difference between the limits of the integral.

Finding a reasonable or good fitting function,  $f(r)$ , and its integral,  $F(\Delta r)$ , is what will be discussed and presented in the following sections.

For the initial part of this project a density profile reconstruction technique developed by Doyle<sup>96,99</sup> was adapted for use with data from phase difference reflectometry. In his technique, Doyle uses a linear function to model the refractive index for the calculation of the phase data (see Figure 6.2). This is the simplest way to solve the problem and this approach will be presented in section 6.2.1. This method provides good results for reconstructing the density profile out of the calculated phase difference data. Nevertheless, a polynomial of any degree can be used to model the missing part of the index of refraction, instead of a linear function as in the case of Doyle's technique. Doyle's method can be considered as the case of a polynomial of first degree. The author decided to try using a polynomial of second degree (i.e., a parabola) to model the missing (or unknown) part of the index of refraction for the calculation of the increment on the radial position. Figure 6.2 shows the index of refraction curve with Doyle's trapezoidal fit (solid straight diagonal line) and the author's Parabolic fit (dash line) together with the real index of refraction (dot-dash line). Both fits are trying to match the area under the fits with the area under the real index of refraction. It must be noticed that since the parabolic fit can curve-up to get closer to the real index of refraction (as compared to the line or trapezoidal fit), then the calculated position for the cutoff of the parabolic fit (i.e., where the parabola intersects the  $x$ -axis) has less error (i.e., it is closer to the cutoff of the real index of refraction) than the calculated position of the cutoff for the trapezoidal fit. More on the error will be presented in section 6.2.2. Unfortunately, there was no noticeable difference between the method using the parabolic fit and the method developed by Doyle using a linear fit. This can be attributed to the derivative of the index of refraction (the derivatives go to infinity) as it approaches the cutoff position. The form of the index of refraction as it approaches the cutoff can be appreciated from Figure 6.3, where the index of refraction as a function of the minor radius is shown for 4 different frequencies (covering the range of the reflectometer) together

with the density profile used. This shows geometrically the form of the index of refraction near the cutoff position. A proof of the convergence of the parabolic approximation solution to Doyle's linear solution will be presented in section 6.2.4. A third technique was developed by the author to fulfill the demands of accuracy on the reconstruction of the profile. This technique uses the real index of refraction function to match the phase difference data and find the position of the cutoff, and will be presented in section 6.2.5.

### 6.2.1 Profile reconstruction based on Doyle's method

The main formula used in this calculation is the equation for the calculation of the phase from the electron density profile, explained previously in section 2.3.5. This phase is given by equation 2.88:

$$\phi = 2 \frac{\omega}{C} \int_{r_1}^{r_2} n(r, \omega) dr - \frac{\pi}{2} \quad (6.7)$$

$$= 2 \int_{r_1}^{r_2} \frac{2\pi n}{\lambda} dr - \frac{\pi}{2} \quad (6.8)$$

where  $\phi$  is the total phase,  $\omega$  is the probing wave frequency,  $C$  is the speed of light,  $\lambda$  is the wavelength, and  $n(r, \omega)$  is the index of refraction. This equation can be expressed as:

$$\phi(\omega_j) = 2 \frac{\omega_j}{C} \int_{r_c(\omega_j)}^{r_0} n(r, \omega_j) dr - \frac{\pi}{2} \quad (6.9)$$

where the reflectometer's probing frequency has been indexed,  $r_0$  is the position of the reference plane, and  $r_c(\omega_j)$  is the position of the cutoff for frequency  $\omega_j$ . The technique assumes knowledge of the electron density profile up to the cutoff frequency,  $\omega_j$  (that is, the density must be assumed or defined from other data), thus, the phase for the cutoff frequency  $\omega_j$  from the reference plane at  $r_0$  to the cutoff position at  $r_c(\omega_j)$  can be calculated. The phase for the next frequency can be calculated by means of equation 6.9 as:

$$\phi(\omega_{j+1}) = 2 \frac{\omega_{j+1}}{C} \int_{r_c(\omega_{j+1})}^{r_0} n(r, \omega_{j+1}) dr - \frac{\pi}{2} \quad (6.10)$$

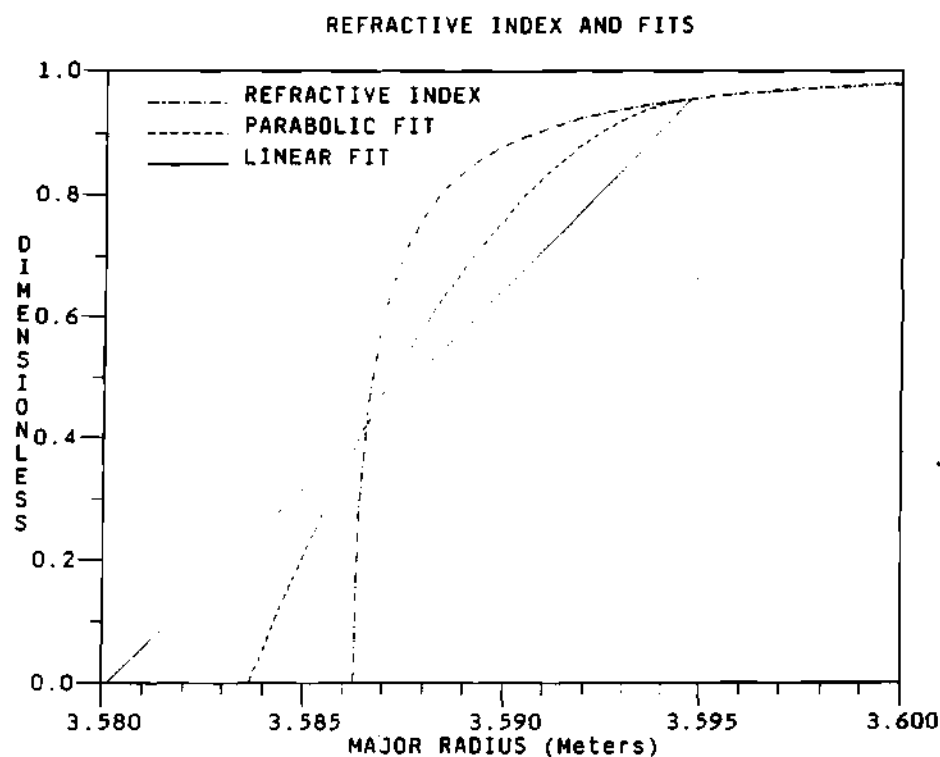
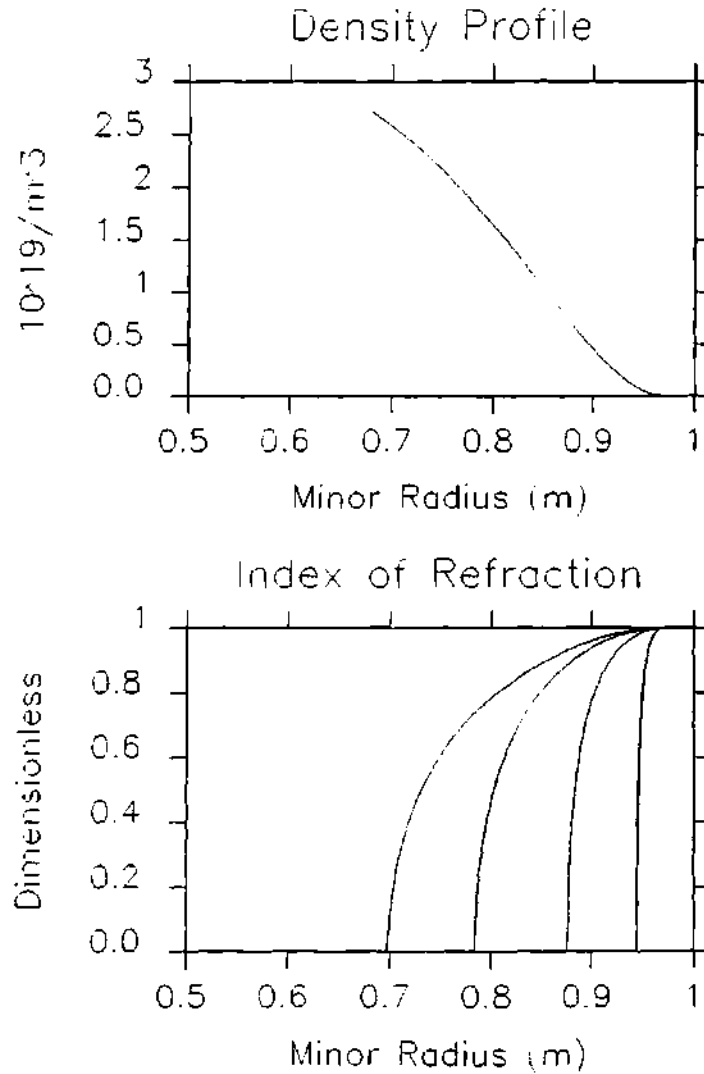


Figure 6.2: Graphical representation of the trapezoidal rule used by Doyle (solid straight diagonal line) to calculate the increment on the radial position and the parabolic method (dash line). The refractive index (dot-dash line) is plotted as a function of the position for the upper frequencies. The error of the technique is the difference in the zero crossing of the curves.



**Figure 6.3:** Examples of the index of refraction as a function of the minor radius for an assumed density profile. The upper plot is the assumed density profile ( $n_e = 3.5 \times 10^{19} \left(1 - \left(\frac{r}{a}\right)^\alpha\right)^\beta$ ) ( $\alpha = 6$  and  $\beta = 2$ ). The lower plot is the calculated index of refraction for the frequencies of 117, 110, 100, and 93 GHz (from most left to most right curve respectively).

where the position for its cutoff,  $r_c(\omega_{j+1})$ , is unknown. The frequency  $\omega_{j+1}$  is given by the formula:

$$\omega_{j+1} = \omega_j + \Delta\omega \quad (6.11)$$

where the frequency  $\omega_j$  is the lower frequency of the dual frequency beam and the frequency  $\omega_{j+1}$  is the upper frequency of the beam.

Using the equations above, the phase difference,  $\Delta\phi(\omega_{j+1})$ , will be given by:

$$\Delta\phi(\omega_{j+1}) = \phi(\omega_{j+1}) - \phi(\omega_j) \quad (6.12)$$

$$= 2\frac{\omega_{j+1}}{C} \int_{r_c(\omega_{j+1})}^{r_0} n(r, \omega_{j+1}) dr - 2\frac{\omega_j}{C} \int_{r_c(\omega_j)}^{r_0} n(r, \omega_j) dr \quad (6.13)$$

where equations 6.9 and 6.10 have been used. Doyle's approximation is given by the equation:

$$\begin{aligned} \int_{r_c(\omega_{j+1})}^{r_0} n(r, \omega_{j+1}) dr &= \int_{r_c(\omega_j)}^{r_0} n(r, \omega_{j+1}) dr \\ &+ \frac{1}{2}\Delta r (n(r_c(\omega_j), \omega_{j+1}) - n(r_c(\omega_{j+1}), \omega_{j+1})) \end{aligned} \quad (6.14)$$

where the increment on the cutoff position,  $\Delta r(\omega_{j+1})$ , is defined by the equation:

$$r_c(\omega_{j+1}) = r_c(\omega_j) + \Delta r(\omega_{j+1}) \quad (6.15)$$

for the next frequency. Doyle's approximation on the previous equation represents the use of a linear function to describe the index of refraction between the last known point of density,  $r_c(\omega_{j+1})$ , and the position of cutoff for the upper frequency wave,  $r_c(\omega_{j+1})$ . This linear function fit is shown in Figure 6.2 as the straight diagonal line. Using the condition for cutoff given by the equation:

$$n(r_c(\omega_{j+1}), \omega_{j+1}) = 0 \quad (6.16)$$

then the final form of Doyle's equation is:

$$\int_{r_c(\omega_{j+1})}^{r_0} n(r, \omega_{j+1}) dr = \int_{r_c(\omega_j)}^{r_0} n(r, \omega_{j+1}) dr + \frac{1}{2}\Delta r n(r_c(\omega_j), \omega_{j+1}) \quad (6.17)$$



which defines the increment on the cutoff position,  $\Delta r$ , as a function of the frequency and index of refraction integrals.

Using Doyle's<sup>96,99</sup> approximation on the first integral of equation 6.13, an equation for  $\Delta r(\omega_{j+1})$  can be obtained, that is:

$$\begin{aligned} \Delta\phi(\omega_{j+1}) = & 2\frac{\omega_{j+1}}{C} \left( \frac{1}{2}\Delta r(\omega_{j+1}) n(r_c(\omega_j), \omega_{j+1}) + \int_{r_c(\omega_j)}^{r_0} n(r, \omega_{j+1}) dr \right) \\ & - 2\frac{\omega_j}{C} \int_{r_c(\omega_j)}^{r_0} n(r, \omega_j) dr \end{aligned} \quad (6.18)$$

where all of the variables have been defined before. Equation 6.18 can be used to solve for the radial spacing,  $\Delta r(\omega_{j+1})$ , which is given by:

$$\Delta r(\omega_{j+1}) = \frac{\Delta\phi - 2\frac{\omega_{j+1}}{C} \int_{r_c(\omega_j)}^{r_0} n(r, \omega_{j+1}) dr + 2\frac{\omega_j}{C} \int_{r_c(\omega_j)}^{r_0} n(r, \omega_j) dr}{\frac{\omega_{j+1}}{C} n(r_c(\omega_j), \omega_{j+1})} \quad (6.19)$$

which defines the radial increment,  $\Delta r(\omega_{j+1})$ , for the cutoff frequency  $\omega_{j+1}$  in terms of the phase difference. This formula can be used to calculate the position of the cutoff in an iterative way, as:

$$r_c(\omega_{j+1}) = r_c(\omega_j) + \Delta r(\omega_{j+1}) \quad (6.20)$$

where  $r_c(\omega_{j+1})$  is the cutoff position for the wave of frequency  $\omega_{j+1}$ . The density at this new cutoff point,  $n_e(r_c(\omega_{j+1}))$ , can be calculated from the cutoff condition on the refractive index, i.e., a density can be found such that the equation:

$$n(r_c(\omega_{j+1}), n_e(r_c(\omega_{j+1})), \omega_{j+1}) = 0 \quad (6.21)$$

has a solution at the cutoff position of  $r_c(\omega_{j+1})$ . Then this cutoff position,  $r_c(\omega_{j+1})$ , and its corresponding cutoff density,  $n_e(r_c(\omega_{j+1}))$ , can be incorporated into a density profile and this process repeated in an iterative way to obtain a full density profile.

### 6.2.2 The parabolic method

There are many types of parabolic fits that have been done to the index of refraction. They are different by the conditions used to calculate the coefficients of the parabola. Only two of them will be presented here. For the first method, the parabola used for the fit passes through the three points. For the second method, the parabola passes through the last two known points of the index of refraction and the condition of matching the slope of the parabola in the last known point of density is used to obtain the equations for the coefficients of the parabola. These will be derived and explained in the following sections. It must be pointed out that the difference between both fits is small and the effect and/or difference on the reconstructed profile for both the modeling and the real data will be insignificant.

**Parabolic fit** Doyle's method fits a linear function to approximate the index of refraction just before the cutoff of the wave for the next cutoff frequency, i.e., in the unknown part of density profile. Nevertheless, a parabolic curve will be a better fit, at least in principle. The derivation starts with the equation:

$$n(r) = a + b(r - r_1) + c(r - r_1)^2 \quad (6.22)$$

where  $n(r) = n(r, \omega_U)$  is the index of refraction corresponding to the curve between cutoff positions  $r_1 = r_c(\omega_U)$  and  $r_2 = r_c(\omega_L)$ , and the coefficients  $a$ ,  $b$ , and  $c$  satisfy the equations:

$$n(r_1) = a + b(r_1 - r_1) + c(r_1 - r_1)^2 \quad (6.23)$$

$$n(r_2) = a + b(r_2 - r_1) + c(r_2 - r_1)^2 \quad (6.24)$$

$$n(r_3) = a + b(r_3 - r_1) + c(r_3 - r_1)^2 \quad (6.25)$$

where the only unknowns are the parabola's coefficients  $a$ ,  $b$ , and  $c$ . Using the condition for cutoff at  $r_1$ , that is:

$$n(r_1) = 0 \quad (6.26)$$

then the value for the coefficient  $a$  is zero, that is:

$$a = 0 \quad (6.27)$$

leaving two equations for the coefficients  $b$  and  $c$ . The equations for these coefficients are:

$$n(r_2) = b \Delta r_1 + c(\Delta r_1)^2 \quad (6.28)$$

$$n(r_3) = b(\Delta r_1 + \Delta r_2) + c(\Delta r_1 + \Delta r_2)^2 \quad (6.29)$$

where  $\Delta r_1$  and  $\Delta r_2$  are given by:

$$\Delta r_1 = r_2 - r_1 \quad (6.30)$$

$$\Delta r_2 = r_3 - r_2 \quad (6.31)$$

Simplifying for the coefficients of the parabola:

$$c = \frac{-n(r_2)(\Delta r_1 + \Delta r_2) + \Delta r_1 n(r_3)}{\Delta r_1 (\Delta r_1 \Delta r_2 + (\Delta r_2)^2)} \quad (6.32)$$

$$b = \frac{n(r_2)}{\Delta r_1} + \frac{\Delta r_1 (n(r_2) - n(r_3)) + \Delta r_2 n(r_2)}{\Delta r_1 \Delta r_2 + (\Delta r_2)^2} \quad (6.33)$$

which are the non-linear equations for the coefficients of the parabola.

For most applications and in much of the literature on polynomial fits, the assumption of equal step size is used when fitting the function to the points. While this can be done and was done and studied for the case of the reflectometer, the more general case of non-equal step size will be presented in the next section.

**Parabolic fit with non-equal step size** It is possible to derive a set of equations for a parabolic fit where no assumption is made about the adjacent steps, i.e., there is no assumption of equal step size. The derivation of the non-equal step size method can be started with the equations for the coefficients of the

parabola,  $b$  and  $c$ , given by equations 6.33 and 6.32 as:

$$c = \frac{-n(r_2)(\Delta r_1 + \Delta r_2) + \Delta r_1 n(r_3)}{\Delta r_1 (\Delta r_1 \Delta r_2 + (\Delta r_2)^2)} \quad (6.34)$$

$$b = \frac{n(r_2)}{\Delta r_1} + \frac{\Delta r_1 (n(r_2) - n(r_3)) + \Delta r_2 n(r_2)}{\Delta r_1 \Delta r_2 + (\Delta r_2)^2} \quad (6.35)$$

where all the variables have been defined before.

The integral in the unknown part of the density profile will be given by:

$$\phi = \frac{2\omega}{C} \int_{r_1}^{r_2} n(r) dr \quad (6.36)$$

where using the parabolic form of the index of refraction, it will give:

$$\phi \frac{C}{2\omega} = \frac{1}{3} c (\Delta r_1)^3 + \frac{1}{2} b (\Delta r_1)^2 \quad (6.37)$$

where substituting the coefficients for  $b$  and  $c$ , it is obtained:

$$\begin{aligned} 0 &= (\Delta r_1)^3 \frac{1}{6} (n(r_2) - n(r_3)) + (\Delta r_1)^2 \frac{2}{3} \Delta r_2 n(r_2) \\ &+ \Delta r_1 \left( \frac{1}{2} (\Delta r_2)^2 n(r_2) - \phi \frac{C}{2\omega} \Delta r_2 \right) - \phi \frac{C}{2\omega} (\Delta r_2)^2 \end{aligned} \quad (6.38)$$

which expresses the increment in the cutoff position in terms of the index of refraction at the two last known points of density and the previous step size,  $\Delta r_2$ , is a known number. For the first step, Doyle's method must be used, since  $\Delta r_2$  is not known.

This method did not provided any improvement on the calculation of the increment on the cutoff position and the overall profile as compared with the parabolic fit with the derivative condition (explained next). This is because the derivative condition allows for a better fit of the parabola to the real index of refraction, as compared with the non-equal step size method.

**Simplifying the non-equal step size** It is possible to simplify the equations for the non-equal method described above. This derivation starts with the equations 6.33 and 6.32.

Instead of using the condition of equal step size, the definition of the difference between adjacent step sizes will be used, given by equation:

$$\Delta r_2 = \Delta r_1 + d \quad (6.39)$$

where  $d$  is the difference between adjacent increments in the cutoff. Assuming that the difference between adjacent increments between the cutoffs is small,  $d \ll \Delta r_1$ , then the equations for the parabolic coefficients can be expanded in the binomial series and simplified to give:

$$c = \frac{-2n(r_2) \left(1 - \frac{d}{\Delta r_1}\right) + n(r_3) \left(1 - \frac{3}{2} \frac{d}{\Delta r_1}\right)}{2(\Delta r_1)^2} \quad (6.40)$$

$$b = \frac{4n(r_2) - n(r_3) + \frac{d}{\Delta r_1} \left(-2n(r_2) + \frac{3}{2}n(r_3)\right)}{2\Delta r_1} \quad (6.41)$$

where all variables have been defined before. Next, using the definition of the phase and the parabolic fit to the index of refraction, the phase integral becomes:

$$\phi \frac{C}{2\omega} = \left(\frac{2}{3}n(r_2) - \frac{1}{12}n(r_3)\right) \Delta r_1 + \frac{1}{12} \left(-2n(r_2) + \frac{3}{2}n(r_3)\right) d \quad (6.42)$$

Now using the definition of the difference between increments, that is:

$$d = \Delta r_2 - \Delta r_1 \quad (6.43)$$

gives:

$$\phi \frac{C}{2\omega} = \left(\frac{-1}{6}n(r_2) + \frac{3}{24}n(r_3)\right) \Delta r_2 + \left(\frac{5}{6}n(r_2) - \frac{5}{24}n(r_3)\right) \Delta r_1 \quad (6.44)$$

where solving for  $\Delta r_1$ , one obtains:

$$\Delta r_1 = \frac{\phi \frac{C}{2\omega} - \left(\frac{-1}{6}n(r_2) + \frac{1}{8}n(r_3)\right) \Delta r_2}{\frac{5}{6}n(r_2) + \frac{-5}{24}n(r_3)} \quad (6.45)$$

which solves for the increment  $\Delta r_1$  in a simpler way than previously.

**Parabolic fit with the derivative condition** The parabolic fit using the derivative condition is done by making a parabola that fits 2 points ( $1^{st}$  and  $2^{nd}$ ) and at the  $2^{nd}$  point matches the slope determined by the  $2^{nd}$  and  $3^{rd}$  points. This will lead to the following equation:

$$n(r) = a + b(r - r_1) + c(r - r_1)^2 \quad (6.46)$$

which is just the equation for the parabolic fit and where the coefficients  $a$ ,  $b$ , and  $c$  need to be calculated from the matching conditions. These conditions are given by the equations:

$$n(r_1) = 0 \quad (6.47)$$

which represents the cutoff condition at the first point and gives the first coefficient,  $a$ , to be:

$$a = 0. \quad (6.48)$$

The next condition is the match at the  $2^{nd}$  point, given by:

$$n(r_2) = b \Delta r_1 + c(\Delta r_1)^2 \quad (6.49)$$

and finally the derivative condition at the  $2^{nd}$  point is given by:

$$\left. \frac{dn(r)}{dr} \right|_{r=r_2} = \frac{n(r_3) - n(r_2)}{\Delta r_2} \quad (6.50)$$

when substituting these condition into the equation for the parabola the following equations for the coefficients  $b$  and  $c$  can be obtained:

$$n(r_1) = b \Delta r_1 + c(\Delta r_1)^2 \quad (6.51)$$

$$\frac{n(r_3) - n(r_2)}{\Delta r_2} = b + 2c \Delta r_1 \quad (6.52)$$

Solving for the coefficient  $b$  one obtains:

$$b = \frac{-\Delta r_1 \frac{n(r_3) - n(r_2)}{\Delta r_2} + 2n(r_2)}{\Delta r_1} \quad (6.53)$$

and solving for the coefficient  $c$ :

$$c = \frac{\Delta r_1 \frac{n(r_3) - n(r_2)}{\Delta r_2} - n(r_2)}{(\Delta r_1)^2} \quad (6.54)$$

where these are still non-linear, but the denominators are in a simple power form.

Next, using the condition of equal step size for adjacent cutoff positions,  $\Delta r_1 \approx \Delta r_2$ , the equations for the coefficients become:

$$b = \frac{3n(r_2) - n(r_3)}{\Delta r_1} \quad (6.55)$$

$$c = \frac{-2n(r_2) + n(r_3)}{(\Delta r_1)^2} \quad (6.56)$$

Finally, substituting the coefficients for the parabola into the integral equation for the phase, one obtains:

$$\phi \frac{C}{2\omega} = \frac{(\Delta r)^2}{2} \frac{(3n(r_2) - n(r_3))}{\Delta r} + \frac{(\Delta r)^3}{3} \frac{(-2n(r_2) + n(r_3))}{(\Delta r)^2} \quad (6.57)$$

$$= \Delta r \left( \frac{3}{2}n(r_2) - \frac{1}{2}n(r_2) + \frac{-2}{3}n(r_2) + \frac{1}{3}n(r_3) \right) \quad (6.58)$$

$$= \Delta r \left( \frac{5}{6}n(r_2) - \frac{1}{6}n(r_3) \right) \quad (6.59)$$

where the  $\Delta r_1$  was changed to  $\Delta r$  to represent the increment in the radial cutoff position.

### 6.2.3 Error on the parabolic method

The following sections will present a derivation describing the propagation of the error from the parabolic fit (applicable to all parabolic fits) to the final density profile. While a full propagation of error may be too complicated to perform because of the complicated nature of the formulas and the recursive nature of the reconstructing technique, the derivation in the following sections can approximate this information in a simple and easy to follow way. The first section will describe the error in the parabolic fit, the second section will describe the error in the increment between cutoffs, and the third section will describe the final error in the reconstructed profile.

**Error in the parabolic fits** The error on the parabolic approximation can be found by using the Taylor's expansion of the index of refraction, that is, by defining the index of refraction as:

$$n(r) = \sum_{j=0}^{\infty} \frac{(r - r_1)^j}{j!} \left. \frac{d^j n(r)}{dr^j} \right|_{r_1} \quad (6.60)$$

which is assumed to converge to  $n(r)$  when all of the term are used. Then the parabolic approximation will be represented as:

$$n(r) = a + b(r - r_1) + c(r - r_1)^2 + R_s \quad (6.61)$$

where the remainder  $R_s$  is given by the equation:

$$R_s = \sum_{j=3}^{\infty} \frac{(r - r_1)^j}{j!} \left. \frac{d^j n(r)}{dr^j} \right|_{r_1} \quad (6.62)$$

for the parabolic approximation. Then the integral of the index of refraction can be expressed as:

$$\int_{r_1}^{r_2} n(r) dr = \int_{r_1}^{r_2} (a + b(r - r_1) + c(r - r_1)^2) dr + \int_{r_1}^{r_2} R_s dr \quad (6.63)$$

where the total error in the phase integral will be given by the integral of the remainder, that is:

$$E = \int_{r_1}^{r_2} R_s dr \quad (6.64)$$

$$= \int_{r_1}^{r_2} \sum_{j=3}^{\infty} \frac{(r - r_1)^j}{j!} \left. \frac{d^j n(r)}{dr^j} \right|_{r_1} dr \quad (6.65)$$

$$= \sum_{j=3}^{\infty} \int_{r_1}^{r_2} \frac{(r - r_1)^j}{j!} \left. \frac{d^j n(r)}{dr^j} \right|_{r_1} dr \quad (6.66)$$

$$= \sum_{j=3}^{\infty} \frac{(r_2 - r_1)^{j+1}}{(j+1)!} \left. \frac{d^j n(r)}{dr^j} \right|_{r_1} \quad (6.67)$$

$$= \sum_{j=3}^{\infty} \frac{(\Delta r)^{j+1}}{(j+1)!} \left. \frac{d^j n(r)}{dr^j} \right|_{r_1} \quad (6.68)$$

where the errors may partially cancel depending on the sign on the derivatives of the index of refraction. The series and its integral will be an exact description



of the index of refraction around the cutoff position since the derivatives are well defined around the cutoff position. The series is not well defined at the cutoff position since at this point the derivatives will go to infinity ( $\infty$ ). Nevertheless, it is possible to get infinitesimally close to the cutoff in such a way that the cutoff is not reached and the integral will be equally close to the real value of the phase. Therefore, for all practical purposes, this is a good description of the index of refraction around the cutoff.

The next standard step is to assume that the higher term derivatives are less than infinity, that is,  $\frac{d^j n}{dr^j} \ll \infty$ , and that only the first term of the summation is the dominant term. This assumption can not be done for the case of the index of refraction. This is because the derivative of the index of refraction goes to infinity at the cutoff position. The reason for this behaviour comes from the expression for the relative permittivity,  $\epsilon_r(r)$ , of the plasma. Since the index of refraction,  $n(r)$ , is equal to the square root of the relative permittivity:

$$n(r) = \sqrt{\epsilon_r} \quad (6.69)$$

then the derivatives of the index of refraction are of the form:

$$\frac{d^j n}{dr^j} = \frac{d^{j-1}}{dr^{j-1}} \left( \frac{1}{2\sqrt{\epsilon_r}} \frac{d\epsilon_r}{dr} \right) \quad (6.70)$$

where the term  $\frac{1}{\sqrt{\epsilon_r}}$  will go to infinity as it approaches the cutoff. Nevertheless, it is possible to calculate the total error due to all of the derivative terms in the limit as  $\Delta r \rightarrow 0$  if the derivatives are expanded using Newtonian finite difference as follows. The derivatives can be expressed as:

$$\frac{d^j n(r)}{dr^j} = \sum_{i=0}^j \frac{j!}{(\Delta r)^j} \frac{(-1)^i n(r+i\Delta r)}{i!(j-i)!} \quad (6.71)$$

where  $\Delta r$  is the increment between points to calculate the  $j^{\text{th}}$  derivative of the index of refraction,  $n(r)$ . Then the error will be given by:

$$E(\Delta r) = \sum_{j=3}^{\infty} \frac{(\Delta r)^{j+1}}{(j+1)!} \left. \frac{d^j n(r)}{dr^j} \right|_{r_1} \quad (6.72)$$

$$= \sum_{j=3}^{\infty} \frac{(\Delta r)^{j+1}}{(j+1)!} \frac{j!}{(\Delta r)^j} \sum_{i=0}^j \frac{(-1)^i n(r_1 + i \Delta r)}{i!(j-i)!} \quad (6.73)$$

$$= \sum_{j=3}^{\infty} \frac{\Delta r}{(j+1)} \sum_{i=0}^j \frac{(-1)^i n(r_1 + i \Delta r)}{i!(j-i)!} \quad (6.74)$$

where all the terms have been defined previously. This series will converge since the terms on the summation over the index,  $i$ , is a series where the terms alternate on sign (due to the  $(-1)^i$  term) and the absolute value of the terms converges to zero as  $i \rightarrow \infty$ . The propagation of this error into the increment of the cutoff positions is calculated in the next section.

**Error in the increment on the cutoff position** The above derivation shows the error on the fit of a parabola to the index of refraction near the cutoff for the propagating beam. The effect of this error on the calculated increment on the cutoff position can be calculated as follows. The parabolic fit with the derivative condition and equal step size will be used in this derivation to show the procedure, but the derivation can be applied to any of the fits described here and obtain the same results. The definition for the phase of the propagating wave is given by:

$$\phi(r_1, \omega) = \frac{2\omega}{C} \int_{r_1}^{r_c} n(r, \omega) dr \quad (6.75)$$

$$= \frac{2\omega}{C} \left( \int_{r_2}^{r_c} n(r, \omega) dr + \int_{r_1}^{r_2} n(r, \omega) dr \right) \quad (6.76)$$

where the integral for the phase has been divided in two pieces. The one for the part of the density profile for which the density profile is known, from the edge of the plasma,  $r_c$ , to the last known position of the density profile,  $r_2$ , and from the last known point of the density profile,  $r_2$ , to the position for the cutoff,  $r_1$ . Now it can be assumed that the index of refraction,  $n(r)$ , is given by a Taylor's series in the interval between the last known point of the density profile and the

position of cutoff,  $r_1$  to  $r_2$ , that is:

$$n(r, \omega) = \sum_{j=0}^{\infty} \frac{1}{j!} (r - r_1)^j \left. \frac{d^j n(r)}{dr^j} \right|_{r_1} \quad r_1 \leq r \leq r_2 \quad (6.77)$$

Substituting Taylor's expansion for the index of refraction into equation 6.76, one obtains:

$$\phi(r_1, \omega) \frac{C}{2\omega} = \int_{r_2}^{r_c} n(r, \omega) dr + \int_{r_1}^{r_2} \sum_{j=0}^{\infty} \frac{(r - r_1)^j}{j!} \left. \frac{d^j n(r)}{dr^j} \right|_{r_1} dr \quad (6.78)$$

$$= \int_{r_2}^{r_c} n(r, \omega) dr + \sum_{j=0}^{\infty} \frac{(r - r_1)^{j+1}}{(j+1)!} \left. \frac{d^j n(r)}{dr^j} \right|_{r_1} \quad (6.79)$$

solving for the increment on the cutoff position,  $\Delta r$ :

$$\phi(r_1, \omega) \frac{C}{2\omega} = \int_{r_2}^{r_c} n(r, \omega) dr + \sum_{j=0}^{\infty} \frac{(\Delta r)^{j+1}}{(j+1)!} \left. \frac{d^j n(r)}{dr^j} \right|_{r_1} \quad (6.80)$$

Using the condition for the cutoff and the definitions for the derivatives in terms of the points of known density, and the coefficients of the parabolic fit, a set of equations can be obtained for the derivatives. For this case, the parabolic index of refraction is given by equation 6.22 as:

$$n(r) = a + b(r - r_1) + c(r - r_1)^2 \quad (6.81)$$

where  $a$ ,  $b$ , and  $c$  are given by equations 6.111, 6.112, and 6.113. Then the derivatives for the Taylor's series expansion in equation 6.80 will be given by:

$$\left. \frac{dn(r)}{dr} \right|_{r_1} = b = \frac{4n(r_2) - n(r_3)}{2\Delta r} \quad (6.82)$$

$$\left. \frac{d^2 n(r)}{dr^2} \right|_{r_1} = 2c = \frac{-2n(r_2) + n(r_3)}{(\Delta r)^2} \quad (6.83)$$

When these are substituted into equation 6.80 one finds:

$$\begin{aligned} \phi(r_1, \omega) \frac{C}{2\omega} &= \int_{r_2}^{r_c} n(r, \omega) dr \\ &+ \frac{\Delta r}{2!} \frac{4n(r_2) - n(r_3)}{2} + \frac{\Delta r}{3!} (-2n(r_2) + n(r_3)) \\ &+ E(\Delta r) \end{aligned} \quad (6.84)$$

where the term  $E(\Delta r)$  contains the error terms from the equation and is given by the remainder of the Taylor series, that is:

$$E(\Delta r) = \sum_{j=3}^{\infty} \frac{\Delta r}{(j+1)} \sum_{i=0}^j \frac{(-1)^i n(r_1 + i \Delta r)}{i!(j-i)!} \quad (6.85)$$

Simplifying equation 6.84 one finds:

$$\begin{aligned} \phi(r_1, \omega) \frac{C}{2\omega} &= \int_{r_2}^{r_c} n(r, \omega) dr \\ &+ \Delta r \left( n(r_2) - \frac{1}{4}n(r_3) - \frac{1}{3}n(r_2) + \frac{1}{6}n(r_3) \right) + E(\Delta r) \\ &= \int_{r_2}^{r_c} n(r, \omega) dr \\ &+ \Delta r \left( \frac{2}{3}n(r_2) - \frac{1}{12}n(r_3) + \frac{E(\Delta r)}{\Delta r} \right) \end{aligned} \quad (6.86)$$

which is the same answer as the one previously obtained for the parabolic fit, equation 6.118, but this one includes an error term.

Now to continue with the derivation and solving for  $\Delta r$ , one finds:

$$\Delta r = \frac{\phi(r_1, \omega) \frac{C}{2\omega} - \int_{r_2}^{r_c} n(r, \omega) dr}{\frac{2}{3}n(r_2, \omega) - \frac{1}{12}n(r_3, \omega) + \frac{E(\Delta r)}{\Delta r}} \quad (6.87)$$

where the new error term,  $\frac{E(\Delta r)}{\Delta r}$ , is given by:

$$\frac{E(\Delta r)}{\Delta r} = \sum_{j=3}^{\infty} \frac{1}{(j+1)} \sum_{i=0}^j \frac{(-1)^i n(r_1 + i \Delta r)}{i!(j-i)!} \quad (6.88)$$

and the only dependance on the increment of the cutoff positions comes from the index of refraction,  $n(r + i \Delta r)$ . Using the binomial theorem:

$$(1+x)^{-1} = 1 - x + \dots \quad x \ll 1 \quad (6.89)$$

then the increment in the cutoff position can be expressed as:

$$\Delta r = \frac{\phi(r_1, \omega) \frac{C}{2\omega} - \int_{r_2}^{r_c} n(r, \omega) dr}{\frac{2}{3}n(r_2, \omega) - \frac{1}{12}n(r_3, \omega)} \left( 1 - \frac{\frac{E(\Delta r)}{\Delta r}}{\frac{2}{3}n(r_2, \omega) - \frac{1}{12}n(r_3, \omega)} \right) \quad (6.90)$$

which contains the error term,  $\frac{E(\Delta r)}{\Delta r}$ , when a parabola is used to approximate the index of refraction near the cutoff.

Next, using the square root dependance of the refractive index around the cutoff, the index of refraction will scale as  $\sqrt{\Delta r}$  near the cutoff, that is,

$$\frac{2}{3}n(r_2) - \frac{1}{12}n(r_3) \propto \sqrt{\Delta r} \quad (6.91)$$

and from equation 6.88, the same can be said about the error term from the fit, that is:

$$\frac{E(\Delta r)}{\Delta r} \propto n(r) \quad (6.92)$$

$$\propto \sqrt{\Delta r} \quad (6.93)$$

then the error term on the increment of the cutoff will become:

$$\frac{\frac{E(\Delta r)}{\Delta r}}{\frac{2}{3}n(r_2, \omega) - \frac{1}{12}n(r_3, \omega)} \propto \frac{\sqrt{\Delta r}}{\sqrt{\Delta r}} \quad (6.94)$$

$$\propto \text{Constant} \quad (6.95)$$

which shows how the error scales to a constant independent of the increment in the cutoff position, as the step size becomes small.

**Error in the density using the parabolic method** The error previously calculated for the reconstruction technique gives the error for the given individual increment on the cutoff position, which helps to give an idea of the accuracy of the technique and shows that in principle the parabolic method is more accurate than Doyle's trapezoidal method, but it is more difficult to calculate the total error for the density profile. The overall error on the density profile (for the modeling calculations) includes the error on the increment of the cutoff position, the error on the calculated density at each calculated cutoff position, and the accumulated error due to the error on all of the previous data points used to calculate the next data point (other major error sources like the uncertainty in the magnetic field and uncertainty on the position of the first cutoff will apply for the real data).

If one tries to include and account for all of these errors the problem becomes harder. Nevertheless, since the core of the calculations and the errors go into the actual calculation of the increment on the cutoff positions, it is clear that for Doyle's method and the parabolic method that the main source of the error will be from the increment on the cutoff position,  $\Delta r$ . This error in the increments of the cutoffs will accumulate in the calculated position of the cutoffs, therefore producing a displacement in the radial position of the real density profile. Defining the error as the difference between the real profile and the calculated (displaced) profile, equation 6.96, then the calculated profile can be expanded in a Taylor series of the real profile and the error be calculated from this equation. This will be presented next.

The total displacement on the density profile is due to the accumulated error on the increment of the cutoff position calculated using the parabolic fit to the index of refraction. Since the increment on the cutoff positions is not a constant through-out the entire density profile ("because the frequency separation,  $\Delta\omega$ , is kept constant"), it can be expected that the main contribution to this displacement comes from the flat part of the edge of the density profile where the increment and/or separation of the cutoff positions is the largest as compared to the one at the steepest part of the density profile. Therefore, the main contribution to the total displacement will come from the error of the parabolic fit at the edge of the profile.

This may be complicated and obscured by the recursive way in which the reconstruction technique re-uses the previously calculated density data points. Since these density data points are used to calculate the next increment on the cutoff position the error from these data points will be passed to the next increment on the cutoff position, thus the overall error on the profile seems to follow the general behaviour of a displacement on the radial position. Then, an estimation

of the fractional error due to the accumulated displacement error on the radial cutoff positions can be expressed as:

$$E_{n_e} = \frac{n_e(r + \Delta r_{total}) - n_e(r)}{n_{e0}} \quad (6.96)$$

where  $\Delta r_{total}$  is the accumulated total displacement due to the accumulated error on the cutoff positions,  $n_e(r)$  is the real density profile,  $n_e(r + \Delta r_{total})$  is the calculated density profile due to the error on the calculated increments on the cutoff positions, and  $n_{e0}$  is the maximum value of the density used here as a normalization constant. A Taylor series expansion around the steepest part of the profile can be used to express  $n_e(r + \Delta r_{total})$  as:

$$n_e(r + \Delta r_{total}) = n_e(r) + \Delta r_{total} \frac{dn_e}{dr} + \dots \quad (6.97)$$

in which case the error can be expressed as:

$$E_{n_e} = \frac{(n_e(r) + \Delta r_{total} \frac{dn_e}{dr} + \dots) - n_e(r)}{n_{e0}} \quad (6.98)$$

$$= \frac{\Delta r_{total} \frac{dn_e}{dr} + \dots}{n_{e0}} \quad (6.99)$$

Using the lowest term only, the error on the profile is proportional to the accumulated total displacement due to the error in the calculated position of the cutoffs and the derivative of the profile, that is:

$$E_{n_e} = \frac{\Delta r_{total} \frac{dn_e}{dr}}{n_{e0}} \quad (6.100)$$

which shows that the error due to the accumulated error in the calculated increment of the cutoff positions is proportional to the total displacement and the derivative of the profile. The increments between cutoff is a strong function of the frequency separation of probing beams. Therefore, by reducing the frequency separation of the probing beams, the increment between the cutoffs will be reduced too. This explains the linear dependance of the error as a function of the

frequency separation of the probing beams as can be seen from Figure 6.4. That is, when the frequency separation of the probing beams is reduced by half, then the separation between the cutoffs will be reduced by half and the separation or displacement between the assumed and reconstructed profiles will be reduced in half, resulting in a reduction of the total error of half of its previous value.

Assuming a hyperbolic density profile of the form:

$$n_e(r) = \frac{n_{e0}}{2} \left( 1 - \tanh \left( \frac{r - r_0}{d} \right) \right) \quad (6.101)$$

where  $r_0$  is the point of maximum slope and  $d$  is a decay constant, then by taking the derivative of the density profile, equation 6.101, and substituting it into the formula for the error, equation 6.96, the error will be given by:

$$E_{n_e} = \frac{\Delta r_{total}}{2d} \frac{1}{1 + \left( \frac{r - r_0}{d} \right)^2} \quad (6.102)$$

where the maximum error is at  $r = r_0$ , which gives:

$$E_{n_e} = \frac{\Delta r_{total}}{2d} \quad (6.103)$$

Then, using typical parameters from the program, where the typical accumulated error for the parabolic method or Doyle's method is:

$$\Delta r_{total} = 0.5 \times 10^{-3} \text{ m} \quad (6.104)$$

and a typical experimental "decay constant" or e-folding length,  $d$ , is:

$$d = 0.03 \text{ m} \quad (6.105)$$

the percent error in the density is:

$$E_{n_e} = \frac{5}{6} \times 10^{-2} \quad (6.106)$$

$$= 0.833\% \quad (6.107)$$



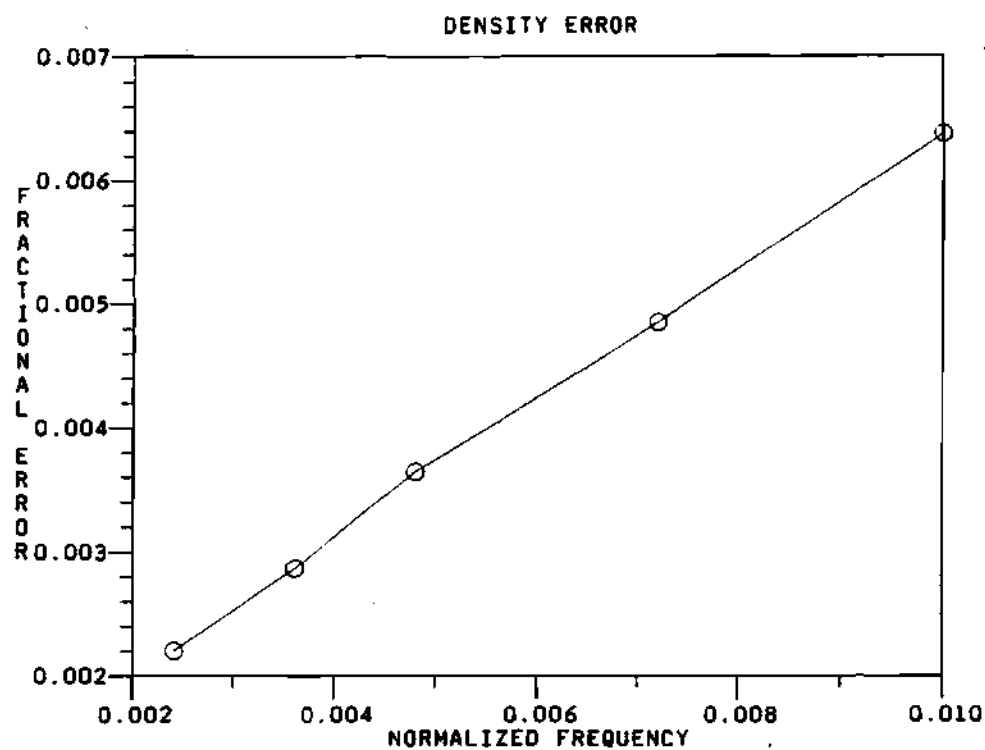


Figure 6.4: Plot of the maximum fractional error as a function of the frequency separation of the probing beams. This is typical for all the parabolic methods presented here.

When compared with the maximum error shown in Figure 6.5, the value from the figure is  $\approx 0.85\%$ , which is reasonably close to the calculated error of equation 6.107. For the accurate method, to be discussed later in section 6.2.5, the error is limited by the round-off error of the computer word-size, in the limit of small step size.

#### 6.2.4 Limits of the parabolic method

It can be expected that under certain circumstances the limit of the parabolic method will approximate or approach the simpler Doyle's method, at the same time that for some other circumstances the two methods will have a bigger difference. These limiting cases will be presented in this section.

**Limit of equal step size** It is possible to simplify greatly the equations for the parabolic coefficients by taking the limit as the difference between the increments in the cutoff goes to zero,  $d \approx 0$ , that is, when the increment between cutoffs is approximately the same (equal step size). Under this limiting case, the derivation starts with the equations for the non-equal step size. To simplify these coefficients, it is assumed that the increments between adjacent cutoffs are approximately the same, that is:

$$\Delta r_1 \approx \Delta r_2 = \Delta r \quad (6.108)$$

then the coefficients become:

$$c = \frac{-2n(r_2) + n(r_3)}{2(\Delta r)^2} \quad (6.109)$$

$$b = \frac{4n(r_2) - n(r_3)}{2\Delta r} \quad (6.110)$$

Finally, the coefficients for the equal step size parabolic fit to the index of

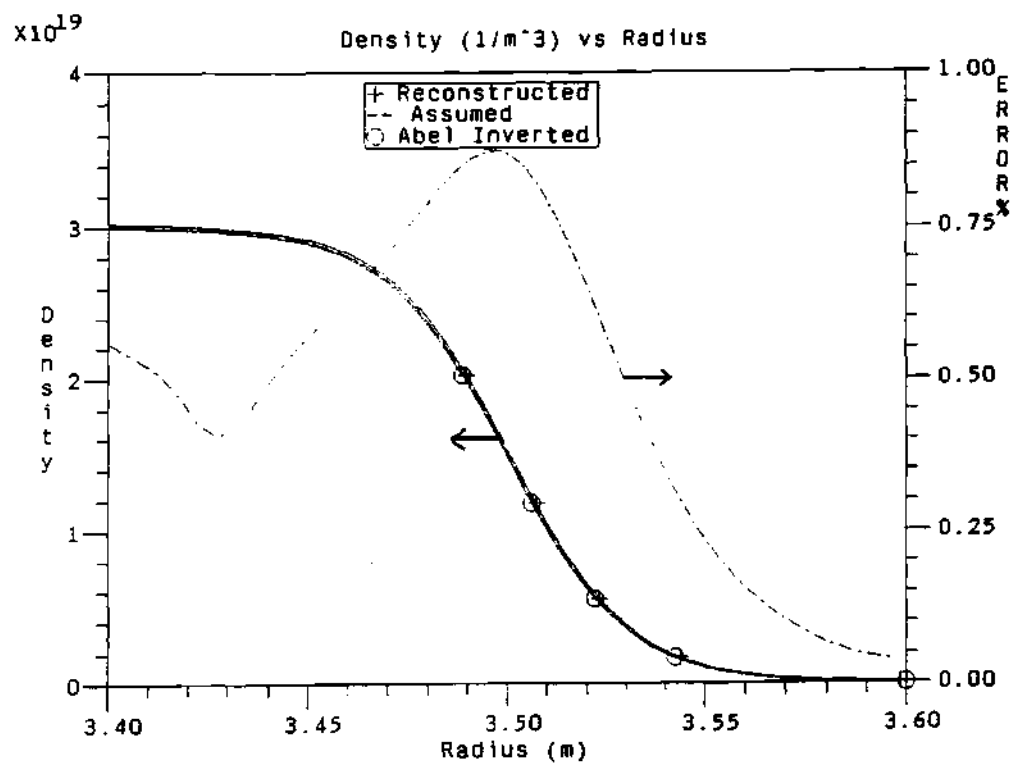


Figure 6.5: Plot of the density profiles and the percent error (dot-dash curve) between the reconstructed and assumed profiles when using the parabolic method with the derivative condition.

refraction in the interval from  $r_1$  to  $r_2$  are given by:

$$a = 0 \quad (6.111)$$

$$b = \frac{4n(r_2) - n(r_3)}{2\Delta r} \quad (6.112)$$

$$c = \frac{-2n(r_2) + n(r_3)}{2(\Delta r)^2} \quad (6.113)$$

where  $r_1, r_2, r_3$  are the radial points used for the fit of the parabola and  $\Delta r$  is given by the relation  $r_2 = r_1 + \Delta r$ . It must be pointed out that the coefficients are still non-linear, but that their denominators are much simpler. Therefore, the area under the refractive index curve is given by:

$$\phi \frac{C}{2\omega} = \int_{r_1}^{r_2} n(r) dr \quad (6.114)$$

$$= \left( a(r - r_1) + \frac{1}{2}b(r - r_1)^2 + \frac{1}{3}c(r - r_1)^3 \right) \Big|_{r_1}^{r_2} \quad (6.115)$$

$$= a\Delta r + \frac{1}{2}b(\Delta r)^2 + \frac{1}{3}c(\Delta r)^3 \quad (6.116)$$

substituting the equations for the coefficients of  $a$ ,  $b$ , and  $c$  in the above equation for the integral of the index of refraction, one obtains:

$$\phi \frac{C}{2\omega} = \frac{(\Delta r)^2}{2} \left[ \frac{4n(r_2) - n(r_3)}{2\Delta r} \right] + \frac{(\Delta r)^3}{3} \left[ \frac{-2n(r_2) + n(r_3)}{2(\Delta r)^2} \right] \quad (6.117)$$

which will linearize since the powers on  $\Delta r$  correspond to the powers on the denominators. Thus, collecting terms with equal coefficients gives:

$$\phi \frac{C}{2\omega} = \Delta r \left( \frac{2}{3}n(r_2) - \frac{1}{12}n(r_3) \right) \quad (6.118)$$

where all the parameters have been defined before. Comparing to Doyle's form given by:

$$\phi \frac{C}{2\omega} = \frac{1}{2} \Delta r n(r_2) \quad (6.119)$$

it can be seen that the quadratic formula weights somewhat more the point  $n(r_2)$  than Doyle's formula, but it compensates with the point  $n(r_3)$ .

**Limit of small step size** There are other fits that can be done to the index of refraction, such as: The square root fit, power law fit, hyperbolic tangent fit, etc. The square root fit is the one that fits the best the index of refraction for the limit of small step size. This is because the index of refraction is proportional to the square root of the relative permittivity,  $\epsilon_r$ . That is, if  $\epsilon_r$  is linear near the cutoff, then the index of refraction,  $n \propto \sqrt{\epsilon_r}$ , will be proportional to the square root near the cutoff. For this limit near the cutoff, the integral for the phase will be given by:

$$\phi_{\text{exact}} = \int_{r_1}^{r_2} n(r) dr \quad (6.120)$$

$$= \int_{r_1}^{r_2} a\sqrt{r - r_1} dr \quad (6.121)$$

$$= \frac{2}{3} n(r_2) \Delta r \quad (6.122)$$

where  $a = \frac{n(r_2)}{\sqrt{\Delta r}}$  is the constant of the square root function. This represents the answer of the integral for the limit of small step size near the cutoff.

The limit of small step size for the linear fit is given by:

$$\phi_{\text{line}} = \int_{r_1}^{r_2} a(r - r_1) dr \quad (6.123)$$

$$= \frac{1}{2} n(r_2) \Delta r \quad (6.124)$$

where  $a = \frac{n(r_2)}{\Delta r}$  is the slope of the line. This is the answer obtained by Doyle, and it differs from the "exact" square root fit by:

$$\frac{\phi_{\text{exact}} - \phi_{\text{line}}}{\phi_{\text{exact}}} \approx \frac{\frac{2}{3} - \frac{1}{2}}{\frac{2}{3}} \quad (6.125)$$

$$\approx 25\% \quad (6.126)$$

which gives an approximated value for the error of the method, but the real error can be smaller depending on the slope and value of the density profile.

For the parabolic method the phase for small step size is given by:

$$\phi_{\text{par}} = \left( \frac{2}{3} n(r_2) - \frac{1}{12} n(r_3) \right) \Delta r \quad (6.127)$$

then the difference between the parabolic and the “exact” solution is given by:

$$\frac{\phi_{exact} - \phi_{par}}{\phi_{exact}} \approx \frac{\frac{2}{3} - \left(\frac{2}{3} - \frac{\sqrt{2}}{12}\right)}{\frac{2}{3}} \quad (6.128)$$

$$\approx 17\% \quad (6.129)$$

where the  $n(r_3) = \sqrt{2}n(r_2)$  was used.

For the parabolic with derivative condition the phase is given by:

$$\phi_{der} = \left( \frac{5}{6}n(r_2) - \frac{1}{6}n(r_3) \right) \Delta r \quad (6.130)$$

then the difference with respect to the “exact” method is:

$$\frac{\phi_{exact} - \phi_{der}}{\phi_{exact}} \approx \frac{\frac{2}{3} - \left(\frac{5}{6} - \frac{\sqrt{2}}{6}\right)}{\frac{2}{3}} \quad (6.131)$$

$$\approx 10\% \quad (6.132)$$

where the  $n(r_3) = \sqrt{2}n(r_2)$  was used again. This shows that the parabolic fit with derivative condition has an improvement of a factor of 2.5 or better over the original linear fit by Doyle, but is still wrong by about 10% as compared to an exact method.

### 6.2.5 An accurate (density expansion) method

As the reader has probably realized by this time, it is possible to fit any function to the index of refraction near the cutoff and solve for the increment between cutoffs. The better the fit of the fitting function to the index of refraction near the cutoff, then the better the calculated increment between cutoffs will be. In principle, the best fitting function is the function of the index of refraction itself. If this function is used to calculate the increments between the cutoffs then a reconstructed profile with nearly zero error can be achieved. This method will have the advantage of showing the non-existence of any other errors in the modeling code. This method was tried by the author and a reconstructed profile is

shown in Figure 6.6 for the far edge of the plasma. The result was a very accurate calculation of the position of the cutoffs at the expense of a long execution time of the method (however, the code has not been numerically optimized).

This new method uses the real index of refraction, given by:

$$n = 1 - \frac{\omega_{pe}^2}{\omega^2} \frac{\omega^2 - \omega_{pe}^2}{\omega^2 - \omega_{pe}^2 - \omega_{ec}^2} \quad (6.133)$$

where  $\omega$  is the frequency of the wave,  $\omega_{ec}$  is the electron cyclotron frequency of the plasma, given by:

$$\omega_{ec}(r) = \frac{q_e B(r)}{m_e} \quad (6.134)$$

and  $\omega_{pe}$  is the plasma resonance frequency of the plasma, given by:

$$\omega_{pe}^2(r) = \frac{q_e^2 n_e(r)}{\epsilon_0 m_e} \quad (6.135)$$

where  $q_e$  is the electron charge,  $m_e$  is the electron mass,  $\epsilon_0$  is the relative permittivity of free space,  $n_e(r)$  is the electron density, and  $B(r)$  is the magnetic field.

Next, given that the phase difference is equal to the difference between the integrals of the index of refraction of the two traveling waves, then the phase difference can be used to find an integral of the index of refraction between the last point of known density and the position of cutoff such that the phase difference and the integral will match. This can be expressed in a formula as a zero finding function, that is:

$$0 = \Delta\phi(\omega) - \frac{\omega}{C} \int_{r_c}^{r_1} n(r, n_e(r), \omega) dr \quad (6.136)$$

where  $r_c$  is the position of cutoff that will be used to find the zero of the function, and  $n_e(r)$  is the density. The density profile will be extended to the point of cutoff by means of an extrapolating polynomial using the previous density knowledge. That is, the density profile near the cutoff and past the position of the last known

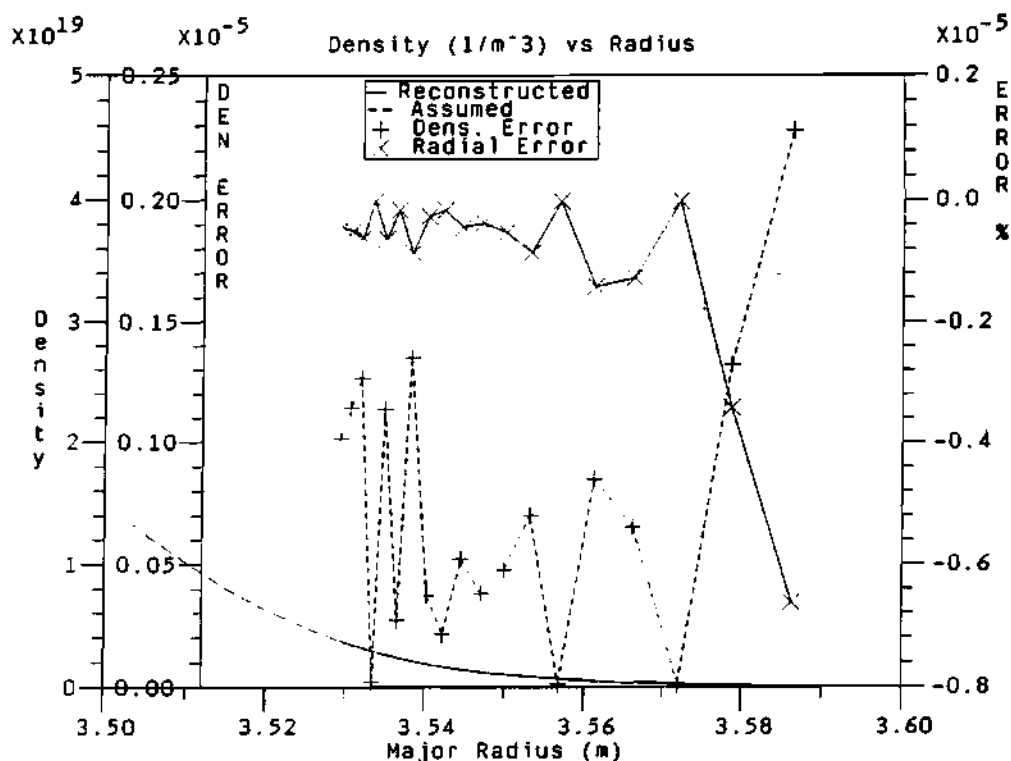


**Figure 6.6:** Reconstructed density profile using a real index of refraction fit near the cutoff to calculate the increments between cutoffs and the density profile. Both the real assumed density and the reconstructed density profile are shown. The percent error due to this method is shown on the right hand side axis for the increment in cutoff and for the calculated density on the left hand side axis. Step size is of the order of  $10^{-6}$  m.



point of density will be assumed to be of the form:

$$n_e(r) = c(r - r_0)^2 + b(r - r_0) + a \quad (6.137)$$

where the coefficients  $a$ ,  $b$ , and  $c$  will be calculated from the known points of the density profile and the cutoff density at the assumed position of cutoff,  $r_c$ . The formulation is as follows. For an assumed position of the cutoff,  $r_c$ , a cutoff density can be calculated using the cutoff condition given by the formula:

$$\omega = \frac{\omega_{ec}}{2} + \left( \omega_{pe}^2 + \frac{\omega_{ec}^2}{4} \right)^{\frac{1}{2}} \quad (6.138)$$

which can be solved for the density at the cutoff as:

$$n_e(r_c) = \frac{\epsilon_0 m_e}{q_e^2} (\omega^2 - \omega_{ec}^2) \quad (6.139)$$

where  $\epsilon_0$  is the relative permittivity of free space,  $\omega_{ec}$  is the electron cyclotron frequency,  $q_e$  is the electron charge, and  $m_e$  is the electron mass. Now that the density at the assumed cutoff position is known, the density between the last known point of density and the position of the assumed cutoff can be interpolated using a parabolic fit (or any other suitable fit) that uses: 1) the assumed position of the cutoff and calculated density at the assumed position of cutoff; and 2) the previously calculated points of density from the reconstructed density profile. Therefore, once a model for the index of refraction and a model for the density near the cutoff has been defined, then the integral of the index of refraction near the cutoff can be calculated numerically and a position of the cutoff can be found that will satisfy the zero finding function.

This method basically finds a match between the phase difference and the integral of the index of refraction in the interval between the last known point of density and the position of the cutoff. This is done by moving the position of the cutoff along the curve of constant cutoff frequency in density profile space.

In the new method, the position of the cutoffs is found by matching the integral of the index of refraction to the phase difference data. Because of this, it is not possible to make an error derivation like the one done for the parabolic fit to the index of refraction in the previous section. Nevertheless, it is safe to say that the error on the method and the calculated position of the cutoffs will be given by the ability of the zero finding function to find a zero for the function on equation 6.136. This will indicate that the zero function can be used as a measurement of the error in the method. That is, the error in the integral of the index of refraction for the zero finding function will be proportional to the error on the calculated position of the cutoff and the increment between cutoffs. With this in mind, an error derivation was done as follows.

The error derivation for this method can be started with the definition of the error as:

$$E = \int_{r_0}^{r_1} n_{real} dr - \int_{r_0}^{r_1} n_{fit} dr \quad (6.140)$$

$$= \int_{r_0}^{r_1} (n_{real} - n_{fit}) dr \quad (6.141)$$

where  $n_{real}$  is the real index of refraction, and  $n_{fit}$  is the index of refraction used for the fit. Then, the indexes of refraction can be expanded in a Taylor series as:

$$n_{real} = n_{real} + \Delta r \frac{dn_{real}}{dr} + \dots \quad (6.142)$$

for the real index of refraction, and as:

$$n_{fit} = n_{real} + \Delta r \frac{dn_{fit}}{dr} + \dots \quad (6.143)$$

for the fitted index of refraction where the matching boundary condition was used. This can be substituted into the error formula, equation 6.141, to obtain:

$$E = \int_{r_0}^{r_1} \left( n_{real} + \Delta r \frac{dn_{real}}{dr} + \dots - \left( n_{real} + \Delta r \frac{dn_{fit}}{dr} + \dots \right) \right) dr \quad (6.144)$$

where the higher terms of the series are dropped, to obtain:

$$E = \int_{r_0}^{r_1} \Delta r \left( \frac{dn_{real}}{dr} - \frac{dn_{fit}}{dr} \right) dr \quad (6.145)$$

$$= (\Delta r)^2 \left( \frac{dn_{real}}{dr} - \frac{dn_{fit}}{dr} \right) \quad (6.146)$$

where all the parameters have been defined before. This simple derivation shows how the error on the new method will scale with the step size. This was observed in the modeling of the method as it can be seen in figure 6.7 where the error for the first 9 points of the reconstruction were plotted as a function of the step size used for 5 different step sizes. As indicated by equation 6.146, the accumulated error can be expressed as:

$$E_N = N (\Delta r)^2 \left( \frac{dn_{real}}{dr} - \frac{dn_{fit}}{dr} \right) \quad (6.147)$$

where  $N$  is the number of steps taken, but  $N = \frac{l}{\Delta r}$ , where  $l$  is the interval length, so that:

$$E_N = l \Delta r \left( \frac{dn_{real}}{dr} - \frac{dn_{fit}}{dr} \right) \quad (6.148)$$

$$= \frac{l^2}{N} \left( \frac{dn_{real}}{dr} - \frac{dn_{fit}}{dr} \right) \quad (6.149)$$

so that as  $N \rightarrow \infty$  then  $E_N \rightarrow 0$ .

## 6.3 Program

### 6.3.1 Density and phase models

A program was written (by the author) to model the reflectometer phase data and reconstruction technique. The program can use two different density profile models. These density profile models are the  $\alpha$ - $\beta$  type profile, defined by the equation:

$$n_e(r) = n_{e0} \left( 1 - \left( \frac{r}{a} \right)^\alpha \right)^\beta \quad (6.150)$$

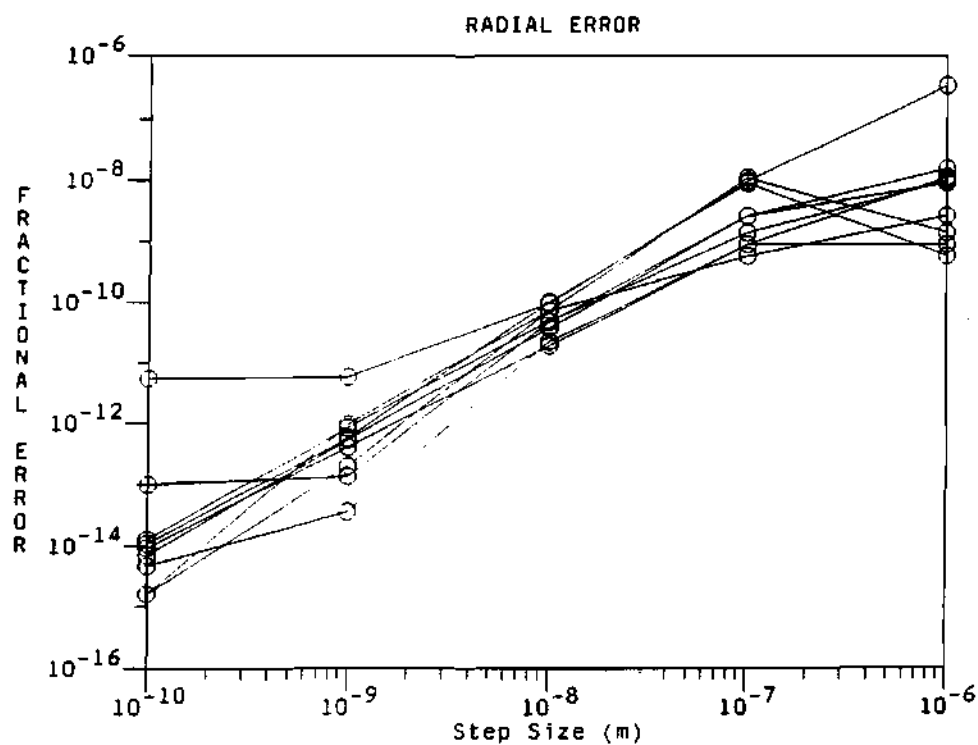


Figure 6.7: Plot of the error as a function of the step size for the new density expansion method. For this plot, the code was run five times with five different increments on the step size. Then the error of the first 9 points of the profile from every run where used as data.

while the other density profile is of the inverse hyperbolic tangent form, defined by the equation:

$$n_e(r) = \frac{n_{e0}}{2} \left( 1 - \tanh \left( \frac{r - r_0}{b} \right) \right) \quad (6.151)$$

where  $a$  is the minor radius,  $n_{e0}$  is the maximum density, and  $\alpha$ ,  $\beta$ ,  $b$ ,  $r_0$  are parameters to change the shape of the assumed electron density profile. Copies and details of this program are presented in appendix B.

As can be seen from Figure 6.8, the program has a relatively simple flow diagram. The code initializes its parameters from a standard ASCII data file. This data file contains such things as the shaping parameters for the assumed density profile ( $a$ ,  $b$ ,  $r_0$ ,  $\alpha$ ,  $\beta$ ,  $n_0$  in equations 6.150 and 6.151), data limits for the plotting windows, etc. The program calculates the position of the cutoff of the reflectometer frequencies. The radial cutoff positions correspond to an equally spaced interval on the frequencies of the reflectometer where the frequency spacing,  $\Delta\omega$ , can be arbitrary, but it is generally set to the frequency spacing of the probing waves.

Using the position of the cutoffs, the full phase for each of the two traveling waves can be calculated using equation 6.9 as:

$$\phi(\omega_L) = 2 \frac{\omega_L}{C} \int_{r_c(\omega_L)}^{r_0} n(r, \omega_L) dr \quad (6.152)$$

$$\phi(\omega_U) = 2 \frac{\omega_U}{C} \int_{r_c(\omega_U)}^{r_0} n(r, \omega_U) dr \quad (6.153)$$

for the particular frequency and cutoff position, where the letters  $L$  and  $U$  correspond to the Lower frequency and Upper frequency waves of the probing beam, and all of the other variables have been defined before. This full phase information is used to calculate the phase difference between the two waves, which is the measurable quantity of the diagnostic, that is:

$$\Delta\phi = \phi(\omega_U) - \phi(\omega_L) \quad (6.154)$$

where  $\Delta\phi$  is the phase difference. Because of the definition of the phase difference, equation 6.154 is in a forward difference form; either the Lower frequency

or the Upper frequency can be used to plot the parameters. Therefore, the Lower frequency was chosen in the program to plot the different parameters.

The same plots for the Upper frequency can be obtained with the addition of an  $\Delta\omega$  to the Lower frequency axis. Using this information the code reconstructs the density profile using the procedure described in the previous section. Typical output of the program is shown in Figure 6.9. The format used in Figure 6.9 for the phase difference data, the assumed density profile and the reconstructed density profile is repeated throughout this chapter for most of the figures. Unless otherwise stated in the caption or in the paragraph quoting the figure, the upper plot of the figure will always be the phase difference data calculated from an assumed density profile which will be plotted on the lower plot of the same figure, together with the reconstructed density profile obtained from the phase difference data in the upper plot. For most of these figures the assumed magnetic field strength is  $B_0 = 4.5$  Tesla, unless otherwise stated. The central density of the profile can be obtained from the density plot (usually dash line curve of the lower plot in the figure). The frequency separation used for the calculation of the phase difference data is  $\Delta\omega = 0.25$  GHz, unless otherwise stated. This type of format was chosen because it provides an easy and fast way to see the goodness or match between the assumed density profile and the reconstructed density profile.

The program can calculate and plot:

1. The reconstructed and assumed density profile vs radius.
2. The index of refraction as a function of the cutoff position.
3. The position of the cutoff vs the reflectometer frequency, which can be used to determine how deep the the reflectometer beam can probe a given plasma profile.

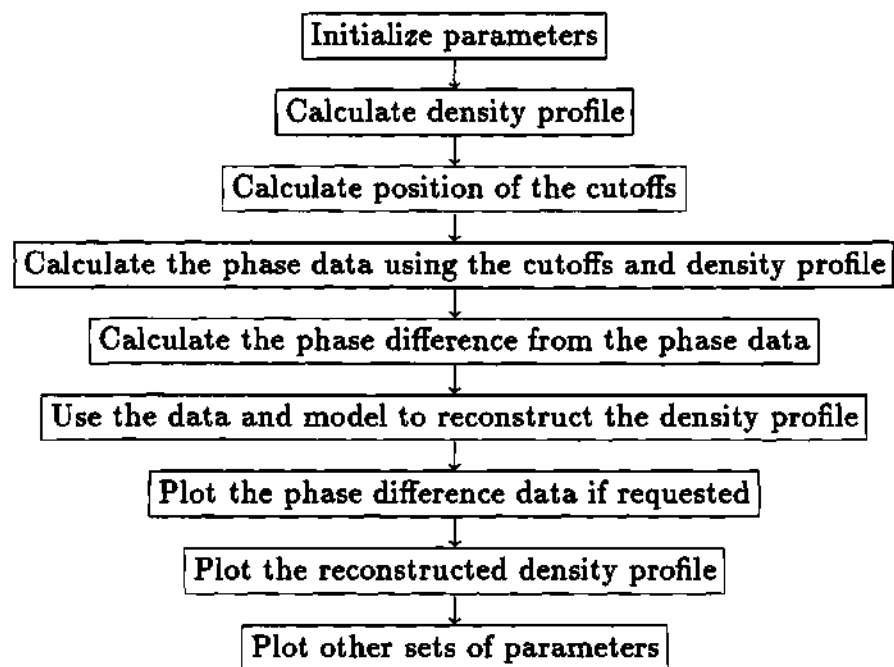


**Figure 6.8:** Flow chart of the modeling program.

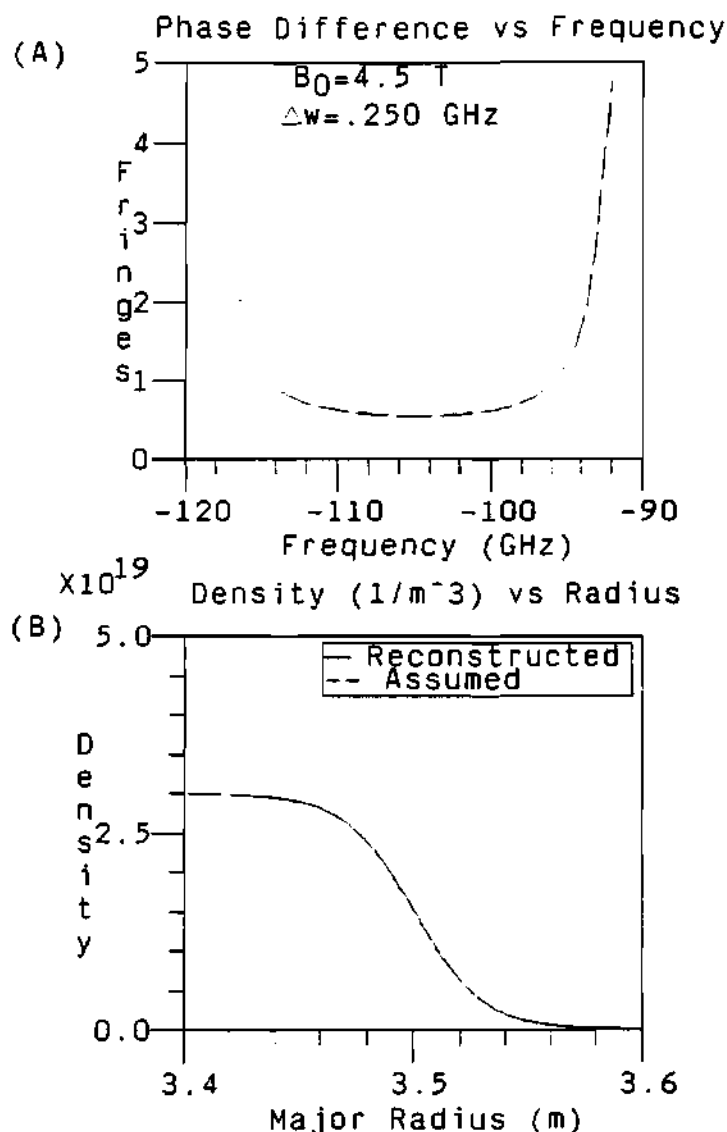


**Figure 6.9:** Typical plotting output for the simulation or modeling code. (A) Plot of the phase difference data calculated from the assumed density profile. Negative frequencies in plot (A) are used to force the plotting routine to write numbers from right to left, thus providing a mapping between the frequency and radial axis. Real frequencies are actually positive. (B) Plot of the assumed density profile (in dash line) and the corresponding reconstructed density profile (solid line) calculated using the phase difference data from plot (A).



4. The spacing between the cutoffs of the lower frequency and the upper frequency waves as a function of the cutoff position can be plotted and studied with this model.
5. The derivative of the phase as a function of the radius.
6. The “real” and reconstructed full phase of the plasma vs the radius. This is used for comparison of the phase from the assumed density profile and the reconstructed density profile.
7. The “real” and reconstructed phase difference of the plasma. This is for comparison of the phase difference obtained from the assumed density profile and the phase difference obtained from the reconstructed density profile.
8. The position of the cutoffs for the reconstructed density profile vs the position of the “real” cutoffs. This is used for comparison of the position of the cutoffs for the assumed density profile and the cutoffs obtained from the reconstructed data. Good agreement of the profile will give a  $45^\circ$  line going through the origin of the coordinate system.

These can provide great insight on the relationship between the phase data and the shape of the density profile.

### 6.3.2 Frequency vs cutoff position mapping

It must be noticed from Figure 6.9 that the lower end of the frequency band corresponds to the lower end of the density profile, and the upper end of the frequency band corresponds to the high end of the density profile. This can be noticed from Figure 6.10, where the frequency as a function of the cutoff radial position is shown. From this plot it is clear that it is not a linear mapping; nevertheless, this plot can be used to obtain the cutoff position of any frequency

(and/or vice versa) for the typical density profile shown in Figure 6.9. Similar plots can be obtained for any given density profile.

### 6.3.3 Integrals calculation

To calculate the different phase integrals (over all the previous points, leaving out only the unknown point at the last step) necessary for the different calculations the program uses a *Cubic* polynomial expansion to approximate the curve between points and to calculate the area between intervals.<sup>66,67</sup> The derivation of the equations used is as follows. There exist two sets of data points,  $(x_i, y_i)$ , which represent a function, or are the sampling points of a function, or the data points of that function. One wishes to calculate the integral of this function over a set of limit points, that is:

$$A = \int_a^b Y(x) dx \quad (6.155)$$

where  $a$  and  $b$  are the limit points. It is not always possible to calculate this integral exactly or analytically. This could be because of the type of function under consideration or because the real form of the function is not known. For instance only its value at specific points is known, as in the case of experimental data. It is possible to approximate the integral of the function by adding the independent contributions of each of the data points to the integral due to the interval of the data points. Since the actual value of the function is not known between the points of the interval, then the function there can be approximated by a polynomial of some degree. For the case of a cubic polynomial type of approximation the piece of curve  $y(x)$  between points  $x_i$  and  $x_{i+1}$  is approximated by the function:

$$y(x) = a_i + b_i x + c_i x^2 + d_i x^3 \quad (6.156)$$

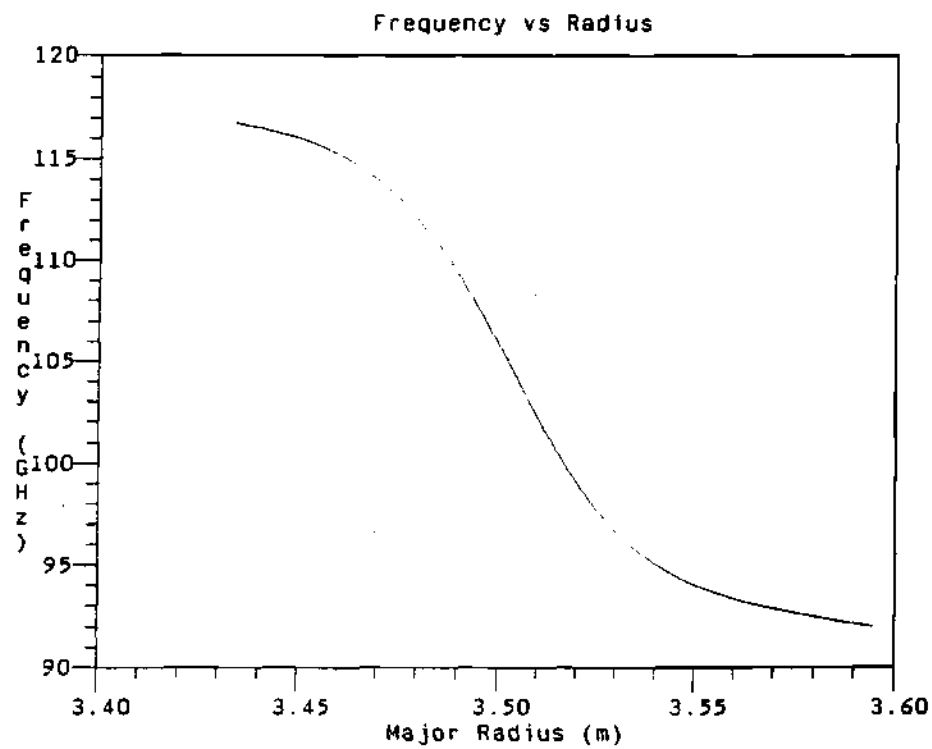


**Figure 6.10:** Cutoff frequency of the propagating wave vs its cutoff radial position (major radius).

for  $x_i \leq x \leq x_{i+1}$  and where the coefficients  $a_i, b_i, c_i, d_i$  are given by:

$$a_i = y_0 \quad (6.157)$$

$$b_i = \frac{-11y_0 + 18y_1 - 9y_2 + 2y_3}{6h} \quad (6.158)$$

$$c_i = \frac{2y_0 - 5y_1 + 4y_2 - y_3}{2h^2} \quad (6.159)$$

$$d_i = \frac{-y_0 + 3y_1 - 3y_2 + y_3}{6h^3} \quad (6.160)$$

where  $h$  is the spacing of the points,  $y_0, y_1, y_2$ , and  $y_3$  are the points used to fit the cubic polynomial. The coefficients  $a_i, b_i, c_i$ , and  $d_i$  are calculated such that the polynomial will satisfy the condition:

$$y(x_i) = y_i \quad (6.161)$$

thus the piece of curve of the polynomial  $y(x)$  is an approximation of the curve  $Y(x)$  in the interval of  $x_i$  to  $x_{i+1}$ . This is called an open approximation of the function, since the points used to calculate the polynomial are outside of interval of integration. Now, the area under the piece of curve in the interval from  $x_i$  to  $x_{i+1}$  is given by:

$$A_1 = \frac{h}{24} (9y_0 + 19y_1 - 5y_2 + y_3) \quad \text{for } i = 1 \quad (6.162)$$

$$A_i = \frac{h}{24} (-y_{i-1} + 13y_i + 13y_{i+1} - y_{i+2}) \quad \text{for } i > 1 \quad (6.163)$$

where  $A_i$  are the areas of the intervals from  $x_i$  to  $x_{i+1}$ . By adding all the areas  $A_i$  of all the intervals the total area of the data is given by:<sup>66,67</sup>

$$A = \frac{h}{3} (y_0 + y_N) + \frac{31h}{24} (y_1 + y_{N-1}) + \frac{5h}{6} (y_2 + y_{N-2}) + \frac{25h}{24} (y_3 + y_{N-3}) + \sum_{i=4}^{N-4} hy_i \quad (6.164)$$

where  $N$  is the total number of points in the array,  $A$  is the total area of the function over the interval from  $x_0$  to  $x_N$ , and  $h = x_{i+1} - x_i$  is the spacing between points.

### 6.3.4 Cubic integrals error

The error in this type of approximation can be calculated as follows. Start with the Taylor's series of the function:

$$f(x) = \sum_{n=0}^{\infty} \frac{(x - x_i)^n}{n!} \left. \frac{d^n f(x)}{dx^n} \right|_{x_i} \quad (6.165)$$

which is exact as long as all of the terms are used, and the derivatives are well defined, and the series is convergent. Then the approximation that has been used in equation 6.156 is of the form:<sup>66,67,311</sup>

$$f(x) = a + bx + cx^2 + dx^3 + R_4 \quad (6.166)$$

where:

$$R_4 = \sum_{n=4}^{\infty} \frac{(x - x_i)^n}{n!} \left. \frac{d^n f(x)}{dx^n} \right|_{x_i} \quad (6.167)$$

is the remainder or error term of the equation. Then the integral can be expressed as:

$$\int_{x_i}^{x_{i+1}} f(x) dx = \int_{x_i}^{x_{i+1}} (a_i + b_i x + c_i x^2 + d_i x^3) dx + \int_{x_i}^{x_{i+1}} R_4 dx \quad (6.168)$$

where the error is given by:<sup>311</sup>

$$E = \int_{x_i}^{x_{i+1}} R_4 dx \quad (6.169)$$

$$= \int_{x_i}^{x_{i+1}} \sum_{n=4}^{\infty} \frac{(x - x_i)^n}{n!} \left. \frac{d^n f(x)}{dx^n} \right|_{x_i} dx \quad (6.170)$$

$$= \sum_{n=4}^{\infty} \int_{x_i}^{x_{i+1}} \frac{(x - x_i)^n}{n!} \left. \frac{d^n f(x)}{dx^n} \right|_{x_i} dx \quad (6.171)$$

$$= \sum_{n=4}^{\infty} \frac{(x_{i+1} - x_i)^{n+1}}{(n+1)!} \left. \frac{d^n f(x)}{dx^n} \right|_{x_i} dx \quad (6.172)$$

where depending on the sign of the derivatives  $\left. \frac{d^n f(x)}{dx^n} \right|_{x_i}$  the errors may cancel.<sup>311</sup> Nevertheless, as long as  $h$  is small the biggest error expected can be for  $n = 4$ , that is:

$$E = \frac{(x_{i+1} - x_i)^5}{5!} \left. \frac{d^4 f(x)}{dx^4} \right|_{x_i} \quad (6.173)$$

and for  $h = x_{i+1} - x_i$  the error is given by:

$$E = \frac{h^5}{5!} \left. \frac{d^4 f(x)}{dx^4} \right|_{\xi} \quad (6.174)$$

where  $x_i \leq \xi \leq x_{i+1}$ . Thus the error with this approximation decreases as a 5<sup>th</sup> power of the step size, and the approximation is exact if the 4<sup>th</sup> derivative or higher terms goes to zero, as for the case of a 3<sup>rd</sup> degree polynomial or lower.<sup>311</sup>

## 6.4 Modeling Results

Before the actual construction of the reflectometer, a modeling program was written to study the behavior of the probing beam on an assumed density profile. The profiles studied were the typical  $\alpha$ - $\beta$  profiles, defined by:

$$n_e = n_{e0} \left( 1 - \left( \frac{r}{a} \right)^\alpha \right)^\beta \quad (6.175)$$

where  $\alpha$  and  $\beta$  are the shaping parameters and a *hyperbolic tangent* density profile. These serve as a test bed for the reconstruction technique. This modeling code allows for the study of things such as:

1. The phase difference data dynamic range.
2. The effect of changes on the central density, the position of the plasma edge and different profile shapes on the phase data.
3. The radial spacing of the cutoff layers for the two probing frequencies.
4. The effect of fluctuations on the measured phase data and on the reconstructing technique.
5. The frequency limits and the penetration range of the probing beam into the plasma for different plasmas.

6. The phase dynamic range limits.
7. The effect of the probing beams frequency spacing on the phase data and reconstructing technique.
8. The effect of the offset of the phase difference data on the reconstructed density profile.

Because of the complicated nature of the equations and procedures involved to calculate the reconstructed density profile, there is no hand calculator test that can be done to show that the program is working correctly or that it is right. On the other hand, the program was written so that it over-plots the reconstructed density profile with the real assumed density profile for comparison. It can also be used to compare the full phase and phase difference for the assumed and reconstructed density profile. Other comparisons or checks to see the accuracy of the program and reconstruction technique were done by comparing the code with another code written by G. R. Hanson, described in section 6.6. The case for zero magnetic field,  $B_0 = 0$  Tesla, was used to compare the result of the reconstruction technique with the Abel inversion result, discussed in section 6.7. These are about the best verification that the reconstruction technique is doing what it is supposed to do and that it is doing the reconstruction accurately.

The modeling of the reflectometer can provide accurate values for important design parameters such as the frequency range necessary to penetrate to a certain depth in the plasma, phase difference dynamic range, accuracy of the reconstructing technique, its limitation, and others. These results will be presented in the following sections.

#### 6.4.1 Phase difference dynamic range

An example of the phase difference data dynamic range is shown in Figure 6.11 for a density profile of the form:

$$n_e(r) = n_0 \left(1 - \left(\frac{r}{a}\right)^\alpha\right)^\beta \quad (6.176)$$

where  $\alpha = 6$  and  $\beta = 2$  are the shape parameters. This example uses a magnetic field of  $B_0 = 4.5$  Tesla and a frequency separation of  $\Delta\omega = 0.25$  GHz. In this model a frequency separation of  $\Delta\omega = 0.25$  GHz will give a phase difference data dynamic range of less than 3 fringes. This compares favorably with the phase dynamic range of a full phase reflectometer which has a phase range of hundreds of fringes. "Systems with only a few fringes of dynamic range are much less likely to 'skip' fringes".

#### 6.4.2 Effect of the density shape

The phase data is a combination of the phase due to the fixed gradient of the magnetic field and the phase due to the gradient of the density profile. Thus the phase difference is more a measurement of the local gradient of the density profile than of the absolute value of the density profile, and therefore, the shape of the density profile determines the phase difference data. That is, as the local slope of the density profile increases or decreases the phase difference will have an opposite response, it will decrease or increase, respectively. This can be seen analytically as follows. The derivative of the density is defined as:

$$\frac{dn_e}{dr} = \frac{\Delta n_e}{\Delta r} \quad (6.177)$$

where the value of  $\Delta r$  can be assumed to be proportional to the phase difference, that is:

$$\Delta r \propto \Delta\phi \quad (6.178)$$



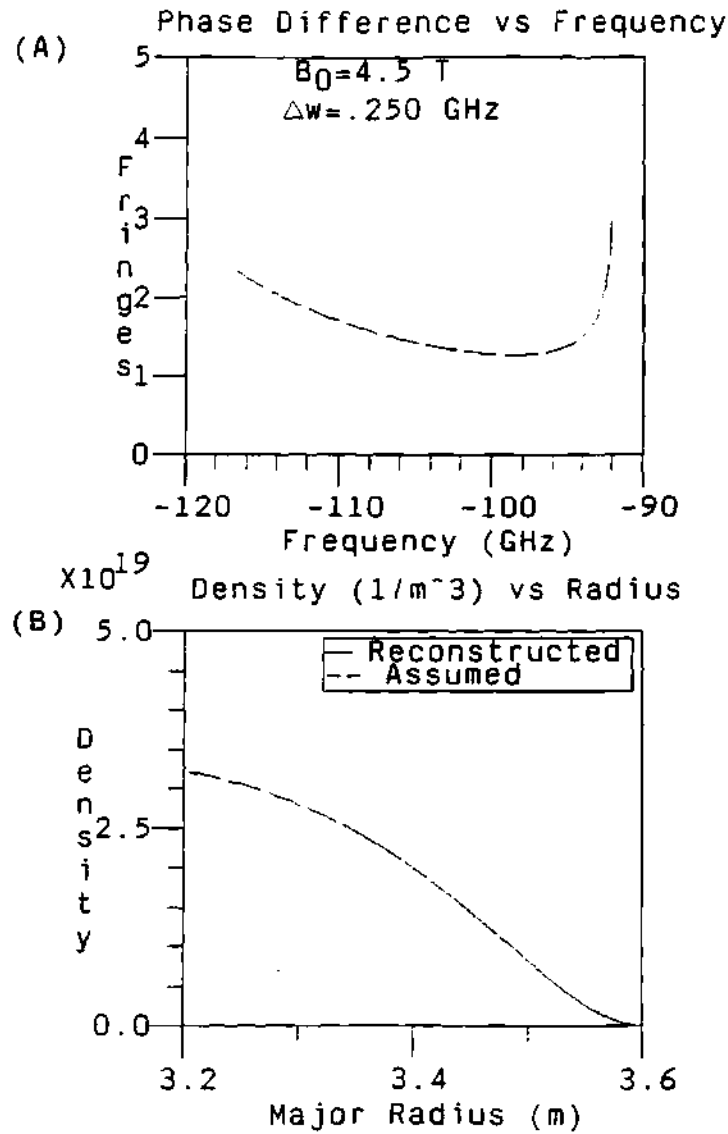


Figure 6.11: (A) Plot of the phase difference dynamic range for a plasma density of the  $\alpha$ - $\beta$  form with  $\alpha = 6$  and  $\beta = 2$ . (B) Plot of the assumed density profile used to calculate the phase data and the reconstructed density using the phase difference data.

thus the derivative can be expressed as:

$$\frac{dn_e}{dr} \propto \frac{\Delta n_e}{\Delta \phi} \quad (6.179)$$

so that if the derivative increases, then  $\Delta \phi$  in equation 6.179 has to decrease; and if the derivative decreases, then  $\Delta \phi$  has to increase.

The following sections will present a series of density profiles with different shape parameters (such as, central density slope, edge slope, and maximum center density) and its corresponding effect on the phase difference data. This will give the reader a feeling for the effects of these shape parameters on the resulting phase difference data, and in particular the role of the local density slope in the phase difference data.

**Central density slope** Figure 6.12 shows the phase difference and the assumed density profile together with its corresponding reconstructed counter part for a hyperbolic density profile with different slopes at the center of the plasma. Notice how the phase difference is a maximum when the slope of the density is a minimum (i.e., when the slope tends to go to 0), as at the edge and the center of the plasma; while the phase difference is a minimum when the slope of the density is a maximum at the center of the step, at  $R = 3.5$  m; as intuitively predicted by equation 6.179. Figure 6.12 is an excellent example to develop an intuitive idea of the effect of the local density slope on the calculated phase difference data. The position and separation of the cutoffs for the reflectometer beam waves depends on the local value of the density and the magnetic field. For the purposes of the phase difference, the change of the local density contributes the most to the separation of the cutoffs. Since the phase difference is proportional to the separation of the cutoffs, then the closer the cutoffs' positions the smaller the phase difference at that position, while the larger the cutoffs' separation, then

the larger the phase difference at that position. A small or flat slope on the density will produce a large separation of the cutoffs' positions, thus producing a large phase difference at that point. This corresponds to the flat center density profile in Figure 6.12(B) (curve 1), which corresponds to the phase difference curve with the largest magnitude at the upper part of the frequency band in Figure 6.12(A)(curve 1). On the other hand, for a density profile which has a very large or steep center slope the position of the cutoffs will be very close together, thus the phase difference will be smaller than the one for the flat profile. This case is seen in Figure 6.12(B) for the steep density profile (curve 3) which corresponds to the phase difference curve in Figure 6.12(A) with the lowest value at the upper part of the frequency band (curve 3). So it can be concluded that the steeper the density profile at any given point at the center of the plasma, then the smaller the phase difference at that point of the corresponding cutoff frequency. A similar and complementary statement is true for the case of a flat profile, that is, the flatter the profile at a given point at the center of the plasma the larger the value for the phase difference at that point.

**Effect of the density edge shape** The shape of the edge density can play an important role in the phase difference data, as can be seen from Figure 6.13, which shows the phase difference data for different edge slopes together with the corresponding assumed and reconstructed density profiles. As the edge slope decreases (i.e., becomes flatter) the radial separation of the cutoffs' layers for the two probing wave increases and therefore the corresponding phase difference data increases, especially at the center part of the frequency band, which corresponds to the rise of the density profile. The phase difference data at the upper part of the frequency band (which corresponds to the center of the plasma) remains about the same. While Figure 6.12 shows the effect of the slope at the

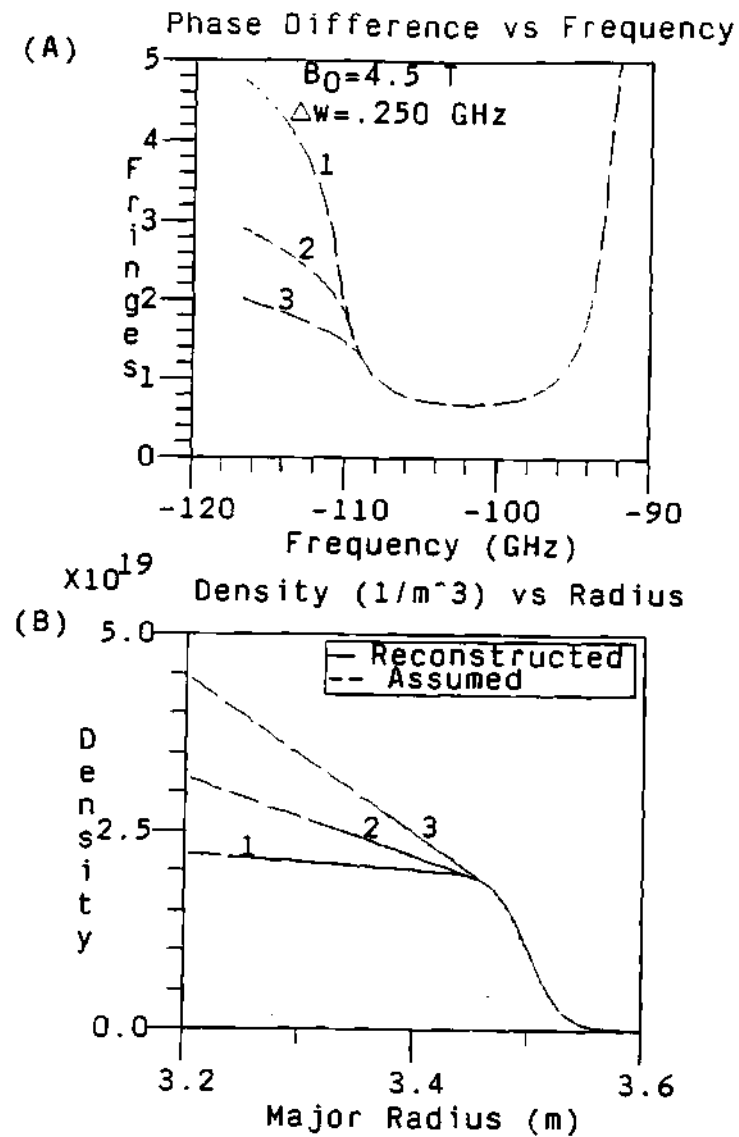


Figure 6.12: Effect of the slope at the center of the density profile on the phase difference data and the reconstructed density profile. (A) The phase difference data calculated from the assumed density profile. (B) The assumed density profile and the reconstructed density profile.

center of the plasma, Figure 6.13 shows the similar or equivalent effect on the edge of the plasma. It can be noticed from plot (B) of Figure 6.13 that as the edge slope of the density profile becomes steeper (curve 1) the calculated phase difference data (curve 1) becomes smaller. Notice how the flat floor of the phase difference data is displaced by a nearly constant offset as the slope of the edge profile becomes flatter. This effect has been noticed in real data on TFTR.

Another important effect of the plasma edge on the phase difference data is the resulting minimum phase difference value of the curve. That is, the flatter the edge the larger will be the minimum of the phase difference curve.

**Effect of the central density** Figure 6.14 shows the effect of different central maximum densities on the phase difference data. Curve 1 in plot (A) of Figure 6.14 corresponds to the density profile with the lowest central density profile, while the lower curve in plot (A) of Figure 6.14 corresponds to the largest central density profile. The assumed density profiles used in Figure 6.14 are different on the central density only. This type of behavior was observed in TFTR data for a central density scan.

#### 6.4.3 **Effect of the edge position**

A *hyperbolic tangent* density profile (given by equation 6.151) was used to study the effects of the change of the edge position on the phase data and the reconstructed density profile. Figure 6.15 shows the phase data and corresponding assumed and reconstructed density profiles for a hyperbolic tangent density profile with different displacements of the profile. The magnetic field is  $B_0 = 4.5$  Tesla and the frequency spacing is  $\Delta\omega = 0.25$  GHz. Notice how the family of curves for the phase difference data in plot (A) are almost identical in shape. This is because the displacement of the density profile does not change the slope of the density

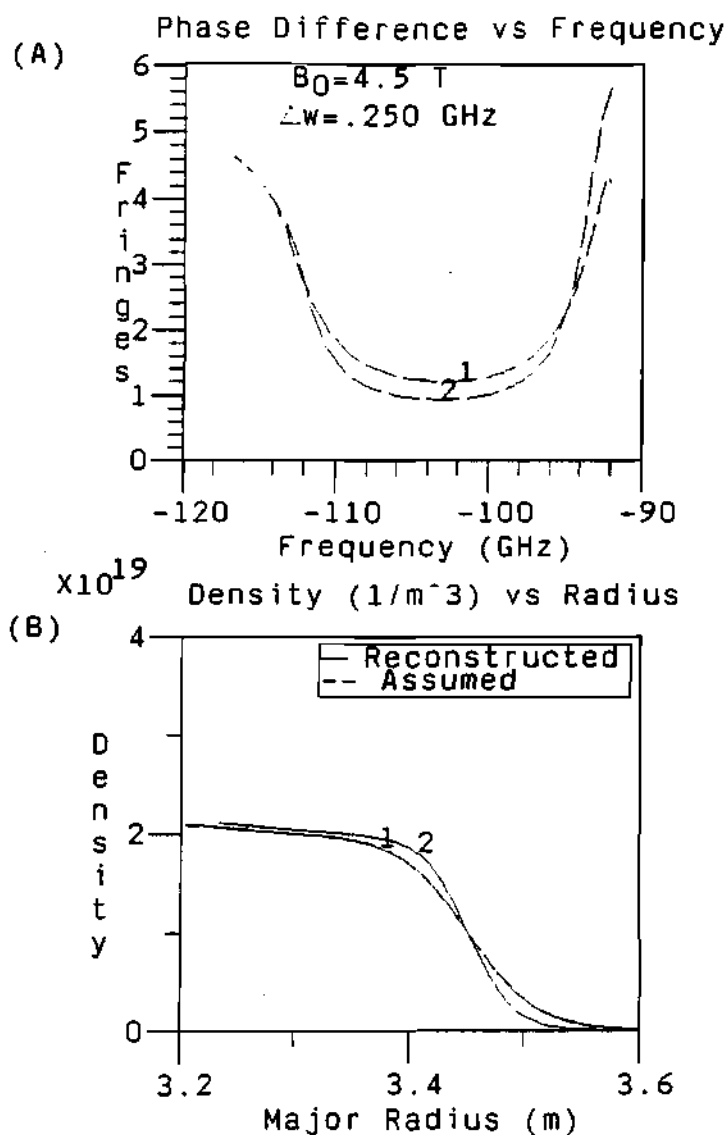


**Figure 6.13:** Effect of the shape of the density edge on the phase difference data and the reconstructed density profile. (A) Calculated phase difference for different plasma edge slopes. (B) Assumed density profile used to calculate the phase difference data over-plotted with the corresponding reconstructed density profile.

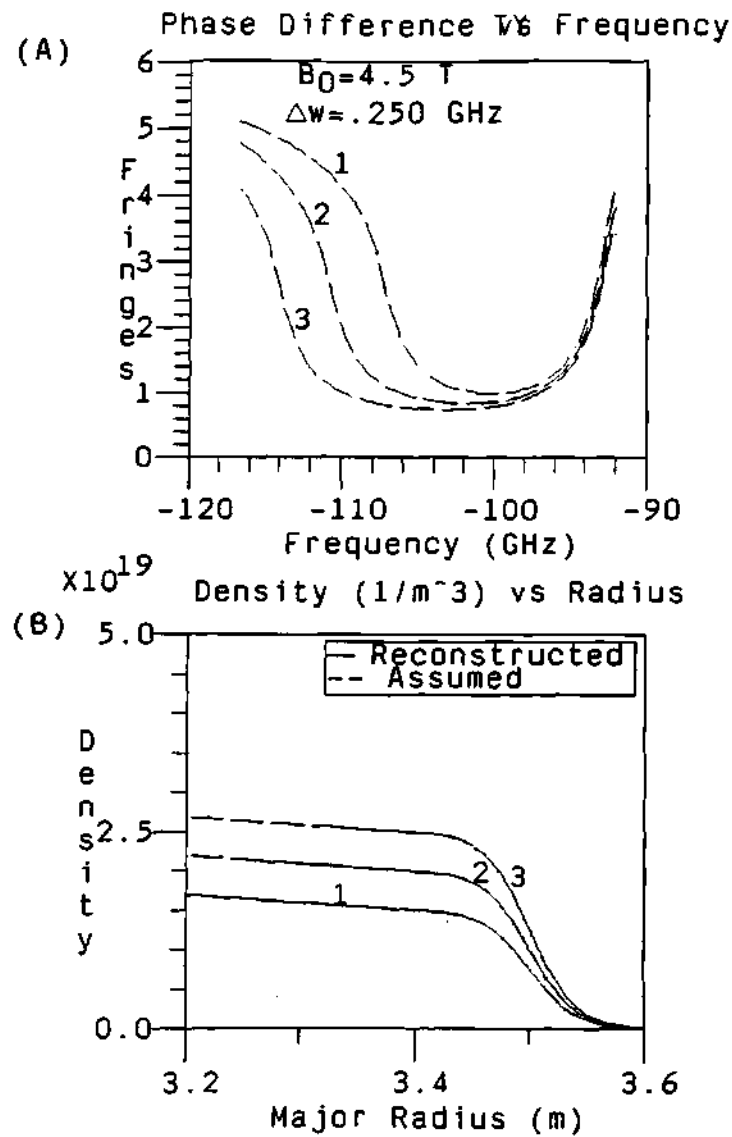


**Figure 6.14:** Effect of the different central density values on the phase difference and the reconstructed profile. Notice how the phase data at the higher part of the frequency band (corresponding to the center area of the profile) increases as the scanned part of the profile becomes flatter. (A) Calculated phase difference for different central maximum densities. (B) Assumed density profiles and corresponding reconstructed density profiles.

profile, but only shifts the cutoff layers' positions inside the plasma. This will have the effect of shifting the phase difference data of plot (A) in the vertical direction by an amount proportional to the phase of the separation frequency, that is:

$$\delta\phi_{shift} \propto 2 \frac{R_{edge} - R_{ref}}{\lambda_m} \quad (6.180)$$

where  $\delta\phi_{shift}$  is the vertical shift on the phase,  $R_{edge}$  is the position of the edge,  $R_{ref}$  is the reference point, and  $\lambda_m$  is the modulation wavelength or the frequency separation wavelength. The horizontal shift at the higher frequencies on plot (A) is due to the higher magnetic field on the inside of the plasma.

#### 6.4.4 Effect of fluctuations

The effect of different fluctuation wavelengths on the assumed density profile are shown in Figure 6.16 for wavelength fluctuations of 1 cm, Figure 6.17 for wavelength fluctuations of 5 cm, and Figure 6.18 for wavelength fluctuations of 10 cm. These fluctuations on the assumed density profile have an amplitude of the form:

$$\delta n_e \propto \frac{\lambda}{2\pi} \sin \left( 2\pi \left( \frac{r-a}{\lambda} \right) \right) \quad (6.181)$$

where  $\lambda$  is the wavelength of the density fluctuation. This form of perturbation was chosen (instead of a pure sinusoidal) because it provides an always negative slope on the density profile, as can be seen from Figures 6.16, 6.17 and 6.18. In this way for any given density there is only one radial position that corresponds to this density, and even more important, for any given probing frequency, there is a cutoff at only one radial location.

The unperturbed density profile is of the  $\alpha = 6$  and  $\beta = 2$  type (described previously) with a magnetic field of  $B_0 = 4.5$  Tesla. It must be noticed how the reconstructed density profile follows the shape of the assumed density profiles, Figure 6.16, 6.17 and 6.18. Therefore, if there are any features in the real TFTR



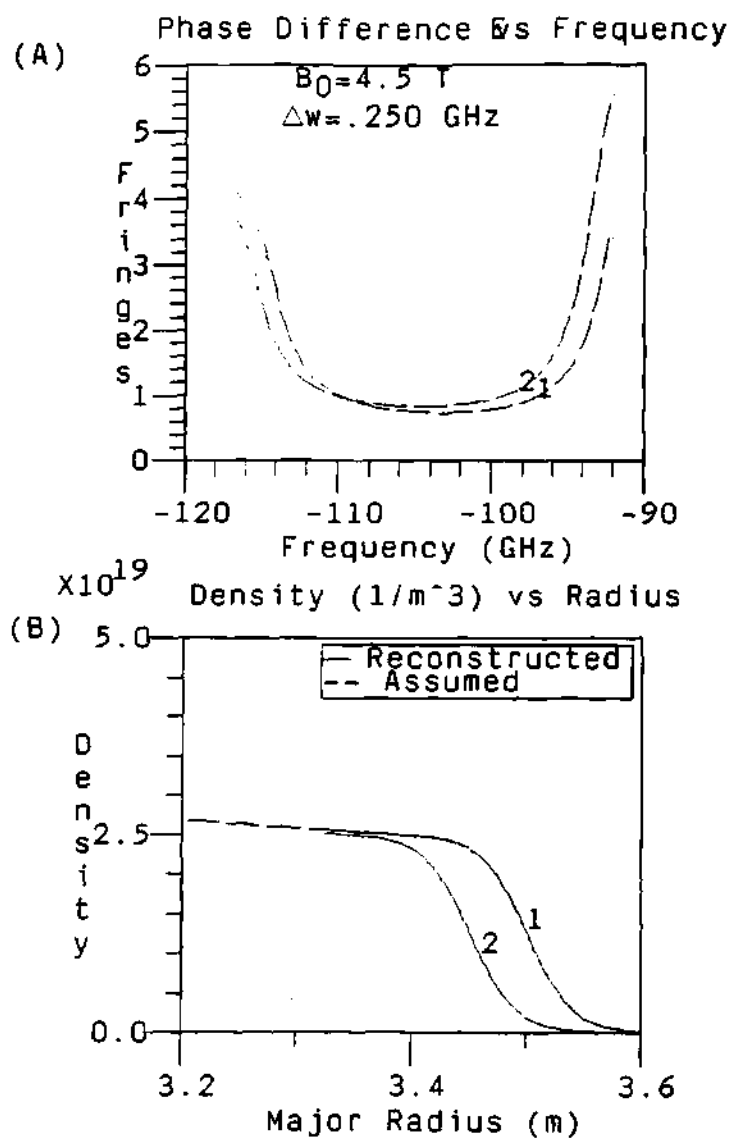


Figure 6.15: Plots showing the effect of the change in the plasma edge position on the phase data and the reconstructed density profile. (A) Calculated phase difference data for different density displacements. (B) Assumed density profile (hyperbolic tangent) and reconstructed density profile from the phase difference data.

plasma which are similar to the density profile in these figures the reconstructed density profile will in general follow the shape of the real density profile. While if the profile has a long wavelength feature like the one in Figure 6.18 then the reconstructed profile will be able to follow this feature. This type of feature shown in the Scrape Off Layer (SOL) of the density profile shown in Figure 6.18 has been seen in TFTR and reported by Hanson.<sup>285-287</sup> In his paper, Hanson calls the feature a *double Scrape Off Layer*. This type of feature (flat spots in the density profile) has been measured for some plasmas by the Thomson Scattering diagnostic, as reported by Boris Grek.<sup>180</sup> The modeling program shows that the reflectometer probing beam can detect this type of change on the density profile and the reconstruction technique can calculate a corresponding density profile that accurately reproduces the assumed density profile. The peaks in the phase difference data are due to the sudden separation of the cutoff layers when the cutoff position for the upper frequency passes the local flat spot of the density perturbation while the cutoff for the lower frequency is still behind this point.

The cases presented above are simple single frequency perturbations to show the response of the phase difference data and the reconstruction technique to such a change in the density profile. For a more realistic treatment of fluctuations on the plasma, fluctuations with a spatial wave-number spectrum and a correlation length were modeled and studied with the simulation program, and the result is shown in Figure 6.19. The assumed wave spectrum has a typical spatial wave-number spectrum for a TFTR plasma, with a typical correlation length of 1-2 cm.<sup>110-114</sup> It was obtained by taking a random fluctuation in position space, taking the fast Fourier transform to the k-space, then multiplying by an exponential function with a decay constant, and finally inverse Fourier transforming the fluctuations back to the position space. The particular wave-number spectrum and spatial correlation function used is based on Fonck<sup>112</sup> (Half Width at Half

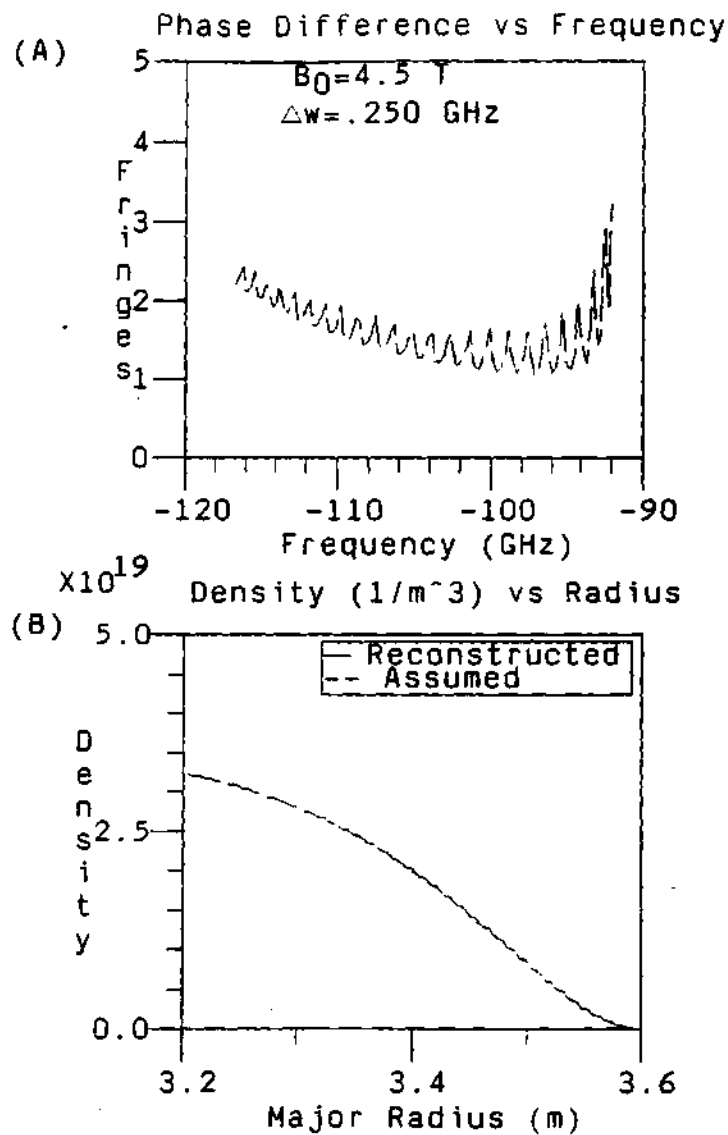


Figure 6.16: (A) The calculated phase difference data for a density profile with a periodic density perturbation with a wavelength of  $\lambda = 1 \text{ cm}$ . (B) The assumed density profile used to calculate the phase difference data and the resulting reconstructed density profile calculated from the phase data.

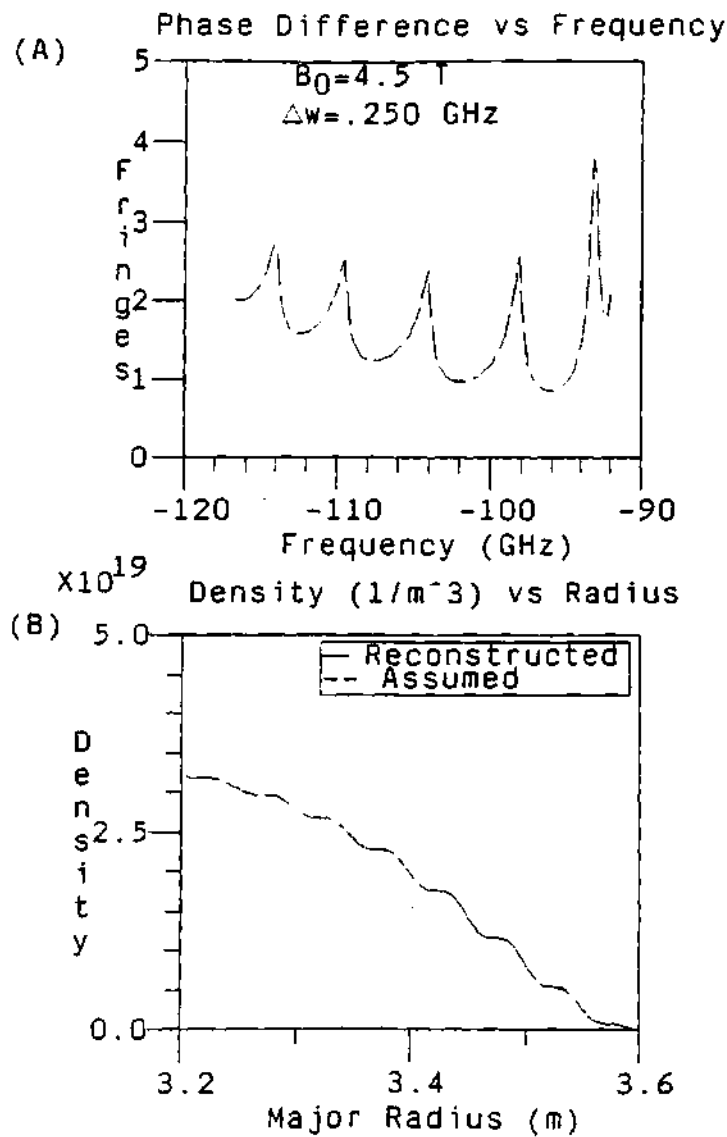


Figure 6.17: (A) Calculated phase difference data for a density profile with a periodic density perturbation with a wavelength of  $\lambda \approx 5 \text{ cm}$ . (B) Assumed density profile and reconstructed density profile.

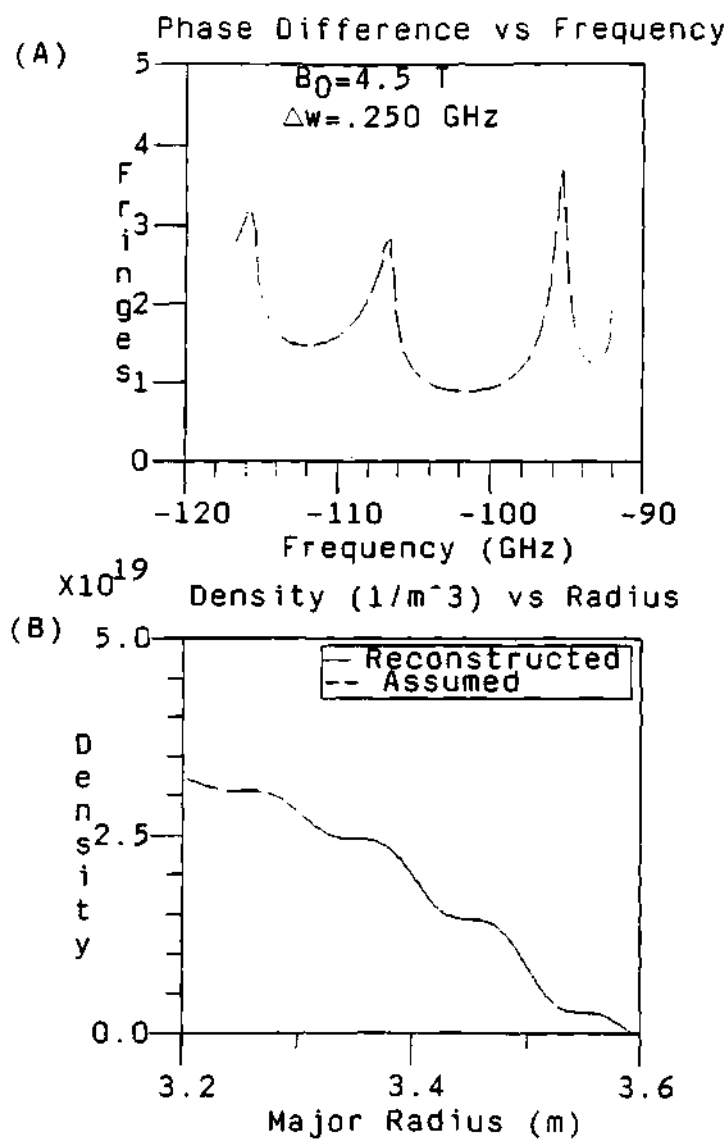


Figure 6.18: (A) Calculated phase difference data for a density profile with a periodic density perturbation with a wavelength of  $\lambda = 10 \text{ cm}$ . (B) Assumed density profile and reconstructed density profile.

Maximums, HWHM, of  $\approx 2$  cm for the spatial correlation length function and  $\approx 1 \text{ cm}^{-1}$  for the spatial wave-number spectrum function), and it uses a Gaussian shape curve for the spatial wave-number spectrum.

The importance of the correlation length of the fluctuations is on its effect on the phase difference fluctuations, described previously in section 2.7.5. That is, if a separation frequency is chosen which corresponds to a cutoff layer separation larger than the correlation length of the fluctuations and the fluctuations cause more than one fringe of jump between measurement intervals, then there is no chance of tracking the phase at that point.<sup>63</sup>

The fluctuations are calculated using a method similar to the one described by Bretz.<sup>110</sup> Fonck<sup>112</sup> shows that the total rms density fluctuations amplitude can change by 1 order of magnitude from the edge of the plasma to the center of the plasma. The rms density fluctuations amplitude at the edge can be as large as  $\frac{\tilde{n}_e}{n_e} \approx 25\%$  and only 1% at the center of the plasma. Other measurements (such as the ones by Durst<sup>113,114</sup>) have shown similar results at the edge and center of the plasma, and with an rms density fluctuation amplitude at the Scrape Off Layer (SOL) of  $\frac{\tilde{n}_e}{n_e} \approx 15\%$ . For this model a worst case situation was assumed, where a constant amplitude for the total rms density fluctuations was used, instead of one whose amplitude decrease with decreasing minor radius.

It must be noted that these large fluctuations on the density profile cause a serious problems for the profile reconstruction code, which assumes that the cutoff frequency is a monotonically decreasing function of the radius. But it is still useful to run the code to show that in spite of these difficulties that the code still works surprisingly well (the following section discusses a way to reduce and/or minimize these difficulties). Figure 6.19 shows the phase difference data with the fluctuation in plot (A) and the reconstructed and assumed density profile in plot (B). It must be noticed that the large fluctuations on the phase data

are mapped into fluctuations on the reconstructed position of the cutoffs on the radial axis of the plot and the resulting reconstructed profile gives a non-physical representation of the density profile. The fluctuation on the radial position of the cutoffs is because the phase data is used to calculate the increment on the cutoff positions and the positions of the cutoffs. Therefore, the fluctuations on the phase will be passed along to the calculated positions of the cutoffs.

#### 6.4.5 Modeling the smoothing

The fluctuations on the data while real in nature have the nasty effect of producing similar fluctuations on the reconstructed increments of the cutoff positions and consequently, on the positions of the cutoffs. The resulting reconstructed profile is consequently non-physical since it gives a multiple valued density profile as a function of the radius. That is, the mapping from radius to density is not one to one (1 to 1). Nevertheless, if the fluctuations on the phase data have a random nature, then the smoothing and averaging will remove the fluctuations from the real data proportional to the square root of the number of data points smoothed or averaged. The reconstructed profile using the smoothed and/or averaged phase data will represent a time averaged profile of the real density profile, as described and discussed in chapter 7, section 7.2.2. Nevertheless, fluctuations or features in the density profile that have a wavelength longer than the separation between cutoffs and that are lower in frequency than the data acquisition rate will remain unchanged.

The fluctuations on the real data as modeled in the previous section are reduced by smoothing and/or averaging the real data. The smoothing will reduce the level of the fluctuations so that the tracking of the phase can be done without much difficulty. This process is especially applicable when there are a large number of data points (over 500 points) and it is convenient to average or smooth the

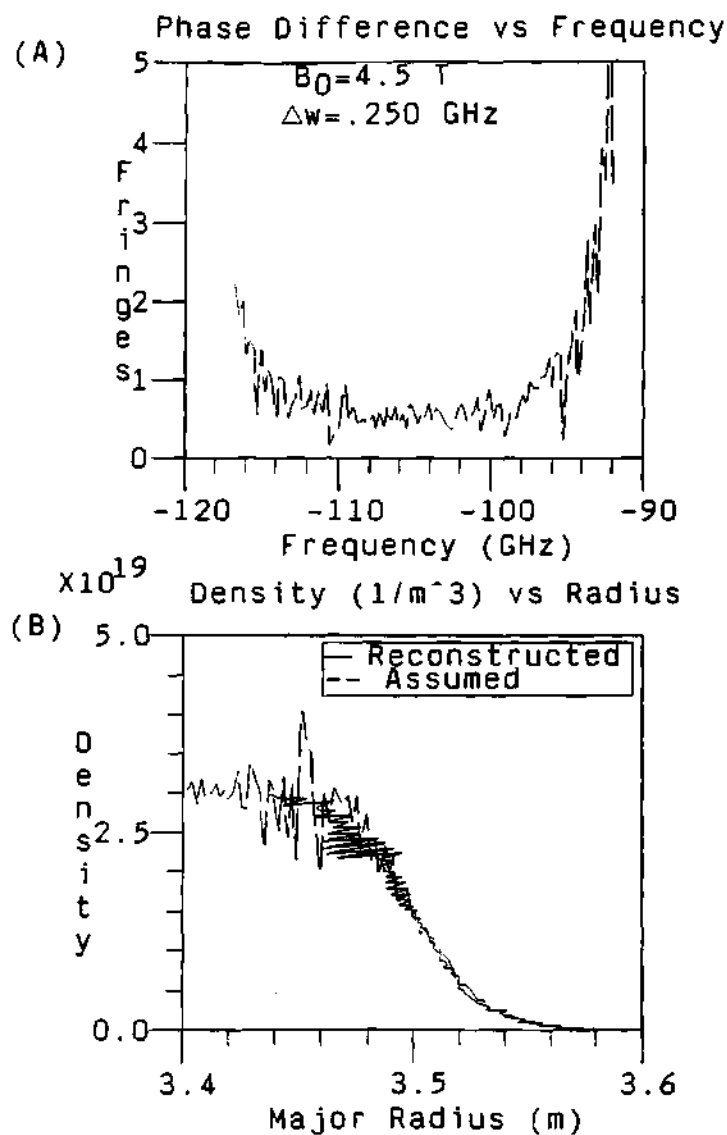


**Figure 6.19:** (A) Plot of the calculated phase difference data for an assumed density profile including density fluctuations ( $\approx 25\%$  rms) with a typical spatial wave-number spectrum. (B) Plot of the assumed and reconstructed density profile for the above phase difference data.



data (by any number of points from 5 to 100 points) in order to reduce the fluctuations and its effects on the reconstructed density. For the modeling, an arbitrary number of data points can be generated, then they can be smoothed by averaging the data points around the center point of the data. Because of the random nature of the fluctuations, this smoothing will allow for a cancelation of the random fluctuations of the data around their central value. Therefore, the smoothed data will have a much smaller fluctuation amplitude as compared with the non-smoothed data. This can be seen in Figure 6.20 where the same data from Figure 6.19 was smoothed over 50 points (details of the smoothing of the real data processes are presented in Section 7.2.2). As expected, the amplitude of the fluctuations was greatly reduced as compared with the data without any smoothing, giving a good match between the assumed and the reconstructed profile.

#### 6.4.6 Frequency range

The first design parameter needed to build the reflectometer was the frequency range necessary to probe some particular part of the plasma. In the case of the TFTR plasma, the radial region of interest was the first 20 to 30 cm of the plasma edge. This first 20 cm of the plasma is of extreme interest to the people in the radio frequency heating group, since this is the area that serves as the interface between the ICRH launching structure and the rest of the plasma. In order to optimize the coupling of the antenna to the plasma and maximize the power deposition, an accurate and detailed knowledge of the plasma edge in front of the antenna structure is necessary. By making a contour plot of the reflection layers for an assumed density profile plasma, the frequency range for the plasma edge can be inferred. This is shown in Figure 6.21 for a plasma with an assumed density profile of the  $\alpha$ - $\beta$  type, with a magnetic field strength of  $B_0 = 4.5$  Tesla ( $I_{tf} = 67$  Kamps) and a maximum density of  $n_0 = 5.0 \times 10^{19} \frac{\text{part}}{\text{m}^3}$  (no relativistic

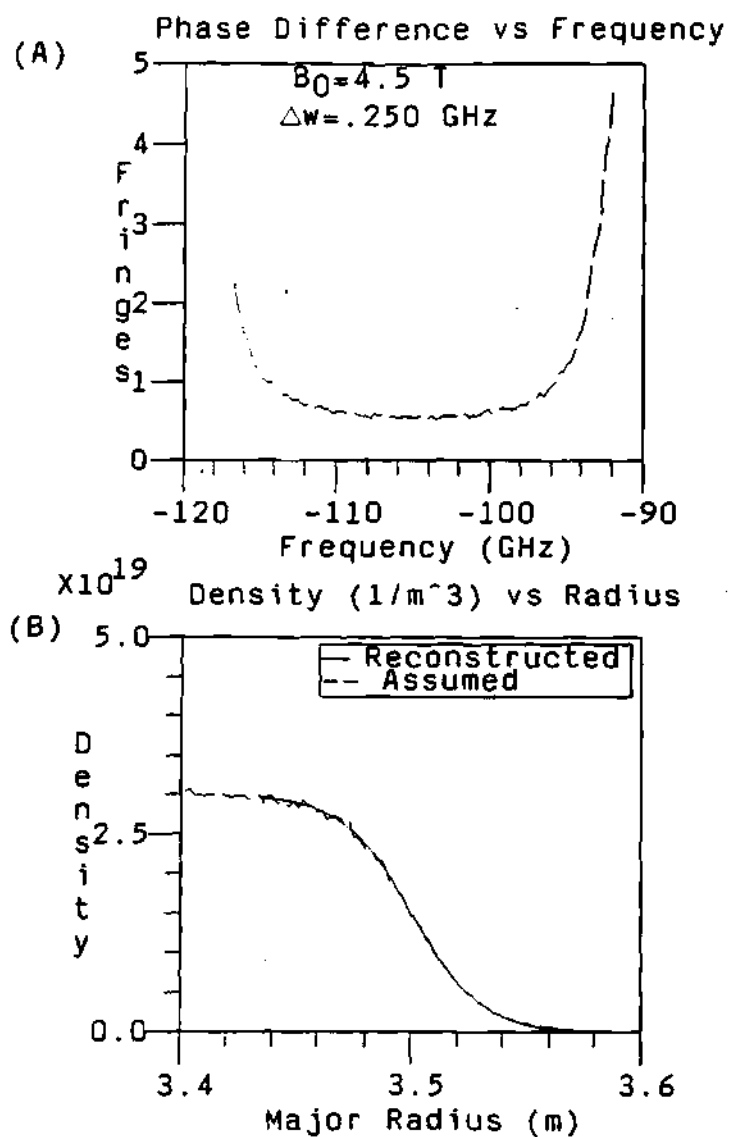


Figure 6.20: (A) Plot of the phase difference data after the smoothing or averaging. (B) Plot of the assumed and reconstructed density profile for the phase difference data after the smoothing.

effects included). This type of density profile is symmetric with respect to the minor radius,  $r$ . A plot of the density for a line in the horizontal midplane of the plasma used to calculate the reflection layers is also shown. The frequency range of 90 to 120 GHz was chosen as a reasonable frequency range for the reflectometer probing beam. For a typical TFTR central magnetic field strength of  $B_0 = 4.5$  Tesla, the cutoff frequency at the plasma edge is equal to the electron cyclotron frequency when the limit as the density goes to zero is taken. Which sets the initial frequency to 90 GHz. The final frequency of 120 GHz was chosen as a reasonable limit to probe the first 20 cm of the plasma edge for the typical TFTR plasma density shown in Figure 6.21.

#### 6.4.7 Analytical limits on the phase difference

There is a way to calculate the analytical limits on the phase difference data for the plasma edge, where the limit of the density and its derivative goes to zero, that is:

$$\lim_{R \rightarrow a} n_e(R) = 0 \quad (6.182)$$

$$\lim_{R \rightarrow a} \frac{dn_e}{dR} = 0 \quad (6.183)$$

as occurs at the plasma edge. The starting point is the equation for the cutoff frequency, equation 2.67, given by:

$$\omega_{X+} = \frac{\omega_{ec}}{2} + \left[ \omega_{pe}^2 + \left( \frac{\omega_{ec}}{2} \right)^2 \right]^{\frac{1}{2}} \quad (6.184)$$

where all the parameters have been defined previously. Next take the derivative with respect to the radial position,  $R$ , to get the equation:

$$\frac{d\omega_{X+}}{dR} = \left( \frac{\omega_{pe}}{\sqrt{\omega_{pe}^2 + \left( \frac{\omega_{ec}}{2} \right)^2}} \right) \frac{d\omega_{pe}}{dR} + \left( \frac{1}{2} + \frac{\frac{\omega_{ec}}{4}}{\sqrt{\omega_{pe}^2 + \left( \frac{\omega_{ec}}{2} \right)^2}} \right) \frac{d\omega_{ec}}{dR} \quad (6.185)$$

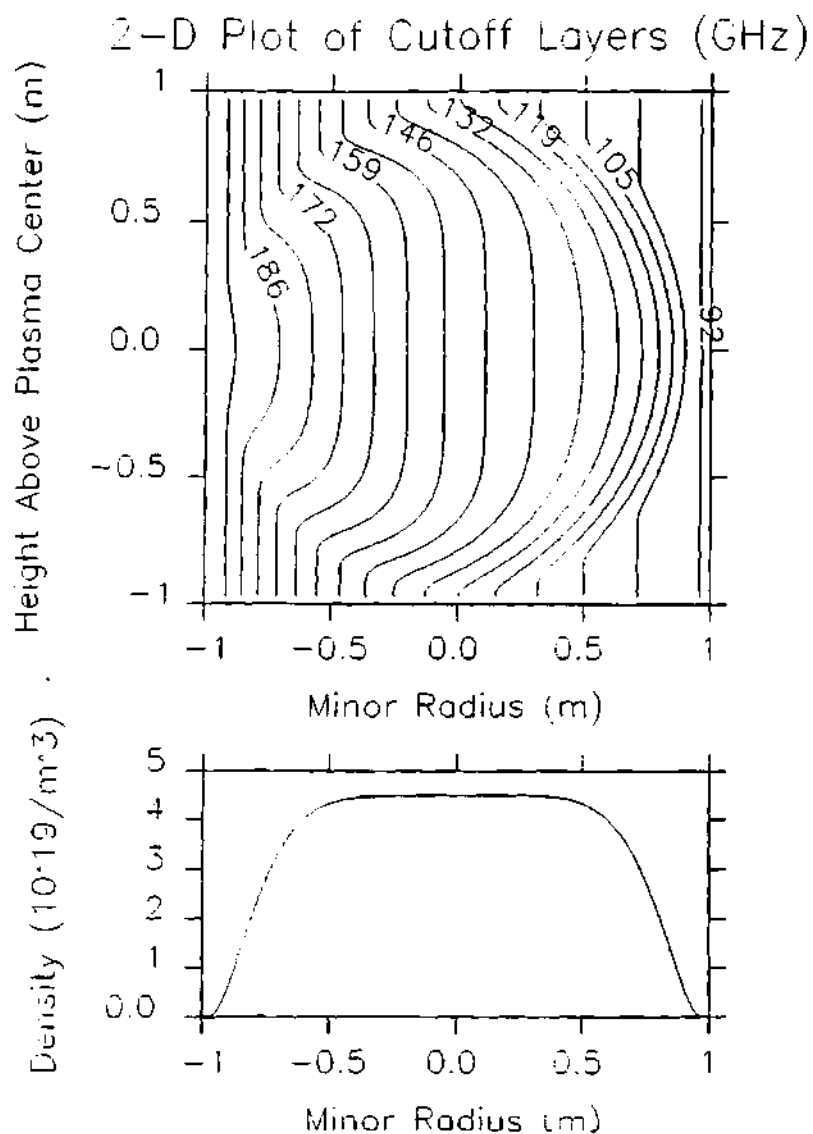


**Figure 6.21:** The upper plot is a contour plot of the cutoff layers for an assumed typical TFTR plasma density profile. The profile assumed is of the  $\alpha$ - $\beta$  type defined previously and with  $B_0 = 4.5$  Tesla. The lower plot shows the assumed density profile at the horizontal midplane.

where all the variables have been defined previously. Now it can be shown that the reflectometer is a truly differential diagnostic. This is done by looking at the ratios of the frequency separation over an average or central frequency of the band:

$$\frac{\Delta\omega}{\omega} = \frac{0.25}{100} = 0.0025 \quad (6.186)$$

and at the ratio of average cutoff separations over the distance to the edge:

$$\frac{\Delta R}{R} = \frac{0.0036}{3.6} = 0.001 \quad (6.187)$$

which are very small values. Therefore, the assumption that:

$$\frac{\Delta\omega}{\Delta R} = \frac{d\omega_{X+}}{dR} \quad (6.188)$$

justified. Thus, substituting equation 6.188 into equation 6.185, an equation for the radial spacing can be obtained as:

$$\Delta R = \frac{\Delta\omega}{\left( \frac{\omega_{pe}}{\sqrt{\omega_{pe}^2 + \left(\frac{\omega_{ec}}{2}\right)^2}} \right) \frac{d\omega_{pe}}{dR} + \left( \frac{1}{2} + \frac{\omega_{ec}}{\sqrt{\omega_{pe}^2 + \left(\frac{\omega_{ec}}{2}\right)^2}} \right) \frac{d\omega_{ec}}{dR}} \quad (6.189)$$

Using this formula for the radial spacing, a formula for the phase difference can be obtained as:

$$\Delta\phi \approx \frac{2\Delta R}{\lambda_{X+}} \quad (6.190)$$

$$\approx \frac{2\Delta R \omega_{X+}}{C} \quad (6.191)$$

$$\approx \frac{2\Delta R}{C} \left( \frac{\omega_{ec}}{2} + \sqrt{\omega_{pe}^2 + \left(\frac{\omega_{ec}}{2}\right)^2} \right) \quad (6.192)$$

which relates the phase difference to the local spacing of the probing beams.

Now, applying the limiting conditions of the plasma edge to the density and the derivative of the density, equations 6.182 and 6.183, to the equation for the cutoff density, equation 6.184, and the equation for the radial spacing of the cutoffs, equation 6.189, will simplify to:

$$\omega_{X+} = \omega_{ec} \quad (6.193)$$

and

$$\Delta R = \frac{\Delta \omega R}{\omega_{ec}} \quad (6.194)$$

which when substituted into the equation for the phase difference, equation 6.192, will yield:

$$\Delta \phi = \frac{2 \Delta \omega R}{C} \quad (6.195)$$

$$= \frac{2 R}{\lambda_m} \quad (6.196)$$

where  $\lambda_m$  is the wavelength of the separation frequency between the probing waves. The value of the phase difference at the edge of the plasma will be the absolute maximum since it is at the edge of the plasma where the gradients of the density and the magnetic field are a minimum, thus, allowing for a maximum separation of the cutoffs. An estimate of this maximum can be obtained by using some typical values of the parameters at the edge, that is:

$$\Delta \phi \approx \frac{2 \times 3.60 \text{ m}}{1.2 \text{ m}} \quad (6.197)$$

$$\approx 6 \quad (6.198)$$

So that the maximum value for the phase difference is 6 fringes. This limit on the phase difference can be seen in Figure 6.22, where the phase difference as the limit of the density going to zero has been plotted. The curves for the phase difference clearly start at a value in the vicinity of 6 fringes, then curve down and start to increase as the slope of the density profile goes flatter.

#### 6.4.8 Effect of the frequency separation

The frequency separation between the probing waves affects two important parameters of the reflectometer. These are: the radial separation of the cutoff positions, and the total dynamic range of the phase difference data. The radial separation of the cutoffs' positions is important for the estimates of the effect of

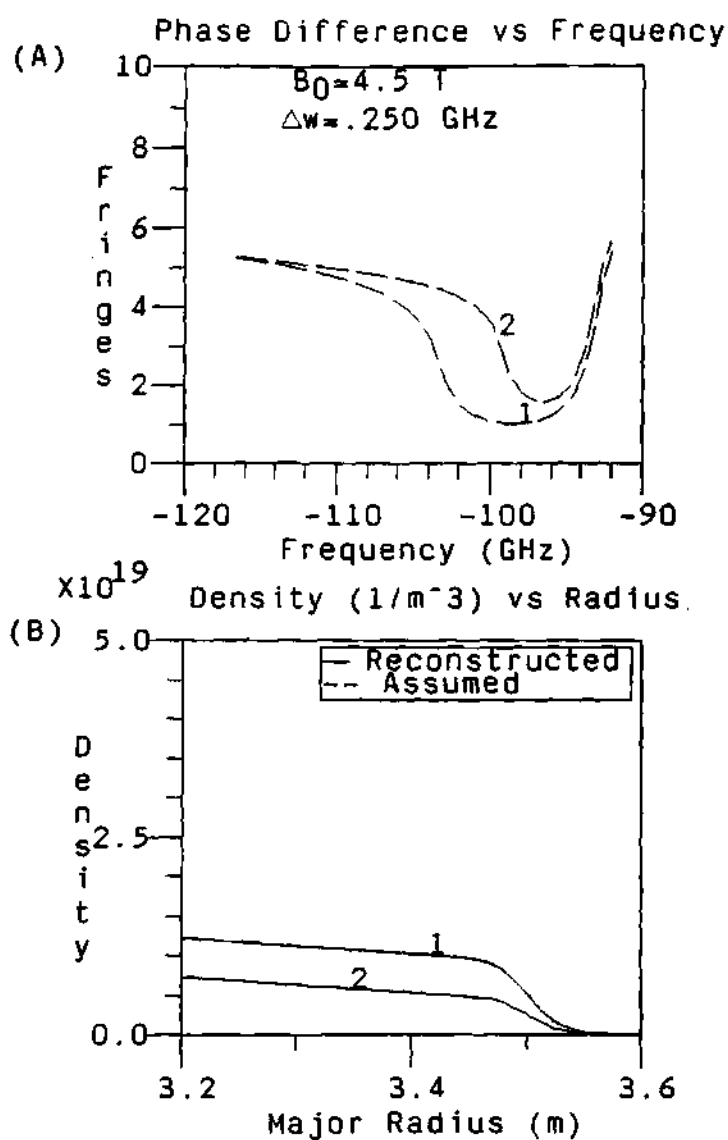


Figure 6.22: Plots showing the limiting value of the phase difference data to be  $\approx 6$  as the density profile goes to 0. (A) Phase difference data calculated from the assumed density profile. (B) Assumed density profile and reconstructed density profile.

coherent or incoherent density fluctuations as discussed previously. That is, the radial separation on the cutoff positions must be smaller than the local density fluctuation correlation length in order to keep the fluctuations on the phase difference below a reasonable level, as discussed in section 2.7.5. The phase difference data is the parameter used to calculate the reconstructed density profile. Because of the multiplicity of fringes and the counting technique used to calculate and track the phase, the limits of the phase difference should be kept to a value of a few fringes. In this way the phase counting is easier and the problems with fringe skipping and multiplicity of fringes are greatly reduced. Fortunately, these are not competing parameters, that is, reducing the frequency separation of the probing waves to improve one parameter will not degrade nor compromise the other. Therefore, reducing the waves' frequency separation helps to reduce both the effect of the density fluctuations on the phase difference data and the dynamic range over which the phase has to be tracked, thus effectively reducing the effect of fringe skips in the phase data.

Figure 6.23 shows the radial spacing and the phase difference data for a typical TFTR plasma (shown in Figure 6.9). For Figure 6.23 the frequency spacing is  $\Delta\omega = 0.25$  GHz, the magnetic field is  $B_0 = 4.5$  Tesla, and the central density is  $n_{e0} = 3.0 \times 10^{19} \frac{\text{part}}{\text{m}^3}$ . This frequency spacing gives a maximum cutoff separation of less than 1 cm, which is below the typical 2-4 cm<sup>110-116</sup> of correlation length for TFTR. For the dynamic range of the phase difference, Figure 6.23 shows a phase difference with a maximum below 5 fringes. To show the effect of reducing the frequency separation on the probing waves, Figure 6.24 shows the same parameters as in Figure 6.23, but with half the frequency separation of Figure 6.23 (i.e.,  $\Delta\omega = 0.125$  GHz). As can be seen, the radial spacing and the phase difference have been reduced to half of their previous values. This is a very important result, and this idea was tested during the phase II of the project, when



the frequency spacing of the probing waves was reduce to  $\Delta\omega = 0.125$  GHz. The data with this new frequency separation showed a strong reduction of the density fluctuations<sup>284,309</sup> and the phase dynamic range was reduce to only 3 fringes of maximum range, making it much easier to track and fringe count the phase. At a later time, in order to reduce the fluctuations more and to reduce the phase dynamic range to the limit of 0 to 2 fringes the frequency separation of the wave was reduce to  $\Delta\omega = 0.080$  GHz.<sup>284,309</sup>

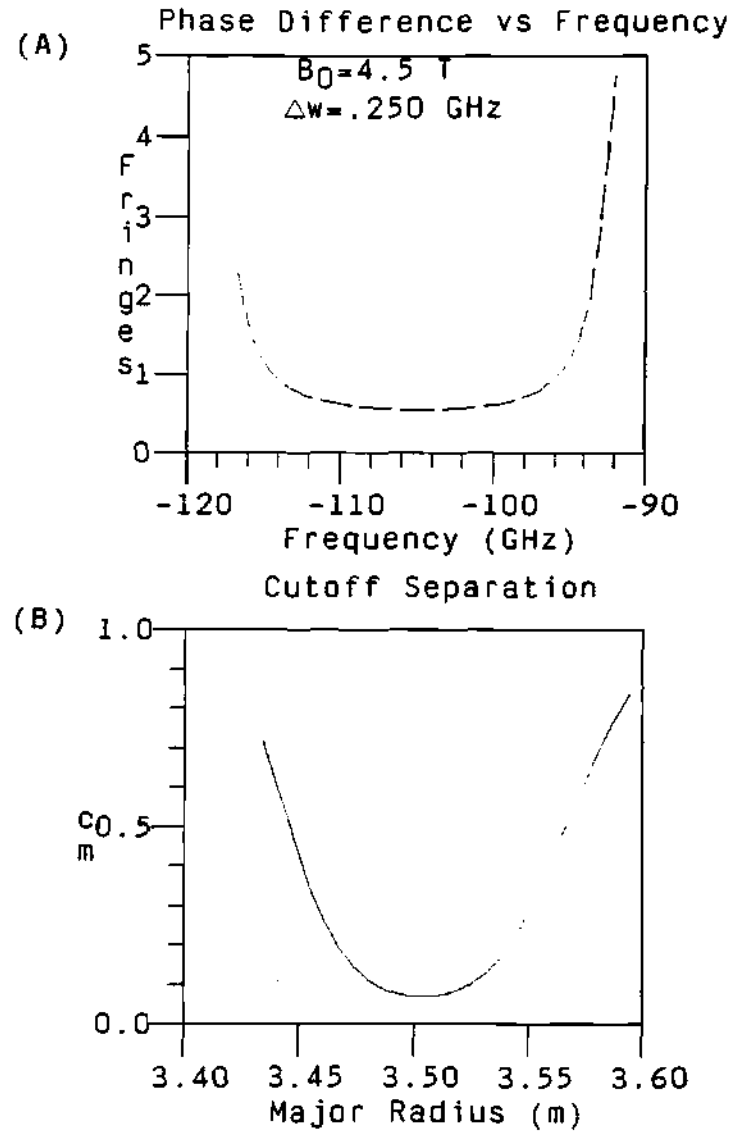
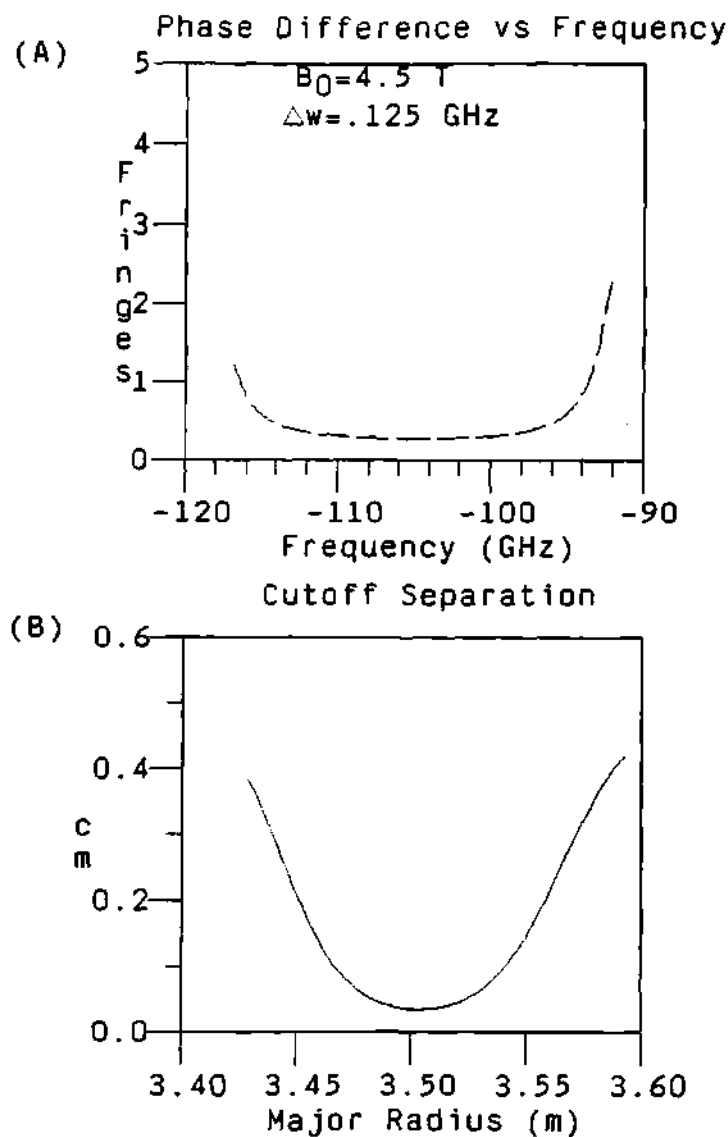


Figure 6.23: Plot of the radial separation of the cutoffs and the phase difference data for a typical TFTR plasma density profile. Frequency separation is  $\Delta\omega = 0.25 \text{ GHz}$ . (A) Plot of the phase difference data dynamic range. (B) Plot of the cutoffs separation as a function of the radial position.



**Figure 6.24: Radial separation of the cutoffs and the phase difference data for a typical TFTR plasma density profile. Frequency separation is  $\Delta\omega = 0.125 \text{ GHz}$ . (A) Plot of the phase difference data. (B) Plot of the cutoff separation as a function of the radial position.**

## 6.5 Sensitivity and Error Analysis

### 6.5.1 Systematic errors in absolute phase calibration

In order to better understand the effect of the calibration phase data and any error in the profile due to it, a study of the effects of different offset functions to the phase difference data was done. The study was done by adding a constant phase offset function or a linear offset function to the real phase difference data. These types of functions seem to be a reasonable approximation of the phase calibration data and the errors introduced by it, as can be seen from the calibration data on Figures 5.6, 5.7 and 5.8 in the chapter on the calibration data. These added offset functions will have the effect of simulating systematic instrumental errors such as the one expected from the calibration phase data of the waveguide run, the instrument calibration phase data, or the uncertainty on the position of the first cutoff. By doing this, a quantitative idea of the error or deviation of the calculated profile to the actual profile can be seen. The functions used were the constant phase offset function, Figure 6.25, and the linear offset function with different slopes, Figures 6.26 and 6.27. From the comparison of these plots it was concluded that the maximum error was obtained when the constant offset function was used, Figure 6.25.

Intuitively, it can be expected that the constant offset function will give the largest error or deviation from the expected reconstructed density profile (Figure 6.25), followed by the linear offset function with the maximum offset error at the lower end of the frequency band (Figure 6.26); the phase data with the linear offset function with the maximum offset error at the high end of the frequency band (Figure 6.27) will be the one with the smallest error or deviation from the expected reconstructed density profile. The intuitive expectations turn out to be true, as can be seen from Figures 6.25, 6.26, and 6.27. The actual expected error

is discussed in sections 5.4 and 5.5 of the corresponding chapter on the calibration.

### 6.5.2 Effect of the magnetic field error

Another source of uncertainty on the reconstructed density profile is the uncertainty of the magnetic field. This is due to the dependence of the index of refraction on both the density and the local magnitude of the magnetic field. Therefore, a change of about 1% can change the position of the cutoff in the plasma and shift the reconstructed density profile. Figure 6.28 shows the effect of a  $\pm 1\%$  change in the magnetic field. Negative changes in the magnetic field will have the effect of moving the reconstructed density profile outward (to the right of plot (B) curve 1), while positive changes in the magnetic field will move the reconstructed profile inward (to the left of plot (B) curve 3).

### 6.5.3 Conclusion on sensitivity/error analysis

From the previous discussions, it can be concluded that the biggest source of error resulting in the biggest discrepancy in the reconstructed profiles comes from the error on the offset of the phase data. This is mainly due to the integral nature of the equations used in the reconstructing process. Therefore, an offset error on the phase difference data will not only increase the uncertainty at the density in its corresponding frequency point, but as the process integrates over this point, the subsequent errors will accumulate and increase the uncertainty and deviation of the reconstructed profiles from the assumed and expected profile. A constant phase error of only  $\pm 0.25$  fringes can produce an error of more than 100% on the reconstructed density profile depending on the edge density gradient of the plasma.

From the examples with sinusoidal and random fluctuations it can be con-

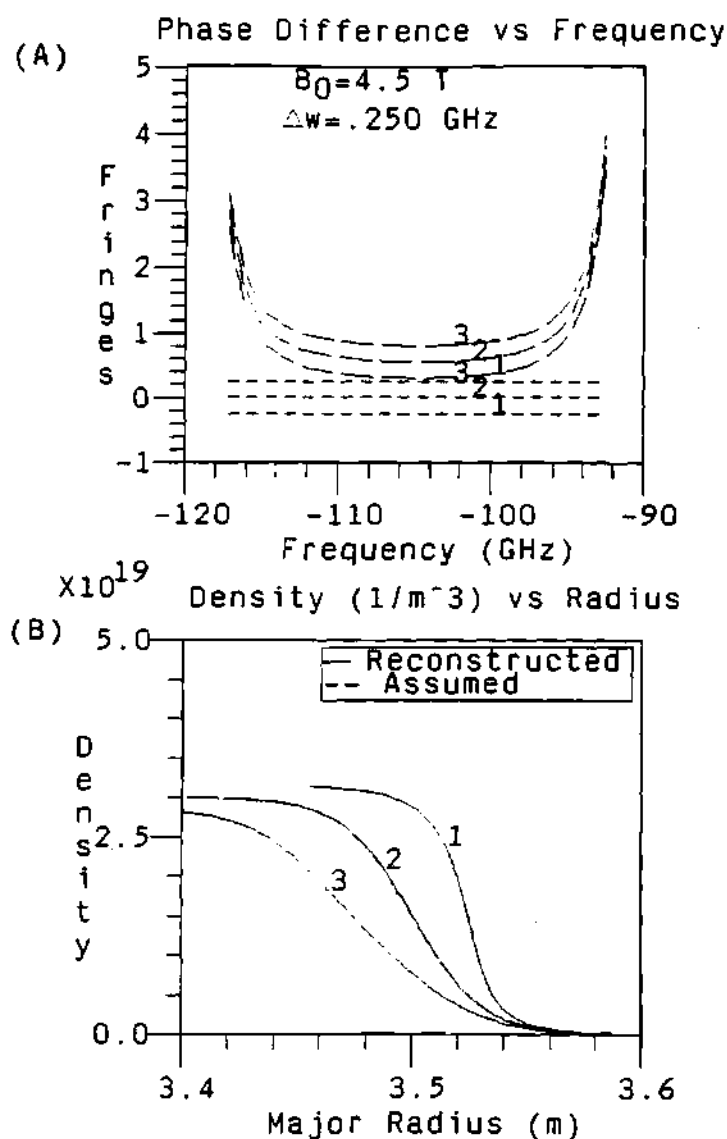
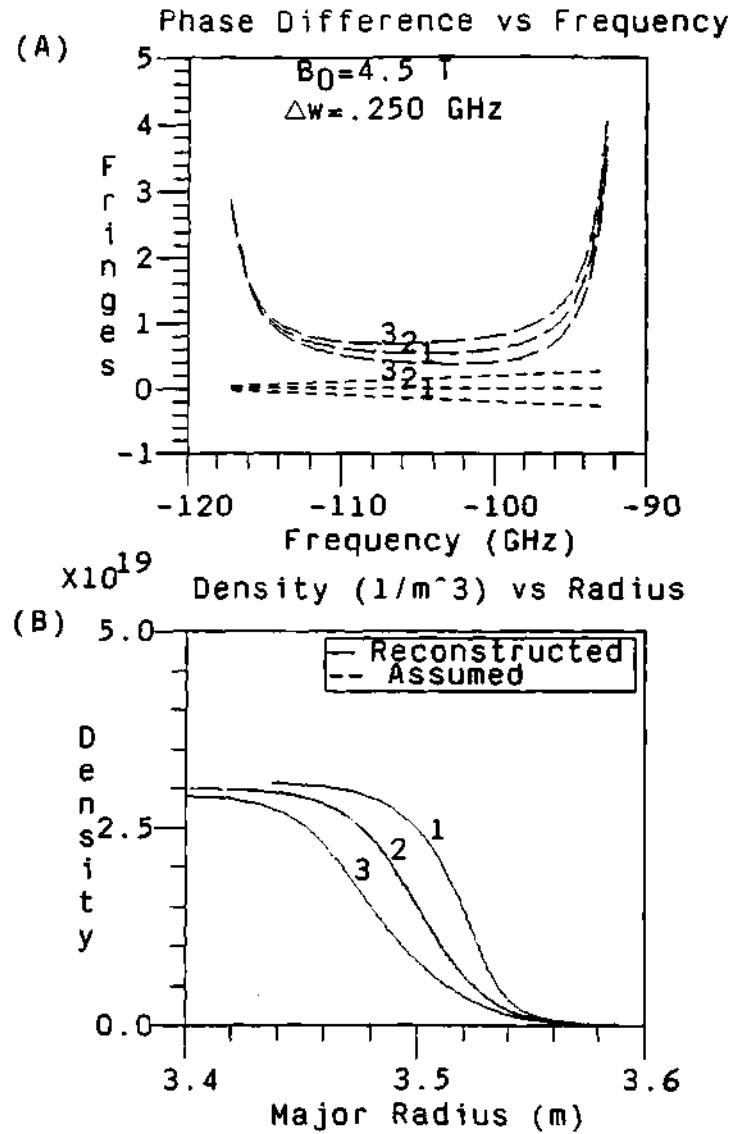


Figure 6.25: Effect of the constant offset function ( $-0.25$ ,  $0$ ,  $+0.25$ ) on the reconstructed density profile. The important feature here is that as the phase offset decreases the profile becomes steeper and as the phase offset increases the profile becomes flatter. (A) Plot of the phase difference data and the associated phase offset added to the phase data. (B) Plot of the assumed density profile and the reconstructed density profile using the phase data above.



**Figure 6.26: Effect of the slope of the offset function (with intersection at 120 GHz) on the reconstructed density profile. (A) Plot of the family of curves for the phase difference and the associated offset functions. (B) Plot of the assumed density profile and the reconstructed density profile for the corresponding phase difference data in plot (A).**

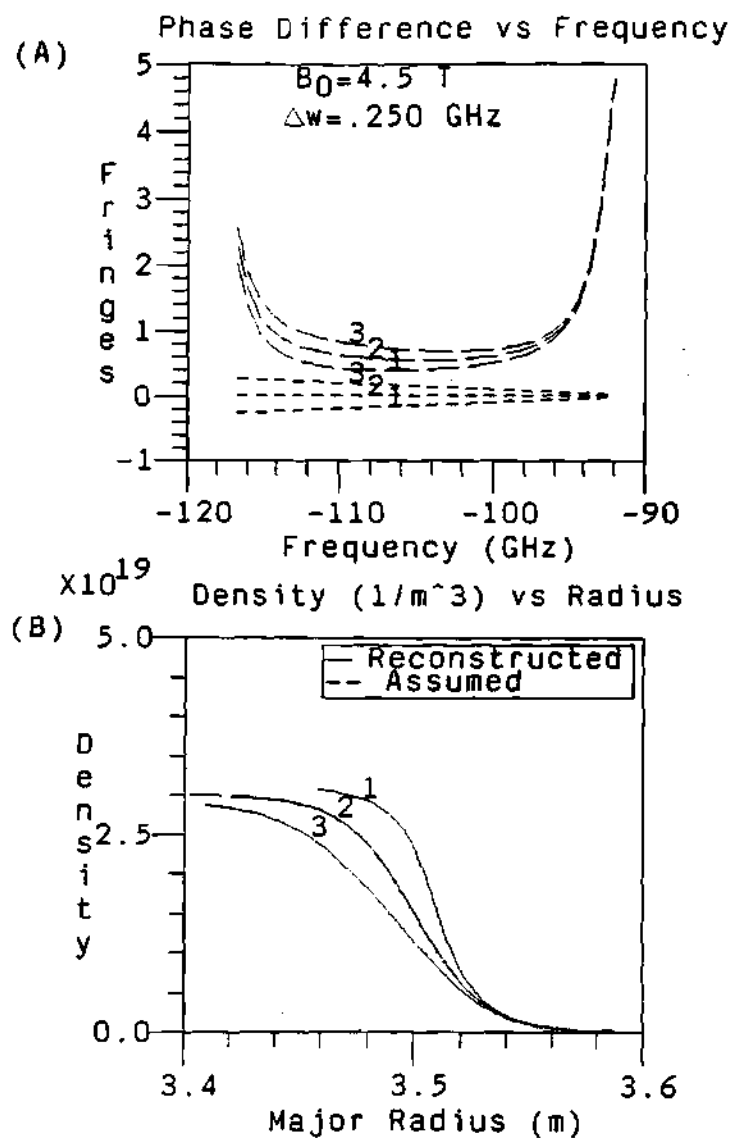


Figure 6.27: Effect of the slope of the offset function (with intersection at 90 GHz) on the reconstructed density profile. (A) Plot of the family of curves for the phase difference data and their corresponding offset functions. (B) Plot of the assumed density profile and the reconstructed density profile for the associated phase difference data.



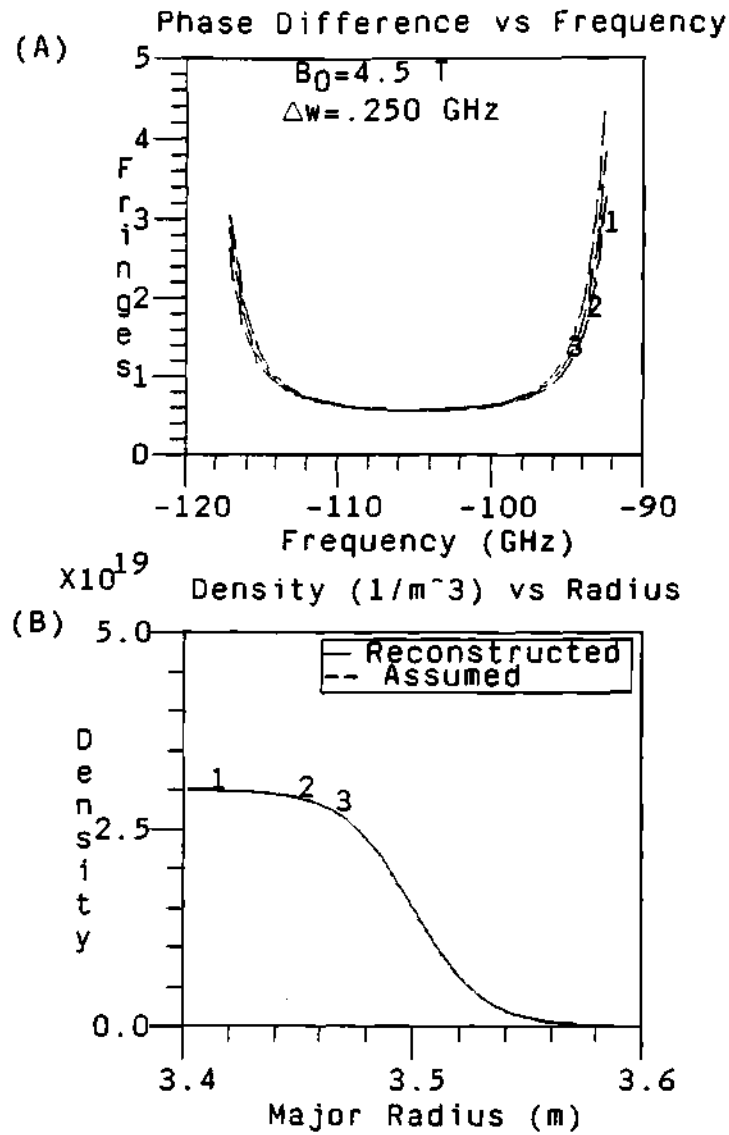


Figure 6.28: Effect of the uncertainty of the magnetic field on the reconstructed density profile. (A) Plot of the phase difference curves calculated with an error on the magnetic field of -1%, 0%, and 1% (corresponding to curves 1, 2, and 3 respectively). (B) Plot of the assumed density profile and the reconstructed density profile for the phase difference data calculated with the error on the magnetic field.

cluded that the reconstruction technique can reproduce the average original density profile for fluctuation errors on the phase difference data that average well to zero as in the case of the sinusoidal and random fluctuations.

## **6.6 Benchmarking: Comparison With Hanson's Code**

A comparison between another profile reconstruction code and the code and techniques developed by the author was performed to benchmark the code. This comparison was done using a similar code written by G. R. Hanson (one of the members of the reflectometer research team) using the Interactive Data Language (IDL) programming language. Hanson provided data files containing the phase difference data vs frequency and the corresponding density profile vs radius, with all of the other necessary parameters. Figure 6.29 shows a plot of the calculated density profile and the density profile from Hanson's code. It can be seen that they match so well that it is difficult to distinguish between the two curves. To have a quantitative calculation of the differences between both curves, the difference between curves is plotted along the radial axis of the plot. It can be seen that the difference on the density (shown by the x-axis) is very close to zero. This differences can be due to small differences in the implementation of the reconstruction technique, differences on the method used to calculate the related integrals, different choice on the position of the first cutoff, different model for the scrape-off layer (linear or exponential), or differences in the model for the magnetic field calculation. These differences will be discussed in the following sections.

### **6.6.1 Differences on the reconstruction technique**

There are several differences in the reconstructing techniques used by the author's program and Hanson's program. The most important is that Hanson's

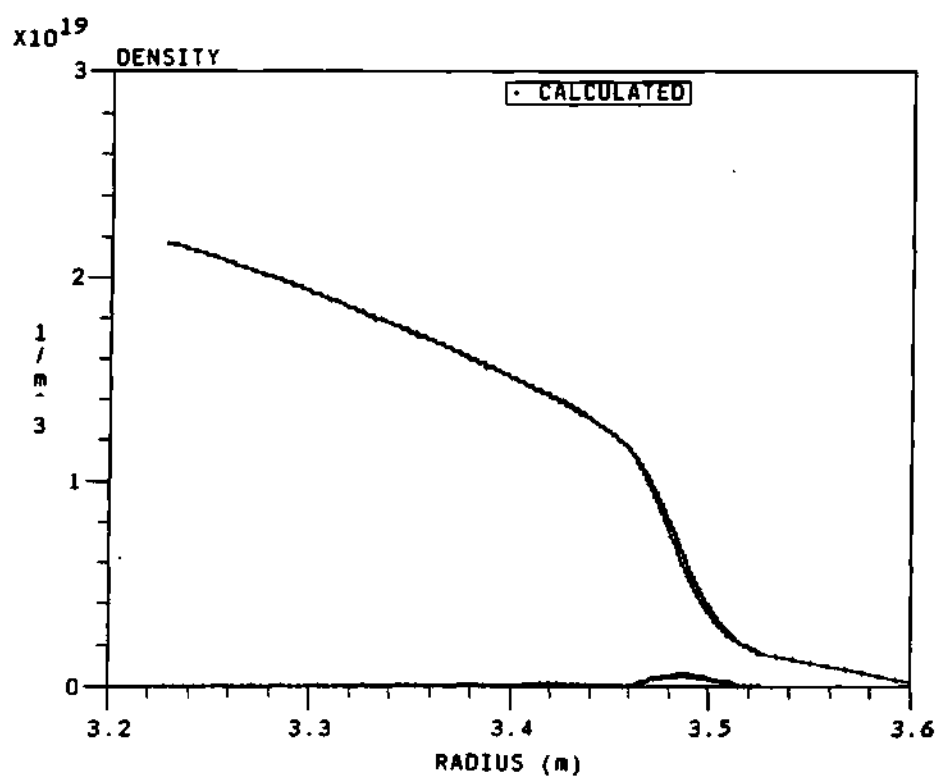


**Figure 6.29:** Plot of the difference between the calculated density profile from author's program and the one provided by Hanson. The two curves seem to blend together. The difference between the density points is shown by the x-axis.

program uses a first degree polynomial fit (i.e., linear fit or trapezoidal fit) to calculate the increment on the position of the cutoff,  $\Delta r$ . It actually uses a correction factor in the calculation of the  $\Delta r$  to try to compensate for the missing area of the integral between the index of refraction curve and the line approximation of Doyle's method. To show this with the formulas for the reconstruction technique, the formula used to calculate the increment on the cutoff radial position is given by equation 6.19 as:

$$\Delta r_{Doyle}(\omega_{j+1}) = \frac{\Delta\phi - 2\frac{\omega_{j+1}}{c} \int_{r_c(\omega_j)}^{r_0} n(r, \omega_{j+1}) dr + 2\frac{\omega_j}{c} \int_{r_c(\omega_j)}^{r_0} n(r, \omega_j) dr}{\frac{\omega_{j+1}}{c} n(r_c(\omega_j), \omega_{j+1})} \quad (6.199)$$

where all the variables have been defined previously. Hanson's correction for Doyle's approximation is given by:

$$\Delta r_G = C_{Hanson} \Delta r_{Doyle} \quad (6.200)$$

where  $\Delta r_{Greg}$  is the new increment with the correction added to it,  $C_{Hanson}$  is Hanson's correction factor generally  $\approx 1.06$ , and  $\Delta r_{Doyle}$  is Doyle's original formula for the increment on the radial position of the cutoff. It is important to notice that Hanson's correction is only 6% away from the answer calculated by Doyle, and in terms of its effect to the radial increment in units of centimeters this is a very small correction. This correction factor can be tuned to some particular type of profile to guarantee convergence of the algorithm and minimize the error of the reconstructed density profile.

### 6.6.2 Differences in integration techniques

Another important difference is the method used to calculate the integrals associated with the calculation of the phase from the index of refraction, that is, equations such as:

$$\phi(\omega_j) = 2\frac{\omega_j}{c} \int_{r_c(\omega_j)}^{r_0} n(r, \omega_j) dr - \frac{\pi}{2} \quad (6.201)$$

used to calculate the phase from the index of refraction. The author's program uses a 3<sup>rd</sup> degree polynomial (described in section 6.3) to calculate all of the integral quantities in the program. This provides errors of the order of  $\propto h^5 \frac{d^4 n}{dr^4}$  for the numerical integrations. Hanson's code uses a trapezoidal rule method with a much different error term.

### **6.6.3 Effect of the choice of the cutoff**

The position of the cutoff for the first frequency can produce shifts of the density profile as explained previously in section 6.4.3. Shifting of the position of the first cutoff will produce a corresponding shift of the density profile. This type of difference is easily eliminated by choosing the same value for the radial position of the first cutoff.

### **6.6.4 Density model before the first cutoff**

The reflectometer can not measure or collect data from the area of the plasma density before the first cutoff position. This area is spatially large for low magnetic field operation and for small size plasmas. For these cases the density profile between the reference plane and the position of the first cutoff must be modeled. The two most common models are the linear density profile and the exponential density profile. The model used by Hanson is the exponential profile, while the model used by the author can be either, with preference for the linear profile. This modeling of the density before the first cutoff appears to be responsible for most of the differences between the codes. This can be seen in Figure 6.30 where the plot of the density for both techniques is shown. The assumed density profile for the density between the reference plane and the first cutoff is the exponential profile. The position of the first cutoff is the same for both density profiles. The difference is mainly at the steep part of the profile, but the general shape of

the reconstructed density profile is the same. The difference can be reduced by shifting the position of the first cutoff (which will shift the entire profile) to make a better match at the steep region of the density profile. This is shown in Figure 6.31 where the position for the first cutoff has been moved 0.5 cm to the right. The corresponding error in the steep part of the profile is greatly reduced because of the match between profiles due to the shift of the position of the first cutoff.

### 6.6.5 Magnetic field model

Another source of differences between the author's code and Hanson's code results is the choice for the model of the magnetic field. This source of error was eliminated by having both codes use the same model to calculate the magnetic field for the reconstruction of the density profile. This model for the magnetic field takes into account the ripple in the magnetic field at the position of the reflectometer launcher and the poloidal field due to the plasma current.

## 6.7 Benchmarking: Comparison Using the $B_0 = 0$ Case

In order to obtain another comparison or test of the reconstruction technique developed for the phase difference reflectometer, the case for  $B_0 = 0$  was considered. Under this condition the index of refraction of the X-mode, given by:

$$n_X^2 = 1 - \frac{\omega_{pe}^2}{\omega^2} \frac{\omega^2 - \omega_{pe}^2}{\omega^2 - \omega_{pe}^2 - \omega_{ec}^2} \quad (6.202)$$

and the index of refraction of the O-mode, given by:

$$n_O^2 = 1 - \frac{\omega_{pe}^2}{\omega^2} \quad (6.203)$$

become the same. This can be seen from equation 6.202 when the condition for  $B_0 = 0$  is used in the electron cyclotron frequency to give  $\omega_{ec} = 0$  and then the

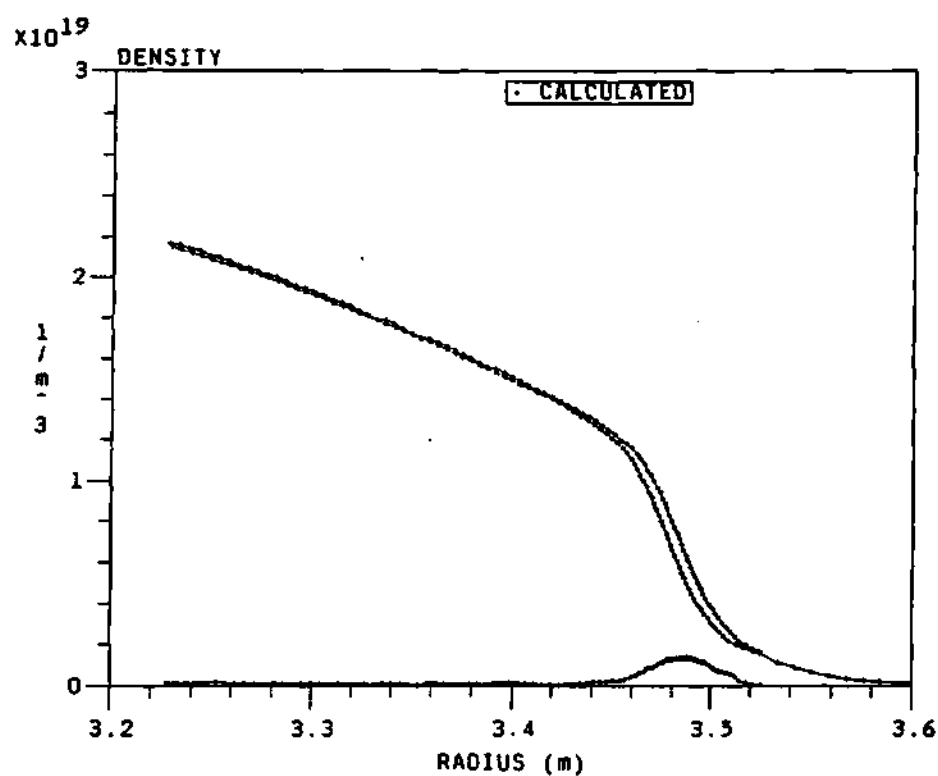
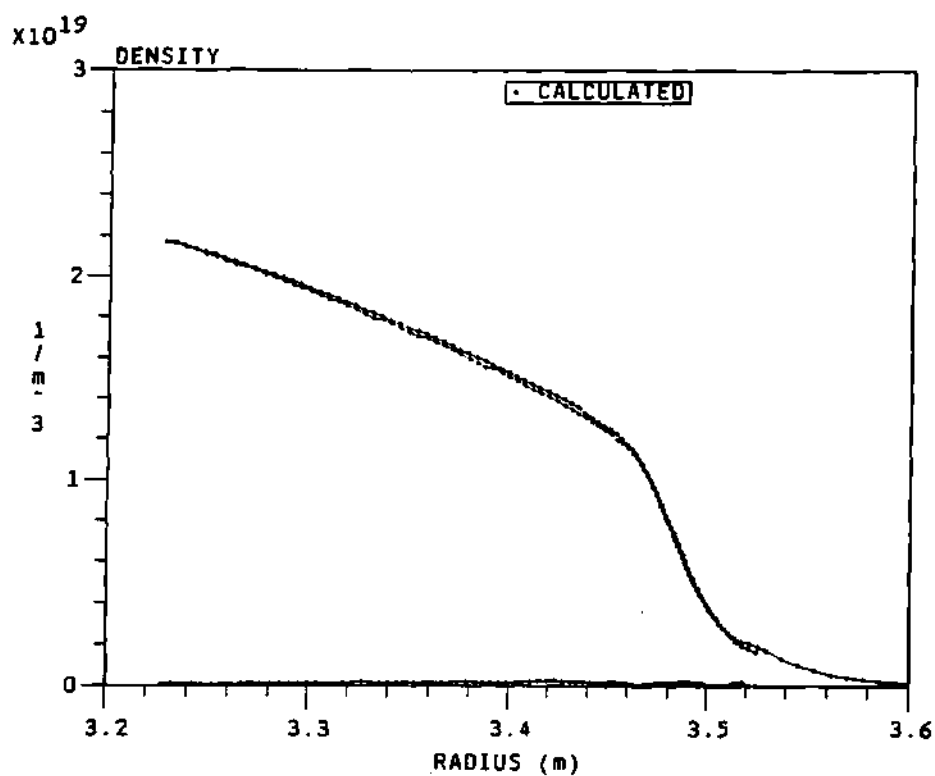


Figure 6.30: Plot of the density profiles for the author's technique and Hanson's technique. The error is shown in the lower curve by the x-axis. The exponential model is used by both codes in this plot.



**Figure 6.31:** Plot of the density profiles for the author's technique and Hanson's technique using an exponential profile for the edge. A shift of the position of the first cutoff in the author's profile provides a much better fit at the steep part of the profile as compared with the previous plot.



second fraction on equation 6.202 becomes unity, that is:

$$\frac{\omega^2 - \omega_{pe}^2}{\omega^2 - \omega_{pe}^2 - \omega_{ec}^2} = 1. \quad (6.204)$$

Using  $B_0 = 0$  is a very simple test of the program and reconstruction technique for the program, since all that is necessary is to set the magnetic field to zero in the code. A typical code calculation with  $B_0 = 0$  can be seen in Figure 6.32 for a plasma with a central density of  $n_{e0} = 4.0 \times 10^{19} \frac{\text{part}}{\text{m}^3}$ . Notice that the phase difference data is much smaller at the steep part of the profile than for the X-mode and the shape of the phase difference data is different. From the plots the small frequency range advantage of the X-mode (92 to 117 GHz) can be compared with the that of the O-mode (10 to 60 GHz). The match between the assumed density profile and the reconstructed density profile is similar to the one seen for the X-mode and what is more important the shape of the reconstructed density profile is the same as the one of the assumed density profile, just as was observed with the X-mode of propagation.

Given that the O-mode of propagation is obtained when the magnetic field is set to zero, then the phase data for this type of plasma can be used to obtain the density profile using the *Abel* inversion technique discussed in section 2.6.1, equation 2.168. This is shown in Figure 6.33 for the same plasma as Figure 6.32, but enlarged to see the details of the three profiles. From the figure it is clear that aside from a very small displacement on the radial position, the curves are very similar to each other. As usual with this type of reconstructed profile, the shape of the profile is the same as the assumed density profile used for the calculation of the phase data.

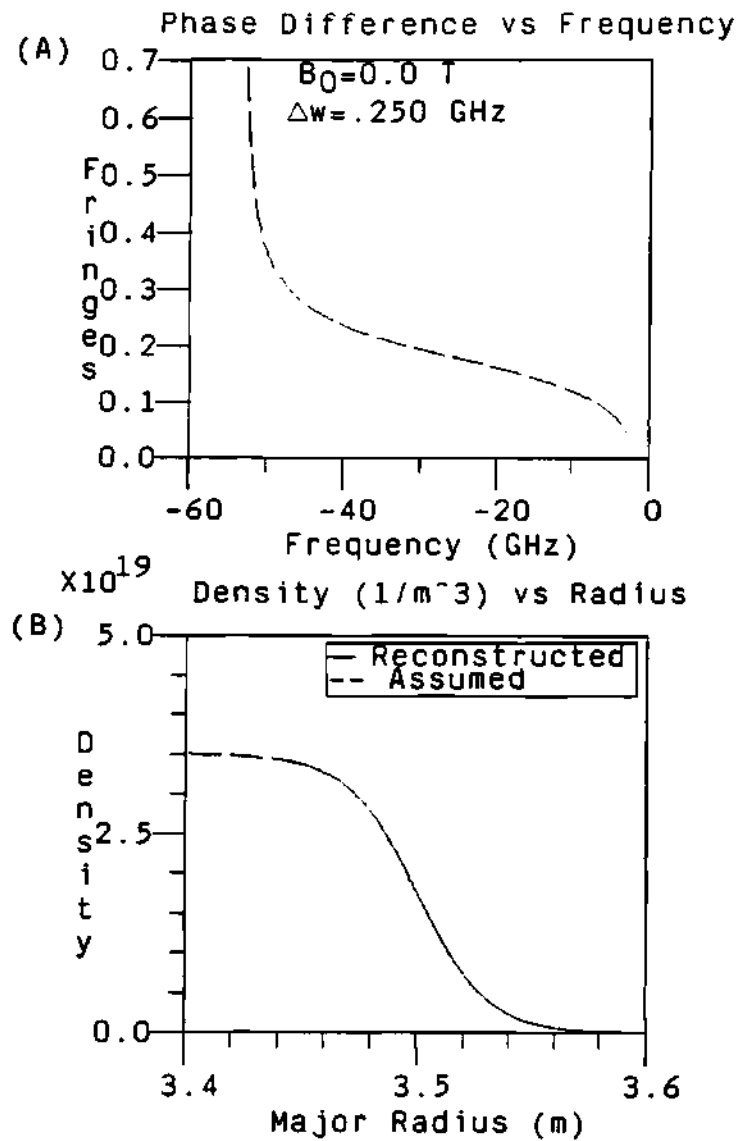


**Figure 6.32:** Plots of (A) the phase difference data and (B) the assumed and reconstructed density profiles for the case of  $B_0 = 0$ .

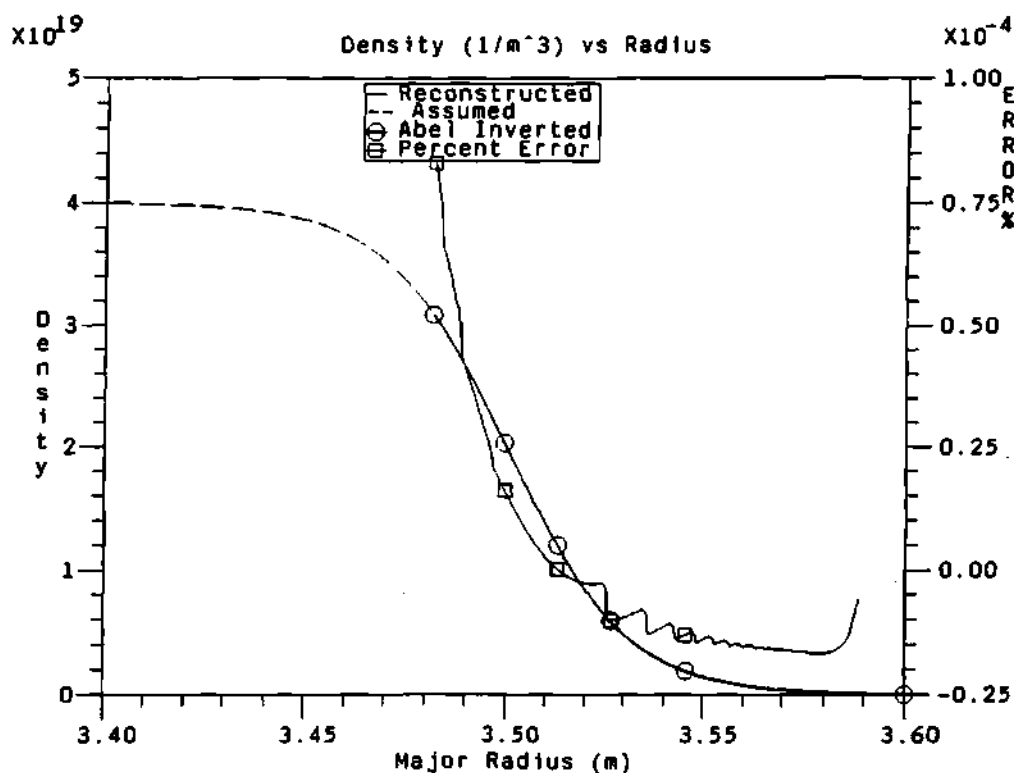


**Figure 6.33:** Plot of the Abel inversion density profile using the phase data from the previous figure, the reconstructed profile using the author's technique, and the assumed profile for comparison and verification. The match between curves makes it difficult to distinguish between them. The percent error is the difference between the reconstructed and Abel inverted profiles.

## 6.8 Summary

This chapter discussed the simulation program used to model the propagation of the probing beam through the plasma, and it tested the reconstruction technique used to calculate the reconstructed density profile. The results obtained from the simulation program are:

1. The phase difference data dynamic range. This is among the most important results since it shows a significant reduction on the fringe count and the phase dynamic range can be obtained using this new technique of phase difference, as compared with other more conventional full phase reflectometer systems.
2. The radial separation between the cutoffs of the two frequencies of the probing beam. This provides an average and typical separation that was used to show and assure that the radial separation between the two cutoffs of the probing waves was smaller than the correlation length of the density fluctuations, therefore effectively reducing the phase fluctuations of the phase difference data.
3. A sensitivity analysis of the reconstruction techniques was presented, together with a discussion of the possible error sources and their effect to the reconstructed profile. It was shown that the largest change on the reconstructed profile can be obtained from a constant shift of the phase difference data, like the one obtained from a constant offset calibration error. The effect of sinusoidal fluctuations and random fluctuations on the reconstructed technique was discussed.
4. The effect of fluctuations on the phase data and on the reconstruction technique studied and presented. From these simulations it was shown that the phase fluctuations due to density fluctuations can be averaged out by the

reconstruction process. This is due to the averaging and smoothing over multiple data sets. Therefore, independent of the noise fluctuations on the phase data, the reconstruction technique was able to follow the main envelope of the assumed density profile, making it resistant to phase fluctuations.

5. The effect of changes on the main density profile shape (such as central density, edge position, profile shape, edge slope, fluctuation level, etc ...) were studied. It was concluded that the local density slope was the key factor in the determination of the phase difference data as expected, and the edge position could add a constant offset phase to the phase difference data.
6. Simulations with different frequency spacings for the probing beams showed that the phase difference data dynamic range and the cutoff radial separation were scaling proportional to the separation frequency of the probing beam. This was especially useful for the second phase of the reflectometer when it was decided to reduce the frequency separation by half in order to reduce the phase difference data dynamic range by half, so that the fringe tracking of the phase could be done in an almost unique way.
7. An idea of the general shape of the phase difference data could be observed from the phase data of the simulation program for a particular density profile shape. This was especially useful when tracking the phase through multi-fringe skips at the edge or where the amplitude of the signal was low, so that false fringe skips could be corrected or discarded.
8. It was shown that both the trapezoidal method (Doyle's) and the parabolic method (or any polynomial expansion of the index of refraction) have inherent errors that are a constant % error in the step size, in the limit of small step size. Furthermore, it was shown that in the limit of small step

size, Doyle's method overestimates the step size by  $\approx 25\%$  and the parabolic method similarly by an error of  $\approx 17\%$ .

9. A density expansion method which achieves round-off limited error accuracy was developed. The main reason for developing this new accurate method was the error in the polynomial fits due to the infinite slope of the real index of refraction at the cutoff described previously. This new method uses a polynomial fit to the density near the cutoff and fits a function that is equal to the real index of refraction near the cutoff, with the density estimated by the parabolic expansion.

Benchmarking of the reconstruction technique developed by the author with other methods was discussed. These include a comparison with G. R. Hanson's code, and a comparison with the O-mode as the magnetic field goes to zero. The resultant density profiles for each case are plotted together with the assumed density profile and compared for the match. In general the difference between the assumed and reconstructed density profiles was very small and within the errors and differences of the codes and techniques used.

From all of this it can be concluded that the simulation program provided great insight into the design and limitations of the dual frequency phase difference reflectometer, and served as a vital tool for the differential reflectometer design. It also pointed out significant and unexpected errors when using Doyle's method or any polynomial approximation for the index of refraction. These errors are due to the infinite slope of the index of refraction at the cutoff. An accurate method based on expanding the density as a polynomial, rather than the index of refraction, was developed.

## CHAPTER VII

### DATA ANALYSIS SOFTWARE

#### 7.1 Introduction

The phase simulation program (discussed in the previous chapter) served as a model for the reflectometer. That is, given a density defined profile, the modeling program will calculate the phase difference data the reflectometer probing beam would produce, and from that phase difference data the density profile could be reconstructed and compared to the original density profile. This would provide an excellent tool for modeling the reflectometer. This chapter will present the program and methods developed to analyze and reduce the actual reflectometer data. This includes the calculation of the final phase data, and the reconstruction of the density profile from the phase data. Table 7.1 shows a simplified description of the input, output, graphics and operations performed by the data analysis and density reconstruction software, and Figure 7.1 shows the flow chart of the data analysis program. The two processes of phase extraction from the data and reconstruction of the density profile have been separated to keep the individual programs and supporting activities as simple as possible. That is, a program was written to read the reflectometer's raw data files, to calculate the phase data, and finally to write it to a data file for the reconstructing density program; and a separate program was written to read this phase data file and calculate the reconstructed density profile from it. This phase data file is the main input for the reconstruction program.

**Table 7.1: A short description of the data analysis and reconstruction programs.**

Program	Input	Operations	Output	Graphics
Data Analysis	General data	Read data to arrays		
	Digitizer data	Convert data to voltages		Ramp voltage
	Reflectometer data			$I$ & $Q$ signals
				Amplitude
		Smooth data		
		Average data		
		Truncate/Compress		
		Calculate $(\omega, \Delta\phi)$		$(\omega, \Delta\phi)$
		Fringe count $\Delta\phi$		$(\omega, \Delta\phi)$
		Calibrate $\Delta\phi$		
Density Calculation	General data	Write $(\omega, \Delta\phi)$ to file	$(\omega, \Delta\phi)$	
	$(\omega, \Delta\phi)$ data	Read $(\omega, \Delta\phi)$ data		$(\omega, \Delta\phi)$
		Calculate phase to 1 <sup>st</sup> cutoff		
		Calculate $\Delta r_j$		
		Calculate $R_{j+1}$		
		Calculate $n_e$ at $R_{j+1}$		
		Write $(R_j, n_e)$ to file	$(R_j, n_e)$	$(R_j, n_e)$



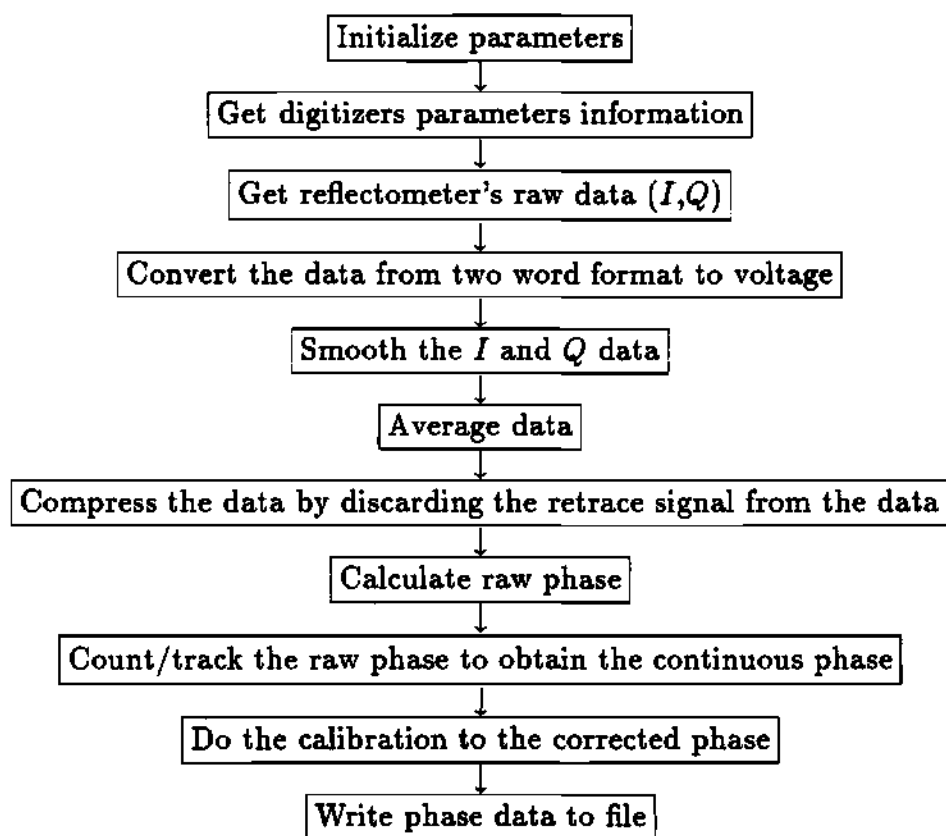


Figure 7.1: Flow chart of the analysis and phase extraction program.

## 7.2 Data Reduction and Phase Extraction

This section will describe the program and methods used for the analysis and extraction of the phase data.

### 7.2.1 Data description

The reflectometer's diagnostic data is contained in two types of file: the parameters file and the Raw Data file. The parameters file contains the settings of the digitizers for a specific plasma shot. The reflectometer's Raw Data files contain the data collected from the reflectometer output ports by the digitizer for a specific shot. These include the  $I$  ( $= \sin \Delta\phi$ ) and  $Q$  ( $= \cos \Delta\phi$ ) voltage signals from the super heterodyne detection system and the sweep voltage of the source sweeper. The  $I$  ( $= \sin \Delta\phi$ ) and  $Q$  ( $= \cos \Delta\phi$ ) signals are used to calculate what is called the *raw phase*, which is the discontinuous phase, before any fringe skips are tracked or counted. This calculation of the raw phase is done by using the simple formula:

$$\Delta\phi = \arctan\left(\frac{I}{Q}\right) \quad (7.1)$$

where  $\Delta\phi$  is the phase difference and  $I$  and  $Q$  have been defined before. The data from the sweep voltage is used to calculate the associated frequency for the corresponding raw phase data points. Assuming a linear sweep voltage, the frequency is calculated as:

$$\omega = m_s x_{sv} + b \quad (7.2)$$

where  $m_s$  is the slope of the sweep (Volts per Hertz),  $x_{sv}$  is the sweep voltage, and  $b$  is the offset or initial frequency of the sweep. This allows organization of the data in the form of an ordered pair  $(\omega, \Delta\phi)$  that it is stored in a file for further processing by the density reconstruction program.

### 7.2.2 Processing the data

A series of operations are performed on the raw data in order to get usable phase difference data. These may include (in order) smoothing, averaging, and truncation of the data, depending on the quality of the data and the type of plasma under study. The smoothing and averaging will have the effect of reducing the fluctuations on the data by the square root of the number of data points used, as expected for random fluctuations and explained by Bevington.<sup>66,67</sup>

The first of these operations is *Smoothing* of the  $I = \sin \Delta\phi$  and  $Q = \cos \Delta\phi$  signals. Smoothing is accomplished by using what is known as the running carriage integral method<sup>309,310</sup> on the data. The equation for this operator has the general form:<sup>310</sup>

$$F(x) = \frac{\int_{x-l}^{x+l} W(y-x) f(y) dy}{\int_{-l}^l W(z) dz} \quad (7.3)$$

where  $l$  is a length representing the width of the smoothing,  $W(y)$  is the weighting function for the smoothing and  $f(y)$  is the function to be smoothed. The factor in the denominator is the normalization constant that accompanies these types of operators. In order to reduce the introduction of other harmonics due to discontinuities of the weighting function during the smoothing process, a Gaussian weighing function was chosen for the smoothing.<sup>308-310</sup> This smoothing is done as a function of the frequency. This equation can be converted to its equivalent in the discrete space of the reflectometer's data sets. For this case the equation used is:<sup>308-310</sup>

$$S_i = \sum_{j=-s}^s \frac{1}{w\sqrt{\pi}} e^{-(\frac{j}{w})^2} D_{i+j} \quad (7.4)$$

where  $D_i$  is the data array to be smoothed,  $S_i$  is the data array after smoothing,  $s$  is the number of elements to smooth by, and the value for  $w$  is given by:

$$w = \frac{s}{\sqrt{\ln(10)}} \quad (7.5)$$

which represents the width of the Gaussian function necessary to have a value of  $\frac{1}{10}$  for the Gaussian at the end points of the summation. This is a way to remove high frequency noise and perturbations on the data by averaging every data point with respect to a number of its neighboring points; as long as the information has a wavelength that is larger than the wavelength of the smoothing, there will be no lost information (this is obviously used to eliminate high frequency noise and random fluctuation noise from the data).

Second is the averaging of the data which can be done in terms of both the frequency and/or the sweep number. The averaging of the data as a function of the frequency is done by averaging the data around one frequency point and using this new averaged data point as the new data, dropping all the points used for the averaging. The averaging over the sweep number is done by taking a set of sweeps and averaging these sweeps into one data set/sweep. Averaging is done in order to reduce the number of data points, to reduce the noise level in the data, and the running time of the reconstructing program. This reduces random and extraneous noise on the data without loss of information, since the digitizers run at a rate much greater than the required time resolution. A step function was used to do the averaging, using anything between 2 to 20 points of averaging.

Truncation of the data is accomplished by removing from the data arrays the data points with signal too low to drive the receiving mixer. The simple idea for this procedure is that in order for the signal to be able to drive the receiving mixer, it needs a minimum voltage. An example of data without the smoothing, averaging and truncating is shown in Figure 7.2 for an average TFTR ohmic plasma shot (67702), with a magnetic field of  $B_0 \approx 4.5$  Tesla and central density of  $n_{e0} \approx 3.5 \times 10^{19} \frac{\text{part}}{\text{m}^3}$  during a quasi steady state part of the shot. For comparison, the same data with the smoothing, averaging and a truncating voltage of 3 volts is shown in Figure 7.3. For the non-smoothed data, the fluctuations of the signal and

phase make it almost impossible to distinguish the different sweep data sets, while in the smoothed data the curves for the different sweeps are clear. In the same way, the raw phase for the non-smoothed data looks like a random set of points, but the raw phase for the smoothed data set looks like a well defined curve with a well defined and easy to track discontinuity at  $\pm\pi$  due to the inverse tangent function.

An example of the typical output plot for the phase extraction code has been shown in Figures 7.2 and 7.3. The main program is highly documented in the code itself. The cycle of work of this code is this: read the raw data from the raw data disk, do the necessary operations on the raw data (i.e., smooth, average and truncate the data as needed), then calculate the raw phase data using the formula:

$$\Delta\phi = \arctan\left(\frac{I}{Q}\right) \quad (7.6)$$

and finally fringe count it to obtain the continuous phase data necessary for the reconstruction program. The final phase data is written to the working disk as an ASCII file that contains a header line followed by the two columns of frequency and phase data. The flow-graph in Figure 7.1 and Table 7.1 shows this process in more detail.

The reconstructing program uses the phase data generated by the data analysis code and the techniques described in sections 2.4.5, 6.2.1, 6.2.2, and 6.2.5 to reconstruct the density profile. Two parameters need to be well defined in order to obtain a density profile. These are the assumed spatial position of the cutoff for the first frequency and the integer fringe offset phase due to transmission to that point. The selection of the position for the first cutoff will influence more the horizontal position of the density profile (like a horizontal offset). The offset phase due to the transmission to the first cutoff will affect the slope of the density profile, that is, adding more offset phase will produce a flatter density profile, while less

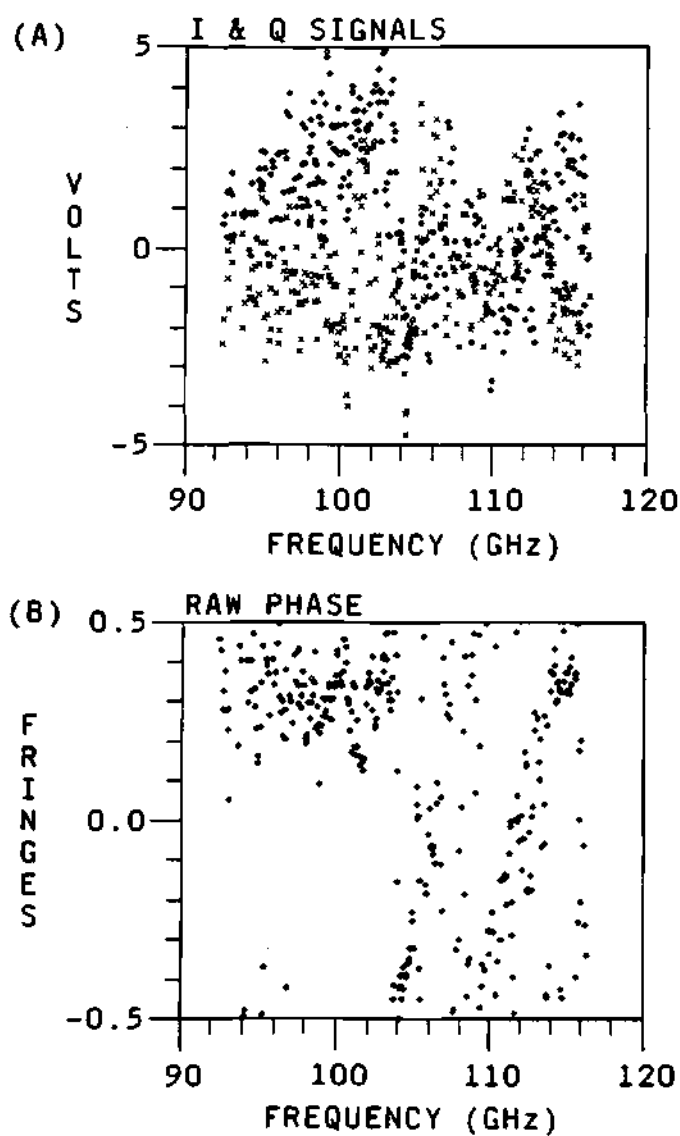


**Figure 7.2:** Raw data for the  $I$  ( $= \sin \Delta\phi$ ,  $\times$  points) and  $Q$  ( $= \cos \Delta\phi$ ,  $\circ$  points) signals and the corresponding calculated raw phase data for the signal. No smoothing is in effect for this data set.

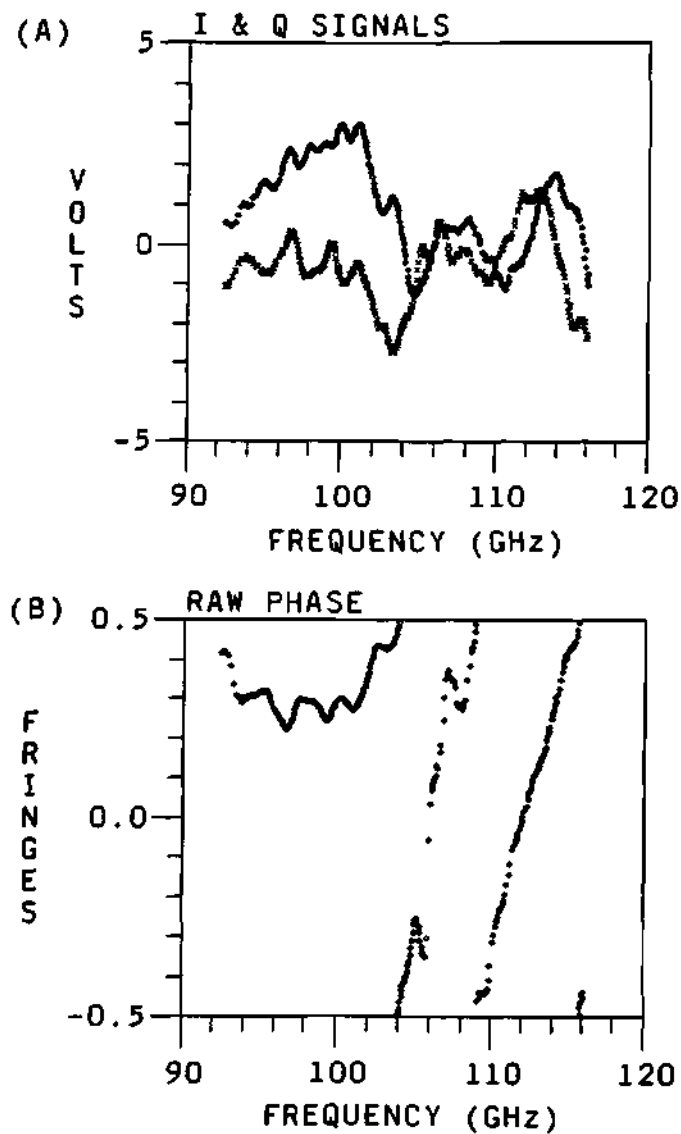


**Figure 7.3:** The same raw data as before, but using smoothing (10 points) and averaging (10 sweeps) on the signal data.

offset phase will make a steeper density profile. This offset is not necessary when a complete set of phase data up to the reference plane is known and when a complete set of phase calibration data is available. For the standard case of probing the edge of the plasma the offset will be equal to zero, and will not be a big source of error. The offset only occurs when the cutoff is deep inside the plasma such as for the case of low field operation and small size plasmas. Propagation over this distance can produce a phase change of one or more fringes which can not be tracked.

The effect of the phase offset was studied with the help of the modeling code and explained in section 6.5. The effect due to the choice on the position of the first cutoff and the phase offset can be seen in Figures 7.4, 7.5, and 7.6. Figure 7.4 shows the reconstructed density profile compared with the Thomson Scattering (TS) density profile. A good match between these can be seen when the proper combination for the values of the position for the first cutoff and the offset phase is chosen. Because of the low magnetic field ( $B_0 \approx 3.3$  Tesla) of this plasma shot, the assumed position of the first cutoff is far way from the edge. This low magnetic field plasma will have a relatively large region where the probing wave is propagating, but there are no reflection layers for the frequency range of the diagnostic. In the region of the plasma that the probing wave can not probe the model assumes a linear profile, noticeable in the figures by the set of points in a straight line at the outmost part of the reconstructed profile. Figure 7.5 shows the same data as before, but the assumed position of the first cutoff has been changed to show how the profile is modified by such a change. In general, it is possible to determine the position of the first cutoff within  $\pm 1$  cm of the real position of the first cutoff. This is especially possible when the density profile and the magnetic field are such that the position of the first cutoff is near or at the edge of the reflectometer launcher (as for the case of full size plasmas). For the case of full size plasmas, both the offset phase and the position of the first cutoff are



calculable and well known. If the plasma configuration is one that has a position for the first cutoff such that it is deep inside the vacuum vessel (as for small size plasmas and low magnetic field), then the uncertainty in the position of the first cutoff is much larger than one centimeter. The uncertainty on the position of the first cutoff will produce a systematic error on the reconstructed profiles for this type of plasmas. Nevertheless, the relative error between consecutive profiles in the same plasma shot will be small. From the figure it can be noticed that the shape of the reconstructed profile with the erroneous position of the cutoff did not change much, but it introduced a horizontal shift of the profile on Figure 7.4. Finally, Figure 7.6 shows the same data as before, but the phase offset due to the propagation through the part of the density profile before the first cutoff has been changed. This change on the offset phase produced a change on the slope of the reconstructed density profile as seen in the figure. This is expected since the slope of the phase difference is proportional to the slope of the density profile.

### **7.3 Density Profile Reconstruction Program**

The reconstructing program uses the frequency and phase data created by the phase extraction program to calculate the density profile.

#### **7.3.1 Description of the density reconstruction program**

The program has the usual straight forward flow chart shown in Figure 7.7. The program starts by initializing all the variables from an initialization file, then it reads the frequency and phase data into the corresponding arrays. With the first cutoff frequency and the position of the first cutoff, an estimate of the phase due to the density before the first cutoff is calculated assuming a linear density profile for this part of the plasma. Then, with all of this information the pro-

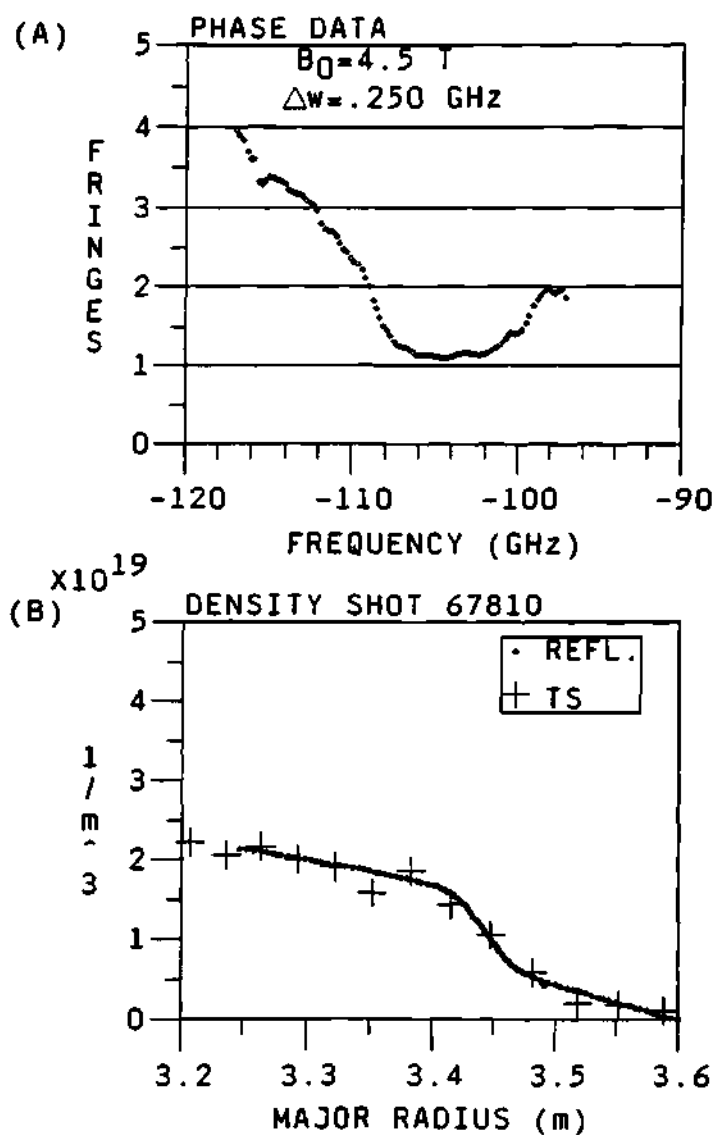


Figure 7.4: Reconstructed density profile (labeled “REFL.” in the legend of the plot) for a good choice on the position of the first cutoff and the initial offset phase. Match to the Thomson Scattering (TS) data is acceptable.

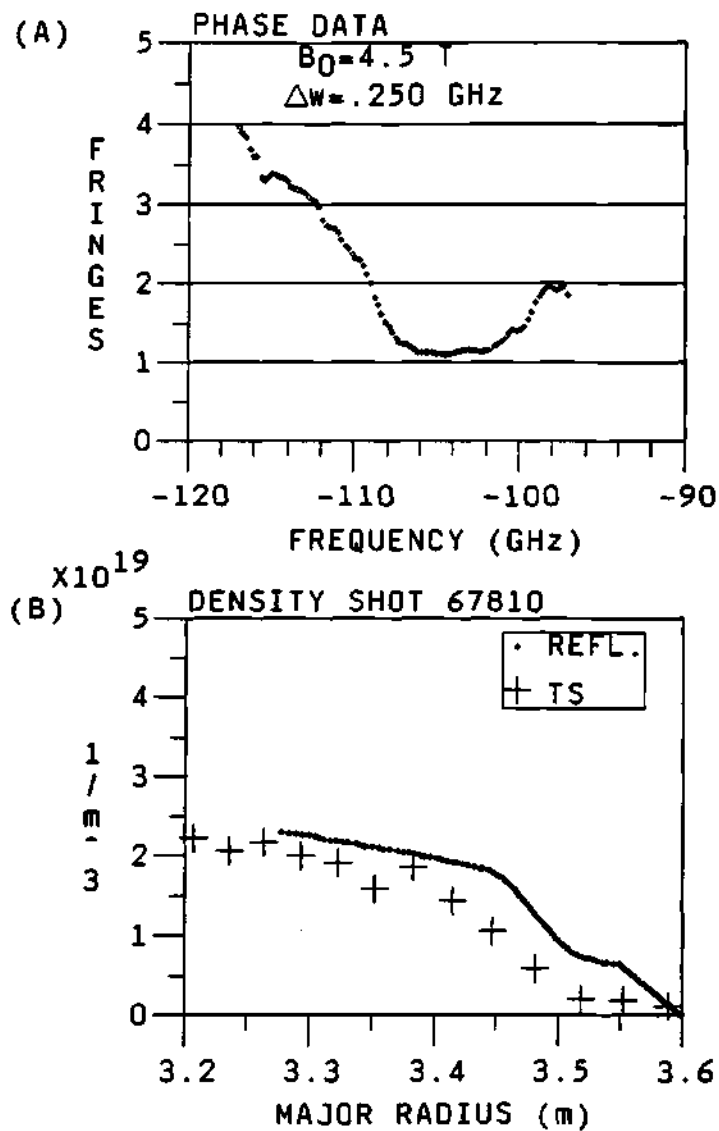


Figure 7.5: Reconstructed density profile for a different choice of the position of the first cutoff.

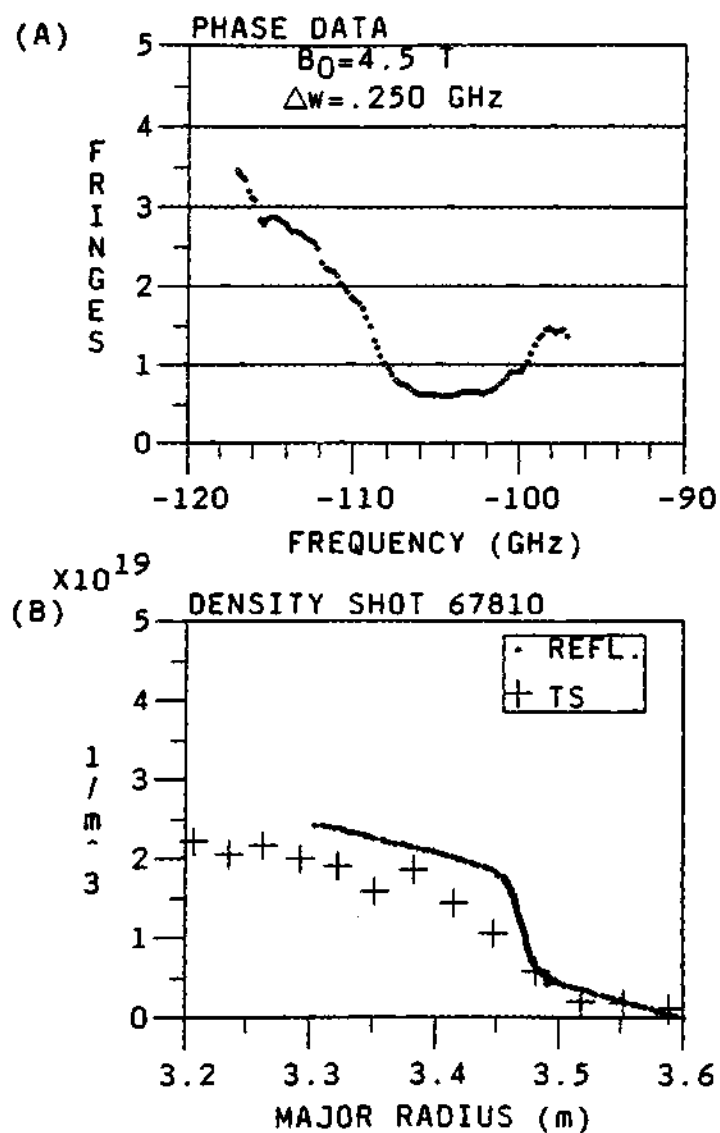
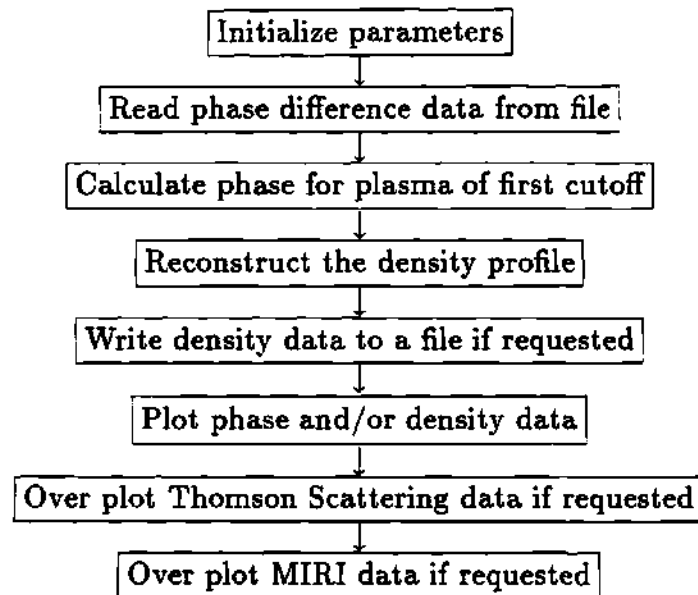


Figure 7.6: Reconstructed density profile for a different choice of the initial offset phase.



**Figure 7.7: Flow chart for the density reconstruction program.**

gram enters the loop to calculate the reconstructed density and the positions of the corresponding cutoffs. The phase data and the reconstructed density profile are plotted with options to over-plot the Thomson Scattering (TS) density profile and/or the Multichannel Infra Red Interferometer (MIRI) density profile to compare for a good match. This match can be changed and/or improved by adjusting the assumed position of the first cutoff and/or the initial integer offset phase due to the propagation to the first cutoff, as previously explained.

The method and theory used to calculate the density profile is the same as used in the simulation program. The main theory involved is the derivation of the phase out of the wave equation. This was explained previously in sections 2.3.5, 6.2.1, 6.2.2, and 6.2.5.

### 7.3.2 Benchmarking the program

In order to verify the reconstructing program used to calculate the density profile for the real data, a comparison was done between the modeling code and the reconstructing code. Both codes use the same reconstructing technique, wave propagation principles and formulas, and model for the magnetic field of the plasma to calculate the reconstructed density profile. The only main difference on the codes and/or data files is that for the reconstruction program the density data before the first cutoff is not known. The program assumes a linear profile in this region of the plasma, and this is how real data is analyzed. While the effect of this linear profile is minimal for most cases, it is there for the real data and it is probably the main cause of error in this comparison. The main reason to do the comparison in this way is to have an idea or estimate of the effect of this error when analyzing real data.

For the purpose of comparing both codes, the modeling code generated a data file containing the data arrays of the frequency vs phase difference and the corresponding radial position vs reconstructed density profile. This data file from the modeling code at the ORNL VAXes was moved to the PPPL VAXes and given to the reconstruction program to use the frequency vs phase difference data to calculate its own reconstructed density profile. Then the reconstructing code plots the density profile that it calculated together with the density profile calculated by the modeling code which is on the data file. When the parameters for the initial conditions and magnetic field are set the same, the result is a good match with less than 1% error between profiles as can be seen from Figure 7.8, where the density profile calculated by the modeling code and the reconstruction code are plotted in the same graph. The difference between the two curves is less than the resolution of the plots, and is plotted with the scale at the right hand side  $y$ -axis of the plot.

The error expected from the calculation and between the two codes can not be of the order of double precision calculation as for the case of the modeling code, because the codes at Princeton are all single precision. There are several reasons and advantages to have a single precision code at the PPPL Vaxes and for the real data. First, the real data as stored in the Vaxes are single precision. This limits the accuracy of the calculations to single precision. Second, in order to have an usable interactive code the time execution has to be kept to a reasonable time to allow iterative calculation with different assumptions of the starting position of the first cutoff. Single precision calculations are more than accurate for the purpose of comparing density plots with any other diagnostics and calculations. Double precision accuracy is too slow to be used in interactive mode and will provide little new information since there is no other diagnostic that can provide with equally accurate data for comparisons.

There are three main regions on the error plot. These are the error on the far edge of the profile, the noisy bell shape error at the steep part of the profile, and the nearly zero constant error at the inner part of the profile. The relatively large error at the edge of the profile is from the the error due to the assumption of the linear density profile at the edge of the profile before the first cutoff. Since the probing beam can not probe this part of the profile, it is assumed that it is of a linear form. While this assumption is a reasonably valid and accurate assumption, the error introduced by it causes the largest error on the plot. This error is still very small compared with systematic errors from the real data (for instance, the error in the position of the first cutoff and the error in the phase difference data). The error in the steep part of the profile is due to the linear assumptions at the edge of the profile, before the first cutoff. The error in the inner part of the profile is due to the accumulated error from the rest of the profile and its effect on the reconstructing technique. This error compares well to the one described in

the modeling chapter if one takes into account the extra error due to the linear assumption of the profile before the first cutoff.

## 7.4 Errors

Every measurement of a real variable or parameter will always have to one extent or another a random error component and a systematic error component. While every effort may be made to reduce one or another source of error, some error will always remain. The following sections will try to separate and explain most, if not all, of the error sources for the diagnostic.

### 7.4.1 Random errors (error bars)

There are different types of random error sources in the data and reconstruction process. The two most important are:

1. Numerical errors. This can include the accumulated error due to the iterative nature of the technique (random error). That is, the calculated density profile points are used to calculate the integrals needed to calculate the next increment on the cutoff position of the propagating wave. Since the calculated density profile points have some error associated with them, this error will propagate along to the next points and calculations.
2. The random error due to the measurement and calculation of the phase difference data in the real experiment. This random error will propagate to the calculation of the position of the cutoffs and consequently to the reconstructed density profile. The measure fluctuations on the phase data are due to the real fluctuations on the density profile, and because of their random nature these fluctuations can be reduced or filtered by smoothing and/or



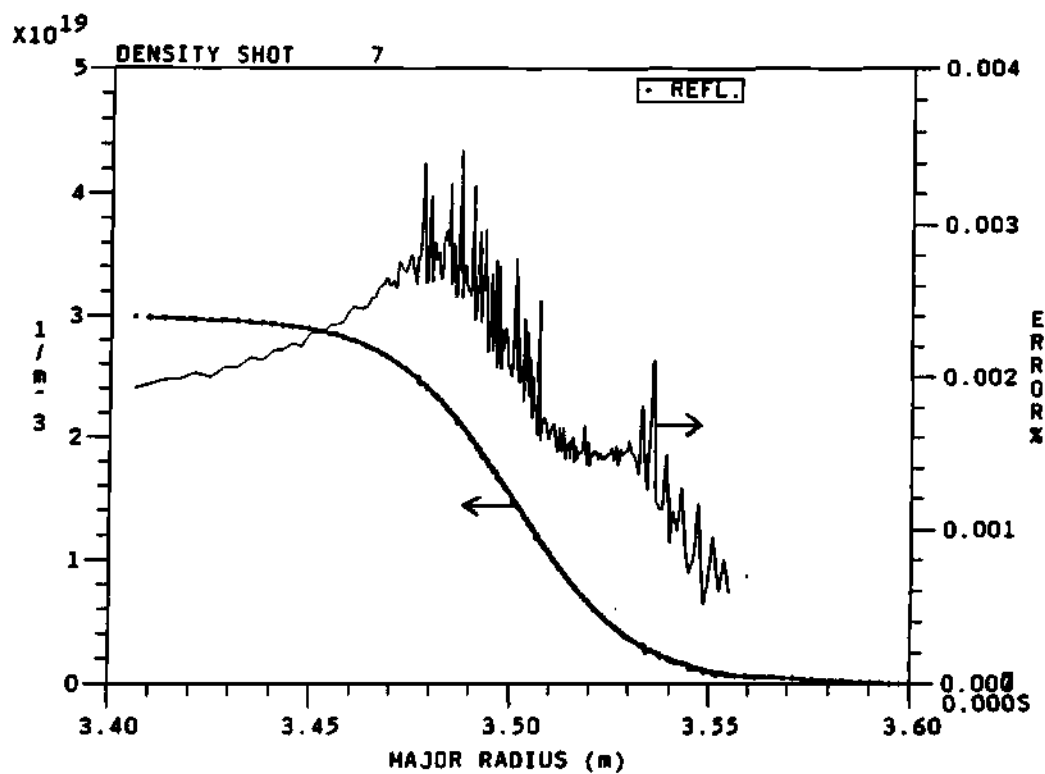


Figure 7.8: Plot of the density profile from the modeling code and the density profile of the reconstructing code. The difference between the curves is shown along the right hand side  $y$ -axis of the plot. Agreement between the curves is acceptable.

averaging of the data. This error is statistical and random (fluctuations) in nature.

3. The random error in the magnetic field. This could be due to uncertainties in the actual measurement of the coil currents (random error), fluctuations on the local magnetic field in the plasma (random error), etc. The main effect of this error is to move and/or oscillate the position of the cutoffs. This error will have its main effect at the edge of the plasma because this is where the density is a minimum and the effect of the magnetic field on the index of refraction is a maximum. It was demonstrated in Section 6.5.2 that the effect is very small.

**Random error formula** The random error sources can be incorporated into a formula for the propagation of random error as described by Bevington,<sup>66,67</sup> that is:

$$\sigma_{n_e}^2 = \sum_i \left( \frac{\partial n_e}{\partial x_i} \right)^2 \sigma_{x_i}^2 \quad (7.7)$$

where  $\sigma_{n_e}$  is the total random error on the density,  $x_i$  are the independent variables of the density, and  $\sigma_{x_i}$  are the corresponding uncertainties of the independent variables. For the error sources of the reflectometer, this equation will give something of the form:

$$\begin{aligned} \sigma_{n_e}^2 = & \left( \frac{\partial n_e}{\partial r} \right)^2 \sigma_r^2 + \left( \frac{\partial n_e}{\partial B} \right)^2 \sigma_B^2 + \left( \frac{\partial n_e}{\partial (\Delta\phi)} \right)^2 \sigma_{\Delta\phi}^2 + \left( \frac{\partial n_e}{\partial n_{ep}} \right)^2 \sigma_{n_{ep}}^2 \\ & + \left( \frac{\partial n_e}{\partial r_1} \right)^2 \sigma_{r_1}^2 + \left( \frac{\partial n_e}{\partial r_0} \right)^2 \sigma_{r_0}^2 + \left( \frac{\partial n_e}{\partial n_{el}} \right)^2 \sigma_{n_{el}}^2 + \left( \frac{\partial n_e}{\partial T} \right)^2 \sigma_T^2 \end{aligned} \quad (7.8)$$

where  $\sigma_r$  is the error in the radial position,  $\sigma_B$  is the error in the magnetic field,  $\sigma_{\Delta\phi}$  is the error in the phase difference,  $\sigma_{n_{ep}}$  is the previous error in the density profile,  $\sigma_{r_1}$  is the error in the first cutoff,  $\sigma_{r_0}$  is the error in the reference plane,  $\sigma_{n_{el}}$  is the error due to the linear profile before the first cutoff, and  $\sigma_T$  is the numerical error of the reconstructing technique.

It is possible to obtain equations and/or estimated values for some of the error terms on the error equation. In particular, for the error on the radial position term, the error due to the magnetic field, the error due to the phase difference, etc. This will be presented next.

**Radial position error formula** The error term due to the radial position can be found using the equation for the cutoff condition, that is:

$$n_e = \frac{m_e \epsilon_0}{q_e^2} (\omega^2 - \omega \omega_{ec}(r)) \quad (7.9)$$

where all the parameters have been defined before. Then the error term will be the derivative of the density and it is given by:

$$\frac{\partial n_e}{\partial r} = \frac{\omega \epsilon_0 B_0 R_0}{q_e R^2} \quad (7.10)$$

where the definition of electron cyclotron emission frequency ( $\omega_{ec} = q_e B(r) / m_e$ ) as a function of the radial position was used. This formula represents the error associated with the calculation of the density at the cutoff. Since this calculation is done based on the calculated position of the cutoff, its contribution to the total error will not be dominant because the error on the calculated positions of the cutoffs is small as shown for the reconstruction technique.

**Phase error formula** The random error due to the uncertainty on the phase difference data can be calculated from the definition of the derivative and the slope of the density profile. That is, the error term is given by:

$$\frac{\partial n_e}{\partial (\Delta\phi)} = \frac{\partial n_e}{\partial r} \frac{\partial r}{\partial (\Delta\phi)} \quad (7.11)$$

where the derivative with respect to the radius can be calculated from the reconstructed density profile, and the derivative of the radius with respect to the phase

difference can be calculated from the definition of the increment on the cutoff position, given by:

$$r = r_0 + \Delta r \quad (7.12)$$

$$= r_0 + \frac{(\phi_0 + \Delta\phi) c}{\omega n(r, \omega)} \quad (7.13)$$

then the derivative of the radius with respect to the phase difference is given by:

$$\frac{\partial r}{\partial (\Delta\phi)} = \frac{c}{\omega n(r, \omega)} \quad (7.14)$$

where  $n(r, \omega)$  is the index of refraction,  $\omega$  is the frequency of the wave, and  $c$  is the speed of light. Finally, the term for the random error due to the previous part of the density profile can be calculated from the definition of the derivative, where the derivative can be calculated numerically from the reconstructing program.

An estimate for the random error due the phase data can be calculated by using worst case scenario values for the variable in equation 7.11. For this case, the values are:

$$\omega \approx 100 \text{ GHz} \quad (7.15)$$

$$c \approx 3 \times 10^8 \frac{\text{meter}}{\text{seconds}} \quad (7.16)$$

$$n \approx 1 \quad (7.17)$$

which are approximately the center frequency of the band, the speed of light, and the index of refraction. The derivative of the density with respect to the radius can be calculated as:

$$\frac{\partial n_e}{\partial r} \approx \frac{\Delta n_e}{\Delta r} \quad (7.18)$$

where  $\Delta n_e \approx 0.1 \times 10^{19} \text{ particles/m}^3$ , and  $\Delta r \approx 0.05 \text{ meters}$ , are typical values for the first 5 cm in the plasma, where the errors will be a maximum. Then, for these values the random error term from the phase is given by:

$$\frac{\partial n_e}{\partial (\Delta\phi)} \approx 10^{16} \frac{\text{particles}}{\text{m}^3} \quad (7.19)$$

which is less than 0.1% for a typical plasma. This would be the absolute worst case error with no averaging or smoothing.

**Calculated phase random error** The random error on the real phase data due to the random phase fluctuations from the density fluctuations can be calculated from the definition of the standard deviation,  $\sigma$ , that is:

$$\sigma_i^2 = \sum_{s=1}^N (x_{is} - \bar{x}_i)^2 \quad (7.20)$$

where  $N$  is the number of sweeps or data sets used for the average,  $x_{is}$  is the data point for frequency  $\omega_i$  and data sweep/set  $s$ , and  $\bar{x}_i$  is the average value of the data point over the sweep number,  $s$ , for the frequency  $\omega_i$ , that is:

$$\bar{x}_i = \frac{1}{N} \sum_{s=1}^N x_{is} \quad (7.21)$$

This calculation is shown in Figure 7.9 for a typical  $B_0 = 4.5$  Tesla plasma. This shot shows a small  $\sigma$  at the steep part of the profile (92 to 102 GHz) and a rather large  $\sigma$  for the starting of the center part of the profile (104 to 108 GHz). As described previously, if the standard deviation of the phase is larger than  $\sigma_{max} = \frac{1}{2\sqrt{3}}$ , then it can not be expected to be able to follow or track the phase. While in the data for Figure 7.9 the  $\sigma$  stays low in most of the frequency band, it can be noticed that it becomes dangerously close to the maximum value around the 106 GHz area. This means that the data around this frequency is not as good as the one with smaller  $\sigma$ , but it is still possible to track the phase through this noisy area of the frequency band as it is shown in the figure.

The above calculations for the random error on the phase data is what people call a “Murphy’s Value” of the random error. The real random error on the phase data can be reduce by smoothing and/or averaging of the real data. Section 7.2.2 explains smoothing in more detail, but the main result of the smoothing

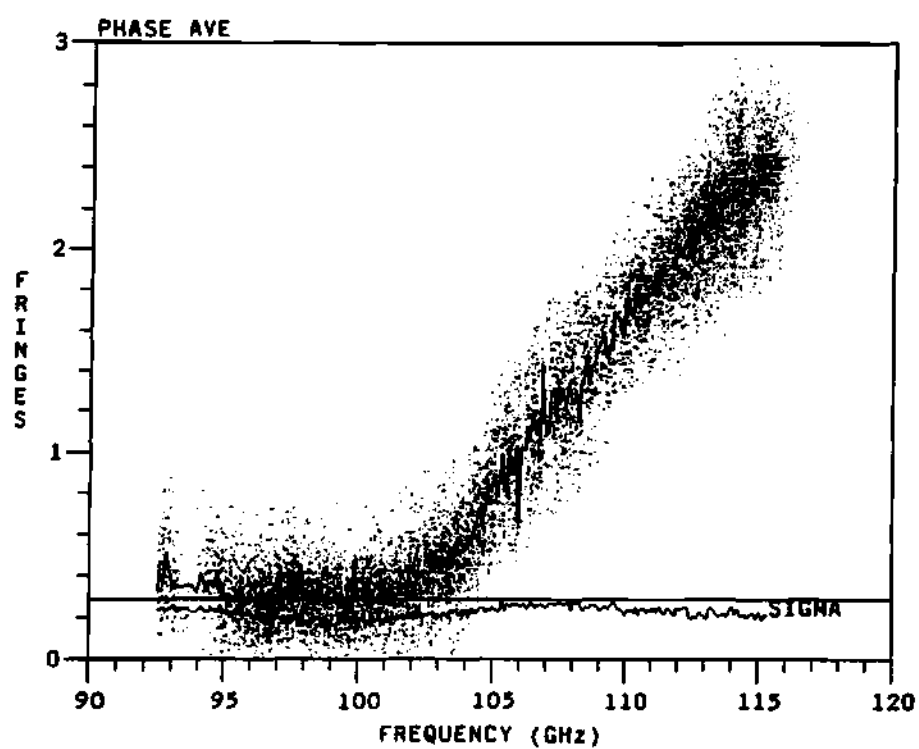


Figure 7.9: Plot of the average phase (solid line) for a set of data points (scattered points), and the standard deviation.

is that it will reduce and/or scale the random error on the phase data as the *square root* of the number of data points used. This can be shown as follows. The definition of the estimated random error for the mean is given by:<sup>66</sup>

$$\sigma_{\bar{f}}^2 = \sum_{i=1}^N \sigma_i^2 \left( \frac{\partial \bar{f}}{\partial x_i} \right)^2 \quad (7.22)$$

where  $\sigma_{\bar{f}}$  is the random error,  $\bar{f}$  is the average and/or smoothed function, and  $x_i$  are the independent variables. The derivatives of the averaged function  $\bar{f}$  are given by:

$$\frac{\partial \bar{f}}{\partial x_i} = \frac{\partial}{\partial x_i} \left( \frac{1}{N} \sum_{j=1}^N x_j \right) \quad (7.23)$$

$$= \frac{1}{N} \quad (7.24)$$

then the random error will become:

$$\sigma_{\bar{f}}^2 = \sum_{i=1}^N \sigma_i^2 \left( \frac{1}{N} \right)^2 \quad (7.25)$$

and using the assumption of equal  $\sigma_i$  given by:

$$\sigma_i = \sigma \quad (7.26)$$

then the random error will simplify to:

$$\sigma_{\bar{f}}^2 = \sum_{i=1}^N \sigma^2 \left( \frac{1}{N} \right)^2 \quad (7.27)$$

$$= \frac{\sigma^2}{N} \quad (7.28)$$

which shows how the random error of the averaged data scales as the square root of the number of data points. This scaling can be noticed in Figure 7.10 where the data was averaged in groups of 16 sweeps. It can be noticed that the standard deviation of the data was reduced significantly and approximately by a factor of  $\frac{1}{4}$  as expected.

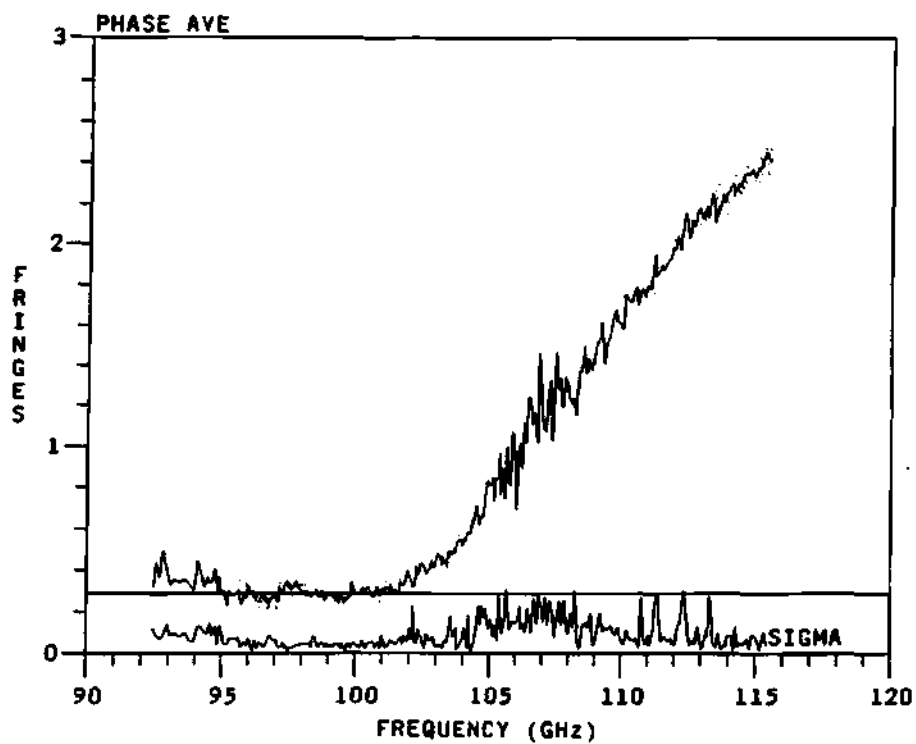


**Figure 7.10:** Plot of the average phase and the standard deviation where a 16 sweep average was done to the data.



For the case of smoothing using a Gaussian function the scaling of the standard deviation can be expected to be similar. This can be shown as follows. The definition of the standard deviation is given by:

$$\sigma_{S_j}^2 = \sum_{i=-N}^N \sigma_{j+i}^2 \left( \frac{\partial S_j}{\partial x_{j+i}} \right)^2 \quad (7.29)$$

where  $S_i$  is the smoothing function with the Gaussian weighting function. Next, the definition of the smoothing is given by the formula:

$$S_j = \sum_{k=-N}^N \frac{1}{\sigma_N \sqrt{2\pi}} e^{-\frac{1}{2} \left( \frac{k}{\sigma_N} \right)^2} x_{j+k} \quad (7.30)$$

where  $\sigma_N$  is defined as:

$$\sigma_N^2 = \frac{N^2}{2 \ln(10)} \quad (7.31)$$

which represents the value of  $\sigma_N$  such that the last point of the smoothing will be weighted by  $\frac{1}{10}^{th}$  of its value. From the definition of the smoothing function its derivative can be calculated as:

$$\frac{\partial S_j}{\partial x_{j+i}} = \frac{1}{\sigma_N \sqrt{2\pi}} e^{-\frac{1}{2} \left( \frac{i}{\sigma_N} \right)^2} \quad (7.32)$$

Then, the standard deviation will become:

$$\sigma_{S_j}^2 = \sum_{i=-N}^N \sigma_{j+i}^2 \left( \frac{1}{\sigma_N \sqrt{2\pi}} e^{-\frac{1}{2} \left( \frac{i}{\sigma_N} \right)^2} \right)^2 \quad (7.33)$$

assuming that  $\sigma_i = \sigma$ , then:

$$\sigma_{S_j}^2 = \frac{\sigma^2}{2N} \quad (7.34)$$

which finally gives the scaling of the standard deviation as:

$$\sigma_{S_j} = \frac{\sigma}{\sqrt{2N}} \quad (7.35)$$

Now that the error propagation for averaging and smoothing has been derived independently for each process, it is relatively easy to derive the effect

of both operations on the standard deviation. The derivation is started with the definition of the standard deviation as:

$$\sigma_{\bar{x}_s}^2 = \sum_{j=1}^N \sum_{i=-M}^M \sigma_{j,s+i}^2 \left( \frac{\partial \bar{x}_s}{\partial x_{j,s+i}} \right)^2 \quad (7.36)$$

where  $\bar{x}_s$  is the average function of the smoothed data, and is given by:

$$\bar{x}_s = \sum_{n=1}^N \sum_{m=-M}^M \frac{x_{n,s+m}}{N} \frac{1}{\sigma_M \sqrt{2\pi}} e^{-\frac{1}{2} \left( \frac{m}{\sigma_M} \right)^2} \quad (7.37)$$

$N$  are the number of averaged sweeps, and  $\sigma_j$  are the standard deviation for the data as described previously. Substituting the definition of the average into the definition of the standard deviation, it is obtained:

$$\sigma_{\bar{x}_s}^2 = \sum_{j=1}^N \sum_{i=-M}^M \sigma_{j,s+i}^2 \left( \frac{\partial}{\partial x_{j,s+i}} \left( \sum_{n=1}^N \sum_{m=-M}^M \frac{x_{n,s+m}}{N} \frac{1}{\sigma_M \sqrt{2\pi}} e^{-\frac{1}{2} \left( \frac{m}{\sigma_M} \right)^2} \right) \right)^2 \quad (7.38)$$

where the derivative can be moved into the summations to give:

$$\sigma_{\bar{x}_s}^2 = \sum_{j=1}^N \sum_{i=-M}^M \sigma_{j,s+i}^2 \left( \sum_{n=1}^N \sum_{m=-M}^M \frac{1}{N} \frac{\partial x_{n,s+m}}{\partial x_{j,s+i}} \frac{1}{\sigma_M \sqrt{2\pi}} e^{-\frac{1}{2} \left( \frac{m}{\sigma_M} \right)^2} \right)^2 \quad (7.39)$$

The derivative term can be simplified using the equation:

$$\frac{\partial x_{n,m}}{\partial x_{j,i}} = \delta_{n,j} \delta_{m,i} \quad (7.40)$$

where  $\delta_{i,j}$  is the Kronecker delta. Now the equation will become:

$$\sigma_{\bar{x}_s}^2 = \sum_{j=1}^N \sum_{i=-M}^M \sigma_{j,s+i}^2 \left( \sum_{n=1}^N \sum_{m=-M}^M \frac{1}{N} \delta_{n,j} \delta_{s+m,s+i} \frac{1}{\sigma_M \sqrt{2\pi}} e^{-\frac{1}{2} \left( \frac{m}{\sigma_M} \right)^2} \right)^2 \quad (7.41)$$

Finally, when the sum over the inner indexes are done, the equation for the standard deviation will simplify to:

$$\sigma_{\bar{x}_s}^2 = \sum_{j=1}^N \sum_{i=-M}^M \sigma_{j,s+i}^2 \left( \frac{1}{\sigma_M N \sqrt{2\pi}} e^{-\frac{1}{2} \left( \frac{i}{\sigma_M} \right)^2} \right)^2 \quad (7.42)$$

which shows how the standard deviation will scale as a function of the number of data points used for the average and the number of data points used in the

smoothing. For the standard deviation of the real data, the standard deviation  $\sigma_{ij}$  will be the difference between the average value of the phase and the value of the data point. This is given as:

$$\sigma_{ij} = x_{ij} - \bar{x}_j \quad (7.43)$$

where  $x_{ij}$  is the value of the data point and  $\bar{x}_j$  is its average value. Then the formula for the standard deviation will become:

$$\sigma_{\bar{x}_j}^2 = \sum_{j=1}^N \sum_{i=-M}^M (x_{j,s+i} - \bar{x}_s)^2 \left( \frac{1}{\sigma_M N \sqrt{2\pi}} e^{-\frac{1}{2} \left( \frac{i}{\sigma_N} \right)^2} \right)^2 \quad (7.44)$$

where all the parameters have been defined before.

The errors presented above have been programed into the modeling code to calculate an estimate of the resulting error when using the method and formulas explained previously. An example reconstructed profile and its corresponding error bars are shown in Figure 7.11 for a typical density profile. It must be noticed that contrary to most diagnostics where they have constant error bars, the error bars for the reconstructed density profile depends strongly on the local slope of the density profile. That is, the error on the profiles are larger at the steep part of the profile and smaller at the flat parts of the profile.

#### 7.4.2 Systematic errors

The theory about systematic errors is not extensively covered in the basic books of error analysis. The book by Bevington says: "Throughout this book we will ignore the problems of systematic errors and concentrate on the random errors resulting from uncertainties in our results."<sup>66</sup> Nevertheless, Bevington describes in chapter 4 a possible procedure to calculate the systematic error in the data. For this particular approach, the systematic error propagation is given by:<sup>66,309</sup>

$$\Delta n_e \approx \sum_i \Delta x_i \frac{\partial n_e}{\partial x_i} \quad (7.45)$$

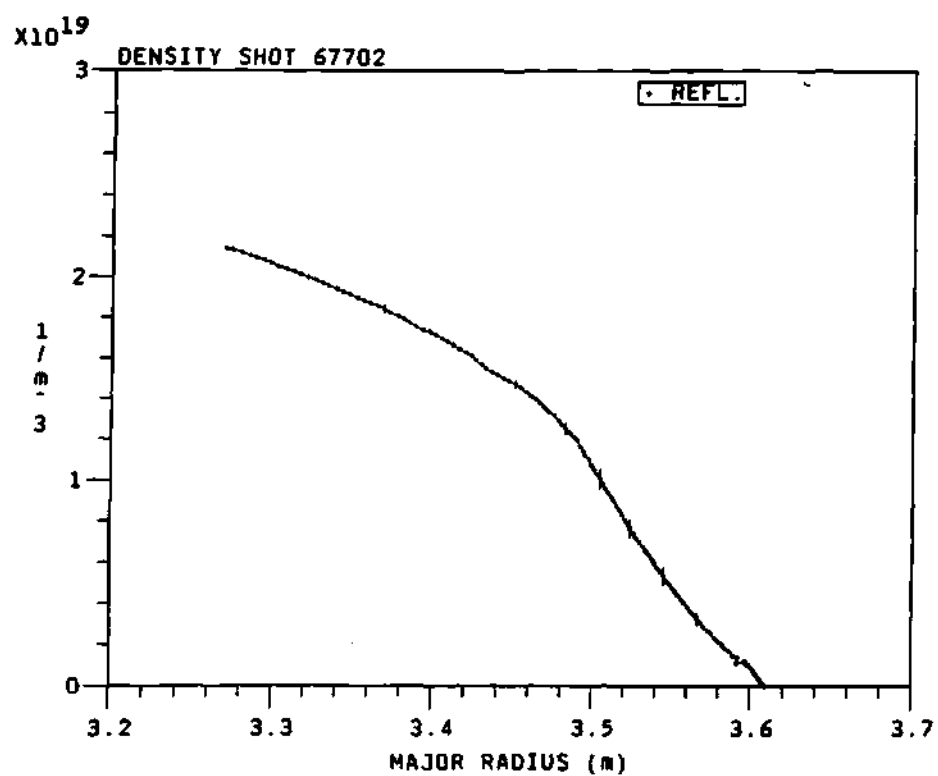


Figure 7.11: Plot of the reconstructed density profile with the corresponding error bars. The error bars in most cases are of the order of the thickness of the lines and are some what hard to see in the plots.

where  $\Delta n_e$  is the error in the density, and  $\Delta x_i$  is the systematic error of the measurements for the different variables  $x_i$ . Another approach was described by Taylor.<sup>67</sup> In his book, Taylor states: "There is no simple theory to tell us what to do about systematic errors. In fact, the only theory of systematic errors is that they must be identified and reduced until they are much less than the required precision."<sup>67</sup> Furthermore, Taylor explains that there are many different approaches to calculate the propagation of the systematic error, but at the same time he states that: "None of these can really be rigorously justified, and we describe just one approach here."<sup>67</sup> Taylor describes the propagation of the systematic error as the sum of the square of the estimated systematic error and the estimated random error, that is:

$$\sigma_f = \sqrt{\sigma_s^2 + \sigma_r^2} \quad (7.46)$$

where  $\sigma_f$  is the error on the function,  $\sigma_s$  is the systematic error, and  $\sigma_r$  is the random error. From the formula it can be noticed that contrary to the random error which can be reduced continuously as the square root of the number of data points, the total systematic error can not be reduced to zero by increasing the number of data points. Therefore, there will always be some systematic error from any measurement which will remain, and the total error can not be reduced or made less than  $\sigma_s$  after the random error is less than the systematic error.

**Systematic error sources** The two main error sources in the reconstruction of the density profile are the offset error in the phase difference data (due to changes in the waveguide system, the multi-fringe value nature of the data, and the propagation from the reference plane to the first cutoff) and the uncertainty in the position of the first cutoff (due to the inability of the diagnostic to probe the plasma before the first cutoff, the phase due to the propagation through the plasma before the first cutoff, etc.). These errors are mainly systematic errors, and

are basically the same for every shot on any given day for any given plasma. They are reproducible errors and do not cause fluctuations on the data at the same time that they will not reduce the reproducibility of the reconstructed density profile. There are other sources of error which may not be considered important, but for completeness will be listed next. These are:

1. The uncertainty in the calculation of the position of the reference plane,  $\sigma_{r_0}$ . This will be equivalent to a systematic error or uncertainty in the phase difference data, since this position is used in the calculation of the phase from the reference plane to the position of the first cutoff. It can be considered a systematic error since it is the same for every data point in the reconstruction process and it will not reduce the reproducibility of the reconstructed profile for adjacent plasma shots.
2. The uncertainty in the position of the first cutoff,  $\sigma_{r_1}$ . This error can be both systematic and random. It is systematic because it is assumed the same for every point in the calculation of the reconstructed profile. At the same time, it is random because for the real data the real position of the first cutoff is fluctuating with the changes and fluctuation of the density profile at the position of the first cutoff.
3. The systematic error in the magnetic field. This could be due to the ripple in the field between magnets (a systematic error). The main effect of this error is to move the position of the first cutoffs at the edge of the profile. That is, the ripple in the field will produce a systematic error on the position of the cutoffs. This error will have its main effect at the edge of the plasma because this is where the density is a minimum and the effect of the magnetic field on the index of refraction is a maximum. It was demonstrated in Section 6.5.2

that the effect is very small. On any given day the magnetic field error is mostly systematic.

4. The systematic error due to the fitting function approximation used by the reconstructing technique. This has been shown to be very small compared with other error sources and therefore it will not be a dominant source of error. It is equivalent to an error in the position of the first cutoff, and it is considered a systematic error.
5. The systematic error due to the assumption of a linear profile for the plasma before the first cutoff. This error will be equivalent to an error in the phase difference since this part of the density profile is used to calculate the phase due to the propagation of the wave to the first cutoff. This is systematic for plasmas of the same type and for all data points in the same sweep since the same linear profile is used for the same sweep.

Most of these errors are difficult to derive or estimate, and the only way to deal with them is to make sure that they are small enough that they can be considered insignificant. Nevertheless, for the purpose of completeness, the derivation of their contribution to the error formula will be presented next.

**Position of the reference plane error** The position of the reference plane was calculated using a wide number of information and measurements available. These include, but not only, copies of "blue prints" and drawings of TFTR and the fluctuation reflectometer system, measuring distances at the fluctuation reflectometer waveguide system with a measuring tape, etc. The different sources of error and uncertainty can be enumerated as follows:

1. Uncertainty in measuring the distance from the waveguide to the viewing flange of the TFTR vacuum vessel port,  $L_1$ . This was done using a measuring

tape and some of the blue prints of the system. Considering all the possible things that can go wrong when measuring with the tape and where to put either end of the tape to make the measurement, the uncertainty on the measurement is of the order of  $L_1 \geq 0.5$  cm.

2. Uncertainty in the estimate of the distance from the flange to the reference plane in the plasma,  $L_2$ . This was based on the drawing available from TFTR. The vacuum vessel and the flange could be displaced from the position shown in the drawing. Dr. Wilgen estimated that the error on the position of the flange was of the order of 0.75 cm.
3. There was no attempt to account for the dielectric constant of the vacuum window. The error due to the window can be calculated from the dielectric constant, that is,  $\Delta \approx (n - 1) L$ , where  $n \approx 1.96$  is the index of refraction, and  $L \approx 7$  mm is the thickness of the window. Then the error is  $\approx 0.67$  cm.
4. The effect of the transmission of the wave through air and not real vacuum. The index of refraction for air is  $\approx 1.0003$ . Therefore, the error due to the propagation in air will be less than  $10^{-3}$ , and it can be assumed insignificant.

If these errors add as described by Taylor,<sup>67</sup> then the final error will be:

$$\sigma = \sqrt{\sum_i \sigma_i^2} \quad (7.47)$$

$$= 1.12 \text{ cm} \quad (7.48)$$

**First cutoff position systematic error** It is possible to estimate a value for the systematic error in the position of the first cutoff from the position of the electron cyclotron emission, the position of the plasma limiter, the other diagnostics (such as Thomson Scattering (TS), the Multichannel Infra Red Interferometer (MIRI), the magnetic diagnostics to obtain the major and minor radii),



etc. For the case when it is possible to obtain data to the lowest frequency and/or the limit of zero density, then the position of the first cutoff will be some where between the position of the electron cyclotron frequency and the position of the plasma limiter. For an average case of an average plasma, the position of the electron cyclotron frequency is within one centimeter to the left of the position of the first cutoff. And the limiter will be about one centimeter to the right of the position of the first cutoff too. Then, for the case of phase data to the limit of zero density, the uncertainty on the position of the first cutoff will be of the order of  $\pm 1$  cm. For the case in which there is not enough data and the first cutoff is far away from the edge and the limiter, then the position of the first cutoff was determined using other diagnostics like TS, MIRI, and the diagnostics to calculate the major and minor radii. Most times, the position of the first cutoff was determined by finding a reasonable match between the TS and/or the MIRI by moving or shifting the position of the first cutoff to find the best possible match to the TS and/or MIRI. The magnetics diagnostics for the major and minor radii were used to get an idea of the approximated position of the first cutoff, and then the match to the TS and MIRI was done. The uncertainty of the major and/or minor radii is approximately of the same order of magnitude as described previously, as stated by Dr. M. Bell in one of his messages: "Depending on the choice of diagnostics which I use to constrain the fit, this outmost point can be shifted by  $\pm 1$  cm." After the match with the TS and MIRI was done, the estimated uncertainty on the position of the first cutoff is about from 1 to 3 cm, depending on the plasma being studied.

**Magnetic field error formula** For the systematic error due to the magnetic field, the same equation for the cutoff (equation 7.9) can be used, that

is:

$$n_e = \frac{m_e \epsilon_0}{q_e^2} (\omega^2 - \omega \omega_{ec}(\tau)) \quad (7.49)$$

but this time the definition of the electron cyclotron emission as a function of the magnetic field is used. Then the error term will be:

$$\frac{\partial n_e}{\partial B} = \frac{\epsilon_0 \omega}{q_e} \quad (7.50)$$

The main effect of the error on the magnetic field is to move the positions of the cutoff of the wave, therefore passing the error to the reconstructed profile in the form of an error on the cutoffs.

While the formulation presented above is probably numerically correct, it is too complicated and impractical to use. Fortunately an alternate method has been developed, and it is explained next.

**Practical approach to systematic error** Because of the complicated form and nature of the integral equations and procedures used to calculate the profile, an analytical formula for the error at every calculated density point is not possible. Instead, a simpler and much easier to implement approach can be used. This consists of calculating the density profile for the data with the given systematic errors on the phase and cutoff position that add-up in the same direction. That is, the density curves:

$$n_e(\phi \pm \sigma_\phi, \tau \pm \sigma_\tau) \quad (7.51)$$

will correspond to the upper (+) and lower (−) error curves for any given systematic errors in the phase,  $\sigma_\phi$ , and the position of the first cutoff,  $\sigma_\tau$ . This is shown in Figure 7.12, where a constant offset of  $\pm 0.084$  fringes has been added to the phase difference data and the position of the first cutoff has been shifted by  $\pm 5$  cm. The value for the offset is calculated from the error due to the shift of the

position of the first cutoff (by  $\pm 5$  cm) as follows. The wave length of the wave at the edge will be approximately:

$$\lambda_m = \frac{C}{\omega_m} \quad (7.52)$$

where  $C$  is the speed of light,  $\omega_m$  is the separation frequency, and  $\lambda_m$  is its wavelength. Then the amount of phase due to the shift of 5 cm will be given by:

$$\phi = \frac{2 \times 5}{\lambda_m} \quad (7.53)$$

$$\approx 0.084 \text{ fringes} \quad (7.54)$$

which is multiplied by two because of the full travel of the wave in the plasma. The center curve of each plot is the unperturbed phase difference data (plot A) and corresponding reconstructed density profile (plot B). The uncertainty in the position of the first cutoff comes from the inability of the wave to scan the plasma before the first cutoff. Finally, assuming that the density function is smooth with respect to the errors in the phase and the position of the first cutoff, then the real density profile curve will be contained within the envelope of the error curves calculated by the method described here. The errors shown in Figure 7.12 are exaggerated to show the general effect of such uncertainties in the reconstructed density profile. The real uncertainties are about  $\frac{1}{5}^{\text{th}}$  the ones used in the figure (*approx* 1 cm), which will correspond to a set of curves which will envelope only  $\frac{1}{5}^{\text{th}}$  of the area shown in the figure. Therefore, the real systematic error of the reconstructing technique is much smaller than the one shown here ( $\approx 1$  cm as described in the previous section) and compares favorably with other diagnostics such as Thomson Scattering (TS) and the Multichannel Infra Red Interferometer (MIRI).

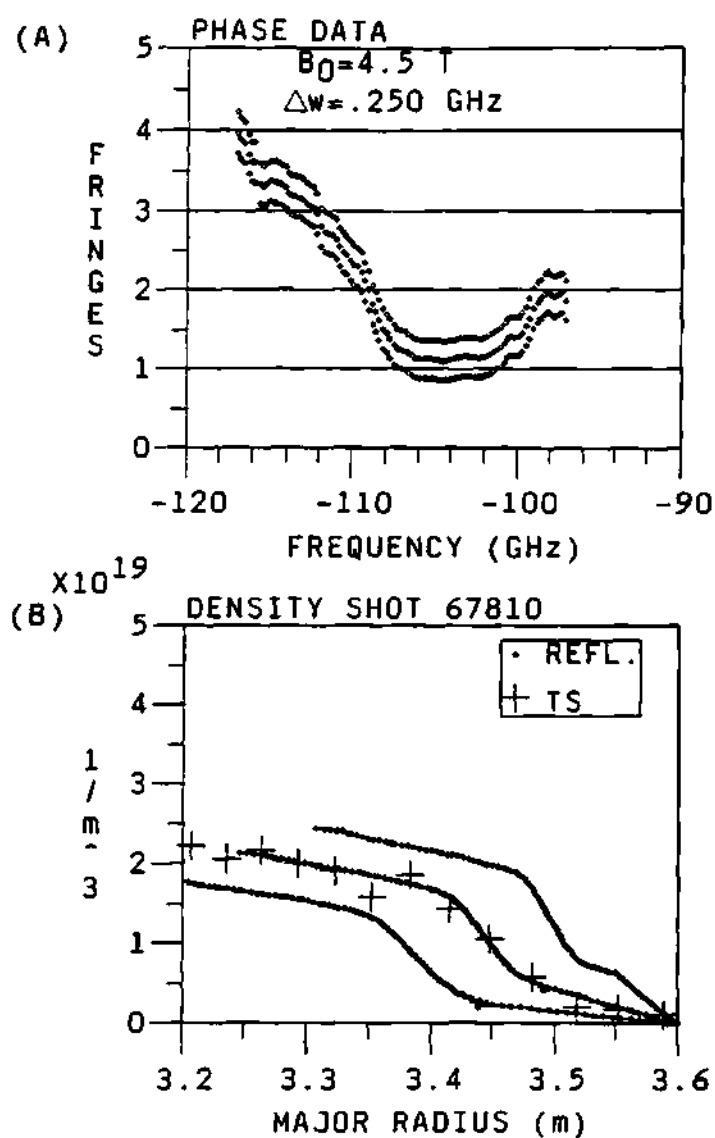


Figure 7.12: Plots of (A) the phase difference data with a  $\pm 0.21$  fringes of systematic error, and (B) the corresponding reconstructed density profiles with a shift in the position of the first cutoff corresponding to an error of  $\pm 5$  cm. This is 5 times the expected systematic error.

## 7.5 Summary

This chapter presented the description of the data analysis program and the reconstructing program used to analyze and calculate the density profiles out of the phase difference data from the reflectometer. The general operation procedures to recall the data, run the programs and analyze the data to obtain the density profiles were discussed. The effect of different variables and parameters of the data analysis and reconstructing procedures was described. This included the smoothing and averaging factors, fringe counting the data, position of the first cutoff layer and effect of the offset phase on the reconstructed profiles. It was shown that the smoothing and/or averaging reduced the error on the data, therefore providing a great improvement of the data and the resulting phase difference. A comparison of the modeling program and the density reconstructing program was presented and the accuracy found to be acceptable. The theory to calculate the random error and the systematic error was presented. The procedure to calculate the error curves for a density profile from the phase difference data and the uncertainty in the phase difference data and position for the first cutoff were described. The error sources were categorized and described. Scaling laws were derived for the effect of the averaging and smoothing on the data. The scaling laws showed that the standard deviation and/or error of the data will scale as the square root of the number of data points smoothed and averaged. Figure 7.11 shows the random error bars associated with typical reflectometer data. The systematic error was analysed and Figure 7.12 plots 5 times the expected systematic error.

## CHAPTER VIII

### EXPERIMENTAL DATA AND INTERPRETATION

#### 8.1 Introduction

This chapter will discuss the results of the reflectometer for both phase I and phase II. As discussed previously in section 4.3, the data for phase I was taken with the reflectometer using the fluctuation reflectometer waveguide system and using a frequency separation of  $\Delta\omega = 0.250$  GHz, while the data for phase II was taken with the reflectometer using the port at the center of the ICRH antenna on the bay-K area of TFTR and the frequency separation of the waves was reduced to  $\Delta\omega = 0.125$  GHz in order to reduce the effect of the density fluctuations. Aside from the frequency separation of the probing waves and the waveguide system/position used to launch the probing beam to the plasma, there were no major changes on the mode of operation of the reflectometer, and for all purposes it was the same diagnostic in both phases of the project. However, any ICRH effects observed might be very different for the two locations, one centered on the ICRH antenna and one far away from it.

#### 8.2 Results of Phase I

This section will present some of the preliminary results of the dual frequency phase difference reflectometer. This reflectometer was intended to measure the electron density profile in front of the ICRH antenna. However, during this

work the reflectometer was located far from the ICRH antenna. The density profile can be used to calculate the antenna loading and the plasma coupling to the ICRH system. Even though no global effects to the density profile were observed from the ICRH power, other interesting results and observations were found that test and prove the performance and accuracy of the reflectometer in the type of environment that it encountered during the second phase of the project, that is, after its relocation to the port in front of the ICRH antenna at the bay-K area. This initial data serves as a base line for the data obtained during the second phase of the project. This initial data allowed a comparison between the measured data and the modeling code developed to study the propagation of the probing waves in the plasma and the reconstruction technique for the reflectometer.

### 8.2.1 Different field strength operation

For a reflectometer using an X-mode wave the position of the cutoff layers depends on both the local density and the magnetic field strength. At lower densities and/or magnetic fields the positions of the cutoff will be further inside the plasma. This allows observation of the plasma behavior in locations other than the plasma edge, for which the reflectometer was designed. These include plasmas with toroidal field currents ( $I_{tf}$ ) of 48, 55, 67 and 72 Kamps, which correspond to magnetic fields strengths ( $B_0$ ) of 3.3, 3.7, 4.5 and 4.8 Tesla. Some examples follow.

**Operation at 3.3 Tesla** For typical operation using a toroidal field current of  $I_{tf} = 48$  Kamps ( $B_0 = 3.3$  Tesla) the cutoff layers start at a major radial position of  $R \approx 3.35$  m and cover a radial distance of  $\approx 0.80$  m. This means that the reflectometer probing beam can probe the center part of the plasma. This was done during shots 67016 to 67024 and the reflectometer was able to measure

the phase delay due to *sawtooth* oscillations. An example of the data and the corresponding reconstructed density profile is shown in Figure 8.1. Notice how the reflectometer originally designed to probe from a major radius of  $R = 3.6$  m to  $R = 3.3$  m (the first 20 to 30 cm of the plasma edge) now is probing from  $R = 3.25$  m to  $R = 2.8$  m, that is, the center of the plasma. The importance of this example is that for low magnetic field operation, the reflectometer can be used to study relative changes of the central density profile, as opposed to changes in the density at the edge.

**Operation at 3.7 Tesla** An example of the data and corresponding reconstructed density profile for one sweep of the reflectometer beam is shown in Figure 8.2 for a plasma with a toroidal field current of 55 Kamps ( $B_0 = 3.7$  Tesla). This particular shot is a low density plasma with a small minor radius of  $a \approx 0.80$  m and central peak density of  $n_{e0} \approx 1.5 \times 10^{19}$  *part/m*<sup>3</sup>, as can be seen in Figure 8.2 from the MIRI density profile and in Figure 8.3 for the toroidal field current and the manor radius. As in the case for a toroidal field current of 48 Kamps ( $B_0 = 3.3$  Tesla), the probing beam of the reflectometer covers the outer center part of the plasma.

**Operation at 4.5 Tesla** The reflectometer was originally designed for operation at a toroidal field current of about 67 Kamps ( $B_0 = 4.5$  Tesla) and maximum central densities of around  $n_{e0} \approx 4.5 \times 10^{19}$  *part/m*<sup>3</sup>. A typical phase data with the corresponding reconstructed density profile is shown in Figure 8.4 for a toroidal field current of 67 Kamps and a central density of  $\approx 3.0 \times 10^{19}$  *part/m*<sup>3</sup>. It can be noticed that under these conditions the probing beam has a penetration of about 30 cm at the edge of the plasma. This is enough to study the effect of the ICRH power on the plasma edge in front of the antenna. Figure 8.4 shows



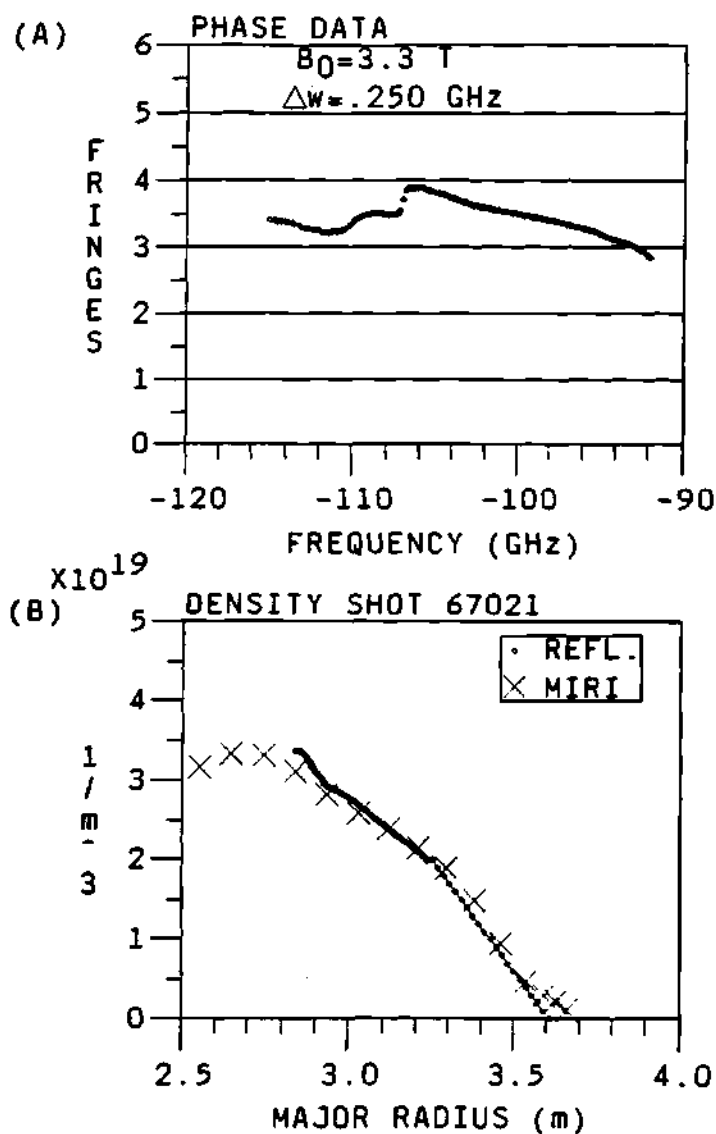


Figure 8.1: Plots of (A) the phase difference data and (B) the corresponding reconstructed density profiles for a plasma with sawtooth oscillations. The MIRI data points used the  $\times$  symbol as noted in the legend of the figure.

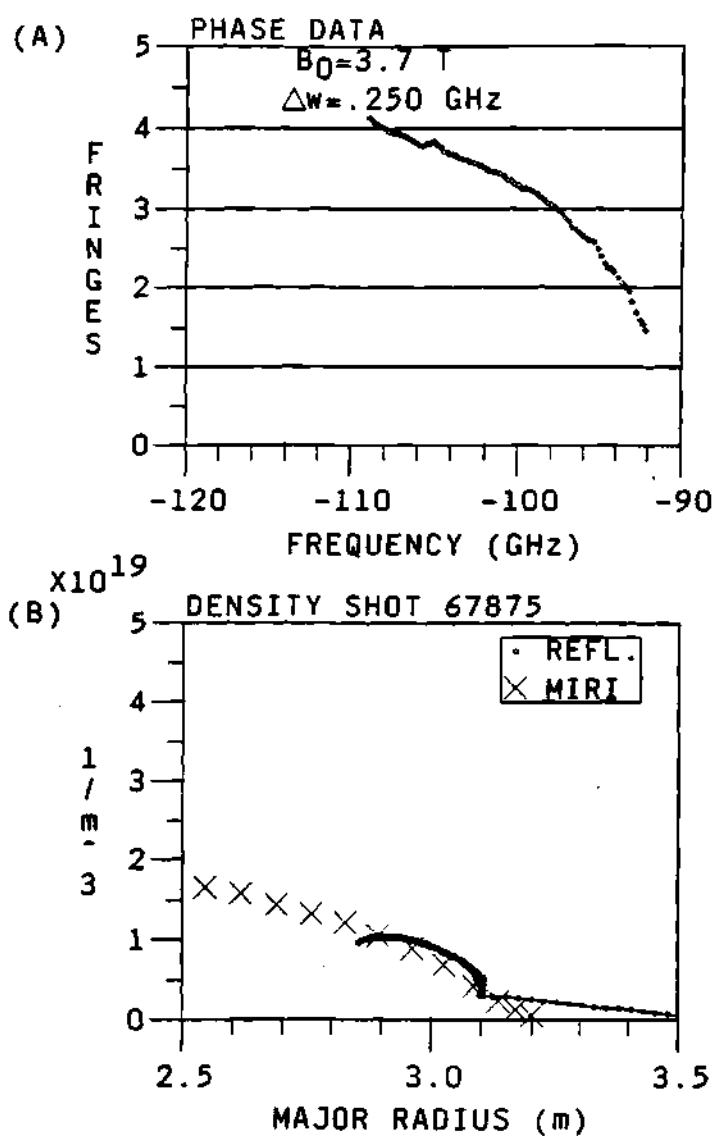


Figure 8.2: (A) Phase data and (B) corresponding reconstructed density profile for a low density plasma and small minor radius at a toroidal field current of 55 Kamps ( $B_0 = 3.7$  Tesla).

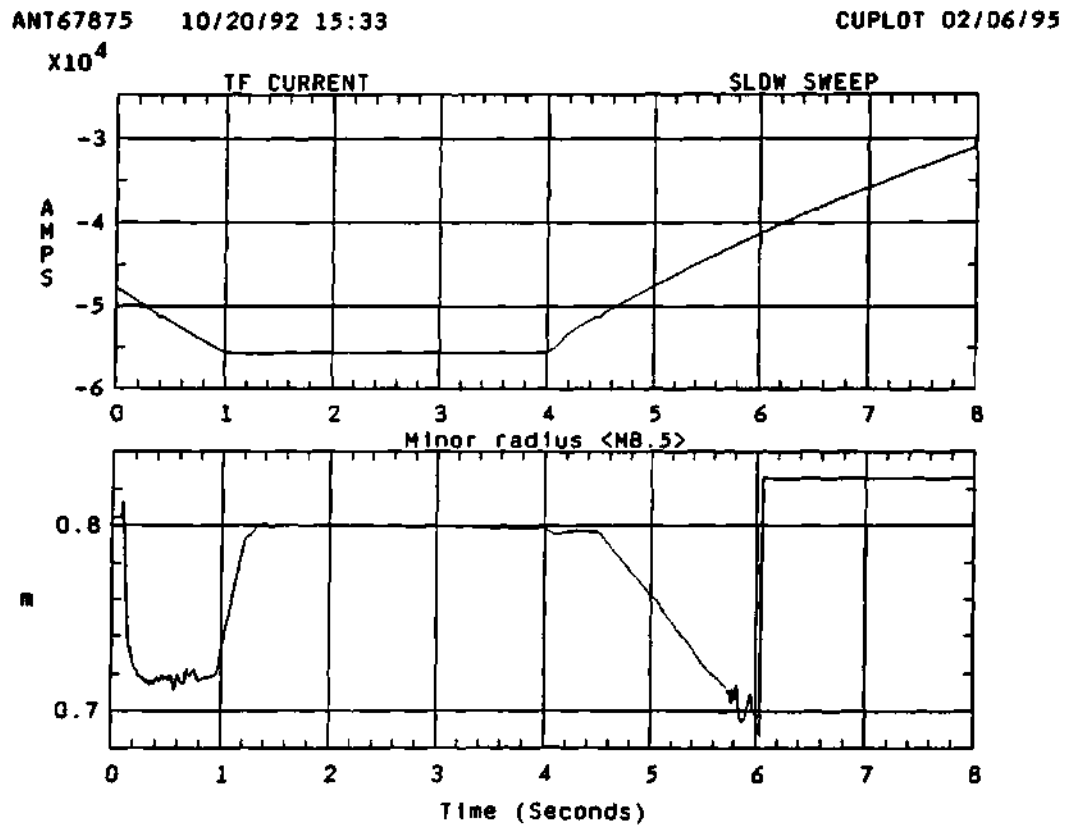


Figure 8.3: Plots of the toroidal field current (upper plot) and the minor radius (lower plot) for plasma shot 67875.

that the MIRI and the reflectometer profile do not agree very well at the far edge of the profile. This is because the MIRI data channels stop just before  $R \approx 3.5$  m. That means that there is no real data after this radial position of the plasma, and that the MIRI data points after the last data channel are calculated from an assumed edge density profile model. The reflectometer data can be used to assist or correct the MIRI density profile past the position of the last MIRI channel. This was done by G. R. Hanson.<sup>92</sup> The motivation for the work on this correction to the MIRI data at the edge was the poor resolution of the MIRI at the scrape-off layer. The separation of the MIRI channels is an average of about 16 cm.<sup>309</sup> The scrape-off layer has a decay length of about 2 cm,<sup>309</sup> while the resolution of the MIRI is about  $\approx 16$  cm.<sup>309</sup> Therefore, the MIRI diagnostic can not provide the resolution and accuracy necessary to do loading calculation studies and scrape-off layer studies.

**Operation at 4.8 Tesla** For high field operation at 72 Kamps ( $B_0 = 4.8$  Tesla) the dynamic range of the probing beam is reduced because the first cutoff is at a much higher frequency. This can be seen from Figure 8.5 where the cutoffs for a model high density plasma are shown, while Figure 8.6 shows the amplitude of a high magnetic field plasma. For the real data the first cutoff starts at a frequency of about 100 GHz as predicted by the contour plot of Figure 8.5. That is, the reflectometer data in Figure 8.6 seems to show a similar trend, since there is very little signal for the frequencies below 100 GHz and a sudden increase in the signal level for signals over 100 GHz. This step function form of the signal level is because for frequencies below the first cutoff of the plasma the separation between the first harmonic and the reflection layer is so small (because of the low local density) that considerable part of the wave can penetrate to the first harmonic layer (through Budden tunneling and exponential decay of the wave at

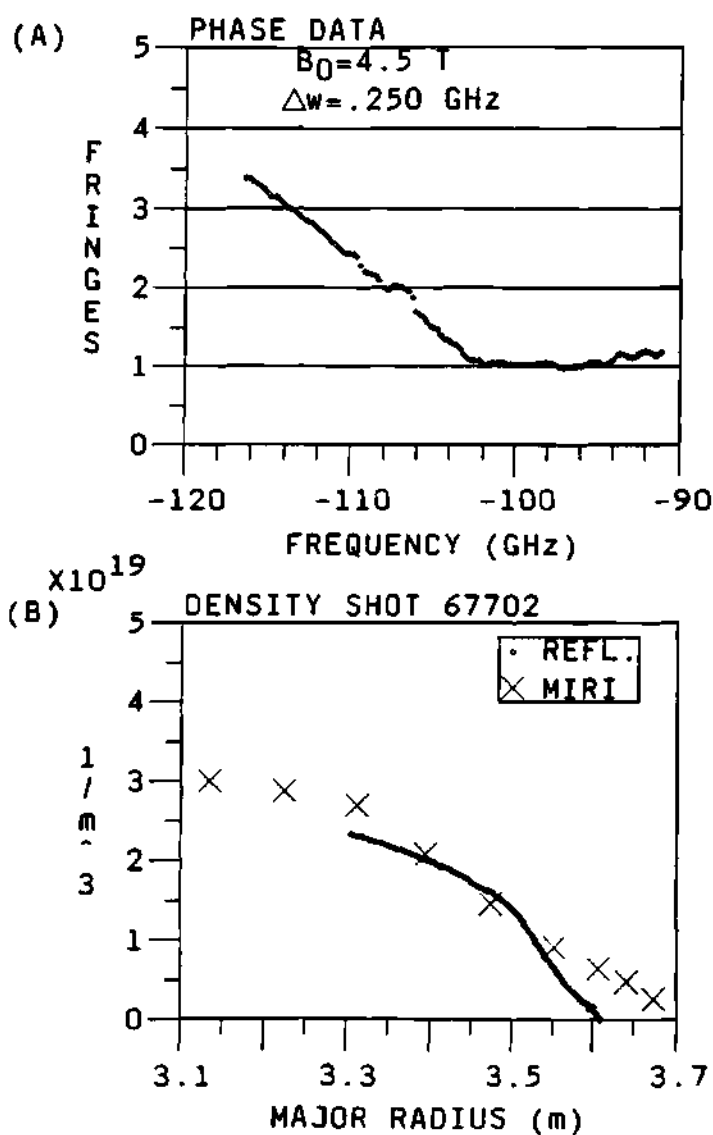


Figure 8.4: (A) Phase data for a typical 67 Kamps ( $B_0 = 4.5$  Tesla) shot, with (B) the corresponding reconstructed density profile.

the evanescent region) and be absorbed or lost in the plasma.

The calculated phase for frequencies below 100 GHz is meaningless and looks rather random when plotted in a Zebra type plot. The phase data and corresponding density profile for the data in Figure 8.6 is shown in Figure 8.7 together with the MIRI density profiles for comparison.

### 8.2.2 Plasma radial scan

An interesting test of the reflectometer can be done when the data for different plasma edge positions are studied together. For this study plasmas with edge positions at  $R_{edge} = 3.30, 3.35, 3.45,$  and  $3.50$  m have been selected. These are shown in Figure 8.8. The plasmas are Neutral Beam Injection (NBI) plasmas ( $P_{NBI} \approx 22.5$  MegaWatts) with a magnetic field of  $B_0 \approx 4.5$  Tesla and maximum central density of  $n_{e0} \approx 5.0 \times 10^{19} \frac{\text{part}}{\text{m}^3}$ . With a shift of the plasma edge, the frequency of the first cutoff will be moved to the center part of the range. This can be observed from the data as the frequencies for the first cutoffs become 102, 100, 97.5 and 95 GHz respectively. From the figures it can be noticed that the phase difference data follows a similar shape, that is, it has well defined and flat floor or minimum at the central part of the frequency band, and past a certain frequency the phase data increases linearly for the upper part of the frequency band. Nevertheless, the phase difference data sets are not exactly the same, but they show a vertical and horizontal displacement. The vertical displacement on the phase difference data is due to the extra amount of length that the probing beam has to travel in order to reach the position of the cutoffs. The horizontal displacement is due to the higher magnetic field at the positions of the cutoffs. That is, at the limit of zero density the cutoff frequency is very close to the electron cyclotron frequency of the plasma, then the frequencies for the first cutoffs will have to be higher for the smaller size plasmas than for the full size plasmas.

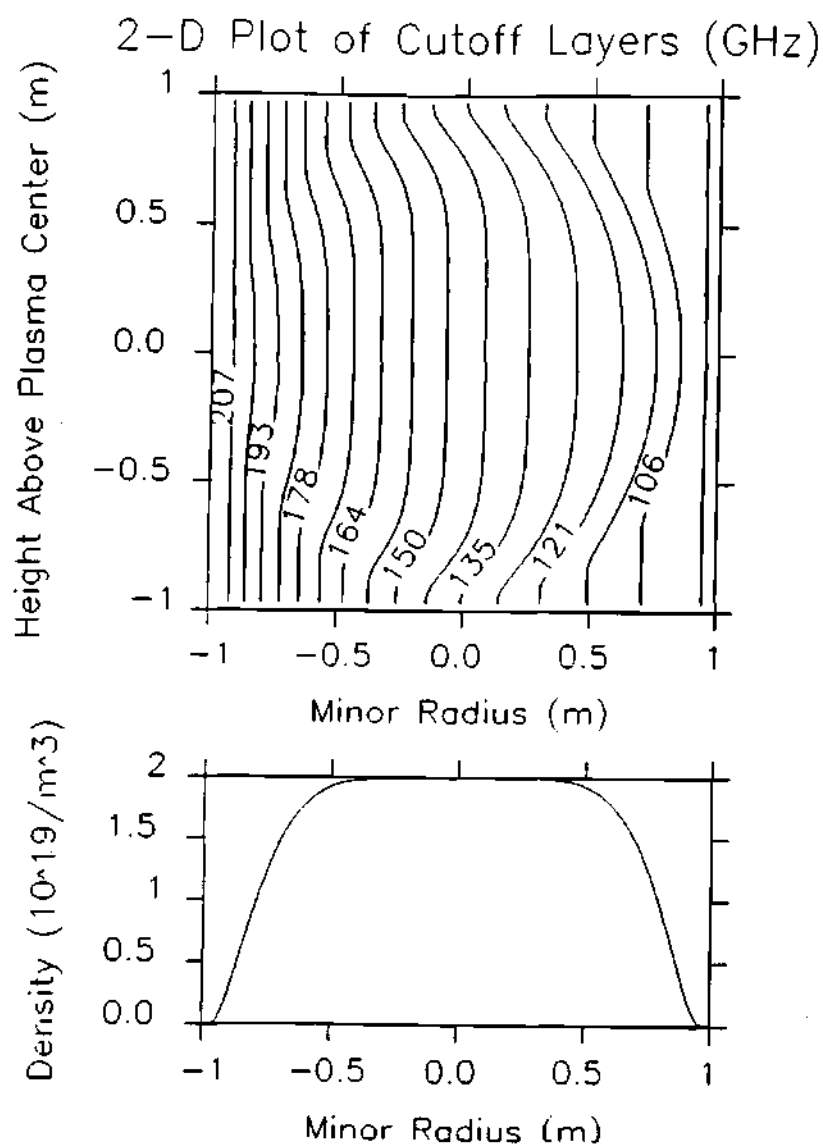


**Figure 8.5:** Contour plot of the reflection layers for a high magnetic field modeled plasma and the center plane line density. Magnetic field is  $B_0 \approx 4.8$  Tesla and the profile model is the typical  $n_e \propto \left(1 - \left(\frac{z}{a}\right)^\alpha\right)^\beta$  profile, where  $\alpha = 6$  and  $\beta = 2$ .

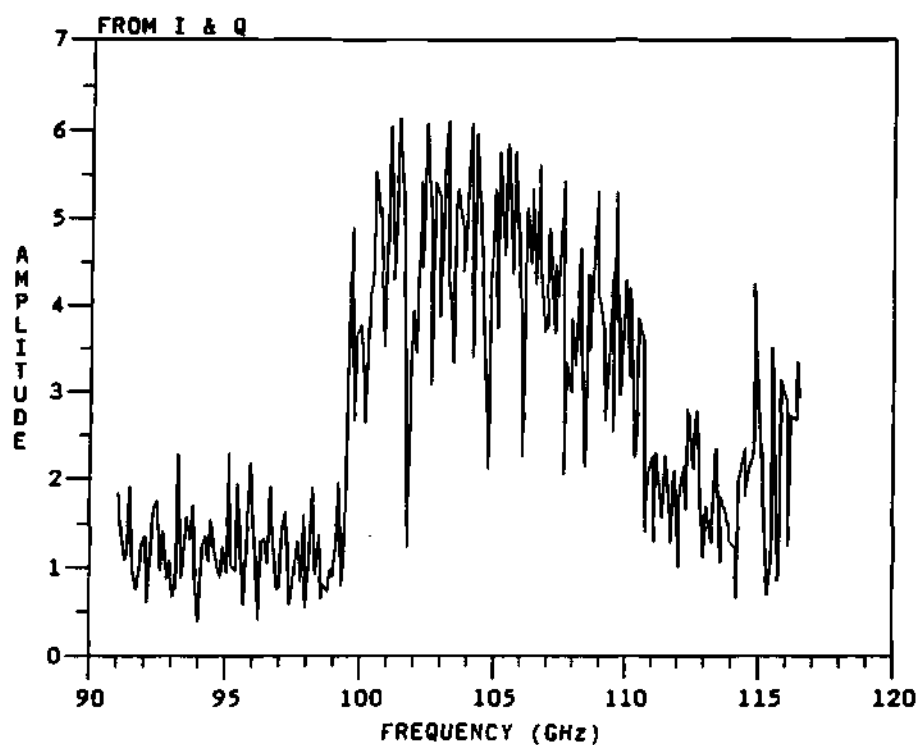


**Figure 8.6:** Signal level for a high magnetic field plasma ( $B_0 \approx 4.8$  Tesla). Notice how the signal level increases rapidly just before 100 GHz.



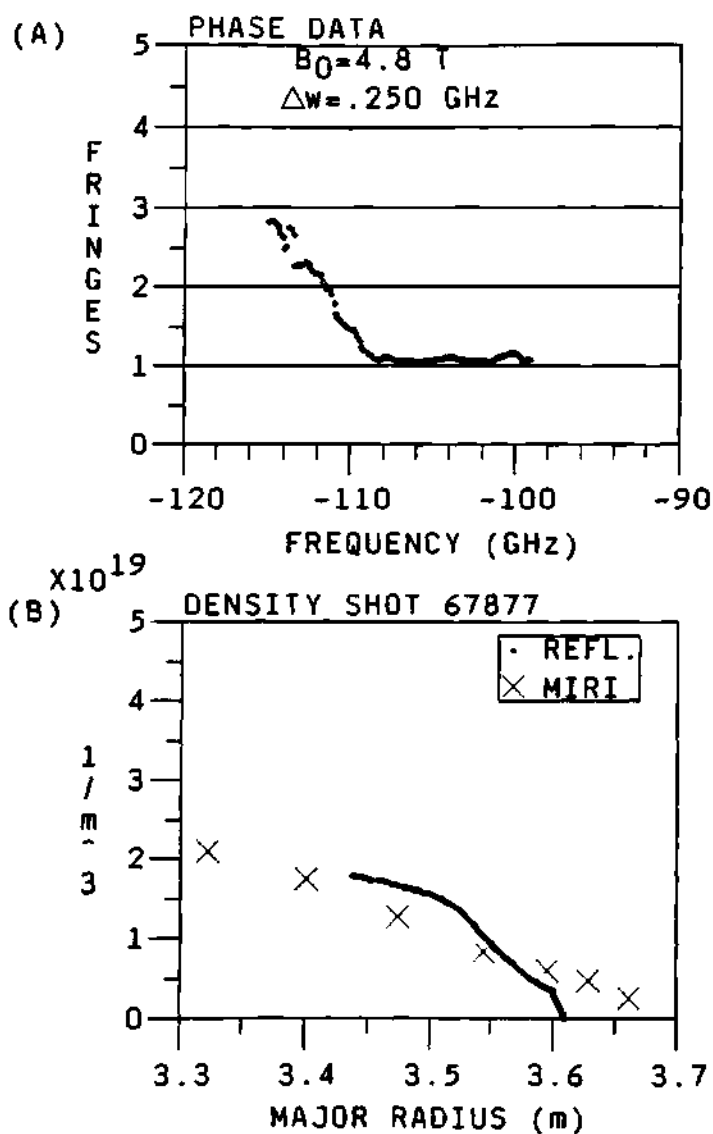


Figure 8.7: (A) Phase difference data and (B) corresponding reconstructed density profile for a plasma with a toroidal field current of  $I_{tf} = 72 \text{ Kamps}$  ( $B_0 = 4.8 \text{ Tesla}$ ) shown before.

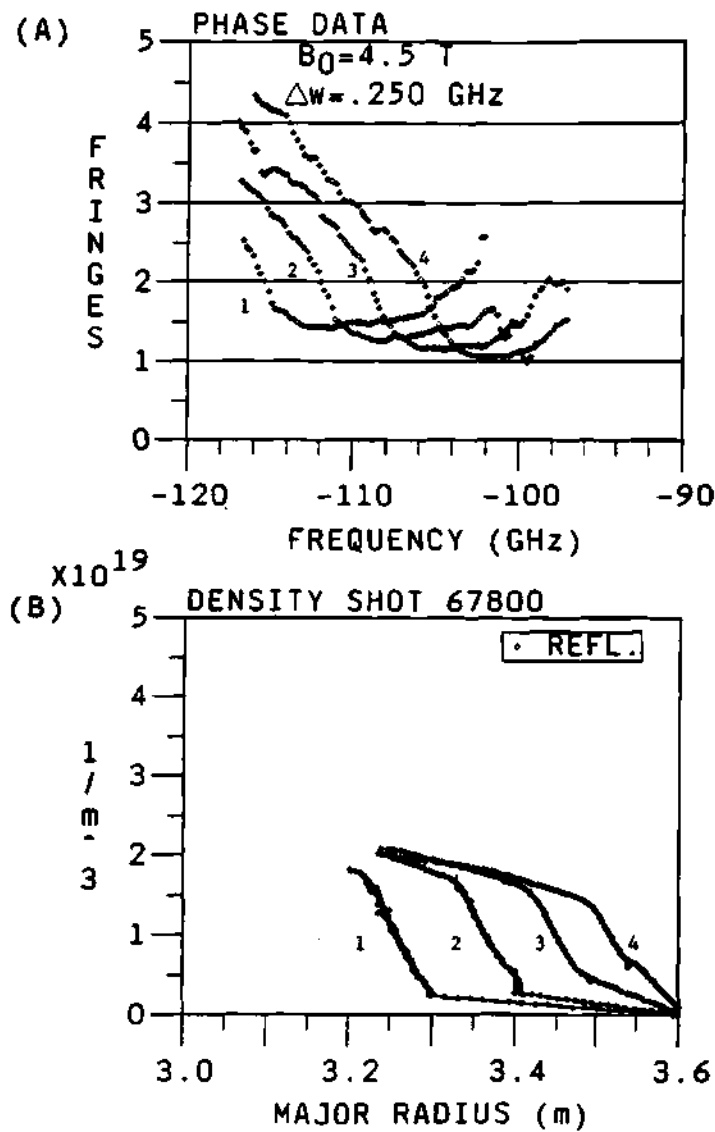


Figure 8.8: (A) Phase difference data and (B) corresponding reconstructed density profile for  $R_{edge} = 3.30, 3.40, 3.50,$  and  $3.55 \text{ m}$  (corresponding to curves 1, 2, 3, and 4 respectively).

### 8.2.3 Central density scan

Another interesting experiment is the central density scan of the plasma. For this density scan, the data for shots of plasmas with different central densities were studied and compared. The central density of the plasma was changed by adjusting the power of the Neutral Beam Injection (NBI) system, from 0 to 27 MegaWatts of beam power. These shots are presented in Figure 8.9. The shape of the phase data is similar for all plasma shots, except for the Ohmic heated plasma ( $P_{NBI} = 0$ , shot 67827) where the central density is significantly smaller than the central density for the other three plasma. Thus, the corresponding phase is larger at the corresponding high frequency part of the band for the Ohmic plasma. The behaviour of the phase is similar to the one predicted and described using the modeling program in section 6.4.2. That is, as the central density increases, the minimum value of the phase difference data decreases and the phase difference data is shifted to the right in the direction of the higher frequencies of the band. It can be noticed too, as expected, that the probing range and the penetration of the probing beam is much greater for the low density plasma in Figure 8.9 than for the high central density plasmas.

### 8.2.4 Effect of the ICRH

The main purpose of the phase difference reflectometer was to measure the changes in the plasma edge due to the power deposition of the ICRH antenna. As discussed previously, the ICRH power can change the density profile in front of the antenna. The change of the density profile will induce a change on the loading and coupling of the power to the plasma. By making a direct measurement of the density profile in front of the antenna, the maximum loading and coupling to the plasma can be calculated, which can be used to help maximize the power deposition in the plasma.

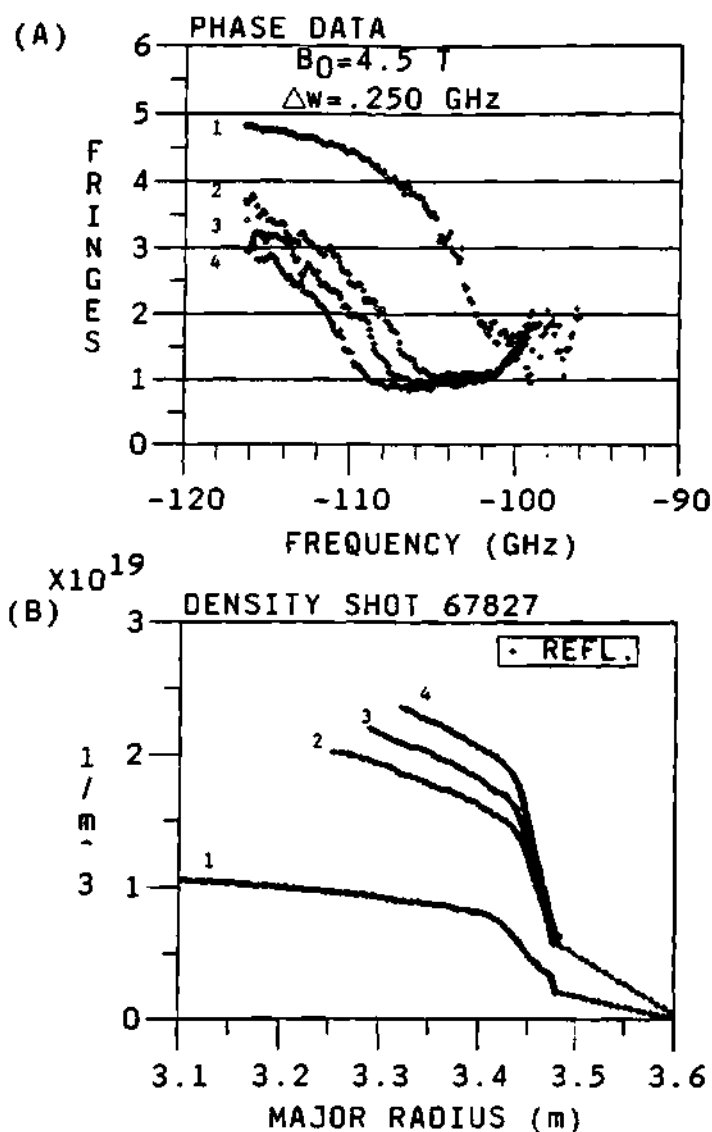
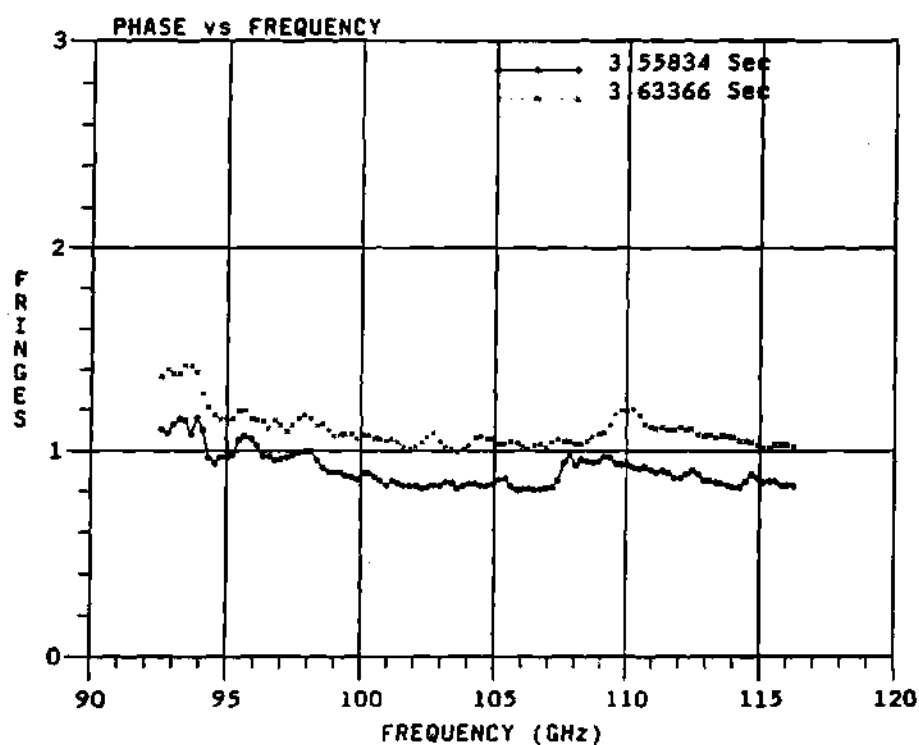


Figure 8.9: (A) Phase data and (B) corresponding reconstructed density profiles for a plasma with central density of  $\approx 2.0, 4.0, 4.5$ , and  $6.0 \times 10^{19} \text{ part/m}^3$ . NBI power is  $P_{NBI} \approx 0.12, 22$ , and  $27 \text{ MegaWatts}$  (corresponding to curves 1, 2, 3, and 4 respectively).

The phase data and corresponding reconstructed density profile during the modulation of the ICRH power are shown in Figures 8.10 and 8.11, with the ICRH power injected to this plasma shown in Figure 8.12. For this particular plasma the ICRH power was modulated as a *square wave* with a maximum amplitude of  $\approx 2.4$  Megawatts and a minimum amplitude of  $\approx 1.2$  Megawatts. The reflectometer covered a time from 3.55 sec to about 3.67 sec. During this time interval the reflectometer collected data for 4 of the step functions of the ICRH power. There was no significant change of the phase data due to the modulation of the ICRH power, as shown in Figure 8.10. The same is true for the reconstructed density profile shown in Figure 8.11, i.e., there is no significant change of the reconstructed density profile due to the modulation of the ICRH power on the plasma. The target plasma for this shot is a typical high density super shot plasma with a steep edge profile at  $R \approx 3.60$  m and a central density of  $n_{e0} \approx 7.0 \times 10^{19}$  part/m<sup>3</sup>. These results can be interpreted to mean that there were no global changes of the density profile due to the ICRH power in the density region covered by the reflectometer frequency beams. If there were any changes they must be local to the area in front of the ICRH antenna and can not be measured from the position of the reflectometer during the first phase of the project. Another possibility could be that the change is too small to be detected at the first position of the reflectometer or that the change is confined to the lower end of the frequency band of the reflectometer, that is, for frequencies less than 92 GHz. The amount of ICRH power deposited in the plasma can have an effect on the magnitude of the induced change on the plasma edge also. It might be necessary to go to higher ICRH powers to be able to see any measurable global change in the plasma edge.



**Figure 8.10:** Plot of the phase difference during an ICRH modulation. The curves have been separated by adding a constant offset of 0.2 fringes in order to distinguish them.

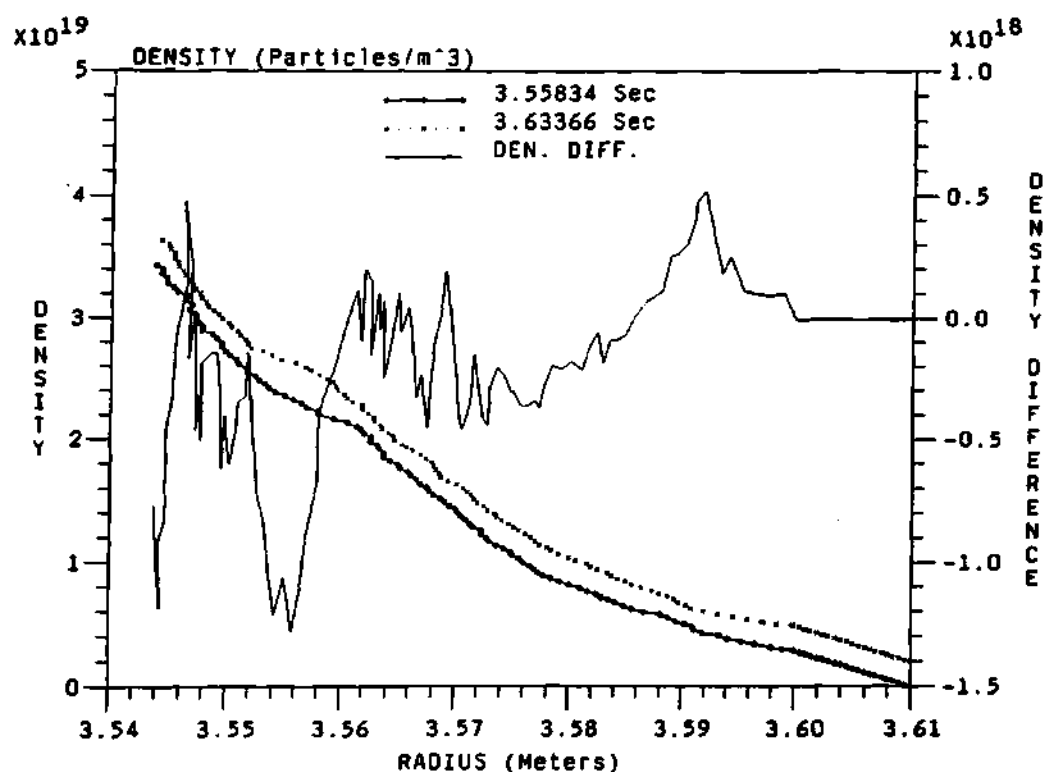


Figure 8.11: Plot of the reconstructed density profile using the phase data in the previous figure. Curves have been separated by adding a constant offset of  $0.2 \times 10^{19} \frac{\text{particles}}{\text{m}^3}$  in order to show the different curves and show any changes in the profiles. As the legend shows, the solid line is the difference between the two curves.

ANT69345 11/08/92 16:30

CUPL0T 08/15/95

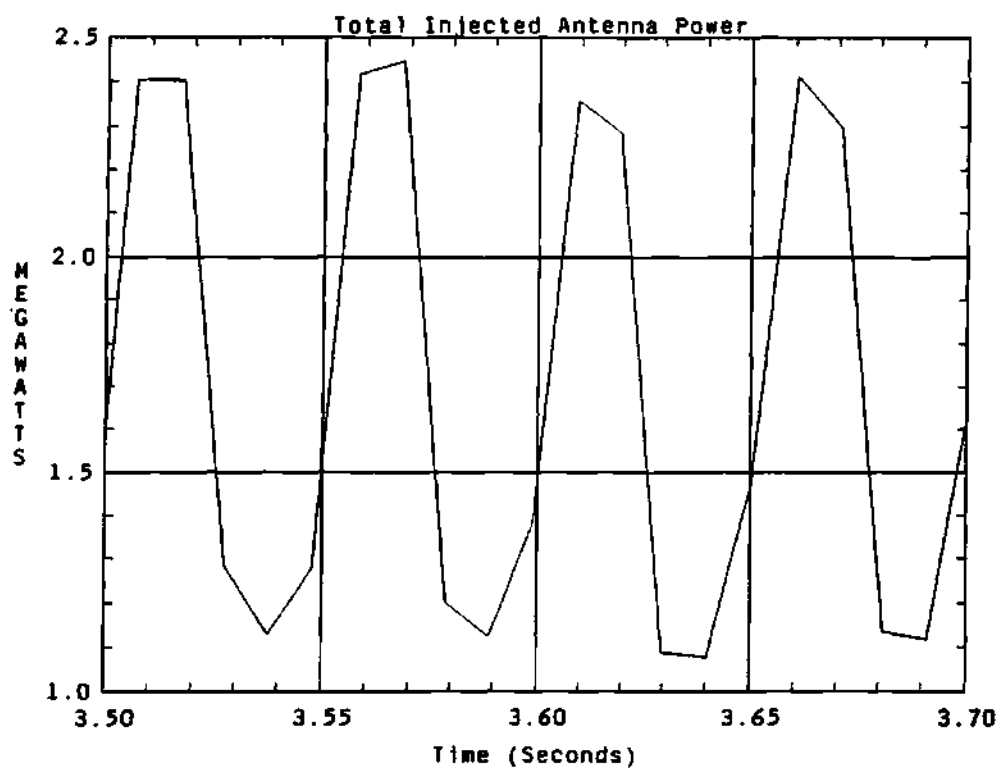


Figure 8.12: Plot of the ICRH power deposition on the plasma for the time interval of the reflectometer.



### 8.2.5 Conclusions of phase I

During the phase I of the reflectometer project the diagnostic was installed on the fluctuation reflectometer waveguide system of TFTR and tested under different scenarios and plasma conditions. From this testing phase of the project it can be safely concluded that:

1. Data during different magnetic field strengths and plasma scenarios was collected and analyzed, showing good agreement with the results and predictions of the modeling code.
2. Verification of the phase difference dynamic range of the real data with the model was observed.
3. A radial scan of the plasma was observed and analyzed to compare the observed response of the reflectometer's phase difference data and that predicted by the modeling code. The real data and the modeled data showed very similar behavior.
4. A central maximum density scan was observed and analyzed to compare the resulting response of the reflectometer's phase difference data with that predicted by the modeling code. The response of the real phase difference data was very similar to the modeled phase difference data.
5. The phase difference data during ICRH plasmas was searched for a possible induced change in the plasma edge density profile. No measurable change was observed at the position of the reflectometer.
6. The reflectometer completed the first phase or the proof of principle phase of the project successfully and it was moved to the ICRH antenna position.

### 8.3 Results of Phase II

With the beginning of TFTR's D-T operation in November 1993, a new phase of reflectometer operation began. For this new data the reflectometer used the waveguide launcher located at the center of the ICRH antenna at bay-K and built specifically for the purpose of measuring the edge density profile in front of the ICRH antenna. This data and its corresponding results are presented and discussed next.

#### 8.3.1 Initial data

Since the reflectometer was moved to a new location, a test to make sure that it worked properly was necessary. This was done by taking data during Ohmic shots, clean-up plasma discharges and test plasma shots used to test and calibrate the many other diagnostics of TFTR. For some of these test shots the plasma was jogged in the major radial direction with the purpose of assisting some of the diagnostics in their calibrations. The jog of the plasma took  $\Delta t_{jog} = 0.1$  sec and it was moved from  $R \approx 3.62$  m to  $R \approx 3.50$  m within this time interval, as can be seen in Figure 8.13. This sudden change of the plasma position provided an excellent opportunity to test the reflectometer, since as the plasma moved away, so did the reflection layers of the reflectometer, thus providing a fast and measurable change of the phase difference data. An example of the changes of the phase difference data due to the jog of the plasma is shown in Figure 8.14 for the same plasma shot as Figure 8.13. For this particular set of data the reflectometer was able to measure one sweep at the center of the jog and two sweeps at each side of the maximum of the jog. These are conspicuously separated on the plot. During the steady state part of the plasma discharge the plasma edge is at  $R \approx 3.62$  m and it is represented by the step in the phase data at Figure 8.14, which is at

the lower end of the frequency band. As the plasma edge starts moving into the radial direction, so do the reflection layers of the plasma. The new location of the reflection layers and the plasma edge will cause the step on the phase data to be shifted to the higher frequency part of the band, as seen in Figure 8.14. As the plasma edge reaches its minimum radial position the phase data shift reaches its maximum and the plasma as well as the phase data start traveling to their corresponding steady state position.

A problem with the timing of digitizer B was discovered thanks to this jog in the plasma. Digitizer B was set to look at the time interval around the jog with a high frequency of digitization, i.e., 0.5 MHz, starting at 3.4 sec, so that a detailed phase data sweep of the jog of the plasma could be obtained. Digitizer A was set at 0.1 MHz starting at 3.0 sec, so that it could take data during most of the steady state part of the plasma shot. Digitizer A showed the effect of the plasma jog, while digitizer B did not show the expected change in the phase data. A careful inspection of the digitizers showed that these were triggered both at the trigger time of digitizer A. So that the data in digitizer B was for the plasma starting at 3.0 sec and not at 3.4 sec. The problem was corrected immediately. Clearly these kinds of test are useful for verifying the reflectometer operation.

### **8.3.2 Effect of the ICRH on the plasma edge**

The initial and main purpose of the Dual Frequency Phase Difference reflectometer was to study the effect of the ICRH deposition on the edge of the plasma. This was done for different plasma scenarios and configurations. The reflectometer phase difference data showed a small, but clear and consistent change at the very low end of the frequency band of the phase difference data. This corresponds to the very edge of the plasma where the plasma interfaces with the antennas. An example of this effect is shown in Figure 8.15 for a plasma with a

ANT72222 10/12/93 15:51

CUPL0T 02/07/95

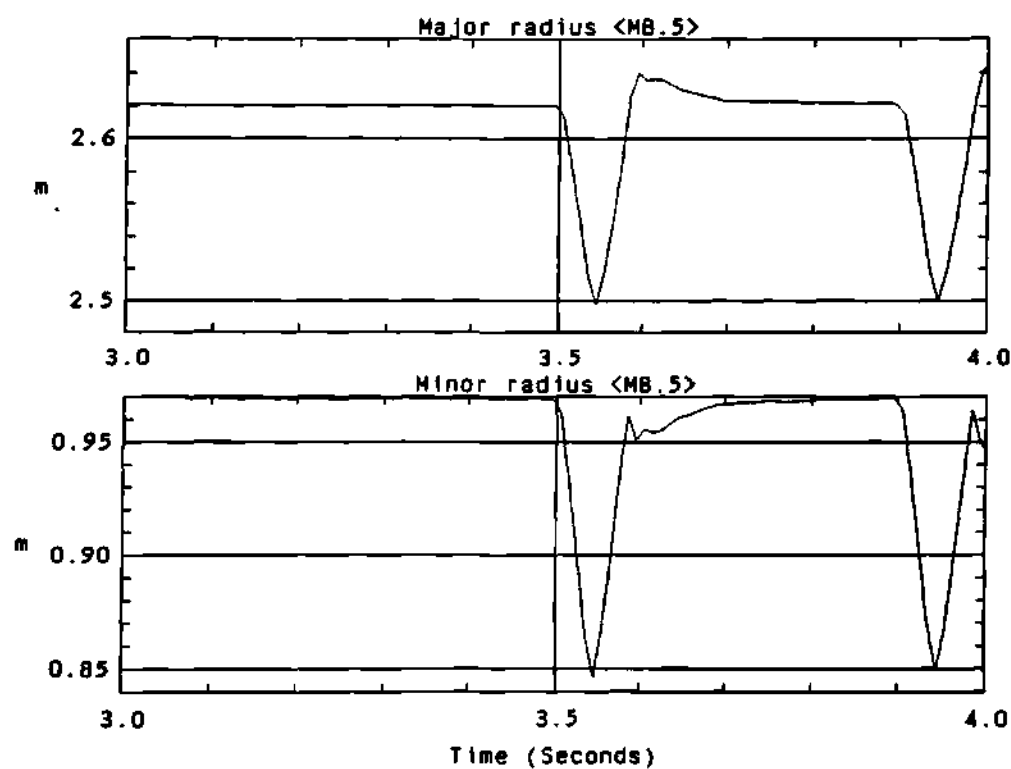


Figure 8.13: Plots of the plasma major and minor radius for the time interval of the jog.

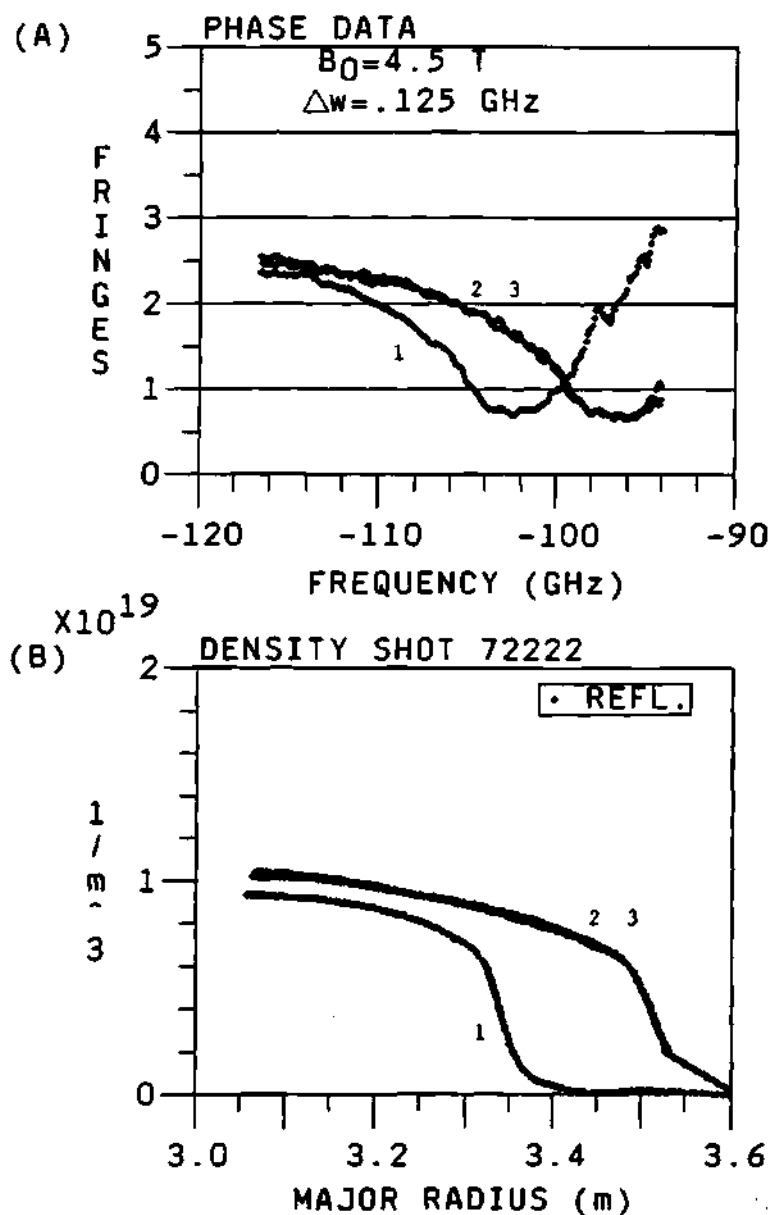


Figure 8.14: (A) Phase data and (B) reconstructed density profile for the time interval of the plasma jog. Data times are before (3.498 sec, curve 2), during (3.548 sec, curve 1), and after (3.598 sec, curve 3). It can be seen that the before (curve 2) and after (curve 3) data are not too different.

magnetic field of  $B_0 = 4.5$  Tesla, a central density of  $n_{e0} = 5.0 \times 10^{19} \frac{\text{part}}{\text{m}^3}$ , and a square wave modulation on the ICRH power with maximum of 2.5 and minimum of 0.5 MegaWatts of power. The data presented in Figures 8.15 and 8.16 show one sweep during the maximum of the square wave and one sweep during the minimum of the square wave, that is, during *on* and *off* times of the ICRH. An enlarged view of the phase difference data and corresponding reconstructed density profile is shown in Figure 8.16. The effect consisted of a small and sudden increase in the phase difference data at the very beginning of the frequency band, as shown in Figure 8.16. This spike on the phase difference data can be due to a displacement of the plasma edge away from the ICRH antenna, that is, the plasma has been pushed away from the antenna during the maximum of the ICRH square wave modulation. This type of behavior of the phase difference and the plasma has been modeled and explained in section 6.4.3. The corresponding reconstructed density profile can be seen in the enlarged plot of Figure 8.16. When plotted at full scale the change on the phase difference data and corresponding reconstructed density profile looks small, but this type of effect was observed during different ICRH and plasmas scenarios and configurations. Therefore, the effect of the ICRH antenna may not be very large and may not go very deep into the plasma, but it seemed to always be present when the ICRH was used.

This case can be compared with its corresponding case during the first phase of the project, when the reflectometer was using the waveguide system of the PPPL fluctuation reflectometer and the probing area in the plasma was away from the ICRH antenna. During the first phase there was no noticeable effect and/or change on the phase difference data due to the ICRH power deposition on the plasma, and at least one reason for this was that the effect was at the frequency range below 92 GHz, where the original reflectometer beam could not probe.

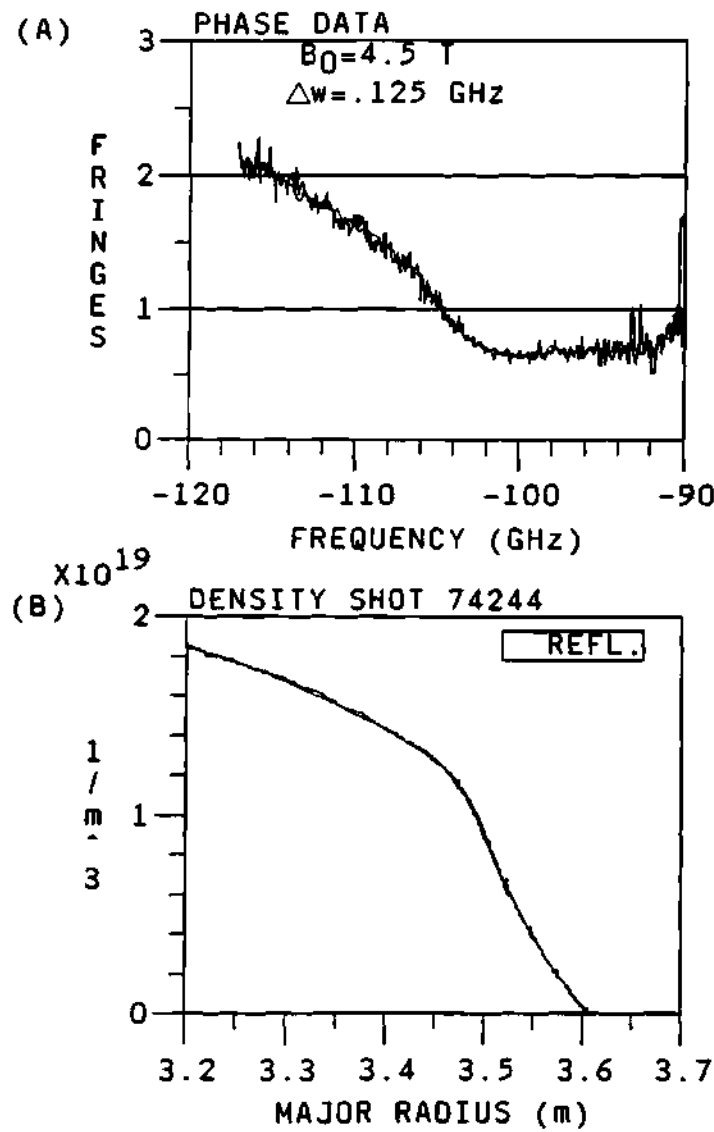


Figure 8.15: Plot of (A) the phase difference data and (B) the corresponding reconstructed density profile for a plasma with a magnetic field of  $B_0 = 4.5$  Tesla and a central density of  $n_{e0} = 5.0 \times 10^{19} \frac{\text{part}}{\text{m}^3}$  during and after the ICRH.

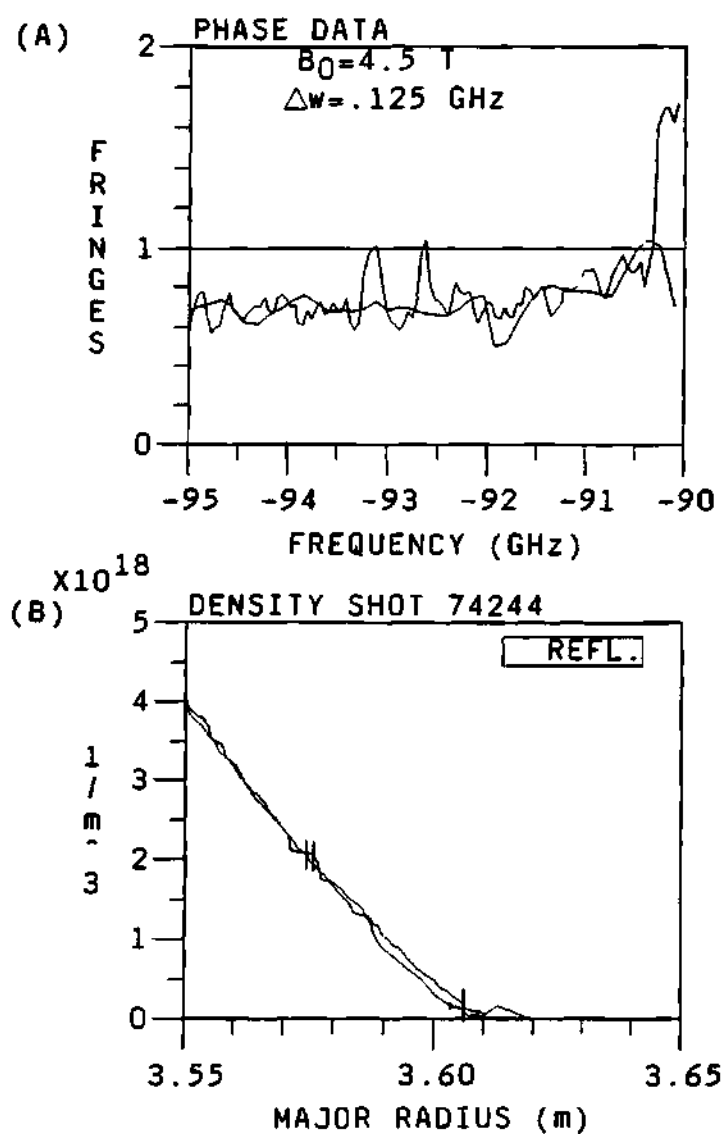


Figure 8.16: Same plot as Figure 8.15, but the lower end of the frequency band and the corresponding far edge of the reconstructed density profile have been enlarge to show the effect of the ICRH on both the phase difference data and the density profile.



### 8.3.3 Conclusions of phase II

For the second phase of the dual frequency difference phase reflectometer diagnostic it can be concluded that:

1. The reflectometer was installed and tested in its new location successfully.
2. First data seems to follow the expectations with respect to phase dynamic range, and reconstructed density profile.
3. Uncertainty due to the position of the first cutoff and the phase offset associated with it has been greatly reduced by using a launcher located at the center of the ICRH antenna.
4. A feature was observed during plasma with ICRH. This feature was small and restricted to the lower end of the frequency band which corresponds to the very edge of the plasma in front of the ICRH antenna, but this is a clear indication that the ICRH deposition of the antenna is pushing the plasma away from the antenna.
5. Considerably more, and varied, experimentation with ICRH will be necessary to understand the cross-influence of the ICRH and edge density on each other.

## 8.4 Summary

This chapter presented some of the results from both operational phases of the reflectometer. These phases were:

1. Phase I: The testing and proof of principle phase. The operation of the reflectometer was tested. Problems and limitations were identified, documented,

and corrected. The reflectometer was used and/or tested during different magnetic fields and density profile scenarios. It was found that the density fluctuations at the edge were at some times large, thus making the tracking of the phase difficult. Smoothing and averaging provide great improvements on the phase data, but it was decided that the best way to reduce the effects of the density fluctuations on the phase difference data was to reduce the frequency separation of the probing beams to half or even a quarter of the original frequency separation. The operation of the reflectometer was tested and verified. It was shown that the reflectometer could provide accurate and high resolution profiles of the density.

2. Phase II: The installation of the reflectometer to a location where it could use the launcher mounted in the ICRH antenna was performed. The frequency separation of the probing beams was reduced in order to reduce the effect of the density fluctuations at the edge of the plasma. During this phase the reflectometer was used to study the effect of the ICRH power on the plasma within the environment of the ICRH antenna. A small effect was observed.

## CHAPTER IX

### SUMMARY

#### 9.1 Discussion

This work presented the development, construction, testing, data acquisition and analysis, and density profile reconstruction of the ORNL Dual Frequency Phase Difference reflectometer for the Tokamak Fusion Test Reactor (TFTR). The first chapter provides an introduction to fusion research, along with a description of TFTR. Chapter two contains a detailed derivation of the formulae required to understand the basics of electromagnetic wave propagation in plasmas and reflectometry theory. The different techniques and approaches used by reflectometry to obtain density information (fluctuations and/or density profiles) were discussed. Chapter three covers the general theory of ICRH and the different phenomena that can induce changes on the plasma edge density. The description of different ICRH antennas used in fusion research was presented. A description and parameters for one of the TFTR antennas was presented. Chapter four presented a description of the dual frequency phase difference reflectometer designed by ORNL for TFTR.

Chapter five presents a discussion of the operation, verification and calibration of the reflectometer system. These include a description of the normal operation of the diagnostic, verification and testing of the system, the absolute bypass loop calibration, and the absolute waveguide run calibration. These operations help verify that the diagnostic is in good working condition.

In chapter six the theory for the modeling of the reflectometer was pre-

sented, together with the different techniques developed to reconstruct the density profile from the phase data and the error and sensitivity analysis for the modeling. Any polynomial or function can be used for the fit of the index of refraction near the cutoff. The standard at the time of the beginning of the project was Doyle's linear fit to the index of refraction near the cutoff. The author developed other methods to improve the fit by using different fits of parabolas, higher order polynomials, and other functions. Nevertheless, it was noticed that the error in the fit did not scale as expected. Further analysis showed that the non-linearity of the index of refraction at the cutoff caused the derivatives to go to infinity. This condition degraded the polynomial fit near the cutoff as the limit of the small step size was taken. For this reason, an accurate method was developed. This accurate method expands the density as a polynomial (instead of the index of refraction), and uses this density expansion in the formula for the index of refraction to calculate the phase.

The modeling program provided a test bed to test some of the novel characteristics of the new reflectometer, such as the phase difference dynamic range, reconstruction techniques, effects of different profiles and magnetic fields strengths, effect of the frequency separation, etc. The maximum limits of the phase difference dynamic range were studied with the modeling code. It was found that the maximum phase difference value for  $\Delta\omega = 0.250$  GHz was 6 fringes and for  $\Delta\omega = 0.125$  GHz was 3 fringes. This showed that the dynamic range of the phase difference and the separation between cutoffs scaled linearly with the frequency separation of the probing beams. This was the first proof that the effects of fluctuations could be reduced by reducing the frequency separation between probing beams. A sensitivity and error analysis of the reconstruction technique was done to study the effect of systematic errors in the absolute phase difference calibration, to simulate systematic errors in the frequency calibration and the error in

the magnetic field, random error and fluctuations on the phase data, and phase noise, etc.

Chapter seven presents the methods and techniques used for the data analysis of the real measured phase difference data from the reflectometer. The smoothing and averaging methods developed to analyse the data and extract the phase difference data was presented. It was found that smoothing and averaging provides a great improvement in noise reduction in the data. A description of the data analysis and the density reconstruction programs were presented. The error analysis for the data and the procedures used to reduce the errors were presented. It was found that the systematic errors dominate the error propagation in the reconstructed density. Nevertheless, these errors are not important when comparing adjacent profiles from the same plasma shot or similar plasma shots on the same day. A procedure to calculate the effect of the systematic errors was developed and explained.

Chapter eight presents some of the data from both operational phases of the reflectometer, i.e., during the testing and proof of principle phase, and during the final phase where the reflectometer launcher was in front of the ICRH antenna. Data from different plasma scenarios was presented, such as different magnetic field strength, different plasma central density, different plasma edge position. This data compared favorably with the modeling data for similar density profiles. During the proof of principle phase, it was found that the level of fluctuations on the data was somewhat high at the lower end of the frequency sweep (corresponding to the edge of the plasma), and it randomized the phase data for those frequencies. While this in general was not a serious problem and could be overcome in most cases by smoothing the data, it was decided to reduce the frequency separation of the probing beams from the original 0.250 GHz (for phase I) to 0.125 GHz (for phase II) in order to reduce and/or eliminate fluctuations on

the phase data during the second phase of the project. The effect of the ICRH on the plasma edge was shown. The change of the density profile due to the ICRH was very well localized to the area in front of the antenna. Data from both phases of the project is presented in this chapter.

In the appendices a discussion of the theory of Gaussian beam optics for lasers and of Gaussian beams in a plasma is presented. This theory is of importance to this work because during the first phase of the project, the reflectometer was using the TFTR fluctuation reflectometer waveguide system. This system uses a set of parabolic mirrors to direct and focus the highly localized Gaussian beam of the waveguide. Thus, this theory is used to calculate the intersection area or cross section of the beams such that an idea of the signal amplitude for the reflectometer can be estimated.

The programs used for the modeling, data analysis, phase extraction, and density profile reconstruction are presented and discussed in the appendices.

## **9.2 Important Results and Accomplishment**

The important results from the thesis are summarized below. These are extensively covered and explained in chapters IV to chapter VIII. The corresponding sections and chapters are referenced in every item.

- A program was written to model the propagation of the probing beams in the plasma (section 6.3) and to test the many different reconstruction techniques developed to reconstruct the density profile (sections 6.2 and 6.2.2). Some of these techniques are:
  1. The trapezoidal technique by Doyle (section 6.2.1).

2. The parabolic fit with non-equal step size (sections 6.2.2).
  3. The parabolic fit with equal step size (section 6.2.2).
  4. The parabolic fit with derivative condition (section 6.2.2).
  5. The accurate (density expansion) method (section 6.2.5).
- The development of an accurate method for calculating the reconstructed density, limited in accuracy only by the chosen stepsize and the round-off error in the computer, was presented (section 6.2.5). This accurate method uses a parabolic expansion of the density to calculate the phase near the cutoff position and reconstruct the density profile.
  - The propagation of error in the reconstruction techniques was extensively studied and developed (sections 6.2.3 and 7.4). It was shown that previous methods of reconstruction, including both Doyle's method and the parabolic methods, have significant calculational errors, exceeding 10%. This error is caused by the impossibility of fitting any integer degree polynomial to the index of refraction at the cutoff, where the slope of the index of refraction is infinite (section 6.2.3).
  - A careful and correct calculation of the error bars for reflectometry, including the effects of Gaussian smoothing and of averaging, was performed (section 7.4). The smoothing and averaging provides a significant reduction in noise and error, and improves the phase tracking.
  - A comparison between the phase data obtained using the new phase difference reflectometer and the modeling was performed for different plasmas (section 8.2). Good agreement was found, which gives confidence in the operation of the reflectometer and equations used to make the physical model used for the reflectometer.

- It was demonstrated that if the cutoff layer separation of the two probing frequencies for the reflectometer is small compared to the density fluctuation correlation length, then the phase fluctuations are greatly reduced (section 6.4.8). This is in comparison with the case when the cutoff separation distance is the same order as or larger than the density fluctuation correlation length. Reduction of phase fluctuations by reducing the cutoff layer separation distance was experimentally verified when the frequency separation of the two probing beams for the reflectometer was reduced from 0.250 GHz to 0.125 GHz. The expected factor of 2 reduction in phase fluctuations was observed, resulting in a more accurate profile (section 8.3).
- The reduction in phase fluctuations observed when the cutoff separation distance is small compared to the density fluctuation correlation length is in agreement with the results of the modeling code (section 6.4.8).
- It was demonstrated that it is possible to measure the electron density profile in the edge region of a high field tokamak where the density fluctuations are large (chapter VIII).
- One effect of the ICRH on the plasma edge was first observed and studied with this new reflectometer (section 8.3). It was observed that the plasma was being pushed away from the antenna during the ICRH operation.

### 9.3 Suggestions for Future Work

The reflectometer at TFTR was designed to study the edge of the plasma, but under some plasma configurations, it can probe the inner part of the profile. Therefore and in principle, it can be used to study the plasma away from the edge.



Some work can be done to find better and faster ways to do the reconstruction of the profile, so that the reconstruction can be done on a real time basis. The main problem to overcome is the non-linearity of the index of refraction at the cutoff. This non-linearity renders any polynomial fit as inefficient near the cutoff and it is the single biggest source of error for any polynomial fit attempted. This forces the more time consuming but accurate density expansion technique.

Further work can be done to reduce the frequency separation between the probing waves. This will improve the reflectometer and the phase data in two ways. First, it will reduce the effect of fluctuations on the phase data allowing for easier, faster and more effective ways to track the phase data. Second, it will reduce the phase dynamic range. For the original system with  $\Delta\omega = 0.25$  GHz the phase dynamic range was about 6 fringes. The modeling showed that the scaling between the frequency separation and the phase dynamic range was the same. Therefore, by reducing the frequency separation by  $\frac{1}{6}$  the phase dynamic range of the data can be reduced to 1 fringe. With a 1 fringe dynamic range system the phase is uniquely determined and there is no need to track the phase and there is no ambiguity due to the discontinuity of the inverse tangent function.

Some work needs to be done to determine an efficient way to reduce the systematic errors due to the uncertainty on the position of the first cutoff and the offset phase of the data. A new waveguide system can be designed and built that will provide with a full waveguide run calibration automatically on every shot.

There has been no proof that the assumptions on the density profile before the first cutoff are optimal. That is, are there other assumptions that will give a better reconstructed profile?

The reconstruction techniques developed in this thesis and explained in chapter 6 can be applied to other types of reflectometers, such as full phase reflectometry and AM reflectometry.

## APPENDIX A

### GAUSSIAN BEAM OPTICS

#### A.1 Introduction

During the first testing phase, the dual frequency reflectometer used TFTR's reflectometer setup.<sup>38</sup> This consists of the waveguide, reflecting mirrors, and focusing mirrors. It was designed for probing highly localized fluctuations at the center of the plasma. This system uses focused Gaussian beams, as shown in Figure A.1, which intersect at the plasma midplane. Figure A.1 shows the gaussian beams as it propagates through the mirror system. The plot has the TFTR major radius coordinate system plotted on the top of the plot, and the parameters for the crossing of the beams can be calculated from the figure. The vacuum windows are located at  $R \approx 400$  cm. The crossing has a maximum diameter of  $\approx 6$  cm, and an intersection length of  $\approx 60$  cm. The wave frequency is 100 GHz and the intersection angle is  $9.75^\circ$ . Because of the optical nature of this setup, an understanding of general optics and Gaussian optics (which governs the propagation of the beam) is necessary. The development of the theory and corresponding formulae has been done in the field of laser beams and resonators. Therefore, a discussion of laser optics and Gaussian beams will be presented from the point of view of laser beams and resonators, but with direct application to the propagation of the reflectometer beam through TFTR's setup. Before continuing, it should be made clear that the words *laser beam* and/or *reflectometer beam* and/or *microwave beam* will be used as synonymous throughout this appendix.

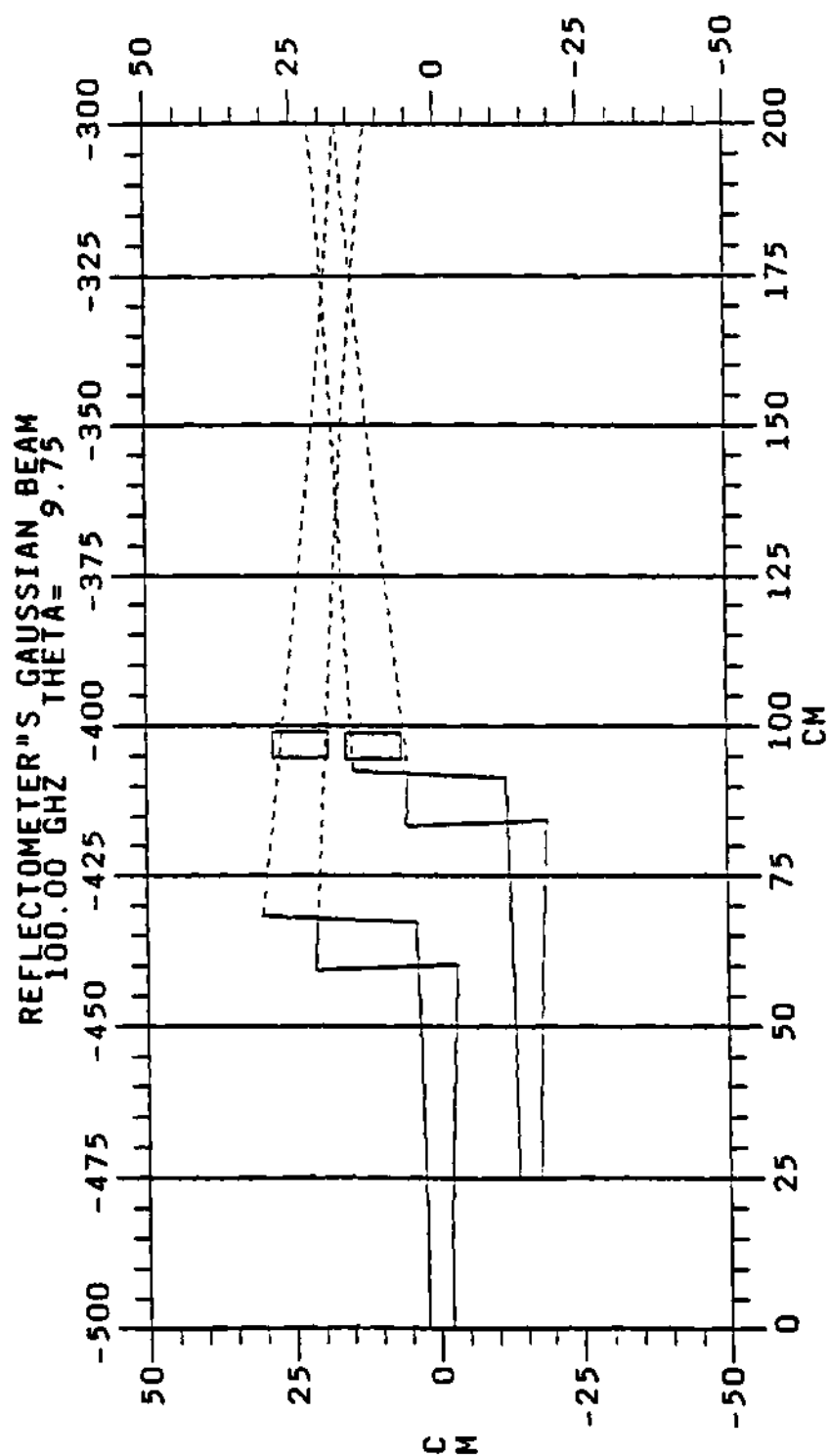


Figure A.1: Calculated TFTR's beam geometry and intersection inside the vacuum chamber.

## A.2 Pre-History of Lasers

The idea of the laser resonator originated when R. Dicke,<sup>263</sup> A. Prokhorov,<sup>264</sup> and A. L. Schawlow and C. H. Townes,<sup>265</sup> independently proposed the use of the Fabry-Perot interferometer as a laser resonator. The modes of propagation of such a structure as determined by diffraction effects was first calculated by A. G. Fox and T. Li.<sup>266,267</sup> G. D. Boyd and J. P. Gordon,<sup>268</sup> and G. D. Boyd and H. Kogelnik,<sup>269</sup> developed the theory for a resonator with spherical mirrors and approximated the modes by wave beams. The concept of electromagnetic wave beams was also introduced by G. Goubau and F. Schwering,<sup>270</sup> who investigated the properties of sequences of lenses for the guided transmission of electromagnetic waves. Another treatment of wave beams was given by J. R. Pierce.<sup>301,272</sup> The behavior of Gaussian beams as they interact with various optical structures has been analyzed by G. Goubau,<sup>273</sup> H. Kogelnik<sup>274</sup> and others.<sup>275</sup>

## A.3 Paraxial Ray Analysis

The study of the propagation of paraxial rays through an optical system with resonators, transmission lines (TFTR's setup in our case), and other similar structures can reveal many important geometrical properties of the system, such as the optical stability of the structure (resonators)<sup>269</sup> and the loss of unstable resonators.<sup>276</sup> The propagation of a paraxial ray and/or of a Gaussian beam through one or more optical structures can be described by the use of ray transfer matrices. The development of H. Kogelnik and T. Li<sup>295</sup> will be followed here. A more detailed treatment of ray propagation can be found in Born and Wolf,<sup>296</sup> W. Brower,<sup>277</sup> and others.<sup>278,279</sup>

### A.3.1 Ray transfer matrix

A paraxial ray in an optical system is characterized by its distance,  $x$ , with respect to the optic  $z$ -axis of the system and its angle or slope,  $x'$ , with respect to the axis of the system, as is shown in Figure A.2.<sup>274</sup> The slope,  $x'$ , is assumed to be small. The optical path of the ray depends on the characteristics of the optical system as well as the initial position and slope of the ray, i.e.,  $(x, x')$ . Assuming that the optical system has linear response, then the output ray in terms of the input ray can be expressed as a matrix times a vector type of equation, that is:

$$\begin{pmatrix} x_2 \\ x_2' \end{pmatrix} = \begin{pmatrix} A & B \\ C & D \end{pmatrix} \cdot \begin{pmatrix} x_1 \\ x_1' \end{pmatrix} \quad (\text{A.1})$$

where the ABCD matrix is called the ray transfer matrix and is defined such that its determinant is equal to unity:

$$\begin{vmatrix} A & B \\ C & D \end{vmatrix} = AD - CB = 1 \quad (\text{A.2})$$

This can be used to express the ray transfer matrix in terms of any 3 given parameters.

The elements of the ray transfer matrix can be related to the focal length,  $f$ , and the location of the principal planes of the system by the formulas:

$$f = \frac{-1}{C} \quad (\text{A.3})$$

$$h_1 = \frac{D - 1}{C} \quad (\text{A.4})$$

$$h_2 = \frac{A - 1}{C} \quad (\text{A.5})$$

where  $h_1$  and  $h_2$  are the distances of the principal planes from the input and output planes as shown in Figure A.2. The transfer matrixes of six elementary optical structures are presented in Table A.1.<sup>295</sup> They represent the following:

1. The ray transfer matrix of a ray over a distance,  $d$ , with input and output planes at positions 1 and 2.

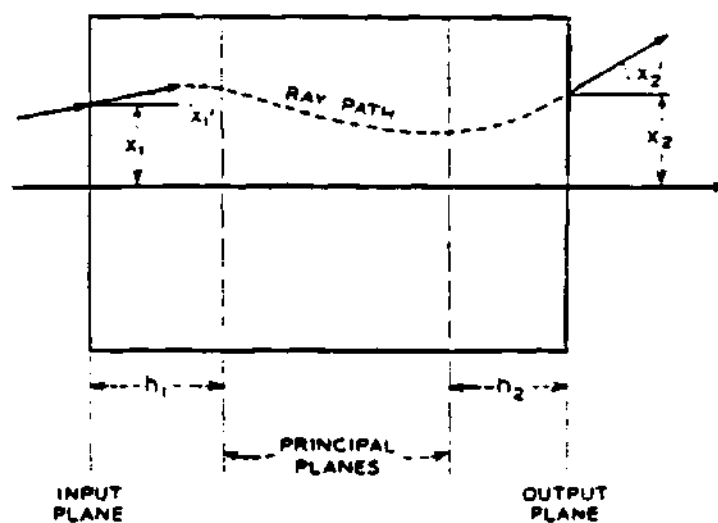
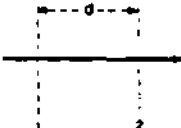
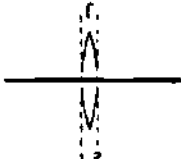
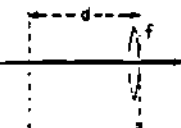
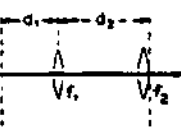
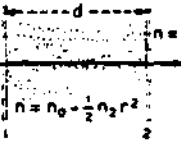
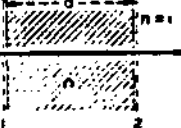


Figure A.2: Optical system diagram and parameters. An arbitrary ray and its corresponding parameters are also shown. ©1966 IEEE

Table A.1: Ray transfer matrices of six elementary structures. ©1966 IEEE

RAY TRANSFER MATRICES OF SIX ELEMENTARY OPTICAL STRUCTURES

NO.	OPTICAL SYSTEM	RAY TRANSFER MATRIX
1		$\begin{bmatrix} 1 & d \\ 0 & 1 \end{bmatrix}$
2		$\begin{bmatrix} 1 & 0 \\ -1/f & 1 \end{bmatrix}$
3		$\begin{bmatrix} 1 & d \\ -1/f & 1 - d/f \end{bmatrix}$
4		$\begin{bmatrix} 1 - d/f_1 & d + d_2 - d d_2/f_1 \\ -1/f_1 - d/f_1 f_2 & 1 - d/f_2 - d d_2/f_2 \end{bmatrix}$
5		$\begin{bmatrix} \cos \theta \sqrt{n_2/n_0} & \frac{1}{\sqrt{n_0 n_2}} \sin \theta \sqrt{n_2/n_0} \\ -\sqrt{n_0 n_2} \sin \theta \sqrt{n_2/n_0} & \cos \theta \sqrt{n_2/n_0} \end{bmatrix}$
6		$\begin{bmatrix} 1 & d/n \\ 0 & 1 \end{bmatrix}$

2. The ray transfer matrix of a ray going through a thin lens of focal length  $f$ .
3. The combination of 1 and 2. The matrix is obtained by multiplying matrix 1 by matrix 2.
4. A beam passing through two structures of type 3.
5. The ray transfer matrix of a lens like medium (like a laser). It is characterized by a parabolic radial density profile.
6. The matrix for a dielectric material of index of refraction  $n$  and length  $d$ .

### A.3.2 Periodic sequences

A laser resonator cavity can be modeled by means of two spherical mirrors facing each other. Such a system will have a focusing effect on the light rays as they bounce back and forth between the two mirrors. The two spherical mirrors facing at each other are equivalent to an infinite sequence of equal lenses, in which the  $n^{\text{th}}$  bounce of the ray on one of the spherical mirrors is equivalent to the same ray passing through the  $n^{\text{th}}$  lens of the infinite sequence of lenses.<sup>272</sup> A schematic of the infinite sequence system is shown in Figure A.3 for an arbitrary ABCD matrix. The ray transfer through the  $n^{\text{th}}$  element (or reflection) is described by the  $n^{\text{th}}$  power of this matrix. This can be evaluated by means of Sylvester's theorem,<sup>274</sup> which is:

$$\begin{vmatrix} A & B \\ C & D \end{vmatrix}^n = \frac{1}{\sin \Theta} \begin{vmatrix} A \sin(n\Theta) - \sin((n-1)\Theta) & B \sin(n\Theta) \\ C \sin(n\Theta) & D \sin(n\Theta) - \sin((n-1)\Theta) \end{vmatrix} \quad (\text{A.6})$$

where the angle  $\Theta$  is defined by:

$$\cos \Theta = \frac{1}{2}(A + D) \quad (\text{A.7})$$



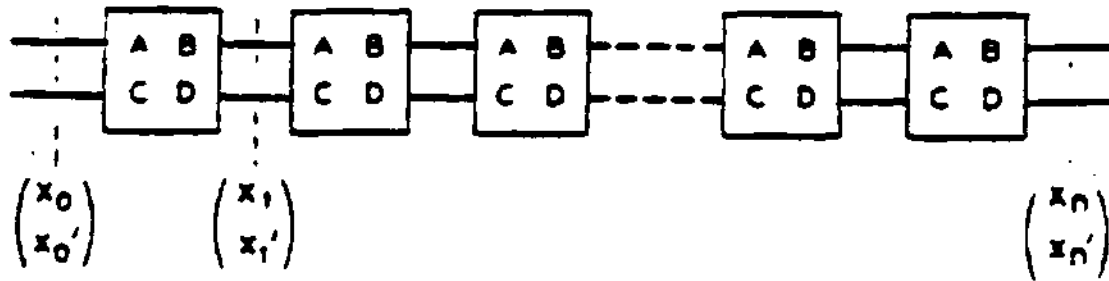


**Figure A.3:** Diagram of an infinite sequence of systems (lenses) each characterized by an equal ray transfer matrix. ©1966 IEEE

Based on equations A.6 and A.7 optical systems can be classified as either stable or unstable. Systems that have a real angle  $\Theta$  are stable, while systems which do not have a real angle  $\Theta$  are unstable. Mathematically speaking, any matrix which satisfies the inequality:

$$-1 < \frac{1}{2}(A + D) < 1 \quad (\text{A.8})$$

is stable, and any system not satisfying the above inequality is unstable.

## A.4 Wave Analysis of Laser Beams

This section will discuss laser beams from the point of view of satisfying a wave equation, thus taking into account the wave nature of the beam. The results derived here are applicable to optical systems with large apertures as compared to the diameter of the beam and/or the wavelength of the wave. This means that edge diffraction effects have not been taken into account. A discussion of the

effects of edge diffraction can be found in the references.<sup>295</sup> The study of “beam waves” was first made by Boyd and Gordon,<sup>268</sup> and by Goubau and Schwering.<sup>270</sup> Here the development of Kogelnik<sup>295</sup> and others<sup>275</sup> will be followed.

#### A.4.1 Solution to the beam’s wave equation

Laser beams are similar to plane waves (since both have to satisfy the wave equation), except that their intensity distribution is not uniform and their phase fronts are slightly curved. Thus, a laser beam traveling in the  $z$ -direction can be expressed as:

$$u = \psi(x, y, z) e^{-ikz} \quad (\text{A.9})$$

where  $\psi(x, y, z)$  is a slow varying function of  $z$  and represents the differences between the laser beam and a plane wave. It incorporates the idea of a non-uniform intensity distribution, the expansion of the beam as it moves away from the source, the curvature of the phase front, and any other difference. This laser beam function is bound to satisfy the wave equation given by:

$$\nabla^2 u + k^2 u = 0 \quad (\text{A.10})$$

assuming harmonic solutions, where  $k = \frac{2\pi}{\lambda}$  is the propagation constant in the medium and  $\lambda$  is its wave length. Substituting the representation of the beam wave, equation A.9, into the wave equation, equation A.10, gives:

$$\frac{\partial^2 \psi}{\partial x^2} + \frac{\partial^2 \psi}{\partial y^2} - 2ik \frac{\partial \psi}{\partial z} = 0 \quad (\text{A.11})$$

where terms of order  $\frac{\partial^2 \psi}{\partial z^2}$  have been ignored because it was assumed that  $\psi(x, y, z)$  was a slow changing function of  $z$ .

The differential “beam equation” has a form similar to the ubiquitous time dependent *Schrödinger* equation. So, borrowing one of the *Schrödinger* solutions

and suiting it to our equation, one obtains:<sup>266-270,273-275,295</sup>

$$\psi = \exp \left( -i \left( P(z) + \frac{kr^2}{2q(z)} \right) \right) \quad (\text{A.12})$$

with

$$r = (x^2 + y^2)^{\frac{1}{2}} \quad (\text{A.13})$$

as a solution to the beam equation. The parameter  $P(z)$  represents a complex phase shift which is associated with the propagation of the light beam and  $q(z)$  is a complex beam parameter which describes the Gaussian dependence of the beam with respect to the distance from the beam's main axis (assumed to be in the  $z$ -axis). Equations for  $P(z)$  and  $q(z)$  can be obtained by substituting the beam function, equation A.12, into the beam equation, equation A.11, and comparing terms of equal powers in  $r$ . This will yield:

$$q'(z) = 1 \quad (\text{A.14})$$

and:

$$P'(z) = \frac{i}{q} \quad (\text{A.15})$$

where the prime symbol, ', indicates differentiation with respect to the argument,  $z$ . Integration of equation A.14 gives:

$$q_2 = q_1 + z \quad (\text{A.16})$$

which relates the parameter  $q_2$  of the output plane to the parameter  $q_1$  of the input plane where the planes are separated by a distance  $z$ .

#### **A.4.2 Propagation law for the fundamental mode**

The beam function, equation A.12, is not the only known solution to the beam equation, but is probably the most important. This beam function is called the fundamental mode. Higher order modes are discussed in the references, such

as: A. G. Fox,<sup>266,267</sup> G. D. Boyd,<sup>268</sup> H. Kogelnik,<sup>274,275,295</sup> E. L. O'Neill<sup>278</sup> and C. S. Williams.<sup>279</sup> Because of the importance of the fundamental mode it will be discussed here in more detail.

Start by redefining the complex  $q(z)$  parameter in terms of two real parameters,  $R$  and  $w$ , as:

$$\frac{1}{q(z)} = \frac{1}{R(z)} - \frac{i\lambda}{\pi w^2(z)} \quad (\text{A.17})$$

where  $R(z)$  represents the radius of curvature of the wave front that intersects the  $z$ -axis at  $z$ , and  $w(z)$  is a measure of the decrease of the intensity with respect to the distance from the axis (i.e., the  $e$ -folding distance of the Gaussian). The new parameter is often called the beam radius or spot size, and  $2w$  is the beam diameter.

A focused Gaussian beam contracts to a minimum diameter of  $2w_0$  at the point that is called the beam waist, where the phase front is plane (so that  $R \rightarrow \infty$ ). If  $z$  is measured from this waist, the  $q$  parameter becomes purely imaginary, that is:

$$q_0 = \frac{i\pi w_0^2}{\lambda} \quad (\text{A.18})$$

and at a distance  $z$  from the waist  $q$  is given by:

$$q(z) = q_0 + z \quad (\text{A.19})$$

or using equation A.18, as:

$$q(z) = \frac{i\pi w_0^2}{\lambda} + z \quad (\text{A.20})$$

where  $z$  is measured from the beam waist. By combining equation A.20 with equation A.17 and equating the real and imaginary parts of each one, one obtains:

$$w^2(z) = w_0^2 \left( 1 + \left( \frac{\lambda z}{\pi w_0^2} \right)^2 \right) \quad (\text{A.21})$$

and

$$R(z) = z \left( 1 + \left( \frac{\pi w_0^2}{\lambda z} \right)^2 \right) \quad (\text{A.22})$$

which expresses the beam radius,  $w(z)$ , and the radius of curvature,  $R(z)$ , of the wave front in terms of the position on the  $z$ -axis and the beam waist.

Equation A.21 is the equation for a hyperbola with asymptote at an angle:

$$\theta = \frac{\lambda}{\pi w_0} \quad (\text{A.23})$$

which is the far-field diffraction angle of the fundamental mode. This can be obtained by taking the limit of equation A.21 as  $z \rightarrow \infty$ , that is:

$$\lim_{z \rightarrow \infty} (w^2(z)) = \lim_{z \rightarrow \infty} \left( w_0^2 \left( 1 + \left( \frac{\lambda z}{\pi w_0^2} \right)^2 \right) \right) \quad (\text{A.24})$$

$$\lim_{z \rightarrow \infty} (w^2(z)) = \lim_{z \rightarrow \infty} \left( \left( \frac{\lambda z}{\pi w_0} \right)^2 \right) \quad (\text{A.25})$$

$$\frac{\lim_{z \rightarrow \infty} (w^2(z))}{\lim_{z \rightarrow \infty} (z^2)} = \left( \frac{\lambda}{\pi w_0} \right)^2 \quad (\text{A.26})$$

$$\tan^2 \theta = \left( \frac{\lambda}{\pi w_0} \right)^2 \quad (\text{A.27})$$

Using the condition that the angle of the beam is small, the approximation  $\tan \theta \approx \theta$  can be used to obtain equation A.23.

Dividing equation A.22 by equation A.21 one can obtain the useful equation:

$$\frac{\lambda z}{\pi w_0^2} = \frac{\pi w^2}{\lambda R} \quad (\text{A.28})$$

which can be used to express  $w_0$  and  $z$  in terms of  $w$  and  $R$ , as:

$$w_0^2 = \frac{w^2}{1 + \left( \frac{\pi w^2}{\lambda R} \right)^2} \quad (\text{A.29})$$

and:

$$z = \frac{R}{1 + \left( \frac{\lambda R}{\pi w^2} \right)^2} \quad (\text{A.30})$$

To obtain the complex phase shift,  $P(z)$ , substitute the solution for  $q$ , equation A.20, into equation A.15 to obtain:

$$P'(z) = \frac{-i}{\frac{i\pi w_0^2}{\lambda} + z} \quad (\text{A.31})$$

which, after integration with respect to  $z$ , yields:

$$iP(z) = \ln \left( 1 - \frac{i\lambda z}{\pi w_0^2} \right) \quad (\text{A.32})$$

$$= \frac{1}{2} \ln \left( 1 + \left( \frac{\lambda z}{\pi w_0^2} \right)^2 \right) - i \arctan \left( \frac{\lambda z}{\pi w_0^2} \right) \quad (\text{A.33})$$

where the real part of  $P(z)$  represent the phase shift difference,  $\Phi$ , between the Gaussian beam and an ideal plane wave. The imaginary part produces an amplitude factor  $\frac{w_0}{w}$  which gives the expected intensity decrease on the axis due to the expansion of the beam.

Substituting all of this into the original beam function, equation A.12 and equation A.9, gives the final form for the beam functions:

$$u(r, z) = \frac{w_0}{w} \exp \left( -i(kz - \Phi) - r^2 \left( \frac{1}{w^2} + \frac{ik}{2R} \right) \right) \quad (\text{A.34})$$

where:

$$\Phi = \arctan \left( \frac{\lambda z}{\pi w_0^2} \right) \quad (\text{A.35})$$

is the phase shift difference in between the Gaussian wave and the plane wave, and is derived from the real part of equation A.33.

## **APPENDIX B**

### **SIMULATION PROGRAM**

#### **B.1 Introduction**

This appendix contains the code for the simulation program and a typical data file. The source for the code is in the computer:

FEDC04.FED.ORNL.GOV

in the area:

USERD:[COLLAZOI.WILGEN]F.FOR

and a copy can be obtained from the author or one of the coworkers of the project. Request can be done by mail, E-mail, or any other way. Transmission of the program can be done via E-mail, diskettes, tape or any other possible way. Section B.2 gives a general description of the code. The theory for the calculation of the phase of the propagating wave has been discussed in Sections 2.3, 2.3.5, 2.4.5, 2.6.2, and others in the thesis.

#### **B.2 Description**

##### **B.2.1 Code description**

The code to model and calculate the phase difference data for the probing beam of the reflectometer is based in the equations for the propagation of

electromagnetic waves in a plasma. This had been presented and discussed in Sections 2.3, 2.3.5, 2.4.5, and 2.6.2 of the thesis, therefore, they will not be discussed here. The heart of the reconstruction technique for the program was described in sections 6.2.1 and 6.2.2, where the program uses equation 6.19 and 6.118 to calculate the increment in the radial position of the cutoffs.

The program was written in Fortran programming language and it uses some of the features of the Vax Fortran common to all Vaxes. Within the program there are extensive comments and details of the variables and their function within the program. The code follows a block structure in all of its parts. This is, extensive use of subroutines and functions was used to reduce the repetition of instructions and ease the readability of the code. Indentation of the statements was used through out all of the codes to ensure a clear, easy to understand and follow code. The code was designed to run in a non-iterative mode. All of the parameters and data are entered from a Fortran "NAMELIST" data file by the use of a block read. An example of one of these data files is shown at the end of the program list in Section B.3. In this type of data file the names of the variables are clearly included in the file, thus making it easier to see the value assigned to the variable after the namelist read. Changes to the data file can be done by editing the file and manually changing the values assigned to the variable.

### **B.2.2 Code graphic subroutines**

Graphics were provided by a version of the famous and ubiquitous Plot-10 or Advance Graphics family of plotting subroutines (available at the Princeton Plasma Physics Laboratory too). These subroutine calls are cluster in blocks which produce entire plots (that is, they are cluster by purpose), thus changing to another plotting package can be easily performed by just changing the plotting subroutine calls in the code. The purpose of every plotting subroutine call is clearly



**Table B.1:** List of the different types of plots that the simulation program can do and its importance.

Y	vs X	Description
Cutoff Position	Frequency	Provides with a scanning range for any particular profile.
Frequencies Radial Spacing	Cutoff Position	Comparison with the density fluctuations correlation length.
Transmission and Reflection Coefficients	Radial Position	Study of the Budden tunneling effect.
Phase Derivative	Radial Position	Comparison with the phase difference data.
Calculated Full Phase	Radial Position	Full phase of the wave from edge to cutoff.
Calculated Phase Difference	Radial Position	Phase difference data due to the propagation of the two waves.
Reconstructed and Assumed Density	Radial Position	Final reconstructed density profile out of the calculated phase difference data.

commented within the code. The plotting subroutines can send the graphics to the screen and a TeKtronics File (TKF) at the same time. This allows for immediate inspection of the results. A hard copy of the plots can be obtained by printing the TKF file in one of the Vax's LN03 printers. A typical graph can have as many as six plots of the different parameters of interest of the propagating beam. This plots can provide with great insight into the dynamics of the propagation and on the effect of a particular density profile on the different parameters and the phase difference data, which is the variable that the reflectometer will finally measure and that can be use to calculate the density profile. A list of these variables and its importance is shown in Table B.1 with a short description of its usefulness.

### B.2.3 Data file

A typical "NAMELIST" data file used for the initialization of the program is shown in Figure B.1. The order of the variables is not important and they can go in any other that is convenient to the programmer. The variables are defined as follows:

- DENN is an array containing the central densities to be used to calculate the phase difference and related parameters. Typical values are from 1.0 to  $5.0 \times 10^{18} \frac{\text{part}}{\text{m}^3}$ .
- RSHIFT is an array containing the position of the edge for the inverted hyperbolic tangent density profile. Its values range from 3.3 to 3.7 meters
- SHAPE is an array containing the parameter that determines the slope at the edge of the inverse hyperbolic tangent density profile. It does not have any physical meaning, but to make the edge steeper for small values of SHAPE and flatter for large values of SHAPE. Values range from 0.02 to 0.10 of arbitrary units.
- DERDEN is an array with the values for the derivatives at the center of the plasma.
- ERROR\_X0 is a floating point variable that sets the intersection point for the family of curves for the offset error function. Its values generally are 90 GHz for intersection at the low end of the band and 120 GHz for intersection at the upper part of the frequency band.
- ERROR\_M is an array of the slope of the offset error function. Nominal values are from -0.01 to 0.01
- ERROR\_B is the constant offset error for the error function. Its values are from -1.0 to +1.0 fringes.

- **ERROR\_A** is the amplitude for the sinusoidal error function. A value of 0 disables the error function, while a value of 1 enables the error function.
- **ERROR\_W** is the wavelength of the sinusoidal error function. A large value used to simulate an constant offset function.
- **B\_ERROR** is an array of the magnetic field error values in fractions of the magnetic field. Nominal values are -0.01 to +0.01, which represent -1% and +1% of the real value for the magnetic field.
- **CG** are fitting parameters for the calculation of the poloidal contribution to the magnetic field.
- **FGREG** is Greg's compensation factor for Doyle's integral method. For  $FGREG = 1$  there is no compensation needed.
- **R0** is the major radius of the plasma.
- **RA** is the minor radius of the plasma.
- **CURRENT** is the current of the toroidal field coils.
- **NTURNS** is the number of turns of the toroidal field coils.
- **POL\_CUR** is the poloidal field current of the plasma.
- **JSTEP** is the number of point used to do the integrations needed to calculate the phase integrals and other related integrals. Its value is generally equal or bigger that the value for **NPOINTS** so that the number of points used for the integral is larger than the number of points for the data arrays, and all of the information from the data arrays is been used.
- **NPOINTS** is the number of points needed for the frequency and phase data arrays. It determines the frequency spacing of the probing beams,  $\approx 1.25$  Ghz.

- IWREF is a code for the AG2 plotting subroutines to determine where in the screen to plot the cutoff frequency as a function of the radial cutoff position. The variables IDELRC, IPHI, ITRANS, IDELPHI IDDPDW, IRREC, IDENREC, and IMU are for similar purposes, that is, they set the screen position for a particular plot. The code and the screen position where the plot will be drawn is explained in Table B.2.
- IDELRC plots the radial separation of the cutoff position as a function of the frequency.
- IPHI plots the full phase as a function of frequency.
- ITRANS plots the reflection and transmission fraction for the probing beam at the edge of the plasma.
- IDELPHI plots the phase difference as a function of the frequency.
- IDDPDW plots the Derivative of the Phase Difference with respect to the frequency ( $\omega$ ) as a function of frequency.
- IRREC plots the reconstructed position of the cutoffs as a function of the real positions of the cutoffs.
- IDENREC plots the assumed density profile as a function of the radius and the reconstructed density profile.
- IMU plots the index of refraction for the assumed density as a function of the cutoff position.
- WFINAL is the final frequency of the sweep.
- WINIT is the initial frequency of the sweep.
- WM is the frequency separation of the two frequencies.

- APERT is the amplitude of a perturbation or fluctuation on the assumed density profile.
- LAMBDA is the wavelength of the perturbation on the assumed density profile.
- RSEED is the seed number for a random number generator to simulate random fluctuations on the phase data.
- EPSILON is another number for the random number generator.
- ANOISE is the amplitude of the noise generated by the random number generator.
- DEN1 is the density at the reference plane for the beginning of the linear density profile between the reference plane position and the position of the first cutoffs.
- RINIT is the position of the first cutoff.
- RGREG is the position of the reference plane.
- RXMIN and RXMAX are the minimum and maximum for the radial axis.
- DPHIMIN and DPHIMAX are the minimum and maximum of the phase difference data axis.
- DYMIN and DYMAX are the minimum and maximum of the density axis.

#### **B.2.4 Subroutine/Functions description**

This section will describe the subroutines and/or functions of the modeling program and their purpose. Table B.3 shows a list of the names of the functions and a short description of their purpose.

```

$DAT
DENN = 3.5E+19
RSHIFT = 3.50
SHAPE = 0.03
DERDEN = -1.0E+19
ERROR_IO = 90.
ERROR_M = .00000001
ERROR_B = .00000001
ERROR_A = 1.0
ERROR_W = 1000000.
B_ERROR = 0.000001
CG = 5.5389 -8.401 6.2041 -2.2861 0.42053 -0.030917
FGREG = 1.0
RO = 2.64 ! METERS
RA = 0.96 ! METERS
CURRENT = 67.0E+03 ! AMPERES
NTURNS = 880 ! TURNS
POL_CUR = 1.98059E+06
JSTEP = 300 ! # OF INTERVALS FOR THE INTEGRATION
NPOINTS = 200
IWREF = 0 IDELRC = 0 IPHI = 0 ITRANS = 0
IDELPHI = 2 IDDPDW = 0 IRREC = 0 IDENREC = 3
IMU = 0
WFINAL = 117.E+09 ! MAXIMUM REFLECTOMETER FREQUENCY
WINIT = 92.E+09 ! MINIMUM REFLECTOMETER FREQUENCY
WM = .125E+09
APERT = 0.0
LAMBDA = .01
RSEED = 0.57
EPSILON = 3.93
ANOISE = 1.0 ! 0.2886751
DEN1 = .1E+14
RINIT = 3.594
RGREG = 3.61 ! POSITION OF GREG'S REFERENCE PLANE
RXMIN = 3.40
RXMAX = 3.60
DPHMIN = 0.0
DPHMAX = 5.0
DYMIN = 0.0
DYMAX = 5.0E+19
$END

```

Figure B.1: "NAMELIST" data file used to initialize the parameters for the modeling program.

**Table B.2:** List of the plotting code for the AG2 plotting subroutines.

Code	Description
0	no plot is drawn
1	one single plot using the entire screen
2	the plot goes in the upper half of the screen
3	the plot goes in the lower half of the screen
4	the plot goes in the upper left corner of the screen
5	the plot goes in the upper right corner of the screen
6	the plot goes in the lower left corner of the screen
7	the plot goes in the lower right corner of the screen

**Table B.3:** List of the function names of the modeling code and a short description of their purpose.

Name	Description
MU2	Calculates the index of refraction out of the assumed density profile.
SN	Calculates the integral of the index of refraction used in the calculation of the phase data.
RZERO	Finds the position of the cutoff for a particular frequency used in the calculation of the phase data.
REZERO	Finds the radial position of the resonance for a given frequency.
MU2REC	Calculates the index of refraction for the reconstructed data.
SNREC	Calculates the integral of the index of refraction for the reconstructed data.
DENSITY	Calculates the real density for the assumed data.
BFIELD	Calculates the magnetic field for the modeling.

**Function MU2** This real valued function provides with a value for the index of refraction given the radial position and the frequency of the wave for the assumed density profile. It is mainly used for the calculation of the integrals of the index of refraction needed to calculate the phase of the waves in the modeling program. The basic formula for the index of refraction is given by the equation:

$$n_X^2 = 1 - \frac{\omega_{pe}^2(n_e(r))}{\omega^2} \cdot \frac{\omega^2 - \omega_{pe}^2(n_e(r))}{\omega^2 - \omega_{pe}^2(n_e(r)) - \omega_{ec}^2(B(r))} \quad (\text{B.1})$$

where  $\omega_{pe}(n_e(r))$  is the plasma electron frequency,  $\omega_{ec}(B(r))$  is the electron cyclotron frequency, and  $\omega$  is the wave's frequency.

**Function SN** This real valued function provides with the integral of the index of refraction from the reference plane to the position of cutoff for a given frequency. The input parameters are the frequency of the wave, the position of the cutoff, and the position of the reference plane. The output is the dimensionless integral of the index of refraction for the given wave frequency and from the reference plane to the cutoff position. The basic formula that this function is trying to calculate is given by the equation:

$$SN = \int_{r_c(\omega)}^{r_0} n(r, n_e(r), \omega) dr \quad (\text{B.2})$$

where  $r_0$  is the position of the reference plane,  $r_c(\omega)$  is the position of the cutoff for the wave with frequency  $\omega$ , and  $n(r, n_e(r), \omega)$  is the index of refraction as a function of radial position for the frequency  $\omega$  of the propagating wave. The subprogram originally used a 3<sup>rd</sup> degree polynomial method<sup>66,67</sup> to calculate the integrals, this was later modified to use a 21 point Gaussian integration method that provides with an error that is less than the precision of the computer. Some of these methods have been discussed in section 6.3 and will not be repeated here. The function "SN" is used to calculate the full phase of the propagating wave in



the plasma, and the formula used in the program is given by:

$$\phi = \frac{2\omega}{c} \int_{r_c(\omega)}^{r_0} n(r, n_e(r), \omega) dr \quad (\text{B.3})$$

where  $\phi$  is the full phase of the wave and all of the other variables have been defined before.

**Function SNREC** This real valued function calculates the integral of the index of refraction for the reconstructing algorithm using the reconstructed density data and the cutoff positions from the reconstructed data. Its input parameters are the frequency of the wave, the reconstructed density profile, and the array of the position of the cutoffs. Its function is the same that the function "SN", but it will use the reconstructed data for the integrals. The integral methods are the similar that of the function "SN" described previously in section 6.3. In specific, the subroutine uses a cubic spline polynomial fit to the reconstructed density data points to calculate the necessary integrals. The equation used in the program is the same equation used for the subroutine "SN" described previously.

**Function MU2REC** This real valued function provides with the index of refraction using the reconstructed data. The formula is the same used for subroutine "MU2" described in the previous sections. It is mainly used by the function "SNREC" to calculate the integral of the index of refraction for the reconstructed data. Input parameters are the radial position, the density at that radial position, and the frequency of the wave. This is the equivalent of the function "MU2", but it uses the reconstructed data for the calculations.

**Function RZERO** This real valued function calculates the radial position for the cutoff given a frequency for the assumed density profile. It uses an IMSL library subroutine that finds the zeros of a given function. The condition

for cutoff, give by:

$$n(r_c(\omega), \omega, n_e) = 0 \quad (\text{B.4})$$

is used to find the positions of the cutoffs for a given frequency  $\omega$  and a density profile  $n_e$ .

**Function REZERO** This real valued function calculates the radial position of the resonance layers. It is not been used at the moment.

**Function DENSITY** This real valued function calculates the density for the assumed density profile. Its input parameters are the radial position at which the density is required and the shape parameters for the density profile. There are two possible density profiles model that the program can use to calculate the phase data and they had been discussed in section 6.3. These density profile models are the  $\alpha$ - $\beta$  type profile, defined by the equation:

$$n_e(r) = n_{e0} \left(1 - \left(\frac{r}{a}\right)^\alpha\right)^\beta \quad (\text{B.5})$$

while the other density profile is of the inverse hyperbolic tangent form, defined by the equation:

$$n_e(r) = n_{e0} \tanh\left(\frac{r - r_0}{b}\right) \quad (\text{B.6})$$

where  $a$  is the minor radius,  $n_{e0}$  is the maximum density, and  $\alpha$ ,  $\beta$ ,  $b$ ,  $r_0$  are parameters to change the shape of the assumed electron density profile.

**Function BFIELD** This real valued function calculates the magnetic field at a given radial position. This model for the magnetic field can correct for the magnetic ripple of TFTR and the poloidal magnetic field. The formula used is the typical  $B \propto \frac{1}{R}$ .

### B.3 Computer Code

```

!
PROGRAM REFLECTO    ! By Ivan Collazo-Lopez
C
C   THIS PROGRAM IS SUPPOSE TO MODEL THE PHASE AND
C   RECONSTRUCTING TECHNIQUE FOR THE DUAL FREQUENCY
C   REFLECTOMETER BUILD AT ORNL FOR THE TFTR REACTOR
C   AT PPPL.
C   THIS IS DONE BY ASSUMING A DENSITY PROFILE OF THE TYPE:
C       = TANH( (R - RSHIFT) / SHAPE )
C   WHERE RSHIFT AND SHAPE ARE THE PARAMETERS THAT CONTROL
C   THE SHAPE OF THE DENSITY PROFILE.
C   USING THIS "REAL" DENSITY PROFILE THE FULL PHASE OF
C   BOTH PROBING BEAMS AND THE PHASE DIFFERENCE CAN BE
C   CALCULATED. WITH THE PHASE DIFFERENCE THE DENSITY
C   PROFILE IS RECONSTRUCTED USING A TRAPEZOIDAL TYPE
C   TECHNIQUE. THUS TESTING AND MODELING THIS IDEA.
C
C   IMPLICIT NONE
C   PARAMETER NN=2000, NN2=22
C
C   THE VARIABLES NAMES ARE INTUITIVE, BUT I WILL DO
C   MY BEST IN TRYING TO DESCRIBE THEM THE BEST THAT
C   I CAN. THESE ARE AS FOLLOWS:
C   DOUBLE PRECISION
C   *   MU2    !FUNCTION GIVES THE "REAL" INDEX OF REF.
C   *   , SNREC    !GIVE THE INTEGRAL OF "MU2REC".
C   *   , MU2REC    !GIVES THE REF. INDEX USING THE RECON. DEN.
C   *   , SN    !GIVES THE INTEGRAL OF INDEX OF REFRACTION.
C   *   , RZERO    !CALCULATES THE POSITION CUT-OFF.
C   *   , DDELPHI(0:NN)    !DOUBLE PRECISION DELTA PHASE.
C   *   , DP1, DP2,MU_1,MU_2,MU_3    !TEMPORARY VARIABLES.
C   *   , DRIND    !TEMPORARY VARIABLES.
C
C   DOUBLE PRECISION
C   *   WREF(0:NN+1)    !REFLECTOMETER'S FREQUENCY ARRAY IN HERTZ.
C   *   , DELREC(0:NN)    !RECONSTRUCTED INCREMENT ON THE RADIUS.
C   *   , DELPHI(0:NN)    !PHASE DIFFERENCE BETWEEN THE PROBING WAVES.
C   *   , DELPHI1(0:NN)    !PHASE DUE TO THE DENSITY GRADIENTS.
C   *   , DELPHI2(0:NN)    !PHASE DUE TO THE POSITION OF THE CUTOFFS.
C   *   , DELWR    !INCREMENT ON THE REFLECTOMETER'S FREQUENCY.
C   *   , RO    !MAJOR RADIUS OF THE TOKAMAK.

```

```

* , RA !MINIR RADIUS OF THE TOKAMAK.
* , DENSO !DENSITY AT THE CENTER OF THE PLASMA.
* , DENN(22)
* , BO !MAGNETIC FIELD AT THE CENTER OF THE PLASMA.
DOUBLE PRECISION
* , ELECHR !CHARGE OF THE ELECTRON IN COULOMBS.
* , ELEMAS !MASS OF THE ELECTRON IN KILOGRAMS.
* , EPSILO !PERMITTIVITY OF THE FREE SPACE.
* , C !SPEED OF LIGHT IN FREE SPACE.
C * , X0, X1, X2, Y1, Y2
* , DELRP, DELPAR, XTEMP, B_PAR, C_PAR
* , XX(3), YY(3) !GENERAL PURPOSE ARRAY FOR PLOTTING.
* , WFINAL !FINAL FREQUENCY OF THE SWEEP.
* , WINIT !STARTING FREQUENCY OF THE SWEEP.
* , RINIT !ASSUMED POSITION FOR FIRST CUT-OFF.
* , RX !GENERAL PURPOSE VARIABLE.
* , DELRX !GENERAL PURPOSE VARIABLE.
* , PI !CONSTANT 3.14159265
DOUBLE PRECISION
* , RK !GENERAL PURPOSE VARIABLE.
* , RK1 !GENERAL PURPOSE VARIABLE.
* , RK2 !GENERAL PURPOSE VARIABLE.
* , DELRK !GENERAL PURPOSE VARIABLE.
* , DEN1 !GENERAL PURPOSE VARIABLE.
* , DEN2 !GENERAL PURPOSE VARIABLE.
* , RKUP !GENERAL PURPOSE VARIABLE.
* , DEN2UP !GENERAL PURPOSE VARIABLE.
* , RK2UP !GENERAL PURPOSE VARIABLE.
* , DELRKUP !GENERAL PURPOSE VARIABLE.
C * , U !EXPONENTIAL DECAY CONSTANT AT THE EDGE.
* , RGREG !GREG'S REFERENCE PLANE.
* , MU2K !TEMPORARY STORAGE ARRAY.
* , DSLOPE !SLOPE OF ASSUMED LINEAR DENSITY.
C * , ZERO !CALCULATES THE DENSITY AT CUT-OFF.
* , RR(0:NN) !RADIAL PLOTTING ARRAY FOR THE ARRAY "MURR".
* , MURR(0:NN) !REFLECTION INDEX FOR THE FIRST CUT-OFF.
* , DENSITY !GIVES THE ASSUMED "REAL" DENSITY PROFILE.
* , DDPDW(0:NN) !DERIVATIVE OF PHASE WITH RESPECT TO FREQ.
DOUBLE PRECISION
* , R1, R2, DELRJ, RJ !GENERAL PURPOSE VARIABLES.
* , WM(22) !FREQUENCY SPACING BETWEEN THE PROBING WAVES.
C * , WW !TEMPORARY STORAGE VARIABLE.
* , COMGET !AG2 FUNCTION, GIVES DATA BLOCK PARAMETERS.
* , RLOW(0:NN+NN2) !RADIUS OF CUT-OFF FOR THE LOWER FREQUENCY.
* , RCUP(0:NN+NN2) !RADIUS OF CUT-OFF FOR THE UPPER FREQUENCY.

```

```

* , DENLOW(0:NN+NN2)!DENSITY OF THE LOWER CUT-OFF.
* , DENUP(0:NN+NN2)!DENSITY OF THE UPPER CUT-OFF.
* , PHILOW(0:NN+NN2)!"REAL" FULL PHASE FOR THE LOWER FREQUENCY.
* , PHIUP(0:NN+NN2)!"REAL" FULL PHASE FOR THE UPPER FREQUENCY.
* , RRLOW(0:NN+NN2)!RECONSTRUCTED RADIUS FOR THE LOWER CUT-OFF.
* , RRUP(0:NN+NN2)!RECONSTRUCTED RADIUS FOR THE UPPER CUT-OFF.
* , PHIRLOW(0:NN+NN2)!RECONSTRUCTED FULL PHASE FOR LOWER FREQ.
* , PHIRUP(0:NN+NN2)!RECONSTRUCTED FULL PHASE FOR UPPER FREQ.
* , DELPREC(0:NN+NN2)!DELTA PHASE RECONSTRUCTED.
C * , PHIUP_2(0:NN) !"REAL" FULL PHASE FOR UPPER FREQ AT RCLOW(I).
* , TEMP1, TEMP2, PHIAVE !TEMPORAL VARIABLES.
* , ER_DELR(0:NN+NN2) !ERRON ON CUTOFF
* , ER_DEN(0:NN+NN2) !ERROR ON DENSITY
* , ER_PAR(0:NN+NN2) !ERROR ON PARABOLIC FIT
* , ERR_MAX !MAXIMUM ERROR
* , ERR_TOM !ERROR FOR THOMAS
* , ERR_B !ERROR IN B
* , ERR_R !ERROR IN R
* , ERR_R1 !ERROR IN R1
* , ERR_PHI !ERROR IN PHI
* , DNDR !DENSITY DERIVATIVE
* , N_REF !INDEX OF REF

```

#### DOUBLE PRECISION

```

* , T1, T2 !GENERAL PURPOSE VARIABLES.
* , WGHZ(0:NN+NN2)!REFLECTOMETER'S FREQUENCIES IN GHz.
* , WGHZ_TOMY(0:NN+NN2)!NEGATIVE FREQUENCIES.
* , CURRENT !CURRENT OF THE TOROIDAL FIELD COILS IN AMPERS.
* , POL_CUR !POLOIDAL CURRENT.
* , DELRC(0:NN+NN2)!RADIAL DIFF. BETWEEN UPPER AND LOWER CUT-OFF.
C * , RRES(0:NN+1) !POSITION OF THE RESONANT LAYERS.
C * , REZERO !GIVES THE POSITION OF THE RESONANCE LAYERS.
* , TRANS(0:NN) !TRANSMISSION COEFFICIENT FOR BUDDEN TUNNELING.
* , REFL(0:NN) !REFLECTION COEFFICIENT FOR BUDDEN TUNNELING.
* , MU !GENERAL PURPOSE VARIABLE.
* , DELDEN !GENERAL PURPOSE VARIABLE.
* , D(0:NN) !GENERAL PURPOSE PLOTTING ARRAY.
* , PRLOWIN !INITIAL RECONSTRUCTED PHASE FOR LOWER FREQ.
C * , PRUPIN !INITIAL RECONSTRUCTED PHASE FOR UPPER FREQ.
* , RXMIN !RADIAL MIN
* , RXMAX !RADIAL MAX
* , DPHMIN !DELTA PHASE MIN
* , DPHMAX !DELTA PHASE MAX
* , DYMIN !DENSITY MIN

```

```

* , DYMAX !DENSITY MAX
* , RZDEL !STEP SIZE FOR FDELTA
DOUBLE PRECISION
* , RSHIFT(22) !PROFILE DISPLACEMENT
* , SHAPE(22) !SHAPING PARAMETER FOR PROFILE
C * , APERTEMP !AMPLITUDE OF PERTURVATION
* , APERT !AMPLITUDE OF PERTURVATION
* , LAMBDA !WAVELENGTH OF PERTURVATION
* , FGREG !GREG'S CORRECTION FACTOR
* , AGREG_(0:NN+NN2) !GREG'S FACTOR
* , SIWREF(99) !ARRAY FOR AG2 DATA BLOCKS
* , SIDELRC(99) !ARRAY FOR AG2 DATA BLOCKS
* , SITRANS(99) !ARRAY FOR AG2 DATA BLOCKS
* , SIDDPDW(99) !ARRAY FOR AG2 DATA BLOCKS
* , SIPHI(99) !ARRAY FOR AG2 DATA BLOCKS
* , SIDELPHI(99) !ARRAY FOR AG2 DATA BLOCKS
* , SIRREC(99) !ARRAY FOR AG2 DATA BLOCKS
* , SIDENREC(99) !ARRAY FOR AG2 DATA BLOCKS
* , SIER_DEN(99) !ARRAY FOR AG2 DATA BLOCKS
* , RLINE !POSITION OF LINEAR DENSITY
* , DERDEN(NN) !DERIVATIVE OF THE PROFILE
* , TEMP !TEMPORAL VARIABLE
* , WCE !ELECTRON CYCLOTRON FREQ.
* , BF !MAGNETIC FIELD
* , ERROR_X0 !ERROR CURVES INTERSECTION POINT
* , ERROR_M(22) !ERROR CURVES SLOPES
* , ERROR_B(22) !ERRORS CURVES INTERSECTIONS
* , ERROR_A(22) !AMPLITUDE ERRORS
* , ERROR_W(22) !FREQUENCY ERRORS
* , OFFSET(0:NN) !OFFSET ARRAY
C * , WORK(0:NN) !GENERAL PURPOSE WORKING ARRAY
* , BFIELD !MAGNETIC FIELD FUNCTION
* , B_ERROR(1:11) !ERRORS IN MAGNETIC FIELD
* , CG(6,6) !MAGNETIC RIPLE CORRECTION COEFICIENTS
* , RRANDOM !RANDOM NUMBER
* , RSEED !SEED FOR RANDOM GENERATOR
* , FRACTAL !VALUE OF FRACTAL
* , RNNOF !RANDOM NUMBER GENERATOR
* , EPSILON !PERMITIVITY OF FREE SPACE
* , SIGN !ALTERNATING SIGN VARIABLE
* , ANOISE !AMPLITUDE OF THE NOISE
* , RNOISE !RANDOM NUMBER FOR NOISE
* , AVENOISE !AVERAGE NOISE
* , DNOISE(0:NN+NN2) !NOISE ARRAY
* , ALPHA, BETA !SHAPING PARAMETER FOR PROFILE

```

```

* , RABEL(0:NN) !ABEL INVERSION RADIAL ARRAY
* , DABEL(0:NN) !ABEL INVERSION DENSITY ARRAY
* , SABEL !INTEGRAL FUNCTION FOR ABEL INVERSION
* , AVE_DIF !AVERAGE DIFFERENCE OF DENSITIES
* , AVE_DIF2 !AVERAGE DIFFERENCE OF DENSITIES
* , R PERT(0:2310)!RADIAL ARRAY OF PERTURVATIONS
* , A PERT(0:2310)!AMPLITUDE ARARY OF PERTURVATIONS
* , DEL_R !INCREMENT ON RADIAL PERTURVATION
* , DBRETZ !FUNCTION TO GET PERTURVATION
* , DELRL !INCREMENT IN LOWER ARRAY
* , DELRU !INCREMENT IN UPPER ARRAY
* , RWLOW(NN+NN2) !PLOTING ARRAY
* , RWUP(NN+NN2) !PLOTING ARRAY
* , WMULOW(NN+NN2) !PLOTING ARRAY
* , WMOUP(NN+NN2) !PLOTING ARRAY
* , WPHILOW(NN+NN2) !PLOTING ARRAY
* , WPHIUP(NN+NN2) !PLOTING ARRAY
* , SPLN !SPLINE FUNCTION
* , WSCALE !SCALING FACTOR FOR FREQUENCY
!

C
C PLOTING ARRAYS AND VARIABLES.
REAL*4 X_DATA(0:NN+NN2), Y_DATA(0:NN+NN2)
* , X_MIN, X_MAX, Y_MIN, Y_MAX
* , X(0:NN) !GENERAL PURPOSE ARRAY FOR PLOTING.
* , Y(0:NN) !GENERAL PURPOSE ARRAY FOR PLOTING.

C
INTEGER
* JSTEP !NUMBER INTERVALS FOR INTERGRATION
* , I, J, K, N !DO LOOPS VARIABLES
* , II, JJ, KK !DO LOOPS VARIABLES
* , LL, IWM, ICG, IDUMY !DO LOOPS VARIABLES
* , IWREF !PLOT POSITION CODE FOR AG2 SUBROUTINE
* , IPHI !PLOT POSITION CODE FOR AG2 SUBROUTINE
* , IDELPHI !PLOT POSITION CODE FOR AG2 SUBROUTINE
* , IDDPDW !PLOT POSITION CODE FOR AG2 SUBROUTINE
* , IRREC !PLOT POSITION CODE FOR AG2 SUBROUTINE
* , IDENREC !PLOT POSITION CODE FOR AG2 SUBROUTINE
* , IDENREAL !PLOT FLAG FOR REAL DENSITY PROFILE
* , IMU !PLOT POSITION CODE FOR AG2 SUBROUTINE
* , IDELRC !PLOT POSITION CODE FOR AG2 SUBROUTINE
* , ITRANS !PLOT POSITION CODE FOR AG2 SUBROUTINE
* , IBASEX !AG2 DATA BLOCK ADDRESS SUBROUTINE
* , IBASEY !AG2 DATA BLOCK ADDRESS SUBROUTINE

```

```

* , IX, IY      !SCREEN POSITION OF PLOT
* , NURNS      !NUMBER OF TURNS OF MAGNETIC COILS
* , IXLEG      !SCREEN X-AXIS POSITION OF LEGEND
* , IYLEG      !SCREEN Y-AXIS POSITION OF LEGEND
* , IYLEG_H    !SCREEN Y-AXIS POSITION OF LEGEND
* , IX1BOX     !X-AXIS POSITION OF LEGEND BOX
* , IY1BOX     !Y-AXIS POSITION OF LEGEND BOX
* , IX2BOX     !X-AXIS POSITION OF LEGEND BOX
* , IY2BOX     !Y-AXIS POSITION OF LEGEND BOX
* , REC_SYMB   !SYMBOL FOR THE RECONSTRUCTED PROFILE
* , ERR_SYMB   !SYMBOL FOR ERROR BARS
* , ERR_ON     !TURN ERROR BARS ON AND OFF
* , N_INDEX    !NUMBER OF DATA POINTS
* , IN_CURVE   !NUMBER OF CURVES FOR THE REFRACTION INDEX
INTEGER
* , IERROR_M   !DO LOOPS VARIABLES
* , IERROR_B   !DO LOOPS VARIABLES
* , IERROR_A   !DO LOOPS VARIABLES
* , IERROR_W   !DO LOOPS VARIABLES
* , IB_ERROR   !DO LOOPS VARIABLES
* , IFILES     !DO LOOPS VARIABLES
* , ISMOOTH    !SMOOTHING VALUE
* , NPOINTS    !NUMBER OF DATA POINTS
* , NIDEAL     !IDEAL NUMBER OF DATA POINTS
* , ISEED      !SEED FOR RANDOM GENERATOR
* , NFILES     !NUMBER OF DATA FILES
* , IDCHOISE   !FLAG FOR THE PROFILE MODEL
* , IPHIMINX   !PLOT AXIS LIMITS
* , IPHIMAXX   !PLOT AXIS LIMITS
* , IPHIMINY   !PLOT AXIS LIMITS
* , IPHIMAXY   !PLOT AXIS LIMITS
* , ISHIFTY    !PLOTS DISPLACEMENT
* , NUMBER     !CURVE NUMBER LABEL
* , ICDELRC    !POSITIONN OF CURVE LABEL
* , ICDELPHI   !POSITIONN OF CURVE LABEL
* , ICDEN      !POSITIONN OF CURVE LABEL
* , IXSMIN     !PLOT AXIS LIMITS
* , IYSMAX     !PLOT AXIS LIMITS
* , IXPARAM    !POSITION OF PARAMETERS OF PLOTS
* , IYPARAM    !POSITION OF PARAMETERS OF PLOTS
* , ICLABEL    !FLAG TO PUT THE CURVE NUMBER
* , IYLOC_DEN_ERR !LABEL LOCATION
* , ISYM_ER    !ERROR SYMBOL
CHARACTER
* , TITLE*77   !TITLE CHARACTER

```



```

* , CHAR*77 !GENERAL USED
* , CHAR2*77 !GENERAL USED
* , TODAY*9 !THE DAYS DATE
* , CFILE*77 !NAME DATA FILE
* , CDIRECTORY*20 !DIRECTORY OF DATA FILE
* , DFILE*77 !COMPLETE ADDRESS OF DATA FILE
* , PLOTFILE*77 !NAME OF PLOTTING FILE
* , PLABEL*3 !PLOT LABEL
* , PARAM*77 !PLOT PARAMETERS LABEL
* , CNUM*3 !NUMBER OF PLOT
C
C
COMMON /COMDAT/ JSTEP
* , RO,RA,DENSO,BO, ELECHR, ELEMAS, EPSILO, C
* , APERT, LAMBDA, PI, RLINE, NTURN, CURRENT
* , POL_CUR, RRANDOM, ALPHA, BETA, IDCHOISE
COMMON /COMBFIELD/ICG, IB_ERROR, B_ERROR, CG
COMMON /PERT_DAT/R_PERT,A_PERT, DEL_R

NAMELIST /DAT/ JSTEP, WFINAL, WINIT, WM
* , RO, RA, DENN, CURRENT, POL_CUR, NTURN, ANOISE
* , RINIT, APERT, LAMBDA, DEN1, RSHIFT, SHAPE, EPSILON
* , IWREF, IPHI, IDELPHI, IDDPDW, IRREC, IDENREC, IMU
* , IDELRC, ITRANS, RGREG, RIMIN, RIMAX, DPHMIN, DPHMAX
* , DYMIN, DYMAX, FGREG, DERDEN, ERROR_XO, B_ERROR
* , ERROR_M, ERROR_B, ERROR_A, ERROR_W, NPOINTS, RZDEL
* , ALPHA, BETA, IDCHOISE, ISMOOTH, CG, RSEED, IDUMY
* , IPHIMINX, IPHIMAXX, IPHIMINY, IPHIMAXY, ISHIFTY
* , ICDELRC, ICDELPHI, ICDEN, ICLABEL, ERR_ON, IDENREAL
* , REC_SYMB, IN_CURVE
!
```

This is the beginning of the executable statements for the program. The basic operations here are to read the necessary data for the program, and proceed.

```

C
C
READ PERTURBATION DATA FILE
OPEN(11,FILE='[COLLAZOI.WILGEN.FF]F.PER',STATUS='OLD')
READ(11,*) R_PERT(0), A_PERT(0)
READ(11,*)( R_PERT(I), A_PERT(I), I=1,R_PERT(0) )
DEL_R = R_PERT(2)-R_PERT(1)
CLOSE(11)
C
OPEN(88,FILE='TOMY.ERR',STATUS='NEW')
C
```

```

C      READ THE DATA FILES FROM THE FILE LIST
      ERR_ON = 0      !DEFAULT
      IDENREAL = 1    !DEFAULT
      OPEN(22,FILE='[COLLAZOI.WILGEN]F.FLS',STATUS='OLD')
      READ(22,*) NFILES, CDIRECTORY
      WRITE(*,*) NFILES, ' ', CDIRECTORY
      DO IFILES = 1, NFILES
      READ(22,120) DFILE
120    FORMAT(A22)
      IF( NFILES .EQ. 1 ) CLOSE(22)

      PLABEL = ' '
      CFILE = CDIRECTORY//DFILE//'.DAT'
      PLOTFILE = CDIRECTORY//DFILE//'.TKF'
      WRITE(*,*) DFILE, CFILE, PLOTFILE

C
C      START READING THE DATA FROM THE NAMELIST DATA FILE.
      REC_SYMB = 0 ! 7=| 8=+
      ERR_SYMB = 7 ! 7=| 8=+
      ERR_ON = 0      !DEFAULT
      IDENREAL = 1    !DEFAULT
      IDUMY = 1      !DEFAULT
      RZDEL = 1.0D-4  !DEFAULT
      IN_CURVE = 20   !DEFAULT
      IYLEG_H = 17    !DEFAULT
      ISYM_ER = 4     !DEFAULT
      OPEN(11,FILE=CFILE,STATUS='OLD')
      READ(11,DAT)     !READ THE DATA FROM THE DATA FILE
      WRITE(*,DAT)     !WRITE TO THE SCREEN WHAT WAS READ
      CLOSE(11)

C      THIS DEFINES SOME CONSTANTS IN MKS UNITS.
      PI      = 3.14159265      ! RADIANS
      ELECHR = 1.60217733D-19    ! COULOMBS
      ELEMAS = 9.1093897D-31     ! Kg
      EPSILO = 8.854187817D-12   ! F/m
      C      = 299792456.2      ! +-1.1 M/SEC, FROM: K. Evenson et al,
C              !Physics Review Letters,
C              !Vol 29, p 1346 (1972)
C      THE FILE F.OUT IS LIKE A LOG FILE OF THE RELEVANT DATA
C      GENERATED ON THE CORRESPONDING LOOPS OF THE PROGRAM.
C      IT IS USED MOSTLY FOR DEBBUGING PURPOSES.
      OPEN(11,FILE='F.OUT',STATUS='NEW')
      WRITE(11,*)CFILE

C      THE FILE F.MER IS ANOTHER DEBBUGING FILE.
      OPEN(66,FILE='F.MER',STATUS='NEW')

```

!

Next it is necessary to initialize the plotting subroutines and to create some headers for the plot.

```

C
C      INITIALIZE THE PLOTTING FILE FOR THE AG2 SUBROUTINES
C      CALL OPNTKF(PLOTFILE)  !INITIALIZE TKF PLOTTING FILE
C
C      INITIALIZE PLOTTING SUBROUTINES.
C      CALL INITT(960)  !INITIALIZE DATA BLOCKS FOR AG2 ROUTINES
C
C      BOTTOM TITLE #2
C      WRITE(CHAR2,135)'WINIT=',WINIT/1.0D+09,' GHz'
*      , ' WFINAL=',WFINAL/1.0D+09,' GHz'
*      , ' WM=',WM(1)/1.0D+09,' GHz'
135  FORMAT(A6,F7.2,A4
*      ,A9,F7.2,A4
*      ,A5,F7.4,A4)
C      CALL AGXICPT(10,CHAR2)  !PLOT THE SECOND LOWER TITLE
C      CALL DATE(TODAY)  !GET DATE FROM THE COMPUTER
C      CALL AGXIMHS(900, 1,TODAY)  !PLOT TODAY'S DATE
C      CALL AGXIMHS( 1, 1,DFILE)  !PLOT THE DATA FILE NAME
C
C      BOTTOM TITLE #1
C      WRITE(CHAR,130)'RINIT=',RINIT,' m', ' FILE =',CFILE
130  FORMAT(A6,F6.3,A2,A8,A33)
C      CALL AGXICPT(35,CHAR)  !PLOT THE LOWER TITLE LABEL.
!
```

This is the main loop to do the different plots when more than one curve is required for the plots.

```

C
      NUMBER = 1
      KK = 1
      DO WHILE(DENN(KK) .NE. 0.0)
      DENSO = DENN(KK)
      II = 1
      DO WHILE(RSHIFT(II) .NE. 0.0)
      JJ = 1
      DO WHILE(SHAPE(JJ) .NE. 0.0)
      LL = 1
      DO WHILE(DERDEN(LL) .NE. 0.0)
      IWM = 1
```

```

DO WHILE(WM(IWM) .NE. 0.0)
  IERROR_M = 1
DO WHILE(ERROR_M(IERROR_M) .NE. 0.0)
  IERROR_B = 1
DO WHILE(ERROR_B(IERROR_B) .NE. 0.0)
  IERROR_A = 1
DO WHILE(ERROR_A(IERROR_A) .NE. 0.0)
  IERROR_W = 1
DO WHILE(ERROR_W(IERROR_W) .NE. 0.0)
  ICG = 1
DO WHILE(CG(1,ICG) .NE. 0.0)
  IB_ERROR = 1
DO WHILE(B_ERROR(IB_ERROR) .NE. 0.0)

C
C   THE VARIABLE "N" CONTAINS THE NUMBER OF ARRAY
C   POINTS THAT WE WILL BE NEEDING.
  N = NPOINTS
C   N = (WFINAL-WINIT) / WM(IWM)
  NIDEAL = (WFINAL-WINIT) / WM(IWM)
C   WSCALE = FLOAT(NPOINTS) / ( (WFINAL-WINIT) / WM(IWM) )
  WSCALE = 1.
  RRANDOM = RSEED
  IF(N.GT.NN) THEN
C     CHECK TO SEE IF THE ARRAYS SIZE ARE LARGE ENOUGH.
C     IF THE ARRAYS ARE TOO SMALL, THE PROGRAM WILL STOP
C     AND THE VALUE FOR "NN" IN THE PARAMETER STATEMENT
C     SHOULD BE INCREASE TO A HIGHER VALUE. THEN THE
C     PROGRAM MUST BE RE-COMPILED TO UP-DATE THE
C     EXECUTABLE FILE.
    WRITE(6,*)
    *   ' *** ERROR:  NN TO SMALL.  INCREASE VALUE OF NN ***'
    WRITE(6,*)
    *   ' *** THEN RE-COMPILE THE PROGRAM          ***'
    STOP
  END IF

C
C   THIS WILL CALCULATE THE POSITION WHERE THE DERIVATIVE
C   OF THE HYPERBOLIC TANGENT DENSITY PROFILE MATCHES THE
C   DERIVATIVE OF THE LINE.
  TEMP = - SQRT( 1. + (2.*SHAPE(JJ)*DERDEN(LL)/DENSO) )
  TEMP2 = (1.0 + TEMP) / (1.0 - TEMP)
  RLINE = RSHIFT(II) + SHAPE(JJ) * 0.5 * LOG(TEMP2)
!

```

Here is where the positions of the cutoffs for the frequency array is calculated. The formula used to calculate the positions of the cutoffs is the condition for cutoff in the index of refraction, given by the equation:

$$0 = 1 - \frac{\omega_{pe}^2}{\omega^2} \frac{\omega^2 - \omega_{pe}^2}{\omega^2 - \omega_{pe}^2 - \omega_{ec}^2} \quad (B.7)$$

where  $\omega$  is the wave frequency,  $\omega_{ec}$  is the electron cyclotron frequency, and  $\omega_{pe}$  is the plasma electron frequency. These parameters depend on the radial position as follows:

$$\omega_{ec} = \frac{q_e B(r)}{m_e} \quad (B.8)$$

$$\omega_{pe}^2 = \frac{q_e^2 n_e(r)}{\epsilon_0 m_e} \quad (B.9)$$

```

C
C      THIS LOOP CALCULATES THE RADIAL POSITION OF THE CRITICAL
C      LAYERS OR CUTOFF LAYERS FOR OUR PLASMA.
CSEP      APERTEMP      = APERT
CSEP      APERT          = 0.0
      DELWR      = (WFINAL - WINIT) / N      !FREQUENCY INCREMENT
      RCLOW(N+1) = RZERO(RO+RA,WINIT-DELWR-WM(IWM)/2.,RSHIFT(II)
*      ,SHAPE(JJ),DERDEN(LL))      !IN METERS
      RCUP(N+1)  = RZERO(RO+RA,WINIT-DELWR+WM(IWM)/2.,RSHIFT(II)
*      ,SHAPE(JJ),DERDEN(LL))      !IN METERS
      WREF(N+1)  = WINIT-DELWR      !WREF AND WINIT ARE IN HERTZ.
      WREF(N+2)  = WINIT-2.*DELWR   !WREF AND WINIT ARE IN HERTZ.
      DO I=N,1,-1
        WREF(I)  = WREF(I+1) + DELWR      !FREQUENCY IN HERTZ
        WGHZ(I)  = WREF(I) / 1.0D+09      !FREQUENCY IN GHz
        WGHZ_TOMY(I) = -WGHZ(I)
        RCLOW(I) = RZERO(RCLOW(I+1),WREF(I)-WM(IWM)/2.,RSHIFT(II)
*        ,SHAPE(JJ),DERDEN(LL))
        RCUP(I)  = RZERO(RCUP(I+1),WREF(I)+WM(IWM)/2.,RSHIFT(II)
*        ,SHAPE(JJ),DERDEN(LL))
        DRIND = RCLOW(I)
        MU_1 = MU2(DRIND,WREF(I)-WM(IWM)/2.
*        ,RSHIFT(II),SHAPE(JJ),DERDEN(LL))
        DRIND = RCLOW(I+1)
        MU_2 = MU2(DRIND,WREF(I)-WM(IWM)/2.
*        ,RSHIFT(II),SHAPE(JJ),DERDEN(LL))
C      WRITE(11,*)I,RCLOW(I), MU_1, MU_2
C      RRES(I)  = RZERO(RRES(I+1),WREF(I),RSHIFT(II)
C      *      ,SHAPE(JJ),DERDEN(LL))
      END DO
C      WREF(N+1)= 0.0      !SET FREQ TO 0 LINEARLY

```

```

C      WGHZ(N+1)= 0.0      !SET FREQ TO 0 LINEARLY
      WREF(0)  = N      !NUMBER OF DATA POINTS FOR AG2
      WGHZ(0)  = N      !NUMBER OF DATA POINTS FOR AG2
      WGHZ_TOMY(0) = WGHZ(0)!NUMBER OF DATA POINTS
      RCLOW(0) = N      !NUMBER OF DATA POINTS FOR AG2
      RCUP(0)  = N      !NUMBER OF DATA POINTS FOR AG2
C      RRES(0)  = N      !NUMBER OF DATA POINTS FOR AG2
CSEP      APERT = APERTEMP
      IF(IWREF.LT.0) WRITE(11,170) (I,WGHZ(I), I=1,N)
170      FORMAT(I5,' WREF=',F11.2,' GHz')
!
```

Here the code plots the cutoff frequencies as a function of the radius if requested in the NAMELIST data file.

```

C
      IF(IWREF.NE.0) THEN
C      AS AN OPTION OF THE DATA FILE, THIS PIECE OF CODE
C      CAN PLOT THE REFLECTOMETER'S FREQUENCY AS A FUNCTION
C      OF THE RADIAL POSITION OF THE CUT-OFF LAYER.
      IF( (KK.EQ.1) .AND. (JJ.EQ.1) .AND. (II.EQ.1) .AND. (LL.EQ.1)
*      .AND. (IWM.EQ.1) .AND. (IERROR_M.EQ.1) .AND. (IERROR_B.EQ.1)
*      .AND. (IERROR_A.EQ.1) .AND. (IERROR_W.EQ.1)
*      .AND. (IB_ERROR.EQ.1) ) THEN
          CALL BINITT()      !INITIALIZE DATA BLOCKS
          CALL PLACE(ABS(IWREF)) !SELECT SCREEN WINDOW
          CALL XFRM(2)      !SELECT X-AXIS TIC STYLE
          CALL YFRM(2)      !SELECT Y-AXIS TIC STYLE
          CALL XDEN(10)     !SET TIC MARKS DENSITY
          CALL XTICS(4)     !SET TIC MARKS
          X_MIN = RXMIN
          X_MAX = RXMAX
          CALL DLIMX(X_MIN,X_MAX) !SET X-AXIS DATA LIMITS
          DO K=0, RCLOW(0)
              X_DATA(K) = RCLOW(K)
              Y_DATA(K) = WGHZ(K)
          END DO
          CALL CHECK(X_DATA,Y_DATA) !SETS DATA LIMITS, ETC...
          CALL DSPLAY(X_DATA,Y_DATA) !DRAW AXIS AND PLOT DATA
          CALL SAVCOM(SIWREF) !SAVE THE COMMON BLOCKS DATA
          CALL FRAME() !FINISHES THE AXIS FRAME
          CALL AGXXGT('Frequency vs Radius') !LABELS
          CALL AGXXCHS('Major Radius (m)')
          CALL AGXXCVS('Frequency (GHz)')
      ELSE
```

```

      CALL RESCOM(SIWREF)      !RESTORE DATA IN COMMON BLOCKS
      CALL XDEN(10)           !SET TIC MARKS DENSITY
      CALL XTICS(4)           !SET TIC MARKS
      X_MIN = RXMIN
      X_MAX = RXMAX
      CALL DLIMX(X_MIN,X_MAX)  !SET X-AXIS DATA LIMITS
      DO K=0, RCLOW(0)
        X_DATA(K) = RCLOW(K)
        Y_DATA(K) = WGHZ(K)
      END DO
      CALL DSPLAY(X_DATA,Y_DATA) !DRAW AXIS AND PLOT DATA
    END IF
  END IF
!
```

Here the code calculates the distance between the cutoff positions and plot them if requested in the NAMELIST data file.

```

C
C      HERE WE CALCULATE THE DISTANCE IN BETWEEN THE REFLECTING
C      POINTS OF THE UPPER AND LOWER FREQUENCIES. THIS IS NOT
C      NEEDED FOR THE RECONSTRUCTION PROCESS, BUT IT WAS NEEDED
C      TO DETERMINE IF THE SPACING IN BETWEEN THE PROBING
C      FREQUENCIES IS SMALLER THAN THE CORRELATION LENGTH
C      OF THE DENSITY FLUCTUATIONS.
      DO I=N,1,-1
        DELRC(I) = ( RCLOW(I) - RCUP(I) ) * 100.    !convert to cm
      END DO
      DELRC(0) = N      !NUMBER OF DATA POINTS FOR AG2
      TRANS(0) = N      !NUMBER OF DATA POINTS FOR AG2
      IF(IDELRC.NE.0) THEN
        IF( (KK.EQ.1) .AND. (JJ.EQ.1) .AND. (II.EQ.1) .AND. (LL.EQ.1)
          * .AND. (IWM.EQ.1) .AND. (IERROR_M.EQ.1) .AND. (IERROR_B.EQ.1)
          * .AND. (IERROR_A.EQ.1) .AND. (IERROR_W.EQ.1)
          * .AND. (IB_ERROR.EQ.1) ) THEN
C
          CALL BINITT()      !INITIALIZE DATA BLOCKS
          IF( (-13 .LE. IDELRC) .AND. (IDELRC .LE. 13) ) THEN
            CALL PLACE(ABS(IDELRC)) !SET SCREEN WINDOW
          ELSE IF((-14.LE.IDELRC).AND.(IDELRC.LE.14)) THEN
            CALL SLIMX(IPHIMINX,IPHIMAXX) !SET UPPER PLOT WINDOW
            CALL SLIMY(IPHIMINY+ISHIFTY,IPHIMAXY+ISHIFTY)
            PLABEL = '(A)' !SET PLOT LABEL
          ELSE !SET LOWER PLOT WINDOW
            CALL SLIMX(IPHIMINX,IPHIMAXX) !SET SCREEN PLOT LIMITS
          END IF
        END IF
      END IF

```

```
      CALL SLIMY(IPHIMINY,IPHIMAXY)  !SET SCREEN PLOT LIMITS
      PLABEL = '(B)'  !SET PLOT LABEL
    END IF
    CALL XFRM(2)  !SET X-AXIS TIC STYLE
    CALL YFRM(2)  !SET Y-AXIS TIC STYLE
    CALL XDEN(10)  !SET TIC MARKS DENSITY
    CALL XTICS(4)  !SET TIC MARKS
    X_MIN = RXMIN
    X_MAX = RXMAX
    CALL DLIMX(X_MIN,X_MAX)  !SET X-AXIS DATA LIMITS
    DO K=0, RCLOW(0)
      X_DATA(K) = RCLOW(K)
      Y_DATA(K) = DELRC(K)
    END DO
    CALL CHECK(X_DATA,Y_DATA)  !SETS DATA LIMITS, ETC...
    CALL DSPLAY(X_DATA,Y_DATA)  !DRAW AXIS AND PLOT DATA
    CALL SAVCOM(SIDELRC)  !SAVE COMMON BLOCKS DATA
    IF(ICLABEL.NE.0) CALL CLABEL(ICDELRC,NUMBER,RCLOW,DELRC)
    CALL FRAME()  !DRAW FRAME AROUND WINDOW
    CALL AGXXGT('Cutoff Separation')  !LABELS
    CALL AGXXCHS('Major Radius (m)')
    CALL AGXXCVS('Centimeters')
    CALL AGXXMHS(IPHIMINX-125,IPHIMAXY,PLABEL)
    IXSMIN = COMGET(IBASEX(13))
    IYSMAX = COMGET(IBASEY(14))
    CALL AGXXMHS(IXSMIN-125,IYSMAX,PLABEL)
  ELSE
    CALL RESCOM(SIDELRC)  !RESTORE COMMON BLOCKS DATA
    CALL XDEN(10)  !SET TIC MARKS DENSITY
    CALL XTICS(4)  !SET TIC MARKS
    X_MIN = RXMIN
    X_MAX = RXMAX
    CALL DLIMX(X_MIN,X_MAX)  !SET X-AXIS DATA LIMITS
    DO K=0, RCLOW(0)
      X_DATA(K) = RCLOW(K)
      Y_DATA(K) = DELRC(K)
    END DO
    CALL DSPLAY(X_DATA,Y_DATA)  !DRAW AXIS AND PLOT DATA
    IF(ICLABEL.NE.0) CALL CLABEL(ICDELRC,NUMBER,RCLOW,DELRC)
  END IF
END IF
!
```



Here is where the phase,  $\phi$ , of the probing beam is calculated from the information know. The phase is calculated using the equation:

$$\phi(\omega_i) = \int_{r_c(\omega_i)}^{r_{edge}} n(r, \omega_i) dr \quad (B.10)$$

where  $r_c(\omega_i)$  is the cutoff position for the probing frequency  $\omega_i$ ,  $r_{edge}$  is the position of the reference plane at the edge, and  $n(r, \omega_i)$  is the index of refraction as a function of the radial position and the probing frequency.

```

C
C      HERE WE CALCULATE THE PHASE OUT OF THE ASSUMED
C      DENSITY PROFILE AND THE PREVIOUS DATA.  THIS IS
C      THE "REAL" CALCULATED FULL PHASE OF THE LOWER AND
C      UPPER PROBING FREQUENCIES, USING THE "REAL" ASSUMED
C      DENSITY PROFILE.  SEE FUNCTION "SN" IN APPENDIX B OF
C      THE THESIS FOR A DESCRIPTION OF FORMULA AND FUNCTION.

      PHIAVE = 0.0
CSEP      TEMP = APERT
CSEP      APERT = 0.0
C      WRITE(11,*) ' I,  PHILOW(I)  WPHILOW(I),  ERR,  PHIUP(I),  '
C      *  ',  WPHIUP(I),  ERR  '      !CWILGEN
      DO I=N,1,-1
          DP1 = 2.*( (WREF(I)-WM(IWM)/2.) /C)
C      *      *SN(RO+RA,RCLOW(I),WREF(I)-WM(IWM)/2.,RSHIFT(II),SHAPE(JJ)
      *      *SN(RGREG,RCLOW(I),WREF(I)-WM(IWM)/2.,RSHIFT(II),SHAPE(JJ)
      *      ,DERDEN(LL))
          PHILOW(I) = DP1
          DP2 = 2.*( (WREF(I)+WM(IWM)/2.) /C)
C      *      *SN(RO+RA,RCUP(I),WREF(I)+WM(IWM)/2.,RSHIFT(II),SHAPE(JJ)
      *      *SN(RGREG,RCUP(I),WREF(I)+WM(IWM)/2.,RSHIFT(II),SHAPE(JJ)
      *      ,DERDEN(LL))
          PHIUP(I) = DP2
          DDELPHI(I) = (DP2 - DP1)
C      DDELPHI(I) = (DP2 - DP1) / WSCALE
C      PHIUP_2(I) = 2.*( (WREF(I)+WM(IWM)) /C)
CC      *      *SN(RO+RA,RCLOW(I),WREF(I)+WM(IWM),RSHIFT(II),SHAPE(JJ)
C      *      *SN(RGREG,RCLOW(I),WREF(I)+WM(IWM),RSHIFT(II),SHAPE(JJ)
C      *      ,DERDEN(LL))
C      TEMP = PHIUP(I) - PHIUP_2(I)
C      DRIND = RCLOW(I)
C      TEMP2 = ( 2. * (WREF(I)+WM(IWM)) / C )
C      *      * DELRC(I) / 100.      ! DELRC(I) in meters
C      *      * SQRT(MU2(DRIND,WREF(I)+WM(IWM),RSHIFT(II),SHAPE(JJ)
C      *      ,DERDEN(LL)))

```

```

CC      WRITE(11,140)I, TEMP, TEMP2, PHILOW(I), PHIUP(I)
C      *      , PHIUP_2(I)
CC      *      , (TEMP-TEMP2)/TEMP
CC      *      , ABS((TEMP-TEMP2)/(PHIUP(I)-PHILOW(I)))
CC      *      , DELRC(I)
CC 140      FORMAT(I5,' ',F5.3,' ',F5.3,' ',F7.3,' ',F7.3,' ',F7.3
CC      *      ,', ',F11.3,' ',F11.3,' ',F11.3)
C      PHIAVE = PHIAVE + (TEMP-TEMP2)/(PHIUP(I)-PHILOW(I))
C
CWILGEN  BEGIN:  CALCULATE PHASE USING CUBIC SPLINE ROUTINE
          DELRL = (RO+RA - RCLOW(I)) / N
          DELRU = (RO+RA - RCUP(I) ) / N
C          DELRL = (RGREG - RCLOW(I)) / N
C          DELRU = (RGREG - RCUP(I) ) / N
          DO K = N, 1, -1
              RWLOW(K) = RO+RA - DELRL * (N-K)
              RWUP(K) = RO+RA - DELRU * (N-K)
C              RWLOW(K) = RGREG - DELRL * (N-K)
C              RWUP(K) = RGREG - DELRU * (N-K)
              DRIND = RWLOW(K)
              TEMP1 = MU2(DRIND,WREF(I)-WM(IWM)/2.,RSHIFT(II)
              *      ,SHAPE(JJ),DERDEN(LL))
C              WMULOW(K) = SQRT(MU2(DRIND,WREF(I),RSHIFT(II)
C              *      ,SHAPE(JJ),DERDEN(LL)))
              WMULOW(K) = TEMP1 / SQRT( ABS( TEMP1 ) )
              DRIND = RWUP(K)
C              WMUUP(K) = SQRT(MU2(DRIND,WREF(I)+WM(IWM),RSHIFT(II)
C              *      ,SHAPE(JJ),DERDEN(LL)))
              TEMP1 = MU2(DRIND,WREF(I)+WM(IWM)/2.,RSHIFT(II),SHAPE(JJ)
              *      ,DERDEN(LL))
              WMUUP(K) = TEMP1 / SQRT( ABS( TEMP1 ) )
C              WRITE(11,*)K, RWLOW(K), RWUP(K), WMULOW(K), WMUUP(K)
          END DO
C      WRITE(11,*) I, WMULOW(1)/WMULOW(2)
          WPHILOW(I) = SPLN(N,RWLOW,WMULOW) * 2.*(WREF(I)-WM(IWM)/2.)/C
          WPHIUP(I) = SPLN(N,RWUP,WMUUP) * 2.*(WREF(I)+WM(IWM)/2.)/C
C      DRIND = RCLOW(I)
C      MU_1 = MU2(DRIND,WREF(I)
C      DRIND = RCUP(I)
C      MU_2 = MU2(DRIND,WREF(I)+WM(IWM)
C      *      ,RSHIFT(II),SHAPE(JJ),DERDEN(LL))
C      *      ,RSHIFT(II),SHAPE(JJ),DERDEN(LL))
C      WRITE(11,*)I, WMULOW(1)**2, WMUUP(1)**2, MU_1, MU_2
C      WRITE(11,260) I
C      *      , PHILOW(I), WPHILOW(I)

```

```

C      *      , ABS( PHILOW(I)- WPHILOW(I) )/PHILOW(I)
C      *      , PHIUP(I) , WPHIUP(I)
C      *      , ABS( PHIUP(I) - WPHIUP(I) )/PHIUP(I)
C 260      FORMAT(I5,2(2F12.7,F12.8))
CWILGEN      END
          END DO
CSEP      APERT = TEMP
C      PHIAVE = ABS(PHIAVE) / N
C      WRITE(11,*)' PHIAVE = ', PHIAVE
          PHILOW(0) = N      !NUMBER OF DATA POINTS FOR AG2
          PHIUP(0) = N      !NUMBER OF DATA POINTS FOR AG2
          IF(IPHI.LT.0) WRITE(11,180) (I,PHILOW(I),PHIUP(I), I=1,N)
180      FORMAT(I5,' PHIUP=',F11.2,' PHILOW=',F11.2)
C
          DEN2 = (WREF(N)-WM(IWM)/2.) * (WREF(N)-WM(IWM)/2.-WCE)
          * * (ELEMAS/ELECHR) * (EPSILO/ELECHR) * (2. * PI)**2
!

```

This part calculates the transmission and reflected fraction of the wave.

```

C
      IF(ITRANS.NE.0) THEN
C      THIS PART CALCULATES THE TRANSMITTED AND REFLECTED
C      COEFFICIENTS OF THE PROBING BEAM. THIS IS TO STUDY
C      THE BUDDEN TUNNELING OF THE PROBING BEAM. SEE THE
C      REFERENCES ON BUDDEN, CHAP 2, EQ. 2.190 AND 2.191
          DELDEN = (DEN2-DEN1) / N
          D(0) = DEN1
          B0 = BFIELD(R0)
          DO I=1,N
              D(I) = D(I-1) + DELDEN
              MU = 2.*PI*PI*((WREF(N)-WM(IWM)/2.)/C)*
*              (0.5*(R0+RA)**3+ELEMAS*D(I)) /
/              (EPSILO*B0*B0*R0*R0)
              TRANS(I) = EXP(-0.5*MU)
              REFL(I) = 1 - EXP(-MU)
          END DO
          D(0) = N      !NUMBER OF DATA POINTS FOR AG2
          TRANS(0) = N      !NUMBER OF DATA POINTS FOR AG2
          REFL(0) = N      !NUMBER OF DATA POINTS FOR AG2
          IF( (KK.EQ.1) .AND. (JJ.EQ.1) .AND. (II.EQ.1) .AND. (LL.EQ.1)
*          .AND. (IWM.EQ.1) .AND. (IERROR_M.EQ.1) .AND. (IERROR_B.EQ.1)
*          .AND. (IERROR_A.EQ.1) .AND. (IERROR_W.EQ.1)
*          .AND. (IB_ERROR.EQ.1) ) THEN
              CALL BINITT()      !INITIALIZED DATA BLOCKS

```

```

      CALL PLACE(ABS(ITRANS))  !SET SCREEN WINDOW
      CALL XFRM(2)  !SET X-AXIS TIC STYLE
      CALL YFRM(2)  !SET Y-AXIS TIC STYLE
C      CALL CHECK(D,REFL)  !CHECK DATA LIMITS, ETC...
C      CALL DSPLAY(D,REFL)  !DRAW AXIS AND PLOT DATA
      CALL DLIMY(0.0,1.0)  !SET Y-AXIS DATA WINDOW
      DO K=0, D(0)
        X_DATA(K) = D(K)
        Y_DATA(K) = REFL(K)
      END DO
      CALL CHECK(X_DATA,Y_DATA)  !SETS DATA LIMITS, ETC...
      CALL DSPLAY(X_DATA,Y_DATA)  !DRAW AXIS AND PLOT DATA
      CALL SAVCOM(SITRANS)  !SAVE DATA BLOCKS

      DO K=0, D(0)
        X_DATA(K) = D(K)
        Y_DATA(K) = TRANS(K)
      END DO
      CALL CPLOT(X_DATA,Y_DATA)  !DRAW AXIS AND PLOT DATA
C      CALL CPLOT(D,TRANS)  !OVER PLOT NEXT DATA SET
      CALL FRAME()  !FRAME THE SCREEN WINDOW
      CALL AGXIGT('Reflection & Transmission')  !LABELS
      CALL AGXICHS('Density part/M**3')  !OUTPUT LABEL
      CALL AGXICVS(' ')  !OUTPUT LABEL
    ELSE
      CALL RESCOM(SITRANS)  !RESTORE DATA BLOCKS
C      CALL DSPLAY(D,REFL)  !OVER PLOT NEXT DATA SET
C      CALL CPLOT(D,TRANS)  !OVER PLOT NEXT DATA SET
      DO K=0, D(0)
        X_DATA(K) = D(K)
        Y_DATA(K) = REFL(K)
      END DO
      CALL DSPLAY(X_DATA,Y_DATA)  !DRAW AXIS AND PLOT DATA
      DO K=0, D(0)
        X_DATA(K) = D(K)
        Y_DATA(K) = TRANS(K)
      END DO
      CALL CPLOT(X_DATA,Y_DATA)  !DRAW AXIS AND PLOT DATA
    END IF
  END IF
!
```

Here is where the code calculates the offsets and oscillations to the phase difference.

C

```

C      CALCULATING:  PHI_p(f+) - PHI_p(f-)
C      THIS IS THE DATA THAT IT IS ACTUALLY USE TO CALCULATE THE
C      RECONSTRUCTED DENSITY PROFILE.
      SIGN = 1.  !SIGN FOR FRACTAL RANDOM NUMBER
      FRACTAL = RSEED  !SEED FOR FRACTAL FUNCTION
      AVENOISE = 0.0  !TEMPORARY VARIABLE
C      ISEED = 9762531  !SEED FOR RANDOM NUMBER GENERATOR
      ISEED = RSEED  !SEED FOR RANDOM NUMBER GENERATOR
      CALL RNSET(ISEED)  !SET THE SEED
      DO I=N,1,-1
        OFFSET(I) =
          *      (ERROR_M(IERROR_M)*(WGHZ(I)-ERROR_XO)+ERROR_B(IERROR_B))
          *      * ERROR_A(IERROR_A)
          *      * COS(2.*PI*(WGHZ(I)-ERROR_XO)/(ERROR_W(IERROR_W)))
          RNOISE = 0.0  !INITIALIZE VARIABLE
          IF(ISMOOTH.EQ.0) ISMOOTH=1
          DO J=1,ISMMOOTH  !BEGIN TOMY SMOOTHING
C            FRACTAL = EPSILON * FRACTAL * (1.- FRACTAL)
C            ISEED = 935721 + ( 900000. / FRACTAL )
C            RRANDOM = RAN(ISEED)
C            RNOISE = SIGN * RRANDOM * ANOISE
C            TEMP = DELRC(I)
            TEMP = RCLOW(N) - RCLOW(I)
            TEMP2 = 0.5
            RNOISE = RNOISE + RNOF()*ANOISE
          *      * (1. - APERT*DBRETZ(RCLOW(I)))
          *      * (0.2+0.8*EXP(-TEMP*TEMP/(TEMP2*TEMP2)))
            END DO
            RNOISE = RNOISE / ISMOOTH
            DNOISE(I) = RNOISE/PI
            DELPHI(I) = DDELPHI(I)  ! (PHIUP(I) - PHILOW(I))
          *      * (1. + RNOISE)
CHERE      *      * (1. + ANOISE * DBRETZ(RCLOW(I)))
CHERE      +      + RNOISE
          +      + OFFSET(I)
C          +      + 0.5 * EXP((WGHZ(I)-97. )**2/-4.)
C          +      + 0.5 * EXP((WGHZ(I)-110. )**2/-4.)
            DELPHI(I) = DELPHI(I) / WSCALE
            AVENOISE = AVENOISE + RNOISE
C          SIGN = -SIGN
        END DO  !END TOMY SMOOTHING
        AVENOISE = AVENOISE / N
C      WRITE(11,*) ' AVENOISE =', AVENOISE
      DELPHI(0) = N  !NUMBER OF DATA POINTS FOR AG2
      OFFSET(0) = N  !NUMBER OF DATA POINTS FOR AG2

```

```

C      CALL SMOOTH(ISMOOTH,DELPHI,WORK)
!

```

Here the code calculates the numerical derivative of the phase. This can be compared with the phase difference and a clear similarity can be seen. The derivative of the phase is used to calculate the density profile when there is no magnetic field and an Abel inversion of the data can be done.

```

C
C      HERE WE CALCULATE THE DERIVATIVE OF THE PHASE
C      WITH RESPECT TO THE PROBING FREQUENCY.
      IF(IDDPDW.NE.0) THEN
        DO I=N,2,-1  !DEFINITION OF DERIVATIVE
          DDPDW(I) = (PHILOW(I)-PHILOW(I-1))/(WREF(I)-WREF(I-1))
        END DO
        DDPDW(1) = DDPDW(2)  !SET SPLINE POINTS
        WGHZ(N+1) = WGHZ(N) - DELWR/1.0D+09
        DDPDW(N+1) = DDPDW(N)  !SET SPLINE POINTS
        WGHZ(N+2) = WGHZ(N+1) - DELWR/1.0D+09
        DDPDW(N+2) = DDPDW(N+1) / 2.  !SET SPLINE POINTS
        WGHZ(N+3) = WGHZ(N+2) - DELWR/1.0D+09
        DDPDW(N+3) = DDPDW(N+2) / 2.  !SET SPLINE POINTS
        WREF(0) = N  !NUMBER OF DATA POINTS FOR AG2
        DDPDW(0) = N  !NUMBER OF DATA POINTS FOR AG2
C
        TEMP = (EPSILO/ELECHR) * (ELEMAS/ELECHR) * 4. * PI * PI
        DO I = N-1, 1, -1  !ABEL INTEGRAL LOOP
C      DO I = N, 1, -1  !ABEL INTEGRAL LOOP
          TEMP2 = SABEL(I,N+3,WGHZ,DDPDW) * C / PI  !INCREMENT
          RABEL(I) = RGREG - TEMP2  !CALCULATE RADIAL POSITION
          DABEL(I) = WREF(I) * WREF(I) * TEMP  !CALCULATE DENSITY
C      WRITE(11,*) I, TEMP2, RABEL(I), DABEL(I), WREF(I)
        END DO
        RABEL(N) = RGREG  !SET LAST DATA POINT
        DABEL(N) = 0.0  !SET LAST DATA POINT
        RABEL(0) = N  !SET NUMBER OF DATA POINTS
        DABEL(0) = N  !SET NUMBER OF DATA POINTS
      END IF
!

```

Here we plot the Abel density if requested.

```

      IF(IDDPDW.GT.0) THEN
        IF( (KK.EQ.1) .AND. (JJ.EQ.1) .AND. (II.EQ.1) .AND. (LL.EQ.1)

```

```

*      .AND. (IWM.EQ.1) .AND. (IERROR_M.EQ.1) .AND. (IERROR_B.EQ.1)
*      .AND. (IERROR_A.EQ.1) .AND. (IERROR_W.EQ.1)
*      .AND. (IB_ERROR.EQ.1) ) THEN
      CALL BINITT()      !INITIALIZE DATA BLOCKS
      CALL PLACE(ABS(IDDPDW)) !SET SCREEN WINDOW
      CALL XFRM(2)      !SET X-AXIS TIC STYLE
      CALL YFRM(2)      !SET Y-AXIS TIC STYLE
C      CALL DLIMX(RXMIN,RXMAX) !SET X-AXIS LIMITS
C      CALL DLIMY(DYMIN,DYMAX) !SET Y-AXIS LIMITS
C      CALL CHECK(RABEL,DABEL) !SET DATA WINDOW, ETC...
C      CALL DSPLAY(RABEL,DABEL) !DRAW AXIS AND PLOT DATA
      X_MIN = RXMIN
      X_MAX = RXMAX
      CALL DLIMX(X_MIN,X_MAX) !SET X-AXIS DATA LIMITS
      Y_MIN = DYMIN
      Y_MAX = DYMAX
      CALL DLIMY(Y_MIN,Y_MAX)
      DO K=0, RABEL(0)
        X_DATA(K) = RABEL(K)
        Y_DATA(K) = DABEL(K)
      END DO
      CALL CHECK(X_DATA,Y_DATA) !SETS DATA LIMITS, ETC...
      CALL DSPLAY(X_DATA,Y_DATA) !DRAW AXIS AND PLOT DATA
      CALL SAVCOM(SIDDPDW) !SAVE DATA BLOCKS
      CALL FRAME() !FRAME THE SCREEN WINDOW
      CALL AGXXGT('Abel Density') !LABELS
      CALL AGXXCHS('Major Radius (m)') !OUTPUT LABEL
      CALL AGXXCVS('part/m^3') !OUTPUT LABEL
    ELSE
C      CALL RESCOM(SIDDPDW) !RESTORE DATA BLOCKS
C      CALL CPLOT(RABEL,DABEL) !OVER PLOT NEXT DATA SET
      DO K=0, RABEL(0)
        X_DATA(K) = RABEL(K)
        Y_DATA(K) = DABEL(K)
      END DO
      CALL CPLOT(X_DATA,Y_DATA) !DRAW AXIS AND PLOT DATA
    END IF
  END IF
!

```

This is the part of the code where the assumption of the linear density profile before the first cutoff is done.

```

C
C      CALL VT$TPMODE() !SET TERMINAL TO ALPHA-NUMERIC MODE

```

```

C      WE CAN ASSUME A LINEAR OR EXPONENTIAL DENSITY PROFILE FOR
C      THE PLASMA BEFORE THE FIRST CUT-OFF AT THE ASSUMED POSITION
C      "RINIT". THIS SECTION OF THE CODE CALCULATES THE DENSITY
C      FOR THAT PART OF THE PROFILE.
      RK1 = RGREG      !POSITION OF GREG'S REFERENCE PLANE
      IF(RINIT.GT. 0) THEN      !USE THE CUTOFF FROM NAMELIST
        RK2 = RINIT      !POSITION OF THE FIRST REFLECTION LAYER
      ELSE      !USE THE REAL CUTOFF POSITION
        RK2 = RZERO(RCLOW(N),WREF(N)-(WM(IWM)/2.)/WSCALE
*      ,RSHIFT(II),SHAPE(JJ),DERDEN(LL))
C      RK2 = RCLOW(N)
      END IF
C      CALCULATED DENSITY FOR THE FIRST CUT-OFF AT THE
C      POSITION RK2
      BF = BFIELD(RK2)      !DEFINES THE MAGNETIC FIELD
C      ELECTRON CYCLOTRON FREQ
      WCE = (BF * ELECHR / ELEMAS) / ( 2. * PI)
      DEN2 = (WREF(N)-WM(IWM)/2.) * (WREF(N)-WM(IWM)/2.-WCE)
*      * (ELEMAS/ELECHR) * (EPSILO/ELECHR) * (2. * PI)**2
      DEN2UP = (WREF(N)+WM(IWM)/2.) * (WREF(N)+WM(IWM)/2.-WCE)
*      * (ELEMAS/ELECHR) * (EPSILO/ELECHR) * (2. * PI)**2
C      RK2UP = (DEN2UP-DEN1) * (RK2-RK1)/(DEN2-DEN1) + RK1
      RK2UP = RZERO(RCUP(N),WREF(N)+(WM(IWM)/2.)/WSCALE
*      ,RSHIFT(II),SHAPE(JJ),DERDEN(LL))
      DELRK = (RK1-RK2) / FLOAT(NN2)
      DELRKUP = (RK1-RK2UP) / FLOAT(NN2)
CE      U = (LOG(DEN2/DEN1)) / (RK1-RK2)      !FOR EXPONENTIAL
      DSLOPE = (DEN1-DEN2) / (RK1-RK2)      !FOR LINEAR PROFILE
      RK = RK1 + DELRK      !INITIALIZE PARAMETER
      RKUP = RK1 + DELRKUP      !INITIALIZE PARAMETER
C      CALCULATE THE PROFILE BEFORE THE FIRST CUTOFF
      DO K=N, NN2+N
        RK = RK2 + DELRK * (K-N)
        RKUP = RK2UP + DELRKUP * (K-N)
        RRLow(K) = RK
        RRUP(K) = RKUP
CE        DENLOW(K) = DEN2 * EXP(-U*(RK-RK2))      !FOR EXPONENTIAL
C        DENLOW(K) = DSLOPE * (RK - RK2) + DEN2!FOR LINEAR PROFILE
C        DENUP(K) = DSLOPE * (RKUP - RK2UP) + DEN2UP
        DENLOW(K) = DENSITY(RK ,RSHIFT(II),SHAPE(JJ),DERDEN(LL))
        DENUP(K) = DENSITY(RKUP,RSHIFT(II),SHAPE(JJ),DERDEN(LL))
        MU2K = MU2REC(RK,DENLOW(K),WREF(N)-(WM(IWM)/2.)/WSCALE)
C        WRITE(11,*) K, RK, RRLow(K), DENLOW(K), MU2K
        RR(K+1-N) = RK
        MURR(K+1-N) = MU2K / SQRT(ABS(MU2K))

```



```

END DO
RR(0)  = NN2+1  !NUMBER OF DATA POINTS
MURR(0) = NN2+1  !NUMBER OF DATA POINTS
RR(1)   = RK2
MURR(1) = 0.0
T1 = 0.
T2 = 0.
!
```

Here is where the loop for the reconstruction process starts. But, before the actual loop starts some definitions and initial conditions need to be calculated.

```

C
C      AFTER CALCULATING AN ASSUMED DENSITY PROFILE FOR
C      THE EDGE OF THE PLASMA BEFORE THE FIRST CUT-OFF
C      POSITION, WE START WITH THE RECONSTRUCTION OF THE
C      DENSITY PROFILE. FIRST WE CALCULATE THE PHASE DUE TO
C      THE ASSUMED DENSITY PROFILE BEFORE THE FIRST CUT-OFF
PRLOWIN = ( 2.*(WREF(N)-(WM(IWM)/2.)/WSCALE) / C )
*      * SNREC(N,N+NN2,RRLOW(1),DENLOW(1)
*      ,WREF(N)-(WM(IWM)/2.)/WSCALE)
C      PRLOWIN = ( 2. * (WREF(N)-WM(IWM)/2.) / C )
C      *      * SNREC(N,N+NN2,RRLOW(1),DENLOW(1),WREF(N)-WM(IWM)/2.)
C      PRLOWIN = 2. * ( WREF(N) + WM(IWM)/2. ) / C
C      *      * SNREC(N,N+NN2,RRUP(1),DENUP(1),WREF(N)+WM(IWM)/2.)
WRITE(11,*) PRLOWIN
C      PHIRLOW(N) = PRLOWIN ! * FGREG
PHIRLOW(N) = PHILOW(N)
WRITE(11,*) PHIRLOW(N), PHILOW(N), RRLOW(N), RCLOW(N)
CC      WRITE(11,*) ' PHIRLOW(N)=', PHIRLOW(N), ' PHIRUP(N)=', PRUPIN
CC      WRITE(11,*) ' PHILOW(N) =', PHILOW(N), ' PHIUP(N) =', PHIUP(N)
WREF(0) = WFINAL
C      WRITE(11,*) ' I ', ' RRLOW ', ' RRUP ', ' PHIL ', ' PHIU '
C      *      , ' DPHI ', ' PHIRL ', ' PHIRU ', ' DPHIR ', ' DENLOW '
C      *      , ' DENUP '
C      THIS IS THE MAIN LOOP OF THE RECONSTRUCTION AND MODELING
C      PROGRAM. THE RECONSTRUCTION FORMULA USED HERE IS
C      DESCRIBED IN APPENDIX B, SECTION B.2, AND CHAPTER 6 IN
C      SECTIONS 6.2.2, EQUATIONS 6.13 AND 6.34 OF THE THESIS.
C****
DO I=N,1,-1
C      CALL THE SUBROUTINE TO CALCULATE THE RECONSTRUCTED PROFILE
      CALL THOMAS(I,N,NN2,RRLOW,DELREC,RRUP,DENLOW,DENUP
*      ,PHIRLOW,DELPHI,PHIRUP,WREF,WM(IWM)/WSCALE,RSHTFT(II)
*      ,SHAPE(JJ),DERDEN(LL),DELRC,AGREG_,IDUMY,RZDEL)
```

```

CC      WRITE(11,200) I, (RCLOW(I)-RCUP(I))/WSCALE
CC      *      , (RCLOW(I)-RCUP(I)-WSCALE*DELREC(I))/(RCLOW(I)-RCUP(I))*100.
CC 200    FORMAT(I4,F16.10,'m',F14.8,'%')
C        WRITE(11,*) I, RCLOW(I), RRLOW(I), (RCLOW(I)-RRLOW(I))/RCLOW(I)
C        WRITE(11,*) I, DELREC(I), RCLOW(I)-RCUP(I)
C      *      , ( DELREC(I) - (RCLOW(I)-RCUP(I)) )
      END DO
      WREF(0)   = N      !NUMBER OF DATA POINTS FOR AG2
      DELREC(0) = N      !NUMBER OF DATA POINTS FOR AG2
      RRLOW(0)  = NN2 + N !NUMBER OF DATA POINTS FOR AG2
      RRUP(0)   = NN2 + N !NUMBER OF DATA POINTS FOR AG2
      DENLOW(0) = NN2 + N !NUMBER OF DATA POINTS FOR AG2
      DENUP(0)  = NN2 + N !NUMBER OF DATA POINTS FOR AG2
      DELPREC(0) = N     !NUMBER OF DATA POINTS FOR AG2
      PHIRLOW(0) = N     !NUMBER OF DATA POINTS FOR AG2
      PHIRUP(0)  = N     !NUMBER OF DATA POINTS FOR AG2
      AGREG_(0)  = N

```

This plots some of the results from the previous calculations. The phase is plotted first if requested in the namelist data file.

```

C
C      PLOT "REAL" AND RECONSTRUCTED FULL PHASE FOR COMPARISON.
C      IF(IPHI.NE.0) THEN
C        IF( (KK.EQ.1) .AND. (JJ.EQ.1) .AND. (II.EQ.1) .AND. (LL.EQ.1)
C          *   .AND. (IWM.EQ.1) .AND. (IERROR_M.EQ.1) .AND. (IERROR_B.EQ.1)
C          *   .AND. (IERROR_A.EQ.1) .AND. (IERROR_W.EQ.1)
C          *   .AND. (IB_ERROR.EQ.1) ) THEN
C          CALL BINITT()      !INITIALIZE DATA BLOCK
C          CALL PLACE(ABS(IPHI)) !SET SCREEN WINDOW
C          CALL XFRM(2)      !SET X-AXIS TIC STYLE
C          CALL YFRM(2)      !SET Y-AXIS TIC STYLE
C          CALL CHECK(WGHZ,PHIRLOW) !SET DATA LIMITS, ETC...
C          CALL DSPLAY(WGHZ,PHIRLOW) !DRAW AXIS AND PLOT DATA
C          DO K=0, WGHZ(0)
C            X_DATA(K) = WGHZ(K)
C            Y_DATA(K) = PHIRLOW(K)
C          END DO
C          CALL CHECK(X_DATA,Y_DATA) !SETS DATA LIMITS, ETC...
C          CALL DSPLAY(X_DATA,Y_DATA) !DRAW AXIS AND PLOT DATA
C          CALL SAVCOM($IPHI) !SAVE COMMON BLOCKS DATA
C          DO K=0, WGHZ(0)
C            Y_DATA(K) = PHIRUP(K)
C          END DO

```

```

CALL CPlot(X_DATA,Y_DATA)  !PLOT NEXT DATA SET
CALL LINE(4)  !SET LINE TYPE
DO K=0,WGHZ(0)
  Y_DATA(K) = PHILOW(K)
END DO
C   CALL CPlot(WGHZ,PHILOW)  !PLOT NEXT DATA SET
CALL CPlot(X_DATA,Y_DATA)  !PLOT NEXT DATA SET
DO K=0,WGHZ(0)
  Y_DATA(K) = PHIUP(K)
END DO
C   CALL CPlot(WGHZ,PHIUP)  !PLOT NEXT DATA SET
CALL CPlot(X_DATA,Y_DATA)  !PLOT NEXT DATA SET

C   THIS WILL PUT 5 EVENLY SPACED "+" FOR USED AS MARKERS.
K = 0  !INITIALIZE INDEX
DO I=WGHZ(0),1, WGHZ(0)/5.
  K = K + 1
  X(K) = WGHZ(I)
  Y(K) = PHIRLOW(I)
END DO
X(0) = K  !NUMBER OF DATA POINTS FOR AG2
Y(0) = K  !NUMBER OF DATA POINTS FOR AG2
CALL LINE(-4)  !SET LINE TYPE TO A POINT PLOT
CALL SYMBL(REC_SYMB)  !SET SYMBOL TYPE TO A "+"
CALL CPlot(X,Y)  !PLOT NEXT DATA SET
CALL FRAME()  !FRAME SCREEN WINDOW
CALL AGXXGT('Phase vs Frequency')  !LABELS
CALL AGXXCHS('Frequency (GHz)')  !OUTPUT LABEL
CALL AGXXCVS('Fringes')  !OUTPUT LABEL
C   PLOTTING THE LEGEND, THIS PIECE OF CODE MAKES A
C   LEGEND ON THE UPPER RIGHT CORNER OF THE DATA WINDOW.
C   THIS DEFINES THE X-AXIS SCREEN COORDINATE OF THE
C   LEGEND LABEL.
IXLEG = COMGET(IBASEX(13)) + 3./5.  !X POSITION
*   * ( COMGET(IBASEX(14)) - COMGET(IBASEX(13)) )
C   THIS DEFINES THE Y-AXIS SCREEN COORDINATE OF THE
C   LEGEND LABEL.
IYLEG = COMGET(IBASEY(14)) - 20  !Y POSITION
IX1BOX = IXLEG - 10  ! CALCULATE LEGEND CORNER
IY1BOX = IYLEG + 10  ! CALCULATE LEGEND CORNER
CALL MOVABS(IXLEG, IYLEG)  !MOVE TO POSITION
CALL SYMOUT(REC_SYMB, 1.)  !OUTPUT LEGEND SYMBOL
C   CALL SYMOUT(45, 3.)  !OUTPUT LEGEND SYMBOL
CALL MOVREL(-10,0)  !MOVE TO DRAW LINE
CALL DRWREL(20,0)  !DRAW LINE

```

```

CALL AGXXMHS(IXLEG+20,IYLEG-6,'Reconstructed')
IX2BOX = IX1BOX + 220    !NEXT LEGEND POSITION
IY2BOX = IY1BOX - 20    !NEXT LEGEND POSITION
CALL AGXXMHS(IXLEG-5,IYLEG-25,'-- Assumed')
IY2BOX = IY2BOX - 25    !NEXT LEGEND POSITION
CALL MOVABS(IX1BOX,IY1BOX)    !MAKE BOX AROUND LEGEND
CALL DRWABS(IX2BOX,IY1BOX)    !MAKE BOX AROUND LEGEND
CALL DRWABS(IX2BOX,IY2BOX)    !MAKE BOX AROUND LEGEND
CALL DRWABS(IX1BOX,IY2BOX)    !MAKE BOX AROUND LEGEND
CALL DRWABS(IX1BOX,IY1BOX)    !MAKE BOX AROUND LEGEND
ELSE
CALL RESCOM(SIPHI)    !RESTORE COMMON BLOCKS DATA
C    CALL DSPLAY(WGHZ,PHIRLOW)    !DRAW AXIS AND PLOT DATA
C    CALL CPLOT(WGHZ,PHIRUP)    !PLOT NEXT DATA SET
DO K=0, WGHZ(0)
    X_DATA(K) = WGHZ(K)
    Y_DATA(K) = PHIRLOW(K)
END DO
CALL CHECK(X_DATA,Y_DATA)    !SETS DATA LIMITS, ETC...
CALL DSPLAY(X_DATA,Y_DATA)    !DRAW AXIS AND PLOT DATA
DO K=0, WGHZ(0)
    Y_DATA(K) = PHIRUP(K)
END DO
CALL CPLOT(X_DATA,Y_DATA)
CALL LINE(4)    !SET LINE TYPE
DO K=0, WGHZ(0)
    X_DATA(K) = WGHZ(K)
    Y_DATA(K) = PHILOW(K)
END DO
CALL CPLOT(X_DATA,Y_DATA)    !DRAW AXIS AND PLOT DATA
DO K=0, WGHZ(0)
    Y_DATA(K) = PHIUP(K)
END DO
CALL CPLOT(X_DATA,Y_DATA)    !DRAW AXIS AND PLOT DATA
C    CALL CPLOT(WGHZ,PHILOW)    !PLOT NEXT DATA SET
C    CALL CPLOT(WGHZ,PHIUP)    !PLOT NEXT DATA SET
C    THIS WILL PUT 5 EVENLY SPACED "+" FOR USED AS MARKERS.
K = 0    !INITIALIZE INDEX
DO I=1,WGHZ(0), WGHZ(0)/5.
    K = K + 1    !INCREASE INDEX
    X(K) = WGHZ(I)    !GET MARKER COORDINATE
    Y(K) = PHIRLOW(I)    !GET MARKER COORDINATE
END DO
X(0) = K    !NUMBER OF DATA POINTS FOR AG2
Y(0) = K    !NUMBER OF DATA POINTS FOR AG2

```

```

      CALL LINE(-4)    !SET LINE TYPE TO A POINT PLOT
      CALL SYMBL(REC_SYMB) !SET SYMBOL TYPE TO A "+"
      CALL CPLOT(X,Y)   !PLOT NEXT DATA SET
    END IF
  END IF

```

This part of the code plots the phase difference for the assumed density profile.

```

C
C   PLOT THE "REAL" AND RECONSTRUCTED DEL-PHI FOR COMPARISON.
  IF(IDELPHI.NE.0) THEN
    IF( (KK.EQ.1) .AND. (JJ.EQ.1) .AND. (II.EQ.1) .AND.(LL.EQ.1)
    *   .AND. (IWM.EQ.1) .AND. (IERROR_M.EQ.1) .AND. (IERROR_B.EQ.1)
    *   .AND. (IERROR_A.EQ.1) .AND. (IERROR_W.EQ.1)
    *   .AND. (IB_ERROR.EQ.1) ) THEN
      CALL BINITT() !INITIALIZE DATA BLOCKS
      IF( (-13 .LE. IDELPHI) .AND. (IDELPHI .LE. 13) ) THEN
        CALL PLACE(ABS(IDELPHI)) !SET SCREEN WINDOW
      ELSE IF((-14.LE.IDELPHI).AND.(IDELPHI.LE.14)) THEN
        CALL SLIMX(IPHIMINX,IPHIMAXX) !SET UPPER PLOT WINDOW
        CALL SLIMY(IPHIMINY+ISHIFTY,IPHIMAXY+ISHIFTY)
        PLABEL = '(A)' !SET PLOT LABEL
      ELSE !SET LOWER PLOT WINDOW
        CALL SLIMX(IPHIMINX,IPHIMAXX) !SET SCREEN PLOT LIMITS
        CALL SLIMY(IPHIMINY,IPHIMAXY) !SET SCREEN PLOT LIMITS
        PLABEL = '(B)' !SET PLOT LABEL
      END IF
      CALL XFRM(2) !SET X-AXIS TIC STYLE
      CALL YFRM(2) !SET Y-AXIS TIC STYLE
      CALL LINE(4) !SET LINE TYPE
      CALL YDEN(5) !SET TICS DENSITY
C     CALL YTICS(DPHMAX-DPHMIN) !SET NUMBER OF Y-AXIS TICS
C     CALL DLIMY(DPHMIN,DPHMAX) !SET Y-AXIS LIMITS
C     CALL CHECK(WGHZ_TOMY,DELPHI) !SET DATA LIMITS, ETC...
C     CALL DSPLAY(WGHZ_TOMY,DELPHI) !DRAW AXIS AND PLOT DATA
      Y_MIN = DPHMIN
      Y_MAX = DPHMAX
      CALL YTICS(Y_MAX-Y_MIN)
      CALL DLIMY(Y_MIN,Y_MAX) !SET X-AXIS DATA LIMITS
      DO K=0, WGHZ_TOMY(0)
        X_DATA(K) = WGHZ_TOMY(K)
        Y_DATA(K) = DELPHI(K)
      END DO
      CALL CHECK(X_DATA,Y_DATA) !SETS DATA LIMITS, ETC...

```

```

CALL DSPLAY(X_DATA,Y_DATA) !DRAW AXIS AND PLOT DATA
CALL SAVCOM(SIDELPHI) !SAVE COMMON BLOCKS DATA
CALL LINE(4) !SET LINE TYPE
IF(ICLABEL.NE.0)
  * CALL CLABEL(ICDELPHI,NUMBER,WGHZ_TOMY,DELPHI)
CET CALL CPlot(WGHZ_TOMY,DELPREC)
offset begin
  IF( DPHMIN .LE. -1) THEN
    CALL LINE(3) !SET LINE TYPE
    DO K=0, WGHZ_TOMY(0)
      X_DATA(K) = WGHZ_TOMY(K)
      Y_DATA(K) = OFFSET(K)
    END DO
  C CALL CPlot(WGHZ_TOMY,OFFSET) !PLOT PHASE OFFSET
    CALL CPlot(X_DATA,Y_DATA) !PLOT PHASE OFFSET
    IF(ICLABEL.NE.0)
      * CALL CLABEL(ICDELPHI,NUMBER,WGHZ_TOMY,OFFSET)
    END IF
  offset end
  ICDELPHI = ICDELPHI - 5
CET THIS WILL PUT 5 EVENLY SPACED "+" TO BE USED AS MARKERS.
CET K = 0
CET DO I=1,WGHZ_TOMY(0), WGHZ_TOMY(0)/5.
CET K = K + 1
CET X(K) = WGHZ_TOMY(I)
CET Y(K) = DELPREC(I)
CET END DO
CET X(0) = K !NUMBER OF DATA POINTS FOR AG2
CET Y(0) = K !NUMBER OF DATA POINTS FOR AG2
CET CALL LINE(-4) !SET LINE TYPE TO A POINT PLOT
CET CALL SYMBL(8) !SET SYMBOL TYPE TO AN "+"
CET CALL CPlot(X,Y) !PLOT NEXT DATA SET
CALL FRAME() !FRAME SCREEN WINDOW
CALL AGXXGT('Phase Difference vs Frequency')!LABELS
CALL AGXXCHS('Frequency (GHz)')
CALL AGXXCVS('Fringes')
C CALL AGXXMHS(IPHIMINX-125,IPHIMAXY+ISHIFTY,PLABEL)
  IXSMIN = COMGET(IBASEX(13)) !GET X POSITION OF WINDOW
  IYSMAX = COMGET(IBASEY(14)) !GET Y POSITION OF WINDOW
  CALL AGXXMHS(IXSMIN-125,IYSMAX,PLABEL)
!
```

This piece of the code prints the magnetic field and the probing waves frequency separation on the top of the plot for the phase difference.

C

```

C      THIS PART PRINTS THE MAGNETIC FIELD AND FREQUENCY
C      SEPARATION ON THE UPPER PART OF THE PLOT.
      WRITE(PARAM,230)'B =',BO,' T'    !WRITE MAGNETIC FIELD
230    FORMAT(A3,F3.1,A2)    !WRITE STRING TO VARIABLE
      IXPARAM = IXSMIN + 75    !SET X POSITION FOR STRING
      IYPARAM = IYSMAX - 16    !SET Y POSITION FOR STRING
      CALL AGXXMHS(IXPARAM,IYPARAM,PARAM)    !OUTPUT STRING
C
      WRITE(PARAM,231)' 0 '    !DO FINAL TOUCHES TO LABEL
231    FORMAT(A3)    !PUT THE "0" TO THE MAGNETIC FIELD
      IYPARAM = IYPARAM - 6    !SET Y POSITION
      CALL AGXXMHS(IXPARAM,IYPARAM,PARAM)    !OUTPUT STRING
C
      WRITE(PARAM,232)'w=',WM(IWM)/1.0D+09,' GHz'
232    FORMAT(A2,F4.3,A4)    !WRITE FREQ SEPARATION STRING
      IYPARAM = IYPARAM - 20    !SET Y POSITION OF STRING
      CALL MOVABS(IXSMIN+75, IYPARAM+5)    !MOVE TO POSITION
      CALL SYMOUT(3, 1.)    !OUTPUT DELTA SYMBOL
      CALL AGXXMHS(IXPARAM+7,IYPARAM,PARAM)    !OUTPUT STRING
C      DO I=1, WGHZ_TOMY(0)
C          DELPHI1(I) = 2.0*(RCLOW(I) -RCUP(I) )*WREF(I)/C
C          DELPHI2(I) = 2.0*(RCLOW(N+1)-RCLOW(I))*DELWR /C
C      END DO
C      DELPHI1(0) = I
C      DELPHI2(0) = I
C      CALL SYMBL(0)
C      CALL LINE(1)
C      CALL CPLOT(WGHZ_TOMY,DELPHI1)
C      CALL CPLOT(WGHZ_TOMY,DELPHI2)
C
C      PLOTTING THE LEGEND, THIS PIECE OF CODE MAKES A
C      LEGEND ON THE UPPER RIGHT CORNER INSIDE THE DATA WINDOW.
C      THIS DEFINES THE X-AXIS SCREEN COORDINATE OF THE LEGEND
C      LABEL.
CET      IXLEG = COMGET(IBASEX(13)) + 1./3.
CET      *      * ( COMGET(IBASEX(14)) - COMGET(IBASEX(13)) )
C      THIS DEFINES THE Y-AXIS SCREEN COORDINATE OF THE LEGEND
C      LABEL.
CET      IYLEG = COMGET(IBASEY(14)) - 20
CET      IX1BOX = IXLEG - 10
CET      IY1BOX = IYLEG + 10
CET      CALL MOVABS(IXLEG, IYLEG)    !MOVE TO POSITION
CET      CALL SYMOUT(8, 1.)    !OUTPUT LEGEND SYMBOL
CET      CALL AGXXMHS(IXLEG,IYLEG-7,'-- Calculated')
CET      IX2BOX = IX1BOX + 200    ! 80

```

```

CET      IY2BOX = IY1BOX - 20
CET      CALL AGXXMHS(IXLEG-5,IYLEG-25,'- Calculated')
CET      IY2BOX = IY2BOX - 25
CET      CALL MOVABS(IX1BOX,IY1BOX)
CET      CALL DRWABS(IX2BOX,IY1BOX)
CET      CALL DRWABS(IX2BOX,IY2BOX)
CET      CALL DRWABS(IX1BOX,IY2BOX)
CET      CALL DRWABS(IX1BOX,IY1BOX)
ELSE
  CALL RESCOM(SIDELPHI)  !RESTORE COMMON BLOCKS DATA
  CALL LINE(4)  !SET LINE TYPE
C  CALL DSPLAY(WGHZ_TOMY,DELPHI)  !DRAW AXIS AND PLOT DATA
  DO K=0, WGHZ_TOMY(0)
    X_DATA(K) = WGHZ_TOMY(K)
    Y_DATA(K) = DELPHI(K)
  END DO
  CALL CHECK(X_DATA,Y_DATA)  !SETS DATA LIMITS, ETC...
  CALL DSPLAY(X_DATA,Y_DATA)  !DRAW AXIS AND PLOT DATA
  IF(ICLABEL.NE.0)
    *      CALL CLABEL(ICDELPHI,NUMBER,WGHZ_TOMY,DELPHI)
CET      CALL LINE(0)  !SET LINE TYPE
CET      CALL CPlot(WGHZ_TOMY,DELPREC)  !PLOT NEXT DATA SET
offset  begin
        IF( DPHMIN .LE. -1) THEN
          CALL LINE(3)  !SET LINE TYPE
          DO K=0, WGHZ_TOMY(0)
            X_DATA(K) = WGHZ_TOMY(K)
            Y_DATA(K) = OFFSET(K)
          END DO
C        CALL CPlot(WGHZ_TOMY,OFFSET)  !PLOT PHASE OFFSET
          CALL CPlot(X_DATA,Y_DATA)  !PLOT PHASE OFFSET
          IF(ICLABEL.NE.0)
            *      CALL CLABEL(ICDELPHI,NUMBER,WGHZ_TOMY,OFFSET)
          END IF
offset  end
        ICDELPHI = ICDELPHI - 5
C      THIS WILL PUT 5 EVENLY SPACED "+" TO BE USED AS MARKERS.
CET      K = 0
CET      DO I=1,WGHZ_TOMY(0), WGHZ_TOMY(0)/5.
CET      K = K + 1
CET      X(K) = WGHZ_TOMY(I)
CET      Y(K) = DELPREC(I)
CET      END DO
CET      X(0) = K  !NUMBER OF DATA POINTS FOR AG2
CET      Y(0) = K  !NUMBER OF DATA POINTS FOR AG2

```



```

CET          CALL LINE(-4)    !SET LINE TYPE TO A POINT PLOT
CET          CALL SYMBL(8)    !SET SYMBOL TYPE TO AN "+"
CET          CALL CPLOT(X,Y)   !PLOT NEXT DATA SET
          END IF
        END IF
      !

```

This part plots the calculated positions of cutoff vs the real positions of cutoff. This is done to compare how well the code has reconstructed the positions of the cutoffs. For a good match, a 45° line will be the result.

```

C
C      THIS PLOTS THE RECONSTRUCTED POSITIONS OF THE CUT-OFFS
C      vs THE "REAL" POSITIONS OF THE CUT-OFFS, FOR COMPARISON.
C      A GOOD RECONSTRUCTION WILL GIVE A STRAIGHT LINE AT
C      45 DEGREES THAT PASSES BY THE ORIGIN.
      IF(IRREC.NE.0) THEN
        IF( (KK.EQ.1) .AND. (JJ.EQ.1) .AND. (II.EQ.1) .AND. (LL.EQ.1)
          * .AND. (IWM.EQ.1) .AND. (IERROR_M.EQ.1) .AND. (IERROR_B.EQ.1)
          * .AND. (IERROR_A.EQ.1) .AND. (IERROR_W.EQ.1)
          * .AND. (IB_ERROR.EQ.1) ) THEN
          CALL BINITT()    !SET DATA BLOCKS
          CALL PLACE(ABS(IRREC)) !SET SCREEN WINDOW
          CALL XFRM(2)     !SET X-AXIS TIC STYLE
          CALL YFRM(2)     !SET Y-AXIS TIC STYLE
C          CALL CHECK(RCLOW,RRLOW) !SET DATA LIMITS, ETC...
C          CALL DSPLAY(RCLOW,RRLOW) !DRAW AXIS AND PLOT DATA
          DO K=0, RCLOW(0)
            X_DATA(K) = RCLOW(K)
            Y_DATA(K) = RRLOW(K)
          END DO
          CALL CHECK(X_DATA,Y_DATA) !SETS DATA LIMITS, ETC...
          CALL DSPLAY(X_DATA,Y_DATA) !DRAW AXIS AND PLOT DATA
          CALL SAVCOM(SIRREC) !SAVE COMMON DATA BLOCKS
          CALL FRAME() !FRAME SCREEN WINDOW
          CALL LINE(1) !SET LINE TYPE
          DO K=0, RCLOW(0)
            Y_DATA(K) = RRUP(K)
          END DO
          CALL CPLOT(X_DATA,Y_DATA) !PLOT NEXT DATA SET
          CALL LINE(2) !SET LINE TYPE
          CALL AGXIGT('Lower Cutoff vs Radius')!LABELS
          CALL AGXICHS('Position (m)')
          CALL AGXICVS('Major Radius (m)')
        ELSE

```

```

      CALL RESCOM(SIRREC)      !RESTORE COMMON DATA BLOCKS
C      CALL DSPLAY(RCLOW,RRLOW) !DRAW AXIS AND PLOT DATA
      DO K=0, RCLOW(0)
        X_DATA(K) = RCLOW(K)
        Y_DATA(K) = RRLOW(K)
      END DO
      CALL CHECK(X_DATA,Y_DATA) !SETS DATA LIMITS, ETC...
      CALL DSPLAY(X_DATA,Y_DATA) !DRAW AXIS AND PLOT DATA
      CALL FRAME()             !FRAME SCREEN WINDOW
      CALL LINE(1)             !SET LINE TYPE
C      CALL CPLOT(RCLOW,RRUP)   !PLOT NEXT DATA SET
      DO K=0, RCLOW(0)
        Y_DATA(K) = RRUP(K)
      END DO
      CALL CPLOT(X_DATA,Y_DATA)
    END IF
  END IF
!
```

This part of the code plots the real/assumed and reconstructed desity profiles together with other information like the Abel inverted profile, the errors between profiles, the index of refraction, etc., for comparison and debugging.

```

C
C      PLOT THE "REAL" AND RECONSTRUCTED DENSITY PROFILE.
C      IF(IDENREC.NE.0) THEN
C        CALCULATE THE ERROR BETWEEN THE REAL, ABEL AND REC PROFILE
        AVE_DIF = 0.0      !INITIALIZE VARIABLE
        AVE_DIF2= 0.0      !INITIALIZE VARIABLE
        OPEN(77,FILE='F.ERR',STATUS='UNKNOWN')
        WRITE(77,*) RABEL(0)-1
        ERR_MAX = 0.0      !INITIALIZE VARIABLE
        DO I = 1, N-1      !CALCULATE THE DENSITY ERROR ARRAY
C          TEMP = (DENLOW(I) - DABEL(I)) / DENLOW(I)
          TEMP = DENSITY(RRLOW(I),RSHIFT(II),SHAPE(JJ),DERDEN(LL))
          TEMP = (TEMP - DENLOW(I)) / DENLOW(1)
CAUG          TEMP = DENSITY(RRUP(I),RSHIFT(II),SHAPE(JJ),DERDEN(LL))
CAUG          TEMP = (TEMP - DENUP(I)) / DENUP(1)
CSEP          TEMP2 = RCLOW(I) - RCUP(I)
CSEP          TEMP = (TEMP2 - WSCALE*DELREC(I)) / TEMP2
C          WRITE(11,*)RCUP(I), RCLOW(I), DELREC(I), TEMP
C          DO J = 1, RABEL(0)
C            IF((RRLOW(I) .LE. RABEL(J)) .AND.
C              *      (RABEL(J) .LT. RRLOW(I+1))) THEN
C              TEMP = (DENLOW(I+1)-DENLOW(I))/(RRLOW(I+1)-RRLOW(I))

```

```

C      *      * (RABEL(J)-RRLOW(I)) + DENLOW(I)
CC      TEMP = (TEMP - DABEL(J)) / TEMP
C      TEMP = (TEMP - DABEL(J)) / DABEL(1)
C      AVE_DIF2 = AVE_DIF2 + ABS(TEMP)
C      END IF
C      END DO
      ER_DEN(I) = TEMP !* 100.
      TEMP2 = RCLOW(I) - RCUP(I)
      IF(TEMP2 .NE. 0.0) THEN
C4-15095      ER_DELR(I) = (DELREC(I) - TEMP2)
C4-15095      ER_DELR(I) = 100.* (DELREC(I) - TEMP2) / (RRLOW(I))
C      ER_DELR(I) = 100.* (RRLOW(I+1)-RRLOW(I) - TEMP2)
      ER_DELR(I) = 100.* (RRLOW(I)-RCLOW(I))/RCLOW(I)
C      ER_DELR(I) = 100.* (DELREC(I)-TEMP2)/(TEMP2*WSCALE)
      ELSE
      ER_DELR(I) = 0.0
      END IF
      DRIND = RRLOW(I+1)
      MU_1 = MU2(DRIND,WREF(I)-WM(IWM)/2.
      *      ,RSHIFT(II),SHAPE(JJ),DERDEN(LL))
      MU_1 = MU_1 / SQRT( ABS( MU_1 ) )
      DRIND = RRLOW(I+2)
      MU_2 = MU2(DRIND,WREF(I)-WM(IWM)/2.
      *      ,RSHIFT(II),SHAPE(JJ),DERDEN(LL))
      MU_2 = MU_2 / SQRT( ABS( MU_2 ) )
      DRIND = RRLOW(I+3)
      MU_3 = MU2(DRIND,WREF(I)-WM(IWM)/2.
      *      ,RSHIFT(II),SHAPE(JJ),DERDEN(LL))
      MU_3 = MU_3 / SQRT( ABS( MU_3 ) )
      ER_PAR(I) = ( 3.*MU_1 - 3.*MU_2 + MU_3 ) * 100.
*      *      * 2.*PI * WREF(I) / C
      WRITE(66,*)I, MU_1, MU_2, MU_3, ER_PAR(I)
166      FORMAT(I5, 5F11.5)
      ERR_MAX = MAX( ERR_MAX , TEMP ) !PICK MAX ERROR
      WRITE(77,*)DELREC(I), ER_DELR(I)
      AVE_DIF = AVE_DIF + TEMP
C      WRITE(11,*)I,TEMP,AVE_DIF,TEMP2,AVE_DIF2
      END DO
      CLOSE(77)
      ER_DEN(0) = I-1 !SET NUMBER OF DATA POINTS
      ER_DELR(0) = ER_DEN(0)
      ER_PAR(0) = ER_DEN(0) !SET NUMBER OF DATA POINTS
      AVE_DIF = AVE_DIF / RRLOW(0) !CALCULATE AVERAGE
      AVE_DIF2 = AVE_DIF2 / RRLOW(0) !CALCULATE AVERAGE
      WRITE(66,*) DELREC(DELREC(0)), ER_DELR(DELREC(0))

```

```

C      OPEN(88,FILE='TOMY.ERR',STATUS='NEW')
      WRITE(88,188)(DELREC(I), ER_DELR(I), I=0,ER_DELR(0))
188    FORMAT(F16.8,E16.8)
C      CLOSE(88)
CC     WRITE(11,*) WM(IWM), AVE_DIF
C      WRITE(11,*) N, AVE_DIF2
C      WRITE(*,*) ' NPOINTS POINT DIF ASSUMED-REC: '
C      WRITE(*,*) N, AVE_DIF
C      WRITE(*,*) ' NPOINTS INTERPOLATED ABEL-REC: '
C      WRITE(*,*) N, AVE_DIF2
      !

```

Here the density is finally plotted.

```

C
      IF( (KK.EQ.1) .AND. (JJ.EQ.1) .AND. (II.EQ.1) .AND. (LL.EQ.1)
*      .AND. (IWM.EQ.1) .AND. (IERROR_M.EQ.1) .AND. (IERROR_B.EQ.1)
*      .AND. (IERROR_A.EQ.1) .AND. (IERROR_W.EQ.1)
*      .AND. (IB_ERROR.EQ.1) ) THEN
        CALL BINITT() !INITIALIZE DATA BLOCKS
        IF( (-13 .LE. IDENREC) .AND. (IDENREC .LE. 13) ) THEN
          CALL PLACE(ABS(IDENREC)) !SET SCREEN WINDOW
        ELSE IF((-14.LE.IDENREC).AND.(IDENREC.LE.14))THEN
          CALL SLIMX(IPHIMINX,IPHIMAXX) !SET UPPER PLOT WINDOW
          CALL SLIMY(IPHIMINY+ISHIFTY,IPHIMAXY+ISHIFTY)
          PLABEL = '(A)' !SET PLOT LABEL
        ELSE !SET LOWER PLOT WINDOW
          CALL SLIMX(IPHIMINX,IPHIMAXX) !SET SCREEN PLOT LIMITS
          CALL SLIMY(IPHIMINY,IPHIMAXY) !SET SCREEN PLOT LIMITS
          PLABEL = '(B)' !SET PLOT LABEL
        END IF
        CALL XFRM(2) !SET X-AXIS TIC STYLE
        CALL YFRM(2) !SET Y-AXIS TIC STYLE
C      CALL DLIMX(RXMIN,RXMAX) !SET X-AXIS DATA LIMITS
C      CALL DLIMY(DYMIN,DYMAX) !SET Y-AXIS DATA LIMITS
C      CALL CHECK(RRLOW,DENLOW) !SET DATA LIMITS, ETC...
C      CALL DDISPLAY(RRLOW,DENLOW) !DRAW AXIS AND PLOT DATA
      X_MIN = RXMIN
      X_MAX = RXMAX
      CALL DLIMX(X_MIN,X_MAX) !SET X-AXIS DATA LIMITS
      Y_MIN = DYMIN
      Y_MAX = DYMAX
      CALL DLIMY(Y_MIN,Y_MAX)
      DO K=0, RRLOW(0)
        X_DATA(K) = RRLOW(K)

```

```

        Y_DATA(K) = DENLOW(K)
    END DO
    CALL CHECK(X_DATA,Y_DATA)  !SETS DATA LIMITS, ETC...
    CALL DSPLAY(X_DATA,Y_DATA) !DRAW AXIS AND PLOT DATA
    CALL SAVCOM(SIDENREC)      !SAVE COMMON BLOCKS DATA
    IF(ICLABEL.NE.0) CALL CLABEL(ICDEN,NUMBER,RRLOW,DENLOW)
    ICDEN = ICDEN + 5
C4-28-95      CALL CPLOT(RRUP,DENUP)  !PLOT NEXT DATA SET
C      THIS WILL PUT 5 EVENLY SPACED "+" TO BE USED AS MARKERS.
        K = 0
        DO I=1, N, N/5.
            K = K + 1
            X(K) = RRLOW(I)
            Y(K) = DENLOW(I)
        END DO
        X(0) = K  !NUMBER OF DATA POINTS FOR AG2
        Y(0) = K  !NUMBER OF DATA POINTS FOR AG2
        CALL LINE(-4)  !SET LINE TYPE TO POINT PLOT
        CALL SYMBL(REC_SYMB)  !SET SYMBOL TYPE TO A "+"
        CALL CPLOT(X,Y)  !PLOT DATA SET
        CALL SYMBL(0)  !SET SYMBOL TYPE TO THE DEFAULT
        CALL FRAME()  !FRAME THE SCREEN WINDOW
        CALL AGXIGT('Density (1/m^3) vs Radius')  !LABELS
        CALL AGXICHS('Major Radius (m)')
        CALL AGXICVS('Density')
C      CALL AGXIMHS(IPHIMINX-125,IPHIMAXY,PLABEL)
        IXSMIN = COMGET(IBASEX(13))
        IYSMAX = COMGET(IBASEY(14))
        CALL AGXIMHS(IXSMIN-125,IYSMAX,PLABEL)
CHERE  TEST OF THE ERROR BARS...
        IF( ERR_ON .EQ. 1 ) THEN
            X(0) = 1
            Y(0) = 1
            CALL LINE(-4)  !SET LINE TYPE TO POINT PLOT
            CALL SYMBL(ERR_SYMB)  !SET SYMBOL TYPE TO A "|"
            TEMP = ( COMGET(IBASEY(14)) - COMGET(IBASEY(13)) )
            /      / ( COMGET(IBASEY(12))-COMGET(IBASEY(11)) )
            /      / 15.
C      *      * 0.2 / 10.
            WRITE(11,*) ' TEMP', TEMP
            DO I=1, N, N/10.
                X(1) = RRLOW(I)
                Y(1) = DENLOW(I)
                DNDR = -(DENLOW(I+1)-DENLOW(I))/(RRLOW(I+1)-RRLOW(I))
                ERR_R = DNDR * 0.01  !Meters

```

```

DRIND = RRLOW(I)
N_REF = MU2(DRIND, WREF(I)+WM(IWM)/2., RSHIFT(II)
*      , SHAPE(JJ), DERDEN(LL))
N_REF = SQRT( N_REF )
ERR_PHI = 0.1 * DNDR * 2. * C / (WREF(I) * N_REF)
ERR_B = (WREF(I) * EPSILO / ELECHR ) * BO * 0.01
ERR_R1 = (WREF(I) * EPSILO * BO * RO) / (ELECHR * RRLOW(I) ** 2) * 0.01
WRITE(11,*) ERR_R, ERR_PHI, ERR_B, ERR_R1
ERR_TOM = SQRT(ERR_R**2+ERR_PHI**2+ERR_B**2+ERR_R1**2)
CALL SIZES(ERR_TOM*TEMP)
C      CALL SIZES(Y(1)*TEMP)
      CALL CPLOT(X,Y)
END DO
CALL SYMBL(0) !SET SYMBOL TYPE TO THE DEFAULT
END IF
CEND TEST OF ERROR BARS
!
```

Here the code prints the legend for the plot of the real/assumed and the reconstructed density.

```

C
C      PLOTTING THE LEGEND, THIS PIECE OF CODE MAKES A
C      LEGEND ON THE UPPER RIGHT CORNER INSIDE THE DATA WINDOW.
C      THIS DEFINES THE X-AXIS SCREEN COORDINATE OF THE LEGEND
C      LABEL.
      IXLEG = COMGET(IBASEX(13)) + 1./3. !SET X POSITION
*      * ( COMGET(IBASEX(14)) - COMGET(IBASEX(13)) )
C      THIS DEFINES THE Y-AXIS SCREEN COORDINATE OF THE LEGEND
C      LABEL.
      IX1BOX = IXLEG - 10 !SET X POSITION OF BOX
      IY1BOX = COMGET(IBASEY(14)) - 5 !SET Y POSITION
      IYLEG = IY1BOX - 10 !SET Y POSITION
      CALL MOVABS(IXLEG, IYLEG) !MOVE TO POSITION
      CALL SYMOUT(REC_SYMB, 1.) !OUTPUT LEGEND SYMBOL
C      CALL SYMOUT(45, 3.) !OUTPUT LEGEND SYMBOL
      CALL MOVREL(-10,0) !MOVE TO DRAW LINE
      CALL DRWREL(20,0) !DRAW LINE
      CALL AGXXMHS(IXLEG+20,IYLEG-6,'Reconstructed')
      IX2BOX = IX1BOX + 220 !SET NEXT X POSITION
      IY2BOX = IY1BOX - 15 - 5 !SET NEXT Y POSITION
C      IXLEG = IXLEG - 10 !SET NEXT X LEGEND POSITION
      IYLEG = IYLEG - IYLEG_H !SET NEXT Y LEGEND POSITION
      CALL AGXXMHS(IXLEG-10,IYLEG-5,'-- Assumed') !OUTPUT LABEL
      IY2BOX = IY2BOX - IYLEG_H !SET NEXT LEGEND LABEL POSITION
```

```

C
C      PLOT THE REAL DENSITY PROFILE.
      RX = RXMIN
      DELRX = (RO+RA - RX) / N      !CALCULATE INCREMENT
      RRANDOM = RSEED      !SET SEED
      DO I=1,N      !CALCULATE DENSITY POINTS
        RX = RX + DELRX      !INCREMENT RADIAL POSITION
        X(I) = RX      !SET ARRAY POSITIONS
        Y(I) = DENSITY(RX,RSHIFT(II),SHAPE(JJ),DERDEN(LL))
        *      * (1. - DNOISE(I)*DBRETZ(RCLOW(I)))
      END DO
      X(0) = N      !NUMBER OF DATA POINTS FOR AG2
      Y(0) = N      !NUMBER OF DATA POINTS FOR AG2
      CALL LINE(4)      !SET LINE TYPE
      CALL CPlot(X,Y)      !PLOT DATA SET
!

```

If the magnetic field is zero,  $B_0 = 0$ , then it is possible to do an Abel inversion of the density profile. This part of the code plots the Abel inverted profile if requested in the NAMELIST data file.

```

C
C      PLOT THE ABEL INVERTION PROFILE
      IF(IDDPDW .LT. 0) THEN
        CALL LINE(0)      !SET LINE TYPE
        DO K=0, RABEL(0)
          X_DATA(K) = RABEL(K)
          Y_DATA(K) = DABEL(K)
        END DO
      C      CALL CPlot(RABEL,DABEL)      !PLOT DATA SET
      CALL CPlot(X_DATA,Y_DATA)
      K = 0      !INITIALIZE INDEX FOR MARKER
      DO I=1, RABEL(0), RABEL(0)/5.      !MAKER LOOP
        K = K + 1      !INCREMENT INDEX FOR MARKER
        X(K) = RABEL(I)      !PASS ABEL DATA TO ARRAY
        Y(K) = DABEL(I)      !PASS ABEL DATA TO ARRAY
      END DO
      X(0) = K      !NUMBER OF DATA POINTS FOR AG2
      Y(0) = K      !NUMBER OF DATA POINTS FOR AG2
      CALL LINE(-4)      !SET LINE TYPE TO POINT PLOT
      CALL SYMBL(1)      !SET SYMBOL TYPE TO A "+"
      CALL CPlot(X,Y)      !PLOT DATA SET
      C      IXLEG = IXLEG + 10      !SET X LEGEND POSITION
      IYLEG = IYLEG - IYLEG_H      !SET Y LEGEND POSITION
      CALL MOVABS(IXLEG, IYLEG)      !MOVE TO POSITION

```

```

CALL SYMOUT(1, 1.)    !OUTPUT LEGEND SYMBOL
CALL MOVREL(-10,0)    !MOVE TO DRAW LINE
CALL DRWREL(20,0)     !DRAW LINE
CALL AGXIMHS(IXLEG+20,IYLEG-5,'Abel Inverted')
IY2BOX = IY2BOX - IYLEG_H    !SET NEXT CORNER POSITION
C
C
PLOT THE FRACTIONAL ERROR ON THE RIGHT AXIS
CALL DINITY()         !INITIALIZE Y-AXIS DATA BLOCK
CALL YLOCRT(0)        !SET AXIS LOCATION TO RIGHT
CALL LINE(0)          !SET LINE TYPE -4=POINTS ONLY
CALL SYMBL(0)         !SET SYMBOL TYPE TO A POINT
C
CALL DLIMX(RXMIN,RXMAX) !SET X-AXIS DATA LIMITS
C
CALL CHECK(RRLOW,ER_DEN)!SET DATA LIMITS, ETC...
C
CALL DSPLAY(RRLOW,ER_DEN)!DRAW AXIS AND PLOT DATA
X_MIN = RXMIN
X_MAX = RXMAX
CALL DLIMX(X_MIN,X_MAX) !SET X-AXIS DATA LIMITS
C
CALL SYMBL(8)
DO K=0, RRLOW(0)
    X_DATA(K) = RRLOW(K)
    Y_DATA(K) = ER_DEN(K)
END DO
CALL CHECK(X_DATA,Y_DATA) !SETS DATA LIMITS, ETC...
CALL DSPLAY(X_DATA,Y_DATA) !DRAW AXIS AND PLOT DATA
CALL SAVCOM(SIER_DEN)     !SAVE COMMON BLOCKS DATA
IX = COMGET(IBASEX(14))+85!CALCULATE POSITION OF LABEL
IF(IX.GT.1022) IX = 1022   !SET TO SCREEN MAXIMUM
IY = COMGET(IBASEY(14))    !CALCULATE POSITION OF LABEL
CALL AGXIMVS(IX,IY,'ERROR%')!LABEL
C
PLOT SYMBOLS
K = 0    !INITIALIZE INDEX
DO I=1,ER_DEN(0), ER_DEN(0)/5.
    K = K + 1
    X(K) = RRLOW(I)
    Y(K) = ER_DEN(I)
END DO
X(0) = K    !NUMBER OF DATA POINTS FOR AG2
Y(0) = K    !NUMBER OF DATA POINTS FOR AG2
CALL LINE(-4) !SET LINE TYPE TO A POINT PLOT
CALL SYMBL(ISYM_ER)
CALL CPLOT(X,Y) !PLOT NEXT DATA SET
C
MAKE LEGEND
C
IXLEG = IXLEG + 10    !SET X LEGEND POSITION
IYLEG = IYLEG - IYLEG_H !SET Y LEGEND POSITION
CALL MOVABS(IXLEG, IYLEG) !MOVE TO POSITION

```



```

      CALL SYMOUT(ISYM_ER, 1.)  !OUTPUT LEGEND SYMBOL
      CALL MOVREL(-10,0)  !MOVE TO DRAW LINE
      CALL DRWREL(20,0)  !DRAW LINE
      CALL AGXIMHS(IXLEG+20,IYLEG-5,'Percent Error')
      IY2BOX = IY2BOX - IYLEG_H  !SET NEXT CORNER POSITION
    END IF
  !

```

The error between profiles is plotted here putting the axis on the right hand side of the plot.

```

C
      IF( IDENREC .LT. 0) THEN
CER_DEN  PLOT THE FRACTIONAL ERROR ON THE LEFT AXIS
          CALL DINITY()  !INITIALIZE Y-AXIS DATA BLOCK
          IYLOC_DEN_ERR = 90 !SET AXIS SHIFT
          CALL YLOC(IYLOC_DEN_ERR)  !SET AXIS LOCATION TO RIGHT
C          CALL YLOCRT(0)  !SET AXIS LOCATION TO RIGHT
          CALL LINE(3)  !SET LINE TYPE
          CALL SYMBL(0)  !SET SYMBOL TYPE TO A POINT
C          CALL DLIMX(RXMIN,RXMAX)  !SET X-AXIS DATA LIMITS
C          CALL CHECK(RRLOW,ER_DEN)!SET DATA LIMITS, ETC...
C          CALL DSPLAY(RRLOW,ER_DEN)!DRAW AXIS AND PLOT DATA
          X_MIN = RXMIN
          X_MAX = RXMAX
          CALL DLIMX(X_MIN,X_MAX)  !SET X-AXIS DATA LIMITS
          CALL SYMBL(8)
          DO K=0, RRLOW(0)
            X_DATA(K) = RRLOW(K)
            Y_DATA(K) = ER_DEN(K)
          END DO
          CALL CHECK(X_DATA,Y_DATA)  !SETS DATA LIMITS, ETC...
          CALL DSPLAY(X_DATA,Y_DATA)  !DRAW AXIS AND PLOT DATA
          CALL SAVCOM(SIER_DEN)  !SAVE COMMON BLOCKS DATA
          IX = COMGET(IBASEX(13))+IYLOC_DEN_ERR+9 !LABEL POSITION
          IF(IX.GT.1022) IX = 1022  !SET TO SCREEN MAXIMUM
          IY = COMGET(IBASEY(14))  !CALCULATE POSITION OF LABEL
          CALL AGXIMVS(IX,IY,'DEN ERROR')!LABEL
C          CALL AGXICVS('DEN ERROR')
C
          IYLEG = IYLEG - IYLEG_H  !SET Y LEGEND POSITION
          CALL MOVABS(IXLEG+5, IYLEG)  !MOVE TO POSITION
          CALL SYMOUT(8, 1.)  !OUTPUT LEGEND SYMBOL
          CALL AGXIMHS(IXLEG+20,IYLEG-5,' Dens. Error')
          IY2BOX = IY2BOX - IYLEG_H  !SET NEXT CORNER POSITION

```

```

C
C      PLOT THE FRACTIONAL ERROR ON THE RIGHT AXIS
      CALL DINITY()    !INITIALIZE Y-AXIS DATA BLOCK
      IF(IMU.NE.0) THEN
        CALL YLOCRT(-90)  !SET AXIS LOCATION TO RIGHT
      ELSE
        CALL YLOCRT(0)   !SET AXIS LOCATION TO RIGHT
      END IF
      CALL LINE(0)       !SET LINE TYPE
      CALL SYMBL(0)      !SET SYMBOL TYPE TO A POINT
C      CALL DLIMX(RXMIN,RXMAX)  !SET X-AXIS DATA LIMITS
C      CALL CHECK(RRLOW,ER_DELR)!SET DATA LIMITS, ETC...
C      CALL DSPLAY(RRLOW,ER_DELR)!DRAW AXIS AND PLOT DATA
      X_MIN = RXMIN
      X_MAX = RXMAX
      CALL DLIMX(X_MIN,X_MAX)  !SET X-AXIS DATA LIMITS
      CALL SYMBL(2)
      DO K=0, RRLOW(0)
        X_DATA(K) = RRLOW(K)
        Y_DATA(K) = ER_DELR(K)
      END DO
      CALL CHECK(X_DATA,Y_DATA) !SETS DATA LIMITS, ETC...
      CALL DSPLAY(X_DATA,Y_DATA) !DRAW AXIS AND PLOT DATA
C      CALL CHECK(RRLOW,AGREG_)!SET DATA LIMITS, ETC...
C      CALL DSPLAY(RRLOW,AGREG_)!DRAW AXIS AND PLOT DATA
      CALL SAVCOM(SIER_DEN)  !SAVE COMMON BLOCKS DATA
C      CALL CPLOT(RRLOW,ER_PAR) !DRAW NEXT DATA SET
      DO K=0, RRLOW(0)
        Y_DATA(K) = ER_PAR(K)
      END DO
      CALL CPLOT(X_DATA,Y_DATA)
      IX = COMGET(IBASEX(14))+85!CALCULATE POSITION OF LABEL
      IF(IX.GT.1022) IX = 1022  !SET TO SCREEN MAXIMUM
      IY = COMGET(IBASEY(14))  !CALCULATE POSITION OF LABEL
      CALL AGXIMVS(IX,IY,'ERROR %')!LABEL

      IYLEG = IYLEG - IYLEG_H  !SET Y LEGEND POSITION
      CALL MOVABS(IXLEG+5, IYLEG) !MOVE TO POSITION
      CALL SYMOUT(2, 1.)  !OUTPUT LEGEND SYMBOL
      CALL AGXIMHS(IXLEG+20,IYLEG-5,' Radial Error')
      IY2BOX = IY2BOX - IYLEG_H  !SET NEXT CORNER POSITION
      END IF
      CALL MOVABS(IX1BOX,IY1BOX) !MAKE BOX AROUND LEGEND
      CALL DRWABS(IX2BOX,IY1BOX) !MAKE BOX AROUND LEGEND
      CALL DRWABS(IX2BOX,IY2BOX) !MAKE BOX AROUND LEGEND

```

```
CALL DRWABS(IX1BOX,IY2BOX)    !MAKE BOX AROUND LEGEND
CALL DRWABS(IX1BOX,IY1BOX)    !MAKE BOX AROUND LEGEND
```

3

Here the real index of refraction can be plotted on the right hand side axis together with the density profiles.

```

C      THIS PLOTS THE "REAL" REFRACTION INDEX FOR THE
C      PROBING WAVE.
      IF(IMU.NE.0) THEN
C      PLOT THE REFRACTION INDEX OF THE FIRST CUT-OFF
      CALL DINITY()      !INITIALIZE Y-AXIS DATA BLOCK
      CALL YLOCRT(0)     !SET AXIS LOCATION TO RIGHT
      CALL LINE(2)       !SET LINE TYPE
      CALL DLIMX(RXMIN,RXMAX) !SET X-AXIS DATA LIMITS
      CALL DLIMY(0.0,1.0)  !SET Y-AXIS DATA LIMITS
C      CALL CHECK(RR,MURR)  !SET DATA LIMITS, ETC...
C      CALL DSPLAY(RR,MURR) !DRAW AXIS AND PLOT DATA
      DO K=0, RR(0)
        X_DATA(K) = RR(K)
        Y_DATA(K) = MURR(K)
      END DO
      CALL CHECK(X_DATA,Y_DATA) !SETS DATA LIMITS, ETC...
      CALL DSPLAY(X_DATA,Y_DATA) !DRAW AXIS AND PLOT DATA
      OPEN(55,FILE='[.INDEX]F2.IND',STATUS='NEW')
      WRITE(55,'(2F16.8)') (X_DATA(J),Y_DATA(J),J=0,X_DATA(0))
      CLOSE(55)
C      CALL CPLOT(RR,MURR)  !PLOT DATA SET
      IX = COMGET(IBASEX(14))+70!CALCULATE POSITION OF LABEL
      IF(IX.GT.1022) IX = 1022 !SET TO SCREEN MAXIMUM
      IY = COMGET(IBASEY(14)) !CALCULATE POSITION OF LABEL
      CALL AGXIMVS(IX,IY,'Refrac Index')!LABEL
C      PLOT THE REFRACTIVE INDEX FOR THE OTHER CUTOFFS.
      R1 = R0+RA !SET INITIAL POSITION
      K = 0 !INITIALIZE INDEX
      N_INDEX = 200
      DO I=N-1,N-IN_CURVE,-1
C      DO I=N,N-20,-1
        R2 = RLOW(I) !SET CUTOFF
        DELRJ = 1.05*(R1-R2) / FLOAT(N_INDEX) !SET INCREMENT
        RJ = R1 + DELRJ !INITIALIZE VARIABLE
        DO J=1,N_INDEX !LOOP OVER RADIAL POINTS
          RJ = RJ - DELRJ !INCREMENT RADIAL POSITION
          X(J) = RJ !SET ARRAY POSITION
        
```

```

DRIND = RJ
C      TEMP1 = MU2(DRIND,WREF(I)-(WM(IWM)/2.)/WSCALE
      TEMP1 = MU2(DRIND,WREF(I)-WM(IWM)/2.    !CALCULATE
      *      ,RSHIFT(II),SHAPE(JJ),DERDEN(LL))    !INDEX OF
C4-6-95      Y(J) = TEMP1                        !REFRACTION
      Y(J) = TEMP1 / SQRT(ABS(TEMP1))          !REFRACTION
END DO
C      Y(N) = 0.0
      X(0) = J-1    !NUMBER OF DATA POINTS FOR AG2
      Y(0) = X(0)   !NUMBER OF DATA POINTS FOR AG2
      CALL SYMBL(0) !SET SYMBOLT TYPE
      CALL LINE(2)  !SET LINE TYPE
      CALL CPLOT(X,Y) !PLOT DATA SET
      OPEN(55,FILE='[.INDEX]F.IND',STATUS='NEW')
      WRITE(55,'(2F16.8)') (X(J), Y(J), J=0, X(0))
      CLOSE(55)
      K = K + 1
      WRITE(CNUM,450) K
450      FORMAT(I2)
C      CALL AGXXHS(CNUM)
!
```

This part of the code plots the parabolic fit used by the reconstruction technique. It shows the goodness of the parabolic fit to the real index of refraction.

```

C
C      PLOT THE PARABOLIC FITS USED IN THE RECONSTRUCTION
C      SET PARAMETERS FOR THE SUBROUTINE
C      XI(1) = RRUP(I+1)    !SET INTERPOLATION POINTS
      XI(2) = RRLOW(I+1)    !SET INTERPOLATION POINTS
      XI(3) = RRLOW(I+2)    !SET INTERPOLATION POINTS
      YY(1) = 0.0    !SET INTERPOLATION POINTS
      TEMP1 = MU2REC( XI(2),DENLOW(I+1)
      *      ,WREF(I)-(WM(IWM)/2.)/WSCALE )
      YY(2) = TEMP1 / SQRT( ABS(TEMP1) )
      TEMP2 = MU2REC( XI(3),DENLOW(I+2)
      *      ,WREF(I)-(WM(IWM)/2.)/WSCALE )
      YY(3) = TEMP2 / SQRT( ABS(TEMP2) )
      DELRP = RCLOW(I) - RCUP(I)
C      PLOT THE PARABOLA USING THE DERIVATIVE CONDITION
      CALL BC_DER(XI,YY,B_PAR,C_PAR)
      DELPAR = (XI(2) - XI(1)) / FLOAT(N-1)
      DO J = 1, N
        XXTEMP = (J-1) * DELPAR
        X(J) = XI(1) + XXTEMP
      
```

```

        Y(J) = B_PAR * XXTEMP + C_PAR * XXTEMP * XXTEMP
      END DO
      X(0) = J-1
      Y(0) = X(0)
      CALL SYMBL(0)    !SET SYMBOLT TYPE
      CALL LINE(1)    !SET LINE TYPE
      CALL CPlot(X,Y)  !PLOT NEXT DATA SET
      OPEN(55,FILE='[.INDEX]F.PAR',STATUS='NEW')
      WRITE(55,'(2F16.8)') (X(J), Y(J), J=0, X(0))
      CLOSE(55)
C      PLOT THE INTERPOLATING POINTS FOR THE DERIVATIVE
      X(0) = 2    !SET INTERPOLATION POINTS
      Y(0) = X(0)  !SET INTERPOLATION POINTS
      X(1) = XX(2)  !SET INTERPOLATION POINTS
      Y(1) = YY(2)  !SET INTERPOLATION POINTS
      X(2) = XX(3)  !SET INTERPOLATION POINTS
      Y(2) = YY(3)  !SET INTERPOLATION POINTS
      CALL SYMBL(2)  !SET SYMBOLT TYPE
      CALL LINE(1)  !SET LINE TYPE
      CALL CPlot(X,Y)  !PLOT NEXT DATA SET
C      PLOT THE OTHER PARABOLIC USING A 3 POINT FIT
      CALL BC_3P(XX,YY,B_PAR,C_PAR)
      DELPAR = (XX(2) - XX(1)) / FLOAT(N-1)
      DO J = 1, N
        XXTEMP = (J-1) * DELPAR
        X(J) = XX(1) + XXTEMP
        Y(J) = B_PAR * XXTEMP + C_PAR * XXTEMP * XXTEMP
      END DO
      X(0) = J-1    !SET NUMBER OF DATA POINTS
      Y(0) = X(0)   !SET NUMBER OF DATA POINTS
      CALL SYMBL(0)  !SET SYMBOLT TYPE
      CALL LINE(0)   !SET LINE TYPE
C      CALL CPlot(X,Y)
      END DO
      END IF
    ELSE
      CALL RESCOM(SIDENREC)  !RESTORE COMMON BLOCKS DATA
C      CALL DSPLAY(RRLOW,DENLOW)  !DRAW AXIS AND PLOT DATA
      DO K=0, RRLOW(0)
        X_DATA(K) = RRLOW(K)
        Y_DATA(K) = DENLOW(K)
      END DO
C      CALL CHECK(X_DATA,Y_DATA)  !SETS DATA LIMITS, ETC...
      CALL DSPLAY(X_DATA,Y_DATA)  !DRAW AXIS AND PLOT DATA
      IF(ICLABEL.NE.0) CALL CLABEL(ICDEN,NUMBER,RRLOW,DENLOW)

```

```

      ICDEN = ICDEN + 5
C      CALL CPlot(RRUP,DENUP)  !PLOT NEXT DATA SET
C      THIS WILL PUT 5 EVENLY SPACED "+" TO BE USED AS MARKERS.
      K = 0
      DO I=1, N, N/5.
        K = K + 1
        X(K) = RRLOW(I)
        Y(K) = DENLOW(I)
      END DO
      X(0) = K  !NUMBER OF DATA POINTS FOR AG2
      Y(0) = K  !NUMBER OF DATA POINTS FOR AG2
      CALL LINE(-4)  !SET LINE TYPE TO POINT PLOT
      CALL SYMBL(REC_SYMB)  !SET SYMBOL TYPE TO A "+"
      CALL CPlot(X,Y)  !PLOT DATA SET
      CALL SYMBL(0)  !SET SYMBOL TYPE TO THE DEFAULT
!
```

This is part that calculates and plots the real density profile.

```

C
C      PLOT THE REAL DENSITY PROFILE IF REQUESTED.
      IF(IDENREAL .GT. 0) THEN
        RX = RXMIN
        DELRX = (RO+RA - RX) / N
        DO I=1,N
          RX = RX + DELRX
          X(I) = RX
          Y(I) = DENSITY(RX,RS SHIFT(II),SHAPE(JJ),DERDEN(LL))
        END DO
        X(0) = N  !NUMBER OF DATA POINTS FOR AG2
        Y(0) = N  !NUMBER OF DATA POINTS FOR AG2
        CALL LINE(4)  !SET LINE TYPE
        CALL CPlot(X,Y)  !PLOT DATA SET
        END IF
C
      IF(IDDPDW .LT. 0) THEN
        CALL LINE(0)
        DO K=0, RABEL(0)
          X_DATA(K) = RABEL(K)
          Y_DATA(K) = DABEL(K)
        END DO
C      CALL CPlot(RABEL,DABEL)
      CALL CPlot(X_DATA,Y_DATA)  !PLOT PHASE OFFSET
      K = 0
      DO I=1, RABEL(0), RABEL(0)/5.

```

```

      K = K + 1
      X(K) = RABEL(I)
      Y(K) = DABEL(I)
    END DO
    X(0) = K    !NUMBER OF DATA POINTS FOR AG2
    Y(0) = K    !NUMBER OF DATA POINTS FOR AG2
    CALL LINE(-4) !SET LINE TYPE TO POINT PLOT
    CALL SYMBL(1) !SET SYMBOL TYPE TO A "+"
    CALL CPLOT(X,Y) !PLOT DATA SET

C
C
    PLOT THE ERROR ON THE RIGHT AXIS
    CALL RESCOM(SIER_DEN) !RESTORE COMMON BLOCKS DATA
C
    CALL DSPLAY(RRLOW,ER_DEN)
    DO K=0, RRLOW(0)
      X_DATA(K) = RRLOW(K)
      Y_DATA(K) = ER_DEN(K)
    END DO
    CALL CHECK(X_DATA,Y_DATA) !SETS DATA LIMITS, ETC...
    CALL DSPLAY(X_DATA,Y_DATA) !DRAW AXIS AND PLOT DATA
  END IF

C
  IF( IDENREC .LT. 0) THEN
C
  PLOT THE ERROR ON THE RIGHT AXIS
  CALL RESCOM(SIER_DEN) !RESTORE COMMON BLOCKS DATA
C
  CALL DSPLAY(RRLOW,ER_DELR)
  DO K=0, RRLOW(0)
    X_DATA(K) = RRLOW(K)
    Y_DATA(K) = ER_DELR(K)
  END DO
  CALL CHECK(X_DATA,Y_DATA) !SETS DATA LIMITS, ETC...
  CALL DSPLAY(X_DATA,Y_DATA) !DRAW AXIS AND PLOT DATA
  END IF
END IF

  OPEN(77,FILE='F.ABEL;1',STATUS='UNKNOWN')
  WRITE(77,177) N, RGREG, ' 0.0 ', ' 0.01 ', ' 007 ', ' 1 '
*   ,POL_CUR, ' 0.0 '
177  FORMAT(I6,F9.1,A5,A6,A5,A3,F16.3,A6)
  WRITE(77,178) (WGHZ(I), DDPDW(I), RRLOW(I)
*   , DENSITY(RRLOW(I),RSHIFT(II),SHAPE(JJ),DERDEN(LL))
*   , I=N,1,-1)
178  FORMAT(F16.8,' ',E16.8,' ',F16.8,' ',E16.7)
  CLOSE(77)
END IF

```

!

This part writes the phase difference to a file is requested.

```

      IF(IDELPHI.LT.0) THEN
        OPEN(33,FILE='F.PHD',STATUS='NEW')
        WRITE(33,155) N, CURRENT, ' 0.0 ', ' 0.01 ', ' 007 ', ' 1 '
    *      ,POL_CUR, ' 0.0 '
155      FORMAT(I6,F9.1,A5,A6,A5,A3,F16.3,A6)
        WRITE(33,160) (WGHZ(I), DELPHI(I)
    *      , RRLow(I), DENLOW(I), I=N,1,-1)
160      FORMAT(G14.5,G18.7,G14.8,G18.8)
C 160      FORMAT(F16.8,' ',F16.8,' ',F16.8,' ',E16.7)
      END IF

```

!

This is the end of the main loop of the program.

```

      NUMBER = NUMBER + 1
      IB_ERROR = IB_ERROR + 1
      END DO
      ICG = ICG + 1
      END DO
      IERROR_W = IERROR_W + 1
      END DO
      IERROR_A = IERROR_A + 1
      END DO
      IERROR_B = IERROR_B + 1
      END DO
      IERROR_M = IERROR_M + 1
      END DO
      IWM = IWM + 1
      END DO
      LL = LL + 1
      END DO
      JJ = JJ + 1
      END DO
      II = II + 1
      END DO
      KK = KK + 1
      END DO
C
C      TOP TITLE
C      DO AN INTERNAL WRITE TO THE VARIABLE "TITLE" USING

```



```

C      THE GIVEN FORMAT.
      WRITE(TITLE,125) ' I=',CURRENT/1000.,' Kamps'
      * , ' B0=',B0,' Teslas '
125    FORMAT(A4,F6.2,A6, A5,F4.1,A8)
C      CALL AGXXCPT(760,TITLE) !PLOT THE TOP TITLE LABEL.

      CALL FINITT(10,100) !CLOSE THE PLOTTING SUBROUTINES
      CLOSE(11) !CLOSE THE DEBUGING FILE "F.OUT"
      END DO ! DO LOOP FOR THE DATA FILES AT "F.FLS"
      CLOSE(66) !CLOSE THE ERROR FILE
      CLOSE(88)

      STOP
      END

```

C

!

Here is where the subroutines are stored.

```

C *****
C
C      FUNCTIONS AND SUBROUTINES
C
C *****
C      ALL SUBROUTINES AND FUNCTIONS ARE DESCRIBED IN THE
C      APPENDIX OF THE THESIS AND INCLUDE THE FORMULAS AND
C      REFERENCES USED IN THE CODE.

```

!

This subroutine calculates the real/assumed index of refraction using the real/assumed density profile. The formula for the index of refraction is given by:

$$n^2(r, \omega) = 1 - \frac{\omega_{pe}^2}{\omega^2} \frac{\omega^2}{\omega^2} - \omega_{pe}^2 \omega^2 - \omega_{pe}^2 - \omega_{ec}^2 \quad (\text{B.11})$$

whese the parameter that depend on the radial position are follows:

$$\omega_{ec} = \frac{m_e B(r)}{q_e} \quad (\text{B.12})$$

$$\omega_{pe}^2 = \frac{q_e^2 n_e(r)}{\epsilon_0 m_e} \quad (\text{B.13})$$

```

      DOUBLE PRECISION FUNCTION MU2(R,WREF, RSHIFT, SHAPE, DERDEN)
C      THIS FUNCTION CALCULATES THE "REAL" INDEX OF REFRACTION

```

```

C      FOR A GIVEN WAVE OF FREQUENCY = WREF AND AT THE RADIAL
C      POINT = R.
      IMPLICIT NONE
      COMMON /COMDAT/ JSTEP
      * , RO, RA, DENSO, BO, ELECHR, ELEMAS, EPSILO, C
      * , APERT, LAMBDA, PI, RLINE, NTURN, CURRENT, POL_CUR
      * , RRANDOM, ALPHA, BETA, IDCHOISE
      DOUBLE PRECISION WREF2, WECE2, WPE2, T1
      * , TEMP1, TEMP2, R
      * , BF !MAGNETIC FIELD VALUE AT POSITION "R".
      * , DENS !"REAL" DENSITY AT "R".
      * , WCE !ELECTRON CYCLOTRON RESONANCE FREQUENCY
      * , WPE !PLASMA ELECTRON RESONANCE FREQUENCY
      * , W !GENERAL PURPOSE VARIABLE
      INTEGER JSTEP, IDCHOISE, NTURN
      DOUBLE PRECISION
      * , RR !RADIUS
      * , WREF !REFLECTOMETER'S FREQUENCY
      * , DENSITY !FUNCTION TO CALCULATE THE "REAL" DENSITY
      * , RSHIFT
      * , SHAPE
      * , BFIELD, RRANDOM
      * , ALPHA, BETA
      DOUBLE PRECISION
      * , RO !MAJOR RADIUS
      * , RA !MINOR RADIUS
      * , DENSO !CENTRAL DENSITY
      * , BO !CENTRAL MAGNETIC FIELD
      * , ELECHR !ELECTRON'S CHARGE
      * , ELEMAS !ELECTRON'S MASS
      * , EPSILO !PERMITTIVITY OF FREE SPACE
      * , C !SPEED OF LIGHT IN FREE SPACE
      * , APERT !AMPLITUDE OF DENSITY FLUCTUATION
      * , LAMBDA !WAVELENGTH OF FLUCTUATION
C      * , DELTA_C !BRETZ CORRELATION LENGTH
C      * , RNNOF !RANDOM NUMBER GENERATOR
      * , PI ! = 3.14159265
      * , RLINE, DERDEN, CURRENT, POL_CUR

      RR = R
      BF = BFIELD(RR) !DEFINES THE MAGNETIC FIELD AT POINT
      DENS = DENSITY(RR,RSHIFT,SHAPE, DERDEN) !DENSITY AT "R"
      TEMP1 =(ELECHR/EPSILO)
      TEMP2= (ELECHR/ELEMAS)
C      FREQUENCIES IN HERTZ.

```

```

C      PLASMA ELECTRON FREQ.
      WPE = SQRT( DENS * TEMP1 * TEMP2 ) / ( 2. * PI)
C      ELECTRON CYCLOTRON FREQ
      WCE = (BF * TEMP2) / ( 2. * PI)
      W = WREF

      WREF2 = W * W
      WECE2 = WCE * WCE
      WPE2 = WPE * WPE
      T1 = (WREF2 - WPE2 - WECE2)
      MU2 = 1.0 - (WPE2/WREF2) * ((WREF2 - WPE2) / T1)
C      WRITE(11,*)WPE,WCE,WREF,T1,MU2

      RETURN
      END

```

!

This subroutine calculates the integral of the index of refraction from the reference plane to the position of cutoff. The formula used here is given by:

$$\phi(\omega_i) = \int_{r_c(\omega_i)}^{r_{edge}} n(r, \omega_i) dr \quad (\text{B.14})$$

where  $r_c(\omega_i)$  is the cutoff position for the probing frequency  $\omega_i$ ,  $r_{edge}$  is the position of the reference plane at the edge, and  $n(r, \omega_i)$  is the index of refraction as a function of the radial position and the probing frequency.

```

C *****
      DOUBLE PRECISION FUNCTION SN(R1,R2,WREF,RSHIFT,SHAPE,DERDEN)
C      THIS FUNCTION CALCULATES THE INTEGRAL OF THE INDEX OF
C      REFRACTION USING THE ASSUMED "REAL" DESITY PROFILE.
C      R1 IS THE REFERENCE POINT OF THE INTEGRAL, WHILE
C      R2 IS THE POINT OF REFLECTION OR POINT OF CUT-OFF, WHERE
C      THE INDEX OF REFRACTION GOES TO 0 (ZERO).

      IMPLICIT NONE
      DOUBLE PRECISION R1, R2, WREF, RSHIFT, SHAPE, DERDEN
      INTEGER ISEED
C      VARIABLES FOR THE FUNCTION TO BE INTEGRATED
      COMMON /FCOM/ FWREF, FRSHIFT, FSHAPE, FDERDEN
      DOUBLE PRECISION FWREF, FRSHIFT, FSHAPE, FDERDEN
      DOUBLE PRECISION ERRABS, ERRREL, RESULT, ERREST, A ,B
      EXTERNAL F
C

```

```

      ISEED = 9572131
      CALL RNSET(ISEED)
C     PASSING THE PARAMETER TO THE FUNCTION'S COMMON BLOCK
      FWREF = WREF
      FRSHIFT = RSHIFT
      FSHAPE = SHAPE
      FDERDEN = DERDEN
C
      A = R2
      B = R1
      ERRABS = 1.0D-10 ! 0.0000001 !ABSOLUTE ERROR CRITERIUM
      ERRREL = 1.0D-10 ! 0.0000001 !RELATIVE ERROR CRITERIUM

      CALL DQDAGS(F,A,B,ERRABS,ERRREL,RESULT,ERREST)

      SN = RESULT
C     WRITE(11,20) A, B, RESULT, ERREST
C 20  FORMAT(2F16.8,2E16.8)

      RETURN
      END

      DOUBLE PRECISION FUNCTION F(R)
      IMPLICIT NONE
      COMMON /FCOM/ FWREF, FRSHIFT, FSHAPE, FDERDEN
      DOUBLE PRECISION FWREF, FRSHIFT, FSHAPE, FDERDEN
      DOUBLE PRECISION TEMP1, R, MU2

      TEMP1 = MU2(R, FWREF, FRSHIFT, FSHAPE, FDERDEN)
      F = SQRT( TEMP1 )

      RETURN
      END

```

!

This subroutine calculates the integral of the index of refraction for the reconstructed profile. For this index of refraction the density is know only to the last position of cutoff.

```

C *****

      DOUBLE PRECISION FUNCTION SNREC(I,N,R,DENS,WREF)
C     THIS FUNCTION CALCULATES THE INTEGRAL OF THE REFRACTIVE
C     INDEX USING THE RECONSTRUCTED DENSITY PROFILE DATA.
      IMPLICIT NONE

```

```

PARAMETER NMAX=2000
INTEGER JSTEP, I, J, K, N, IDCHOISE, NDATA, NINTV, NTURNS
COMMON /COMDAT/ JSTEP
* , RO, RA, DENSO, BO, ELECHR, ELEMAS, EPSILO, C
* , APERT, LAMBDA, PI, RLINE, NTURNS, CURRENT, POL_CUR
* , RRANDOM, ALPHA, BETA, IDCHOISE
DOUBLE PRECISION R(N), DENS(N), WREF, RJ, DELRJ, DENRJ
* , RRANDOM, ALPHA, BETA
DOUBLE PRECISION
*   RO   !MAJOR RADIUS
*   , RA   !MINOR RADIUS
*   , DENSO !CENTRAL DENSITY
*   , BO   !CENTRAL MAGNETIC FIELD
*   , ELECHR !ELECTRON'S CHARGE
*   , ELEMAS !ELECTRON'S MASS
*   , EPSILO !PERMITTIVITY OF FREE SPACE
*   , C   !SPEED OF LIGHT IN FREE SPACE
*   , APERT !AMPLITUDE OF THE FLUCTUATION
*   , LAMBDA !WAVELENGTH OF FLUCTUATION
*   , PI   ! = 3.14159265
*   , RLINE, CURRENT, POL_CUR, TEMP

DOUBLE PRECISION X(NMAX), Y(NMAX), MU2REC
* , BREAK(NMAX), CSCOE(4*NMAX), A, B, DCSITG

C   DOUBLE PRECISION   SUMY

C   FIVE POINT CUBIC INTERPOLATION INTEGRATION OF THE
C   INDEX OF REFRACTION.  SEE CHAPTER 6, SECTION 6.3
DELRJ = ( R(N) - R(I) ) / FLOAT( N )
RJ = R(I) - DELRJ
DO J = 1, N
  RJ = RJ + DELRJ
  X(J) = RJ
  DO K = I+1, N
    IF( (R(K-1).LE.RJ) .AND. (RJ.LT.R(K)) ) THEN
      DENRJ = (DENS(K)-DENS(K-1))/(R(K)-R(K-1))
      *   * (RJ-R(K-1)) + DENS(K-1)
      TEMP = MU2REC(RJ,DENRJ,WREF)
C   Y(J) = SQRT( ABS( TEMP ) )
      Y(J) = TEMP / SQRT( ABS( TEMP ) )
      GOTO 11
    END IF
  END DO
11  CONTINUE

```

```

C      WRITE(11,20)J, K, RJ, DENRJ, X(J), Y(J)
C 20   FORMAT(I5,I5,F11.6,3D18.8)
      END DO

      NDATA = J
      CALL DCSINT(NDATA, X, Y, BREAK, CSCOEFF)
C      INTEGRATE THE SPLINE USING THE COEFFICIENTS
      NINTV = NDATA - 1
      A = R(I)
      B = R(N)
      SNREC = DCSITG(A, B, NINTV, BREAK, CSCOEFF)

      RETURN
      END

```

!

This function calculates the reconstructed index of refraction using the data from the reconstructed density profile.

```

C *****

      DOUBLE PRECISION FUNCTION MU2REC(R,DENS,WREF)
C      THIS FUNCTION CALCULATES THE INDEX OF REFRACTION USING
C      THE RECONSTRUCTED DENSITY PROFILE DATA.
      IMPLICIT NONE
      DOUBLE PRECISION
      *   BF      !MAGNETIC FIELD VALUE AT POSITION "R"
      *   , WCE    !ELECTRON CYCLOTRON RESONANCE FREQUENCY
      *   , WPE    !PLASMA ELECTRON RESONANCE FREQUENCY
      *   , TEMP1, TEMP2  !TEMPORAL STORAGE VARIABLES
      *   , WPE2
      *   , WCE2
      *   , W2
      COMMON /COMDAT/ JSTEP
      *   , RO, RA, DENSO, BO, ELECHR, ELEMAS, EPSILO, C
      *   , APERT, LAMBDA, PI, RLINE, NURNS, CURRENT, POL_CUR
      *   , RRANDOM, ALPHA, BETA, IDCHOISE
      INTEGER JSTEP, IDCHOISE, NURNS
      DOUBLE PRECISION
      *   RO      !MAJOR RADIUS
      *   , RA      !MINOR RADIUS
      *   , DENSO   !CENTRAL DENSITY
      *   , BO      !CENTRAL MAGNETIC FIELD
      *   , ELECHR  !ELECTRON'S CHARGE

```

```

* , ELEMAS !ELECTRON'S MASS
* , EPSILO !PERMITIVITY OF FREE SPACE
* , C !SPEED OF LIGHT IN FREE SPACE
* , APERT !AMPLITUDE OF THE FLUCTUATION
* , LAMBDA !WAVELENGTH
* , PI ! = 3.14159265
* , RLINE, CURRENT, POL_CUR
* , ALPHA, BETA
* , BFIELD, RRANDOM
* , R !RADIAL POSITION
* , DENS !RECONSTRUCTED DENSITY
* , WREF !REFLECTOMETER'S FREQUENCY

BF = BFIELD(R) !MAGNETIC FIELD AT POINT "R".
TEMP1 =(ELECHR/EPSILO)
TEMP2= (ELECHR/ELEMAS)
IF(DENS.LT. 0.0) THEN
  WRITE(*,*) ' NEGATIVE DENSITY = ',DENS,R,'=R ',WREF,'=WREF'
END IF
C FREQUENCIES IN HERTZ.
C PLASMA ELECTRON FREG.
WPE = SQRT( DENS * TEMP1 * TEMP2 ) / ( 2. * PI)
C ELECTRON CYCLOTRON FREG
WCE = (BF * TEMP2) / (2. * PI)
WPE2 = WPE * WPE
WCE2 = WCE * WCE
W2 = WREF * WREF

C MU2REC = 1.0 - WPE*WPE/(WREF*WREF) * (WREF*WREF-WPE*WPE) /
C / (WREF*WREF - WPE*WPE - WCE*WCE)

MU2REC = 1.0 - (WPE2/W2) * (W2-WPE2) / (W2-WPE2-WCE2)

RETURN
END

```

!

This function calculates the radial position where the index of refraction of the real density profile is equal to zero.

```

C *****

DOUBLE PRECISION FUNCTION RZERO(R,WREF,RSHIFT,SHAPE,DERDEN)
C THIS FUNCTION CALCULATES THE POINT IN THE RADIUS AT

```

```

C      WHICH THE INDEX OF REFRACTION IS EQUAL TO ZERO.
      IMPLICIT NONE
      INTEGER IDUMMY, NROOT, ITMAX
      DOUBLE PRECISION R, WREF, RSHIFT, SHAPE, DERDEN
      COMMON /CRZERO/  CWREF, ZRSHIFT, ZSHAPE, ZDERDEN
      DOUBLE PRECISION CWREF, ZRSHIFT, ZSHAPE, ZDERDEN
      DOUBLE PRECISION ERRABS, ERRREL, EPS, ETA, XGUESS, RZ
C      *, DMU, DMUOLD, MU2, RZOLD, RZDEL
      EXTERNAL ZWRX
      !

```

This function uses the index of refraction to calculate the position of cutoff for the propagating wave. The position of the cutoff is used to calculate the phase of the propagating wave from the reference plane to the cutoff position.

```

      CWREF = WREF
      ZRSHIFT = RSHIFT
      ZSHAPE = SHAPE
      ZDERDEN = DERDEN
      ERRABS = 1.0D-10 ! 1.0D-8 ! 0.0000001
      ERRREL = 1.0D-10 ! 1.0D-8 ! 0.0000001
      EPS = 0.0
      ETA = 0.0
      NROOT = 1
      ITMAX = 100000
      XGUESS = R
C      ZREAL IS AN IMSL FUNCTION THAT FINDS THE ZERO OF A
C      GIVEN FUNTION "F"
      CALL DZREAL(ZWRX,ERRABS,ERRREL,EPS,ETA,NROOT,ITMAX,XGUESS
*      ,RZ,IDUMMY)

      RZERO = RZ

C      RZDEL = 0.0001
C      RZ = RZ + 0.005      ! + RZDEL*2.
C      RZOLD = RZ
C      DMU = MU2(RZ,WREF,RSHIFT,SHAPE,DERDEN)
C      DMUOLD = DMU
C      WRITE(11,*)RZ,RZDEL,DMU
C      DO WHILE( DMU / SQRT( ABS( DMU ) ) ) .GT. 1.0D-4 )
C          RZOLD = RZ
C          DMUOLD = DMU
C          RZ = RZ - RZDEL
C          DMU = MU2(RZ,WREF,RSHIFT,SHAPE,DERDEN)

```



```

CC      WRITE(11,*)RZ,RZDEL,DMU
C      IF( DMU .LT. 0.0 ) THEN
C          RZ = RZOLD
C          DMU = DMUOLD
C          RZDEL = RZDEL / 2.
C      END IF
C  END DO
C      WRITE(11,*)RZ,RZDEL,DMU
C      RZERO = RZ

```

```

RETURN
END

```

```

DOUBLE PRECISION FUNCTION ZWRI(RR)
C  THIS FUNCTION CALCULATES THE FREQUENCY OF THE RIGHT HAND
C  CUT-OFF FOR THE X-MODE.
IMPLICIT NONE
DOUBLE PRECISION TEMP1, TEMP2, WCE, WPE, WREF
* , DENS, BF, RR
DOUBLE PRECISION DENSITY
INTEGER JSTEP, IDCHOISE, NURNS
COMMON /CRZERO/  CWREF, RSHIFT, SHAPE, DERDEN
DOUBLE PRECISION CWREF, RSHIFT, SHAPE, DERDEN, RRANDOM
COMMON /COMDAT/ JSTEP
* , RO,RA,DENSO,BO, ELECHR, ELEMAS, EPSILO, C
* , APERT, LAMBDA, PI, RLINE, NURNS, CURRENT, POL_CUR
* , RRANDOM, ALPHA, BETA, IDCHOISE
DOUBLE PRECISION
*   RO   !MAJOR RADIUS
*   , RA   !MINOR RADIUS
*   , DENSO   !CENTRAL DENSITY
*   , BO   !CENTRAL MAGNETIC FIELD
*   , ELECHR   !ELECTRON'S CHARGE
*   , ELEMAS   !ELECTRON'S MASS
*   , EPSILO   !PERMITIVITY OF FREE SPACE
*   , C   !SPEED OF LIGHT IN FREE SPACE
*   , APERT   !AMPLITUDE OF THE FLUCTUATION
*   , LAMBDA   !WAVELENGTH
*   , PI   ! = 3.14159265
*   , RLINE, CURRENT, POL_CUR, BFIELD, ALPHA, BETA

BF = BFIELD(RR)   !MAGNETIC FIELD AT THE POINT "RR"
DENS = DENSITY(RR,RSHIFT,SHAPE, DERDEN) !DENSITY AT "RR"
TEMP1 =(ELECHR/EPSILO)

```

```

      TEMP2= (ELECHR/ELEMAS)
C      FREQUENCIES IN HERTZ
      WPE = SQRT(DENS*TEMP1*TEMP2)/(2.*PI)  !PLASMA ELECTRON FREQ.
      WCE = BF*TEMP2/(2.*PI)  !CYCLOTRON ELECTRON FREQ
      WREF = CWREF
      ZWRX = 0.5 * ( WCE + SQRT(WCE*WCE + 4.0*WPE*WPE) ) - WREF
C      TEMP1 = MU2(RR,CWREF,RSHIFT,SHAPE,DERDEN)
C      TEMP2 = SQRT( ABS( MU2(RR,CWREF,RSHIFT,SHAPE,DERDEN) ) )
C      ZWRX = TEMP1 / TEMP2
C      ZWRX = MU2(RR,WREF,RSHIFT,SHAPE,DERDEN)
      RETURN
      END

```

!

This function calculates the position where the reconstructed index of refraction is equal to zero.

```

C *****
      DOUBLE PRECISION FUNCTION RECZERO(R, DENS, WREF)
C      THIS FUNCTION CALCULATES THE POINT IN THE RADIUS AT
C      WHICH THE INDEX OF REFRACTION IS EQUAL TO ZERO.
      IMPLICIT NONE
      INTEGER IDUMMY, NROOT, ITMAX
      DOUBLE PRECISION R, WREF, DENS, CWREF, CDENS
      COMMON /CRZERO/      CWREF, CDENS
      DOUBLE PRECISION ERRABS, ERRREL, EPS, ETA, IGUESS, RZ
      EXTERNAL MUREC

```

!

This function calculate the cutoff position using the reconstructed density profile data.

```

      CWREF = WREF
      CDENS = DENS

      ERRABS = 1.0D-10  ! 0.0000001
      ERRREL = 1.0D-10  ! 0.0000001
      EPS = 0.0
      ETA = 0.0
      NROOT = 1
      ITMAX = 100000
      IGUESS = R
C      ZREAL IS AN IMSL FUNCTION THAT FINDS THE ZERO OF A

```

```

C      GIVEN FUNTION "F"
      CALL DZREAL(MUREC,ERRABS,ERRREL,EPS,ETA,NROOT,ITMAX,IGUESS
*      ,RZ,IDUMMY)

      RECZERO = RZ
      RETURN
      END

      DOUBLE PRECISION FUNCTION MUREC(QRR)
C      CALCULATES THE CUTOFF FOR THE WAVE
      IMPLICIT NONE
C      THIS DEFINES SOME CONSTANTS IN MKS UNITS.
      DOUBLE PRECISION TEMP1, TEMP2, TEMP3, WCE, WPE, BF
*      , WCE2, WPE2, WREF2, QRR
      DOUBLE PRECISION RR, BFIELD, WREF, DENS
      COMMON /CRZERO/ WREF, DENS
      COMMON /COMDAT/ JSTEP
*      , RO,RA,DENSO,BO, ELECHR, ELEMAS, EPSILO, C
*      , APERT, LAMBDA, PI, RLINE, NURNS, CURRENT
*      , POL_CUR, RRANDOM, ALPHA, BETA, IDCHOISE
      INTEGER JSTEP, IDCHOISE, NURNS
      DOUBLE PRECISION
*      RO,RA,DENSO,BO, ELECHR, ELEMAS, EPSILO, C
*      , APERT, LAMBDA, PI, RLINE, CURRENT
*      , POL_CUR, RRANDOM, ALPHA, BETA

      RR = QRR
      BF = BFIELD(RR)      !MAGNETIC FIELD AT THE POINT "RR"
      TEMP1 = (ELECHR/EPSILO)
      TEMP2 = (ELECHR/ELEMAS)
C      FREQUENCIES IN HERTZ
      WPE = SQRT(DENS*TEMP1*TEMP2)/(2.*PI)      !PLASMA ELECTRON FREQ.
      WCE = BF*TEMP2/(2.*PI)      !CYCLOTRON ELECTRON FREQ
      WCE2 = WCE * WCE
      WPE2 = WPE * WPE
      WREF2 = WREF * WREF
      TEMP3 = 1. - (WPE2/WREF2) * (WREF2-WPE2)/(WREF2-WPE2-WCE2)
C      IF( TEMP3 .NE. 0.0 ) THEN
C          MUREC = TEMP3 / ABS(TEMP3)
C      ELSE
C          MUREC = TEMP3
C      END IF
      MUREC = WCE/2. + SQRT(WPE2 + WCE2/4.) - WREF
      WRITE(11,*) RR,BF,WREF, WCE, WPE, MUREC, TEMP3

```

```

      RETURN
      END

```

```

!

```

This subroutine calculates the increment on the cutoff positions using the non-linearize version of the radial increment in the cutoff positions.

```

C *****
      DOUBLE PRECISION FUNCTION DELTA_R(DEL1,DEL2,MUR2,MUR3)
C      THIS FUNCTION CALCULATES THE POINT IN THE RADIUS AT
C      WHICH THE INDEX OF REFRACTION IS EQUAL TO ZERO.
      IMPLICIT NONE
      INTEGER IDUMMY, NROOT, ITMAX
      DOUBLE PRECISION DEL1,      DEL2,  MUR2,  MUR3
      *      , CDEL2, CMUR2, CMUR3
      COMMON /CPARABOLA/ CDEL2, CMUR2, CMUR3
      DOUBLE PRECISION ERRABS, ERRREL, EPS, ETA, XGUESS, RZ
      EXTERNAL PARABOLA
      !

```

This subroutine uses the no-linearizer version of the parabolic approximation to calculate a no-linearize increment on the cutoff positions.

```

      CDEL2 = DEL2
      CMUR2 = MUR2
      CMUR3 = MUR3

      ERRABS = 1.0D-10 ! 0.0000001
      ERRREL = 1.0D-10 ! 0.0000001
      EPS = 0.0
      ETA = 0.0
      NROOT = 1
      ITMAX = 100000
      XGUESS = DEL1
C      ZREAL IS AN IMSL FUNCTION THAT FINDS THE ZERO OF A
C      GIVEN FUNTION "F"
      CALL DZREAL(PARABOLA,ERRABS,ERRREL,EPS,ETA,NROOT,ITMAX,XGUESS
      *      ,RZ,IDUMMY)

      DELTA_R = RZ
      RETURN

```

END

```

      DOUBLE PRECISION FUNCTION PARABOLA(DELR1)
C      THIS FUNCTION CALCULATES THE ERROR ON THE PARABOLIC COEFFICIENTS
      IMPLICIT NONE
      DOUBLE PRECISION DELR1, BB, CC
      DOUBLE PRECISION DENOMI, DELR2, MUR2, MUR3
      COMMON /CPARABOLA/ DELR2, MUR2, MUR3

      DENOMI = (DELR1 + DELR2) * DELR2
C      BB = MUR2/DELR1 + (DELR1*(MUR2-MUR3)+DELR2*MUR2) / DENOMI
C      CC = (-MUR2*(DELR1+DELR2) + DELR1*MUR3) / (DENOMI*DELR1)
      BB = ( (MUR2-MUR3) * DELR1 / DELR2 + 2. * MUR2 ) / DELR1
      CC = ( (MUR3-MUR2) * DELR1 / DELR2 - MUR2 ) / (DELR1*DELR1)
      PARABOLA = BB*DELR1 + CC*DELR1*DELR1 - MUR2

      RETURN
      END

```

!

This subroutine calculates the position of where the resonances ocure.

```

C *****
      DOUBLE PRECISION FUNCTION REZERO(R,WREF, RSHIFT, SHAPE, DERDEN)
C      THIS FUNCTION CALCULATES THE RADIUS AT WHICH THE
C      RESONANCE OCCURES.
      IMPLICIT NONE
      INTEGER IDUMMY
      DOUBLE PRECISION R, WREF, RZ, RSHIFT, SHAPE, DERDEN
      COMMON /CREZERO/ CWREF, ZRSHIFT, ZSHAPE, ZDERDEN
      DOUBLE PRECISION CWREF, ZRSHIFT, ZSHAPE, ZDERDEN
      EXTERNAL ZWRES

      CWREF = WREF
      ZRSHIFT = RSHIFT
      ZSHAPE = SHAPE
      ZDERDEN = DERDEN
C      ZREAL IS AN IMSL FUNCTION THAT FINDS THE ZERO OF A
C      GIVEN FUNTION "F"
      CALL ZREAL(ZWRES,0.000001,0.000001,0.,0.,1,100000,R,RZ,IDUMMY)

      REZERO = RZ

```

```

RETURN
END

```

```

DOUBLE PRECISION FUNCTION ZWRES(RR)
C THIS FUNCTION CALCULATES THE FREQUENCY OF THE UPPER
C HYBRID RESONANCE. IT IS ONLY USED BY THE FUNCTION
C "REZERO" TO CALCULATE THE RADIAL POINT WHERE THE
C RESONANCE OCCURES.
IMPLICIT NONE
DOUBLE PRECISION RR, BF, DENS, WCE, WPE, TEMP1, TEMP2, DENSITY
INTEGER JSTEP, IDCHOISE, NURNS
COMMON /CREZERO/ CWREF, RSHIFT, SHAPE, DERDEN
DOUBLE PRECISION CWREF, RSHIFT, SHAPE, DERDEN, RRANDOM
COMMON /COMDAT/ JSTEP
* , RO, RA, DENSO, BO, ELECHR, ELEMAS, EPSILO, C
* , APERT, LAMBDA, PI, RLINE, NURNS, CURRENT, POL_CUR
* , RRANDOM, ALPHA, BETA, IDCHOISE
DOUBLE PRECISION
* RO !MAJOR RADIUS
* , RA !MINOR RADIUS
* , DENSO !CENTRAL DENSITY
* , BO !CENTRAL MAGNETIC FIELD
* , ELECHR !ELECTRON'S CHARGE
* , ELEMAS !ELECTRON'S MASS
* , EPSILO !PERMITTIVITY OF FREE SPACE
* , C !SPEED OF LIGHT IN FREE SPACE
* , APERT !AMPLITUDE OF THE FLUCTUATION
* , LAMBDA !WAVELENGTH
* , PI ! = 3.14159265
* , RLINE, CURRENT, POL_CUR
* , BFIELD
* , ALPHA, BETA

BF = BFIELD(RR) !MAGNETIC FIELD AT THE POINT "RR"
DENS = DENSITY(RR, RSHIFT, SHAPE, DERDEN) !DENSITY AT "RR"
TEMP1 = (ELECHR/EPSILO)
TEMP2 = (ELECHR/ELEMAS)
C FREQUENCIES IN HERTZ.
C PLASMA ELECTRON FREQ.
WPE = SQRT( DENS * TEMP1 * TEMP2 ) / (2. * PI)
C CYCLOTRON ELECTRON FREQ
WCE = BF * TEMP2 / (2. * PI)
ZWRES = SQRT(WCE*WCE + WPE*WPE) - CWREF
RETURN

```

END

!

This function gives the real/assumed density profile for any given radius  $R$ . It can use the inverse hyperbolic density profile or the famous  $\alpha - \beta$  profile favorite of many theorists, and given by:

$$n_e(r) = n_0 \left( 1 - \left( \frac{r}{a} \right)^\alpha \right)^\beta \quad (\text{B.15})$$

where  $n_0$  is the central density,  $r$  is the radius,  $a$  is the minor radius,  $\alpha$  and  $\beta$  are the shaping parameters.

```

C
C *****
C
      DOUBLE PRECISION FUNCTION DENSITY(RR, RSHIFT, SHAPE, DERDEN)
C      THIS FUNCTION CALCULATES THE "REAL" DENSITY PROFILE.
      IMPLICIT NONE
      COMMON /COMDAT/ JSTEP
      * , RO,RA,DENSO,BO, ELECHR, ELEMAS, EPSILO, C
      * , APERT, LAMBDA, PI, RLINE, NTURN, CURRENT, POL_CUR
      * , RRANDOM, ALPHA, BETA, IDCHOISE
      INTEGER JSTEP, IDCHOISE, NTURN
      DOUBLE PRECISION RR, RSHIFT, SHAPE, RRANDOM, TEMP
      * , RO,RA,DENSO,BO, ELECHR, ELEMAS, EPSILO, C
      * , APERT, LAMBDA, PI, D, RLINE, DERDEN, CURRENT
      * , POL_CUR, ALPHA, BETA, DENS1, DENS2, DERDENS, DENSPER
C      * , DBRETZ

      IF( IDCHOISE .EQ. 0 )THEN      ! ELSE DO ALPHA-BETA PROFILE
        TEMP = ( 1.0 - TANH((RR-RSHIFT)/SHAPE) ) / 2.0
        IF( RR .GE. RLINE ) THEN
          DENSITY = DENSO * TEMP
        ELSE
          D = DENSO * ( 1.0 - TANH((RLINE-RSHIFT)/SHAPE) ) / 2.
          DENSITY = DERDEN * (RR - RLINE) + D
        END IF
      CHERE      CORRELATION FLUCTUATION BEGIN
C      DENSITY = DENSITY * (1. + APERT * DBRETZ(RR) )
C      CORRELATION FLUCTUATION END
      ELSE      ! DO ALPHA-BETA PROFILE
        IF ( (RR.GE.(RO-RA)) .AND. (RR.LE.(RO+RA)) ) THEN
C      WRITE(11,*)RR,RO,RA,ALPHA, BETA
          DENS1 = DENSO*(ABS(1.0-(ABS(RR-RO)/RA)**ALPHA))**BETA

```

```

      DENSPER = APERT * (LAMBDA/(2.*PI))
*      * SIN(-2.0*PI*(RR-RO-RA)/LAMBDA)

      DERDENS = DENSO
*      * BETA * (ABS(1.0-(ABS(RR-RO)/RA)**ALPHA))**(BETA-1)
*      * ALPHA * (ABS(RR-RO)/RA)**(ALPHA-1) / RA

      DENS2 = DENSPER * DERDENS

      DENSITY = ABS( DENS1 + DENS2 )
C      WRITE(11,*)RR, APERT, RO, RA, LAMBDA
C      WRITE(11,*)DENS1,'=D1 ',DENSPER,'=PER ',DENS2,'=D2 ',DENSITY
      ELSE
      DENSITY = 0.00001 * DENSO
      END IF

END IF      ! *****

RETURN
END

```

C  
!

This subroutine is a smoothing subroutine like the one that is used in the PPPL computers. It uses a Gaussian envelope to weight the point around the center point in order to reduce the inception of high frequencies due to discontinuities in the weighting function, like it will happen if a square function was used to do the smoothing.

C \*\*\*\*\*  
C

```

      SUBROUTINE SMOOTH2(ICONV, DATA, DATAS)
C      THIS SUBROUTINE SMOOTHS THE DATA BY USING THE FAMOUS
C      RUNNING CARIAGE INTRGRAL METHOD. THIS IS DONE BY AVERAGING
C      EVERY POINT ON THE ARRAY/FUNCTION AGAINST THE SURROUNDING
C      NEIGHBOR POINTS OF THE ARRAY/FUNCTION.
      IMPLICIT NONE
      DOUBLE PRECISION
*      DATA(0:*) ! DATA TO BE SMOOTHED
*      , DATAS(0:*) ! WORKING ARRAY
*      , SUM ! WORKING VARIABLE
*      , C ! DECAY CONSTANT FOR THE GAUSSIAN
*      , X ! WORKING VARIABLE
*      , PI ! = 3.14159265

```



```

      INTEGER
      *   I   ! DO LOOP INDEX
      *   , ICONV   ! NUMBER OF POINTS TO AVERAGE BY
      *   , I1   ! LIMITS FOR THE DO LOOP
      *   , I2   ! LIMITS FOR THE DO LOOP
      *   , J   ! DO LOOP INDEX
      *   , IJ   ! INDEX
C
      IF( ICONV .LE. 0 ) RETURN
      PI = 3.14159265
C   I DECIDED TO USE A GAUSSIAN ENVELOPE OR WEIGHTING FUNCTION TO DO
C   THE SMOOTHING, AS OPPOSED TO USING A SQUARE STEP FUNCTION.  THIS
C   WILL HELP TO REDUCE THE INTRODUCTION OF HIGHER HARMONICS INTO
C   THE DATA, AS COMPARED TO A SQUARE STEP FUNCTION.
      C = FLOAT(ICONV) / SQRT(LOG(10.))
      DO I = 1, ICONV
        SUM = 0.0
        DO J = 1-I , ICONV
          IJ = I + J
          X = FLOAT(J) / C
          SUM = SUM + DATA(IJ) * EXP(-X*X) / ( C * SQRT(PI))
        END DO
        DATAS(I) = SUM
      END DO
      I1 = ICONV + 1
      I2 = DATA(0) - ICONV - 1
      DO I = I1 , I2
        SUM = 0.0
        DO J = -ICONV , ICONV
          IJ = I + J
          X = FLOAT(J)/C
          SUM = SUM + DATA(IJ) * EXP(-X*X) / ( C * SQRT(PI))
        END DO
        DATAS(I) = SUM
      END DO
      DO I = I2+1, DATA(0)
        SUM = 0.0
        DO J = -ICONV , ICONV - (I - I2)
          SUM = SUM + DATA(J)
        END DO
        DATAS(I) = SUM / (DATA(0)-(I-ICONV)+1)
      END DO
C
      DO I = 1, DATA(0)
        DATA(I) = DATAS(I)
      END DO

```

```

      END DO
C
      RETURN
      END
C
!
```

This subroutine makes the running carriage integral of a given function or array of points. It is a simple and effective way of smoothing the data.

```

C *****
C
      SUBROUTINE SMOOTH(ICONV,DATA)
      IMPLICIT NONE
      DOUBLE PRECISION DATA(0:*), SUM
      INTEGER ICONV, I, J
      IF(ICONV .LE. 0) RETURN
      DO I = DATA(0), ICONV, -1
        SUM = 0.0
        DO J = I, I-ICONV+1, -1
          SUM = SUM + DATA(J)
        END DO
        DATA(I) = SUM / ICONV
      END DO
      RETURN
      END
C
!
```

This function calculates the magnetic field. It has a correctio factor for the modeling of the ripple in the magnetic field between the magnetic coils.

```

C *****
C
      DOUBLE PRECISION FUNCTION BFIELD(R)
C      THIS FUNCTION CALCULATES THE MAGNETIC FIELD.
      IMPLICIT NONE
      DOUBLE PRECISION R, CR, CG(6,6), BF, BPOL
      * , RO, RA, BO, DENSO, ELECHR, ELEMAS, EPSILO, C
      * , APERT, LAMBDA, PI, RLINE, CURRENT, POL_CUR, B_ERROR(11)
      * , ALPHA, BETA, RRANDOM
      COMMON /COMDAT/ JSTEP
      * , RO,RA,DENSO,BO, ELECHR, ELEMAS, EPSILO, C
      * , APERT, LAMBDA, PI, RLINE, NURNS, CURRENT
      * , POL_CUR, RRANDOM, ALPHA, BETA, IDCHOISE
```

```

COMMON /COMBFIELD/I, J, B_ERROR, CG
INTEGER NURNS, I, JSTEP, J, IDCHOISE
C
BO = 2.0D-07 * NURNS * CURRENT / RO
CR = CG(1,I) + R*(CG(2,I) + R*(CG(3,I) + R*(CG(4,I)
* + R*(CG(5,I) + R*CG(6,I))))
BF = CR * BO * RO/R
BPOL = 2.0D-07 * POL_CUR / (R-RO) * (RO/R)
BFIELD = SQRT( BF*BF + BPOL*BPOL ) + B_ERROR(J)
RETURN
END
C
!
```

This subroutine simply prints a number on the corresponding curve for a give plot.

```

C *****
C
SUBROUTINE CLABEL(IWHERE, NUMBER, X, Y)
C THIS SUBROUTINE WRITES THE CURVE NUMBER ON THE PLOT.
IMPLICIT NONE
INTEGER IWHERE, NUMBER
CHARACTER LABEL*1
DOUBLE PRECISION X(0:*), Y(0:*)
REAL*4 XLABEL(0:1), YLABEL(0:1)
C
XLABEL(0) = 1
YLABEL(0) = 1
XLABEL(1) = X(IWHERE)
YLABEL(1) = Y(IWHERE)
WRITE(LABEL,10) NUMBER
10 FORMAT(I1)
C
CALL SYMBL(0)
CALL CPlot(XLABEL,YLABEL)
CALL AGXHS(LABEL)
RETURN
END
```

!

This subroutine is the Abel inversion subroutine used to calculate the density profile the magnetic field is zero. The Abel inversion technique was presented, discussed and derived in the second chapter of the thesis.

C

```

C *****
C
      DOUBLE PRECISION FUNCTION SABEL(I,N,WREF,DDPDW)
C      THIS FUNCTION CALCULATES THE INTEGRAL OF THE ABEL
C      INVERSION USING THE DERIVATIVE OF THE PHASE DATA.
      IMPLICIT NONE
      PARAMETER NMAX=2000
C      DOUBLE PRECISION SUMY, Y(NMAX), DERWJ, X1,X2,Y1,Y2
C      REAL SUMY, DERWJ, X1,X2,Y1,Y2, WJ, DELWJ
C      REAL
      DOUBLE PRECISION WREF(0:*), DDPDW(0:*)
      DOUBLE PRECISION BREAK(NMAX),CSCOE(4*NMAX),A,B,DCSITG
*      , X(NMAX), Y(NMAX), DELW, TEMP, WK
      INTEGER I, J, N, K, NDATA, NINTV
!
```

This is the Abel inversion subroutine used when the magnetic field is set to zero,  $B_0 = 0$ .

```

C      WRITE(*,*)' '
C      WRITE(*,*)' K, J, WK, TEMP, Y(K) '
      DELW = (WREF(I) - WREF(N)) / N
      WK = WREF(N) - DELW
      DO K = 1, N
        WK = WK + DELW
        DO J = I+1, N
          IF( (WREF(J) .LE. WK ) .AND. (WK .LT. WREF(J-1)) ) THEN
            X(K) = WK
            TEMP = (DDPDW(J-1)-DDPDW(J))/(WREF(J-1)-WREF(J))
*            * (WK - WREF(J)) + DDPDW(J)
            Y(K) = TEMP / SQRT(WREF(I) * WREF(I) - WK * WK)
C            WRITE(*,*) K, J, WK, TEMP, Y(K)
            GOTO 10
          END IF
        END DO
      10    CONTINUE
      END DO
      NDATA = K
      CALL DCSINT(NDATA, X, Y, BREAK, CSCOE)
C      INTEGRATE THE SPLINE USING THE COEFFICIENTS
      NINTV = NDATA - 1
      A = WREF(N)
      B = WREF(I) + DELW/2.
      SABEL = DCSITG(A, B, NINTV, BREAK, CSCOE)
C      WRITE(*,*)' SABEL =', SABEL
```

```

      RETURN
      END

```

```

C
!

```

This subroutine calculates the perturbation for the phase data.

```

C *****
C
      DOUBLE PRECISION FUNCTION DBRETZ(R)
      IMPLICIT NONE
      DOUBLE PRECISION R, R PERT(0:2310), A PERT(0:2310), DEL_R
      COMMON /PERT_DAT/R PERT,A PERT, DEL_R
      DBRETZ = A PERT( (R - R PERT(1)) / DEL_R)

      RETURN
      END
C
!

```

This subroutine calculates the increment on the cutoff position and the density at that point. It is the main part of the reconstruction process and it was put in a subroutine to ease the readability of the program.

```

C *****
C
      SUBROUTINE THOMAS(I,N,NN2,RRLOW,DELREC,RRUP,DENLOW,DENUP
      * ,PHIRLOW,DELPHI,PHIRUP,WREF,WM,AFIT,BFIT,CFIT,RCOMP
      * ,ATMP_,IDUMY,RZDEL)
      IMPLICIT NONE
      PARAMETER NDATA=4
      INTEGER I, N, NN2,IDUMY !, J
      DOUBLE PRECISION DTEMP1, DTEMP2, DTEMP3, DTEMP4, RZDEL
      * , MU2REC, SNREC, MUR_1, MUR_2, MUR_3, ERR_DR, ERR_DOYLE
      * , DELR1 !, DELR2, DELTA_R, TEMP5, RECZERO
C      * , D_WILGEN
C      * , C_DAVE, B_DAVE !, DAVE1, DAVE2
C      * , XSIM, F1, F2, DSIM, DELRSIM
C      * , T1, T2
      DOUBLE PRECISION PI,ELECHR,ELEMAS,EPSILO,C,RCOMP(0:*)
      * ,TMP,ATMP_(0:*)
C      * , BREAK(NDATA), CSCOE(4,NDATA), CSVAL, X(NDATA), Y(NDATA)
      * , RRLOW(0:*), DELREC(0:*), RRUP(0:*), DENLOW(0:*), DENUP(0:*)
      * , PHIRLOW(0:*), DELPHI(0:*), PHIRUP(0:*), WREF(0:*),WM!,DENSITY

```

```

* , BF, BFIELD, WCE, WW, AFIT,BFIT,CFIT,FDELTA,FDELTA1,DRGES
!

```

This is the subroutine that calculates the increment in the cutoff positions. It was put in a subroutine so that it will make the program easier to read and work with it. The formula for the increment in the cutoff position has been derived and explained in detail in the thesis. There are different linear and parabolic fits that can be done to the unknown part of the index of refraction in order to obtain a formula for the increment on the positions of the cutoffs. It was found that the one using the condition of the derivative or slope that the last two points of the index of refraction was the one that provided with the best fit to the index of refraction. That is the one used here, even though that the formulas for the other cases have been commented out and left here to allow for future work if necessary.

```

C
C      THIS SUBROUTINE CALCULATES THE INCREMENT ON THE RADIAL
C      POSITION OF THE CUTOFF, THE POSITION OF THE CUTOFF, AND
C      THE DENSITY AT THE CALCULATED CUTOFF POSITION FOR THE
C      RECONSTRUCTION PROCESS.
C      THIS DEFINES SOME CONSTANTS IN MKS UNITS.
C      PI      = 3.14159265      ! RADIANS
C      ELECHR = 1.60217733D-19 ! COULOMBS
C      ELEMAS = 9.1093897D-31    ! Kg
C      EPSILO = 8.854187817D-12 ! F/m
C      C      = 299792456.2      ! +-1.1 M/SEC, FROM: K. Evenson et al,
C              !Physics Review Letters,
C              !Vol 29, p 1346 (1972)
C      BEGINS IVAN'S METHOD
C      MUR_1 = SQRT(MU2REC(RRLOW(I), DENLOW(I), WREF(I)+WM/2.))
C      MUR_2 = SQRT(MU2REC(RRLOW(I+1), DENLOW(I+1), WREF(I)+WM/2.))
C      MUR_3 = SQRT(MU2REC(RRLOW(I+2), DENLOW(I+2), WREF(I)+WM/2.))
C      MUR_1 = MU2REC(RRLOW(I), DENLOW(I), WREF(I)+WM/2.)
C      MUR_2 = MU2REC(RRLOW(I+1), DENLOW(I+1), WREF(I)+WM/2.)
C      MUR_3 = MU2REC(RRLOW(I+2), DENLOW(I+2), WREF(I)+WM/2.)
C      MUR_1 = MUR_1 / SQRT(ABS(MUR_1))
C      MUR_2 = MUR_2 / SQRT(ABS(MUR_2))
C      MUR_3 = MUR_3 / SQRT(ABS(MUR_3))
C      DTEMP1 = (PHIRLOW(I)+DELPHI(I)) * (C/(2.*(WREF(I)+WM/2.)))
C      DTEMP2 = SNREC(I,N+NN2,RRLOW(1),DENLOW(1),WREF(I)+WM/2.)
C      WRITE(11,*)I,MUR_1,MUR_2
C      WRITE(11,*)'      ',' DTEMP1 ',' DTEMP2 '
C      *      ',' DTEMP3 ','/ DTEMP4 ',' = DELR1 '
C3POINTS CONDITION
C      DTEMP3 = (DTEMP1 - DTEMP2)
C      DTEMP4 = ( MUR_1 * 2./3. - MUR_2 / 12. )
C      DELR1 = DTEMP3 / DTEMP4

```

```

C      WRITE(11,11)'3POIN ', DTEMP1, DTEMP2, DTEMP3, DTEMP4, DELR1
11      FORMAT(A6,5D12.5)
CUN-EQUAL STEP CONDITION
C      DTEMP4 = ( MUR_1 * 5./6. - MUR_2 * 5./24. )
C      DELR2 = RRLOW(I+1) - RRLOW(I)
C      DTEMP3 = (DTEMP1 - DTEMP2) - (-MUR_1/6. + MUR_2/8.)*DELR2
C      DELR1 = DTEMP3 / DTEMP4
C      WRITE(11,11)'UN-EQ ', DTEMP1, DTEMP2, DTEMP3, DTEMP4, DELR1
C4POINTS CONDITION
C      DTEMP3 = (DTEMP1 - DTEMP2)
C      DTEMP4 = ( MUR_1 * 19./24. - MUR_2 * 5./24. + MUR_3 /24.)
C      DELR1 = DTEMP3 / DTEMP4
C      WRITE(11,11)'4POIN ', DTEMP1, DTEMP2, DTEMP3, DTEMP4, DELR1
CSQUARE ROOT FIT
C      DTEMP3 = (DTEMP1 - DTEMP2)
C      DTEMP4 = MUR_1 * 2./3.
C      DELR1 = DTEMP3 / DTEMP4
C      WRITE(11,11)'SQRT ', DTEMP1, DTEMP2, DTEMP3, DTEMP4, DELR1
IF( IDUMY .EQ. 2 ) THEN
C      REAL INDEX FIT
      DTEMP3 = (DTEMP1 - DTEMP2)
      DTEMP4 = ( MUR_1 * 5./6. - MUR_2 / 6. )
      DELR1 = FDELTA1(RRLOW(I),DENLOW(I),RRLOW(I+1),DENLOW(I+1)
*      ,WREF(I)+WM/2.,DTEMP1,DTEMP2,RZDEL)
      WRITE(11,11)'INDEX1', DTEMP1, DTEMP2, DTEMP3, DELR1
ELSE IF( IDUMY .EQ. 1 ) THEN
C      REAL INDEX FIT
      DTEMP3 = (DTEMP1 - DTEMP2)
      DTEMP4 = ( MUR_1 * 5./6. - MUR_2 / 6. )
      DRGES = DTEMP3 / DTEMP4
      DELR1 = FDELTA(RZDEL,RRLOW(I),WREF(I)+WM/2.,DTEMP1
*      ,DTEMP2,AFIT,BFIT,CFIT)
      WRITE(11,11)'INDEX ', DTEMP1, DTEMP2, DTEMP3, DRGES, DELR1
ELSE
C      DERIVATIVE CONDITION
      DTEMP3 = (DTEMP1 - DTEMP2)
      DTEMP4 = ( MUR_1 * 5./6. - MUR_2 / 6. )
      DELR1 = DTEMP3 / DTEMP4
      WRITE(11,11)'DERIV ', DTEMP1, DTEMP2, DTEMP3, DTEMP4, DELR1
END IF
!

CPower FIT
C      B_POWER = LOG(MUR_2/MUR_1)/LOG(2.)
C      DTEMP3 = (DTEMP1 - DTEMP2)

```

```

C      DTEMP4 = MUR_1 / ( 1. + B_POWER )
C      DELR1 = DTEMP3 / DTEMP4
C      WRITE(11,11)'POWER ', B_POWER, DTEMP2, DTEMP3, DTEMP4, DELR1
C
C      DELR2 = RRLOW(I+1) - RRLOW(I)
C      CONS1 = LOG(MUR_2/MUR_1)
C      DELR1 = ABS( DELR1 / 100. )
C      DELH = 0.0000001
C      B_POWER = 1. + CONS1 / LOG((DELR1+DELR2)/DELR1)
C      ZERO = DTEMP3 - DELR1 * MUR_1 / B_POWER
C      DO WHILE(ABS(ZERO) .GT. 1.0D-9)
C          DELR1OLD = DELR1
C          DELR1 = DELR1 + DELH
C          B_POWER = 1. + CONS1 / LOG((DELR1+DELR2)/DELR1)
C          ZERO = DTEMP3 - DELR1 * MUR_1 / B_POWER
C          IF( ZERO .LT. 0.0 ) THEN
C              DELR1 = DELR1OLD
C              DELH = DELH / 2.
C          END IF
C      END DO
C      WRITE(11,*)DELR1, DELH, ZERO, B_POWER
C
C      DELREC(I) = DELR1
C
C      CHERE 2-24-95
C      D_WILGEN = ( DTEMP3 - DTEMP4 * DELR1 ) /
C      /      ( ( -2. * MUR_1 + MUR_2 * 2./3. ) / 12. )
C      DELREC(I) = DELR1 - D_WILGEN
C      WRITE(11,*)I,'DELREC=DELR1+D_WILGEN ',DELREC(I),DELR1,D_WILGEN
C      CEND HERE
C      TEMP5 = DELTA_R(DELR1,DELR2,MUR_1,MUR_2)
C      DELREC(I) = TEMP5
CC      WRITE(11,*) ' '
C      WRITE(11,*) I, DELR1,DELR1-TEMP5,(DELR1-TEMP5)/DELR1
C      MUR_4 = SQRT(MU2REC(RRLOW(I+3),DENLOW(I+3),WREF(I)+WM/2.))
C      ERR_DR = (MUR_4-3.*MUR_3+3.*MUR_2-MUR_1) / (24.*DTEMP4)
C      ERR_DR = (MUR_3 - 3.*MUR_2 + 3.*MUR_1) / (24.*DTEMP4)
C      ERR_DOYLE = (MUR_2 - 2.*MUR_1) / (6.*(0.5*MUR_1))
CC      WRITE(11,60) I, DENLOW(I), DENLOW(I+1),DENLOW(I+2),DENLOW(I+3)
CC 60      FORMAT(I4,6D17.8)
CC      WRITE(11,70) I, RRLOW(I),RRLOW(I+1),RRLOW(I+2),RRLOW(I+3)
CC 70      FORMAT(I4,4(F16.8,'m'))
CC      WRITE(11,80) I, MUR_3, MUR_2, MUR_1
CC 80      FORMAT(I4,D17.8,' -3*',D16.8,' +3*',D16.8)
CC      WRITE(11,85)I,MUR_3 - 3.*MUR_2 + 3.*MUR_1, DTEMP4

```



```

CC      *      ,      (MUR_3 - 3.*MUR_2 + 3.*MUR_1)/(DTEMP4*24)
CC 85      FORMAT(I4,D17.8,' / ( 24*',D17.8,')',',',D17.8)
CC      WRITE(11,90) I,PHIRLOW(I),DELPHI(I),WREF(I)/1.E09,WM/1.E09
CC 90      FORMAT(I4,2F17.8,2(F14.6,'GHz'))
CC      WRITE(11,10) '(',DTEMP1,'-',DTEMP2,'=',DTEMP3,')/'
CC      *      ,DTEMP4,'=',DELREC(I)
CC 10      FORMAT(A1,F13.10,A1,F13.10,A1,F13.10,A2,F13.10,A1,F13.10,'m')
CC      WRITE(11,40)I,MUR_1,MUR_2,MUR_3,ERR_DR*100.,ERR_DOYLE*100.
CC 40      FORMAT(I4,3F11.8,2(F11.4,'%'))
C      ENDS IVAN'S METHOD
C
      IF(DELR1 .NE. 0.0) THEN
          TMP = RCOMP(I) / ( DELR1*100.)
          ATMP_(I) = TMP
C      DELREC(I) = DELR1 * TMP
      END IF
C      WRITE(11,*) TMP,DELREC(I),RCOMP(I)
C      BEGINS WILGEN'S SHIFTING METHOD
C      SNF1=SNREC(I,N+NN2,RRLOW(1),DENLOW(1),WREF(I)+WM/2.)
C      DELREC(I) = (DELPHI(I)*C - SNF1*2.*WM )
C      /      / (2.*(WREF(I)+WM/2.))
C      ENDS WILGEN'S SHIFTING METHOD

      RRUP(I)  = RRLOW(I) - DELREC(I)
      BF = BFIELD(RRUP(I))  !DEFINES THE MAGNETIC FIELD
      WCE = (BF*ELECHR/ELEMAS)/(2.*PI)  !ELEC CYCLOTRON FREQ
      DENUP(I) = (WREF(I)+WM/2.) * (WREF(I)+WM/2.-WCE)
      *      * (ELEMAS/ELECHR) * (EPSILO/ELECHR) * (4.*PI*PI)
      PHIRUP(I) = PHIRLOW(I) + DELPHI(I)

      WW      = (WREF(I-1) - WM/2.) - (WREF(I) + WM/2.)
      RRLOW(I-1) = (RRUP(I)-RRLOW(I)) * WW/WM + RRUP(I)
C      RRLOW(I-1) = RECZERO(RRLOW(I-1),DENLOW(I),WREF(I-1))
C      RRLOW(I-1) = RECZERO(RRLOW(I), DENLOW(I), WREF(I-1))

C      TMP = RCOMP(I-1) / RRLOW(I-1)
C      WRITE(11,*) I,RRLOW(I-1), RCOMP(I-1), TMP
C      RRLOW(I-1) = RRLOW(I-1)*TMP
      BF = BFIELD(RRLOW(I-1))  !MAGNETIC FIELD
      WCE = (BF*ELECHR/ELEMAS)/(2.*PI)  !ELEC CYCLOTRON FREQ
      DENLOW(I-1) = (WREF(I-1)-WM/2.) * (WREF(I-1)-WM/2.-WCE)
      *      * (ELEMAS/ELECHR) * (EPSILO/ELECHR) * (4.*PI*PI)
C      WRITE(11,*) I, DENLOW(I-1)
C      DENLOW(I-1) = DENSITY(RRLOW(I-1),AFIT,BFIT,CFIT)
C      WRITE(11,*) I, DENLOW(I-1)

```

```

C      PHIRLOW(I-1) = 2. * (WREF(I-1)-WM/2.) / C
C      *      * SNREC(I-1,N+NN2,RRLOW(1),DENLOW(1),WREF(I-1)-WM/2.)
      PHIRLOW(I-1) = DELPHI(I) * WW/WM + PHIRUP(I)

      RETURN
      END

C
!
```

The subroutine SPLN calculates the integral of a given spline fit from the coefficients of the fit.

```

C *****
C
      DOUBLE PRECISION FUNCTION SPLN(N,X,Y)
C      THIS FUNCTION CALCULATES THE INTEGRAL OF THE REFRACTIVE
C      INDEX USING THE RECONSTRUCTED DENSITY PROFILE DATA.
      IMPLICIT NONE
      PARAMETER NMAX=2000
      DOUBLE PRECISION X(NMAX), Y(NMAX)
      *      , A, B, BREAK(NMAX), CSCOE(4*NMAX), DCSITG
      INTEGER NINTV, NDATA, N

      NDATA = N
C      CALCULATE THE COEFFICIENTS OF THE SPLINE
      CALL DCSINT(NDATA, X, Y, BREAK, CSCOE)
C      INTEGRATE THE SPLINE USING THE COEFFICIENTS
      NINTV = NDATA - 1
      A = X(1)
      B = X(N)
      SPLN = DCSITG(A, B, NINTV, BREAK, CSCOE)

      RETURN
      END

C
!
```

The subroutine FDELTA calculates the increment on the cutoff using a zero finding function to the index of refraction.

```

C *****
C
      DOUBLE PRECISION FUNCTION FDELTA(DEL_H,R2,WREF
      *      ,DTEMP1,DTEMP2,A,B,C)
```

```

      IMPLICIT NONE
      DOUBLE PRECISION DEL_H, R2, WREF, DTEMP1,DTEMP2, A, B ,C

      DOUBLE PRECISION RZ, RZDEL, ZERO !, ZERO_OLD
      *, MU, MU2, MU_1, MU_2, R

      RZDEL = DEL_H
      RZ =R2
      MU = MU2(RZ,WREF,A,B,C)
      MU = MU / SQRT( ABS( MU ) )
      ZERO = ( DTEMP1 - DTEMP2 ) - MU * RZDEL / 2.
      WRITE(11,*) 'RZ',RZ,' RZDEL',RZDEL,' ZERO',ZERO
      DO WHILE((MU .GE. 0.0) .AND. (ZERO .GT. 1.0D-10))
        RZ = RZ - RZDEL
        MU = MU2(RZ,WREF,A,B,C)
        MU = MU / SQRT(ABS(MU))
        ZERO = ZERO - RZDEL * MU
      END DO
      WRITE(11,*) 'RZ',RZ,' RZDEL',RZDEL,'ZERO', ZERO,' MU',MU
      RZ = RZ + RZDEL
C      HERE WE FIT A SQUARE ROOT TO THE LAST 2 DATA POINTS
C      AND SOLVE FOR DEL_R
      MU_1 = MU2(RZ,WREF,A,B,C)
      MU_1 = MU_1/SQRT(ABS(MU_1))
      MU_2 = MU_1
      DO WHILE(MU_1 .EQ. MU_2)
        RZDEL = RZDEL+RZDEL
        R = RZ + RZDEL
        MU_2 = MU2(R,WREF,A,B,C)
        MU_2 = MU_2/SQRT(ABS(MU_2))
        WRITE(11,*)'RZDEL',RZDEL,' R', R,'MU_2', MU_2
      END DO
      WRITE(11,*)'MU_1',MU_1,' MU_2',MU_2
      RZ = RZ - RZDEL / ( (MU_2*MU_2) / (MU_1*MU_1) - 1. )
      FDELTA = R2 - RZ
      WRITE(11,*) 'FDELTA4', RZDEL, RZ, MU_1, MU_2, FDELTA

      RETURN
      END

C
C      THIS SUBROUTINE CALCULATES THE FUNCTION TO FIND A ZERO FOR
      DOUBLE PRECISION FUNCTION Z2(RQUESS)
      IMPLICIT NONE
C      INTEGER N_FIT, I
      DOUBLE PRECISION  DTEMP, MU2, DRIND

```

```

      DOUBLE PRECISION RQUESS
C      , X(1000), Y(1000), S_INDEX, SPLN, DEL_R
      DOUBLE PRECISION R2,WREF,A,B,C
      COMMON /ZBLOCK/ R2,WREF,A,B,C
      DOUBLE PRECISION DTEMP1,DTEMP2
      COMMON /ZDBLOCK/ DTEMP1,DTEMP2

C      WRITE(11,*)' RQUESS=', RQUESS
      DRIND = RQUESS
      DTEMP = MU2(DRIND,WREF,A,B,C)
      Z2 = DTEMP / SQRT(ABS(DTEMP))

      WRITE(11,*)' R=',RQUESS,' Z2=', Z2,' MU2='
*      , MU2(DRIND,WREF,A,B,C)

      RETURN
      END

C
C      THIS SUBROUTINE CALCULATES THE FUNCTION TO FIND A ZERO FOR
      DOUBLE PRECISION FUNCTION Z(RQUESS)
      IMPLICIT NONE
      INTEGER N_FIT, I
      DOUBLE PRECISION DTEMP, MU2, DRIND
      DOUBLE PRECISION RQUESS,X(1000),Y(1000),S_INDEX,SPLN,DEL_R
      DOUBLE PRECISION R2,WREF,A,B,C
      COMMON /ZBLOCK/ R2,WREF,A,B,C
      DOUBLE PRECISION DTEMP1,DTEMP2
      COMMON /ZDBLOCK/ DTEMP1,DTEMP2

C      WRITE(11,*)' RQUESS=', RQUESS
      N_FIT = 100
      DEL_R = (R2 - RQUESS) / (N_FIT-1.)
      DO I = 1, N_FIT
        X(I) = RQUESS + DEL_R * (I-1.)
        DRIND = X(I)
        DTEMP = MU2(DRIND,WREF,A,B,C)
        Y(I) = DTEMP / SQRT(ABS(DTEMP))
C        WRITE(11,*)I,RQUESS,R2,DEL_R,X(I),Y(I)
      END DO

      S_INDEX = SPLN(N_FIT,X,Y)
      Z = DTEMP1 - DTEMP2 - S_INDEX
C      WRITE(11,*)' R=',RQUESS,' Z=', Z,' MU2='
C      *      , MU2(X(1),WREF,A,B,C)

```

```

      RETURN
      END

```

```

C
!

```

The subroutine FDELTA calculates the increment on the cutoff using a zero finding function to the index of refraction.

```

C
C *****
C
      DOUBLE PRECISION FUNCTION FDELTA1(R2,DENR2,R3,DENR3
*      ,WREF,DTEMP1,DTEMP2,RZDEL)
      IMPLICIT NONE
      DOUBLE PRECISION R2, DENR2, WREF, ZERO_OLD
      DOUBLE PRECISION DTEMP1,DTEMP2,RZDEL, DELRK
      DOUBLE PRECISION ZERO, X_PAR(3), Y_PAR(3), AA, BB, CC
      DOUBLE PRECISION DELR1, R1, DENR1, R1OLD, R3, BF, BFIELD
*      , WCE, DENR3, M_SLOPE, DELH, RH, DEN_RH, MU_RH, MU2REC

      INTEGER JSTEP, K, IDCHOISE, K_POINTS, NURNS

      DOUBLE PRECISION
*      RO,RA,DENSO,BO, ELECHR, ELEMAS, EPSILO, C_SPEED
*      , APERT, LAMBDA, PI, RLINE, CURRENT
*      , POL_CUR, RRANDOM, ALPHA, BETA
      COMMON /COMDAT/ JSTEP
*      , RO,RA,DENSO,BO, ELECHR, ELEMAS, EPSILO, C_SPEED
*      , APERT, LAMBDA, PI, RLINE, NURNS, CURRENT
*      , POL_CUR, RRANDOM, ALPHA, BETA, IDCHOISE

      K_POINTS = 100
      ZERO = DTEMP1 - DTEMP2
      ZERO_OLD = ZERO
      DELR1 = RZDEL
      DELH = DELR1 / 100. ! 1.0D-6
      R1 = R2
      WRITE(11,*)' '
      WRITE(11,*)'O R1=',R1,' ZERO=',ZERO
      DO WHILE((ZERO .GE. 1.0D-6) .AND. (DELR1 .GE. 1.0D-6)
*      .AND. (ZERO .LE. ZERO_OLD ))
          ZERO = DTEMP1 - DTEMP2
          ZERO_OLD = ZERO
          R1OLD = R1
C          SET UP LINEAR FIT TO THE DENSITY

```

```

      R1 = R1 - DELR1
C      R3 = R1
      BF = BFIELD(R1)
      WCE = BF * (ELECHR/ELEMAS) / ( 2. * PI )
      DENR1 = WREF * (WREF-WCE) * (ELEMAS/ELECHR)
      * (EPSILO/ELECHR) * (4.*PI*PI)
C      IF(DENR1 .LT. DENR2) DENR1 = DENR2
      M_SLOPE = ( DENR2 - DENR3 ) / ( R2 - R3 )
C      WRITE(11,*)' '
C      WRITE(11,*) DENR1, DENR2, DENR1-DENR2
C      WRITE(11,*) R1, R2, R1-R2
C
C      SET FIRST POINT FOR PARABOLIC FIT TO THE DENSITY
      X_PAR(1) = R1
      Y_PAR(1) = DENR1
C      SET SECOND POINT FOR PARABOLIC FIT TO THE DENSITY
      X_PAR(2) = R2
      Y_PAR(2) = DENR2
C      SET LAST POINT FOR PARABOLIC FIT
      X_PAR(3) = R2
      Y_PAR(3) = (DENR2-DENR3) / (R2-R3)
C      PASS PARAMETERS TO SUBROUTINE TO CALCULATE PARABOLIC COEF.
      CALL GETABC(X_PAR,Y_PAR,AA,BB,CC)
C      WRITE(11,524)( K, X_PAR(K), Y_PAR(K), K=1,3 )
524      FORMAT(I3,' X_PAR=',F20.16,' Y_PAR=',D25.16)
C      WRITE(11,*)' AA BB CC '
C      WRITE(11,*) AA, BB, CC
C
C      DELH = 1.0D-6
      RH = R2 + DELH
      MU_RH = 1.
C      WRITE(11,*)'1', R1, R2, DENR1, DENR2
C      WRITE(11,*)'2' RH, DEN_RH, MU_RH, ZERO '
C      DO WHILE( MU_RH .GE. 0.0 )
      DELRK = (R2 - R1) / (K_POINTS-1)
      DO K = 1, K_POINTS
C          RH = RH - DELH
          RH = R2 - DELRK * (K-1)
          DEN_RH = CC + ( BB + AA * RH ) * RH !PAR. DENSITY FIT
C          WRITE(11,*)' PARABOLIC DENSITY = ',DEN_RH
          DEN_RH = M_SLOPE * (RH - R2) + DENR2 !LINEAR DENS. FIT
C          WRITE(11,*)' LINEAR DELSITY = ',DEN_RH
          MU_RH = MU2REC(RH, DEN_RH, WREF)
          IF(MU_RH .NE. 0.0) MU_RH = MU_RH / SQRT( ABS(MU_RH) )
C          ZERO = ZERO - DELH * MU_RH

```

```

      ZERO  = ZERO - DELRK * MU_RH
C      WRITE(11,*) RH, DEN_RH, MU_RH, ZERO
      END DO
C      WRITE(11,*)'4 ZERO = ',ZERO,' DELR1=', DELR1
      IF( ZERO .LT. 0.0 ) THEN
        DELR1 = DELR1 / 2.
        R1 = R1OLD
      END IF
      END DO
C      WRITE(11,*)'5', R1, R2, DELR1
C      WRITE(11,*)'5', DENR1, DENR2
      WRITE(11,*)'6 R1=',R1,' ZERO=',ZERO

      FDELTA1 = R2 - R1

      RETURN
      END

C
C
!
```

The subroutine GETABC calculates the coefficients for the parabolic fit when using the assumption of equal step size for the positions of the cutoffs.

```

C *****
C
      SUBROUTINE GETABC(X,Y,A,B,C)
      DOUBLE PRECISION Y(3), X(3), A, B, C
      DOUBLE PRECISION DELX1

      DELX1 = X(2) - X(1)

      A = ( ( Y(1) - Y(2) ) / DELX1 + Y(3) ) / DELX1

      B = ( Y(2) - Y(1) ) / DELX1 - A * ( X(2) + X(1) )

      C = Y(1) - B * X(1) - A * X(1)*X(1)

      RETURN
      END

C
!
```

The subroutine BC\_DER calculates the parabolic coefficients using the derivative condition and assuming an un-equal step size for the calculation.

```

C *****
C
      SUBROUTINE BC_DER(X,Y,BB,CC)
      IMPLICIT NONE
      DOUBLE PRECISION X(3), Y(3), BB, CC, DELX1, DELX2, DERIVA

C Coefficients when using the derivative condition with un-equal
C spacing.
      DELX1 = X(2) - X(1)
      DELX2 = X(3) - X(2)
      DERIVA = (Y(3)-Y(2)) / DELX2
      BB = ( -DELX1 * DERIVA + 2.*Y(2) ) / DELX1
      CC = ( DELX1 * DERIVA - Y(2) ) / (DELX1*DELX1)

      RETURN
      END

```

```

C
!

```

The subroutine BC\_3P calculates the coefficients of the parabolic fit when using the condition of equal spacing. To calculate the coefficients for the condition of the slope at the last two know points of the profile all what needs to be done is to comment and de-comment the corresponding lines and/or statements.

```

C *****
C
      SUBROUTINE BC_3P(X,Y,BB,CC)
      IMPLICIT NONE
      DOUBLE PRECISION X(3), Y(3), BB, CC, DELX1, DELX2

C Coefficients when passing through the 3 points with equal spacing.
      DELX1 = X(2) - X(1)
      DELX2 = X(3) - X(2)
      BB = ( 4.*Y(2) - Y(3) ) / (2.*DELX1)
      CC = (-2.*Y(2) + Y(3)) / (2.*DELX1*DELX1)
C Coefficients when using the derivative conditions.
CC      BB = ( 3.*Y(2) - Y(3) ) / (DELX1)
CC      CC = (-2.*Y(2) + Y(3)) / (DELX1*DELX1)

      RETURN
      END

```

```

!

```



## APPENDIX C

### DATA ANALYSIS PROGRAM

#### C.1 Introduction

This appendix contains the code for the data analysis program and a typical data file. The source for the code is in the computer:

RAX.PPPL.GOV

in the area:

[ICOLLAZO.WILGEN]W.FOR

and a copy can be obtained from the author or one of the coworkers of the project. Request can be done by mail, E-mail, or any other way. Transmission of the program can be done via E-mail, diskettes, tape or any other possible way.

#### C.2 Reflectometer Data Files

The reflectometer's data is contained in two types of file: the Parameters file (PFT) and the Raw Data file (RDT). The parameters file contains specific setting of the digitizers when the digitizers were triggered during the plasma shot. The raw data file contains the actual reflectometer signal data. The name of the parameters file is of the form "PFT*shot\_number*.YO", while the name for the raw

data file is of the form "RDTshot.number.YO", and they are both temporally stored in the directory TFTR\$RAW:[TFTR.YO] of the TFTR computer system. This is the disk area where the data is made accessible to the programs and utilities. The information contained in the parameters file include such things as:

1. Start time of the digitizers sampling window.
2. The digitizers sampling rate.
3. Number of active channels of the digitizers.
4. Number of sampling channels for each digitizer.
5. Voltage limits of each channel.
6. 4 comments lines.

The information on the parameters file and the raw data file are accessible through subroutines calls provided by the PPPL computer support group.

The data traffic on the PPPL computer system is as follows. The data is recorded on the CAMAC modules in the diagnostic area. From there it is moved to the corresponding disk area of the diagnostic. For the ORNL reflectometer (called YO by PPPL) this disk area is in the directory "TFTR\$RAW:[TFTR.YO]", where "YO" refers to the reflectometer (other diagnostics have similar code names, like TFTR\$RAW:[TFTR.TS] for Thomson Scattering, etc). This disk area is a temporary area, since as more data files keep on accumulating the computer copies them to the optical disk area and then deletes them to create working space for the incoming new files. The old data file can be recalled using the "GETSHOTS" utility, which retrieves the data files from the optical disks and puts them in the "TFTR\$RAW:[TFTR.YO]" area, where it can be accessed by the corresponding data reading subroutines.

### C.3 Description

The program is designed to run on a batch mode form. This allows for a better use of the time while the code is running. The parameters for the analysis are passed to the program via a namelist data file. All of the variables have intuitive names and the data file is internally documented for the novice user.

#### C.3.1 Generation of the phase data files

The phase data is stored in a standard ASCII data file. The name of this file follows the form "*DShotNumber\_Time*", where the "*ShotNumber*" is the standard 5 digits plasma shot number and "*Time*" is the time in seconds of that particular data sweep. Thus, the file name "D67890.3.849" is the phase data for the plasma shot 67890 starting at the time of 3.849 sec into the beginning of the shot. This format allows for an ordered display of the phase data on the Vax directory system, this is, it displays all the data in numerical order of time and shot number. A list of all the phase data files created during the last run of the phase generation program is stored in the file "F.FLS" in the directory of the reconstructing program described next. The first line of the phase data file contains what can be called a header and it contains some general information like the number of data points, the shot toroidal field coil current, the initial and final time of the sweep, and the shot number. This information is used to identify and characterize the phase data. From the second line to the last line is the frequency and phase data arrays, where the first column is the frequency array in GHz and the second column is the phase array in fringes. Thus, the first lines of the phase data file will look like the following:

```
352  66967.1  3.42778  3.42865  67702  0.0
```

92.22481	4.453421
92.32542	4.874972
92.38291	4.788904
92.55538	5.064823

:

### C.3.2 Subroutine/Function description

There are a number of subroutines, functions, and subprograms used by the code in order to recall the data and calculate the phase difference data from the signals. These subprograms will be discussed in the following sections.

**Graphic package** The program uses a version of the ubiquitous Plot 10 or Advance Graphics II available at the Princeton Plasma Physics Laboratory (PPPL) computer system. The only difference between these version and the version available at the Oak Ridge National Laboratory is on the names used for the string handling subroutines. All of the other plotting subroutines and the calling sequence are the same for both versions.

**Subroutine YO\_INFO** This is a subroutine provided by the PPPL to read the parameters file and obtain the digitizers setting for a particular shot. It provides with such information as: starting time of the digitizers, the maximum peak voltage of the digitizer, the sampling rate, number of active channels, and 4 comment lines. This subroutine was written by Tom Eck of the computer division at PPPL.

**Subroutine YO\_DATA** This subroutine provided with the actual data from the digitizers as it is stored in the Raw Data file at the PPPL computer system. The raw data is stored in 4 arrays that correspond to the I and Q signals, the ramp voltage of the sweeper for the Backward Wave Oscillator (BWO) and the Amplitude of the signal. This data is in some type of compress format, that is, there are two data points of data from the reflectometer for each integer number of the array. Therefore, the data has to be decompress and converted into a real voltage from the reflectometer signal that was measured by the digitizers. This is done by the subroutine CONVERT.

**Subroutine CONVERT** This subroutine uses the raw data arrays from the subroutine YO\_DATA and converts it into real voltages that can be used to calculate the phase difference data, the time of each data point, the ramp voltage from the sweeper, the frequency of the wave, and the amplitude of the reflected signal.

**Subroutine GET\_INDEX** This subroutine scans the wave's frequency array and finds out the array starting and ending position for all the sweeps of the reflectometer. This information is used to delete the part of the data arrays that corresponds to the dead time of the sweeper or the reset time of the Backward Wave Oscillator. This information is used by the subroutine COMPRES to delete the array points for the time corresponding to the dead time of the sweeper and reduce the total number of points needed to process.

**Subroutine COMPRES** This subroutine uses the array positions calculated by the subroutine GET\_INDEX to delete the array points corresponding to the dead time of the sweeper. By deleting these data points the total number

of data points are reduced and the data arrays are effectively compressed.

**Subroutine SMOOTH** This subroutine carries out the smoothing of the data by using the running carriage smoothing method with a Gaussian weighting function. This has been discussed in section 7.2.2.

Smoothing is accomplished by using what is known as the running carriage integral method<sup>309,310</sup> on the data. The equation for this operator has the general form:<sup>310</sup>

$$f(x) = \frac{\int_{x-l}^{x+l} W(y-x) f(y) dy}{\int_{-l}^l W(z) dz} \quad (C.1)$$

where  $l$  is a length representing the width of the smoothing,  $W(y)$  is the weighting function for the smoothing and  $f(x)$  is the function to be smoothed. The factor in the denominator is the normalization constant that accompanies these types of operators. This equation can be converted to its equivalent in the discrete space of the reflectometer's data sets. For this case the equation that was used is:

$$S_i = \sum_{j=-s}^s \frac{1}{w\sqrt{\pi}} e^{-(\frac{j}{w})^2} D_{i+j} \quad (C.2)$$

where  $s$  is the number of elements to smooth by and the value for  $w$  is given by:

$$w = \frac{s}{\sqrt{\ln(10)}} \quad (C.3)$$

which represent the width of the Gaussian function necessary to have a value of  $\frac{1}{10}$  for the Gaussian at the end points of the summation. This is a way to remove high frequency noise and perturbations on the data by averaging every data point with respect to a number of its neighboring points, and as long as the information has a wavelength that is larger than the wavelength of the smoothing, there will be no lost of information. In order to reduce the introduction of other harmonics due to discontinuities of the weighting function during the smoothing process, a Gaussian weighing function was chosen for the smoothing.<sup>308,309</sup>

**Subroutine DAT\_AVE** This subroutine average the data per number of sweeps of the reflectometer sweeper. This is done to reduce the random fluctuations on the data when the data is collected during the steady state part of a plasma shot.

**Subroutine YO\_PHASE** This subroutine is the one that uses the I and Q signal of the reflectometer's data to calculate the raw phase of the propagating wave probing the plasma. It simply calculates the raw uncounted phase using the formula:

$$\Delta\phi = \tan^{-1} \left( \frac{I}{Q} \right) \quad (\text{C.4})$$

where all of the variables have been defined before.

**Subroutine IQ\_AVE** This subroutine calculates the total average of all of the sweeps for a given shot. It is specially useful when all of the data has been collected during the steady state part of the plasma shot and it is expected that all of the phase data sweeps are the same within the random error of the diagnostic. This average I and Q data is used to do some statistical analysis and have a feeling of the random and fluctuation error of the data. The standard deviation,  $\sigma$  can be calculated from this data and it is described in the next section.

**Subroutine PH\_SIGMA** This subroutine calculates the standard deviation of the data for a particular plasma shot. From the averaged I and Q data and the resultant average phase data it calculates the standard deviation,  $\sigma$  as given by the formula:

$$\sigma = \sqrt{\sum_{j=1}^n \frac{(x_j - \bar{x})^2}{n}} \quad (\text{C.5})$$

where  $n$  is the number of points,  $x_j$  is the data point, and  $\bar{x}$  is the average value of the variable.

**Subroutine MATCH\_TO\_AVE** This subroutine tracks the phase for the raw phase using the averaged counted phase. The phase counted and/or tracked in this way can be used to calculate the standard deviation of the data.

## C.4 Computer Code

```

!
PROGRAM ECK ! BY Ivan Collazo-Lopez
C
C THIS PROGRAM IS INTENDED FOR THE READING, EXTRACTION AND COMPRESSION
C OF THE REFLECTOMETER'S DATA (KNOWN TO THE PPPL SYSTEM AS "YO").
C THERE IS BASICALLY ONE MAIN LOOP THAT RUNS OVER THE LIST OF SHOTS
C AND THE DATA ARRAY OPERATIONS ARE CONTAINED IN SUBROUTINES WITH
C CONSPICUOUS NAMES LIKE:
C     YO_INFO    GETS DIGITIZERS INFORMATION FROM THE INFO FILE
C     YO_DATA    GETS THE DATA FROM DISK IN PPPL "WORD" FORMAT
C     CONVERT    CONVERTS "WORD" DATA INTO VOLTAGE DATA
C     GET_INDEX  FINDS OUT WHERE THE DATA SWEEP STARTS AND ENDS
C     SMOOTH     SMOOTHS BY USING THE RUNNING CARRIAGE INTEGRAL
C     COMPRES    COMPRES DATA BY ELIMINATING THE TRACE POINTS
C     DAT_AVE    DO AVERAGE OF MANY SWEEPTS TO REDUCE NOISE, ETC
C     YO_PHASE   CALCULATE PHASE OUT OF THE I AND Q VOLTAGE DATA
C     PH_COUNT   PHASE COUNT AND TRACK THE PHASE
C     YO_CAL     SUBTRACT THE CALIBRATION DATA IF REQUESTED
C AT THE END OF THE LOOP, THE PHASE AS A FUNCTION OF FREQUENCY IS
C WRITTEN TO A FILE FOR PROCESSING BY THE RECONSTRUCTION CODE AND
C CALCULATION OF THE ACTUAL DENSITY PROFILE.
C
C
C I WILL LIKE TO GIVE THANKS TO TOM ECK FOR HIS HELP WITH THE
C ROUTINES TO GET THE INFORMATION AND THE DATA FROM THE DISK
C (THIS ARE YO_INFO AND YO_DATA)
C
C THANKS GOES TOO TO DR WILGEN, HOW GAVE ME EXCELENT SUGESTIONS
C ABOUT HOW TO GO ON SMOOTHING AND ANALYSING THE DATA.
C
C
C IMPLICIT NONE
C
C INTEGER MAXRAW !IT IS USED TO DEFINE THE ARRAY SIZE
C PARAMETER (MAXRAW=2*65536) !true for most devices

```



```

REAL
*   W1 !INITIAL SWEEPING FREQUENCY
*   , W2 !FINAL SWEEPING FREQUENCY
*   , WGHZ(0:2*MAXRAW) !REFLECTOMETER'S FREQUENCY IN GHz
*   , RIDATA(0:2*MAXRAW) !REAL VOLTAGE OF THE I SIGNAL
*   , RQDATA(0:2*MAXRAW) !REAL VOLTAGE OF THE Q SIGNAL
*   , RVDATA(0:2*MAXRAW) !REAL VALUE OF THE RAMP VOLTAGE FOR THE SWEEPER
*   , RADATA(0:2*MAXRAW) !REAL VALUE OF THE AMPLITUDE OF THE SIGNAL
C   *   , RASMOOTH(0:2*MAXRAW) ! ARRAY OF SMOOTHED SIGNAL AMPLITUDE
*   , RASIG(0:2*MAXRAW) !STANDARD DIVIATION OF THE AVERAGED DATA
*   , TIME(0:2*MAXRAW) !TIME ARRAY OF THE SWEEPTS
*   , PHASE(0:2*MAXRAW) !CALCULATED PHASE
*   , PI ! = 3.14159265
*   , WORK(0:2*MAXRAW) !TEMPORARY WORKING ARRAY
*   , VMIN !MINIMUM STARTING VOLTAGE OF THE RAMP VOLTAGE
*   , VMAX !MAXIMUM ENDING VOLTAGE OF THE RAMP VOLTAGE
*   , BO !MAGNETIC FIELD
*   , TCURRENT !TOROIDAL CURRENT
*   , XSTART !START TIME OF THE TOROIDAL FIELD COIL CURRENT
*   , XDELTA !INCREMENT IN TIME FOR "XSTART"
*   , WFDATA(MAXRAW) !Wave Form DATA FOR THE TOROIDAL CURRENT
*   , POL_START !START TIME FOR THE POLOIDAL CURRENT
*   , POL_DEL !INCREMENT IN TIME FOR POL_START
*   , POL_CUR(MAXRAW) !Wave Form DATA FOR THE POLOIDAL CURRENT
*   , WPHASE(0:MAXRAW) !VARIABLE USED TO DO THE ZEBRA STRIP PLOTS
*   , RAD_MIN !MINIMUM VOLTAGE FOR CLIP-OFF
*   , X(0:11), Y(0:11) !GENERAL PURPOSE ARRAYS
*   , COMGET !AG2 ACCESS FUNCTION
*   , PHMAX !MAXIMUM FOR THE PHASE Y-AXIS
*   , DER1 !VALUE FOR THE DERIVATIVE CRITERIUM
*   , AMP1 !VALUE FOR THE AMPLITUDE CRITERIUM
*   , PHSIG(0:2*MAXRAW) !PHASE SIGMA ARRAY
*   , WGHZAVE(0:2*MAXRAW) !FREQUENCY ARRAY FOR THE PHASE SIGMA
*   , PHAVE(0:2*MAXRAW) !AVERAGE PHASE ARRAY
C   *   , RWGHZ(0:2*MAXRAW) !RESORTED FREQUENCY DATA
C   *   , RPHASE(0:2*MAXRAW) !RESORTED PHASE DATA
*   , RIAVE(0:1000) !AVERAGED I SIGNAL
*   , RQAVE(0:1000) !AVERAGED Q SIGNAL
*   , PHAVE_C(0:2*MAXRAW) !PHASE DATA ARRAY
*   , RAMPMIN !RAMP VOLTAGE MINIMUM
*   , RAMPMAX !RAMP VOLTAGE MAXIMUM
*   , RAWPHSIZE !SET SYMBOL SIZE
*   , IQSIZE !SET SYMBOL SIZE
C   *   , PHTEMP !TEMP PHASE

```

```

* , SIG_MAX(0:3)          !MAXIMUM SIGMA
* , WSIG_MAX(0:3)        !FREQUENCY ARRAY OF MAX SIG
!
C
  INTEGER
*   IERR ! ERROR CODE
*   , I_SHOT(100) ! SHOT NUMBER LIST ARRAY
*   , IS ! INDEX FOR THE SHOT NUMBER LIST ARRAY
*   , I ! GENERAL PURPOSE INDEX
*   , II ! GENERAL PURPOSE INDEX
*   , J ! GENERAL PURPOSE INDEX
*   , JJ ! GENERAL PURPOSE INDEX
*   , K ! GENERAL PURPOSE INDEX
*   , I_GOT ! NUMBER OF DATA POINTS THAT IS RETRIEVED FROM DISK
*   , IVDATA2 ! SETS THE SCREEN WINDOW FOR THE RAMP VOLTAGE DATA
*   , IVDATA ! SETS THE SCREEN WINDOW FOR THE RAMP VOLTAGE DATA
*   , IVTYPE ! SETS THE LINE TYPE FOR THE RAMP VOLTAGE DATA
*   , IPHASE ! SETS THE SCREEN WINDOW FOR THE PHASE DATA
*   , IPHTYPE ! SETS THE LINE TYPE FOR THE PHASE DATA
*   , IWILGEN ! SETS WHERE TO PUT THE SCREEN WINDOW FOR THE RAW DATA
*   , IWTYPE ! SETS THE LINE TYPE FOR THE RAW DATA PLOT
*   , IPOLAR ! SETS THE SCREEN WINDOW FOR THE POLAR DATA
*   , IPTYPE ! SETS LINE TYPE FOR THE POLAR DATA
*   , ITIME ! SETS THE SCREEN WINDOW FOR THE TIME DATA
*   , ITTYPE ! SETS THE LINE TYPE FOR THE TIME DATA PLOT
*   , IAMP ! SETS THE SCREEN WINDOW FOR THE AMPLITUDE DATA
*   , IAMPTYPE ! SETS THE LINE TYPE FOR THE PLOT
*   , IIQ ! SETS THE SCREEN WINDOW FOR THE I/Q DATA
*   , IIQTYPE ! SETS THE LINE TYPE FOR THE I/Q DATA
*   , ISIGMA ! SETS THE SCREEN WINDOW FOR THE STANDARD DEVIATION DATA
*   , ISIGTYPE ! SETS THE LINE TYPE FOR THE STANDARD DEVIATION DATA
*   , IDAT1 ! INITIAL DATA POINT FOR THE ANALYSIS
*   , IDAT2 ! FINAL DATA POINT FOR THE ANALYSIS
*   , INDEX(0:1000) ! ARRAY OF POINTERS FOR THE BEGINING OF THE DATA
*   , INDEX2(0:1000)! ARRAY OF POINTERS FOR THE ENDING OF THE DATA
*   , IOFFSET ! OFFSET FOR THE DATA READING/CONVERSION
*   , ICONV ! NUMBER OF POINTS FOR THE RUNNING CARIAGE INTEGRAL
*   , IAVER ! NUMBER OF POINTS FOR THE AVERAGING ROUTINE
C
*   , IDUMMY ! DUMMY WORKING VARIABLE
*   , NNDATA ! THE NUMBER OF DATA POINTS OF EVERY SWEEP
*   , IQUAL ! WAVE FORM QUALITY CODE
*   , NUMGOT ! NUMBER OF DATA POINTS FROM THE WAVE FORM ROUTINE
*   , NPICK ! NUMBER OF DATA POINTS TO BE WRITTEN TO FILE
*   , IWILY ! NUMBER OF STRIPES IN THE ZEBRA PLOT

```

```

* , IBASEX ! X-AXIS COMMON SECTION POINTER FUNCTION
* , IBASEY ! Y-AXIS COMMON SECTION POINTER FUNCTION
* , IPHAVE ! POSITION FOR THE PLOT OF THE PHASE AVERAGE
* , IAVETYPE ! SET LINE TYPE FOR THE AVERAGED PHASE
* , IPHSIG ! POSITION FOR THE PLOT OF THE SIGMA
* , IPH2 ! FLAG TO PLOT THE RESORTED PHASE DATA
* , INDEXAVE(0:1000) ! INDEX FOR THE AVERAGED DATA
INTEGER
*   IP ! GENERAL PURPOSE INDEX
* , IPHAVE_C ! SET POSITION OF COUNTED AVERAGED PHASE
* , IRAWPHA ! SET POSITION OF RAW PHASE PLOT
* , IRAWPHTYPE ! SET TYPE OF PLOT FOR RAW PHASE PLOT
* , IRAWPHSYMBL ! SET TYPE OF SYMBOL FOR THE PLOT
* , IDIGIT ! DIGITIZER NUMBER: 1 OR 2
* , IQSYMBL ! SET SYMBOL TYPE
* , MAXRAW_POL
* , NUMGOT_POL, IQUAL_POL
* , IPHIMINX, IPHIMAXX, IPHIMINY, IPHIMAXY, ISHIFTY
* , AUTOLIM, ITITLE
* , IXSMIN !PLOT SCREEN MINIMUM
* , IYSMAX !PLOT SCREEN MAXIMUM
* , IXPARAM !SCREEN COORDINATES FOR PARAMETERS
* , IYPARAM !SCREEN COORDINATES FOR PARAMETERS
* , IPARAM !SCREEN COORDINATES OF CORNER LEGEND
C   * , ITEMP
C
C   THIS INTEGER DATA IS FOR THE STORAGE OF THE DATA IN FORM OF
C   "WORDS", WHICH IS THE WAY IN WHICH THE RAW DATA IS STORED IN
C   THE OPTICAL DISK AT PPPL. ONE WORD CONTAINS TWO DATA POINTS.
C   INTEGER*4
*   WIDATA(2*MAXRAW) ! I SIGNAL DATA IN PPPL "WORDS"
*   , WQDATA(2*MAXRAW) ! Q SIGNAL DATA IN PPPL "WORDS"
*   , WVDATA(2*MAXRAW) ! RAMP VOLTAGE DATA FROM THE SWEEPER
*   , WADATA(2*MAXRAW) ! AMPLITUDE DATA ON THE FORTH DIGITIZER
C
C   CHARACTER
*   CTITLE*80 ! CHARACTER VARIABLE FOR THE TITLE
*   , CTITLE2*80 ! CHARACTER VARIABLE FOR THE BOTTOM TITLE
*   , CFILE*77 ! STRING FOR THE FILE NAME OF THE CALIBRATION FILE
*   , C3I*3 ! CHARACTER CODE FOR THE DATA SET NUMBER
*   , T_FLS*55 ! WHERE TO STORE THE FILES DATA
*   , DATA_FLS*55 ! WHERE TO STORE THE PHASE DATA FILES
*   , WFDESC*77 ! WAVE FORM DESCRIPTION STRING
*   , XUNITS*16 ! X-AXIS UNITS FOR THE WAVE FORM
*   , WFUNITS*16 ! Y-AXIS UNITS FOR THE WAVE FORM

```

```

* , POL_DESC      ! POLOIDAL FIELD DESCRIPTION
* , POL_UNITS*16  ! POLOIDAL RADIAL  UNITS
* , WFUNITS_POL*16! POLOIDAL UNITS
* , TODAY*9      ! TODAY'S DATE
* , C1TYPE*1     ! USED FOR ASYNCRUNUS AND SYNCRUNUS DATA TAKING
* , PFILE*77     ! PLOTTING OUTPUT FILE FOR THE GRAPHS
* , CORNER*11    ! CORNER INFORMATION
* , CORNER2*11   ! CORNER INFORMATION
* , DIGIT*1      ! DIGITIZER: 'A' OR 'B'
* , CRAMP        ! PORT NUMBER FOR THE RAMP VOLTAGE
* , PLABEL*3     ! PLOT LABEL
* , PARAM*22     ! PARAMETER CHARACTER
* , CTIME*44     ! TIME OF SWEEP CHARACTER
* , SIG_FILE*77  ! FILE FOR THE SIGMA DATA

```

C

## LOGICAL

```

*   CAL_DAT ! TRUE = THIS IS CALIBRATION DATA, CREATE CAL. FILE
* , CAL_ON  ! TRUE = SUBTRACT CALIBRATION DATA TO PHASE DATA
* , T_DATA  ! TRUE = WRITE PHASE VS FREQUENCY DATA TO A FILE
* , W_TIME  ! TRUE = WRITE THE TIME DATA TO THE W.TIME FILE

```

!

C

CTOM

C

BEGINS TOM'S INSTRUCTIONS

C

THIS CODE COMES FROM TOM ECK'S PROGRAMS

```

INTEGER*4 MAX_DEV ! NUMBER OF DEVICES IN DEVICE LIST
PARAMETER (MAX_DEV = 20)
INTEGER N_MEMORY  ! TOTAL MEMORY PER 6810 (IN K)
PARAMETER (N_MEMORY=512) ! 9/91 (CHANGE ALSO YRIXDAT)
INTEGER N_6810    ! # 6810 MODULES (MAX =4 IN DSM)
PARAMETER (N_6810=2)
INTEGER N_TMOD    ! # TIMING MODULE CHANNELS
PARAMETER (N_TMOD=2)
INTEGER N_MAXSEG  ! MAX # SEGMENTS ALLOWED IN 6810
PARAMETER (N_MAXSEG=16)
INTEGER N_MAXCHAN ! MAX # CHANNELS PER 6810
PARAMETER (N_MAXCHAN=4)
INTEGER N_COMMENT ! MAX # COMMENT LINES IN PFT
PARAMETER (N_COMMENT=4)
INTEGER N_COMLNTH ! NUMBER OF CHARACTERS IN EACH COMMENT LINE
PARAMETER (N_COMLNTH=40)

```

C -----

C DECLARATIONS

C

```

      INTEGER*4
      .      I_STIMES( N_TMOD ),      ! TIMING MODULE TRIG TIMES, MSEC
      .      I_OFSETS( N_6810*N_MAXCHAN ), ! 6810 CHANNEL OFFSETS
      .      I_RATES( N_6810 ),      ! 6810 DIGITIZING RATES, KHZ
      .      I_ACTCHN (N_6810 ),      ! 6810 ACTIVE CHANNELS
      .      I_SMPCHN (N_6810 )      ! 6810 SAMPLES/CHANNEL

      CHARACTER*40
      .      C_COMNTS(N_COMMENT)

      REAL*4
      .      R_VOLTS( N_6810*N_MAXCHAN ) ! 6810 CHANNEL FULL-SCALE VOLTS

C
CTOM  END TOM'S INSTRUCTIONS
C

      NAMELIST /DAT/
      *      I_SHOT !THIS IS THE SHOT NUMBER ARRAY LIST
      *      , CAL_DAT !TRUE = THIS IS CALIBRATION DATA, CREATE CAL. FILE
      *      , CAL_ON !TRUE = SUBTRACT CALIBRATION DATA FROM PHASE DATA
      *      , W_TIME !TRUE = WRITE TIME DATA TO THE FILE W.TIME
      *      , IVDATA2 !SETS SCREEN WINDOW TO PLOT THE RAMP VOLTAGE DATA
      *      , IVDATA !SETS SCREEN WINDOW TO PLOT THE RAMP VOLTAGE DATA
      *      , IVTYPE !SETS LINE TYPE FOR THE RAMP VOLTAGE DATA
      *      , IPHASE !SETS SCREEN WINDOW TO PLOT THE PHASE DATA
      *      , IPHTYPE !SETS LINE TYPE FOR THE PHASE DATA
      *      , IDAT1 !START OF DATA CONVERSION
      *      , IDAT2 !END OF DATA CONVERSION
      *      , IOFFSET !OFFSET FOR THE DATA READING/CONVERSION
      *      , IAMP !SETS SCREEN WINDOW TO PLOT THE AMPLITUDE DATA
      *      , IAMPType !SETS THE LINE TYPE FOR THE AMPLITUDE DATA
      *      , IWILGEN !SETS SCREEN WINDOW TO PLOT THE RAW PHASE DATA
      *      , IWTYPE !SETS LINE TYPE FOR THE WILGEN DATA
      *      , IPOLAR !SETS SCREEN WINDOW TO PLOT THE POLAR DATA
      *      , IPTYPE !SETS POLAR DATA LINE TYPE
      *      , ICONV !NUMBER OF POINTS IN THE RUNNING CARIAGE INTEGRAL
      *      , IAVER !NUMBER OF POINTS IN THE AVERAGE OF THE DATA
      *      , ITIME !SETS SCREEN WINDOW TO PLOT THE TIME DATA
      *      , ITTYPE !SETS THE TIME DATA LINE TYPE
      *      , IIQ !SETS SCREEN WINDOW TO PLOT THE I/Q DATA
      *      , IIQTYPE !SETS THE LINE TYPE FOR THE I/Q DATA
      *      , W1 !INITIAL FREQUENCY
      *      , W2 !FINAL FREQUENCY
      *      , T_FLS !WHERE TO STORE THE PHASE DATA FILES NAMES
      *      , DATA_FLS !WHERE TO STORE THE PHASE DATA FILES
      *      , VMIN !MINIMUM TRUNCATION VOLTAGE FOR THE COMPRESION SUB.

```

```

* , VMAX !MAXIMUM TRUNCATION VOLTAGE FOR THE COMPRESION SUB.
* , C1TYPE !VARIABLE FOR SUBROUTINE YO_DATA
* , T_DATA !ON/OFF VARIABLE TO WRITE PHASE VS FREQUENCY ON FILE
* , NPICK !NUMBER OF DATA POINTS TO BE WRITTEN TO FILE
* , IWILY !SET SCREEN WINDOW FOR THE DENSITOMETER DIAGRAM
* , ISIGMA !SET SCREEN WINDOW FOR THE SIGMA DATA
* , ISIGTYPE !SET THE LINE TYPE
* , RAD_MIN !MINIMUM VOLTAGE FOR CLIP-OFF
* , PFILE !PLOTING FILE OUTPUT
* , PHMAX !MAXIMUM FOR THE PHASE Y-AXIS
* , DER1 !VALUE FOR THE DERIVATIVE CRITERIUM
* , AMP1 !VALUE FOR THE AMPLITUDE CRITERIUM
* , IPHAVE !POSTION OF THE AVERAGE PHASE
* , IAVETYPE !SET LINE TYPE FOR AVERAGED PHASE
* , IPHSIG !POSITION OF THE SIGMA PLOT
* , IPH2 !FLAG TO PLOT THE RESORTED PHASE DATA
* , IPHAVE_C !SET POSITION OF COUNTED AVERAGED PHASE
* , IRAWPHA !SET POSITION OF RAW PHASE
* , IRAWPHTYPE !SET PLOT TYPE FOR RAW PHASE
* , IRAWPHSYMBL ! SET TYPE OF SYMBOL FOR THE PLOT
* , RAWPHSIZE, IQSYMBL, IQSIZE, DIGIT, CRAMP, ITITLE
* , IPHIMINX, IPHIMAXX, IPHIMINY, IPHIMAXY, ISHIFTY, AUTOLIM
C
!

C READ THE DATA FROM THE DATA FILE
OPEN(11,FILE='[ICOLLAZO.WILGEN]W.DAT',STATUS='OLD')
READ(11,DAT)
WRITE(*,DAT)
CLOSE(11) ! FREE THE Logical Unit Number

C
IF(DIGIT.EQ.'A') THEN
  IDIGIT = 1
ELSE
  IDIGIT = 2
END IF
WRITE(*,*) ' DIGITIZER=', DIGIT, IDIGIT

C
PI = 3.14159265

C
C INITIALIZE THE I_SHOT INDEX
IS = 1
C
C LOOP OVER THE SHOT LIST
CALL RINITT(PFILE) ! INITIALIZE THE PLOTING FILE
DO WHILE(I_SHOT(IS).NE. 0)

```

```

C
C      OPEN THE DEBUGING FILE "W.RUN". IT CONTAINAINS INFORMATION ABOUT
C      THE DIFFERENT VARIABLES AS THE PROGRAM RUNS.
C      OPEN(11,FILE='[ICOLLAZO.WILGEN]W.RUN;1',STATUS='UNKNOWN')
C      WRITE(11,*) ' I_SHOT = ', I_SHOT(IS)
C
C      YO_INFO GETS THE INFORMATION DATA STORED IN THE INFORMATION FILE.
C      THIS INCLUDE THE INFOMATION MARKED WITH AN "O" FOR "OUTPUT".
C      WRITE(*,*) ' '
C      WRITE(*,*) ' '
C      WRITE(*,*) ' '
C      CALL YO_INFO( ! GET THE FOLLOWING INFORMATION:
I      I_SHOT(IS), ! SHOT NUMBER
O      I_STIMES, ! STARTING TIMES OF THE SAMPLING
O      R_VOLTS, ! MAXIMUN PEAK VOLTAGE OF THE DIGITIZERS
O      I_OFFSETS, ! OFFSETS FROM THE DIGITIZERS
O      I_RATES, ! SAMPLING RATES OF THE DIGITIZERS
O      I_ACTCHN, ! ACTIVE CHANNELS OF THE DIGITIZERS
O      I_SMPCHN, ! NUMBER OF SAMPLING CHANNELS OF EACH DIGITIZER
O      C_COMNTS, ! COMMENT LINES
O      IERR ) ! ERROR CODE, 0=NO ERROR
C      WRITE(*,*) ' I_SHOT = ', I_SHOT(IS)
C      WRITE (*, '(1X,A13,2I6)') 'START TIMES: ', I_STIMES
C      WRITE (*, '(1X,A12,2I11)') 'DIG. RATES: ', I_RATES
C      WRITE (*, '(1X,A12,2I6)') 'ACT. CHANS :', I_ACTCHN
C      WRITE (*, '(1X,A12,2I6)') 'KSAMP/CHAN.:', I_SMPCHN
C      WRITE (*, '(1X,A12,8F6.2)') 'F.S. VOLTS: ', R_VOLTS
C      WRITE (*, '(1X,A9,8I6)') 'OFFSETS :', I_OFFSETS
C      WRITE(*,*)' IERR = ', IERR
C      ! ==== DISPLAY COMMENTS
C      DO I = 1, N_COMMENT
C          WRITE (*, '(1X,A40)') C_COMNTS( I )
C      ENDDO ! I = 1, N_COMMENT
C      IF( (IERR .NE. 0) .AND. (C1TYPE .EQ. 'T') ) GOTO 1
C
C      THIS IS THE ROUTINE THAT READS THE DATA FROM THE OPTICAL DISK AND
C      PUTS IT IN THE INTEGER ARRAYS. THE DATA COMES IN A FORMAT THAT
C      IT IS KNOWN AS THE PPPL "WORD" FORMAT. IT CONTAINS TWO DATA POINTS
C      IN ONE INTEGER MEMORY SPACE.
C      WRITE(11,*) 'YO_DATA: I_SHOT = ', I_SHOT(IS)
C      *      , ' MAXRAW = ', MAXRAW
C      CALL YO_DATA(
I      I_SHOT(IS) ! THE SHOT NUMBER
I      , MAXRAW ! THE SIZE OF THE INTEGER WAVEFORM DATA ARRAYS
I      , C1TYPE ! USED FOR ASYNCRONUS AND SYNCRONUS DATA TAKING

```

```

I      , DIGIT  ! DIGITIZER LETTER
I      , CRAMP  ! PORT NUMBER FOR THE RAMP VOLTAGE
O      , I_GOT  ! NUMBER OF DATA POINTS THAT WE ACTUALLY GOT
O      , WIDATA ! DATA ARRAY FOR THE WAVEFORM OF CHANNEL 1
O      , WQDATA ! DATA ARRAY FOR THE WAVEFORM OF CHANNEL 2
O      , WVDATA ! DATA ARRAY FOR THE WAVEFORM OF CHANNEL 3
O      , WADATA ! DATA ARRAY FOR THE WAVEFORM OF CHANNEL 4
O      , IERR ) ! ERROR CODE
      IF( IERR .NE. 0 ) THEN
          GO TO 1
      END IF
!
C
C      WRITE TO THE DEBUGGING FILE SOME VARIABLE VALUES.
      WRITE(11,*)' CONVERT: '
I      , ' MAXRAW = ', MAXRAW
I      , ' W1 = ', W1
I      , ' W2 = ', W2
I      , ' I_STIMES = ', I_STIMES(IDIGIT)
I      , ' R_VOTS = ', R_VOLTS
I      , ' I_RATES = ', I_RATES(IDIGIT)
I      , ' IOFFSET = ', IOFFSET
I      , ' IDAT1 = ', IDAT1
I      , ' IDAT2 = ', IDAT2
I      , ' I_GOT = ', I_GOT
C
C      HERE IS WHERE THE WORD DATA IS CONVERTED INTO THE REAL VOLTAGE
C      DATA THAT THE DIGITIZERS READ.  THE SAME ROUTINE CALCULATES THE
C      CORRESPONDING FREQUENCY ARRAYS.
      CALL CONVERT( ! CONVERT FROM WORD DATA TO VOLTAGE DATA
I          MAXRAW ! SIZE OF THE DATA ARRAYS
I          , W1 ! INITIAL SWEEPING FREQUENCY
I          , W2 ! FINAL SWEEPING FREQUENCY
I          , IDIGIT ! DIGITIZER NUMBER
I          , I_STIMES ! STARTING TIMES FOR THE DIGITIZERS (TRIGER TIME)
I          , R_VOLTS ! MAXIMUM PEAK VOLTAGES FOR EACH CHANNEL OF THE DIGITI.
I          , I_RATES ! SAMPLING RATES OF EACH DIGITIZER
I          , IOFFSET ! DIGITIZERS OFFSETS
O          , RAMPMIN ! RAMP VOLTAGE MINIMUM
O          , RAMPMAX ! RAMP VOLTAGE MAXIMUM
I          , IDAT1 ! FIRST DATA POINT TO START CONVERSION
I          , IDAT2 ! LAST DATA POINT TO END CONVERSION
I          , I_GOT ! NUMBER OF DATA POINTS THAT WE ACTUALLY GOT
I          , WIDATA ! WORD INTEGER DATA

```



```

I      , WQDATA      ! WORD INTEGER DATA
I      , WVDATA      ! WORD INTEGER DATA
O      , RIDATA      ! REAL VOLTAGE NUMBER DATA
O      , RQDATA      ! REAL VOLTAGE NUMBER DATA
O      , RVDATA      ! REAL VOLTAGE NUMBER DATA
O      , RADATA      ! REAL VOLTAGE NUMBER DATA
O      , WGHZ        ! FREQUENCY ARRAY DATA IN GHz
O      , TIME         ! CORRESPONDING TIME DATA
O      , II)         ! GENERAL PURPOSE INDEX

C
      WRITE(11,*) 'AFTER CALLING CONVERT'
      WRITE(11,*) 'WGHZ(0)=', WGHZ(0), 'WGHZ(1)=', WGHZ(1)

C
      IF( IVDATA2 .EQ. 1 ) THEN
      CALL INITT(960) ! INITIALIZE PLOTTING SUBROUTINES
      CALL BINITT()  ! INITIALIZE DATA BLOCKS
      CALL XFRM(2)   ! SET X-AXIS FRAMES
      CALL YFRM(2)   ! SET Y-AXIS FRAMES
      CALL DLIMY(0.0,15.0) ! SET Y-AXIS LIMITS
      CALL CHECK(TIME,RVDATA) ! CHECK DATA LIMITS
      CALL DDISPLAY(TIME,RVDATA) ! PLOT DATA
      CALL FRAME()   ! DRAW FRAME AROUND PLOT
      CALL AGTCHS('TIME (SEC)') ! LABELS
      CALL AGTCVS('VOLTS') ! LABELS
      CALL GTITLE(5,'SWEEPER VOLTAGE') ! PUT A TITLE ON THE PLOT
      CALL FINITT(10,770) ! CLOSE PLOTTING FILE
      END IF

C
      WRITE(11,*) ' GET_INDEX:',
I      I_RATES(IDIGIT) ! SAMPLING RATES OF THE DIGITIZERS
I      , R_VOLTS      ! MAXIMUM PEAK VOLTAGE OF THE DIGITIZERS
I      , MAXRAW       ! SIZE OF ARRAYS

C
      GET_INDEX FINDS OUT WHERE THE USEFULL DATA STARTS AND ENDS.
C      IT DOES THIS BY USING THE RAMP VOLTAGE DATA TO SEE WHERE IS THAT
C      THE SWEEP STARTS AND ENDS. THE DATA THAT IS NOT ON THE SWEEP IS
C      THE RETRACE DATA OF THE RAMP VOLTAGE GENERATOR. THIS DATA IS
C      LATER DISCHARTED USING THE SUBROUTINE COMPRES.
      CALL GET_INDEX(
I      I_RATES(IDIGIT) ! SAMPLING RATES OF THE DIGITIZERS
I      , VMIN          ! MINIMUM TRUNCATION VOLTAGE
I      , VMAX          ! MAXIMUM TRUNCATION VOLTAGE
I      , MAXRAW        ! SIZER OF ARRAYS
I      , WGHZ          ! FREQUENCY DATA

```

```

C      I      , RVDATA ! VOLTAGE DATA OF THE RAMP VOLTAGE
I      , AUTOLIM ! SET AUTOMATICALLY THE MIN/MAX FOR THE SWEEP
O      , INDEX ! ARRAY WITH THE LOCATION OF THE BEGINING OF THE DATA
O      , INDEX2) ! ARRAY WITH THE LOCATION OF THE END OF THE DATA
C
      WRITE(11,*)'AFTER CALLING GET_INDEX'
      WRITE(11,*)'WGHZ(0)=',WGHZ(0),'WGHZ(INDEX(1))=',WGHZ(INDEX(1))
C
      WRITE(*,*) ' DATA TIME INTERVAL = '
*      , FLOAT(INDEX2(1)-INDEX(1))/FLOAT(I_RATES(IDIGIT)), ' SEC'
C
      IF(W_TIME .EQ. .TRUE.) THEN
C      HERE WE WRITE DIFFERENT DATA LIKE THE BEGINING TIME OF THE SWEEP,
C      AND OTHER DATA FOR EVERY SWEEP OF THE DATA. IT IS USED MOSTLY
C      AS A DEBUGGING FILE.
      OPEN(33,FILE='[ICOLLAZO.WILGEN]W.TIME;1',STATUS='UNKNOWN')
      WRITE(33,*)I_SHOT(IS),'=ISHOT ',IDAT1,'=IDAT1 '
*      ,IDAT2,'=IDAT2 '
      WRITE(33,*)' J ',' TIME ',' INDEX ',' INDEX2 '
*      , ' DELTA ',' WGHZ ',' RVDATA1 ',' RVDATA2 '
      DO J = 0,INDEX(0)
        WRITE(33,33)J, TIME(INDEX(J)), INDEX(J), INDEX2(J)
*      , INDEX2(J)-INDEX(J)
*      , WGHZ(INDEX(J)), RVDATA(INDEX(J)), RVDATA(INDEX2(J))
33      FORMAT(I4, F8.4, I8, I8
*      , I8
*      , F8.3, F9.4, F9.4)
      END DO
      CLOSE(33)
      END IF
C
C      SMOOTH THE DATA BY USING THE RUNNING CARIAGE INTEGRAL METHOD.
      IF( ICONV .GT. 1 ) THEN
C      CALL SMOOTHIQ(ICONV, RIDATA, RADATA, WORK)
C      CALL SMOOTHIQ(ICONV, RQDATA, RADATA, WORK)
      CALL SMOOTH(ICONV, RIDATA, WORK)
      CALL SMOOTH(ICONV, RQDATA, WORK)
      CALL SMOOTH(ICONV, RADATA, WORK)
      END IF
!
CHERE
C      DO I = 0, RADATA(0)
C      RASMOOTH(I) = RADATA(I)
C      END DO

```

```

C      CALL SMOOTH(ICONV*5,RASMOTH,WORK)
C
C      COMPRESS THE DATA TO GET RID OF THE RETRACE POINTS ON THE DATA.
C      CALL COMPRES(
I      NPICK ! NUMBER OF DATA POINTS TO BE WRITTEN TO FILE
I      , MAXRAW ! SIZE OF ARRAYS
I      , INDEX ! ARRAY OF POINTERS FOR THE BEGINING OF THE DATA
I      , INDEX2 ! ARRAY OF POINTERS FOR THE END OF THE DATA
I      , RAD_MIN ! MINIMUM VOLTAGE FOR CLIP-OFF
C      N      , RASMOTH ! ARRAY OF SMOOTHED SIGNAL AMPLITUDE
O      , RIDATA ! ARRAY OF I SIGNAL VOLTAGE DATA
O      , RQDATA ! ARRAY OF Q SIGNAL VOLTAGE DATA
O      , RVDATA ! ARRAY OF RAMP VOLTAGE DATA
O      , RADATA ! ARRAY OF SIGNAL VOLATAGE AMPLITUDE
O      , WGHZ ! ARRAY OF THE FREQUENCY POINTS
O      , TIME) ! ARRAY OF THE TIME DATA
!
C
C      WRITE(11,*)'AFTER CALLING COMPRES'
C      WRITE(11,*)'WGHZ(0)=',WGHZ(0),'WGHZ(INDEX(1))=',WGHZ(INDEX(1))
C
C      IF((IAVER.GT.INDEX(0)).AND.(INDEX(0).GE. 1)) IAYER = INDEX(0)
C
C      CALL INITT(960) ! INITIALIZE THE PLOTTING DATA BLOCKS
C
C      GET WAVE FORM DATA FOR THE TOROIDAL MAGNETIC FIELD
C      CALL WF_GET(I_SHOT(IS),'MB-TF-SL', WFDESC, IQUAL, XSTART
*      , XDELTA, XUNITS, WFDATA, MAXRAW, NUMGOT, WFUNITS, IERR)
C
C      CALL WF_GET(I_SHOT(IS),'MB-IP-SL', POL_DESC, IQUAL_POL
*      , POL_START, POL_DEL, POL_UNITS, POL_CUR, MAXRAW_POL
*      , NUMGOT_POL, WFUNITS_POL, IERR)
C
C      MAKE SOME KIND OF A TITLE
C      WRITE(CTITLE,10)
*      ' SHOT=',I_SHOT(IS)
*      , ' CURENT=',ABS(WFDATA((TIME(INDEX(1)+1)-XSTART)/XDELTA))
/      /1000.
*      , ' TIME=',TIME(INDEX(1)+1),' TO '
*      , TIME(INDEX(INDEX(0))+TIME(INDEX(INDEX(0))))
10      FORMAT(A6,I6, A10,F5.1, A8,F5.3,A4,F5.3)
IF(ITITLE .EQ. 1) CALL AGTMHS(100,780,CTITLE)
C      MAKE A TITLE AT THE BOTTOM OF THE PAGE
C      WRITE(CTITLE2,20)

```

```

*      'ICONV=',ICONV
*      , ' IAVR=',IAVR
*      , ' NPICK=',NPICK
*      , ' DIGIT=',DIGIT
20      FORMAT(A6,I2, A8,I2, A8,I2,A8,A1)
C      CALL AGTMHS(300,1,CTITLE2)
C      WRITE THE TOROIDAL FIELD CURRENT AND SHOT NUMBER AT THE CORNER
      WRITE(CORNER,30)I_SHOT(IS)
30      FORMAT(I5)
      IPARAM = 1
      CALL AGTMHS(950,IPARAM,CORNER)    ! OUTPUT SHOT NUMBER
      TCURRENT = ABS(WFDATA((TIME(INDEX(1)+1)-XSTART)/XDELTA))
      BO = 2.0E-07 * 880 * TCURRENT / 2.60
      WRITE(CORNER2,40) TCURRENT / 1000.
40      FORMAT(F3.0)
      IPARAM = IPARAM + 17
      CALL AGTMHS(985,IPARAM,CORNER2)    ! OUTPUT MAGNETIC FIELD
C
      IPARAM = IPARAM + 60
      DO I = 1, INDEX(0)
        WRITE(CTIME,50)TIME(INDEX(I)+1),'s'
50      FORMAT(F6.3,A1)
        CALL AGTMHS(920,IPARAM,CTIME)
        IPARAM = IPARAM + 20
      END DO
C
      IF (IVDATA.NE.0) THEN
C      PLOT THE RAMP VOLTAGE DATA IF REQUESTED
      CALL BINITT()    ! INITIALIZE DATA BLOCKS
      CALL XFRM(2)    ! SET X-AXIS FRAMES
      CALL YFRM(2)    ! SET Y-AXIS FRAMES
      CALL PLACE2(ABS(IVDATA))! SET SCREEN WINDOW
      CALL LINE(IVTYPE) ! SET LINE TYPE
C      SET X-AXIS DATA LIMITS
      CALL DLIMX(TIME(INDEX(1)+1), TIME(INDEX2(INDEX2(0)))) )
C      SET PLOT PARAMETERS
      CALL CHECK(TIME(INDEX(1)),RVDATA(INDEX(1)))
C      PLOT THE DATA
      CALL DSPLAY(TIME(INDEX(1)),RVDATA(INDEX(1)))
      CALL FRAME()    ! DRAW FRAME AROUND SCREEN WINDOW
      CALL AGTCHS('TIME SEC') ! LABELS
      CALL AGTCVS('SWEEP VOL') ! LABELS
      CALL GTITLE(5,'DY01-6810-B-3') ! PUT A TITLE ON THE PLOT
      DO I = 2, INDEX(0) ! PLOT NEXT DATA SETS
        CALL CPLOT(TIME(INDEX(I)),RVDATA(INDEX(I)))

```

```

        END DO
        CALL AGSALF ! SWITCH TERMINAL TO ALPHA-NUMERIC MODE
    END IF

!

C
C
    AVERAGE PHASE DATA SETS IN GROUPS OF "IAVER" NUMBERS
    CALL DAT_AVE(
I      MAXRAW ! SIZE OF ARRAYS
I      , IAVR ! NUMBER OF AVERAGES
I      , INDEX ! ARRAY OF POINTERS
I      , INDEX2 ! ARRAY OF POINTERS
O      , RIDATA ! I SIGNAL VOLTAGE DATA ARRAY
O      , RQDATA ! Q SIGNAL VOLTAGE DATA ARRAY
O      , RVDATA ! RAMP VOLTAGE DATA ARRAY
O      , RADATA ! AMPLITUDE DATA ARRAY
O      , RASIG ! STANDARD DEVIATION DATA ARRAY
O      , ISIGMA ! PLOTTING FLAG VARIABLE
O      , WGHZ ! FREQUENCY DATA ARRAY
O      , TIME) ! TIME DATA ARRAY

C
    IF(IIQ.NE.0) THEN
C
        PLOT THE I/Q VOLTAGE DATA IF REQUESTED
        CALL BINITT() ! INITIALIZE DATA BLOCKS
        CALL XFRM(2) ! SET X-AXIS STYLE
        CALL YFRM(2) ! SET Y-AXIS STYLE
        IF( IIQ .LE. 13) THEN
            CALL PLACE2(ABS(IIQ))! SET SCREEN WINDOW
        ELSE
            IF( IIQ .EQ. 14 ) THEN
                CALL SLIMX(IPHIMINX,IPHIMAXX)
                CALL SLIMY(IPHIMINY+ISHIFTY,IPHIMAXY+ISHIFTY)
                PLABEL = '(A)'
            ELSE
                CALL SLIMX(IPHIMINX,IPHIMAXX)
                CALL SLIMY(IPHIMINY,IPHIMAXY)
                PLABEL = '(B)'
            END IF
        END IF
        END IF
        CALL LINE(IIQTYPE) ! SET LINE TYPE
        CALL SYMBL(IQSMBL+1)! SET SYMBOL TYPE
        CALL SIZES(IQSIZE) ! SET SYMBOL SIZE
        CALL DLIMY(-5.,5.) ! SET Y-AXIS DATA LIMITS
C
        CALL DLIMX(W1,W2) ! SET X-AXIS DATA LIMITS
C
        SET DATA BLOCK PARAMETERS

```

```

      CALL CHECK(WGHZ(INDEX(1)),RIDATA(INDEX(1)))
C      PLOT AXIS AND DATA
      CALL DSPLAY(WGHZ(INDEX(1)),RIDATA(INDEX(1)))
      CALL FRAME() ! FRAME SCREEN WINDOW
      CALL AGTCHS('FREQUENCY (GHz)') ! LABELS
      CALL AGTCVS('VOLTS') ! LABELS
      CALL GTITLE(5,'I & Q SIGNALS') ! PUT A TITLE ON THE PLOT
      IXSMIN = COMGET(IBASEX(13)) ! GET SCREEN MINIMUM
      IYSMAX = COMGET(IBASEY(14)) ! GET SCREEN MAXIMUM
      CALL AGTMHS(IXSMIN-125,IYSMAX,PLABEL)!PLOT LABEL
C      PLOT NEXT DATA SET
      CALL SYMBL(IQSYMBL) ! SET SYMBOL TYPE
      CALL CPLOT(WGHZ(INDEX(1)),RQDATA(INDEX(1)))
      DO I = 2, INDEX(0) ! PLOT NEXT DATA SETS
        CALL SYMBL(IQSYMBL+1) ! SET SYMBOL TYPE
        CALL CPLOT(WGHZ(INDEX(I)),RIDATA(INDEX(I)))
        CALL SYMBL(IQSYMBL) ! SET SYMBOL TYPE
        CALL CPLOT(WGHZ(INDEX(I)),RQDATA(INDEX(I)))
      END DO
      CALL AGSALF ! SWITCH TERMINAL TO ALPHA-NUMERIC MODE
END IF

C
IF (IPOLAR.NE.0) THEN
C      WRITE THE DATA IN POLAR FORM
      CALL BINITT() ! INITIALIZE DATA BLOCKS
      CALL XFRM(2) ! SET X-AXIS STYLE
      CALL YFRM(2) ! SET Y-AXIS STYLE
      CALL PLACE2(ABS(IPOLAR))! SET SCREEN WINDOW
      CALL LINE(IPTYPE) ! SET LINE TYPE
      CALL DLIMX(-10.0,10.0) ! SET X-AXIS DATA LIMITS
      CALL DLIMY(-10.0,10.0) ! SET Y-AXIS DATA LIMITS
C      SET DATA LIMITS
      CALL CHECK(RIDATA(INDEX(1)),RQDATA(INDEX(1)))
C      PLOT AXIS AND DATA
      CALL DSPLAY(RIDATA(INDEX(1)),RQDATA(INDEX(1)))
      CALL FRAME() ! DRAW FRAME
      CALL AGTCHS('I DATA ') ! LABELS
      CALL AGTCVS('Q DATA ') ! LABELS
      CALL GTITLE(5,'POLAR FORM') ! PUT A TITLE ON THE PLOT
      DO I = 2, INDEX(0) ! PLOT NEXT DATA SETS
        CALL CPLOT(RIDATA(INDEX(I)),RQDATA(INDEX(I)))
      END DO
      CALL AGSALF ! SWITCH TERMINAL TO ALPHA-NUMERIC MODE
END IF

```

```

      IF (ITIME.NE. 0) THEN
C      PLOT RAMP VOLTAGE DATA AS A FUNCTION OF TIME
      CALL BINITT() ! INITIALIZE DATA BLOCKS
      CALL XFRM(2) ! SET X-AXIS STYLE
      CALL YFRM(2) ! SET Y-AXIS STYLE
      CALL PLACE2(ABS(ITIME))! SET SCREEN WINDOW
      CALL LINE(ITTTYPE) ! SET LINE TYPE
C      SET X-AXIS DATA LIMITS
      CALL DLIMX(TIME(INDEX(1)+1), TIME(INDEX2(INDEX(0))))
C      SET DATA LIMITS
      CALL CHECK(TIME(INDEX(1)),RVDATA(INDEX(1)))
C      PLOT AXIS AND DATA
      CALL DSPLAY(TIME(INDEX(1)),RVDATA(INDEX(1)))
      CALL FRAME() ! DRAW FRAME
      CALL AGTCHS('TIME ') ! LABELS
      CALL AGTCVS('RAMP VOL ') ! LABELS
      CALL GTITLE(6,'SWEEP VOLTALGE') ! PUT A TITLE ON THE PLOT
      DO I = 2, INDEX(0) ! PLOT NEXT DATA SETS
        CALL CPLOT(TIME(INDEX(I)),RVDATA(INDEX(I)))
      END DO
      CALL AGSALF ! SWITCH TERMINAL TO ALPHA-NUMERIC MODE
END IF

!

C
IF(IAMP.NE.0) THEN
C      PLOT AMPLITUDE OF THE SIGNAL IF REQUESTED
      CALL BINITT() ! SET DATA BLOCKS
      CALL XFRM(2) ! SET X-AXIS STYLE
      CALL YFRM(2) ! SET Y-AXIS STYLE
      IF( IAMP .LE. 13 ) THEN
        CALL PLACE2(ABS(IAMP))! SET SCREEN WINDOW
      ELSE
        IF( IAMP .EQ. 14 ) THEN
          CALL SLIMX(IPHIMINX,IPHIMAXX)
          CALL SLIMY(IPHIMINY+ISHIFTY,IPHIMAXY+ISHIFTY)
          PLABEL = '(A)'
        ELSE
          CALL SLIMX(IPHIMINX,IPHIMAXX)
          CALL SLIMY(IPHIMINY,IPHIMAXY)
          PLABEL = '(B)'
        END IF
      END IF
      CALL LINE(IAMPTYPE) ! SET LINE TYPE
C      CALL DLIMY(0.,10.) ! SET Y-AXIS DATA LIMITS

```

```

C      CALL DLIMX(W1,W2) ! SET X-AXIS DATA LIMITS
C      SET DATA LIMITS
      CALL CHECK(WGHZ(INDEX(1)),RADATA(INDEX(1)))
C      PLOT AXIS AND DATA
      CALL DISPLAY(WGHZ(INDEX(1)),RADATA(INDEX(1)))
      CALL FRAME() ! DRAW FRAME
      CALL AGTCHS('FREQUENCY (GHz)') ! LABELS
      CALL AGTCVS('AMPLITUDE') ! LABELS
      CALL GTITLE(5,'FROM I & Q') ! PUT A TITLE ON THE PLOT
      IXSMIN = COMGET(IBASEX(13)) ! GET SCREEN MINIMUM
      IYSMAX = COMGET(IBASEY(14)) ! GET SCREEN MAXIMUM
      CALL AGTMHS(IXSMIN-125,IYSMAX,PLABEL)!PLOT LABEL
      DO I = 2, INDEX(0) ! PLOT NEXT DATA SETS
        CALL CPLOT(WGHZ(INDEX(I)),RADATA(INDEX(I)))
      END DO
      X(0) = 2. ! THIS SMALL PIECE OF CODE DRAWS A LINE WHERE THE
      Y(0) = 2. ! MINIMUM SIGNAL VOLTAGE OF THE DIGITIZERS IS.
      X(1) = COMGET(IBASEX(26)) ! GET X-AXIS LOWER DATA LIMIT
      Y(1) = RAD_MIN ! SET MINIMUM VOLTAGE
      X(2) = COMGET(IBASEX(27)) ! GET X-AXIS UPPER DATA LIMIT
      Y(2) = RAD_MIN ! SET MINIMUM VOLTAGE
      CALL LINE(0) ! SET LINE TYPE
      CALL CPLOT(X,Y) ! DRAW THE MINIMUM VOLTAGE LINE
      CALL AGSALF ! SWITCH TERMINAL TO ALPHA-NUMERIC MODE
      END IF
!
C
C      IF(ISIGMA.NE.0) THEN
C      PLOT STANDARD DEVIATION OF THE SIGNAL IF REQUESTED
      CALL BINITT() ! SET DATA BLOCKS
      CALL XFRM(2) ! SET X-AXIS STYLE
      CALL YFRM(2) ! SET Y-AXIS STYLE
      CALL PLACE2(ABS(ISIGMA))! SET SCREEN WINDOW
      CALL LINE(ISIGTYPE) ! SET LINE TYPE
      CALL DLIMY(0.,2.) ! SET Y-AXIS DATA LIMITS
C      CALL DLIMX(W1,W2) ! SET X-AXIS DATA LIMITS
C      SET DATA LIMITS
      CALL CHECK(WGHZ(INDEX(1)),RASIG(INDEX(1)))
C      PLOT AXIS AND DATA
      CALL DISPLAY(WGHZ(INDEX(1)),RASIG(INDEX(1)))
      CALL FRAME() ! DRAW FRAME
      CALL AGTCHS('FREQUENCY (GHz)') ! LABELS
      CALL AGTCVS('SIGMA') ! LABELS
      CALL GTITLE(5,'FROM RADATA')! PUT A TITLE ON THE PLOT

```



```

DO I = 2, INDEX(0) ! PLOT NEXT DATA SETS
  CALL CPLOT(WGHZ(INDEX(I)),RASIG(INDEX(I)))
END DO
X(0) = 2. ! THIS SMALL PIECE OF CODE DRAWS A LINE FOR
Y(0) = 2. ! THE RANDOM NOICE LEVEL
X(1) = COMGET(IBASEX(26)) ! GET THE X-AXIS DATA MINIMUM
Y(1) = PI / SQRT(3.) ! RANDOM NOISE VALUE
X(2) = COMGET(IBASEX(27)) ! GET THE X-AXIS DATA MAXIMUM
Y(2) = Y(1) ! RANDOM NOISE VALUE
CALL LINE(0) ! SET LINE TYPE
CALL CPLOT(X,Y) ! PLOT RANDOM NOISE LINE LEVEL
CALL AGSALF ! SWITCH TERMINAL TO ALPHA-NUMERIC MODE
END IF

C
C THIS SUBROUTINE CALCULATES THE RAW PHASE OUT OF THE I AND Q DATA
CALL YO_PHASE(
  I INDEX ! ARRAY OF POINTERS FOR THE BEGINING OF THE DATA
  I , RIDATA ! I VOLTAGE DATA ARRAY
  I , RQDATA ! Q VOLTAGE DATA ARRAY
  O , PHASE) ! CALCULATED DATA ARRAY
!

C
C IF (IRAWPHA .NE. 0) THEN

C
  CALL BINITT() ! INITIALIZE DATA BLOCKS
  CALL XFRM(2) ! SET X-AXIS STYLE
  CALL YFRM(2) ! SET Y-AXIS STYLE
  IF( IRAWPHA .LE. 13 ) THEN
    CALL PLACE2(ABS(IRAWPHA)) ! SET SCREEN WINDOW
  ELSE
    IF( IRAWPHA .EQ. 14 ) THEN
      CALL SLIMX(IPHIMINX,IPHIMAXX)
      CALL SLIMY(IPHIMINY+ISHIFTY,IPHIMAXY+ISHIFTY)
      PLABEL = '(A)'
    ELSE
      CALL SLIMX(IPHIMINX,IPHIMAXX)
      CALL SLIMY(IPHIMINY,IPHIMAXY)
      PLABEL = '(B)'
    END IF
  END IF
  CALL LINE(IRAWPHTYPE) ! SET LINE TYPE
  CALL SYMBL(IRAWPHSYMBL) ! SET SYMBOL TYPE
  CALL SIZES(RAWPHSIZE) ! SET SYMBOL SIZE
C CALL DLIMX(W1,W2) ! SET X-AXIS DATA LIMITS

```

```

      CALL DLIMY(-0.49,0.49) ! SET Y-AXIS DATA LIMITS
      CALL CHECK(WGHZ(INDEX(1)),PHASE(INDEX(1)))! SET DATA LIMITS
      CALL DPLAY(WGHZ(INDEX(1)),PHASE(INDEX(1)))! PLOT AXIS AND DATA
      CALL FRAME() ! DRAW FRAME
      CALL AGTCHS('FREQUENCY (GHz)') ! LABELS
      CALL AGTCVS('FRINGES') ! LABELS
      CALL GTITLE(5,'RAW PHASE')! PUT A TITLE ON THE PLOT
      IXSMIN = COMGET(IBASEX(13)) ! GET SCREEN MINIMUM
      IYSMAX = COMGET(IBASEY(14)) ! GET SCREEN MAXIMUM
      CALL AGTMHS(IXSMIN-125,IYSMAX,PLABEL)!PLOT LABEL
      DO I = 2, INDEX(0) ! PLOT NEXT DATA SETS
        CALL CPLT(WGHZ(INDEX(I)),PHASE(INDEX(I)))
      END DO
      CALL AGSALF ! SWITCH TERMINAL TO ALPHA-NUMERIC MODE
END IF

C
IF ( (IPHAVE .NE. 0) .OR. (IPHSIG .NE. 0) ) THEN
C
  IF REQUESTED, DO THE TOTAL AVERAGE OF THE DATA
  CALL IQ_AVE(INDEX,WGHZ,RIDATA,RQDATA,WGHZAVE,RIAVE,RQAVE)
  INDEXAVE(0) = 1
  INDEXAVE(1) = 0
  CALL YO_PHASE(
    I   INDEXAVE ! ARRAY OF POINTERS FOR THE BEGINING OF THE DATA
    I   , RIAVE ! I VOLTAGE DATA ARRAY
    I   , RQAVE ! Q VOLTAGE DATA ARRAY
    0   , PHAVE) ! CALCULATED DATA ARRAY
C
    IF ( IPHAVE .NE. 0 ) THEN
C
      COUNT THE PHASE TO CALCULATE THE SIGMA
C
      CALL PH_COUNT(
C      I   DER1 ! VALUE FOR THE DERIVATIVE CRITERIUM
C      I   , AMP1 ! VALUE FOR THE AMPLITUDE CRITERIUM
C      I   , INDEX ! ARRAY OF POINTERS FOR THE BEGINING OF THE DATA
C      0   , PHASE ! PHASE DATA ARRAY
C      0   , WORK) ! WORKING DATA ARRAY
C
      COUNT THE AVERAGE PHASE
      DO IP = 0, PHAVE(0)
        PHAVE_C(IP) = PHAVE(IP)
      END DO
      CALL PH_COUNT(
C      I   DER1 ! VALUE FOR THE DERIVATIVE CRITERIUM
C      I   , AMP1 ! VALUE FOR THE AMPLITUDE CRITERIUM
C      I   , INDEXAVE ! ARRAY OF POINTERS FOR THE BEGINING OF THE DATA
C      0   , PHAVE_C ! PHASE DATA ARRAY

```

```

0      , WORK) ! WORKING DATA ARRAY
C
C      USE THE AVERAGED PHASE DATA TO MATCH OR COUNT THE
C      NON-AVERAGED DATA.
C      CALL MATCH_TO_AVE(INDEX,PHASE,PHAVE_C)
C
C      CALL BINITT() ! INITIALIZE DATA BLOCKS
C      CALL XFRM(2) ! SET X-AXIS STYLE
C      CALL YFRM(2) ! SET Y-AXIS STYLE
C      CALL PLACE2(ABS(IPHAVE))! SET SCREEN WINDOW
C      CALL LINE(IAVETYPE) ! SET LINE TYPE
C      CALL DLIMX(W1,W2) ! SET X-AXIS DATA LIMITS
C      CALL DLIMY(0.0,3.0) ! SET Y-AXIS DATA LIMITS
C      CALL CHECK(WGHZAVE,PHAVE) ! SET DATA LIMITS
C      CALL DSPLAY(WGHZAVE,PHAVE)! PLOT AXIS AND DATA
C      CALL CHECK(WGHZAVE,PHAVE_C)! SET DATA LIMITS
C      CALL DSPLAY(WGHZAVE,PHAVE_C)! PLOT AXIS AND DATA
C      IF( IPH2 .NE. 0 ) THEN
C          CALL PH_SORT(INDEX,WGHZ,PHASE,RWGHZ,RPHASE) !RESORT PHASE DATA
C          CALL LINE(-4) ! SET LINE TYPE
C          DO JJ = 1, INDEX(0) ! PLOT OTHER DATA SETS
C              CALL CPlot(WGHZ(INDEX(JJ)),PHASE(INDEX(JJ)))
C          CALL CPlot(WGHZAVE,PHASE(INDEX(JJ)))
C          END DO
C      END IF
C      CALL FRAME() ! DRAW FRAME
C      CALL AGTCHS('FREQUENCY (GHz)') ! LABELS
C      CALL AGTCVS('FRINGES') ! LABELS
C      CALL GTITLE(5,'PHASE AVE')! PUT A TITLE ON THE PLOT
C      CALL AGSALF ! SWITCH TERMINAL TO ALPHA-NUMERIC MODE
C      END IF
C
C      IF ( IPHSIG .NE. 0 ) THEN ! DRAW THE PHASE SIGMA DATA
C          CALL PH_SIGMA(INDEX,PHASE,PHAVE_C,PHSIG)
C          CALL BINITT() ! INITIALIZE DATA BLOCKS
C          CALL XFRM(2) ! SET X-AXIS STYLE
C          CALL YFRM(2) ! SET Y-AXIS STYLE
C          WRITE(*,*) IPHSIG
C          CALL PLACE('LOH')! SET SCREEN WINDOW
C          CALL PLACE2(ABS(IPHSIG))! SET SCREEN WINDOW
C          CALL LINE(-4) ! SET LINE TYPE
C          CALL DLIMX(W1,W2) ! SET X-AXIS DATA LIMITS
C          CALL DLIMY(0.,0.5) ! SET Y-AXIS DATA LIMITS
C          CALL CHECK(WGHZAVE,PHSIG) ! SET DATA LIMITS
C          CALL DSPLAY(WGHZAVE,PHSIG)! PLOT AXIS AND DATA

```

```

      CALL LINE(0) ! SET LINE TYPE
      CALL CPLOT(WGHZAVE,PHSIG)! PLOT AXIS AND DATA
      CALL AGTHS('SIGMA')
      SIG_MAX(0) = 2
      WSIG_MAX(0) = 2
      SIG_MAX(1) = 1. / (2.*SQRT(3.))
      WSIG_MAX(1) = 90.
      SIG_MAX(2) = SIG_MAX(1)
      WSIG_MAX(2) = 120.
      CALL CPLOT(WSIG_MAX,SIG_MAX)
C      CALL FRAME() ! DRAW FRAME
C      CALL AGTCHS('FREQUENCY (GHz)') ! LABELS
C      CALL AGTCVS('FRINGES') ! LABELS
C      CALL GTITLE(5,'PHASE SIGMA') ! PUT A TITLE ON THE PLOT
      CALL AGSALF ! SWITCH TERMINAL TO ALPHA-NUMERIC MODE
      IF(IPHSIG .LT. 0) THEN
C      WRITE SIGMA DATA TO FILE
      WRITE(SIG_FILE,188) DATA_FLS,I_SHOT(IS),'.SIG'
188      FORMAT(A26,I5,A4)
      OPEN(88,FILE=SIG_FILE,STATUS='NEW')
      WRITE(88,189) ( WGHZAVE(I),PHSIG(I), I=0,WGHZAVE(0))
189      FORMAT(' ',F16.8,' ',F16.8)
      CLOSE(88)
      END IF
      END IF
!

      IF( IPHAVE_C .NE. 0) THEN
      DO IP = 0, PHAVE(0)
      PHAVE_C(IP) = PHAVE(IP)
      END DO
      CALL PH_COUNT(
I      DER1 ! VALUE FOR THE DERIVATIVE CRITERIUM
I      , AMP1 ! VALUE FOR THE AMPLITUDE CRITERIUM
I      , INDEXAVE ! ARRAY OF POINTERS FOR THE BEGINING OF THE DATA
0      , PHAVE_C ! PHASE DATA ARRAY
0      , WORK) ! WORKING DATA ARRAY
      CALL BINITT() ! INITIALIZE DATA BLOCKS
      CALL XFRM(2) ! SET X-AXIS STYLE
      CALL YFRM(2) ! SET Y-AXIS STYLE
      CALL PLACE2(ABS(IPHAVE_C))! SET SCREEN WINDOW
      CALL LINE(0) ! SET LINE TYPE
C      CALL DLIMX(W1,W2) ! SET X-AXIS DATA LIMITS
C      CALL DLIMY(0.,0.5) ! SET Y-AXIS DATA LIMITS

```

```

      CALL CHECK(WGHZAVE,PHAVE_C)! SET DATA LIMITS
      CALL DSPLAY(WGHZAVE,PHAVE_C)! PLOT AXIS AND DATA
      CALL FRAME() ! DRAW FRAME
      CALL AGTCHS('FREQUENCY (GHz)') ! LABELS
      CALL AGTCVS('FRINGES') ! LABELS
      CALL GTITLE(5,'AVERAGE PHASE AND SIGMA')! PUT A TITLE
      CALL AGSALF ! SWITCH TERMINAL TO ALPHA-NUMERIC MODE

C
C      COUNT THE PHASE TO CALCULATE THE SIGMA
      CALL PH_COUNT(
I      DER1 ! VALUE FOR THE DERIVATIVE CRITERIUM
I ,      AMP1 ! VALUE FOR THE AMPLITUDE CRITERIUM
I ,      INDEX ! ARRAY OF POINTERS FOR THE BEGINING OF THE DATA
O ,      PHASE ! PHASE DATA ARRAY
O ,      WORK) ! WORKING DATA ARRAY

C
C      PLOT THE COUNTED PHASE USED FOR THE CALCULATION OF THE SIGMA
C      AS A GROUP OF SCATTERED POINTS.
      IF( IPH2 .NE. 0 ) THEN
C          CALL PH_SORT(INDEX,WGHZ,PHASE,RWGHZ,RPHASE) !RESORT PHASE DATA
          CALL LINE(-4) ! SET LINE TYPE
          DO JJ = 1, INDEX(0) ! PLOT OTHER DATA SETS
              CALL CPLOT(WGHZ(INDEX(JJ)),PHASE(INDEX(JJ)))
          END DO
      END IF

C
C      CALCULATE THE SIGMA
      CALL PH_SIGMA(INDEX,PHASE,PHAVE,PHSIG)
C      PLOT SIGMA
      CALL LINE(1) !SET LINE TYPE
      CALL CPLOT(WGHZAVE,PHSIG)! PLOT SIGMA DATA

C
      END IF
      END IF

C
      IF (IWILGEN .NE. 0) THEN
C          DRAW THE RAW PHASE DATA IN THE FORM OF A ZEBRA STRIPE PLOT
          CALL BINITT() ! INITIALIZE DATA BLOCKS
          CALL XFRM(2) ! SET X-AXIS STYLE
          CALL YFRM(5) ! SET Y-AXIS STYLE
          IF( IWILGEN .LE. 13 ) THEN
              CALL PLACE2(ABS(IWILGEN)) ! SET SCREEN WINDOW
          ELSE
              IF( IWILGEN .EQ. 14 ) THEN
                  CALL SLIMX(IPHIMINX,IPHIMAXI)
              
```

```

        CALL SLIMY(IPHIMINY+ISHIFTY,IPHIMAXY+ISHIFTY)
        PLABEL = '(A)'
    ELSE
        CALL SLIMX(IPHIMINX,IPHIMAXX)
        CALL SLIMY(IPHIMINY,IPHIMAXY)
        PLABEL = '(B)'
    END IF
END IF
CALL LINE(IWTYPE) ! SET LINE TYPE
CALL SYMBL(IRAWPHSYMBL) ! SET SYMBOL TYPE
CALL SIZES(RAWPHSIZE) ! SET SYMBOL SIZE
CALL DLIMY(0.,FLOAT(IWILY)) ! SET Y-AXIS DATA LIMITS
C CALL DLIMX(W1,W2) ! SET X-AXIS DATA LIMITS
C SET DATA LIMITS
CALL CHECK(WGHZ(INDEX(1)),PHASE(INDEX(1)))
C PLOT AXIS AND DATA FOR THE FIRST STRIPE
CALL DSPLAY(WGHZ(INDEX(1)),PHASE(INDEX(1)))
CALL FRAME() ! DRAW FRAME
CALL AGTCHS('FREQUENCY (GHz)') ! LABELS
CALL AGTCVS('RAW PH CY') ! LABELS
CALL GTITLE(5,'RAW PHASE') ! PUT A TITLE ON THE PLOT
IXSMIN = COMGET(IBASEX(13)) ! GET SCREEN MINIMUM
IYSMAX = COMGET(IBASEY(14)) ! GET SCREEN MAXIMUM
CALL AGTMHS(IXSMIN-125,IYSMAX,PLABEL)!PLOT LABEL
DO I = 2, INDEX(0) ! PLOT NEXT DATA SET
    CALL CPLOT(WGHZ(INDEX(I)),PHASE(INDEX(I)))
END DO
DO I = 1, IWILY ! PLOT THE NEXT STRIPES
    DO J = 1, INDEX(0)
        DO K = 1, PHASE(INDEX(J))
            WPHASE(K) = PHASE(K+INDEX(J)) + I
        END DO
        WPHASE(0) = PHASE(INDEX(J))
        CALL CPLOT(WGHZ(INDEX(J)), WPHASE ) ! PLOT NEXT DATA SET
    END DO
END DO
CALL AGSALF ! SWITCH TERMINAL TO ALPHA-NUMERIC MODE
END IF
IF( (IPHASE .NE. 0) .OR. (T_DATA.EQ. .TRUE.) ) CALL PH_COUNT(
I DER1 ! VALUE FOR THE DERIVATIVE CRITERIUM
I , AMP1 ! VALUE FOR THE AMPLITUDE CRITERIUM
I , INDEX ! ARRAY OF POINTERS FOR THE BEGINING OF THE DATA
O , PHASE ! PHASE DATA ARRAY
O , WORK) ! WORKING DATA ARRAY
!
```

```

C      IF ( CAL_DAT .EQ. .TRUE. ) THEN
C      IF THIS IS CALIBRATION DATA, THEN PUT IT ON THE
C      CALIBRATION DIRECTORY
      WRITE(CFILE,222) '[.CAL]SH',I_SHOT(IS),'.CAL'
222      FORMAT(A8,I5,A4)
      OPEN(55,FILE=CFILE,STATUS='NEW')
      WRITE(55,*)' 0.0 ',I_SHOT(IS),'=ISHOT ',TIME(2)
      *      ,'=TIME CALIBRATION DATA'
      WRITE(55,*) PHASE(INDEX(1)), INDEX2(1)-INDEX(1)
      DO I = INDEX(1)+1, INDEX2(1)
        WRITE(55,*) WGHZ(I), PHASE(I)
      END DO
      CLOSE(55)
    ELSE
C      CONTINUE
      IF( (CAL_ON .EQ. .TRUE.) .AND.
      *      ((IPHASE .NE. 0) .OR. (T_DATA .EQ. .TRUE.))) THEN
C      IF CALIBRATION IS REQUESTED THEN DO THE CALIBRATION BY
C      SUBTRACTING THE CALIBRATION DATA TO THE COUNTED DATA
      CALL YO_CAL(
      I      INDEX ! ARRAY OF POINTERS FOR THE BEGINING OF THE DATA
      *      , WGHZ ! ARRAY OF THE FREQUENCIES
      *      , PHASE) ! ARRAY OF THE PHASE DATA
      END IF
      IF (IPHASE.NE.0) THEN
C      PLOT PHASE DATA IF REQUESTED
      CALL BINITT() ! SET DATA BLOCKS
      CALL XFRM(2) ! SET X-AXIS STYLE
      CALL YFRM(5) ! SET Y-AXIS STYLE
      IF( IPHASE .LE. 13 ) THEN
        CALL PLACE2(ABS(IPHASE))! SET SCREEN WINDOW
      ELSE
        IF( IPHASE .EQ. 14 ) THEN
          CALL SLIMX(IPHIMINX,IPHIMAXX)
          CALL SLIMY(IPHIMINY+ISHIFTY,IPHIMAXY+ISHIFTY)
          PLABEL = '(A)'
        ELSE
          CALL SLIMX(IPHIMINX,IPHIMAXX)
          CALL SLIMY(IPHIMINY,IPHIMAXY)
          PLABEL = '(B)'
        END IF
      END IF
      CALL SYMBL(IRAWPHSYMBL) ! SET SYMBOL TYPE
      CALL SIZES(RAWPHSIZE) ! SET SYMBOL SIZE
    
```

```

      CALL LINE(IPHTYPE) ! SET LINE TYPE
C      CALL DLIMX(W1,W2) ! SET X-AXIS LIMITS
      CALL DLIMY(0.0, PHMAX) ! SET Y-AXIS LIMITS
C      SET DATA LIMITS
      CALL CHECK(WGHZ(INDEX(1)),PHASE(INDEX(1)))
C      PLOT AXIS AND DATA
      CALL DSPLAY(WGHZ(INDEX(1)),PHASE(INDEX(1)))
C      CALL AGTHS('1') ! LABELS
      CALL FRAME() ! DRAW FRAME
      CALL AGTCHS('FREQUENCY (GHz)') ! LABELS
      CALL AGTCVS('FRINGES') ! LABELS
      CALL GTITLE(5,'COUNTED PHASE') ! PUT A TITLE ON THE PLOT
      IXSMIN = COMGET(IBASEX(13)) ! GET SCREEN MINIMUM
      IYSMAX = COMGET(IBASEY(14)) ! GET SCREEN MAXIMUM
      CALL AGTMHS(IXSMIN-125,IYSMAX,PLABEL)!PLOT LABEL
C
      WRITE(PARAM,230)'B = ',BO,' T'
230      FORMAT(A3,F3.1,A2)
      IXPARAM = IXSMIN + 75
      IYPARAM = IYSMAX - 16
      CALL AGTMHS(IXPARAM,IYPARAM,PARAM)
C
      WRITE(PARAM,231)' 0 '
231      FORMAT(A3)
      IYPARAM = IYPARAM - 6
      CALL AGTMHS(IXPARAM,IYPARAM,PARAM)
C
      DO I = 2, INDEX(0) ! PLOT NEXT DATA SETS
        CALL CPLOT(WGHZ(INDEX(I)),PHASE(INDEX(I)))
        WRITE(C3I,110) I
110        FORMAT(1X,I2)
C        CALL AGTHS(C3I) ! OUTPUT CURVE NUMBER
      END DO
      CALL AGSALF ! SWITCH TERMINAL TO ALPHA-NUMERIC MODE
      END IF
      END IF
!
C
      IF ( T_DATA .EQ. .TRUE. ) THEN
C      IF REQUESTED WRITE THE PHASE VS FREQUENCY DATA ON A FILE
      OPEN(33,FILE=T_FLS,STATUS='NEW')
      WRITE(33,*) INDEX(0)
      DO I = 1, INDEX(0)
C      WRITE(*,*) ' TIME(', INDEX(I)+1,')= ', TIME(INDEX(I)+1)

```



```

        WRITE(CFILE,130) DATA_FLS,I_SHOT(IS),DIGIT,'_'
        *      ,TIME(INDEX(I)+1)
130      FORMAT(A26,I5,A1,A1,F5.3,F16.4)
C        WRITE(*,*) CFILE
C        *      ,ABS( WFDATA((TIME(INDEX(I)+1)-XSTART)/XDELTA) )
        OPEN(22,FILE=CFILE,STATUS='NEW')
        WRITE(33,*) CFILE
        NNDATA = WGHZ(INDEX(I))
        WRITE(22,25)NNDATA
        *      ,ABS( WFDATA((TIME(INDEX(I)+1)-XSTART)/XDELTA) )
        *      ,TIME(INDEX(I)+1),TIME(INDEX(I)+TIME(INDEX(I)))
        *      ,I_SHOT(IS)
        *      ,IDIGIT
        *      ,',',ABS( POL_CUR((TIME(INDEX(I)+1)-POL_START)/POL_DEL) )
        *      ,', 0.0 '
25      FORMAT(I9, F9.1, F9.5,F9.5, I9, I3, A1, F9.1, A6)
        DO J = INDEX(I)+1, INDEX2(I)
            WRITE(22,*) WGHZ(J), PHASE(J)
        END DO
        CLOSE(22)
        END DO
        CLOSE(33)
        END IF
C
C        PLOT TODAY'S DATE
        CALL DATE(TODAY)
        CALL AGTMBS(900,780,TODAY)
C
        CALL AGSALF ! SWITCH TERMINAL TO ALPHA-NUMERIC MODE
        CALL TSEND() ! SEND WHAT IS LEFT ON THE BUFFER TO TERMINAL
C
1      CLOSE(11) ! CLOSE THE DEBUGGING FILE
        IS = IS + 1 ! INCREMENT TO THE NEXT SHOT ON THE LIST
        END DO ! LOOP OVER THE DATA LIST IN "I_SHOTS(IS)"
C
        CALL FINITT(10,770) ! CLOSE THE PLOTTING SUBROUTINES
C
        STOP
        END
C
!
!
C

```

```

C *****
C
C FUNCTIONS AND SUBROUTINES
C
C *****
C

```

```

SUBROUTINE GTITLE(N,TITLE)
C THIS SUBROUTINE WRITES A TITLE ABOVE THE GRAPH.  IT DOES THIS
C BY READING THE GRAPH'S SCREEN COORDINATES FROM THE DATA BLOCK
C AND USING IT TO KNOW WHERE TO BUT THE TITLE STRING.
IMPLICIT NONE
INTEGER
    *   N ! NUMBER OF RASTER UNITS ABOVE GRAPH TO PUT THE TITLE
    *   , IBASEX ! AG2 FUNCTION TO GET ADDRESS OF DATA ON DATA BLOCK
    *   , IBASEY ! AG2 FUNCTION TO GET ADDRESS OF DATA ON DATA BLOCK
REAL COMGET ! AG2 FUNCTION TO GET DATA FROM DATA BLOCK
CHARACTER TITLE*77

    CALL AGTMHS(INT(COMGET(IBASEX(13))),INT(COMGET(IBASEY(14)))+N
    *           , TITLE)

```

```

RETURN
END
!

```

```

C
C *****
C

```

```

SUBROUTINE SMOOTH(ICONV, DATA, DATAS)
C THIS SUBROUTINE SMOOTHS THE DATA BY USING THE FAMOUS
C RUNNING CARIAGE INTRGRAL METHOD.  THIS IS DONE BY AVERAGING
C EVERY POINT ON THE ARRAY/FUNCTION AGAINST THE SURROUNDING
C NEIGHBOR POINTS OF THE ARRAY/FUNCTION.
IMPLICIT NONE
REAL
    *   DATA(0:*) ! DATA TO BE SMOOTHED
    *   , DATAS(0:*) ! WORKING ARRAY
    *   , SUM ! WORKING VARIABLE
    *   , C ! DECAY CONSTANT FOR THE GAUSSIAN
    *   , X ! WORKING VARIABLE
    *   , PI ! = 3.14159265
INTEGER
    *   I ! DO LOOP INDEX

```

```
* , ICONV ! NUMBER OF POINTS TO AVERAGE BY
* , I1 ! LIMITS FOR THE DO LOOP
* , I2 ! LIMITS FOR THE DO LOOP
* , J ! DO LOOP INDEX
* , IJ ! INDEX

C
IF( ICONV .LE. 0 ) RETURN
PI = 3.14159265
C I DECIDED TO USE A GAUSSIAN EMVELOPE OR WEIGHTING FUNCTION TO DO
C THE SMOOTHING, AS OPPOSED TO USING A SQUARE STEP FUNCTION. THIS
C WILL HELP TO REDUCE THE INTRODUCTION OF HIGHER HARMONICS INTO
C THE DATA, AS COMPARED TO A SQUARE STEP FUNCTION.
C = FLOAT(ICONV) / SQRT(LOG(10.))
DO I = 1, ICONV
  SUM = 0.0
  DO J = 1-I , ICONV
    IJ = I + J
    X = FLOAT(J) / C
    SUM = SUM + DATA(IJ) * EXP(-X*X) / ( C * SQRT(PI))
  END DO
  DATAS(I) = SUM
END DO
I1 = ICONV + 1
I2 = DATA(0) - ICONV - 1
DO I = I1 , I2
  SUM = 0.0
  DO J = -ICONV , ICONV
    IJ = I + J
    X = FLOAT(J)/C
    SUM = SUM + DATA(IJ) * EXP(-X*X) / ( C * SQRT(PI))
  END DO
  DATAS(I) = SUM
END DO
DO I = I2+1, DATA(0)
  SUM = 0.0
  DO J = -ICONV , ICONV - (I - I2)
    SUM = SUM + DATA(J)
  END DO
  DATAS(I) = SUM / (DATA(0)-(I-ICONV)+1)
END DO
C
DO I = 1, DATA(0)
  DATA(I) = DATAS(I)
END DO
C
```

```

RETURN
END
!
```

```

C
C *****
C
```

```

SUBROUTINE SMOOTHIQ(ICONV, DATA, RADATA, DATAS)
C THIS SUBROUTINE SMOOTHS THE DATA BY USING THE FAMOUS
C RUNNING CARIAGE INTRGRAL METHOD. THIS IS DONE BY AVERAGING
C EVERY POINT ON THE ARRAY/FUNCTION AGAINST THE SURROUNDING
C NEIGHBOR POINTS OF THE ARRAY/FUNCTION.
C THIS VERSION OF THE SMOOTHING SUBROUTINE USES THE AMPLITUDE
C OF THE SIGNAL TO WEIGHT THE DATA POINTS IN FAVOR OF THE
C DATA POINTS WITH THE HIGHEST AMPLITUDES. THIS IS A WAY TO
C REDUCE THE EFFECT OF THE LOW AMPLITUDE DATA POINTS TO THE
C TOTAL SMOOTHED DATA POINTS.
```

```

IMPLICIT NONE
```

```

REAL
```

```

*   DATA(0:*) ! DATA TO BE SMOOTHED
*   , DATAS(0:*) ! WORKING ARRAY
*   , RADATA(0:*) ! AMPLITUDE DATA
*   , SUM ! WORKING VARIABLE
*   , C ! DECAY CONSTANT FOR THE GAUSSIAN
*   , X ! WORKING VARIABLE
*   , PI ! = 3.14159265
*   , TEMP ! DUMMY VARIABLE
*   , RA_AVE ! AMPLITUDE DATA RUNNING AVERAGE
```

```

INTEGER
```

```

*   I ! DO LOOP INDEX
*   , ICONV ! NUMBER OF POINTS TO AVERAGE BY
*   , I1 ! LIMITS FOR THE DO LOOP
*   , I2 ! LIMITS FOR THE DO LOOP
*   , J ! DO LOOP INDEX
*   , IJ ! INDEX
```

```

C
```

```

IF( ICONV .LE. 0 ) RETURN
```

```

PI = 3.14159265
```

```

C I DECIDED TO USE A GAUSSIAN ENVELOPE OR WEIGHTING FUNCTION TO DO
C THE SMOOTHING, AS OPPOSED TO USING A SQUARE STEP FUNCTION. THIS
C WILL HELP TO REDUCE THE INTRODUCTION OF HIGHER HARMONICS INTO
C THE DATA, AS COMPARED TO A SQUARE STEP FUNCTION.
```

```

C = FLOAT(ICONV) / SQRT(LOG(10.))
```

```

DO I = 1, ICONV
```

```

SUM = 0.0
DO J = 1-I , ICONV
  IJ = I + J
  X = FLOAT(J) / C
  SUM = SUM + DATA(IJ) * EXP(-X*X) / ( C * SQRT(PI))
END DO
DATAS(I) = SUM
END DO
I1 = ICONV + 1
I2 = DATA(0) - ICONV - 1
DO I = I1 , I2
  SUM = 0.0
  RA_AVE = 0.0
  DO J = -ICONV , ICONV
    IJ = I + J
    X = FLOAT(J)/C
    TEMP = RADATA(IJ) * RADATA(IJ)
    SUM = SUM + DATA(IJ) * EXP(-X*X) / (C * SQRT(PI))
    * * TEMP
    RA_AVE = RA_AVE + TEMP
  END DO
  DATAS(I) = SUM / RA_AVE
END DO
DO I = I2+1, DATA(0)
  SUM = 0.0
  DO J = -ICONV , ICONV - (I - I2)
    SUM = SUM + DATA(J)
  END DO
  DATAS(I) = SUM / (DATA(0)-(I-ICONV)+1)
END DO
C
DO I = 1, DATA(0)
  DATA(I) = DATAS(I)
END DO
C
RETURN
END
!

C
C *****
C
SUBROUTINE SMOOTH_PH(ICONPH, INDEX, PHASE, WORK)
REAL PHASE(0:*), WORK(0:*)
INTEGER I, ICONPH, INDEX(0:1000)

```

```

C
DO I = 1, INDEX(0)
    CALL SMOOTH(ICONPH, PHASE(INDEX(I)), WORK)
END DO
C
RETURN
END
!

C
C *****
C
SUBROUTINE YO_DATA(
    I   I_SHOT ! THE SHOT NUMBER
    I , MAXRAW ! THE SIZE OF THE INTEGER WAVEFORM DATA ARRAYS
    I , C1TYPE ! SINCRONOUS / ASINCRONOUS SWITCH
    I , DIGIT  ! DIGITIZER LETTER
    I , CRAMP  ! PORT NUMBER FOR THE RAMP VOLTAGE
    O , I_GOT  ! NUMBER OF DATA POINTS THAT WE ACTUALY GOT
    O , WIDATA ! DATA ARRAY FOR THE WAVEFORM OF CHANNEL 1
    O , WQDATA ! DATA ARRAY FOR THE WAVEFORM OF CHANNEL 2
    O , WVDATA ! DATA ARRAY FOR THE WAVEFORM OF CHANNEL 3
    O , WADATA ! DATA ARRAY FOR THE WAVEFORM NOT IN USE
    O , IERR) ! ERROR CODE
C
C THIS SUBROUTINE READS THE DATA FROM THE DISK AND PUTS IT ON THE
C CORRESPONDING INTEGER ARRAYS
IMPLICIT NONE
INTEGER I_SHOT, I_LFC, I_START, IERR, NUMKEYS, ERRSTATUS
    * , I_GOT, MAXRAW
INTEGER*4 WIDATA(2*MAXRAW), WQDATA(2*MAXRAW), WVDATA(2*MAXRAW)
    * , WADATA(2*MAXRAW)
CHARACTER C2DIGRPH*2, C8DATE*8, MESSAGE*80, C16KEY*16, C1TYPE*1
    * , DIGIT*1, CRAMP*1

I_LFC = 9 ! LOGICAL FILE UNIT USED FOR THE READ
I_START = 1 ! STARTING DATA POINT TO BE READ FROM DISK
C2DIGRPH = 'YO' ! DIGRAPH NAME
C
C OPEN THE FILE TO READ
CALL CM_RROPN(I_LFC, C2DIGRPH, C1TYPE, I_SHOT, C8DATE, NUMKEYS, IERR)
    IF (IERR .NE. 0) THEN
        CALL CM_ERR(IERR, MESSAGE, ERRSTATUS)
        WRITE(*,*) IERR, MESSAGE, ERRSTATUS
    END IF

```

```

WRITE(*,*)I_LFC, C2DIGRPH, I_SHOT, C8DATE, NUMKEYS, IERR
C
WRITE(*,*)'      ','      ' DIGRAPH      ','      ' START TIME      ','      '
      * , ' MAXRAW      ','      ' I_GOT      ','      ' ERROR      '
C
C READ THE DATA FROM THE FILE
C16KEY = 'DY01-6810-'//DIGIT//'-1' ! CHANNEL 1 TO THE I SIGNAL
CALL CM_RRDAT(I_LFC,C16KEY,WIDATA,I_START,MAXRAW,I_GOT,IERR)
      IF (IERR .NE. 0) THEN
        CALL CM_ERR(IERR, MESSAGE, ERRSTATUS)
        WRITE(*,*)IERR, MESSAGE, ERRSTATUS
      END IF
WRITE(*,10)I_LFC, C16KEY, I_START, MAXRAW, I_GOT, IERR
      10 FORMAT(I4,2X,A15,2X,I11,2X,I11,2X,I11,2X,I11)
C16KEY = 'DY01-6810-'//DIGIT//'-2' ! CHANNEL 2 TO THE Q SIGNAL
CALL CM_RRDAT(I_LFC,C16KEY,WQDATA,I_START,MAXRAW,I_GOT,IERR)
      IF (IERR .NE. 0) THEN
        CALL CM_ERR(IERR, MESSAGE, ERRSTATUS)
        WRITE(*,*)IERR, MESSAGE, ERRSTATUS
      END IF
WRITE(*,10)I_LFC, C16KEY, I_START, MAXRAW, I_GOT, IERR
C
WRITE(C16KEY,20) 'DY01-6810-',DIGIT,'-',CRAMP
      20 FORMAT(A10,A1,A1,A1)
C C16KEY = 'DY01-6810-'//DIGIT//'-3' ! CHANNEL 3 RAMP VOLTAGE SIGNAL
CALL CM_RRDAT(I_LFC,C16KEY,WVDATA,I_START,MAXRAW,I_GOT,IERR)
      IF (IERR .NE. 0) THEN
        CALL CM_ERR(IERR, MESSAGE, ERRSTATUS)
        WRITE(*,*)IERR, MESSAGE, ERRSTATUS
      END IF
WRITE(*,10)I_LFC, C16KEY, I_START, MAXRAW, I_GOT, IERR

C CHANNEL 4 IS NOT USED ANY MORE FOR THE SIGNAL AMPLITUDE.  NOW
C THE AMPLITUDE SIGNAL IS CALCULATED FROM THE I AND Q SIGNALS
C BY USING THE PITAGORA'S SQUARE ROOT LAW.
C C16KEY = 'DY01-6810-'//DIGIT//'-4'
C CALL CM_RRDAT(I_LFC,C16KEY,WADATA,I_START,MAXRAW,I_GOT,IERR)
C IF (IERR .NE. 0) THEN
C   CALL CM_ERR(IERR, MESSAGE, ERRSTATUS)
C   WRITE(*,*)IERR, MESSAGE, ERRSTATUS
C   END IF
C WRITE(*,10)I_LFC, C16KEY, I_START, MAXRAW, I_GOT, IERR

RETURN
END

```

!

C

C \*\*\*\*\*

C

SUBROUTINE CONVERT(

```

    I  MAXRAW ! ARRAY SIZE
    I , W1 ! INITIAL FREQUENCY
    I , W2 ! FINAL FREQUENCY
    I , IDIGIT ! DIGITIZER NUMBER
    I , I_STIMES ! STARTING TIME OF THE DIGITIZERS IN MILI SECONDS
    I , R_VOLTS ! VOLTAGES COMVERSION FACTORS FOR THE CHANNELS
    I , I_RATES ! DIGITIZATION RATE FOR THE DIGITIZERS
    I , IOFFSET ! OFFSET OF THE DIGITIZERS
    O , RAMPMIN !
    O , RAMPMAX !
    I , IDAT1 ! INITIAL DATA POINT
    I , IDAT2 ! FINAL DATA POINT
    I , I_GOT ! NUMBER OF POINTS ON THE "WORD" DATA
    I , WIDATA ! I SIGNAL WORD DATA
    I , WQDATA ! Q SIGNAL WORD DATA
    I , WVDATA ! RAMP VOLTAGE SIGNAL WORD DATA
    O , RIDATA ! REAL VOLTAGE OF THE I SIGNAL
    O , RQDATA ! REAL VOLTAGE OF THE Q SIGNAL
    O , RVDATA ! REAL VOLTAGE OF THE RAMP VOLTAGE
    O , RADATA ! REAL VOLAGE AMPLITUDE OF THE SIGNAL, NOT IN USE NOW
    O , WGHZ ! CORRESPONDING FREQUENCY ARRAY FOR THE SWEEPS
    O , TIME ! CORRESPONDING FREQUENCY ARRAY FOR THE SWEEPS
    O , II) ! GENERAL PURPOSE INDEX

```

C

C THIS SUBROUTINE CONVERTS THE WORD DATA INFORMATION INTO VOLTAGE DATA  
 IMPLICIT NONE

```

INTEGER I_GOT, MAXRAW, IDAT1, IDAT2, II, I, IOFFSET

```

```

    * , I_STIMES(2), I_RATES(2)
    * , IDIGIT ! DIGITIZER NUMBER
    * , ISHIFT

```

```

INTEGER*4 WIDATA(2*MAXRAW), WQDATA(2*MAXRAW), WVDATA(2*MAXRAW)

```

```

INTEGER*4 WITEMP, WQTEMP, WVTEMP, WATEMP

```

C

C THIS IS USED TO EXTRACT THE INFORMATION FROM THE WORD DATA.

C THE WORD DATA IS PASS TO THE TEMPORAL VARIABLES W\*TEMP WHICH

C ARE EQUIVALENT TO THE ARRAYS H\*TEMP(\*). SINCE THE

C INTEGER\*2 SIZE DEFINITION IS DIFFERENT, THE Half WORD CAN BE

C EXTRACTED BY CALLING THE DATA WITH THE ARRAY VARIABLES H\*TEMP(\*),

C THUS BREAKING THE 4 BYTES WORD IN W\*TEMP INTO 2 VARIABLES OF



```

C 2 BYTES NAMED H*TEMP(1) AND H*TEMP(2).
INTEGER*2 HITEMP(2), HQTEMP(2), HVTEMP(2), HATEMP(2)
EQUIVALENCE (WITEMP,HITEMP), (WQTEMP,HQTEMP), (WVTEMP,HVTEMP)
      * , (WATEMP,HATEMP)

REAL W1, W2, WDEL, WGHZ(0:2*MAXRAW), RIDATA(0:2*MAXRAW)
      * , RQDATA(0:2*MAXRAW), RVDATA(0:2*MAXRAW), RADATA(2*MAXRAW)
      * , TIME(0:2*MAXRAW), R_VOLTS(8), RAMPMIN, RAMPMAX
C
RAMPMAX = 0.0
RAMPMIN = 5.0
II = 0
IF (IDAT2 .GT. I_GOT) IDAT2 = I_GOT
ISHIFT = (IDIGIT - 1) * 4
DO I=IDAT1,IDAT2,1
  WITEMP = WIDATA(I)
  WQTEMP = WQDATA(I)
  WVTEMP = WVDATA(I)
  II = II + 1
  TIME(II) = FLOAT(2*IDAT1+II)/FLOAT(I_RATES(IDIGIT))
C    +    + I_STIMES(1)/1000.
    +    + I_STIMES(IDIGIT)/1000.
  RIDATA(II) = HITEMP(1)
  RQDATA(II) = HQTEMP(1)
  RVDATA(II) = HVTEMP(1)
  RIDATA(II) = R_VOLTS(ISHIFT+1) * (RIDATA(II)-IOFFSET) / 4096.
  RQDATA(II) = R_VOLTS(ISHIFT+2) * (RQDATA(II)-IOFFSET) / 4096.
  RVDATA(II) = R_VOLTS(ISHIFT+3) * (RVDATA(II)-IOFFSET) / 4096.
  RADATA(II) = SQRT(RIDATA(II)*RIDATA(II) + RQDATA(II)*RQDATA(II))
  RAMPMAX = MAX(RAMPMAX,RVDATA(II))
  RAMPMIN = MIN(RAMPMIN,RVDATA(II),0.0)
  II = II + 1
  TIME(II) = FLOAT(2*IDAT1+II)/FLOAT(I_RATES(IDIGIT))
C    +    + I_STIMES(1)/1000.
    +    + I_STIMES(IDIGIT)/1000.
  RIDATA(II) = HITEMP(2)
  RQDATA(II) = HQTEMP(2)
  RVDATA(II) = HVTEMP(2)
  RIDATA(II) = R_VOLTS(ISHIFT+1) * (RIDATA(II)-IOFFSET) / 4096.
  RQDATA(II) = R_VOLTS(ISHIFT+2) * (RQDATA(II)-IOFFSET) / 4096.
  RVDATA(II) = R_VOLTS(ISHIFT+3) * (RVDATA(II)-IOFFSET) / 4096.
  RADATA(II) = SQRT(RIDATA(II)*RIDATA(II) + RQDATA(II)*RQDATA(II))
  RAMPMAX = MAX(RAMPMAX,RVDATA(II))
  RAMPMIN = MIN(RAMPMIN,RVDATA(II))
END DO

```

```

1110 CONTINUE
RAMPMIN = MAX(RAMPMIN,0.0)
RIDATA(0) = II-4
RQDATA(0) = II-4
RVDATA(0) = II-4
RADATA(0) = II-4
TIME(0) = II-4
WGHZ(0) = II-4
C
WDEL = (W2-W1) / (RAMPMAX - RAMPMIN)
WRITE(11,*) W1,'=W1 ',RAMPMIN,'=RMIN ',RAMPMAX,'=RMAX '
      * ,WDEL,'=WDEL'
DO I = 1, WGHZ(0)
      WGHZ(I) = W1 + (RVDATA(I)-RAMPMIN) * WDEL
END DO
C
RETURN
END
!

C
C*****
C
SUBROUTINE GET_INDEX(
      I   I_RATE ! DIGITIZERS SAMPLING RATE
      I   , VMIN ! LOWER CLIPPING VOLTAGE
      I   , VMAX ! UPPER CLIPPING VOLTAGE
      I   , MAXRAW ! SIZE OF THE ARRAYS
      I   , DATA ! RAMP VOLTAGE DATA
      I   , AUTOLIM ! SET AUTOMATIC MIN/MAX LIMITS FOR SWEEP
      O   , INDEX ! ARRAY OF POINTERS FOR THE BEGINING OF THE DATA
      O   , INDEX2) ! ARRAY OF POINTERS FOR THE END OF THE DATA
C
C THIS SUBROUTINE DETERMINES WHERE THE REAL DATA STARTS AND ENDS
C BY USING THE RAMP VOLTAGE OF THE SWEEPER SOURCE.
IMPLICIT NONE
INTEGER MAXRAW, II, ISCAN, IMINOLD, IMINDEL, I, J, NSAMPLE
      * , I_RATE, NAVE, JMAX, AUTOLIM
INTEGER INDEX0(0:1000),INDEX(0:1000),INDEX2(0:1000),INDEX3(0:1000)
REAL DATA(0:2*MAXRAW), DER, VMIN, VMAX, DATMAX, AVEO
LOGICAL GOT_0, GOT_MIN, GOT_MAX, GOT_MAX3
C Which one came first: the Chicken or the Egg ?
C How comes first to give you presents: Santa Clauss or the 3 Wise Man ?
GOT_0 = .FALSE.
GOT_MIN = .TRUE.

```

```
GOT_MAX = .TRUE.
GOT_MAX3 = .TRUE.
C
J = 1
DO I = 1 , DATA(0)
C
  IF ( (GOT_0 .EQ. .FALSE.)
    * .AND. (DATA(I) .GE. VMIN )
    * .AND. (DATA(I+1) .LT. VMIN )
    * ) THEN
    INDEX0(J) = I
    GOT_0 = .TRUE.
    GOT_MIN = .FALSE.
  END IF
C
  IF ( (GOT_MIN .EQ. .FALSE.)
    * .AND. (DATA(I) .LE. VMIN )
    * .AND. (DATA(I+1) .GT. VMIN )
    * ) THEN
    INDEX(J) = I
    GOT_MIN = .TRUE.
    GOT_MAX = .FALSE.
  END IF
C
  IF ( (GOT_MAX .EQ. .FALSE. )
    * .AND. (DATA(I) .LE. VMAX )
    * .AND. (DATA(I+1) .GT. VMAX )
    * ) THEN
    INDEX2(J) = I
    GOT_MAX = .TRUE.
    GOT_MAX3 = .FALSE.
  END IF
C
  IF ( (GOT_MAX3 .EQ. .FALSE. )
    * .AND. (DATA(I) .GE. VMAX )
    * .AND. (DATA(I+1) .LT. VMAX )
    * ) THEN
    INDEX3(J) = I
    GOT_MAX3 = .TRUE.
    GOT_0 = .FALSE.
    J = J + 1
  END IF
END DO
INDEX0(0) = J - 1
INDEX(0) = J - 1
```

```

INDEX2(0) = J - 1
INDEX3(0) = J - 1

WRITE(11,*)' VMIN=',VMIN,' VMAX=',VMAX
WRITE(11,*)(DATA(INDEX(I)),DATA(INDEX2(I)), I=1,INDEX(0) )
CHERE
IF( AUTOLIM .EQ. 1 )THEN

NAVE = 20
DO I = 1, INDEX0(0)
  AVEO = 0.0
  DO J = INDEX0(I), INDEX(I), (INDEX(I)-INDEX0(I))/NAVE
    AVEO = AVEO + DATA(J)
  END DO
  AVEO = AVEO / (NAVE+1)
  WRITE(11,*)I,AVEO,'=AVEO '
  DO J = INDEX(I)-1, INDEX0(I), -1
    IF( (DATA(J).LE.AVEO) .AND. (AVEO.LT.DATA(J+1)) ) GOTO 10
  END DO
  10  INDEX(I) = J
  WRITE(11,*)I, INDEX(I),'=INDEX',DATA(INDEX(I))
C
  DATMAX = DATA(INDEX2(I))
  DO J = INDEX2(I)+1, INDEX3(I)
    IF(DATA(J) .GT. DATMAX) THEN
      DATMAX = DATA(J)
      JMAX = J
    END IF
  END DO
  INDEX2(I) = JMAX
  WRITE(11,*)I, INDEX2(I),'=INDEX2 ',DATA(INDEX2(I))
END DO

END IF
C
RETURN
END
!

C
C *****
C
SUBROUTINE YO_CAL(
  *   INDEX ! ARRAY OF POINTERS FOR THE BEGINING OF THE DATA
  *   , WGHZ ! ARRAY OF FREQUENCY DATA

```

```

      * , PHASE ) ! ARRAY OF THE PHASE DATA
C
C READ AND SUBTRACT THE CALIBRATION DATA FROM THE REAL DATA.
IMPLICIT NONE
REAL WGHZ(0:*), PHASE(0:*), CAL_WG(0:1000), CAL_PH(0:1000)
      * , BYPAS1, BYPAS2, CALDAT, W1, W2, W3, SUM, CALO
INTEGER INDEX(0:1000), I, J, K, ICAL
C
C THIS IS THE DATA FOR BYPASS WAVEGUIDE #1
OPEN(55,FILE='[ICOLLAZO.WILGEN.CAL]WBYPAS1.CAL',STATUS='OLD')
READ(55,*) ! JUMP THE FIRST LINE, i.e., THE DATA HEADER
READ(55,*) BYPAS1 ! READ THE NUMBER OF DATA POINTS IN THE FILE
C THIS IS THE DATA FOR BYPASS WAVEGUIDE #2
OPEN(56,FILE='[ICOLLAZO.WILGEN.CAL]WBYPAS2.CAL',STATUS='OLD')
READ(56,*) ! JUMP THE FIRST LINE, i.e., THE DATA HEADER
READ(56,*) BYPAS2 ! READ THE NUMBER OF DATA POINTS IN THE FILE
C THIS IS THE DATA FOR THE CALIBRATION OF THE FULL WAVEGUIDE
OPEN(57,FILE='[ICOLLAZO.WILGEN.CAL]WAVEGUIDE.CAL',STATUS='OLD')
READ(57,*)CALO ! JUMP THE FIRST LINE, i.e., THE DATA HEADER
READ(57,*) CALDAT ! READ THE NUMBER OF DATA POINTS IN THE FILE
CAL_PH(0) = MIN(BYPAS1, BYPAS2, CALDAT) ! FIND THE MINIMUM DATA POINTS
CAL_WG(0) = CAL_PH(0)
CAL_WG(1) = 0.0
CAL_PH(1) = 0.0
DO I = 2, CAL_PH(0) ! CALCULATE CALIBRATION DATA
  READ(55,*) W1, BYPAS1
  READ(56,*) W2, BYPAS2
  READ(57,*) W3, CALDAT
  CAL_WG(I) = (W1+W2+W3) / 3.
  CAL_PH(I) = BYPAS1 - BYPAS2 + CALDAT + CALO
END DO
CLOSE(55)
CLOSE(56)
CLOSE(57)
CAL_PH(0) = CAL_PH(0) + 1
CAL_PH(1) = CAL_PH(2)
CAL_WG(CAL_PH(0)) = 130.
CAL_PH(CAL_PH(0)) = CAL_PH(CAL_PH(0)-1)
DO I = 1, INDEX(0)
C ICAL = MIN( PHASE(INDEX(I)) , CAL_PH(0) )
  DO J = 1, PHASE(INDEX(I))
    DO K = 1, CAL_PH(0)
      IF ( (WGHZ(INDEX(I)+J) .GE. CAL_WG(K))
*        .AND. (WGHZ(INDEX(I)+J) .LT. CAL_WG(K+1)) )
*        THEN ! INTERPOLATE TO GET ACURATE VALUE FOR CALIBRATION

```

```

PHASE(INDEX(I)+J) = PHASE(INDEX(I)+J) - (
    + (CAL_PH(K+1)-CAL_PH(K)) / (CAL_WG(K+1)-CAL_WG(K)) *
    * (WGHZ(INDEX(I)+J) - CAL_WG(K)) +
    + CAL_PH(K) )
    END IF
    END DO
    END DO
END DO
C
RETURN
END
!

C
C *****
C
SUBROUTINE COMPRES(
    I    NPICK ! SKIP ON THE NUMBER OF POINTS
    I , MAXRAW ! SIZE OF THE ARRAYS
    I , INDEX ! ARRAY OF POINTERS FOR THE BEGINING OF THE DATA
    I , INDEX2 ! ARRAY OF POINTERS FOR THE END OF THE DATA
    I , RAD_MIN ! MINIMUM VOLATAGE FOR CLIP-OFF
C    N , RASMOTH ! ARRAY OF SMOOTHED SIGNAL AMPLITUDE
    O , RIDATA ! ARRAY OF THE I SIGNAL REAL VOLTAGE DATA
    O , RQDATA ! ARRAY OF THE Q SIGNAL REAL VOLTAGE DATA
    O , RVDATA ! ARRAY OF THE RAMP VOLTAGE DATA
    O , RADATA ! ARRAY OF THE SIGNAL AMPLITUDE VOLTAGE DATA
    O , WGHZ ! ARRAY OF THE FREQUENCY DATA
    O , TIME) ! ARRAY OF THE TIME DATA
C
C THIS SUBROUTINE COMPRESSES THE DATA BY WRITING OVER THE
C RETRACE DATA POINTS
IMPLICIT NONE
INTEGER MAXRAW, INDEX(0:1000), INDEX2(0:1000), I, J, IJ
    * , ISTART, NPICK, K, NCOUNT, JK
REAL RIDATA(0:MAXRAW), RQDATA(0:MAXRAW), RVDATA(0:MAXRAW)
    * , RADATA(0:MAXRAW), WGHZ(0:MAXRAW), TIME(0:MAXRAW)
    * , SUMRI, SUMRQ, SUMRA, SUMRV, SUMW, SUMT, RAD_MIN
C    N , RASMOTH(0:MAXRAW) ! ARRAY OF SMOOTHED SIGNAL AMPLITUDE
C
IJ = 0
DO I = 1, INDEX(0)
    IJ = IJ + 1
    ISTART = IJ
    DO J = INDEX(I), INDEX2(I), NPICK

```

```
SUMRI = 0.0
SUMRQ = 0.0
SUMRA = 0.0
SUMRV = 0.0
SUMW = 0.0
SUMT = 0.0
NCOUNT = 0
DO K = 0, NPICK-1
  JK = J + K
  IF( RADATA(JK) .GE. RAD_MIN ) THEN
C    IF( RADATA(JK) .GE. RASMOTH(JK) ) THEN
      NCOUNT = NCOUNT + 1
      SUMRI = SUMRI + RIDATA(JK)
      SUMRQ = SUMRQ + RQDATA(JK)
      SUMRA = SUMRA + RADATA(JK)
      SUMRV = SUMRV + RVDATA(JK)
      SUMW = SUMW + WGHZ(JK)
      SUMT = SUMT + TIME(JK)
    END IF
  END DO
  IF( NCOUNT .GT. 0 ) THEN
    IJ = IJ + 1
    RIDATA(IJ) = SUMRI / NCOUNT
    RQDATA(IJ) = SUMRQ / NCOUNT
    RVDATA(IJ) = SUMRV / NCOUNT
    RADATA(IJ) = SUMRA / NCOUNT
    WGHZ(IJ) = SUMW / NCOUNT
    TIME(IJ) = SUMT / NCOUNT
  END IF
END DO
  RIDATA(ISTART) = IJ - ISTART
  RIDATA(ISTART) = IJ - ISTART
  RVDATA(ISTART) = IJ - ISTART
  RADATA(ISTART) = IJ - ISTART
  WGHZ(ISTART) = IJ - ISTART
  TIME(ISTART) = IJ - ISTART
INDEX(I) = ISTART
INDEX2(I) = IJ
END DO
RIDATA(0) = IJ
RQDATA(0) = IJ
RVDATA(0) = IJ
RADATA(0) = IJ
WGHZ(0) = IJ
TIME(0) = IJ
```

```

C
RETURN
END
!

C
C *****
C
SUBROUTINE IQ_AVE(INDEX,WGHZ,RIDATA,RQDATA,WGHZAVE,RIAVE,RQAVE)
IMPLICIT NONE
INTEGER INDEX(0:1000), I, J, JO, NDAT(1000)
REAL RMAX, WGHZ(0:*), RIDATA(0:*), RQDATA(0:*), WGHZAVE(0:*)
    * , RIAVE(0:*), RQAVE(0:*)
DO J = 1, WGHZAVE(0)
    WGHZAVE(J) = 0.0
    RIAVE(J) = 0.0
    RQAVE(J) = 0.0
    NDAT(J) = 0
END DO
RMAX = RIDATA(INDEX(1))
DO I=1, INDEX(0)
    RMAX = MIN(RMAX,RIDATA(INDEX(I)))
    JO = INDEX(I)
    DO J=1, RIDATA(JO)
        WGHZAVE(J) = WGHZAVE(J) + WGHZ(J+JO)
        RIAVE(J) = RIAVE(J) + RIDATA(J+JO)
        RQAVE(J) = RQAVE(J) + RQDATA(J+JO)
        NDAT(J) = NDAT(J) + 1
    END DO
END DO
C CALCULATE THE AVERAGE FREQUENCY AND PHASE
DO J = 1, RMAX
    WGHZAVE(J) = WGHZAVE(J) / NDAT(J)
    RIAVE(J) = RIAVE(J) / NDAT(J)
    RQAVE(J) = RQAVE(J) / NDAT(J)
END DO
    WGHZAVE(0) = J-1
    RIAVE(0) = J-1
    RQAVE(0) = J-1

RETURN
END
!

C

```



```

C *****
C
SUBROUTINE PH_SORT(INDEX,WGHZ,PHASE,RWGHZ,RPHASE)
IMPLICIT NONE
INTEGER INDEX(0:1000), I, J, NC, JJ, NMIN, INDEXI
REAL WGHZ(0:*), PHASE(0:*), RWGHZ(0:*), RPHASE(0:*)
    * , WMIN, RP
C MOVE DATA TO THE SORTING ARRAY
NC = 0
DO I = 1, INDEX(0)
    INDEXI = INDEX(I)
    DO J = 1, WGHZ(INDEXI)
        NC = NC + 1
        JJ = J + INDEXI
        RPHASE(NC) = PHASE(JJ)
        RWGHZ(NC) = WGHZ(JJ)
    END DO
END DO
RPHASE(0) = NC
RWGHZ(0) = NC
C
C SORT THE NUMBERS
DO I = 1, RWGHZ(0)
    NMIN = I
    WMIN = RWGHZ(NMIN)
    DO J = I+1, RWGHZ(0)
        IF( RWGHZ(J) .LT. WMIN ) THEN
            NMIN = J
            WMIN = RWGHZ(NMIN)
        END IF
    END DO
    RWGHZ(NMIN) = RWGHZ(I)
    RWGHZ(I) = WMIN
    RP = RPHASE(I)
    RPHASE(I) = RPHASE(NMIN)
    RPHASE(NMIN) = RP
C WRITE(*,*) I, RWGHZ(I), RPHASE(I)
END DO

RETURN
END
!

C
C *****

```

C

```

SUBROUTINE DAT_AVE(
  I   MAXRAW ! SIZE OF ARRAYS
  I , IAYER ! NUMBER OF SWEEPS TO AVERAGE BY
  I , INDEX ! ARRAY OF POINTERS FOR THE BEGINING OF THE DATA
  I , INDEX2 ! ARRAY OF POINTERS FOR THE END OF THE DATA
  O , RIDATA ! ARRAY OF I SIGNAL VOLTAGE DATA
  O , RQDATA ! ARRAY OF Q SIGNAL VOLTAGE DATA
  O , RVDATA ! ARRAY OF RAMP VOLTAGE SIGNAL VOLTAGE DATA
  O , RADATA ! ARRAY OF THE SIGNAL AMPLITUDE VOLTAGE DATA
  O , RASIG ! STANDARD DEVIATION DATA ARRAY
  O , ISIGMA ! PLOTTING FLAG VARIABLE
  O , WGHZ ! ARRAY OF THE FREQUENCY
  O , TIME) ! ARRAY OF THE TIME DATA

```

C

```

C THIS SUBROUTINE MAKES AN AVERAGE OF THE SWEEPTS TO REDUCE THE
C NOICE AND THE EFFECT OF FLUTUATIONS
IMPLICIT NONE

```

```

INTEGER MAXRAW, INDEX(0:1000), INDEX2(0:1000)
  * , I, II, J, K, IAYER, MPTS, ISIGMA
REAL RIDATA(0:2*MAXRAW), RQDATA(0:2*MAXRAW), RVDATA(0:2*MAXRAW)
  * , RADATA(0:2*MAXRAW), WGHZ(0:2*MAXRAW), TIME(0:2*MAXRAW)
  * , RASIG(0:2*MAXRAW), SUMSIG, RA, RAI1
  * , SUMI, SUMQ, SUMV, SUMA, SUMW, SUMT

```

C

```

IF ( IAYER .EQ. 1 ) RETURN
IF ( IAYER .LE. 0 ) THEN
  WRITE(*,*) ' ***** ERROR FROM SUBROUTINE DAT_AVE: '
  WRITE(*,*) ' ***** ', IAYER, '=IAYER MOST BE = 1 OR BIGGER.'
  WRITE(*,*) ' ***** NO AVERAGING DONE TO THE DATA. '
ELSE
  II = 0
  DO I = 1, (INDEX(0)-IAYER) , IAYER
    MPTS = RIDATA(INDEX(I))
    DO K = I+1 , I+IAYER-1
      MPTS = MIN(FLOAT(MPTS),RIDATA(INDEX(K)))
    END DO

    II = II + 1
    RIDATA(II) = MPTS
    RQDATA(II) = MPTS
    RVDATA(II) = MPTS
    RADATA(II) = MPTS
    RASIG(II) = MPTS
    WGHZ(II) = MPTS
  END DO

```

```

TIME(II)  = MPTS
DO J = 1 , MPTS
  SUMI = 0.0
  SUMQ = 0.0
  SUMV = 0.0
  SUMA = 0.0
  SUMW = 0.0
  SUMT = 0.0
  II = II + 1
  DO K = 0 , IAVR-1
    SUMI = SUMI + RIDATA(J + INDEX(I+K))
    SUMQ = SUMQ + RQDATA(J + INDEX(I+K))
    SUMV = SUMV + RVDATA(J + INDEX(I+K))
    SUMA = SUMA + RADATA(J + INDEX(I+K))
    SUMW = SUMW +  WGHZ(J + INDEX(I+K))
    SUMT = SUMT +  TIME(J + INDEX(I+K))
  END DO
  RIDATA(II) = SUMI / IAVR
  RQDATA(II) = SUMQ / IAVR
  RVDATA(II) = SUMV / IAVR
  RADATA(II) = SUMA / IAVR
  WGHZ(II)   = SUMW / IAVR
  TIME(II)   = SUMT / IAVR
END DO
INDEX(1+I/IAVR) = II - MPTS
INDEX2(1+I/IAVR) = II
END DO
INDEX(0) = INDEX(0) / IAVR
INDEX2(0) = INDEX(0)
END IF
RETURN
END
!

C
C *****
C
SUBROUTINE YO_PHASE(
  I  INDEX ! ARRAY OF POINTERS OF THE BEGINING OF THE DATA
  I , RIDATA ! ARRAYS OF I SIGNAL DATA
  I , RQDATA ! ARRAYS OF Q SIGNAL DATA
  O , PHASE) ! RAW PHASE DATA
C
C THIS SUBROUTINE CALCULATES THE RAW PHASE OUT OF THE I/Q SIGNAL
IMPLICIT NONE

```

```

REAL RIDATA(0:*), RQDATA(0:*), PHASE(0:*), SKIP, PMIN, PI
INTEGER I, J, K, INDEX(0:1000), INDEX2(0:1000)
C
PI = 3.14159265
DO I = 1, INDEX(0)
  PHASE(INDEX(I)) = RIDATA(INDEX(I))
  DO K = 1, RIDATA(INDEX(I))
    J = K + INDEX(I)
    IF ((RIDATA(J).EQ. 0.0) .AND. (RQDATA(J).EQ. 0.0)) THEN
      WRITE(*,*) ' PHASE DATA IS ALL ZERO, PATCHING UP TO CONTINUE'
      WRITE(*,*) I, J
      PHASE(J) = 0.0
    ELSE
      PHASE(J) = ATAN2(RQDATA(J), RIDATA(J)) / (2.*PI)
    END IF
  END DO
END DO
PHASE(0) = INDEX(INDEX(0)) + RIDATA(INDEX(INDEX(0)))
C
RETURN
END
!

C
C *****
C
SUBROUTINE PH_COUNT(
  I DER1 ! VALUE FOR THE DERIVATIVE CRITERIUM
  I , AMP1 ! VALUE FOR THE AMPLITUDE CRITERIUM
  * , INDEX ! ARRAY OF POINTERS FOR THE BEGINING OF THE DATA
  * , PHASE ! PHASE DATA
  * , PHDER) ! PHASE DERIVATIVE
C
C THIS SUBROUTINE DOES THE PHASE TRACKING AND PHASE COUNTING ON
C THE RAW PHASE DATA
REAL PHASE(0:*), PHDER(0:*), SKIP, PMIN, DER1, AMP1, PHTEMP
INTEGER I, J, K, INDEX(0:1000), INDEXI

DO I = 1, INDEX(0)
  INDEXI = INDEX(I)
  PHDER(INDEXI) = PHASE(INDEXI)
  DO K = 1, PHASE(INDEXI) - 1
    J = K + INDEXI
    PHDER(J) = PHASE(J+1) - PHASE(J)
  END DO

```

```

      PHDER(J+1) = PHDER(J)
END DO
PHDER(0) = PHASE(INDEX(0))
C
DO I = 1, INDEX(0)
  SKIP = 0.0
  INDEXI = INDEX(I)
  DO K = 1, PHASE(INDEXI)
    J = K + INDEXI
    PHTEMP = PHASE(J)
    PHASE(J) = PHTEMP + SKIP
    IF((PHDER(J).LT.-DER1) .AND. (PHTEMP.GT.AMP1)) THEN
      SKIP = SKIP + 1.
    ELSE
      IF((PHDER(J).GT.DER1) .AND. (PHTEMP.LT.-AMP1)) THEN
        SKIP = SKIP - 1.
      END IF
    END IF
  END DO
C
  PMIN = PHASE(INDEX(I)+1)
  DO K = 1, PHASE(INDEX(I))
    PMIN = MIN(PMIN,PHASE(K+INDEX(I)))
  END DO
  IF ( PMIN .LT. 0.0) THEN
    DO J = 1, PHASE(INDEX(I))
      PHASE(J+INDEX(I)) = PHASE(J+INDEX(I)) + INT(-PMIN) + 1
    END DO
  END IF
END DO
C
RETURN
END
!

C
C *****
C
      SUBROUTINE YO_INFO (
      I I_SHOT, ! SHOT NUMBER
      O I_STIMES, ! STARTING TIMES FOR THE DIGITIZERS
      O R_VOLTS, ! VOLTAGE CONVERSION FACTORS
      O I_OFFSETS, ! DIGITIZERS OFFSETS
      O I_RATES, ! DIGITIZERS SAMPLING RATES
      O I_ACTCHN, ! ACTIVE CHANNELS

```

```

      0 I_SMPCHN, ! SAMPLING CHANNELS
      0 C_COMNTS, ! COMMENTS LINES
      0 IERR ) ! ERROR CODE
*
*   THIS SUBROUTINE RETURNS THE TIMING AND SETUP INFORMATION STORED
*   IN THE PFT CORRESPONDING TO I_SHOT FOR THE YO DIGRAPH.
*
*   INPUT:      I_SHOT -- THE SHOT NUMBER IN QUESTIONS
*
*   OUTPUT:     IERR      - ERROR RETURN STATUS; 0=NO ERROR
*               I_STIMES  - THE START TIMES OF THE TIMING MODULES (MSEC)
*               R_VOLTS   - THE FULL SCALE VOLTAGES FOR EACH CHANNEL (V)
*               I_OFSETS  - THE OFFSETS FOR EACH CHANNEL
*               I_RATES   - THE DIGITIZATION RATES (KHZ) FOR EACH 6810
*               I_ACTCHN  - NUMBER OF ACTIVE CHANNELS FOR EACH 6810
*               I_SMPCHN  - NUMBER OF SAMPS/CHANNEL FOR EACH 6810, KHZ
*               C_COMNTS  - PFT COMMENTS
*
*   RETURNS:    NONE
*
*   PROGRAMMER:  J. THOMAS ECK
*
*   MODIFICATIONS: 09/14/92 JTE -- INITIAL RELEASE
*
*   CALLS:       CM_NAME
*               CM_KROPE
*               YO__GT2S
*               YO__GTDV
*               CM_KRINT
*               CM_KCLOS
*
*****
      IMPLICIT NONE
C
C-----/INCLUDE FILES
C
      INCLUDE 'USER2:[ICOLLAZO.YO]YOIPAR.'
      INCLUDE 'USER2:[ICOLLAZO.YO]YOIDVLST.'
C-----
C PARAMETERS
C
      INTEGER*4 N_68WRDS      ! NUMBER OF WORDS IN 6810 BUFFERS
      PARAMETER (N_68WRDS = 36)
C

```

C-----/DECLARATIONS  
C

```

      CHARACTER*1
      L          C1IDENT,
      I          C1_FTYPE

      CHARACTER*2
      L          C2DIGRPH

      CHARACTER*16
      L          C16KEY,
      L          C16TYPE,
      L          C16PNAME,
      L          C16TMODS (N_TMOD)

      CHARACTER*(*)
      O          C_COMNTS (N_COMMENT) ! PFT COMMENTS

      INTEGER*4
      I          I_SHOT,
      O          I_STIMES (N_TMOD),      ! TIMING MODULE TRIG TIMES, MSEC
      O          I_RATES (N_6810),      ! 6810 DIGITIZATION RATES
      O          I_OFFSETS (N_6810*N_MAXCHAN), ! 6810 CHANNEL OFFSETS
      O          I_ACTCHN (N_6810),      ! ACTIVE CHANNELS FOR EACH 6810
      O          I_SMPCHN (N_6810),      ! SAMPLES/CHANNEL FOR EACH 6810
      O          IERR,
      L          IERR2,
      L          I, J, K,
      L          I_INDEX,
      L          I_START,
      L          I_GOT,
      L          I_LFC,
      L          I_TOTAL,
      L          NUMKEYS,
      L          NUMWORDS,
      L          ISPECIAL (5, MAX_DEV),
      L          I_6810_A (N_68WRDS),
      L          I_6810_B (N_68WRDS),
      L          I_DRATES (0:17)          ! 6810 DIGITIZATION RATE CODES

      INTEGER*2
      L          IDIGITAL (MAX_DEV + 1)

      REAL*4
      L          R_DELMS,

```

```

      L          R_VCODES (0:7),          ! 6810 CHANNEL VOLTAGE CODES
      L          R_VOLTS (N_6810 * N_MAXCHAN) ! 6810 CHANNEL FULL SCALE VOLTAGE

C -----
C EQUIVALENCES
C
INTEGER*4 I_DSM( 90 )
CHARACTER*1 C1_DSM( 4*90 )
      EQUIVALENCE (I_DSM, C1_DSM)
!

C
C-----/DATA FOR KEYWORD FILE
C
      DATA
+      C2DIGRPH   / 'Y0'   /,
+      C1IDENT    / 'T'    /,
+      C16TYPE     / 'PARAMETER' /,
+      I_LFC       / 8      /,
+
+      I_TOTAL     / MAX_DEV /

      DATA C16TMDS
      . /
      . 'DY01-TM-CH1' ,
      . 'DY01-TM-CH2' ,
      . /

C
C-----/DATA FOR CLOCK CODES
C
      DATA ( I_DRATES(I), I=0, 17 )
+ /
+      0,          ! REALLY MEANS EXTERNAL CLOCK
+      20,          50,   100,   200,   500,
+      1000,        2000,  5000,  10000, 20000,
+      50000,       100000, 200000, 500000, 1000000,
+      2000000, 5000000
+ /

C
C-----/DATA FOR FULL-SCALE VOLTAGE CODES
C
      DATA ( R_VCODES(I), I=0,7 )
      . /
      . 0.4096,
```



```

.    1.024,
.    2.048,
.    4.096,
.   10.24,
.   25.60,
.   51.20,
.  102.4
.    /

!

*****
*           *
* EXECUTABLE CODE *
*           *
*****

I_START = 1
C
C-----/CREATE PFT FILENAME
C
    CALL CM_NAME (
I          C2DIGRPH,
I          C16TYPE,
I          C1IDENT,
I          I_SHOT,
O          C16PNAME,
O          IERR )

    IF (IERR .NE. 0) THEN
        CALL AA_ERR ('CM_NAME', 'YO_INFO', IERR)
    END IF
C
C-----/OPEN THE PARAMETER FILE
C
    CALL CM_KROPE (
I          I_LFC,
I          C2DIGRPH,
I          C16PNAME,
O          NUMKEYS,
O          NUMWORDS,
O          IERR)
    IF (IERR .NE. 0) THEN
        IF (IERR .EQ. 8) WRITE(*, '(1XA25)')

```

```

      'PFT FILE IS NOT AVAILABLE'
      CALL AA_ERR ('CM_KROPE', 'YO_INFO', IERR)
      GOTO 999 ! FATAL ERROR -----G-O-T-O----->
    END IF

C
C-----/GET 2SEC DATA
C
      CALL YO_GET2S
      I      (I_LFC,
      0      ISPECIAL,
      0      IDIGITAL)

C
C-----/READ THE DEVICE LIST
C
      CALL YO_GETDV
      I      (I_LFC ,
      I      I_TOTAL,
      0      I_DVLST)

C
C-----/READ DSM KEY
C
      C16KEY = 'DIGRAPH_MEMORY__'

      CALL CM_KRINT (
      I      I_LFC      ,
      I      C16KEY      ,
      0      I_DSM      ,
      I      I_START     ,
      I      90          ,      !# OF POINTS TO READ
      0      I_GOT       ,
      0      IERR        )

!

      IF (IERR .NE. 0) THEN
        CALL AA_ERR ('CM_KRINT', C16KEY // ' FROM YO_INFO', IERR)
      END IF

C
C-----/LOAD DIGITIZER PARAMETERS
C
      ! ==== LOAD PARAMETERS FOR 6810'S
      C16KEY = 'L6810_A_-----'

      CALL CM_KRINT (
      I      I_LFC      ,

```

```

I          C16KEY      ,
O          I_6810_A    ,
I          I_START     ,
I          N_68WRDS    ,      !# OF POINTS TO READ
O          I_GOT       ,
O          IERR        )

IF (IERR .NE. 0) THEN
    CALL AA_ERR ('CM_KRINT', C16KEY // ' FROM YO_INFO', IERR)
END IF

C16KEY = 'L6810_B_-----'

CALL CM_KRINT (
I          I_LFC       ,
I          C16KEY      ,
O          I_6810_B    ,
I          I_START     ,
I          N_68WRDS    ,      !# OF POINTS TO READ
O          I_GOT       ,
O          IERR        )

IF (IERR .NE. 0) THEN
    CALL AA_ERR ('CM_KRINT', C16KEY // ' FROM YO_INFO', IERR)
END IF

C
C-----/CONVERT AND STORE DIGITIZATION RATES
C
I_RATES( 1 ) = I_DRATES( I_6810_A( 31 ) )
I_RATES( 2 ) = I_DRATES( I_6810_B( 31 ) )
C
C-----/STORE ACTIVE CHANNELS
C
I_ACTCHN( 1 ) = I_6810_A( 17 )
I_ACTCHN( 2 ) = I_6810_B( 17 )
C
C-----/STORE SAMPLES/CHANNEL
C
I_SMPCHN( 1 ) = 2**I_6810_A( 27 )
I_SMPCHN( 2 ) = 2**I_6810_B( 27 )
C
C-----/STORE THE FULL SCALE VOLTAGES & OFFSETS
C
! ===== FOR EACH 6810 CHANNEL...
DO I = 1, N_MAXCHAN

```

```

      ! ==== STORE THE F.S.V. AND OFFSET FOR DIGITIZER A
      R_VOLTS( I ) = R_VCODES( I_6810_A( I+1 ) )
      I_OFFSETS( I ) = I_6810_A( I+17 )

      ! ==== STORE THE F.S.V. AND OFFSET FOR DIGITIZER B
      R_VOLTS( I+N_MAXCHAN ) = R_VCODES( I_6810_B( I+1 ) )
      I_OFFSETS( I+N_MAXCHAN ) = I_6810_B( I+17 )

      ENDDO ! I = 1, N_MAXCHAN

C
C-----/STORE COMMENTS
C
! ==== FLIP WORDS TO CONVERT FROM SEL->VAX BYTE ORDERING
CALL CM_FLIP( I_DSM, 90 )

      I_START = 34 ! START OF COMMENTS IN I1_DSM: MUST BE CHANGED IF
                   ! SEL DSM INCLUDE FILE (YOIDSM) IS MODIFIED

! ==== STORE CHARS FOR RETURN
DO J = 1, N_COMMENT
DO K = 1, N_COMLNGTH
I_INDEX = ( ( K-1 ) * N_COMMENT ) + J ) + I_START
C_COMNTS( J )( K:K ) = C1_DSM( I_INDEX )
ENDDO ! K = 1, N_COMLNGTH
ENDDO ! J = 1, N_COMMENT

C
C-----/DECODE AND STORE TIMING MODULE
C                                TRIGGER TIMES
! ==== FOR EACH TIMING MODULE...
DO I = 1, N_TMOD
      C16KEY = C16TMODS( I )

      ! ==== LOCATE NAME IN DEVICE LIST
      CALL YO_INDEX (
I              C16KEY,
O              I_INDEX,
O              IERR )

      ! ==== DECODE THE TRIGGER TIME
      CALL AA_TMTM (
I              ISPECIAL( 1, I_INDEX ),
O              R_DELMS,
O              IERR )

```

```

        IERR = 0

        ! ==== CONVERT AND STORE FOR RETURN
        I_STIMES( I ) = INT( R_DELMs )
        ENDDO ! I = 1, N_TMOD
C
C-----/CLOSE THE PFT
C
!

        CALL CM_KCLOS (
            I           I_LFC,
            0           IERR2)

        IF (IERR2 .NE. 0) THEN
            CALL AA_ERR ('CM_KCLOS', 'FROM YO_INFO', IERR2)
        END IF
C
C-----/END OF YO_INFO
C
999  CONTINUE
      RETURN
      END
!

C
*****
*
*      SUBROUTINE YO_GET2S (
*          I           I_LFC,
*          0           ISPECIAL,
*          0           IDIGITAL)
*
*      THIS SUBROUTINE READS THE OPEN PFT ASSOCIATED WITH I_LFC AND
*      RETURNS THE SPECIAL AND DIGITAL ARRAYS
*
*      INPUT:      I_LFC -- THE LFC FOR THE CURRENTLY OPEN PFT
*
*      OUTPUT:     ISPECIAL
*                  IDIGITAL
*
*      RETURNS:
*
*      PROGRAMMER:  J. THOMAS ECK

```

```

*
* LAST MODIFIED:      9/14/92 JTE -- CLONED FROM RP__GT2S
*
*****

C
C-----/DECLARATIONS
C
    IMPLICIT NONE

    INTEGER*4    MAX_KEYS

    PARAMETER (MAX_KEYS = 2)

C
C-----/INCLUDE FILE
C
    INCLUDE 'USER2:[ICOLLAZO.YO]YOIPAR.'          !CONTAINS MAX_DEV

C -----
C DECLARATIONS
C
    CHARACTER*16
    +          KEY (MAX_KEYS)

    INTEGER*4
    +          IERR, I_LFC, I,
    +          I4_DATA (MAX_DEV),
    +          ISPECIAL (5,MAX_DEV),
    +          NUMGOT,
    +          ISTART,
    +          LENGTH (MAX_KEYS)

    INTEGER*2
    +          I2_DUM,
    +          IDIGITAL (MAX_DEV + 1),
    +          I2_DATA (MAX_DEV + 1)

C
C-----/EQUIVALENCE
C
    EQUIVALENCE
    +          (I4_DATA, I2_DATA)

C
C-----/DATA FOR KEYWORD FILE

```

C

```

      DATA KEY
      . /
      .      'GETPD_SPECIAL___',
      .      'GETPD_DIGITAL___'
      . /

      LENGTH (1) = MAX_DEV*5
      LENGTH (2) = MAX_DEV

      DATA ISTART / 1 /

!

*****
*                               *
* EXECUTABLE CODE *
*                               *
*****

      ! ==== READ ISPECIAL
      CALL CM_KRINT (I_LFC,
      +             KEY (1),
      +             ISPECIAL (1,1),
      +             ISTART,
      +             LENGTH (1),
      +             NUMGOT,
      +             IERR)
      IF (IERR .NE. 0) THEN
         CALL CI_ERR ('CM_KRINT', KEY (1) //' FROM YO_GET2S', IERR)
      END IF

!

      ! ==== READ IDIGITAL
      CALL CM_KRINT (I_LFC,
      +             KEY (2),
      +             I4_DATA,
      +             ISTART,
      +             LENGTH (2),
      +             NUMGOT,
      +             IERR)
      IF (IERR .NE. 0) THEN
         CALL CI_ERR ('CM_KRINT', KEY (2) //' FROM YO_GET2S', IERR)

```

```

      END IF
C
C-----/UNPACK AND FLIP HALFWORDS
C
      DO I=1, MAX_DEV, 2                !UNPACK I*4 DATA TO I*2
        I2_DUM = I2_DATA (I)
        IDIGITAL (I) = I2_DATA (I+1)
        IDIGITAL (I+1) = I2_DUM
      END DO
C
C-----/END OF YO_GET2S
C
      RETURN
      END
!

C
*****
*
      SUBROUTINE YO_GETDV (
      I          I_LFC,
      I          I_TOTAL,
      O          I_DVLIST)
*
*   THIS SUBROUTINE RETURNS THE DEVICE LIST STORED IN THE CURRENTLY
*   OPEN PFT ASSOCIATED WITH I_LFC.
*
*   INPUT:      I_LFC -- LFC OF CURRENTLY OPEN PFT
*               I_TOTAL- TOTAL NUMBER OF DEVICES IN DEVICE LIST
*
*   OUTPUT:     I_DVLIST-THE DEVICE LIST
*
*   RETURNS:
*
*   PROGRAMMER: J. THOMAS ECK
*
*   LAST MODIFIED: 9/14/92 JTE -- CLONED FROM RP__GTDV
*
*****

      IMPLICIT NONE
C
C-----/INCLUDE FILES
C
      INCLUDE 'USER2:[ICOLLAZO.YO]YOIPAR.'    !CONTAINS MAX_DEVICE

```



```

C
C-----/DECLARATIONS
C
      CHARACTER*16
+           KEY

      INTEGER*4
+           IERR, I_LFC, I, J, I4,
+           I_DVLIST (4,*),
+           I_TOTAL,
+           NUMGOT,
+           ISTART,
+           LENGTH

      BYTE           I1 (4),
+           I1_1DUM,
+           I1_2DUM
C
C-----/EQUIVALENCE
C
      EQUIVALENCE (I1, I4)
C
C-----/DATA FOR KEYWORD FILE
C
      DATA
+           KEY           / 'DEVICE_LIST____' /,
+           ISTART       / 1 /

      LENGTH = I_TOTAL * 4

!

*****
*                               *
* EXECUTABLE CODE *
*                               *
*****

      CALL CM_KRINT (I_LFC,
+           KEY ,
+           I_DVLIST (1,1),
+           ISTART,
+           LENGTH,
+           NUMGOT,

```

```

+           IERR)
  IF (IERR .NE. 0) THEN
    CALL CI_ERR ('CM_KRINT', KEY //' FROM YO_GETDV', IERR)
  END IF

C
C-----/FLIP THE BYTES
C           BYTE 4 -> 1
C           "    3 -> 2
C           "    2 -> 3
C
C
C           "    1 -> 4

  DO I = 1, NUMGOT / 4
    DO J = 1, 4
      I4 = I_DVLIST (J,I)
      I1_1DUM = I1 (1)
      I1_2DUM = I1 (2)

      I1 (1) = I1 (4)
      I1 (2) = I1 (3)
      I1 (3) = I1_2DUM
      I1 (4) = I1_1DUM

      I_DVLIST (J,I) = I4
    END DO          !J
  END DO          !I

C
C-----/END OF YO_GETDV
C
  RETURN
END

!

C
*****
*
*       SUBROUTINE AA_TMTM
*
*  THIS S/R DECODES THE ISPECIAL ARRAY FOR EVENT CODE AND DELAY AND
*  RETURN THE DELAY WRT TO
*
*  ERRORS RETURNED
*    IERR = 1  EVENT CODE NOT TO OR T-1
*    IERR = 2  CLOCK = 0

```

```

*
*  AUTHOR VAL FEBRUARY, 1986
*
*          CALLS:    AA_INDXX
*
*****

      SUBROUTINE AA_TMTM ( ISPECIAL,
+                        RDEL_MS,
+                        IERR)

C
C-----/DECLARATIONS
C
      IMPLICIT NONE

      INTEGER*4      IERR,
+
+                  I,
+                  ISPECIAL (5)

      REAL*4         RDEL_MS,
+
+                  RCOUNT,
+                  RCLOCK,
+                  RDELAY

*****
*
*  EXECUTABLE CODE *
*
*****

      IERR = 0

      RCOUNT = FLOAT (ISPECIAL(2))      !NO OF COUNTS
      RCLOCK  = FLOAT (ISPECIAL(3))      !CLOCK USED

      IF (RCLOCK .NE. 0) THEN
         RDELAY = RCOUNT * 1000 / RCLOCK      !WANT RESULT IN MILLISEC.
         IERR = 2
      END IF

      IF (BTEST (ISPECIAL (1),5)) THEN      !EVENT T-1
         RDEL_MS = -1000.0 + RDELAY
      ELSE IF (BTEST (ISPECIAL (1),6)) THEN  !EVENT TO
         RDEL_MS = 0.0 + RDELAY

```

```

      ELSE
        IERR = 1                                ! ONLY FINDS T-1 OR TO
        RDEL_MS = 1 000 000.0
      END IF
C
C-----/END OF AA:TMTM
C
      RETURN
      END
!

C
*****
*
*       SUBROUTINE AA_ERR
*
*  AUTHOR VAL JAN., 1987
*****

      SUBROUTINE AA_ERR (C8SUB,
+                        CIN,
+                        IERR)

      IMPLICIT NONE
C
C-----/DECLARATIONS
C
      CHARACTER*8 C8SUB

      CHARACTER*(*) CIN

      CHARACTER*61 C61OUT

      INTEGER*4    IERR

*****
*
*  EXECUTABLE CODE *
*
*****

      C61OUT = '
+
      C61OUT (2:61) = CIN

```

```

C      WRITE (*, '(A10)') '. '

      WRITE (*,100) C8SUB, IERR
100    FORMAT (' ERROR FROM S/R ', A8, ' ERROR = ',I3)

C      WRITE (*, '(A60)') C61OUT
C
C-----/END OF AA_ERR
C
      RETURN
      END

!

*****
*
* THIS S/R IS USED TO GENERATE THE INDEX OF A DEVICE IN A DEVICE LIST
*
* ENTERING ARGUMENTS
* I_DVLIST - INTEGER*4 (4,ITOTAL) ARRAY CONTAINING THE DEVICE LIST
* ITOTAL   - INTEGER*4 - TOTAL NUMBER OF DEVICES
* I_DVNAM  - INTEGER*4 (4) - NAME OF THE DEVICE
*
* RETURNED ARG.
* I_INDEX  - INTEGER*4 POSITIONS OF THE DEVICE IN THE DEVICE LIST
* IERR     - INTEGER*4 IERR = 0 IF NAME WAS FOUND, 1 IF NOT FOUND
*
* AUTHOR VAL JANUARY, 1987
*
*****

      SUBROUTINE AA_INDX (I_DVLIST,
+                        I_TOTAL,
+                        I_DVNAM,
+                        I_INDEX,
+                        IERR)

      IMPLICIT NONE

C-----/DECLARATIONS
C
      INTEGER*4
+      I, IERR,
+      I_DVLIST (4,*),

```

```

+          I_DVNAM (4),
+          I_TOTAL,
+          I_INDEX

*****
*          *
* EXECUTABLE CODE *
*          *
*****

C
C-----/INITIALIZE IERR
C
      IERR = 0
C
C-----/PARSE FOR THE DEVICE NAME
C
      DO I = 1,I_TOTAL
        IF (I_DVLIST (3,I) .EQ. I_DVNAM (3)) THEN
          IF (I_DVLIST (2,I) .EQ. I_DVNAM (2)) THEN
            IF (I_DVLIST (4,I) .EQ. I_DVNAM (4)) THEN
              IF (I_DVLIST (1,I) .EQ. I_DVNAM (1)) THEN
                I_INDEX = I
                RETURN          !----->ALL DONE - SO RETURN
              END IF
            END IF
          END IF
        END IF
      END DO

C
C-----/LEFT LOOP W/O INDEX
C
      IERR = 1
C
C-----/END OF AA__INDX
C
      RETURN
      END

!

*****
*
```

```

      SUBROUTINE YO_INDEX (
      I          C16DVNAM,
      O          I_INDEX,
      O          IERR)
*
*
*      INPUT:      C16DVNAM -- THE DEVICE NAME TO SCAN FOR
*
*      OUTPUT:     I_INDEX -- INDEX OF C16DVNAM IN DEVICE LIST YOADEV1
*
*      RETURNS:
*
*      PROGRAMMER:  J. THOMAS ECK
*
*      LAST MODIFIED: 9/14/92 JTE -- CLONED FROM RP__INDX
*
*****

      IMPLICIT NONE
C
C-----/INCLUDE FILES
C
      INCLUDE 'USER2:[ICOLLAZO.YO]YOIPAR.'
      INCLUDE 'USER2:[ICOLLAZO.YO]YOIDVLST.'
C
C-----/DECLARATIONS
C
      CHARACTER*16 C16DVNAM,
      +           C16NAME

      INTEGER*4
      +         IERR,
      +         ITOTAL,
      +         I_INDEX,
      +         I_NAME (4)
C
C-----/EQUIVALENCE
C
      EQUIVALENCE (C16NAME, I_NAME)
C
C-----/MISC DATA
C
      DATA ITOTAL / MAX_DEV /

```

```

*****
*
* EXECUTABLE CODE *
*
*****

```

```

C
C-----/GET THE DEVICE INDEX
C

```

```

      C16NAME (1:16) = C16DVNAM (1:16)
      CALL AA_INDY (I_DVLST,
+                ITOTAL,
+                I_NAME,
+                I_INDEX,
+                IERR)

```

```

C
C-----/END OF YO_INDEX
C

```

```

      RETURN
      END

```

```

!

```

```

C
C *****
C

```

```

      SUBROUTINE PLACE2(IPLACE)
      INTEGER IPLACE

      character*3 places(13)
      data places /'STD','UPH','LOH','UL4','UR4','LL4','LR4',
>                'UL6','UC6','UR6','LL6','LC6','LR6'/
      WRITE(11,*) IPLACE, PLACES(IPLACE)
      call place(places(IPLACE))

```

```

      RETURN
      END

```

```

!

```

```

C
C *****
C

```

```

      SUBROUTINE MATCH_TO_AVE(INDEX,PHASE,PHAVE_C)
      IMPLICIT NONE
      REAL PHASE(0:*), PHAVE_C(0:0), PHTEMP
      INTEGER INDEX(0:*), I, II, J, K !,ITEMP

```



```

C
C      COUNT THE RAW PHASE USING THE COUNTED AVERAGE PHASE
C      DO I=1,INDEX(0)
C          DO J=1,PHASE(INDEX(I))
C              K = J + INDEX(I)
C              ITEMP = (PHAVE_C(J)/PHASE(K) - 1. ) * PHASE(K)
C              PHASE(K) = PHASE(K) + ITEMP
C              PHTEMP = PHASE(K)
C              DO II=-2,4
C                  PHASE(K) = PHTEMP + II
C                  IF( ( (PHAVE_C(J)-0.5) .LT. PHASE(K) ) .AND.
*                      (PHASE(K) .LE. (PHAVE_C(J)+0.5) ) ) GOTO 1221
C              END DO
1221          CONTINUE
C          END DO
C          PHASE(INDEX(I)) = PHAVE_C(0)
C      END DO
C
C      RETURN
C      END

```

```

C
!
```

```

!
```

```

C
C *****
C
SUBROUTINE PH_SIGMA(INDEX,PHASE,PHAVE,RPSIGMA,KSMOOTH)
IMPLICIT NONE !DECLARE ALL VARIABLES
C      INDEXES FOR THE LOOPS
INTEGER I, J, K, KMIN, KMAX, JO, KSMOOTH
*      , NDAT(1000), INDEX(0:1000)
C      INPUT PARAMETERS
REAL RMAX, PHASE(0:*), PHAVE(0:*), RPSIGMA(0:*), CONS
*      , SUM1, SUM2, SIGMA_K
C      OPEN DEBUGGING FILE
C      OPEN(55,FILE='PH_SIGMA.OUT',STATUS='UNKNOWN')
C      LOOP TO INITIALIZE PARAMETERS
DO I = 0, RPSIGMA(0)
    RPSIGMA(I) = 0.0 !INITIALIZE VARIABLE FOR THE LOOP
    NDAT(I) = 0 !INITIALIZE VARIABLE FOR THE LOOP
END DO
C      SET MAXIMUM NUMBER OF POINTS
RMAX = PHASE(INDEX(1))

```

```

C      START LOOP FOR THE SIGMA
DO I=1, INDEX(0)
  JO = INDEX(I) !SET NUMBER OF POINTS
  RMAX = MAX(RMAX,PHASE(JO)) !SEARCH FOR MAXIMUM
C  WRITE(11,*) JO,PHASE(JO), RMAX
C      LOOP OVER DATA POINTS
DO J=1, PHASE(JO) !LOOP OVER THE SMOOTHING
C  CHECK THE LOWER LIMIT FOR THE LOOP
  IF(J .LE. KSMOOTH) THEN
    KMIN = -J+1 !SET THE PROPER LIMIT FOR LOOP
  ELSE !THIS IS THE SMALLEST VALUE FOR LOWER LIMIT
    KMIN = -KSMOOTH !SET MINIMUM LIMIT FOR LOOP
  END IF
C  CHECK THE MAXIMUM LIMIT FOR THE LOOP
  IF(J .GT. (PHASE(JO)-KSMOOTH)) THEN
    KMAX = PHASE(JO) - J !SET PROPER LIMIT FOR LOOP
  ELSE !SET MAXIMUM UPPER LIMIT
    KMAX = KSMOOTH
  END IF
  SUM1 = 0.0 !INITIALIZE VARIABLE
  SUM2 = 0.0 !INITIALIZE VARIABLE
C  DEFINE WIDTH FOR THE GAUSSIAN
  SIGMA_K = KSMOOTH / SQRT(LOG(10.))
C  CALCULATE SIGMA
DO K=KMIN,KMAX
  CONS = EXP(-(K/SIGMA_K)**2) !EXP. GAUSSIAN FACTOR
C  CALCULATE SIGMA WITH GAUSSIAN WEIGHTING FACTOR
  SUM1 = SUM1 + CONS * (PHASE(K+J+JO) - PHAVE(J))**2
  SUM2 = SUM2 + CONS !CALCULATE NORMALIZATION FACTOR
C  WRITE(55,51)I,J,K,CONS,SUM1,SUM2
C 51  FORMAT(3I8,3F16.8)
  END DO
C  WRITE(55,*)' '
C  CALCULATE NORMALIZE SIGMA
  RPSIGMA(J) = RPSIGMA(J) + SUM1/SUM2
C  RPSIGMA(J) = RPSIGMA(J)+CONS*(PHASE(J+JO)-PHAVE(J))**2
  NDAT(J) = NDAT(J) + 1 !INCREMENT NUMBER OF DATA POINT
C  WRITE(11,*) PHASE(J+JO), PHAVE(J), RPSIGMA(J),NDAT(J)
END DO
END DO
C  AVERAGE SIGMAS
DO J = 1, RMAX
  IF(NDAT(J).LE. 1) NDAT(J) = 2
  WRITE(11,*) J, RPSIGMA(J), NDAT(J)
  RPSIGMA(J) = SQRT(RPSIGMA(J)/FLOAT(NDAT(J)-1))

```

```
      WRITE(11,*) J, RPSIGMA(J), NDAT(J)
END DO
      RPSIGMA(0) = J-1 !SET NUMBER OF DATA POINTS
C      CLOSE(55) !CLOSE FILE

RETURN
END
C
!
```

## APPENDIX D

### DENSITY RECONSTRUCTION PROGRAM

#### D.1 Introduction

This appendix contains the code for the density reconstruction program and a typical data file. The source for the code is in the computer:

RAX.PPPL.GOV in the area:

[ICOLLAZO.GREG]T.FOR

and a copy can be obtained from the author or one of the coworkers of the project. Request can be done by mail, E-mail, or any other way. Transmission of the program can be done via E-mail, diskettes, tape or any other possible way.

The phase data files are stored in the directory “[.DATA]” and a list of the data files created during the last run can be found in the file “T.FLS”, which serves as the input list of data file names for the reconstructing program.

#### D.2 Description

The program was written to run in a non-iterative mode or as a batch mode if necessary. In this way a large number of profiles can be done without the direct intervention of the user. This type of arrangement was chosen to provide

a platform for an automated calculation of the density profiles in a continuous fashion for every day use at TFTR.

The program initialize its parameters through a "NAMELIST" read to the data file. The phase difference data files are stored in the sub-directory "[.DATA]" in the directory where the program is. To provide with an easy implementation for automatization, there is a file named "F.FLS", which contains a list of the names of the phase difference data file. This is the file that the program uses to know where to read the phase difference data. The program reads the phase data file name from the file "F.FLS", then using this file name it reads the phase data arrays from the corresponding file to the arrays in the program. With all of the parameters initialized and the phase data the program proceeds to calculate the reconstructed density profile for the given parameter set.

The theory and operation of the program is exactly the same as for the modeling program described previously. As a fact, the density reconstructing program was started from the modeling code, by striping the unnecessary code from the modeling code and adding the necessary code to read the phase data and plot the resulting reconstructed density profile. Therefore, the theory and related material of the reconstructed process will not be repeated here.

### D.3 Computer Code

```
!  
PROGRAM TIM !BY Ivan Collazo-Lopez  
C  
C THIS PROGRAM READS THE PHASE VS FREQUENCY DATA FROM THE DATA FILES  
C AND USES IT TO RECONSTRUCT THE DENSITY PROFILE.  
IMPLICIT NONE  
PARAMETER NN=1000, NP=20  
REAL  
* WREF(0:NN+NP+1) ! FREQUENCY ARRAY IN HERTS
```

```

* , DELREC(0:NN+NP) ! ARRAY OF DELTA RECONSTRUCTED ON THE RADIUS
* , DELPHI(0:NN+NP) ! ARRAY OF THE DELTA PHASE IN CYCLES = FRINGES
* , RO ! MAJOR RADIUS
* , RA ! MINOR RADIUS
* , BO ! MAGNETIC FIELD AT RO
* , ELECHR ! ELECTRON CHARGE IN COULOMBS
* , ELEMAS ! ELECTRON MASS IN KILO GRAMS
* , EPSILO ! PERMITTIVITY OF FREE SPACE IN F/M
* , C ! SPEED OF LIGHT IN FREE SPACE METERS/SECONDS
* , WINIT ! INITIAL FREQUENCY
* , WFINAL ! FINAL FREQUENCY
C * , MU2REC ! RECONSTRUCTED INDEX OF REFRACTION
* , SNREC ! RECONSTRUCTED INTEGRAL OF THE INDEX OF REFRA.
* , RPLANE ! POSITION OF THE REFERENCE PLANE
* , RCUTINI(NP) ! ASSUMED POSITION OF THE FIRST CUT-OFF
* , PI ! = 3.14159265
* , RK ! GENERAL PURPOSE VARIABLE
* , RK1 ! GENERAL PURPOSE VARIABLE
* , RK2 ! GENERAL PURPOSE VARIABLE
* , DELRK ! GENERAL PURPOSE VARIABLE
* , DEN1 ! INITIAL DENSITY FOR THE RAMP DENSITY
* , DEN2 ! FINAL DENSITY FOR THE RAMP DENSITY
C * , U ! DECAY CONSTANT FOR THE DENSITY AT THE EDGE
* , DSLOPE ! SLOPE FOR THE FAR EDGE RAMP DENSITY
* , WM ! FREQUENCY SPACING OF THE PROBING BEAMS
C * , WW ! GENERAL PURPOSE VARIABLE
* , TEMP ! TEMP VARIABLE
REAL
* , DENLOW(0:NN+NP) ! RECONSTRUCTED DENSITY OF LOWER FREQUENCY
* , DENUP(0:NN+NP) ! RECONSTRUCTED DENSITY OF UPPER FREQUENCY
* , PHILOW(0:NN+NP) ! FULL PHASE OF LOWER FREQ
* , PHIUP(0:NN+NP) ! FULL PHASE OF UPPER FREQ
* , RRLOW(0:NN+NP) ! RECONSTRUCTED CUT-OFF POSITIONS OF LOWER FREQ
* , RRUP(0:NN+NP) ! RECONSTRUCTED CUT-OFF POSITIONS OF UPPER FREQ
* , WGHZ(0:NN+NP) ! FREQUENCY ARRAY IN GHz
* , WGHZ_TOMY(0:NN+NP) ! FREQUENCY ARRAY IN GHz
* , COMGET ! AG2 FUNCTION, GETS VALUES FROM THE DATA BLOCK
* , CURRENT ! PLASMA CURRENT IN AMPERS
* , DPHIO ! INITIAL PHASE INCREMENT
* , TIME1 ! TIME OF THE SWEEP
* , TIME2 ! TIME OF THE SWEEP
C * , RETIME(0:NN+NP) ! TIME ARRAY DATA FOR THE EDGE POSITION
* , RPDATA(0:NN+NP) ! EDGE RADIAL POSITON ARRAY DATA
* , APDATA(0:NN+NP) ! EDGE RADIAL POSITON ARRAY DATA
* , REDATA(0:NN+NP) ! EDGE RADIAL POSITON ARRAY DATA

```

```

* , WFR(0:NN+NP) ! WAVE FORM RADIAL ARRAY
* , WFDATA(0:NN+NP) ! WAVE FORM DATA ARRAY
* , XSTART ! START POINT OF THE WAVE FORM ARRAY
* , XDELTA ! INCREMENT OF THE WAVE FROM ARRAY
* , R1REC ! LIMITS FOR THE PLOTS OF THE RECONS. RADIUS
* , R2REC ! LIMITS FOR THE PLOTS OF THE RECONS. RADIUS
* , D1REC ! LIMITS FOR THE PLOTS OF THE RECONS. DENSITY
* , D2REC ! LIMITS FOR THE PLOTS OF THE RECONS. DENSITY
* , XWGHZ1 ! LIMITS FOR THE PLOTS OF THE PHASE
* , XWGHZ2 ! LIMITS FOR THE PLOTS OF THE PHASE
* , XWGHZ1_TOMY ! LIMITS FOR THE PLOTS OF THE PHASE
* , XWGHZ2_TOMY ! LIMITS FOR THE PLOTS OF THE PHASE
* , YPHI1 ! LIMITS FOR THE PLOTS OF THE PHASE
* , YPHI2 ! LIMITS FOR THE PLOTS OF THE PHASE
* , OFFSET ! INDIVIDUAL OFFSET FOR THE DATA SETS
* , WCE, BF
* , REOFFSET
* , BFIELD ! MAGNETIC FIELD FUNCTION
* , POL_CUR ! POLOIDAL CURRENT
* , FUDGE !
* , PHSIZE ! SET SYMBOL SIZE
* , DENSIZE ! SET SYMBOL SIZE
* , RGREG(0:NN+NP) ! RADIAL POSITON ARRAY FOR GREG'S DATA
* , DENGREG(0:NN+NP) ! DENSITY DATA FOR GREG'S DATA
* , DENDIF(0:NN+NP) ! GREG'S AND MY DENSITY DIFFERENCE
* , RDIF(0:NN+NP) ! GREG'S AND MY RADIAL DIFFERENCE

```

C

## INTEGER

```

* , I, J, K ! GENERAL PURPOSE LOOP INDICES
* , IDELPHI ! SET SCREEN WINDOW FOR THE DELTA PHASE DATA
* , IDENREC ! SET SCREEN WINDOW FOR THE RECONSTRUCTED DENSITY
* , IPHTYPE ! SET THE LINE TYPE FOR THE PHASE DATA
* , IDENTYPE ! SET THE LINE TYPE FOR THE DENSITY DATA
* , IBASEX ! AG2 FUNCTION, GIVES THE ADDRESSES ON THE DATA BLOCKS
* , IBASEY ! AG2 FUNCTION, GIVES THE ADDRESSES ON THE DATA BLOCKS
* , NURNS ! NUMBER OF TURNS ON THE MAGNET COILS
* , NNDATA ! NUMBER OF PHASE/FREQUENCY DATA POINTS ON THE FILE
* , IPLOTS ! NUMBER OF DATA FILE NAMES ON THE FILE "F.FLS"
* , I_SHOT ! SHOT NUMBER
* , FM ! 1 = PLOT MIRI DENSITY DATA
* , TS ! 1 = PLOT THOMSON SCATTERING DENSITY DATA
* , IQUAL ! QUALITY FACTOR NUMBER FROM SUBROUTINE "WF_GET"
* , NUMGOT ! NUMBER OF POINTS ON THE WAVE FORM
* , IERR ! ERROR CODE
* , IXLEG ! X-AXIS POSITION OF THE LEGEND

```

```

* , IYLEG ! Y-AXIS POSITION OF THE LEGEND
* , KK ! GENERAL PURPOSE INDEX
* , IX1BOX ! X-AXIS POSITION OF LEGEND BOX
* , IY1BOX ! Y-AXIS POSITION OF LEGEND BOX
* , IX2BOX ! X-AXIS POSITION OF LEGEND BOX
* , IY2BOX ! Y-AXIS POSITION OF LEGEND BOX
* , ITITLE ! Y-AXIS POSITION OF THE TITLE
* , ICHANEL ! CHANNEL NUMBER
* , IPHIMINX, IPHIMAXX, IPHIMINY, IPHIMAXY, ISHIFTY
* , IPHSYMBL ! SET SYMBOL TYPE
* , IDENSYMBL ! SET SYMBOL TYPE
* , ITOI ! POSITION OF THE TIME OF INTEREST
* , IXSMIN ! SCREEN COORDINATES FOR MAG. FIELD LABEL
* , IYSMAX ! SCREEN COORDINATES FOR MAG. FIELD LABEL
* , IXPARAM ! SCREEN COORDINATES FOR FREQUENCY SEPARATION
* , IYPARAM ! SCREEN COORDINATES FOR FREQUENCY SEPARATION
* , IYTIME ! SCREEN POSITION OF THE SWEEP TIME
* , IXERR ! LABEL POSITION
* , IYERR ! LABEL POSITION
* , ERR_ON ! ERROR BARS FLAG
* , IDUMY ! GENERAL PURPOSE VARIABLE

```

#### CHARACTER

```

* TITLE*77 ! PAGE TITLE
* , CHAR2*77 ! SECOND LOWER TITLE
* , TODAY*9 ! TODAYS DATE
* , CFILE*77 ! STRING WITH THE PHASE DATA FULL FILE NAME
* , PFILE*77 ! PLOTTING FILE NAME
* , FMNE*8 ! DIGRAPH STRING FOR THE MIRI DENSITY DATA
* , FMXR*8 ! DIGRAPH STRING FOR THE MIRI RADIAL DATA
* , TSNE*8 ! DIGRAPH STRING FOR THE TS DENSITY DATA
* , TSXR*8 ! DIGRAPH STRING FOR THE TS RADIAL DATA
C * , WFNAME*77 ! WAVE FORM NAME STRING
* , WFUNITS*77 ! WAVE FORM UNITS STRING
* , WFDESC*77 ! WAVE FORM DESCRIPTION STRING
* , XUNITS*77 ! WAVE FORM UNITS STRING
* , DEN_FILE*77 ! STRING WITH FULL NAME OF THE RECONSTRUCTED DATA FILE
* , CORNER*11 ! STRING WITH THE SHOT NUMBER
* , CTIME*11 ! SWEEP TIME
* , TOI*4 ! STRING WITH THE TIME OF INTEREST
* , MIRILEG*22 ! STRING FOR THE MIRI LEGEND
* , MIRILEG2*22 ! STRING FOR THE MIRI LEGEND
* , PLABEL*3 ! PLOT LABEL

```



```
* , PARAM*22 ! MAGNETIC FIELD LABEL
* , CDENSITY*77 ! DENSITY PLOT TITLE
* , T_FLS*77 ! LIST FILE
```

```
LOGICAL IDENS ! IF TRUE, GENERATES THE DENSITY DATA FILES
```

C

```
COMMON /COMDAT/ RO, RA, BO, ELECHR, ELEMAS, EPSILO, C, PI
* , NTURN, CURRENT, POL_CUR
```

```
NAMELIST /DAT/
```

```
* WM ! SPACING FREQUENCY
* , RPLANE ! POSITION OF THE EDGE/BUMPER LIMITER, REFERENCE PLANE
* , RCUTINI ! POSITION OF THE FIRST CUT-OFF
* , DEN1 ! DENSITY AT RK1
* , DEN2 ! DENSITY AT THE FIRST CUT-OFF, AT "RK2"
* , RO ! MAJOR RADIUS
* , RA ! MINOR RADIUS
* , NTURN ! NUMBER OF COIL TURNS
* , IDELPHI ! SET THE SCREEN WINDOW
* , IDENREC ! SET THE SCREEN WINDOW
* , DPHIO ! DELTA PHI INITIAL
* , R1REC ! LIMITS FOR THE DATA WINDOW
* , R2REC ! LIMITS FOR THE DATA WINDOW
* , D1REC ! LIMITS FOR THE DATA WINDOW
* , D2REC ! LIMITS FOR THE DATA WINDOW
* , FMNE ! DIGRAPH CHARACTER CODE FOR THE MIRI DENSITY DATA
* , FMXR ! DIGRAPH CHARACTER CODE FOR THE MIRI RADIAL DATA
* , FM ! ON/OFF SWITCH FOR THE PLOTTING OF THE MIRI DATA
* , TSNE ! DIGRAPH CHARACTER CODE FOR THE THOMSON SCATERING DATA
* , TSXR ! DIGRAPH CHARACTER CODE FOR THE TS RADIAL DATA
* , TS ! ON/OFF SWITCH FOR THE PLOTTING OF THE TS DATA
* , IPHTYPE ! SET THE PHASE LINE TYPE
* , IDENTYPE ! SET THE DENSITY LINE TYPE
* , YPHI1 ! LIMITS FOR THE DATA WINDOW
* , YPHI2 ! LIMITS FOR THE DATA WINDOW
* , IWGHZ1 ! LIMITS FOR THE PLOTS OF THE PHASE
* , IWGHZ2 ! LIMITS FOR THE PLOTS OF THE PHASE
* , IDENS ! LOGICAL, IF TRUE, GENERATES THE DENSITY DATA FILES
* , PFILE ! PLOTTING FILE
* , REOFSET !
* , FUDGE !
* , IPHIMINX, IPHIMAXI, IPHIMINY, IPHIMAXY, ISHIFTY
* , IPHSYMBL ! SET SYMBOL TYPE
* , IDENSYMBL ! SET SYMBOL TYPE
* , PHSIZE ! SET SYMBOL SIZE
```

```

* , DENSIZE ! SET SYMBOL SIZE
* , ERR_ON !ERROR FLAG
* , IDUMY !SET METHOD
* , T_FLS ! LIST FILE
C
C READ THE DATA IN THE DATA FILE
ERR_ON = 1
IDUMY = 0
OPEN(11,FILE='T.DAT',STATUS='OLD')
READ(11,DAT)
WRITE(*,DAT)
CLOSE(11) ! CLOSE THE FILE AND FREE THE LOGICAL UNIT NUMBER
C
C SOME UNIVERSAL PHYSICAL CONSTANTS
PI = 3.14159265 ! RADIANS
ELECHR = 1.60217733E-19 ! COULOMBS
ELEMAS = 9.1093897E-31 ! Kg
EPSILO = 8.854187817E-12 ! F/m
C = 299792456.2 ! +- 1.1 M/SEC
ITITLE = 760
C
C THE FILE T.ERR IS ANOTHER DEBBUGING FILE. IT HAS INFORMATION
C FROM THE SUBROUTINE "SNREC".
OPEN(66,FILE='T.ERR;1',STATUS='UNKNOWN')
C
C OPEN THE FILE THAT HAS THE NAMES OF THE DELTA PHASE DATA FILES
C OPEN(22,FILE='[ICOLLAZO.TIM]T.FLS',STATUS='OLD')
OPEN(22,FILE=T_FLS,STATUS='OLD')
C READ THE NUMBER OF DELTA PHASE DATA FILE NAMES IN THE FILE "F.FLS"
READ(22,*) IPLOTS
C
C INITIALIZE AND OPEN THE PLOTTING FILE
CALL RINITT(PFILE)
CALL INITT(960)
!
C
C MAIN LOOP THAT LOOPS OVER THE DELTA PHASE DATA FILE NAMES
IYTIME = 80
DO KK=1,IPLOTS
C
C THE FILE T.OUT IS LIKE A LOG FILE OF THE RELEVANT DATA
C GENERATED ON THE CORRESPONDING LOOPS OF THE PROGRAM. IT IS USE
C MOSTLY FOR DEBBUGING PURPOSES. IT CONTAINS THE RECONSTRUCED
C DATA AS IT IS BEEN CALCULATED IN THE LOOP. IF THE PROGRAM ABORTS,

```

```

C      THE INFORMATION ON THIS FILE CAN BE HELPFULL TO DETERMINE THE
C      POSSIBLE CAUSE OF THE PROBLEM.
      OPEN(11,FILE='T.OUT;1',STATUS='UNKNOWN')
C      READ THE NAME OF A DATA FILE TO BE OPENED FOR READING AND
C      PROCESSING OF THE PHASE DATA
      READ(22,22)CFILE
22      FORMAT(A44)
      WRITE(11,*)KK, CFILE
      OPEN(44,FILE=CFILE,STATUS='OLD')
C      READ THE DATA ON THE HEADER OF THE PHASE DATA FILE
C      NNDATA IS THE NUMBER OF PHASE/FREQUENCY DATA POINTS ON THE FILE
      READ(44,*) NNDATA,CURRENT,TIME1,TIME2,I_SHOT,ICHANEL,POL_CUR
*      ,OFFSET
C
C      WF_GET GETS THE WAVE FORM DATA FOR THE POSTION OF THE EDGE
      CALL WF_GET(I_SHOT,'MB-RP-SL', WFDESC, IQUAL, XSTART, XDELTA
*      , XUNITS, RPDATA(1), NN, NUMGOT, WFUNITS, IERR)
      RPDATA(0) = NUMGOT ! SET NUMBER OF DATA POINTS
C      WF_GET GETS THE WAVE FORM DATA FOR THE POSTION OF THE EDGE
      CALL WF_GET(I_SHOT,'MB-AP-SL', WFDESC, IQUAL, XSTART, XDELTA
*      , XUNITS, APDATA(1), NN, NUMGOT, WFUNITS, IERR)
      APDATA(0) = NUMGOT ! SET NUMBER OF DATA POINTS
      DO K = 1, RPDATA(0)
          REDATA(K) = RPDATA(K) + APDATA(K) ! METERS
C          WRITE(*,*) K, RPDATA(K), APDATA(K), REDATA(K)
C      *      , REDATA(TIME1/10.0E-03)
      END DO
C
C      NOW START TO READ THE PHASE/FREQUENCY DATA. AS WE READ,
C      WE LOOK FOR THE MIN AND MAX FREQUENCIES FROM THE DATA.
      READ(44,160) WGHZ(NNDATA), DELPHI(NNDATA)
C      READ(44,* ) WGHZ(NNDATA), DELPHI(NNDATA)
*      ,RGREG(NNDATA), DENGREG(NNDATA) !BENCH_MARK
160      FORMAT(G14.5,G18.7,G14.5,G18.7)
      DELPHI(NNDATA) = DELPHI(NNDATA) + DPHIO + OFFSET
      WREF(NNDATA) = WGHZ(NNDATA) * 1.0E+09
      WGHZ_TOMY(NNDATA) = -WGHZ(NNDATA)
      XWGHZ1_TOMY = -XWGHZ1 ! LIMITS FOR THE PLOTS OF THE PHASE
      XWGHZ2_TOMY = -XWGHZ2 ! LIMITS FOR THE PLOTS OF THE PHASE
      WINIT = WREF(NNDATA) ! INITIALIZE THE MINIMUM FREQUENCY
      WFINAL = WREF(NNDATA) ! INITIALIZE THE MAXIMIM FREQUENCY
      DO I=NNDATA-1,1,-1
          READ(44,160) WGHZ(I), DELPHI(I) ! READ THE DATA
C          READ(44,* ) WGHZ(I), DELPHI(I) ! READ THE DATA
*          ,RGREG(I), DENGREG(I) !BENCH_MARK

```

```

WREF(I) = WGHZ(I) * 1.0E+09 ! CONVERT FROM GHz TO HERTZ
WGHZ_TOMY(I) = -WGHZ(I) ! MAKE PLOTTING DATA
DELPHI(I) = DELPHI(I)+DPHI0+OFFSET ! ADD THE INITIAL PHASE
WINIT = MIN(WINIT,WREF(I)) ! LOOK FOR THE MINIMUM
WFINAL = MAX(WFINAL,WREF(I)) ! LOOK FOR THE MAXIMUM
END DO
WGHZ(0) = NNDATA ! SET THE NUMBER OF FREQUENCY DATA POINTS
WGHZ_TOMY(0) = NNDATA ! SET THE NUMBER OF FREQUENCY DATA POINTS
DELPHI(0) = NNDATA ! SET THE NUMBER OF DELTA PHI DATA POINTS
WREF(0) = NNDATA ! SET THE NUMBER OF FREQUENCY DATA POINTS
RGREG(0) = NNDATA ! SET THE NUMBER OF DATA POINTS !BENCH_MARK
DENGREG(0)= NNDATA ! SET THE NUMBER OF DATA POINTS !BENCH_MARK
CLOSE(44) ! CLOSE PHASE/FREQUENCY DATA FILE
WRITE(CTIME,50)TIME1,'S'
50 FORMAT(F5.3,A1)
IYTIME = IYTIME + 20
CALL AGTMHS(930,IYTIME,CTIME)
WRITE(CORNER,51)I_SHOT
51 FORMAT(I5)
IYTIME = IYTIME + 20
CALL AGTMHS(930,IYTIME,CORNER)
C
IF(IDELPHI.NE.0) THEN
  IF( (KK.EQ. 1) ) THEN
    C WITH THE INFORMATION ON THE HEADER WE CAN MAKE A NICE TITLE
    WRITE(TITLE,140) ' I=',CURRENT/1000., 'Kamps ', ICHANEL
    * , ' TIME=',TIME1, ' sec '
    * , ' SHOT=', I_SHOT
    140 FORMAT(A4,F6.2,A6,I1, A6,F5.3,A13, A6,I6)
    C CALL AGTMHS(75,ITITLE,TITLE) ! PLOT THE TITLE
    CALL DATE(TODAY) ! GET TODAY'S DATE
    CALL AGTMHS(900,ITITLE,TODAY) ! PLOT TODAY'S DATE
    WRITE(CORNER,30)I_SHOT
    30 FORMAT(I5)
    CALL AGTMHS(950,1,CORNER) ! OUTPUT SHOT NUMBER
    WRITE(CORNER,40)CURRENT/1000
    40 FORMAT(F4.0)
    CALL AGTMHS(950,20,CORNER)
C
C WRITE A BOTTOM TITLE
C WRITE(CHAR,130)'RCUTINI=',RCUTINI,' m'
C * , ' DEDGE=',DEN1,' part/m^3'
C 130 FORMAT(A8,F6.3,A2
C * ,A8,1PE9.2,A9)
C CALL AGTMHS(200,30,CHAR) ! PLOT BOTTOM TITLE

```

```

C
C      WRITE A SECOND BOTTOM TITLE
WRITE(CHAR2,135)'WINIT=',WINIT/1.0E+09,' GHz'
*      , ' WFINAL=',WFINAL/1.0E+09,' GHz'
*      , ' WM=',WM/1.0E+09,' GHz'
135      FORMAT(A6,F7.2,A4
*      ,A9,F7.2,A4
*      ,A5,F7.4,A4)
C      CALL AGTMHS(140,10,CHAR2)! PLOT BOTTOM TITLE
END IF
!
C
IF( KK .EQ. 1 ) THEN
  CALL BINITT() ! INITIALIZE DATA BLOCKS
  CALL XFRM(2) ! SET X-AXIS STYLE
  CALL YFRM(5) ! SET Y-AXIS STYLE
  IF( (-13 .LE. IDELPHI) .AND. (IDELPHI .LE. 13) ) THEN
    CALL PLACE2((ABS(IDELPHI))) ! SET SCREEN WINDOW
  ELSE IF( IDELPHI .EQ. 14 ) THEN
    CALL SLIMX(IPHIMINX,IPHIMAXX)
    CALL SLIMY(IPHIMINY+ISHIFTY,IPHIMAXY+ISHIFTY)
    PLABEL = '(A)'
  ELSE
    CALL SLIMX(IPHIMINX,IPHIMAXX)
    CALL SLIMY(IPHIMINY,IPHIMAXY)
    PLABEL = '(B)'
  END IF
  CALL DLIMX(XWGHZ2_TOMY,XWGHZ1_TOMY)! SET X-AXIS DATA LIMITS
  CALL DLIMY(YPHI1,YPHI2) ! SET Y-AXIS DATA LIMITS
  CALL LINE(IPHTYPE) ! SET LINE TYPE
  CALL SYMBL(IPHSYMBL) ! SET SYMBOL TYPE
  CALL SIZES(PHSIZE) ! SET SYMBOL SIZE
  CALL CHECK(WGHZ_TOMY,DELPHI) ! SET LIMITS FROM DATA
  CALL DSPLAY(WGHZ_TOMY,DELPHI) ! PLOT AXIS AND DATA
  CALL FRAME() ! DRAW FRAME
  CALL LINE(-4) ! SET LINE TYPE
  CALL SYMBL(0) ! SET SYMBOL TYPE
  CALL AGTCHS('FREQUENCY (GHz)') ! LABELS
  CALL AGTCVS('FRINGES')
  CALL AGTMHS(INT(COMGET(IBASEX(13)))
*      ,INT(COMGET(IBASEY(14))+5), 'PHASE DATA')
  IXSMIN = COMGET(IBASEX(13))
  IYSMAX = COMGET(IBASEY(14))
  CALL AGTMHS(IXSMIN-125,IYSMAX,PLABEL)

```

```

C
      BF = BFIELD(RCUTINI(KK))
      WRITE(PARAM,230)'B =',BO,' T'
230    FORMAT(A3,F3.1,A2)
      IXPARAM = IXSMIN + 75
      IYPARAM = IYSMAX - 16
      CALL AGTMHS(IXPARAM,IYPARAM,PARAM)

C
      WRITE(PARAM,231)' 0 '
231    FORMAT(A3)
      IYPARAM = IYPARAM - 6
      CALL AGTMHS(IXPARAM,IYPARAM,PARAM)

C
      WRITE(PARAM,232)'w=',WM/1.0E+09,' GHz'
232    FORMAT(A2,F4.3,A4)
      IYPARAM = IYPARAM - 20
      CALL MOVABS(IXSMIN+75, IYPARAM+5)  !MOVE TO POSITION
      CALL SYMOUT(3, 1.)                !OUTPUT SYMBOL
      CALL AGTMHS(IXPARAM+7,IYPARAM,PARAM)
      ELSE
      CALL BINITT()  ! INITIALIZE DATA BLOCKS
      IF( IDELPHI .LE. 13 ) THEN
        CALL PLACE2((ABS(IDELPHI)))! SET SCREEN WINDOW
      ELSE
        IF( IDELPHI .EQ. 14 ) THEN
          CALL SLIMX(IPHIMINX,IPHIMAXX)
          CALL SLIMY(IPHIMINY+ISHIFTY,IPHIMAXY+ISHIFTY)
        ELSE
          CALL SLIMX(IPHIMINX,IPHIMAXX)
          CALL SLIMY(IPHIMINY,IPHIMAXY)
        END IF
      END IF
      CALL DLIMX(XWGHZ2_TOMY,XWGHZ1_TOMY)! SET X-AXIS DATA LIMITS
      CALL DLIMY(YPHI1,YPHI2)  ! SET Y-AXIS DATA LIMITS
      CALL LINE(IPHTYPE)  ! SET LINE TYPE
      CALL SYMBL(IPHSYMBL)  ! SET SYMBOL TYPE
      CALL SIZES(PHSIZE)  ! SET SYMBOL SIZE
      CALL CHECK(WGHZ_TOMY,DELPHI)  ! SET LIMITS FROM DATA
      CALL CPLOT(WGHZ_TOMY,DELPHI)  ! PLOT NEXT DATA SET
      END IF
    END IF
  !

C
C      HERE WE GENERATE THE DATA FOR THE ASSUMED LINEAR DENSITY

```

```

C      PROFILE AT THE EDGE OF THE BUMPER LIMITER.
      RK1 = RPLANE ! POSITION OF THE REF. PLANE
C      RK2 = REDATA(TIME1/10.0E-03)+REOFSET ! POSITION OF FIRST CUT-OFF
      RK2 = RCUTINI(KK) ! POSITION OF FIRST CUT-OFF
      BF = BFIELD(RK2) !DEFINES THE MAGNETIC FIELD ON THE RADIAL POINT.
      WCE = (BF * ELECHR / ELEMAS) / (2.*PI) !ELECTRON CYCLOTRON FREQUENCY
      DEN2 = WREF(NNDATA) * (WREF(NNDATA) - WCE)
      * (ELEMAS/ELECHR) * (EPSILO/ELECHR)
      * (2. * PI)**2
      DELRK = (RK1-RK2) / NP ! DELTA IN THE RADIUS
CE      U = (LOG(DEN2/DEN1)) / (RK1-RK2) ! EXPONENTIAL PROFILE CONSTANT
      DSLOPE = (DEN1-DEN2) / (RK1-RK2) ! SLOPE FOR LINEAR PROFILE
C      WRITE(66,*)RK1,DEN1, RK2,DEN2, DSLOPE
      RK = RK1 + DELRK ! INITIALIZE "RK"
      DO K=NNDATA+NP,NNDATA,-1
        RK = RK - DELRK ! NEXT RADIAL POSITION
        RRLOW(K) = RK ! RADIAL POSITION ARRAY
CE        DENLOW(K) = DEN2 * EXP(-U*(RK-RK2)) ! EXPONENTIAL PROFILE
        DENLOW(K) = DSLOPE*(RK-RK2) + DEN2 ! LINEAR PROFILE
        RRUP(K) = RK ! RADIAL POSITION ARRAY
        DENUP(K) = DENLOW(K) ! DENSITY PROFILE
      END DO

C
!

C      PHASE DUE TO THE LINEAR (OR EXP) PROFILE BEFORE THE FIRST CUT-OFF
      PHILOW(NNDATA) = 2.*(WREF(NNDATA))/C * FUDGE *
      * SNREC(NNDATA,NNDATA+NP,RRLOW(1),DENLOW(1),WREF(NNDATA))
      WRITE(11,*) ' PHILOW(NNDATA) =', PHILOW(NNDATA)
      WRITE(11,*) ' I ', ' RRLOW ', ' RRUP ', ' DENLOW '
      * ' DENUP '
C****      LOOP TO RECONSTRUCT THE DENSITY PROFILE
      DO I = NNDATA, 2, -1
        CALL THOMAS(I,NNDATA,NP,RRLOW,DELREC,RRUP,DENLOW,DENUP
      * ,PHILOW,DELPHI,PHIUP,WREF,WM,IDUMY)
C11      WRITE(11,150)I,RRLOW(I),RRUP(I),DENLOW(I),DENUP(I), WGHZ(I)
C11 150      FORMAT(I4,2F11.4,2(E11.3),F11.3)

      END DO
      RRLOW(1) = RRLOW(2) ! SET THE LAST ELEMENT OF THE ARRAY
      RRUP(1) = RRUP(2) ! SET THE LAST ELEMENT OF THE ARRAY
      DENLOW(1) = DENLOW(2) ! SET THE LAST ELEMENT OF THE ARRAY
      DENUP(1) = DENUP(2) ! SET THE LAST ELEMENT OF THE ARRAY
      DELREC(0) = NNDATA ! SET THE NUMBER OF DATA POINTS
      RRLOW(0) = NNDATA + NP ! SET THE NUMBER OF DATA POINTS
      RRUP(0) = NNDATA ! SET THE NUMBER OF DATA POINTS

```

```

DENLOW(0) = NNDATA + NP ! SET THE NUMBER OF DATA POINTS
DENUP(0) = NNDATA ! SET THE NUMBER OF DATA POINTS
CLOSE(11) ! CLOSE FILE "T.OUT;1"

C
C   GENERATE DENSITY/RADIUS DATA FILES IF REQUESTED
IF(IDENS.EQ..TRUE.) THEN
  WRITE(DEN_FILE,33)'.DENSITY'D',I_SHOT,'_',TIME1
  33   FORMAT(A11,I5,A1,F5.3) ! CREATE FILE NAME
  OPEN(33,FILE=DEN_FILE,STATUS='NEW') ! OPEN FILE
  WRITE(33,*) I_SHOT, CURRENT, TIME1 ! WRITE SOME TYPE OF A HEADER
  DO I=0,RRLOW(0)
    WRITE(33,*) RRLOW(I), DENLOW(I) ! WRITE DATA TO FILE
  END DO
  CLOSE(33) ! CLOSE FILE AND FREE LOGICAL UNIT NUMBER
END IF

C
C   PLOT DENSITY PROFILES
IF(IDENREC.NE.0) THEN
  C   WRITE RECONSTRUCTED DENSITY DATA TO FILE
  OPEN(55,FILE='T.DEN;1',STATUS='UNKNOWN')
  WRITE(55,*)RRLOW(0), I_SHOT
  DO K = 1, RRLOW(0)
    WRITE(55,*)RRLOW(K), DENLOW(K)
  END DO
  CLOSE(55)
  IF( KK.EQ. 1) THEN
    CALL BINITT() ! INITIALIZE DATA BLOCKS
    CALL XFRM(2) ! SET X-AXIS STYLE
    CALL YFRM(2) ! SET Y-AXIS STYLE
    IF( IDENREC.LE. 13 ) THEN
      CALL PLACE2((ABS(IDENREC)))! SET SCREEN WINDOW
    ELSE
      IF( IDENREC.EQ. 14 ) THEN
        CALL SLIMX(IPHIMINX,IPHIMAXX)
        CALL SLIMY(IPHIMINY+ISHIFTY,IPHIMAXY+ISHIFTY)
        PLABEL = '(A)'
      ELSE
        CALL SLIMX(IPHIMINX,IPHIMAXX)
        CALL SLIMY(IPHIMINY,IPHIMAXY)
        PLABEL = '(B)'
      END IF
    END IF
  END IF
  CALL DLIMX(R1REC,R2REC) ! SET X-AXIS DATA LIMITS
  CALL DLIMY(D1REC,D2REC) ! SET Y-AXIS DATA LIMITS
  CALL LINE(IDENTYPE) ! SET LINE TYPE

```



```

      CALL SYMBL(IDNSYMBL) ! SET SYMBOL TYPE
      CALL SIZES(DENSIZE) ! SET SYMBOL SIZE
      CALL CHECK(RRLOW,DENLOW) ! SET DATA BLOCKS
      CALL DSPLAY(RRLOW,DENLOW)! PLOT AXIS AND DATA
      CALL FRAME() ! DRAW FRAME
C      CALL CPLOT(RRUP,DENUP) ! PLOT NEXT DATA SET
      CALL LINE(-4) ! SET LINE TYPE
      CALL SYMBL(IDNSYMBL) ! SET SYMBOL TYPE
C      CALL SYMBL(0) ! SET SYMBOL TYPE
      CALL AGTCHS('MAJOR RADIUS (m)')! LABELS
      CALL AGTCVS('1/m^3') ! LABELS
      IF(ERR_ON .NE. 0) CALL ERR_BAR(RRLOW,DENLOW,WREF)
!

      IF( RGREG(RGREG(0)/2) .GT. 0.0 ) THEN
C !BENCH_MARK BEGIN
      CALL CPLOT(RGREG,DENGREG)! PLOT NEXT DATA SET
      DO I = 1, RGREG(0) ! CALCULATE THE DIFFERENCES
      DO J = 1, RGREG(0)
      IF( (RGREG(J).LE.RRLOW(I))
*      .AND. (RRLOW(I).LT.RGREG(J+1))) THEN
      DENDIF(I) = ABS(DENLOW(I) - DENGREG(J)
*      - (DENGREG(J+1)-DENGREG(J))/(RGREG(J+1)-RGREG(J))
*      * (RRLOW(I)-RGREG(J))) / DENLOW(1) !*100.
      GOTO 420
      END IF
      END DO
420      CONTINUE
C      DENDIF(I) = ABS(DENGREG(I) - DENLOW(I))
C      RDIF(I) = ABS(RGREG(I) - RRLOW(I)) + COMGET(IBASEX(11))
C      WRITE(11,430)I,RRLOW(I),RGREG(I),DENLOW(I),DENGREG(I)
C      *      , RDIF(I), DENDIF(I)
C 430      FORMAT(I4,F7.3,F7.3,E14.3,E14.3,F7.4,E14.3)
      END DO
      DENDIF(0) = RGREG(0) ! SET NUMBER OF DATA POINTS
      RDIF(0) = RGREG(0) ! SET NUMBER OF DATA POINTS
      DO I=DENDIF(0),1,-1
      TEMP = 0.0
      DO J=0,9
      TEMP = TEMP + DENDIF(I+J)
      END DO
      DENDIF(I) = TEMP/J
      END DO
C      CALL CPLOT(RGREG,DENDIF)! PLOT THE DIFFERENCE IN DENSITY
C      CALL CPLOT(RDIF,DENLOW) ! PLOT THE DIFFERENCE IN POSITION

```

```

C          PLOT THE FRACTIONAL ERROR ON THE RIGHT AXIS
          CALL DINITY()          !INITIALIZE Y-AXIS DATA BLOCK
          CALL YLOCRT(0)         !SET AXIS LOCATION TO RIGHT
          CALL LINE(0)           !SET LINE TYPE -4=NOLINE
          CALL SYMBL(0)          !SET SYMBOL TYPE TO A POINT
C          CALL DLIMX(RXMIN,RXMAX) !SET X-AXIS DATA LIMITS
          CALL CHECK(RGREG,DENDIF) !SET DATA LIMITS, ETC...
          CALL DSPLAY(RGREG,DENDIF) !DRAW AXIS AND PLOT DATA
C          CALL SAVCOM(SIER_DEN)  !SAVE COMMON BLOCKS DATA
          IXERR = COMGET(IBASEX(14))+85 !CALCULATE POSITION OF LABEL
          IF(IXERR.GT.1022) IXERR = 1022
          IYERR = COMGET(IBASEY(14)) !CALCULATE POSITION OF LABEL
C          CALL AGTMVS(IXERR,IYERR,'ERROR%      ') !LABEL
          CALL AGTCVS('ERROR%') !LABEL
C !BENCH_MARK END
          END IF
          WRITE(CDENSITY,630) 'DENSITY SHOT ',I_SHOT
630          FORMAT(A13,I5)
          IXSMIN = COMGET(IBASEX(13))
          IYSMAX = COMGET(IBASEY(14))
          CALL AGTMHS(IXSMIN-125,IYSMAX,PLABEL)
          CALL AGTMHS(INT(COMGET(IBASEX(13)))
*          ,INT(COMGET(IBASEY(14))+5),CDENSITY)
C          PLOTTING THE LEGEND, CALCULATE THE X-Y POSITION OF THE LEGEND
          IXLEG = COMGET(IBASEX(13)) + 2./3.
*          * ( COMGET(IBASEX(14)) - COMGET(IBASEX(13)) )
          IYLEG = COMGET(IBASEY(14)) - 20
          CALL MOVABS(IXLEG, IYLEG) ! MOVE TO POSITON
          CALL SYMOUT(IDENSYMBL,DENSIZ) ! DRAW SYMBOL AT POSITION
          CALL AGTMHS(IXLEG+20, IYLEG-6, 'REFL.')
          IX1BOX = IXLEG - 10 ! SET POSITION OF THE LEGEND BOX
          IY1BOX = IYLEG + 10 ! SET POSITION OF THE LEGEND BOX
          IX2BOX = IX1BOX + 100 ! SET POSITION OF THE LEGEND BOX
          IY2BOX = IY1BOX - 20 ! SET POSITION OF THE LEGEND BOX
C
C          PLOT THE MIRI DATA IF REQUESTED
          IF (FM.NE.0) THEN
C          WF_GET GETS THE WAVE FORM DATA FOR THE MIRI DIAGNOSTIC
          CALL WF_GET(I_SHOT,FMNE, WFDESC, IQUAL, XSTART, XDELTA
*          , XUNITS, WFDATA(1), NN, NUMGOT, WFUNITS, IERR)
          WFDATA(0) = NUMGOT ! SET NUMBER OF DATA POINTS
C          PLOTS THE MIRI TITLE TO THE GRAPH
C          CALL AGTMHS(INT(COMGET(IBASEX(13)))
C          ,INT(COMGET(IBASEY(14))+20), WFDESC)
C          *
C          GET THE DATA ARRAY FOR THE RADIUS OF THE MIRI DATA

```

```

      CALL WF_GET(I_SHOT,FMXR, WFDESC, IQUAL, XSTART, XDELTA
*      , XUNITS, WFR(1), NN, NUMGOT, WFUNITS, IERR)
      WFR(0) = NUMGOT ! SET THE NUMBER OF DATA POINTS
      OPEN(55,FILE='T.MIRI;1',STATUS='UNKNOWN')
      WRITE(55,*)WFR(0), I_SHOT
      DO K = 1, WFR(0)
        WFR(K) = WFR(K) / 100. ! CHANGE UNITS TO METERS
        WFDATA(K) = WFDATA(K)*1.E06 ! CHANGE UNITS TO PART/METERS^3
        WRITE(55,*)WFR(K), WFDATA(K)
      END DO
      CLOSE(55)
      CALL SYMBL(2) ! CHANGE SYMBOL TYPE
      CALL SIZES(1.0) ! SET SYMBOL SIZE
      CALL CPlot(WFR,WFDATA) ! PLOT NEXT DATA SET
C      PLOTTING THE LEGEND
      IYLEG = IYLEG - 25 ! MOVE TO NEXT LEGEND LINE
      CALL MOVABS(IXLEG, IYLEG) ! MOVE TO POSITION
      CALL SYMOUT(2, 1.) ! OUTPUT SYMBOL
      ITOI = INDEX(WFDESC,'=')
      TOI = WFDESC(ITOI+1:ITOI+4)
      MIRILEG2 = 'MIRI@' // TOI //'S'
      MIRILEG = 'MIRI'
      CALL AGTMHS(IXLEG+20, IYLEG-8, MIRILEG)
      IY2BOX = IY2BOX - 25 ! MOVE THE CORNER OF THE BOX
      CALL AGTMHS(880,50,MIRILEG2)
END IF

!

C      HERE WE PLOT THE THOMSON SCATTERING DATA IF REQUESTED
      IF (TS.NE.0) THEN
C      GET THE THOMSON SCATTERING DATA
      CALL WF_GET(I_SHOT,TSNE, WFDESC, IQUAL, XSTART, XDELTA
*      , XUNITS, WFDATA(1), NN, NUMGOT, WFUNITS, IERR)
      WFDATA(0) = NUMGOT ! SET THE NUMBER OF DATA POINTS
C      PLOT THE HEADER FOR THE THOMSON SCATTERING DATA
      WFDESC = WFDESC(1:35)
CHERE
      ITOI = INDEX(WFDESC,' MS')
      TOI = WFDESC(ITOI-4:ITOI-1)
      MIRILEG2 = 'TS@' // TOI //'MS'
      CALL AGTMHS(900,70,MIRILEG2)
C      CALL AGTMHS(INT(COMGET(IBASEI(13))),INT(COMGET(IBASEY(14)))
C      , WFDESC)
C      *
C      GET THE RADIAL DATA ARRAY FOR THE THOMSON SCATTERING DATA
      CALL WF_GET(I_SHOT,TSXR, WFDESC, IQUAL, XSTART, XDELTA

```

```

*      , XUNITS, WFR(1), NN, NUMGOT, WFUNITS, IERR)
      WFR(0) = NUMGOT ! SET THE NUMBER OF DATA POINTS
      OPEN(55,FILE='T.TS;1',STATUS='UNKNOWN')
      WRITE(55,*)WFR(0), I_SHOT
      DO K = 1, WFR(0)
        WFR(K) = WFR(K) / 100. ! CHANGE UNITS TO METERS
        WFDATA(K) = WFDATA(K)*1.0E19 ! CHANGE UNITS TO PART/METERS^3
        WRITE(55,*)WFR(K), WFDATA(K)
      END DO
      CLOSE(55)
      CALL SYMBL(8) ! SET SYMBOL TYPE
      CALL SIZES(1.0) ! SET SYMBOL SIZE
      CALL CPLOT(WFR,WFDATA) ! PLOT NEXT DATA SET
C      PLOTTING THE LEGEND
      IYLEG = IYLEG - 30 ! MOVE TO NEXT LEGEND LINE
      CALL MOVABS(IXLEG, IYLEG) ! MOVE TO POSITION
      CALL SYMOUT(8, 1.) ! OUTPUT SYMBOL
      CALL AGTMHS(IXLEG+20, IYLEG-10, 'TS')
      IY2BOX = IY2BOX - 33 ! MOVE THE CORNER OF THE BOX
      END IF
      CALL MOVABS(IX1BOX,IY1BOX)
      CALL DRWABS(IX2BOX,IY1BOX)
      CALL DRWABS(IX2BOX,IY2BOX)
      CALL DRWABS(IX1BOX,IY2BOX)
      CALL DRWABS(IX1BOX,IY1BOX)
    ELSE
      CALL BINITT() ! INITIALIZE DATA BLOCKS
      IF( IDENREC .LE. 13 ) THEN
        CALL PLACE2((ABS(IDENREC)))! SET SCREEN WINDOW
      ELSE
        IF( IDENREC .EQ. 14 ) THEN
          CALL SLIMX(IPHIMINX,IPHIMAXX)
          CALL SLIMY(IPHIMINY+ISHIFTY,IPHIMAXY+ISHIFTY)
        ELSE
          CALL SLIMX(IPHIMINX,IPHIMAXX)
          CALL SLIMY(IPHIMINY,IPHIMAXY)
        END IF
      END IF
      CALL DLIMX(R1REC,R2REC) ! SET X-AXIS DATA LIMITS
      CALL DLIMY(D1REC,D2REC) ! SET Y-AXIS DATA LIMITS
      CALL LINE(IDENTYPE) ! SET LINE TYPE
      CALL SYMBL(IDENSYMBL) ! SET SYMBOL TYPE
      CALL SIZES(DENSIZE) ! SET SYMBOL SIZE
      CALL CHECK(RRLOW,DENLOW) ! SET DATA BLOCKS
      CALL CPLOT(RRLOW,DENLOW) ! PLOT DATA

```

```

                IF(ERR_ON .NE. 0) CALL ERR_BAR(RRLOW,DENLOW,WREF)
            END IF
        END IF
C
        CALL TSEND() ! EMPTY DATA BUFFER
        END DO ! LOOP OVER KK = 1 TO IPLOTS
        WRITE(TITLE,415) ' - ',TIME2
415        FORMAT(A4,F5.3) ! PLOT THE LAST TIME
C        CALL AGTMHS(450,ITITLE,TITLE)
        CALL FINITT(10,100) ! CLOSE PLOTTING SUBROUTINES
        CLOSE(22) ! CLOSE FILE "T.FLS"
        CLOSE(66) ! CLOSE FILE "T.ERR"

        STOP
        END
!
```

The subroutine "PLACE2" simply sets the screen coordinates for the plotting subroutines.

```

C
C *****
C
        SUBROUTINE PLACE2(IPLACE)
            INTEGER IPLACE

            character*3 places(13)
            data places /'STD','UPH','LOH','UL4','UR4','LL4','LR4',
>                    'UL6','UC6','UR6','LL6','LC6','LR6'/
            call place(places(IPLACE))

            RETURN
            END
!
```

C

!

This subroutine calculates the increment on the cutoff position and the density at that point. It is the main part of the reconstruction process and it was put in a subroutine to ease the readability of the program.

```

C *****
C
        SUBROUTINE THOMAS(I,N,NN2,RRLOW,DELREC,RRUP,DENLOW,DENUP
```

```

      * ,PHIRLOW,DELPHI,PHIRUP,WREF,WM,IDUMY)
      IMPLICIT NONE
      PARAMETER NDATA=4
      INTEGER I, N, NN2,IDUMY
C      DOUBLE PRECISION
      REAL
      * DTEMP1, DTEMP2, DTEMP3, DTEMP4, RZDEL
      * , MU2REC, SNREC, MUR_1, MUR_2, MUR_3, DELR1
C      DOUBLE PRECISION
      REAL
      * PI,ELECHR,ELEMAS,EPSILO,C
      * , RRLOW(0:*), DELREC(0:*), RRUP(0:*), DENLOW(0:*), DENUP(0:*)
      * , PHIRLOW(0:*), DELPHI(0:*), PHIRUP(0:*), WREF(0:*), WM
      * , BF, BFIELD, WCE, WW, FDELTA1
      !

```

This is the subroutine that calculates the increment in the cutoff positions. It was put in a subroutine so that it will make the program easier to read and work with it. The formula for the increment in the cutoff position has been derived and explained in detail in the thesis. There are different linear and parabolic fits that can be done to the unknown part of the index of refraction in order to obtain a formula for the increment on the positions of the cutoffs. It was found that the one using the condition of the derivative or slope that the last two points of the index of refraction was the one that provided with the best fit to the index of refraction. That is the one used here, even though that the formulas for the other cases have been commented out and left here to allow for future work if necessary.

```

C
C      THIS SUBROUTINE CALCULATES THE INCREMENT ON THE RADIAL
C      POSITION OF THE CUTOFF, THE POSITION OF THE CUTOFF, AND
C      THE DENSITY AT THE CALCULATED CUTOFF POSITION FOR THE
C      RECONSTRUCTION PROCESS.
C      THIS DEFINES SOME CONSTANTS IN MKS UNITS.
      PI      = 3.14159265      ! RADIANS
      ELECHR = 1.60217733D-19 ! COULOMBS
      ELEMAS = 9.1093897D-31   ! Kg
      EPSILO = 8.854187817D-12 ! F/m
      C      = 299792456.2     ! +-1.1 M/SEC, FROM: K. Evenson et al,
C              !Physics Review Letters,
C              !Vol 29, p 1346 (1972)
C      BEGINS IVAN'S METHOD
      MUR_1 = MU2REC(RRLOW(I), DENLOW(I), WREF(I)+WM/2.)
      MUR_2 = MU2REC(RRLOW(I+1), DENLOW(I+1), WREF(I)+WM/2.)
      MUR_3 = MU2REC(RRLOW(I+2), DENLOW(I+2), WREF(I)+WM/2.)
      MUR_1 = MUR_1 / SQRT(ABS(MUR_1))
      MUR_2 = MUR_2 / SQRT(ABS(MUR_2))

```

```

MUR_3 = MUR_3 / SQRT(ABS(MUR_3))
DTEMP1 = (PHIRLOW(I)+DELPHI(I)) * (C/(2.*(WREF(I)+WM/2.)))
DTEMP2 = SNREC(I,N+NN2,RRLOW(1),DENLOW(1),WREF(I)+WM/2.)
IF( IDUMY .EQ. 1 ) THEN
C   REAL INDEX FIT
      DTEMP3 = (DTEMP1 - DTEMP2)
      DTEMP4 = ( MUR_1 * 5./6. - MUR_2 / 6. )
      RZDEL = 10.0E-5
      DELR1 = FDELTA1(RRLOW(I),DENLOW(I),RRLOW(I+1),DENLOW(I+1)
*      ,WREF(I)+WM/2.,DTEMP1,DTEMP2,RZDEL)
      WRITE(11,11)'INDEX1', DTEMP1, DTEMP2, DTEMP3, DELR1
11  FORMAT(A6,5E12.5)
      ELSE
C   DERIVATIVE CONDITION
      DTEMP3 = (DTEMP1 - DTEMP2)
      DTEMP4 = ( MUR_1 * 5./6. - MUR_2 / 6. )
      DELR1 = DTEMP3 / DTEMP4
      WRITE(11,11)'DERIV ', DTEMP1, DTEMP2, DTEMP3, DTEMP4, DELR1
END IF

C
      DELREC(I) = DELR1

C
      RRUP(I) = RRLOW(I) - DELREC(I)
      BF = BFIELD(RRUP(I)) !DEFINES THE MAGNETIC FIELD
      WCE = (BF*ELECHR/ELEMAS)/(2.*PI) !ELEC CYCLOTRON FREQ
      DENUP(I) = (WREF(I)+WM/2.) * (WREF(I)+WM/2.-WCE)
*      * (ELEMAS/ELECHR) * (EPSILO/ELECHR) * (4.*PI*PI)
      PHIRUP(I) = PHIRLOW(I) + DELPHI(I)

      WW = (WREF(I-1) - WM/2.) - (WREF(I) + WM/2.)
      RRLOW(I-1) = (RRUP(I)-RRLOW(I)) * WW/WM + RRUP(I)

C
      BF = BFIELD(RRLOW(I-1)) !MAGNETIC FIELD
      WCE = (BF*ELECHR/ELEMAS)/(2.*PI) !ELEC CYCLOTRON FREQ
      DENLOW(I-1) = (WREF(I-1)-WM/2.) * (WREF(I-1)-WM/2.-WCE)
*      * (ELEMAS/ELECHR) * (EPSILO/ELECHR) * (4.*PI*PI)
      PHIRLOW(I-1) = DELPHI(I) * WW/WM + PHIRUP(I)

RETURN
END
!
C
!
```

The subroutine FDELTA calculates the increment on the cutoff using a zero finding function to the index of refraction.

```

C
C *****
C
      REAL FUNCTION FDELTA1(R2,DENR2,R3,DENR3
*      ,WREF,DTEMP1,DTEMP2,RZDEL)
      IMPLICIT NONE
      REAL    R2, DENR2, WREF, ZERO_OLD
      REAL    DTEMP1,DTEMP2,RZDEL, DELRK, ZERO
      REAL    DELR1, R1, DENR1, R1OLD, R3, BF, BFIELD
*      , WCE, DENR3, M_SLOPE, DELH, RH, DEN_RH, MU_RH, MU2REC

      DOUBLE PRECISION  X_PAR(3), Y_PAR(3), AA, BB, CC

      REAL              RO, RA, BO, ELECHR, ELEMAS, EPSILO, C, PI
*      , CURRENT, POL_CUR
      INTEGER  NTURN
      COMMON /COMDAT/ RO, RA, BO, ELECHR, ELEMAS, EPSILO, C, PI
*      , NTURN, CURRENT, POL_CUR

      INTEGER  K, K_POINTS

      K_POINTS = 100
      ZERO = DTEMP1 - DTEMP2
      ZERO_OLD = ZERO
      DELR1 = RZDEL
      DELH = DELR1 / 100. ! 1.0D-6
      R1 = R2
      WRITE(11,*)' '
      WRITE(11,*)'O R1=',R1,' ZERO=',ZERO
      DO WHILE((ZERO .GE. 1.0D-6) .AND. (DELR1 .GE. 1.0D-6)
*      .AND. (ZERO .LE. ZERO_OLD ))
          ZERO = DTEMP1 - DTEMP2
          ZERO_OLD = ZERO
          R1OLD = R1
C      SET UP LINEAR FIT TO THE DENSITY
          R1 = R1 - DELR1
C
          R3 = R1
          BF = BFIELD(R1)
          WCE = BF * (ELECHR/ELEMAS) / ( 2. * PI )
          DENR1 = WREF * (WREF-WCE) * (ELEMAS/ELECHR)
*          * (EPSILO/ELECHR) * (4.*PI*PI)
          IF(DENR1 .LT. 0.0) WRITE(11,*)'NEGATIVE DEN', DENR1

```



```

C      IF(DENR1 .LT. DENR2) DENR1 = DENR2
C      IF(R2 .EQ. R3) R2 = R2*1.00001
C      M_SLOPE = ( DENR2 - DENR3 ) / ( R2 - R3 )
C      WRITE(11,*)' '
C      WRITE(11,*) DENR1, DENR2, DENR1-DENR2
C      WRITE(11,*) R1, R2, R1-R2
C
C      SET FIRST POINT FOR PARABOLIC FIT TO THE DENSITY
C      X_PAR(1) = R1
C      Y_PAR(1) = DENR1
C      SET SECOND POINT FOR PARABOLIC FIT TO THE DENSITY
C      X_PAR(2) = R2
C      Y_PAR(2) = DENR2
C      SET LAST POINT FOR PARABOLIC FIT
C      X_PAR(3) = R2
C      Y_PAR(3) = (DENR2-DENR3) / (R2-R3)
C      PASS PARAMETERS TO SUBROUTINE TO CALCULATE PARABOLIC COEF.
C      CALL GETABC(X_PAR,Y_PAR,AA,BB,CC)
C      WRITE(11,524)( K, X_PAR(K), Y_PAR(K), K=1,3 )
524  FORMAT(I3,' X_PAR=',F20.16,' Y_PAR=',D25.16)
C      WRITE(11,*)' AA BB CC '
C      WRITE(11,*) AA, BB, CC
C
C      DELH = 1.0D-6
C      RH = R2 + DELH
C      MU_RH = 1.
C      WRITE(11,*)'1', R1, R2, DENR1, DENR2
C      WRITE(11,*)'2' RH, DEN_RH, MU_RH, ZERO '
C      DO WHILE( MU_RH .GE. 0.0 )
C      DELRK = (R2 - R1) / (K_POINTS-1)
C      DO K = 1, K_POINTS
C      RH = RH - DELH
C      RH = R2 - DELRK * (K-1)
C      DEN_RH = CC + ( BB + AA * RH ) * RH !PAR. DENSITY FIT
C      WRITE(11,*)' PARABOLIC DENSITY = ',DEN_RH
C      DEN_RH = M_SLOPE * (RH - R2) + DENR2 !LINEAR DENS. FIT
C      WRITE(11,*)' LINEAR DELSITY = ',DEN_RH
C      MU_RH = MU2REC(RH, DEN_RH, WREF)
C      IF(MU_RH .NE. 0.0) MU_RH = MU_RH / SQRT( ABS(MU_RH) )
C      ZERO = ZERO - DELH * MU_RH
C      ZERO = ZERO - DELRK * MU_RH
C      WRITE(11,*) RH, DEN_RH, MU_RH, ZERO
C      END DO
C      WRITE(11,*)'4 ZERO = ',ZERO,' DELR1=', DELR1
C      IF( ZERO .LT. 0.0 ) THEN

```

```

        DELR1 = DELR1 / 2.
        R1 = R1OLD
    END IF
END DO
C      WRITE(11,*)'5', R1, R2, DELR1
C      WRITE(11,*)'5', DENR1, DENR2
      WRITE(11,*)'6 R1=',R1,' ZERO=',ZERO

      FDELTA1 = R2 - R1

      RETURN
      END

```

```

C
!

```

```

C
!

```

The subroutine GETABC calculates the coefficients for the parabolic fit when using the assumption of equal step size for the positions of the cutoffs.

```

C *****
C
      SUBROUTINE GETABC(X,Y,A,B,C)
      DOUBLE PRECISION Y(3), X(3), A, B, C, DELX1

      DELX1 = X(2) - X(1)

      A = ( ( Y(1) - Y(2) ) / DELX1 + Y(3) ) / DELX1

      B = ( Y(2) - Y(1) ) / DELX1 - A * ( X(2) + X(1) )

      C = Y(1) - B * X(1) - A * X(1)*X(1)

      RETURN
      END
!

```

This is one version of the reconstruction subroutine used during the development of the program.

```

C
C
C *****
C

```

```

SUBROUTINE THOMAS1(I,N,NN2,RRLOW,DELREC,RRUP,DENLOW,DENUP
* ,PHIRLOW,DELPHI,PHIRUP,WREF,WM)
IMPLICIT NONE
INTEGER I, N, NN2
REAL PI, ELECHR, ELEMAS, EPSILO, C
* , RRLOW(0:*), DELREC(0:*), RRUP(0:*), DENLOW(0:*), DENUP(0:*)
* , PHIRLOW(0:*), DELPHI(0:*), PHIRUP(0:*), WREF(0:*), WM
* , TEMP, TEMP2, MU2REC, SNREC, SNF1, BF, BFIELD, WCE, WW

C      THIS DEFINES SOME CONSTANTS IN MKS UNITS.
PI      = 3.14159265      ! RADIANS
ELECHR  = 1.60217733E-19 ! COULOMBS
ELEMAS  = 9.1093897E-31  ! Kg
EPSILO  = 8.854187817E-12 ! F/m
C       = 299792456.2     ! +-1.1 M/SEC, FROM: K. Evenson et al,
C                                     !Physics Review Letters,
C                                     !Vol 29, p 1346 (1972)
C      BEGINS IVAN'S METHOD
C      SNF1=SNREC(I,N+JSTEP,RRLOW(1),DENLOW(1),WREF(I)+WM)
C      SNF1=SNREC(I,N+NN2,RRLOW(1),DENLOW(1),WREF(I)+WM) !,STEP(KK))
C      TEMP = SQRT(MU2REC(RRLOW(I), DENLOW(I) ,WREF(I)+WM))
C      TEMP2 = SQRT(MU2REC(RRLOW(I+1),DENLOW(I+1),WREF(I)+WM))
C      DELREC(I) = (PHIRLOW(I)*C/(2.*(WREF(I)+WM))-SNF1)
/      / ( TEMP * 2./3. - TEMP2 / 12. )
C      ENDS IVAN'S METHOD

C      BEGINS WILGEN'S SHIFTING METHOD
C      SNF1=SNREC(I,N+NN2,RRLOW(1),DENLOW(1),WREF(I)+WM)
CC     SNF1=SNREC(I,N+JSTEP,RRLOW(1),DENLOW(1),WREF(I)+WM)
C      DELREC(I) = (DELPHI(I)*C - SNF1*2.*WM )
C      /      / (2.*(WREF(I)+WM))
C      ENDS WILGEN'S SHIFTING METHOD

RRUP(I)  = RRLOW(I) - DELREC(I)
BF = BFIELD(RRUP(I)) !DEFINES THE MAGNETIC FIELD
WCE = (BF*ELECHR/ELEMAS)/(2.*PI)      !ELEC CYCLOTRON FREQ
DENUP(I) = (WREF(I)+WM) * (WREF(I)+WM-WCE)
*      * (ELEMAS/ELECHR) * (EPSILO/ELECHR) * (2. * PI)**2
PHIRUP(I) = PHIRLOW(I) + DELPHI(I)

WW      = WREF(I-1) - (WM + WREF(I))
RRLOW(I-1) = (RRUP(I)-RRLOW(I))/WM * WW + RRUP(I)
BF = BFIELD(RRLOW(I-1))      !MAGNETIC FIELD
WCE = (BF*ELECHR/ELEMAS)/(2.*PI)      !ELEC CYCLOTRON FREQ
DENLOW(I-1) = WREF(I-1) * (WREF(I-1)-WCE)

```

```

      *      * (ELEMAS/ELECHR) * (EPSILO/ELECHR) * (2. * PI)**2
      PHIRLOW(I-1) = DELPHI(I)/WM * WW + PHIRUP(I)

C      THIS IS TO CHECK THE CALCULATED RESULTS WITH THE ASSUMED.
C      VERY USEFULL FOR DEBUGING PURPOSES.
C      T2 = 2.*(WREF(I)+WM)/C
C      *      * SNREC(I,NN2+N,RRUP(1),DENUP(1),WREF(I)+WM)
CC     *      * SNREC(I,JSTEP+N,RRUP(1),DENUP(1),WREF(I)+WM)
C      T1 = 2.* WREF(I) /C
C      *      * SNREC(I,NN2+N,RRLOW(1),DENLOW(1),WREF(I))
CC     *      * SNREC(I,JSTEP+N,RRLOW(1),DENLOW(1),WREF(I))
C      DELPREC(I) = T2 - T1
C
C      WRITE(11,150)I,RRLOW(I),RRUP(I),T2,T1,DELPREC(I)
C      WRITE(11,150)I,RRLOW(I),DELREC(I),T2,T1,DELPREC(I)
C      *      , PHIRLOW(I), PHIRUP(I), PHIRUP(I)-PHIRLOW(I)
C      *      , DENLOW(I), DENUP(I)
C 150  FORMAT(I4, 2F7.4, 2F6.1, F7.3, 2F6.1, F6.3, 2(' ',P1E10.3) )

      RETURN
      END

```

This subroutine calculates and plots the error bars for the density profile.

```

C
C*****
C
C      SUBROUTINE ERR_BAR(RRLOW,DENLOW,WREF)
C      THIS SUBROUTINE CALCULATES THE ERROR BARS FOR TOMY.
C      REAL RRLOW(0:*), DENLOW(0:*), I(0:1), Y(0:1), TEMP, COMGET
C      *      , DNDR, ERR_R, ERR_TOM, N_REF, WREF(0:*), WTEMP, PH_SIG(0:1000)
C
C      REAL RO, RA, BO, ELECHR, ELEMAS, EPSILO, C, PI
C      *      , CURRENT, POL_CUR
C      INTEGER NTURNS
C
C      COMMON /COMDAT/ RO, RA, BO, ELECHR, ELEMAS, EPSILO, C, PI
C      *      , NTURNS, CURRENT, POL_CUR
C
C      INTEGER ERR_SYMB, IBASEY
C

```

```

      OPEN(88,FILE='T.SIG',STATUS='OLD')
      READ(88,*) WTEMP, PH_SIG(0)
      READ(88,*)(WTEMP, PH_SIG(I), I=1,PH_SIG(0))
      CLOSE(88)
      OPEN(11,FILE='T.BAR;1',STATUS='UNKNOWN')
      ERR_SYMB = 7
CHERE  TEST OF THE ERROR BARS...
      X(0) = 1
      Y(0) = 1
      CALL LINE(-4)  !SET LINE TYPE TO POINT PLOT
      CALL SYMBL(ERR_SYMB)  !SET SYMBOL TYPE TO A "|"
      TEMP = ( COMGET(IBASEY(14)) - COMGET(IBASEY(13)) )
      /      / ( COMGET(IBASEY(12))-COMGET(IBASEY(11)) )
      /      *3./15.
C      *      * 0.2 / 10.
      WRITE(11,*)' TEMP', TEMP
C      DO I=1+1, RRLOW(0), RRLOW(0)/10
      DO I=1+1, WREF(0)-WREF(0)/10, WREF(0)/10
          X(1) = RRLOW(I)
          Y(1) = DENLOW(I)
          IF(RRLOW(I+1).EQ.RRLOW(I)) WRITE(*,*) I, RRLOW(I)
          DNDR = -(DENLOW(I+1)-DENLOW(I))/(RRLOW(I+1)-RRLOW(I))
          ERR_R = DNDR * 0.001  !Meters
C          N_REF = MU2(RRLOW(I), WREF(I)+WM(IWM)/2., RSHIFT(II)
C      *      , SHAPE(JJ), DERDEN(LL))
C          N_REF = SQRT( N_REF )
          N_REF = 1.
          WRITE(11,*) I, WREF(I),'=W', PH_SIG(I),'=PHI_SIG'
          ERR_PHI = PH_SIG(I) * DNDR * 2. * C / (WREF(I) * N_REF)
          ERR_B = (WREF(I) * EPSILO / ELECHR ) * B0 * 0.001
          ERR_R1 = (WREF(I) * EPSILO * B0 * R0) / (ELECHR * RRLOW(I) ** 2) * 0.001
          WRITE(11,*) ERR_R,'=R', ERR_PHI,'=PHI', ERR_B,'=B'
      *      , ERR_R1,'=R1'
          ERR_TOM = SQRT(ERR_R**2+ERR_PHI**2+ERR_B**2+ERR_R1**2)
C          ERR_TOM = SQRT(ERR_R*ERR_R + ERR_PHI*ERR_PHI)
          CALL SIZES(ERR_TOM*TEMP)
C          CALL SIZES(Y(1)*TEMP)
          CALL CPLOT(X,Y)
      END DO
      CALL SYMBL(0)  !SET SYMBOL TYPE TO THE DEFAULT
CEND TEST OF ERROR BARS
      CLOSE(11)
      RETURN
      END
C

```

```

!
!
C
C *****
C
C FUNCTIONS AND SUBROUTINES
C
C *****
C
C *****
C
REAL FUNCTION SNREC(I,N,R,DENS,WREF)
C THIS FUNCTION CALCULATES THE INTEGRAL OF THE REFRACTIVE INDEX
C USING THE RECONSTRUCTED DENSITY PROFILE DATA.
C2APR93 This new version of SNREC is a more efficient and fast way to
C calculate the integral of the refractive index for the
C reconstructed density profile. It interpolates on the
C reconstructed density profile data to integrate using a fixed
C number of points given by N.
IMPLICIT NONE
INTEGER I, N, K, J, NK, NURNS, IIERR
COMMON /COMDAT/ RO, RA, BO, ELECHR, ELEMAS, EPSILO, C, PI, NURNS
* , CURRENT, POL_CUR, IIERR, BERR(11)
REAL R(N), DENS(N), WREF, RJ, DELRJ, TJ, MU2REC, DENRJ, BFIELD
* , CURRENT, POL_CUR, BERR
REAL
* RO !MAJOR RADIUS
* , RA !MINOR RADIUS
* , BO !CENTRAL MAGNETIC FIELD
* , ELECHR !ELECTRON'S CHARGE
* , ELEMAS !ELECTRON'S MASS
* , EPSILO !PERMITIVITY OF FREE SPACE
* , C !SPEED OF LIGHT IN FREE SPACE
* , PI ! = 3.14159265

TJ = 0.0
SNREC = 0.0
DELRJ = ( R(N) - R(I) ) / N
RJ = R(N) + DELRJ
NK = N
C OPEN(44,FILE='T.SNR;1',STATUS='UNKNOWN')
C WRITE(44,*)I,N,WREF
DO J = 1, N

```

```

      RJ = RJ - DELRJ
      DO K = I+1, NK
        IF( (R(K-1).LE.RJ) .AND. (RJ.LT.R(K)) )THEN
          DENRJ = (DENS(K)-DENS(K-1))/(R(K)-R(K-1))
            * * (RJ-R(K-1)) + DENS(K-1)
          TJ = SQRT( MU2REC(RJ,DENRJ,WREF) )
          GOTO 11
        END IF
      END DO
      11  CONTINUE
      C  WRITE(44,*)K,'=K ',RJ,'=RJ ',DENRJ,'=DENRJ ',SNREC,'=SNREC '
      SNREC = SNREC + TJ
    END DO
    SNREC = SNREC * DELRJ
    C CLOSE(44)

  RETURN
  END
  !

  C
  C *****
  C
  REAL FUNCTION MU2REC(R,DENS,WREF)
  C THIS FUCNTION CALCULATES THE INDEX OF REFRACTION USING THE
  C RECONSTRUCTED DENSITY PROFILE
  IMPLICIT NONE
  REAL R, BF, DENS, WCE, WPE, WREF,PI
    * , RO,RA,BO, ELECHR, ELEMAS, EPSILO, C
    * , TEMP1, TEMP2, BFIELD
    * , CURRENT, POL_CUR, BERR
  COMMON /COMDAT/ RO,RA,BO, ELECHR, ELEMAS, EPSILO, C, PI, NURNS
    * , CURRENT, POL_CUR, IIERR, BERR(11)
  INTEGER NURNS, IIERR

  BF = BFIELD(R) ! MAGNETIC FIELD AT "R"
  TEMP1 =(ELECHR/EPSILO)
  TEMP2= (ELECHR/ELEMAS)
  IF(DENS.LT. 0.0) THEN ! CHECK FOR ERRONEUS DENSITY INFORMATION
    WRITE(*,10) DENS,R,WREF/1.0E+09
    10  FORMAT(' NEGATIVE DENSITY= ',E16.4,F11.4,'=R ',F11.4,'=WREF')
    WRITE(*,*)' PATCHING UP TO CONTINUE'
    DENS = ABS(DENS)
    STOP
  END IF

```

```

WPE = SQRT( ABS(DENS) * TEMP1 * TEMP2 ) / ( 2. * PI)
WCE = (BF * TEMP2) / ( 2. * PI)

```

```

MU2REC = 1.0 - WPE*WPE/(WREF*WREF) * (WREF*WREF-WPE*WPE) /
      / (WREF*WREF - WPE*WPE - WCE*WCE)

```

```

RETURN
END
!

```

```

C
C *****
C

```

```

      REAL FUNCTION BFIELD(R)
IMPLICIT NONE
      REAL R
      REAL CR, MO,M1,M2,M3,M4,M5, BF, BPOL, BERR
REAL RO, RA, BO, ELECHR, ELEMAS, EPSILO, C, PI, CURRENT, POL_CUR
COMMON /COMDAT/ RO, RA, BO, ELECHR, ELEMAS, EPSILO, C, PI, NTURNS
      * , CURRENT, POL_CUR, IIERR, BERR(11)
INTEGER NTURNS, IIERR
      DATA MO/5.5389/, M1/-8.401/, M2/6.2041/, M3/-2.2861/
      * , M4/0.42053/, M5/-0.030917/
BO = 2.0E-07 * NTURNS * CURRENT / RO
      CR = MO+R*(M1+R*(M2+R*(M3+R*(M4+R*M5))))
BF = CR * BO * RO/R
BPOL = 2.0E-07 * POL_CUR / (R-RO) * (RO/R)
BFIELD = SQRT( BF*BF + BPOL*BPOL ) + BERR(IIERR)
      RETURN
      END

```

```

!

```



## APPENDIX E

### CALL NUMBERS FOR THE BIBLIOGRAPHY

We have taken the liberty of including the library call numbers for the books and magazines mentioned in this report, in the best interest to help an interested reader to find the references. The titles of most articles have been included for the same purpose.

1. Bulletin of the American Physical Society ..... QC 1.A56
2. Fusion Technology ..... TK 9204.N82
3. IEEE Transactions on Plasma Science ..... TA 2110.I18A
4. International Journal of Infrared and Millimeter Waves ..... TA 1570.I6
5. Journal of Physics E: Scientific Instruments ..... Q 184.J6
6. Nuclear Fusion ..... QC 791.N8
7. Plasma Physics and Controlled Fusion ..... QC 770.P5
8. Physical Review Letters ..... QC 1.P43
9. Physics Today ..... QC 1.P658
10. Radio Frequency Power in Plasmas ..... QC 718.5.H5 R36X
11. Review of Scientific Instruments ..... Q 148.R5
12. Soviet Physics JETP ..... QC 1.Z472

13. Soviet Physics – Technical Physics ..... QC 1.Z482X

## BIBLIOGRAPHY

- 1 Weston M. Stacey, Jr.  
"Fusion  
An Introduction to the Physics and Technology of Magnetic Confinement  
Fusion"  
John Wiley & Sons, New York, 1984  
QC 791.73.S73
- 2 Meyerhof  
"Elements of Nuclear Physics"  
McGraw-Hill, New York, 1967  
QC 776.M4.
- 3 J. G. Cordey, et al.  
"Progress Toward a Tokamak Fusion Reactor"  
Physics Today, Vol. 45 No. 1, p. 22, Jan. 1992
- 4 John W. Willis  
"Confinement Systems Program Summary"  
July 1990, DOE/ER-0478T  
U.S. Government Printing Office: 1990 O-862-957
- 5 K. G. Budden  
"Radio Waves in the Ionosphere"  
Cambridge U. P., Cambridge, 1961  
QC 973.4.I6 B82X.
- 6 J. O. Thomas  
Proceedings of the Institute of Radio Engineering, Vol. 47, p. 162 (1959)
- 7 D. Davies  
"Ionospheric Radio Waves"  
Chapters 3 and 8  
Ginn and Blaisdell, 1969  
TK 6553.D293
- 8 V. I. Ginzburg  
"The Propagation of Electromagnetic Waves in Plasmas"  
sec. 16, pp. 229-231, Series solution  
sec. 17, pp. 240-242, Exact solution for linear  $\epsilon$   
2<sup>nd</sup> ed., Pergamon Press, Oxford, 1970  
QC 661.G533

- 9 J. F. Lyon  
"The Advanced Toroidal Facility"  
Fusion Tech., Vol. 10, pp. 179-226, Sept. 1986
- 10 Fritz Rau  
"Ninth International Workshop on Stellarators"  
Stellarator News, Issue #28, July 1993  
Published by Fusion Energy Division, Oak Ridge National Laboratory  
Building 9201-2, P.O. Box 2009, Oak Ridge, TN 37831-8071, USA  
Editor: James A. Rome, Phone: (615) 574-1306  
E-Mail: JAR@ORNL.GOV
- 11 B. A. Carreras, et al.  
"Progress in Stellarator/Heliotron Research: 1981-1986"  
Nuclear Fusion, Vol. 28, No. 9, pp. 1613-1694 (1988)
- 12 K. M. Young, et al.  
"TFTR Initial Operations"  
Plasma Physics and Controlled Fusion, Vol. 26, No. 1A, pp. 11-22 (1984)
- 13 K. V. Orlinskij and G. Magyar  
"Plasma Diagnostics on Large Tokamaks"  
Nuclear Fusion, Vol. 28(4), pp. 611-697 (1988)
- 14 Earl C. Tanner  
"Project Matterhorn: an Informal History"  
Princeton Plasma Physics Laboratory Publications, 1982  
QC 718.615.U62 P747
- 15 Earl C. Tanner  
"First Princeton Tokamaks: an Informal History"  
Princeton Plasma Physics Laboratory Publications, 1982  
QC 718.615.U62 P7474
- 16 Earl C. Tanner  
"Model C Decade: an Informal History"  
Princeton Plasma Physics Laboratory Publications, 1980  
QC 718.615.U62 P7475
- 17 A. I. Anisimov, et al.  
"Method of Investigating Electron Spatial Distribution in a Plasma"  
Soviet Physics - Tech. Phys. Vol. 5, No. 9, pp. 939-948, March 1961

- 18 V. A. Anoshkin, et al.  
"Microwave Investigations of Plasma on the 'Alpha' Device"  
Soviet Physics - Tech. Phy. Vol. 5, No. 12, pp. 1370-1377, June 1961
- 19 R. J. Colchin  
Intra-Laboratory Correspondence  
ORMAK Technical Memo No. 105  
Oak Ridge National Laboratory, May 3, 1973
- 20 R. J. Colchin  
Intra-Laboratory Correspondence  
ORMAK Technical Memo No. 93  
Oak Ridge National Laboratory, January 17, 1973
- 21 F. Simonet  
"Measurement of Electron Density Profile by Microwave Reflectometry on Tokamaks"  
Review of Scientific Instruments, Vol. 56(5), pp. 664-669, May 1985
- 22 F. Simonet  
Ph.D. Thesis  
Univesité de Nancy, 1985
- 23 TFR Group, presented by F. Simonet  
"Measurements of Electron Density Profile and Local Density Fluctuations by Microwave Reflectometry on TFR"  
Proceedings of the 11<sup>th</sup> European Conference on Controlled Fusion and Plasma Physics, Aachen, 1983  
pp. 85-88, Vol. 7D, Part I
- 24 S. H. Heijnen, et al.  
"A Multichannel Reflectometer for the RTP Tokamak"  
19<sup>th</sup> EPS Conference on Confined Fusion and Plasma Physics  
pp. 1059-1062, June 1992
- 25 M. A. G. Calderon and F. Simonet  
"Experimental Study of a Swept Reflectometer with a Single Antenna for Plasma Density Profile Measurement"  
Int. J. Infrared and Millimeter Waves, Vol. 6, No. 7, pp. 605-628 (1985)
- 26 J. Sánchez, et al.  
"Observation of Density Fluctuations Associated with the Resonant  $q = 2$

- Surface on the Wendelstein VII-AS Stellarator"  
Nuclear Fusion, Vol. 30, No. 11, pp. 2383-2391 (1990)
- 27 J. Sánchez, et al.  
"Radial Distribution of Turbulence Correlation Lengths Obtained by Reflectometry in the TJ-1 Tokamak"  
9<sup>th</sup> Topical Conference on High-Temperature Plasma Diagnostics  
March 15-19, 1992  
and/or  
Review of Scientific Instruments, Vol. 63(10), p. 4657, Oct. 1992
- 28 J. Sánchez, et al.  
"Amplitude Modulation Reflectometry for Large Fusion Devices"  
9<sup>th</sup> Topical Conference on High-Temperature Plasma Diagnostics  
March 15-19, 1992  
and/or  
Review of Scientific Instruments, Vol. 63(10), pp. 4654-4656, Oct. 1992
- 29 J. Sánchez, et al.  
Nuclear Fusion, Vol. 30, p. 2383 (1990)
- 30 J. Sánchez, et al.  
"Reflectometry Observations of Density Fluctuations in Wendelstein VII-AS Stellarator"  
Proceedings of the 17<sup>th</sup> European Conference on Controlled Fusion and Plasma Physics, Amsterdam, 1990  
pp. 1572-1575, Vol. 14B, Part VI
- 31 J. Sánchez, et al.  
"Broadband Microwave Reflectometry on Wendelstein VII-AS Stellarator"  
Proceedings of the 16<sup>th</sup> European Conference on Controlled Fusion and Plasma Physics, Venice, 1989  
pp. 1565-1568, Vol. 13B, Part VI
- 32 J. Sánchez, et al.  
"Amplitude Modulation Reflectometry for Large Fusion Devices"  
19<sup>th</sup> EPS Conference on Confined Fusion and Plasma Physics  
pp. 1075-1078, June 1992
- 33 J. B. Wilgen, et al.  
"An AM Reflectometer on PBX-M for Edge Density Profile Measurements"  
Bulletin of the American Physical Society, Vol. 38(6), Nov. 1993

- 34 I. H. Hutchinson  
"One-Dimensional Full-Wave Analysis of Reflectometry Sensitivity and Correlations"  
Plasma Physics and Controlled Fusion, Vol. 34, No. 7, pp. 1225-1251 (1992)
- 35 I. Stakgold  
"Green's Functions and Boundary Value Problems"  
John Wiley & Sons, New York (1979)
- 36 M. L. V. Pitteway  
Proceedings of the Royal Society, Vol. 254, p. 86 (1959)
- 37 E. Mazzucato  
Princeton Plasma Physics Laboratory  
Report No. MATT-1151, Sept. 1975
- 38 E. Mazzucato, et al.  
"TFTR Microwave Reflectometer"  
9<sup>th</sup> Topical Conference on High-Temperature Plasma Diagnostics  
March 15-19, 1992  
and/or  
Review of Scientific Instruments, Vol. 63(10), p. 4657, Oct. 1992
- 39 J. B. Wilgen, et al.  
"Microwave Reflectometry for ICRF Coupling Studies on TFTR"  
Princeton Plasma Physics Laboratory Report  
PPPL-2915, Publically available from:  
National Technical Information Service  
Department of Commerce  
5285 Port Royal Road  
Springfield, Virginia 22161
- 40 G. R. Hanson, et al.  
"A Swept Frequency Amplitude Modulated Reflectometer for Measuring the Edge Density Gradient on TFTR"  
9<sup>th</sup> Topical Conference on High-Temperature Plasma Diagnostics  
March 15-19, 1992  
and/or  
Review of Scientific Instruments, Vol. 63(10), pp. 4658-4660, Oct. 1992
- 41 C. Domier, et al.  
"Development of Technology and Techniques for Reflectometry"

- 9<sup>th</sup> Topical Conference on High-Temperature Plasma Diagnostics  
March 15-19, 1992  
and/or  
Review of Scientific Instruments, Vol. 63(10), pp. 4666-4668, Oct. 1992
- 42 S. M. Hamberger, et al.  
Physics Review Letters, Vol. 37, p. 1345 (1976)
- 43 G. Bottollier-Curtet and G. Ichtchenko  
"Microwave Reflectometry with the Extraordinary Mode on Tokamaks: Determination of the Electron Density Profile on Petula-B"  
Review of Scientific Instruments, Vol. 58(4), pp. 539-546, April 1987
- 44 G. Ichtchenko, et al.  
"Density Profile From Microwave Reflectometry and Confinement Properties of a Lower Hybrid Current Drive Sustained Tokamak Discharge"  
Proceedings of the 13<sup>th</sup> European Conference on Controlled Fusion and Plasma Heating, 1986  
pp. 419-422, Vol. 10C, Part I
- 45 R. N. Ó. Dubhghaill, et al.  
"The Characterization of High-Speed Swept Reflectometer for Plasma Diagnostics on the RFX Reversed-Field Pinch"  
International Journal of Infrared and Millimeter Waves, Vol. 13, No. 3, 1992
- 46 J. H. Irby and P. Stek  
"Simulation of Experimental Data From the Proposed C-Mod Reflectometer"  
Review of Scientific Instruments, Vol. 61(10), pp. 3052-3054, Oct. 1990
- 47 G. Arfken  
"Mathematical Methods for Physicists"  
Academic Press, New York  
QA37.2 .A74 1985  
Library of Congress Catalog Card Number: 73-119611
- 48 D. G. Swanson  
"Plasma Waves"  
Academic Press Inc., 1989  
QC 718.5.W3S43
- 49 J. D. Jackson  
"Classical Electrodynamics"



- John Wiley & Sons, New York, 1975  
QC 631.J3
- 50 K. Evenson et al.  
Physics Review Letters, Vol. 29, p. 1346, 1972
- 51 M. Bornatici  
"Electron Cyclotron Emission and Absorption in Fusion Plasmas"  
Nuclear Fusion, Vol. 23, No. 9, pp. 1153-1257 (1983)
- 52 W. P. Allis  
"Waves in Anisotropic Plasmas"  
Cambridge: MIT Press 1963  
QC 718.A4.
- 53 T. H. Stix  
"The Theory of Plasma Waves"  
McGraw-Hill, New York, 1962  
QC 718.S7  
Library of Congress Catalog Number: 62-17376
- 54 T. H. Stix  
Physics Review Letters, Vol. 15, p. 878, 1965
- 55 T. H. Stix  
"Fast-Wave Heating of a Two-Component Plasma"  
Nuclear Fusion, Vol. 15, pp. 737-754 (1975)
- 56 E. T. Whittaker and G. N. Watson  
"A Course of Modern Analysis"  
4<sup>th</sup> edition, Cambridge University Press, New York, 1927  
QA 401.W62
- 57 D. B. Batchelor, et al.  
Physics of Fluids, Vol. 27, p. 2835 (1984)
- 58 H. Bindslev  
"Relativistic Effects in Plasma Reflectometry"  
JET Report: JET-P (92) 35
- 59 H. Bindslev  
Plasma Physics and Controlled Fusion, Vol. 33, p. 1775 (1991)

- 60 H. Bindslev  
Proceedings of the International School of Plasma Physics, Piero Caldirola  
p. 779, Varenna (1991)
- 61 H. Bindslev  
Proceedings of the 18<sup>th</sup> EPS Conference on Controlled Fusion and Plasma  
Physics  
15C, Part IV, p. 9, Berlin (1991)
- 62 H. Bindslev  
"Relativistic Effects in Plasma Reflectometry"  
Plasma Physics and Controlled Fusion, Vol. 34(11), pp.1601-1618 (1992)
- 63 N. Bretz  
Private communication with Dr. Bretz.
- 64 B. A. Trubnikov  
"Plasma Physics and The Problem of Controlled Thermonuclear Reactions"  
Vol. 3, p. 122, Pergamon Press (1959)
- 65 I. P. Shkarofsky  
Journal of Plasma Physics, Vol. 35, p. 319 (1986)
- 66 P. H. Bevington  
"Data Reduction and Error Analysis for the Physical Sciences"  
McGraw-Hill Inc., New York, 1969  
QA278 .B48 (1992)  
Library of Congress Catalog Number: 69-16942
- 67 John R. Taylor  
"An Introduction to Error Analysis"  
University Science Books, 20 Edgehill Rd., Mill Valley, CA 94941  
Library of Congress Catalog Number: 81-51269
- 68 E. Anabitarte, E. G. Bustamante, et al.  
"Characterization of a Q-Band Microwave Reflectometer for Plasma Diagnosis  
in the Tokamak TJ-1"  
Int. J. Infrared and Millimeter Waves, Vol. 8, No. 7, pp. 733-751 (1987)
- 69 E. Anabitarte, et al.  
"Determination of the Electron Density Profile and its Fluctuation by Broad  
Band Microwave Reflectometry in the TJ-1 Tokamak"  
Journal of Physics D: Applied Physics

Vol. 21, pp. 1384-1390, March 1988  
IOP Publishing Ltd., March 1988, pp. 1384-1390

- 70 A. E. Costley, et al.  
"Recent Developments in Microwave Reflectometry at JET"  
Review of Scientific Instruments, Vol. 61(10), pp. 2823-2828, Oct. 1990
- 71 A. E. Costley  
Proc. Course and Workshop, Basic and Advanced Diagnostic Techniques for Fusion Plasmas  
EUR 10797, Varenna, Vol. 2, pp. 379-396 (1986)
- 72 Mase, et al.  
"Measurement of Alfvén Ion-Cyclotron Wave Using Both X- and O-Mode Reflectometers"  
Physics of Fluids B, Vol. 5(6), pp. 1677-1680, June 1993
- 73 F. Engelmann and M. Curatolo  
Nuclear Fusion, Vol. 13, p. 497 (1973)
- 74 I. Fidone and G. Granata  
"Propagation of Electromagnetic Waves in a Plasma With a Sheared Magnetic Field"  
Nuclear Fusion, Vol. 11, pp. 133-139 (1971)
- 75 D. A. Boyd  
"What is the Limiting Polarization of Electron Cyclotron Emission Leaving a Fusion Plasma?"  
5<sup>th</sup> Conference on Electron Cyclotron Emission, pp. 77-87, Nov. 1985, San Diego Ca.
- 76 F. J. Stauffer, et al.  
"Electron Cyclotron Emission Measurement on TFTR"  
5<sup>th</sup> Conference on Electron Cyclotron Emission, pp. 18-36, Nov. 1985, San Diego Ca.
- 77 TFR Group  
"Local Density Fluctuations Measurements by Microwave Reflectometry on TFR"  
Plasma Physics and Controlled Fusion, Vol. 27, No. 11, pp. 1299-1306 (1985)
- 78 TFR Group  
Nuclear Fusion 18, 647 (1978)

- 79 M. A. Heald and C.B. Wharton  
"Plasma Diagnostics with Microwaves"  
New York: Wiley  
QC 718.H36
- 80 J. L. Doane, et al.  
"Plasma Density Measurements Using FM-CW Millimeter Wave Radar Techniques"  
Review of Scientific Instruments, Vol. 52(1), pp. 12-15, Jan. 1981
- 81 A. C. C. Sips  
"Reflectometry and Transport in Thermonuclear Plasmas in the Joint European Torus"  
Ph.D. Thesis, Stichting voor Fundamenteel Onderzoek der Materie, 1991
- 82 A. C. C. Sips, et al.  
"Measurements of the Electron Particle Diffusion Coefficient With the JET Multichannel Reflectometer"  
Proceedings of the 16<sup>th</sup> European Conference on Controlled Fusion and Plasma Physics, Venice, 1988  
pp. 99-102, Vol. 13B, Part I
- 83 C. A. J. Hugenholtz  
"Microwave Interferometer and Reflectometer Techniques"  
Ph.D. Thesis, Stichting voor Fundamenteel Onderzoek der Materie' (FOM), 1990
- 84 C. A. J. Hugenholtz  
"Pulse Radar Technique for Reflectometry on Thermonuclear Plasmas"  
Review of Scientific Instruments, Vol. 62(4), pp. 1100-1101, April 1991
- 85 G. R. Hanson, et al.  
"ATF Two-Frequency Correlation Reflectometer"  
Review of Scientific Instruments, Vol. 61(10), pp. 3049-3051, Oct. 1990
- 86 G. R. Hanson  
"Microwave Reflectometry on the Advanced Toroidal Facility to Measure Density Fluctuations and Their Radial Correlation Lengths"  
Ph.D. Thesis, Georgia Institute of Technology, Atlanta Georgia, 1991
- 87 G. R. Hanson, et al.  
"Density Fluctuation Measurement in ATF Using Correlation Reflectometry"  
Nuclear Fusion, Vol. 32, No. 9, pp. 1593-1608 (1992)

- 88 H. Jeffreys  
Proc. London Mathematical Society, **23**, p. 428 (1923)
- 89 G. Wentzel  
Z. Physik **38**, p. 518 (1926)
- 90 H. A. Kramers  
Z. Physik **39**, p. 828 (1926)
- 91 L. Brillouin  
Compt. Rend. **183**, p. 24 (1926)
- 92 G. R. Hanson, et. al.  
"Microwave Reflectometry for Edge Density Profile Measurements on TFTR"  
Plasma Physics and Controlled Fusion, Vol. **36**, pp. 2073-2082, 1994
- 93 E. Anabitarte, G. R. Hanson, et al.  
"Density Fluctuation Measurements on ATF Using a Two-Frequency Reflectometer"  
Proceedings of the 17<sup>th</sup> European Conference on Controlled Fusion and Plasma Physics, Amsterdam, 1990  
pp. 1492-1494, Vol. 14B, Part VI
- 94 T. Lehecka, W. A. Peebles, et al.  
"Reflectometry System for the DIII-D Tokamak"  
Review of Scientific Instruments, Vol. 59(8), pp. 1620-1622, August 1988
- 95 T. Lehecka, et al.  
"Results From the DIII-D Millimeter-wave Reflectometer"  
Proceedings of the 16<sup>th</sup> Conference on Controlled Fusion and Plasma Physics, Venice, 1989  
pp. 123-126, Vol. 13B, Part I
- 96 E. J. Doyle, T. Lehecka, et al.  
"X-Mode Broadband Reflectometry Density Profile Measurements on DIII-D"  
Review of Scientific Instruments, Vol. 61(10), pp. 2896-2898, Oct. 1990
- 97 E. J. Doyle, et al.  
"Reflectometer Density Fluctuation Measurements on DIII-D"  
Review of Scientific Instruments, Vol. 61(10), pp. 3016-3018, Oct. 1990

- 98 E. J. Doyle, et al.  
"New Reflectometer Systems for the DIII-D Tokamak"  
9<sup>th</sup> Topical Conference on High-Temperature Plasma Diagnostics  
March 15-19, 1992  
and/or  
Review of Scientific Instruments, Vol. 63(10), p. 4665, Oct. 1992
- 99 E. J. Doyle, et al.  
"X-Mode Broadband Reflectometric Density Profile Measurements on DIII-D"  
Proceedings of the 17<sup>th</sup> European Conference on Controlled Fusion and Plasma Heating, Amsterdam, 1990  
pp. 1596-1599, Vol. 14B, Part VI
- 100 E. Mazzucato and R. Nazikian  
"Microwave Reflectometry for the Study of Density Fluctuations in Tokamak Plasmas"  
Plasma Physics and Controlled Fusion, Vol. 33, No. 3, pp. 261-274 (1991), Great Britain
- 101 E. Mazzucato  
"Relativistic Effects on Microwave Reflectometry"  
Physics of Fluids B, Vol. 4(10), pp. 3460-3461, Oct. 1992
- 102 E. Mazzucato, et al.  
"The Application of X-mode Reflectometry to the Study of Large Scale Fluctuations in TFTR"  
19<sup>th</sup> EPS Conference on Confined Fusion and Plasma Physics  
pp. 1055-1058, June 1992
- 103 R. Nazikian, et al.  
"Density Fluctuation Measurements from Microwave Scattering on TFTR"  
Proceedings of the 17<sup>th</sup> European Conference in Controlled Fusion and Plasma Physics, Amsterdam, 1990  
pp. 1544-1547, Vol. 14B, Part VI
- 104 R. Nazikian  
"Modulational Sources, Sideband Correlations and Non-Stationary Interference for Waves Scattered From Random Media"  
Review of Scientific Instruments, Vol. 63(11), pp. 5326-5331, Nov. 1992

- 105 P. Cripwell, A. E. Costly and A. E. Hubbard  
"Correlation Reflectometry"  
Proceedings of the 16<sup>th</sup> European Conference on Controlled Fusion and  
Plasma Physics, Venice, 1989  
pp. 75-78, Vol. 13B, Part I
- 106 T. Estrada, et al.  
Review of Scientific Instruments, Vol. 61, p. 3034 (1992)
- 107 N. Bretz, et al.  
"X-Mode Scattering for the Measurement of Density Fluctuations on TFTR"  
Review of Scientific Instruments, Vol. 59(8), pp. 1538-1543, August 1988
- 108 N. Bretz  
"The Interpretation of Reflectometry Measurements of Plasma Fluctuations"  
Princeton Plasma Physics Laboratory  
Princeton, NJ 08543
- 109 N. Bretz  
"Instrumental Aspects of Extraordinary Mode Scattering on TFTR"  
Review of Scientific Instruments, Vol. 61(10), pp. 3031-3033, Oct. 1990
- 110 N. Bretz  
"One-Dimensional Modeling of the Wavelength Sensitivity, Localization, and  
Correlation in Reflectometry Measurements of Plasma Fluctuations"  
Physics of Fluids B, Vol. 4(8), pp. 2414-2422, Aug. 1992
- 111 E. Mazzucato and R. Nazikian  
"Radial Scale Length of Turbulent Fluctuations in the Main Core of TFTR  
Plasmas"  
Physical Review Letters, Vol. 71, Num 12, pp. 1840-1843, Sept. 1993
- 112 R. J. Fonck, et al.  
"Long-Wavelength Density Turbulence in the TFTR Tokamak"  
Physical Review Letters, Vol. 70(24), pp. 3736-3739, June 1993
- 113 R. D. Durst, et al.  
"BES Observations of Internal Coherent and Quasi-Coherent MHD Modes in  
TFTR"  
University of Wisconsin Publications, Madison WI

- 114 R. D. Durst, et al.  
"Observation of a Localized Transition From Edge and Core Density Fluctuations in TFTR"  
Princeton Plasma Physics Laboratory Publications, Princeton NJ
- 115 R. J. Groebner, et al.  
"Role of Edge Electric Field and Poloidal Rotation in the L-H Transition"  
Physical Review Letters, Vol. 64(25), pp. 3015-3018, June 1990
- 116 S. F. Paul, et al.  
"Measurements of Long-Wavelength Density Fluctuations in TFTR"  
Physics of Fluids B, Vol. 4(9), pp. 2922-2928, Sept. 1992
- 117 I. Collazo-López  
Fortran computer program on the ORNL Fusion Energy Division Vax Cluster.  
Available upon request. E-Mail: COLLAZOI@FEDC06.FED.ORN.L.GOV
- 118 L. Vahala, et al.  
"Measurement of Magnetic Fluctuations by  $O \rightarrow X$  Mode Conversion"  
Review of Scientific Instruments, Vol. 61 (10), pp. 3022-3024, Oct. 1990
- 119 L. Vahala, et al.  
"Electromagnetic Wave Scattering from Magnetic Fluctuations in Tokamaks"  
Physics of Fluids B, Vol. 4(3), pp. 619-629, March 1992
- 120 G. D. Conway  
"Scattering of Reflectometer Signals from Rippled Surfaces"  
Accepted for publication by Review of Scientific Instruments  
Prepared January 1993, revised March 1993.
- 121 J. P. García, et al.  
"Scattering Effects of Small-Scale Density Fluctuations on Reflectometric Measurements in a Tokamak Plasma"  
Proceedings of the 16<sup>th</sup> European Conference on Controlled Fusion and Plasma Physics, Venice, 1989  
pp. 1521-1524, Vol. 13B, Part VI
- 122 A. Hubbard, D. Ward and T. E. Stringer  
"Direct Measurement of the Electron Diffusion Coefficient on JET Using a Microwave Reflectometer"  
Proceedings of the 13<sup>th</sup> European Conference on Controlled Fusion and Plasma Heating, Schliersee, 1986  
pp. 232-235, Vol. 10C, Part I



- 123 Paul Michelsen  
"Simulation of Correlation Reflectometry"  
19<sup>th</sup> EPS Conference on Confined Fusion and Plasma Physics  
pp. 1067-1070 , June 1992
- 124 L. Rhodes, et al.  
"The UCLA Correlation Reflectometer System on DIII-D"  
9<sup>th</sup> Topical Conference on High-Temperature Plasma Diagnostics  
March 15-19, 1992  
and/or  
Review of Scientific Instruments, Vol. 63(10), pp. 4661-4664, Oct. 1992
- 125 T. L. Rhodes, et al.  
"Microwave Reflectometry as a Density Fluctuation Diagnostic: a Comparison Between a Controlled Laboratory Experiment and a One Dimensional Numerical Model"  
19<sup>th</sup> EPS Conference on Confined Fusion and Plasma Physics  
pp. 1071-1073, June 1992
- 126 H. J. Hartfuss  
"Broadband Heterodyne Reflectometry on the W7-AS Stellarator"  
9<sup>th</sup> Topical Conference on High-Temperature Plasma Diagnostics  
March 15-19, 1992  
and/or  
Review of Scientific Instruments, Vol. 63(10), p. 4653, Oct. 1992
- 127 S. Martini, et al.  
"Interferometry and Reflectometry Diagnostics for RFX"  
Proceedings of the 16<sup>th</sup> European Conference on Controlled Fusion and Plasma Physics, Venice, 1989  
pp. 1493-1496, Vol. 13B, Part VI
- 128 Anatoly Skibenko and Rostislav Pavlichenko  
"Electron Density Profile Reconstruction for the Uragan-3M Torsatron Via Upper X-Mode reflectometry"  
Stellarator News, Issue #25, January 1993  
Published by the ORNL Fusion Energy Division  
Building 9201-2, P.O. Box 2009  
Oak Ridge, TN 37831-8071  
Editor: James A. Rome  
E-Mail: JAR@ORNL.GOV

- 129 M. E. Manso, et al.  
"Broadband Microwave Reflectometry on ASDEX"  
Proceedings of the 16<sup>th</sup> European Conference on Controlled Fusion and Plasma Physics, Venice, 1989  
pp. 1517-1520, Vol. 13B, Part VI
- 130 M. E. Manso, et al.  
"Localized Density Measurements on ASDEX Using Microwave Reflectometry"  
Proceedings of the 17<sup>th</sup> European Conference on Controlled Fusion and Plasma Physics, Amsterdam, 1990  
pp. 1560-1563, Vol. 14B, Part VI
- 131 R. Schubert, et al.  
"Edge Density X-Mode Reflectometry of RF-Heated Plasmas on ASDEX"  
Proceedings of the 17<sup>th</sup> European Conference on Controlled Fusion and Plasma Physics, Amsterdam, 1990  
pp. 1552-1555, Vol. 14B, Part VI
- 132 A. Silva, et al.  
"A Microwave Reflectometric System for Tokamak ASDEX Upgrade"  
19<sup>th</sup> EPS Conference on Confined Fusion and Plasma Physics  
pp. 1063-1066 , June 1992
- 133 F. Serra, et al.  
"Reflectometry Measurements of the  $m = 1$  Satellite Mode in L- and H-mode Plasmas in ASDEX"  
19<sup>th</sup> EPS Conference on Confined Fusion and Plasma Physics  
pp. 231-234 , June 1992
- 134 P. Millot, et al.  
Proceedings of the 14<sup>th</sup> European Conference on Controlled Fusion and Plasma Physics, Madrid, Spain  
pp. 1303-1304, Vol. 11D, Part III (1987)
- 135 W. A. Peebles, et al.  
"Fluctuation Measurements in the DIII-D and TEXT Tokamaks Via Collective Scattering and Reflectometry"  
Review of Scientific Instruments 61 (11), pp. 3509-3519, Nov. 1990

- 136 T. Fukuda, et al.  
"Broadband Reflectometry for the Density Profile and Fluctuation Measurements in the JT-60 Tokamak"  
Review of Scientific Instruments, Vol. 61(11), pp. 3524-3527, Nov. 1990
- 137 H. Meuth and E. Sevillano  
"Microwave Plasma Diagnostics"  
PFC/JA-87-42
- 138 V. E. Golant  
Zh. Tekh. Fiz., Vol. 30, p. 1261, 1960  
Soviet Physics - Technical Physics, Vol. 5, p. 1240 (1961)
- 139 V. A. Vershkov and V. A. Zhuravlev  
"Plasma Diagnostics Experiments on the T-10 Tokamak by Means of a Reflected Microwave Signal"  
Soviet Physics - Technical Physics, Vol. 32(5), pp.523-526 (1987)
- 140 O. S. Pavlichenko, et al.  
ITER Diagnostic Workshop, Garching, Germany  
ITER-IL-Ph-07-0-15, Feb. 12-23 (1990)
- 141 A. E. Hubbard, et al.  
"A Simple Fixed-Frequency Reflectometer for Plasma Density Profile Measurements on JET"  
Journal of Physics E: Scientific Instruments, 20 pp. 423-427 (1987)
- 142 A. E. Hubbard  
"Measurement of Electron Density on JET by Microwave Reflectometry"  
Ph. D. Thesis, May 1987  
University of London  
Imperial College of Science and Technology
- 143 K. Tomabechi  
Proceedings of the 12<sup>th</sup> International Conference on Plasma Physics and Controlled Nuclear Fusion Research, NICE (1988)  
pp. 215, Vol. 3
- 144 M. Abramowitz and I. A. Stegun  
"Handbook of Mathematical Functions"  
5<sup>th</sup> ed., DOVER, New York, 1968  
C 13.32:55/2

- 145 R. Cano and C. Cavallo  
Proceedings of the 5<sup>th</sup> International Conference on Infrared and Millimeter Waves  
Würzburg, 1980
- 146 M. Brambilla and M. Moresco  
"The Influence of Mode Mixing on Reflectometry Density Measurements in a Reversed Field Pinch"  
Plasma Physics and Controlled Fusion, Vol. 29, No. 3, pp. 381-393 (1987)
- 147 J. Lohr  
"Electron Density Measurements From Cutoff of Electron Emission in the DIII-D Tokamak"  
Review of Scientific Instruments, Vol. 59(8), pp. 1608-1610, Aug. 1988
- 148 J. Adam, et al.  
"Wave Generation and Heating in the ST-Tokamak at the Fundamental and Harmonic Cyclotron Frequencies"  
Plasma Physics and Controlled Nuclear Fusion Research  
Vol. 1, IAEA, Vienna (1975)
- 149 J. C. Hosea, et al.  
"Fast Wave Heating in the Princeton Large Torus"  
Princeton Plasma Physics Laboratory Report-1588, October 1979
- 150 TFR Group  
"Impurity Pump-Out at the Two Ion Hybrid Resonance During ICRF Experiments in TFR Tokamak Plasmas"  
EUR-CEA-FC-1131, October 1981
- 151 R. J. Taylor, et al.  
"Observation of Short ICRF Waves in Microtor/Macrotor"  
4<sup>th</sup> Topical Conference in RF Heating, Austin, TX (1981)
- 152 A. P. Biddle and J.C. Sprott  
"High Power Heating in the Ion Cyclotron Range of Frequencies in the Wisconsin Tokapole II"  
University of Wisconsin report UC-20f, September 1980
- 153 A. W. Molvik, et al.  
"Initial TMX Central-Cell ICRH Experiments"  
Lawrence Livermore Laboratory Report UCID-18866, December 1980

- 154 T. Watari, et al.  
"A Slow-Wave Heating Experiment on RFC-XX Using an Array of Phased Antennas"  
Nuclear Fusion, Vol. 22, No. 10 (1982)
- 155 D. K. Smith and B. D. McVay  
"Low Frequency RF Pumping of Electrons for Potential Enhancement in Tandem Mirrors"  
Bulletin of the American Physical Society, Vol. 27, No. 8, Part II
- 156 K. Steinmetz, et al.  
"Observation of a High-Confinement Regime in a Tokamak Plasma with Ion Cyclotron-Resonance Heating"  
Physical Review Letters, Vol. 58, No. 2, pp. 124-127, Jan. 1987
- 157 N. J. Fisch  
Rev. Mod. Phys., Vol. 59, p. 175 (1987)
- 158 N. J. Fisch  
"Heating in Toroidal Plasmas"  
Brussels: Commission of the European Communities  
Proc. 3<sup>th</sup> Joint Varenna-Grenoble Int. Symp. Vol. 3, p. 841
- 159 N. J. Fisch  
Nuclear Fusion, Vol. 21, p. 15 (1981)
- 160 Dave Rasmussen  
Private communication with Dr. Rasmussen
- 161 T. J. Wade, et al.  
"High Power (22MW) ICRH at JET and Developments for Next Step Devices"  
14<sup>th</sup> IEEE/NPSS Symposium, Sept. 1991, San Diego, Ca.  
pp. 902-907, 91CH3035-3 ©IEEE
- 162 K. Steinmetz  
"ICRF Heating in Fusion Plasmas"  
AIP Conference Proceedings 1987  
Radio Frequency Power in Plasmas, pp. 211-219 (1987)
- 163 G. Schilling  
"Overview of TFTR ICRF Results"  
10<sup>th</sup> Topical Conference on Radio Frequency Power in Plasmas  
April, 1993, Boston, Massachusetts

- 164 J. M. Noterdaeme  
"First Results of Ion Cyclotron Resonance Heating in ASDEX Upgrade"  
10<sup>th</sup> Topical Conference on Radio Frequency Power in Plasmas  
April, 1993, Boston, Massachusetts
- 165 B. Saoutic  
"High Power ICRH and LHCD Experiments on Tore Supra"  
10<sup>th</sup> Topical Conference on Radio Frequency Power in Plasmas  
April, 1993, Boston, Massachusetts
- 166 T. Fujii  
"Lower Hybrid Current Drive and ICRH Heating Experiments on JT-60U"  
10<sup>th</sup> Topical Conference on Radio Frequency Power in Plasmas  
April, 1993, Boston, Massachusetts
- 167 DIII-D team, presented by T. C. Simonen  
"Recent Results From DIII-D and Future Plans"  
14<sup>th</sup> IEEE/NPSS Symposium on Fusion Engineering  
pp. 1068-1076, Sept. 1991, San Diego, Ca.
- 168 D. Baker and the DIII-D group  
"DIII-D Research Operations: Annual Report to the U.S. Department of Energy"  
October 1, 1991 through September 30, 1992  
Date Published: May 1993  
Available to DOE from:  
Office of Scientific and Technical Information  
P.O. Box 62  
Oak Ridge, TN 37831
- 169 R. A. Cairns  
"Radiofrequency Heating of Plasmas"  
Adam Hilger, Bristol, Philadelphia and New York  
QC718.5.H5C35 1991  
ISBN 0-7503-0034-5
- 170 D. R. Baker, et al.  
"Tests of an ICRH Resonant Cavity Launcher with Faraday Shield"  
IEEE Transactions on Plasma Science, Vol. PS-14, No. 1, pp. 53-58, Feb. 1986
- 171 L. K. Kuznetsova, et al.  
"Electron Cyclotron Current Drive and Tearing Mode Stabilization in ITER"

- EPS 17<sup>th</sup> Conference on Controlled Fusion and Plasma Heating, Amsterdam, 1990, pp. 1247-1250, Vol. 14B, Part III
- 172 F. X. Söldner, et al.  
"Profile Control with Lower Hybrid Waves on ASDEX"  
EPS 17<sup>th</sup> Conference on Controlled Fusion and Plasma Heating, Amsterdam, 1990, pp. 1323-1326, Vol. 14B, Part III
- 173 R. H. Goulding, et al.  
"Development of Fast-Wave ICRF Current Drive Systems at ORNL"  
EPS 17<sup>th</sup> Conference on Controlled Fusion and Plasma Heating, Amsterdam, 1990, pp. 1311-1314, Vol. 14B, Part III
- 174 J. Adam  
"Review of Tokamak Plasma Heating by Wave Damping in the Ion Cyclotron Range of Frequency"  
Plasma Physics and Controlled Fusion, Vol. 29, pp. 443-472 (1987)
- 175 D. M. Manos, et al.  
"Studies of the Edge Plasma of RF Heated PLT Discharges"  
Journal of Nuclear Materials, Vol. 129, pp. 319-324 (1985)
- 176 J. R. Wilson, et al.  
"The Evolution of Plasma Parameters as Governed by Edge Phenomena During Ion Bernstein Wave Heating"  
Journal of Nuclear Materials, Vol. 145-147, pp. 161-620 (1987)
- 177 C. E. Thomas, et al.  
"ICH/Edge Interactions on Tore Supra: First Data"  
Oral presentation on Tuesday, 5 January 1993  
Fusion Energy Division, ORNL
- 178 Private communication with Dr. C. E. Thomas.
- 179 N. Noda, et al.  
"Impurity Origin During ICRF Heating in the JIPP T-IIU Tokamak"  
Journal of Nuclear Materials, Vol. 128-129, pp. 304-309 (1984)
- 180 H. Tamai, et al.  
"Edge Plasma Characteristics During ICRF Heating on JFT-2M"  
Fusion Engineering and Design, Vol. 12, pp. 25-29 (1990)

- 181 L. I. Grigoreva, et al.  
"A Study of the Mechanics of Metal Impurity Release During ICRF Heating in the URAGAN-3 Torsatron"  
Journal of Nuclear Materials, Vol. 162-164, pp. 458-461 (1989)
- 182 E. D. Volkov, et al.  
"On the Mechanisms of Light and Heavy Impurity Release During RF Plasma Heating in the URAGAN-3 Torsatron"  
Fusion Engineering and Design, Vol. 12, p. 237 (1990)
- 183 H. L. Manning, et al.  
"Impurity Generation During ICRF Heating Experiments on Alcator-C"  
Nuclear Fusion, Vol. 26, pp. 1665-1678 (1986)
- 184 A. S. Wan, et al.  
"The Effects of ICRF on the Alcator-C Scrape-off Layer Plasma"  
Journal of Nuclear Materials, Vol. 162-164, pp. 292-299
- 185 C. Janeschitz, et al.  
"Impurity Production During ICRF Heating"  
Europhysics Conference Abstracts, Vol. 10C, pp. 678-681, EPS (1986)
- 186 B. Schweer, et al.  
"Effects of ICRF Heating on the Plasma Edge in TEXTOR"  
Europhysics Conference Abstracts, Vol. 10C, pp. 399-402, EPS (1985)
- 187 U. Samm, et al.  
"Plasma Edge Physics in the TEXTOR Tokamak With Poloidal and Toroidal Limiters"  
Journal of Nuclear Materials, Vol. 162-164, pp. 24-27 (1989)
- 188 R. Van Nieuwenhove, et al.  
"Experimental Evidence for Sheath Effects at the ICRF Antenna and Ensuing Changes in the Plasma Boundary During ICRF on TEXTOR"  
Journal of Nuclear Materials, Vol. 162-164, pp. 288-291 (1989)
- 189 R. Van Nieuwenhove, et al.  
"Influence of ICRF on the Edge Plasma of Tokamaks"  
Ph.D. Thesis, University of Antwerp, B-2610, Antwerp (1989)
- 190 M. Bures, et al.  
"The Modification of the Plasma Edge and Impurity Production by Antenna Phasing During ICRF Heating on JET"  
Plasma Physics and Controlled Fusion, Vol. 30, pp. 149-167 (1988)



- 191 J. A. Tagle, et al.  
"The Effect of Different ICRF Heating Scenarios on the JET Scrap-Off Layer"  
Journal of Nuclear Materials, Vol. 162-164, pp. 282-287 (1989)
- 192 T. Fujii, et al.  
"Interaction Between RF and Edge Plasma During ICRF Heating in JT-60"  
Fusion Engineering and Design, Vol. 12, pp. 139-148 (1990)
- 193 D. B. Batchelor, et al.  
"ICRF Heating"  
Fusion Technology, Vol. 21, pp. 1214-1242 (1992)
- 194 P. P. Colestock  
"Review of ICRF Experiments"  
IEEE Trans. of Plasma Science, PS-12, p. 64 (1984)
- 195 H. Takahashi  
"ICRF Heating in Tokamaks"  
J. de Physique, Vol. 38, C6 (1977)
- 196 S. Yoshikawa  
"Ion Heating in the C-Stellarator"  
Plasma Physics and Controlled Nuclear Fusion Research  
2<sup>nd</sup> International Conference, Culham 1965  
Vol. 2, IAEA, p. 925 (1965)
- 197 J. I. Lodge and R.W. Steward  
"Studies in High Frequency Discharges"  
Canadian J. of Res., Vol. 26, section A, p. 205 (1948)
- 198 H. S. Butler and G. S. Kino  
"Plasma Sheath Formation by Radio Frequency Fields"  
Physics of Fluids, Vol. 6, p. 1346 (1963)
- 199 V. L. Vdovin, et al.  
"Excitation of Magnetosonic Resonance in the Tokamak Plasma"  
JETP Letter, Vol. 14, p. 149 (1971)
- 200 V. L. Vdovin, et al.  
"Magnetosonic Plasma Heating"  
JETP Letter, Vol. 17, p. 2 (1973)

- 201 V. L. Vdovin, et al.  
"Investigation of the Magnetosonic Plasma Heating in the Tokamak"  
Controlled Fusion and Plasma Physics,  
6<sup>th</sup> European Conference, Moscow, p. 553 (1973)
- 202 V. L. Vdovin, et al.  
"Plasma Heating with an Azimuthally Non-Symmetrical Ion Cyclotron Wave  
in Tokamak TM-1-HF"  
Plasma Physics and Controlled Nuclear Fusion Research  
5<sup>th</sup> IAEA Conference, Tokyo, 1974  
Nuclear Fusion Suppl. IAEA,  
English translation of the Russian paper, p. 21 (1975)
- 203 J. C. Hosea, et al.  
"Ion Cyclotron and Fast Hydromagnetic Wave Generation in the ST Tokamak"  
Physics Review Letters, Vol. 31, p. 150 (1973)
- 204 J. Adam, et al.  
"Wave Generation and Heating in the ST-Tokamak at the Fundamental and  
Harmonic Ion Cyclotron Frequencies"  
Plasma Physics and Controlled Nuclear Fusion Research  
5<sup>th</sup> IAEA Conference, Tokyo, 1974, Vol. 1, IAEA 65
- 205 J. C. Hosea  
"Fast and Slow Ion Cyclotron Wave Generation and Heating in the ST Tokamak"  
Symp., Varenna, 1974, CNR, Milano, p. 61 (1973)
- 206 TFR Group  
"TFR Experiments on Superbanana Particle Diffusion, Small Scale Turbulence and Transport"  
Plasma Physics and Controlled Nuclear Fusion Research  
8<sup>th</sup> IAEA Conference, Brussels, 1980, IAEA, p. 425 (1981)
- 207 TFR Group  
"ICRF Heating in TFR and the Problem of Impurity Release"  
Plasma Physics and Controlled Fusion, Vol. 26, p. 165 (1984)
- 208 TFR Group  
"Plasma Edge Measurements During Additional Heating in the TFR Tokamak"

- Plasma Physics and Controlled Fusion  
11<sup>th</sup> EPS Conference, Aachen (1983)  
Europhysics Conference Abstracts, Vol. 7D(II), EPS, p. 493 (1983)
- 209 TFR Group  
"ICRF Results on TFR at Megawatt Power Levels"  
Plasma Physics, Vol. 24, p. 615 (1981)
- 210 TFR Group  
"ICRF Heating in TFR"  
CEA, DRFC-SCP EUR-CEA-FC-1186, June 1983
- 211 TFR Group  
"Graphite Limiter Used in TFR"  
Journal of Nuclear Materials, Vol. 128-129, p. 292 (1984)
- 212 TFR Group and Sand F.  
"ICRF Heating Experiments in TFR Using a Low-Field-Side Antenna"  
Nuclear Fusion, Vol. 25, p. 1719 (1985)
- 213 J. C. Hosea, et al.  
"Fast Wave Heating in the Princeton Large Torus"  
Princeton University, NJ(USA)  
Princeton Plasma Physics Lab., Experimental Report PPPL-1588, Oct .1979
- 214 P. L. Colestock, et al.  
"The Effects of ICRF Heating on Plasma Edge Conditions in PLT"  
Journal of Vacuum Science and Technology, A. Vol. 3, pp. 1211-1217 (1985)
- 215 H. Ogawa, et al.  
"Impurity Behaviour During ICRF Heating in JFT-2M"  
Journal of Nuclear Materials, Vol. 128-129, p. 298 (1984)
- 216 S. I. Itoh, et al.  
"Three-dimensional Study of Coupling Efficiency of ICRF Wave Heating. Antenna Launcher and Wave Guide Launcher"  
Heating in Toroidal Plasmas, 4<sup>th</sup> International Symposium, Rome (1984)  
Vol. 1, p. 407, Nuclear Energy Agency (1984)
- 217 K. Itoh, et al.  
"A Possible Origin of Metal Impurities in ICRF Heating Experiments"  
Comments Plasma Physics and Controlled Fusion, Vol. 10, p. 91 (1986)

- 218 M. Mori, et al.  
"High-Power ICRF Heating Experiments in the JFT-2M Tokamak"  
Plasma Physics and Controlled Nuclear Fusion Research  
10<sup>th</sup> IAEA International Conference, London, Vol. 1, p. 445, IAEA (1984)
- 219 H. Tamai, et al.  
"Impurity Reduction During ICRF Heating in JFT-2M Tokamak"  
Nuclear Fusion, Vol. 26, p. 365 (1986)
- 220 H. Tamai, et al.  
"Suppression of the Metal Impurity Release During ICRF Heating by the Installation of Carbon Blocks"  
Japan Atomic Energy Research Institute, Tokyo  
Experimental Report JAERI-M-86-143, Oct. 1986
- 221 M. Bures, et al.  
"Role of the Antenna Screen Angle During ICRF Heating in JET"  
Nuclear Fusion, Vol. 30, p. 251 (1990)
- 222 M. Brambilla, et al.  
"Theoretical and Experimental Investigation of a Mechanism for Impurity Production by ICRF Fields"  
Plasma Physics and Controlled Nuclear Fusion Research  
13<sup>th</sup> IAEA Conference, Washington, 1990  
Vol. 1, p. 723, IAEA, Vienna (1991)
- 223 M. Brambilla, et al.  
"Introduction of Parallel Electric Fields at the Plasma Edge During ICRF Heating"  
Controlled Fusion and Plasma Heating  
17<sup>th</sup> EPS Conference, Amsterdam, 1990  
Vol. 14B(III), p. 1056, EPS (1990)
- 224 F. W. Perkins  
Princeton Plasma Physics Laboratory Report No. 2571, Princeton (1988)
- 225 F. W. Perkins  
"Radiofrequency Sheaths and Impurity Generation by ICRF Antennas"  
Nuclear Fusion, Vol. 29, No. 4, pp. 583-592 (1989)
- 226 J. R. Myra, et al.  
Physics of Fluids B1, Vol. 6, p. 1193 (1989)

- 227 J. B. O. Caughman II, et al.  
"Experimental Evidence of Increased Electron Temperature, Plasma Potential, and Ion Energy Near an ICRF Antenna Faraday Shield"  
Fusion Engineering and Design, Vol. 12, pp. 179-183 (1990)
- 228 J. B. O. Caughman  
"The Distribution of Ion Energies Incident on a ICRH Antenna Faraday Shield"  
Ph.D. Thesis, University of Illinois, Urbana, IL (1989)
- 229 I. S. Lehrman  
"A Study of Coupling and Edge Processes for ICRF Antennas"  
Ph.D. Thesis, University of Wisconsin, Madison, WI (1988)
- 230 J. M. Noterdaeme, et al.  
"Experimental Results on Edge Effects During ICRF Heating of ASDEX Plasmas"  
Fusion Engineering and Design, Vol. 12, pp. 127-137 (1990)
- 231 M. D. Carter, et al.  
"Electron Heating and Static Sheath Enhancement in Front of Energized RF Antennas"  
Fusion Engineering and Design, Vol. 12, pp. 105-110 (1990)
- 232 D. A. D'Ippolito, et al.  
"Impurity Release by ICRF Antennas in JET"  
Fusion Engineering and Design, Vol. 12, pp. 209-216 (1990)
- 233 R. J. Taylor, et al.  
"Particle Transport Due to ICRF Waves and Radial Electric Fields in Tokamaks"  
Plasma Physics and Controlled Nuclear Fusion  
9<sup>th</sup> International Conference, Baltimore, Vol. 3, pp. 251-261, IAEA (1982)
- 234 L. I. Grigor'eva, et al.  
"Plasma Potential Formation Under the Influence of an External RF Field and the Effect of this Potential on Particle Transport"  
Journal of Nuclear Materials, Vol. 128-129, p. 317 (1984)
- 235 J. M. Noterdaeme, et al.  
"Plasma Edge Effects with ICRF in ASDEX"  
Controlled Fusion and Plasma Physics

- 14<sup>th</sup> European Conference, Madrid, 1987  
Europhysics Conference Abstracts, Vol. 11D(pt 2), p. 678, EPS, Geneva
- 236 R. Van Nieuwenhove, et al.  
"Observation of a Localized RF Electric Field Structure in the Scrape-Off Layer During ICRF on TEXTOR and ASDEX"  
European Conference on Controlled Fusion and Plasma Physics  
Europhysics Conference Abstract, Vol. 13B(pt.3), p. 3, EPS, Geneva (1989)
- 237 R. Van Nieuwenhove, et al.  
"Effect of RF Heating on D.C. Electric Fields in the SOL of TEXTOR"  
Fusion Engineering and Design, Vol. 12, p. 231 (1990)
- 238 D. A. D'Ippolito, et al.  
"ICRF-Driven Convective Cells in the Tokamak Edge Plasma"  
Presented at the Sherwood Fusion Theory Conference (1991)
- 239 I. A. Moyer, et al.  
"Effects of Auxiliary Heating on D.C. Electric Fields in the TEXTOR Boundary"  
Plasma Surface Interaction  
9<sup>th</sup> International Conference, Bournemouth (1990)
- 240 D. Bora, et al.  
"Effects of ICRH on Electrostatic Fluctuations and Particle Transport in the Boundary Plasma of TEXTOR"  
To be published in Nuclear Fusion
- 241 S. K. Erents, et al.  
Journal of Nuclear Materials, Vol. 145-147, p. 231 (1987)
- 242 I. S. Lehrman, et al.  
Proceedings of the 7<sup>th</sup> APS Topical Conference on Applications of Radio Frequency Power to Plasmas, Kissimmee, Fl (1987)
- 243 G. J. Greene  
International Conference on Plasma Physics, Lausanne, p. 5 (1984)
- 244 R. Van Nieuwenhove, et al.  
8<sup>th</sup> International Conference on Plasma Surface Interactions, Jülich (1988)
- 245 I. L. Lehrman, et al.  
Fusion Engineering Design, Vol. 12, pp. 51-62 (1990)

- 246 D. J. Hoffman  
"Experimental Measurements of the Ion Cyclotron Antennas Coupling and RF Characteristics"  
Fusion Technology, Vol. 8, pp. 411-419 (1985)
- 247 D. J. Hoffman  
"The Design of High-Power ICRF Antennas for TFTR and Tore Supra"  
Applications of Radio-Frequency Power to Plasmas  
Proc. 7<sup>th</sup> Topical Conference, Kissimmee, Florida, p. 302 (1987)
- 248 J. R. Wilson  
"TFTR ICRF Antenna Design"  
AIP Conference Proceedings 1987, pp. 294-297
- 249 J. E. Stevens  
"The Effect of ICRF Antenna Phasing on Metal Impurities in TFTR"  
Plasma Physics and Controlled Fusion (G.B.), Vol. 32, No. 3, pp. 189-196 (1990)
- 250 J. E. Stevens, C. Bush and P.L. Colestock  
Princeton Plasma Physics Laboratory Internal Report  
PPPL-2640, Princeton (1989)
- 251 G. L. Chen  
"Resonant Loop Antenna Design with a 2-D Steady-State Analysis"  
AIP Conference Proceedings 1987, pp. 382-385
- 252 F. W. Baity  
"Modeling of Compact Loop Antennas"  
AIP Conference Proceedings 1987, pp. 378-381
- 253 W. L. Gardner  
"ICH Antenna Development of the ORNL RF Test Facility"  
AIP Conference Proceedings 1987, pp. 306-309
- 254 V. L. Granatstein and P. L. Colestock  
"Wave Heating and Current Drive in Plasmas"  
Gordon and Breach Science Publishers  
QC 718.5.H5W38 (1985)
- 255 A. Bers  
IEEE Trans. Plasma Science, PS-12 No. 2 (1984)  
Special Issue on RF Heating and Current Generation

- 256 J. F. King  
"Materials Test and Analysis of Faraday Shield Tubes for ICRF Antennas"  
Fusion Technology, Vol. 15, Mar. 1989, pp. 1093-1096
- 257 D. J. Taylor  
"Resonant Double Loop Antenna Developments at ORNL"  
Fusion Technology, Vol. 15, Mar. 1989, pp. 1088-1092
- 258 M. Goniche, et al.  
"Lower Hybrid Wave Experiments in Tore Supra"  
EPS 17<sup>th</sup> Conference on Controlled Fusion and Plasma Heating, Amsterdam, 1990, pp. 1231-1234, Vol. 14B, Part III
- 259 M. Kwon, et al.  
"Measurement of the Effects of Faraday Shields on ICRH Antenna Coupling"  
IEEE Transactions on Plasma Science, Vol. 18, No. 2, pp. 184-189, April 1990
- 260 B. D. Blackwell  
"The Alcator-C ICRF Experiment"  
Bulletin of the American Physical Society, 29, p. 1219 (1984)
- 261 J. B. O. Caughman II  
"Measurements of the Transmission Characteristics of the Alcator-C ICRH Antenna"  
Bulletin of the American Physical Society, 29, p. 1221 (1984)
- 262 McDonnell Douglas Co.  
"Technical Proposal for TFTR/Big Dee ICRH Launcher Development"  
Vol. 1, MDC E2675, McDonnell Douglas Corporation (1983)
- 263 R. H. Dicke  
"Molecular Amplification and Generation Systems and Methods"  
U.S. Patent 2,851,652 - Sept. 9, 1958
- 264 A. M. Prokhorov  
"Molecular Amplifier and Generator for Sub-Millimeter Waves"  
JETP (USSR), Vol. 34, pp.1658-1659, June 1959  
Soviet Physics JETP, Vol. 7, pp. 1140-1141, Dec. 1958
- 265 A. L. Schawlow and C. H. Townes  
"Infrared and Optical Masers"  
Physics Review, Vol.29 pp. 1940-1949, Dec. 1958



- 266 A. G. Fox and T. Li  
"Resonant Modes in an Optical Maser"  
Proc. IRE (Correspondence), Vol. 48, pp. 1904-1905, Nov. 1960
- 267 A. G. Fox and T. Li  
"Resonant Modes in a Maser Interferometer"  
Bell Sys. Tech. J., Vol. 40, pp. 453-488, March 1961
- 268 G. D. Boyd and J. P. Gordon  
"Confocal Multi-Mode Resonator for Millimeter Through Optical Wavelength Lasers"  
Bell Sys. Tech. J., Vol. 40, pp. 489-508, March 1961
- 269 G. D. Boyd and H. Kogelnik  
"Generalized Confocal Resonator Theory"  
Bell Sys. Tech. J., Vol. 41, pp. 1347-1369, July 1962
- 270 G. Goubau and F. Schwing  
"On the Guided Propagation of Electromagnetic Wave Beams"  
IRE Trans. on Antennas and Propagation, Vol. AP-9, pp. 248-256, May 1961
- 271 J. R. Pierce  
"Modes in Sequences of Lenses"  
Proc. NAT'L Acad. Sci., Vol. 47, pp. 1808-1813, Nov. 1961
- 272 J. R. Pierce  
"Theory and Design of Electron Beams"  
New York, Van Nostrand, 1954, p. 194  
TK 7815.P5
- 273 G. Goubau  
"Optical Relations for Coherent Wave Beams  
Electromagnetic Theory and Antennas"  
New York, MacMillan, 1963, pp. 907-918
- 274 H. Kogelnik  
"Imaging of Optical Mode-Resonators With Internal Lenses"  
Bell Sys. Tech. J., Vol. 44, pp. 455-494, March 1965
- 275 H. Kogelnik, et al.  
"On the Propagation of Gaussian Beams of Light Through Lens-Like Media Including Those With a Loss or Gain Variation"  
Applied Optics, Vol. 4, pp. 1562-1569, Dec. 1965

- 276 A. E. Siegman  
"Unstable Optical Resonators for Laser Applications"  
Proceedings IEEE, Vol. 53, pp. 277-287, March 1965
- 277 W. Brouwer  
"Matrix Methods in Optical Instruments Design"  
New York, Benjamin, 1964  
QC 371.B847
- 278 E. L. O'Neill  
"Introduction to Statistical Optics"  
Mass., Addison-Wesley, 1963
- 279 C. S. Williams  
"Gaussian Beam Formulas From Diffraction Theory"  
Applied Optics, Vol. 12, No. 4, pp. 872-876, April 1973
- 280 T. S. Bigelow  
"Design of a Reflectometer System for Measurement of the Plasma Edge Density Profile on TFTR"  
APS Conference, Nov. 1992, Seattle, Washington
- 281 I. Collazo-López  
"Preliminary Results of the ORNL Swept Two-Frequency X-Mode Reflectometer for TFTR"  
APS Conference, Nov. 1992, Seattle, Washington
- 282 Greg Hanson, et al.  
"Microwave Reflectometry for Edge Density Profile Measurements on TFTR"  
To be published. Available from the author at:  
Fusion Energy Div., Y-12 Bldg. 9201-2  
Oak Ridge, TN 37831-8072
- 283 S. Raftopoulos, et al.  
"Design of ICRF antennas for TFTR"  
14<sup>th</sup> IEEE/NPSS Symposium, Sept. 1991, San Diego, Ca.  
pp. 111-114, 91CH3035-3 ©IEEE
- 284 G. R. Hanson  
Drawing provided by Dr. Hanson  
Private communication with Dr. Hanson

- 285 G. R. Hanson  
"Edge Density Profile Measurements in Front of an ICRF antenna"  
Bulletin of the American Physical Society, Vol. 38, No. 10, p.2033 Nov. 1993
- 286 G. R. Hanson  
Private communication with Dr. Hanson.
- 287 G. R. Hanson  
"Results for the TFTR Edge Profile Reflectometer"  
IAEA Technical Meeting on Microwave Reflectometry for Fusion Plasma Diagnostics, Jan. 25-27, 1994.  
Princeton Plasma Physics Laboratory, Princeton, NJ 08543
- 288 S. A. Maas  
"Microwave Mixers"  
Artech House, Dedham, Mass., 1986
- 289 S. Y. Yngvesson  
"Microwave Semiconductor Devices"  
Kluwer Academic Publishers, 1991
- 290 E. R. Collin  
"Foundations for Microwave Engineering"  
McGraw-Hill, N.Y., 1966
- 291 G. L. Matthaei, et al.  
"Microwave Filters, Impedance-Matching Networks, and Coupling Structures"  
Artech House, Dedham, Mass., 1980
- 292 J. A. G. Halherbe  
"Microwave Transmission Line Filters"  
Artech House, Dedham, Mass., 1979
- 293 W. A. Davis  
"Microwave Semiconductor Circuit Design"  
Van Nostrand Reinhold, N.Y., 1984
- 294 M. McCarthy, et al.  
"TFTR Microwave Reflectometer Diagnostic"  
14<sup>th</sup> IEEE/NPSS Symposium, Sept. 1991, San Diego, Ca.  
pp. 1192-1194, 91CH3035-3 ©IEEE

- 295 H. Kogelnik and T. Li  
"Laser Beams and Resonators"  
Proceedings of the IEEE, Vol. 54, No. 10, pp. 1312-1329, Oct. 1966
- 296 Born and Wolf  
"Principles of Optics"  
Pergamon Press, New York, 1959  
QC 355.B63
- 297 David M. Pozar  
"Microwave Engineering"  
Addison-Wesley Publishing Company, New York, 1990  
TK 7876.P69
- 298 J. T. Coleman  
"Microwave Devices"  
Reston Publishing Company, Inc.  
Reston, Virginia 22090  
TK7876.C64  
ISBN 0-8359-4386-0
- 299 O. P. Gandhi  
"Microwave Engineering and Applications"  
Pergamon Press, New York  
TK 7876-G36  
ISBN 0-08-025589-2
- 300 S. N. Van Voorhis  
"Microwave Receivers"  
Massachusetts Institute of Technology Radiation Laboratory Series  
McGraw-Hill Book Company, Inc., 1948
- 301 J. R. Pierce  
"Traveling Wave Tubes"  
D. Van Nostrand Co., Inc., 1950  
Princeton, NJ
- 302 Alfred Electronics and The Singer Company  
"Instruction Manual: Using Stewart BWO Tubes with Grid Leveling"  
3176 Porter Drive, Palo Alto, California 94304  
(415)326-6496

- 303 J. Wilgen, T. Bigelow, G. R. Hanson, I. Collazo  
Material obtained from: "The Reflectometer's Look Book"  
Private communication
- 304 Sierra Milliwave Technolowy (SMT)  
SMT catalog
- 305 Millitech Co.  
Millitech catalog
- 306 Merrimac Co.  
Merrimac catalog
- 307 Walter Joswick  
"I/Q Networks Deliver Various Modulation Formats"  
Microwaves & RF, pp 81-94, March 1994
- 308 R. Nazikian  
Private communication with Dr. Rafi Nazikian
- 309 J. B. Wilgen  
Private communication with Dr. Wilgen
- 310 E. A. Lord and C. B. Wilson  
"The Mathematical Description of Shape and Form"  
Ellis Horwood Series *Mathematics and Its Applications*  
Halsted Press: a division of JOHN WILEY & SONS  
605 Third Avenue, New York, N.Y. 10158  
QA445  
Library of Congress Card No. 83-26685
- 311 Brice Carnahan, H. A. Luther, James O. Wilkes  
"Applied Numerical Methods"  
John Wiley & Sons, Inc.  
Library of Congress Catalog #67-27555  
SBN 471 13507 0

## VITA

Iván Collazo López is the second son of Francisco Collazo González and María Del Carmen López Pujolz, and was born December 20, 1961, in Aquadilla, Puerto Rico, U.S.A.; he is the brother of Humberto and Francisco, Jr. He graduated from the Domingo Aponte Collazo High School at Lares, Puerto Rico, in May 1979, where he earned the honor medals in Mathematics, Best All Round Student, and Services to the Graduating Class. Immediately after high school, he was admitted to the University of Puerto Rico, Rio Piedras campus, where he scored in the top 100 on the entrance test for the School of Natural Science. Mr. Collazo studied physics and mathematics during his four years at the university, finishing a dual bachelor's degree in these fields. After completing his studies at the university, Mr. Collazo started work at the Arecibo Observatory as an assistant engineer, doing real-time test programs for testing data taking equipment. Mr. Collazo was accepted in the graduate program of the Department of Physics, Michigan State University, in the fall 1984. He obtained his Master's degree in the spring of 1986. In 1986, Mr. Collazo also obtained a summer internship with Los Alamos National Laboratory, at Los Alamos, New Mexico. In the fall 1986 he returned to Michigan State University and obtained his second Master's degree in Applied Mathematics in spring 1988. In 1987 he obtained another internship to work with the Lawrence Livermore National Laboratory, Livermore, California. Mr. Collazo started his studies at the Georgia Institute of Technology in 1988, and obtained his third Master's degree in Nuclear Engineering in 1989. In 1990 he moved to the Oak Ridge National Laboratory, Oak Ridge, Tennessee, and started to work on the design of the Novel Dual Frequency Differential Phase reflectometer, which he used to do his Doctoral thesis. On May 14, 1994, Mr. Collazo married Miss Stephanie A. May, whom he met during his first year at Michigan State University.